

MASARYKOVA UNIVERZITA
LÉKAŘSKÁ FAKULTA
BIOCHEMICKÝ ÚSTAV

M U N I
M E D

STUDIUM BIOLOGICKY AKTIVNÍCH AMIDŮ
JAKO
POTENCIÁLNÍCH LÉČIV

*Habilitační práce
(komentář souboru publikovaných článků)*

PharmDr. Jiří Kos, Ph.D.

Název vědního oboru: Lékařská chemie a biochemie

Brno 2022

Na tomto místě bych rád poděkoval Prof. PharmDr. Josefu Jampílkovi, Ph.D. za cenné rady a připomínky, dále PharmDr. Tomáši Goňcovi, Ph.D. za všestrannou podporu a vytvoření podmínek pro tvůrčí práci.

Za toleranci, morální podporu a pochopení chci zvláště poděkovat svým rodičům.

Obsah

1. ÚVOD	4
Antibakteriální látky	6
MRSA a antistafylokokové látky	6
Tuberkulóza a antimykobakteriální léčiva.....	7
Africká trypanosomiáza a antitrypasomální látky.....	9
Virus ptačí chřipky a antivirotika	10
Zánět a antiflogistika	11
Rakovina a protinádorová léčiva	13
Inhibice fotosyntézy xenobiotiky	14
Lipofilita.....	16
2. KOMENTÁŘ K PUBLIKOVANÝM PRACÍM	18
3. ZÁVĚR	21
4. SEZNAM KOMENTOVANÝCH PUBLIKACÍ	22
5. SEZNAM POUŽITÉ LITERATURY	25
6. KOMENTOVANÉ PUBLIKACE	

1. ÚVOD

Syntézou a studiem biologicky aktivních látek jsem se začal zabývat v roce 2007 v rámci mé diplomové práce, kdy mým zaměřením byla příprava biologicky aktivních kokystalů a následně už jako student doktorského studijního programu na Ústavu chemických léčiv Farmaceutické fakulty Veterinární a farmaceutické univerzity v Brně, kde jsem se zaměřil na biologicky aktivní anilidy, které se pak staly stálým objektem mého zájmu v rámci testování antimikrobiální, antitrypanosomální, antivirotické, protizánětlivé, antineoplastické a herbicidní aktivity.

Antibakteriální aktivita s důrazem především na působení proti meticilin rezistentním kmenům *Staphylococcus aureus* testovaly Dr. Iveta Zadražilová, Ph.D., Dr. Šárka Pospíšilová a Dr. Hana Michnová v laboratořích Veterinární a farmaceutické univerzity v Brně.

Antimykobakteriální aktivita proti *Mycobacterium tuberculosis* byla testována ve spolupráci s Prof. Aidanem Coffeyem, Ph.D. z Department of Biological Sciences, Cork Institute of Technology v Irsku. Později potom testování (včetně atypických mykobakteriálních kmenů - *Mycobacterium kansasii*, *Mycobacterium avium*, *Mycobacterium paratuberculosis*, *Mycobacterium marinum*) zajišťovaly Dr. Iveta Zadražilová, Ph.D., Dr. Šárka Pospíšilová a Dr. Hana Michnová v laboratořích Veterinární a farmaceutické univerzity v Brně.

Dr. Carol Clements, Ph.D. ze Strathclyde Institute of Pharmacy and Biomedical Sciences, University of Strathclyde, Glasgow ve Skotsku studovala **antitrypanosomální aktivitu** připravených látek.

Antivirotickou aktivitu proti vybraným kmenům chřipky zjišťoval Prof. H.-J. Zhang ze School of Chinese Medicine, Hong Kong Baptist University.

Od roku 2017 na Katedře farmaceutické chemie Farmaceutické fakulty Univerzity Komenského v Bratislavě jsem se začal zabývat deriváty kyseliny skořicové. Výzkum jsem potom převedl na nové pracoviště Regionální centrum pokročilých technologií a materiálů Univerzity Palackého v Olomouci, kde **protizánětlivou aktivitu** testoval docent Jan Hošek, Ph.D.

Protinádorová aktivita zejména hydroxynaftanilidů byla testována Doc. Peterem Kollárem, Ph.D. na Farmaceutické fakultě Veterinární a farmaceutické univerzity v Brně a také Prof. Ricardo D. Enrizem, Ph.D. na Faculty of Chemistry, Biochemistry and Pharmacy &

Institute of Multidisciplinary of Biological Research, National University of San Luis v Argentině.

Nedílnou součástí screeningu biologické aktivity připravených látek bylo i zjišťování jejich **lipofility** metodou HPLC jakožto důležitého fyzikálně-chemického parametru pro studia vztahu struktury a účinku.

Předkládaná habilitační práce je souhrnem dosavadních výsledků vědecké činnosti, které byly publikovány v odborné literatuře, prezentovány na tuzemských a zahraničních konferencích prostřednictvím plakátových sdělení (46 konferenčních abstraktů), elektronických konferencích^{1,2,3,4,5,6,7,8,9,10,11,12,13} a byly součástí dvou patentových přihlášek^{14,15}. Studium nových látek bylo rovněž podpořeno čtyřmi úspěšně řešenými grantovými projekty, jichž jsem byl buď řešitelem, nebo členem řešitelského týmu.

Antibakteriální látky

Přizpůsobování mikroorganismů vnějším vlivům, a tím i vývoj jejich rezistence vůči antimikrobiálním látkám, není překvapením. Tento proces je bohužel rychlejší a rychlejší. Vznikající rezistence mikrobiálních patogenů na klinicky užívaná léčiva, včetně léčiv druhé a třetí volby, a vývoj křížově rezistentních nebo multirezistentních kmenů je tedy alarmující. Mikrobiální patogeny byly schopné vyvinout řadu mechanismů pro přizpůsobení se účinkům prostředí. Ačkoli objev nových molekul je prioritou, od 90. let minulého století je na trhu pouze zanedbatelný počet skutečně nových protinfekčních léčiv pro systémové podání.¹⁶

MRSA a antistafylokokové látky

Vzrůstající rezistence vůči stávající antimikrobiální léčbě vyvstává zejména u patogenu *Staphylococcus aureus*, grampozitivní bakterii patřící do rodu stafylokoků, způsobující závažné a dlouhodobě přetrvávající celosvětové zdravotní problémy. Methicilin rezistentní *Staphylococcus aureus* (MRSA) může způsobovat řadu orgánově specifických infekcí. Nejčastěji se jedná o postižení kožní a podkožní tkáně, které následují invazivní infekce, jako je osteomyelitida, meningitida, pneumonie, plicní absces a empyém. MRSA je rovněž závažnou příčinou bakteriální endokarditidy, která může zapříčinit smrt přibližně u třetiny infikovaných pacientů. MRSA byl poprvé popsán v roce 1961 a od té doby se stal jedním z nejvýznamnějších bakteriálních patogenů v klinické praxi, který byl izolován po celém světě. Původně byl jeho výskyt omezen pouze na nemocniční zařízení, kde byl původcem nozokomiálních infekcí.^{17,18} V dnešní době je ale častou příčinou infekcí ve společnosti. Je často přítomen asymptomaticky u zdravých jedinců na různých částech lidského těla, jako je kůže, kožní žlázy a sliznice, včetně nosu a střev. Klíčovým důvodem rezistence MRSA k beta-laktamovým antibiotikům je přítomnost genové sekvence *mecA*, o které je známo, že vytváří transpeptidasu PB2a, která snižuje afinitu organismu k vazbě na beta-laktamová antibiotika. Poslední studie ukazují, že i přes dostupnou antibakteriální terapii infekce MRSA způsobují vážné klinické následky. Vlivem častých změn kvalitativních vlastností MRSA, se jedná o jednu z nejhůře klinicky léčitelných bakterií. U většiny nekomplikovaných infekcí měkkých tkání se volí empirická léčba pomocí perorálních antibiotik (trimethoprim/sulfamethoxazol, doxycyklin, minocyklin, klindamycin). Parenterálně jsou antibiotika indikována u komplikovanějších infekcí a při hrozbě systémového postižení. Lékem volby je vankomycin, který může být nahrazen při špatné toleranci daptomycinem. Mezi další krátkodobě působící látky patří ceftarolin a telavancin. Dlouhodobě působící možnosti léčby zahrnují dalbavancin

a oritavancin. Při bakterémii se jako adekvátní léčba volí rovněž vankomycin a daptomycin. Při alergii, toxicitě nebo rezistenci se volí jako alternativa telavancin a ceftarolin případně vhodně volené kombinace zmíněných antibiotik. Jako další možnost léčby bakterémie MRSA je použití bakteriostatického glykopeptidu teikoplaninu. V aktivitě a účinnosti se vyrovná vankomycinu, na rozdíl od kterého je lépe snášen. Problém je ale často jeho omezená dostupnost. Vzhledem ke zmiňované toxicitě, obecné nedostupnosti léků a rezistenci k dostupným perorálním léčivům, je nutné se rovněž soustředit na nové anti-MRSA účinné preparáty.¹⁹

Tuberkulóza a antimykobakteriální léčiva

Jak bylo popsáno výše, rostoucí počet bakteriálních a mykobakteriálních infekcí podtrhuje důležitost výzkumu nových protiinfekčních a protiinvazních chemoterapeutik. Tuberkulóza (TB) a jiná mykobakteriální onemocnění jsou časté, v mnoha případech život ohrožující, choroby způsobené různými druhy mykobakterií. Samotné onemocnění vyvolané bakteriemi *Mycobacterium tuberculosis* (Mtb) představuje globální hrozbu pro zdraví lidstva. Zvláště pro rychle rostoucí počet tuberkulózních kmenů multirezistentních (MDR-TB), extenzivně rezistentních (XDR-TB), totálně rezistentních (TDR-TB), různých latentních forem Mtb a mykobakteriálních infekcí způsobených atypickými kmeny mykobakterií (NTM) nebo smrtelných kombinací HIV pozitivních pacientů s mykobakteriálními infekcemi je nutné hledat nové léky a nové racionální postupy léčby.²⁰ Tuto situaci umocňuje fakt, že jako léky první volby se stále používají několik desetiletí stará léčiva rifampicin a isoniazid. Léčba jedním preparátem vzhledem k rozsáhlým genetickým mutacím mykobakterií a vznikem mnohačetných lékových rezistencí nestačí. Proto je v současné době využívána troj až čtyřkombinace léčiv.^{21,22} Celosvětově za rok 2018 onemocnělo tuberkulózou přibližně 10 milionů lidí. Tento nárůst se v posledních letech ustálil. Prevalence tuberkulózního onemocnění se v jednotlivých zemích značně liší, od méně než pěti do více než 500 nových případů na 100 000 obyvatel za rok, s celosvětovým průměrem kolem 130. Odhaduje se, že v roce 2018 došlo přibližně k 1,2 milionu úmrtí na tuberkulózu u HIV-negativních lidí, což je o 27 % nižší hodnota než v roce 2000. Dalších přibližně 251 000 úmrtí na toto onemocnění bylo za rok 2018 uvedeno mezi HIV pozitivními lidmi, což znamenalo až 60% snížení oproti počtu 620 000 v roce 2000. Tuberkulóza postihuje lidi obou pohlaví ve všech věkových skupinách, ale nejvyšší zatížení je u mužů (ve věku ≥ 15 let), kteří v roce 2018 tvořili 57 % všech

případů TBC. Pro srovnání, ženy představovaly 32 % a děti (ve věku <15 let) 11 %. Ve všech případech TBC bylo 8,6% lidí žijících s HIV (PLHIV).²⁰

Tabulka 1. Rozdělení klinicky užívaných antituberkulotik.

Perorální anti-TB první řady	INH, RIF a rifabutin, PZA, EMB
Parenterální anti-TB druhé volby	amikacin, kapreomycin, KAN, STM, (viomycin)
Fluorochinolony	ofloxacin, levofloxacin, moxifloxacin, (gatifloxacin)
Perorální anti-TB druhé řady	cykloserin, terizidon, ethionamid, prothionamid, PASA
Léčiva s nejasnou úlohou v léčbě MDR-TB	amoxicilin/klavulanát, imipenem, klarithromycin, klofazimin, thioacetazon, linezolid, vysoké dávky INH

Patogenní role netuberkulózních (atypických) mykobakterií (NTM) nebyla vždy v popředí zájmu. Nicméně tyto atypické mykobakterie mohou způsobovat onemocnění lymfatického systému, infekce kůže a měkkých tkání a dále netuberkulózní, v dnešní době časté a od TB těžko rozpoznatelné infekce plic. Kromě *Mycobacterium tuberculosis* a *Mycobacterium leprae* je většina mykobakterií široce rozšířena v půdě a ve vodě ve venkovských i městských prostředích po celém světě, zahrnující přírodní i užitkové vodní zdroje (*Mycobacterium kansasii*, *Mycobacterium xenopi*, a *Mycobacterium simiae* jsou izolovány téměř výhradně z komunálních odpadních zdrojů). Vzhledem k tomu, že jsou tyto mikroorganismy chráněny na lipidy bohatou buněčnou stěnou, jsou odolné vůči dezinfekčním prostředkům a přípravkům na úpravu vod. Převládá názor, že původ těchto onemocnění pochází z životního prostředí. Jedná se např. o vdechování či požití aerosolů, prachu, přenos při chirurgických zákrocích, poraněních nebo zavedení katetrů. Přesný zdroj je nicméně velmi složité identifikovat.^{23,24,25}

Tabulka 2. NTM druhy/komplexy rozdělené podle rychlosti růstu.

Pomalou rostoucí kmeny	Středně rychle rostoucí kmeny	Rychle rostoucí kmeny
<i>M. avium komplex</i>	<i>M. marinum</i>	<i>M. abscessus</i>
<i>M. kansasii</i>		<i>M. chelonae</i>
<i>M. xenopi</i>		<i>M. fortuitum</i>
<i>M. malmoense</i>		<i>M. smegmatis</i>
<i>M. simiae</i>		
Pomalou rostoucí je definováno jako >7 dní potřebných pro viditelný nárůst ze subkultury		

Počet mykobakteriálních infekcí, které mohou být spojovány s konkrétními druhy, stejně jako počet nových druhů jako etiologických agens v posledních několika letech prudce stoupl v důsledku nárůstu počtu imunokompromitovaných pacientů.²⁰ Vzhledem k MDR-TB a NTM je výzkum nových antimykobakteriálních látek prioritou k dosažení účinné kontroly TB i NTM.

Africká trypanosomiáza a antitrypanosomální látky

Spavá nemoc, lidská africká trypanozomiáza (Human African Trypanosomiasis, HAT), je tropické onemocnění přenášené mouchami tse-tse (*Glossina spp.*). Je způsobena protozoálními parazity *Trypanosoma brucei*. V závislosti na typu parazita má dvě formy. *T. b. gambiense* HAT (gHAT) je chronické onemocnění přenášené mezi lidmi kontaktem člověk-tsetse-člověk a udržované vertikálním přenosem. Představuje 98% všech hlášených případů. *T. b. rhodesiense* HAT (rHAT) je akutní onemocnění se složitou epidemiologií zahrnující přenos mezi divokými či hospodářskými zvířaty a lidmi. Představuje 2% všech hlášených případů. Obě neléčené formy mohou mít pro pacienta fatální konec, kdy se paraziti množí v těle, procházejí hematoencefalickou bariérou a napadají centrální nervový systém.^{26,27, 28}

Afrika jako nejčastější místo výskytu je mnohdy příčinou nezájmu farmaceutických firem. Tato oblast totiž neoplývá dostatečným množstvím finančních prostředků k tomu, aby byla schopna výzkum, vývoj i distribuci léčiv finančně zabezpečit. Ať už spavá nemoc u lidí (africká trypanosomiáza) nebo Nagana u zvířat, v obou případech se jedná o jedno z nejnebezpečnějších onemocnění postihujících Africký kontinent. Problém v podobě neúspěšnosti léčby je přikládána přítomnosti VSG glykoproteinu, pomocí kterého parazit dokáže modifikovat svou antigenní výbavu. Díky tomu pak dokáže obcházet imunitní systém hostitele.^{29,30}

Pro léčbu je v současné době k dispozici pouze pět léčiv: amidinový derivát pentamidin (proti *T. b. gambiense*) a polysulfonovaný naftalenový derivát suramin (proti *T. b. rhodesiense*) se používají v první fázi léčby, arzenový, dimerkaptopropanolový derivát melarsoprol (používá se k léčbě obou typů), analog aminokyseliny ornitinu eflornitin a nifurtimox (proti *T. b. gambiense*) se používají pro druhou fázi léčby. Kromě toho, že je nutné léčiva podávat parenterálně, je léčba provázena řadou mnohdy život ohrožujících nežádoucích účinků. U suraminu riziko představují anafylaktický šok, selhání ledvin, neurologické anomálie, vyrážky, hypokalcémie a hyperglykémie. Pentamidin až u 10 % pacientů způsobuje snížení krevního tlaku a hladinu glykémie, dále potom může vyvolat nefrotoxicitu, leukopenii a tvorbu jaterních abnormalit. Melarsoprol, který je schopný procházet hematoencefalickou bariérou, způsobuje u 5-10 % léčených pacientů reaktivní encefalopatie, které mohou vyústit až v koma. Eflornitin je jako inhibitor ornitin dekarboxylázy relativně bezpečnějším léčivem ve srovnání s melarsoprolem. Přesto se během jeho aplikaci při léčbě trypanozomiáz často vyskytují nežádoucí účinky jako gastrointestinální potíže či poškození kostní dřeně. Vzhledem k tomu, že nové léčivo bez nežádoucích účinků nebylo v posledních desetiletích objeveno a s přihlédnutím k výše zmíněným faktům, je důležité hledat nové a levné typy léčiv pro dosažení účinné kontroly afrických trypanosom.^{30,31,32,33,34,35,}

3-Hydroxynaftalen-2-karboxanilidy, cyklické analogy salicylanilidů s přítomnou amidovou skupinou a prostorově blízkou hydroxylovou částí na naftalenovém skeletu, byly připraveny a publikovány jako sloučeniny s prokázanou biologickou aktivitou.^{36,37} Salicylanilidy jsou známé jako látky se širokým spektrem biologických aktivit.^{38,39} Vlastnosti amidové skupiny lze snadno modifikovat různými substitucemi. Amidová skupina se také vyskytuje v mnoha antiprotosoálních léčivech. V důsledku tvorby vodíkových vazeb mezi skupinou amidů CONH a cílovými proteiny CONH mohou nastat změny v konformaci proteinů, což vede k usmrcení protozoí.^{26,30,40,41,}

V souvislosti s výše uvedenými skutečnostmi byla série substituovaných 3-hydroxynaftalen-2-karboxanilidů³⁶ testována na jejich *in vitro* antitrypanosomální aktivitu proti modelovému nepatogennímu druhu *T. b. brucei*.

Virus ptačí chřipky a antivirotika

Virus chřipky A je celosvětově hlavní příčinou sezónní nebo pandemické chřipky, onemocnění s vysokou morbiditou a signifikantní úmrtností. Patří do rodiny RNA virů, které se

označují termínem *Orthomyxoviridae*. Díky tomu, že se virus chřipky A neustále vyvíjí důsledkem své antigenní mutace a adaptace, způsobuje epidemie a celosvětové pandemie jako např. v letech 1918 H1N1 (španělská chřipka), 1957 H2N2 (asijská chřipka), 1968 H3N2 (Hongkongská chřipka), 2005 H5N1 (ptačí chřipka), 2009 H1N1 (prasečí chřipka) a v poslední době H7N9 (ptačí chřipka) z roku 2013. Mezi dvě základní strategie v boji proti chřipce A patří vakcinace a používání malých molekul antivirotik. Ta jsou účinná zejména v časném stádiu onemocnění během epidemie.⁴²

Chřipkové onemocnění způsobené vysoce patogenním virem ptačí chřipky H5N1 je jedním z nejničivějších virových infekčních onemocnění způsobených zoonózami na celém světě. V současnosti jsou pro prevenci a léčbu těchto infekcí schváleny pouze dvě třídy antivirotik. Jsou to blokátory iontových kanálů M2 a inhibitory neuraminidasy. Jejich prospěch byl omezen nízkou účinností při eradikaci viru, jejich vedlejšími účinky a rychlým vznikem virových kmenů rezistentních na léčivo.⁴³ Proti ptačí chřipce se používá oseltamivir komerčně dostupný pod názvem Tamiflu®. Jeho aktivita spočívá v inhibici virové neuraminidasy, enzymu, který prostřednictvím odštěpení kyseliny sialové z glykoproteinů nově vznikajícího obalu umožňuje uvolňování nových virových částic z hostitelských buněk. Klinický přínos oseltamiviru je největší, pokud je podán do 48 hodin od nástupu příznaků chřipky. Po uplynutí této doby se účinnost léčiva významně snižuje. Benifit oseltamiviru je ale diskutabilní. Studie z roku 2014 přinesla údaje o omezeném přínosu léčiva. Autoři v ní došli k závěru, že užívání oseltamiviru má u dospělých jen nespecifický a nízký vliv na příznaky a neexistují dostatečné důkazy o snížení rizika komplikací chřipky, jakou je např. pneumonie. V poměru risk/benefit tak převažují nežádoucí účinky (nauzea, zvracení, psychiatrické účinky) nad malým klinickým přínosem oseltamiviru.⁴⁴

Ačkoli byla studována řada různých skupin přírodních sloučenin na jejich anti-H5N1 aktivitu, proti ptačí chřipce nebyly zkoumány žádné chinolonové alkaloidy.⁴⁵ V nedávných studiích bylo popsáno, že sloučeniny na bázi chinolinu vykazují antivirové vlastnosti^{46,47,48,49}, a proto byly v souvislosti s výše uvedenými skutečnostmi podrobeny primárnímu screeningu na antivirotickou aktivitu látky typu 8-hydroxychinolin-2-karboxanilidů.

Záněť a antiflogistika

Záněť je fyziologická imunitní reakce spuštěná při poranění nebo při obraně organismu proti infekčním agens. Hlavní úlohou zánětu je eradikace škodlivého původce a obnovení

homeostázy tkáně.⁵⁰ Za normálních podmínek je regulován pomocí negativní zpětné vazby. V opačném případě však může dojít k nekontrolovanému kontinuálnímu průběhu s vyústěním do chronické fáze. Chronický zánět je charakteristickým znakem mnoha chorob, včetně aterosklerózy,⁵¹ revmatoidní artritidy,⁵² psoriázy,⁵³ rakoviny,⁵⁴ chronických onemocnění dýchacích cest⁵⁵ a diabetu 2. typu⁵⁶. Dokázat modulovat a řídit zánětlivou odpověď a zánět samotný je velkou výzvou pro současnou medicínu. Ač se dosáhlo značného pokroku v porozumění buněčných a molekulárních jevů, které se podílejí na akutní zánětlivé reakci při infekci, o příčinách a mechanismech systémového chronického zánětu, který se vyskytuje u celé řady nemocí, včetně již zmiňovaných diabetu 2. typu a kardiovaskulárních chorob, je však známo mnohem méně.⁵⁰ Uvažuje se, že tyto chronické zánětlivé stavy nejsou způsobeny klasickými podněty zánětu (infekce a poranění). Místo toho se zdá, že jsou spojeny s poruchou funkce tkáně; to znamená s homeostatickou nerovnováhou jednoho z několika fyziologických systémů, které nejsou přímo funkčně spojeny s obranou hostitele nebo opravou tkáně. Příkladem takového chronického postižení může být i revmatoidní artritida (RA), onemocnění ne zcela objasněné etiologie, jehož léčba je pouze symptomatická. Projevuje se zánětlivými změnami synoviální tkáně kloubů, chrupavek a kostí. Může docházet i k mimokloubním projevům, jakou jsou různé systémové a orgánové postižením (kožní, plicní, cévní abnormality, anémie...), proto je toto onemocnění zařazeno mezi systémové autoimunitní onemocnění. Zánět se projevuje především bolestí kloubů, otokem a následnou destrukcí chrupavky a kostí, jakož i systémovými projevy způsobenými metabolity kyseliny arachidonové a různými zánětlivými cytokiny.^{57,58}

Naději v léčbě RA znamenalo zavedení methotrexátu. Jedná se o syntetické, chorobu modifikující léčivo (DMARD). I do současné doby si zachovává důležité postavení v rámci léčby RA a v neposlední řadě je součástí kombinované terapie. I přes tento úspěch bylo nutné zavést do praxe cílenější léčbu. To přinesl až pokrok výzkumu molekulárních a hybridomových technologií. Pomocí biologické léčby lze dosáhnout remise choroby a navrátit pacienta do plnohodnotného života. Přes nepochybně lepší účinnost těchto látek je závažnou otázkou jejich bezpečnost a riziko infekčních onemocnění při dlouhodobém užívání, neboť biologická léčba je již součástí komplexní terapie pacientů s RA. Právě z těchto důvodů je důležité hledat stále nové léky, ať už syntetické nebo biologické, které by mohly pomoci v léčbě revmatických onemocnění.^{59,60,61,62}

Jednou z cest je použití přírodních léčiv a z nich připravených derivátů. Přírodní látky jsou velkým zdrojem bioaktivních sloučenin a je známa řada klinicky užívaných léčiv, které byly získány z rostlin či hub. Jednou takovou látkou je kyselina skořicová, malá molekula vyskytující se v různých rostlinách buď v čisté formě, nebo jako součást složitějších struktur. V minulé době bylo prokázáno její široké spektrum biologické aktivity, jako je např. antimikrobiální, protinádorová, anti-oxidační a v neposlední řadě také protizánětlivá.^{63,64,65,66,67}

N-Arylcinnamidy představují skupinu syntetických derivátů kyseliny skořicové. Tyto molekuly obsahují několik zajímavých potenciálně aktivních částí. Jedná se o styryl, amid a aryl. Z toho důvodu mohou být anilidy kyseliny skořicové považovány za privilegované struktury.^{68,69,70,71}

Rakovina a protinádorová léčiva

Na základě dostupných informací International Agency for Research on Cancer při WHO je odhadován celosvětový nárůst onemocnění rakovinou na 18,1 milionu nových případů a 9,6 milionu úmrtí. Uvádí se, že se statisticky rakovina vyvinula během života u jednoho z pěti mužů a u jedné z šesti žen, přičemž u mužů jeden z osmi a u žen jedna z jedenácti na tuto chorobu umírá. Celosvětově potom žije 43,8 milionu lidí v tzv. pětileté prevalenci, což znamená pět let života od zjištěné diagnózy onemocnění. Nárůst zátěže způsobenou rakovinou může být způsoben několika faktory včetně neustálého růstu a současného stárnutí populace.^{72,73}

Z hlediska incidence se řadí mezi tři hlavní typy rakoviny kolorektální karcinom, karcinom prsu a plic. Celosvětově jsou tyto formy zodpovědné za jednu třetinu celkového počtu výskytu rakoviny. Rakovina prsou u žen a rakovina plic jsou celosvětově vedoucím typem rakoviny v počtu nových případů. V roce 2018 se odhaduje přibližně 2,1 milionu nových diagnóz, což představuje asi 11,6% z celkového počtu případů rakoviny. Rakovina tlustého střeva a konečníku (1,8 milionu případů, 10,2% z celkového počtu) je třetí nejčastěji diagnostikovanou rakovinou, rakovina prostaty je čtvrtá (1,3 milionu případů, 7,1 %) a rakovina žaludku je pátá (1,0 milionu případů, 7,1%). Rakovina plic je potom odpovědná za nejvyšší počet úmrtí (1,8 milionu úmrtí, 18,4% z celkového počtu).⁷³

Jedním ze stále neúčinnějších nástrojů v léčbě nádorových onemocnění je chemoterapie. V rámci výzkumu jsou pak hledány nové léky a zároveň zkoumány stávající pro

nové využití. Nové studie potom pomohly zlepšit naše porozumění mechanismu účinku těchto látek, někdy rozšířily spektrum aktivity a v neposlední řadě našly nové cesty jak zlepšit prognózu pacientů. Hlavní myšlenkou vývoje je cílená terapie, kdy jsou molekuly chemoterapeutik navrhovány tak, aby napadaly pouze rakovinné buňky, zatímco normální poškozovaly co nejméně.⁷²

V rámci výzkumu nových protirakovinných látek se zjišťují jejich antiproliferační účinky. Pro naše účely byly použity THP-1 a MCF-7 buněčné nádorové linie. THP-1 je lidská monocytární buněčná linie, která je používána ke studiu monocyto/makrofágových funkcí, mechanismů, signálních drah a transportu živin a léčiv. Podle studií se THP-1 buňky podobají morfologicky a ve funkčních vlastnostech monocytům a makrofágům, které patří k přirozené imunitní výbavě. Hlavními funkcemi jsou (1) identifikace cizorodých patogenů, (2) podpora tvorby buněk eliminující patogeny, (3) regulace zánětu prostřednictvím tvorby chemokinů a citokinů a (4) fagocytóza. Buněčná linie MCF-7 byla odvozena z pleurálního výpotku odebraného 69-ti leté pacientce s metastatickým karcinomem prsu a stala se standardním modelem ve statisících laboratořích po celém světě.^{74,75}

V dalších studiích látek připravených naší skupinou byly hledány potenciální inhibitory BRAF. Jedná se o onkogenní mutantní protein, který je exprimován v několika typech rakovinných buněk, včetně buněk melanomu. V případě mutace trvale vysílá signály, které podporují růst buněk a jejich dělení. US Food and Drug Administration (FDA) schválil dva léky ze třídy malých molekul, které se používají na léčbu metastatického melanomu. Jsou to vemurafenib a dabrafenib. Jejich použití však není ideální, neboť u pacientů dochází k trvalé rezistenci a k projevům sekundárních toxických účinků. Tato omezení zdůrazňují důležitost navrhování nových a lepších inhibitorů.⁷⁶

Inhibice fotosyntézy xenobiotiky

Společným principem při vývoji nových pesticidů a humánních je snaha o cílené působení látek na určité buněčné struktury se snahou ovlivnit jen konkrétní funkce. Samozřejmě pak může docházet k situaci, kdy se tyto cíle překrývají pro obě skupiny a farmaka a pesticidy tak ovlivňují totožné molekulární procesy. Zároveň je nutné dodat, že dopad působení těchto látek může být u rostlin a zvířat zcela odlišný. Na rostlinu herbicidně působící látka tak může mít i příznivý mikrobiologický efekt u savců.⁷⁷ Na základě těchto poznatků potom farmaceutické společnosti hodnotí biologicky aktivní sloučeniny jednak jako

agrochemikálie a druhak jako farmaka a na základě výsledků dochází k tomu, že se z pesticidů stávala léčiva a naopak.^{77,78,79,80} S ohledem na tato fakta je třeba zmínit, že používáním herbicidů může být ovlivněna účinnost některých antibiotik (snížení či zvýšení MIC) a zároveň může dojít k vývoji rezistence na antibiotika u lidí. Známa je schopnost herbicidů indukovat adaptivní fenotypový typ rezistence proti vícero antibiotikům. Ta potom může být způsobená např. zvýšenou expresí efluxních pump nebo znesnadněním vstupu molekul antibiotika do buněk.⁸¹

Na základě dříve provedených vědeckých prací je možné konstatovat, že přítomnost uskupení –NHCO– (alternace peptidové vazby) a rovněž i hydroxylové, resp. fenolické skupiny v molekule studovaných látek umožňují snazší interakci studovaných látek s proteiny buňky, které rovněž jako polypeptidy obsahují segment –NHCO–.^{82,83} Interakce se tak nejpravděpodobněji uskutečňuje prostřednictvím vodíkových vazeb. Děje se tak prostřednictvím reverzibilní vazby na proteinový komplex v membránách tylakoidů, který katalyzuje oxidaci vody a redukci plastochinonu.⁸⁴ S přihlédnutím k těmto důvodům byly vybrané látky testovány na jejich schopnost inhibovat elektronový transport (PET) v chloroplastech špenátu (*Spinacia oleracea* L.) pomocí Hillovy reakce.⁸⁵ Jako porovnávací látka byl použit účinný inhibitor fotosyntézy (PS II) ze skupiny herbicidů 3-(3,4-dichlorophenyl)-1,1-dimethylurea, DCMU, (Diuron®). Při vlastním experimentu byla stanovena hodnota IC₅₀, tedy koncentrace látky, která způsobí pokles aktivity chloroplastů na polovinu. Tato hodnota je potom mírou herbicidní aktivity zkoumané látky. Jako elektronakceptor byl použit roztok barviva 2,6-dichlorfenolindofenolu (DCPIP). Při spektrofotometrickém vyhodnocení byl pokles jeho absorbance při dané vlnové délce (600 nm) mírou poklesu samotného elektronového transportu v chloroplastech špenátu.

V poslední době bylo do praxe zavedeno jen malé množství herbicidů. Tím pádem se staré látky aplikovaly dlouhodobě a ve větších množstvích. Tento proces samozřejmě znamenal nárůst rezistence na herbicidně působící látky. Zároveň se objevily nové rezistentní rostlinné druhy a u některých látek jsou pozorované toxické účinky na různé živočišné druhy včetně člověka. Pro všechna tato negativní fakta v rámci používání herbicidních látek je nutné hledat nové s lepším profilem účinnosti a bezpečnosti. Široký screening biologických vlastností nových sloučenin se zkoušením herbicidní aktivity je rovněž potřebný pro zjišťování jejich dopadu na životní prostředí ve smyslu negativního vlivu na „necílové“ organismy.^{86,87,88,89,90}

Lipofilita

V rámci závěrečného hodnocení vztahu struktury a účinku (SAR) připravených látek se používá různých molekulárních deskriptorů, topologických indexů nebo parametrů popisujících fyzikálně-chemické vlastnosti sloučenin. Pomocí těchto číselných parametrů pak lze charakterizovat vlastnosti, které ovlivňují biologickou aktivitu látek nebo také navrhnout způsob budoucího zpracování nových léčiv do vhodné galenické formy. Velmi důležitou fyzikálně-chemickou vlastností látek je lipofilita, která stojí v popředí zájmu při QSAR studiích. Přímo souvisí s rozpustností látek ve vodné fázi či membránové permeabilitě a ovlivňuje tak farmakokinetiku látky během absorpce, distribuce, metabolismu a exkrece (ADME). Transport přes biologické membrány je nejčastěji zprostředkován pasivní difuzí, proto má hydrofobicita látky zásadní význam.^{91,92}

Lipofilita bývá nejčastěji charakterizována pomocí rozdělovacího koeficientu $\log P$. Jedná se o podíl látkové koncentrace léčiva v organické a vodné fázi dvousložkového systému. Vyjadřuje tak amfifilní charakter látky *in vitro*. $\log P$ lze poměrně snadno stanovit pro každou molekulu bez náboje, látky v iontovém a amfiontovém stavu potom omezeně. Pro hodnocení je stěžejní výběr rozdělovací soustavy tak, aby co nejlépe odpovídala systému vodné a organické biofáze. Vzhledem k tomu, že v biologických membránách, které představují hlavní lipidovou biofázi, je velké množství amino a hydroxy skupin, a protože jsou tyto biofáze nasycené vodou, ukázala se jako velmi praktická soustava vyšší *alkohol/voda* (např. *n*-oktanol/voda).^{93,94,95,96}

V současné době se určují hodnoty $\log P$ z retenčních parametrů vysokoúčinné kapalinové chromatografie (High Performance Liquid Chromatography - HPLC) s použitím reverzní fáze, kdy je proces zadržování analytu řízen hydrofobními interakcemi mezi analytem a reverzním separačním systémem. Právě retence látek v kapalinové chromatografii je zapříčiněna a současně ovlivněna jejich hydro/lipofiními vlastnostmi. Rovněž byla zjištěna dobrá korelace s *n*-oktanol/voda rozdělovacím koeficientem $\log P$. Výhodou této metody je zároveň její značná automatizace a možnost separace analytu od případných nečistot. Při samotném stanovení se odečítá retenční čas analytu při použití různého množství organické frakce v mobilní fázi a chromatografické kolony se silikagelem modifikovaným oktadecylovými řetězci (tzv. C_{18} endkapovaná RP-HPLC kolona). Ze získaných hodnot retenčních se vypočítá parametr lipofility logaritmus kapacitního faktoru ($\log k$), který je možné porovnávat s $\log P$.^{97,98}

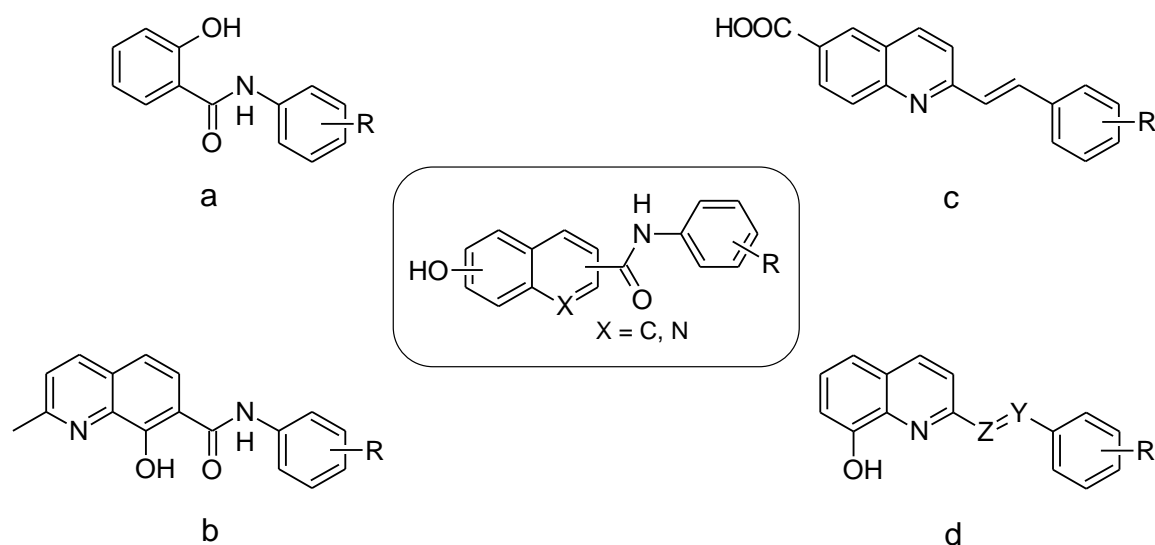
Lipofiní vlastnosti látek je možné současně predikovat pomocí vhodného softwaru. Ve výsledných hodnotách $\log P$ /Clog P je zahrnut příspěvek všech fragmentů molekuly (atomy, funkční skupiny). Každý software má databáze těchto fragmentů, ze kterých výpočet probíhá. Nevýhodou je, že tyto programy často nedokáží odlišit polohové izomery a také to, že různí výrobci mají různé knihovny, a proto se výsledné hodnoty lipofility mohou lišit. Proto je nutné provádět měření rovněž experimentálně.^{99,100}

2. KOMENTÁŘ K PUBLIKOVANÝM PRACÍM

Předkládaný přehled publikací zahrnutý do habilitační práce představuje dvanáct let mé vědecké činnosti. Společným tématem pro většinu prací je příprava biologicky aktivních molekul.

Během odborné stáže ve společnosti ZENTIVA jsem dostal za úkol přípravu kokrystalů vybraných bisfosfonátů s cílem zlepšit jejich biologickou dostupnost. Gastrointestinální absorpce bisfosfonátů je obecně pouze asi 1 %. K řešení tohoto problému byly navrženy směsi monosodné soli risedronátu a ibandronátu s různými cukernými alkoholy, furanózami, pyranózami a gluko-, manno- a galaktopyranosidovými deriváty jako protiionty ve snaze připravit kokrystaly (nové entity se zlepšenou absorpcí ze střeva). Krystalické formy byly generovány pomocí kineticky a/nebo termodynamicky řízených krystalizačních procesů.^{101, 102}

Během postgraduálního studia se můj zájem zúžil na přípravu strukturně jednoduchých biologicky aktivních amidů. Naši inspirací se staly salicylanilidy, u kterých studie odhalily zajímavé fyzikálně-chemické vlastnosti a široké spektrum biologické aktivity zahrnující vlastnosti antibakteriální, antimykobakteriální, herbicidní, anthelmintické, antifungální, antivirotické či antineoplastické.^{103,104,105,106,107,108} Námi navržené struktury tak vycházejí ze strukturní analogie, bioisosterie, resp. polohové izomerie s již zmiňovanými salicylanilidy resp. hydroxyarylkarboxanilidy (Obrázek 1a), dále pak s hydroxychinolinkarboxanilidy¹⁰⁹ (Obrázek 1b) a styrylchinoliny^{110,111,112,113,114} (Obrázek 1c,d).



Obrázek 1

Pomocí mikrovlnné syntézy jsme v širším týmu s Dr. Tomášem Goňcem, Ph.D. a Prof. Josefem Jampálkem, Ph.D. principem „click chemistry“ dokázali vytvořit velmi obsáhlou sérii látek, jejichž následným studiem jsme přispěly v poznání vztahu struktury a účinku tohoto typu molekul a dané poznatky jsme mohli prezentovat prostřednictvím plakátových sdělení, elektronických konferencí^{3,4,5,6,7,8,10,11} a zejména pak časopisecky^{28,37,76,115,116,117,118,119,120,121,122,123,124,125,126,127,128,129,130,131,132,133,134}.

Primárním cílem naší skupiny bylo testování antimikrobiální aktivity připravených derivátů. MRSA je jedním z nejvýznamnějších bakteriálních patogenů v klinické praxi, který byl izolován po celém světě. V **publikacích č. 1, 9 a 15** je toto téma diskutováno. Deriváty 8-hydroxychinolin-2-karboxanilidu, byly pak testovány na schopnost ovlivňovat viabilitu a metabolismus síry u bakterie *Desulfovibrio piger* (**publikace č. 7 a 10**), která je ve zvýšené míře izolována u pacientů s gastrointestinálními potížemi, které mohou být příčinou zánětlivých procesů ve střevech.¹³⁵

Tuberkulóza (TB) a jiné mykobakteriální onemocnění jsou časté, v mnoha případech život ohrožující, choroby způsobené různými druhy mykobakterií. Zvláště pro rychle rostoucí počet tuberkulózních kmenů multirezistentních (MDR-TB), extenzivně rezistentních (XDR-TB) a mykobakteriálních infekcí způsobených atypickými kmeny mykobakterií (NTM). Studiem antimykobakteriálních hydroxy(aza)naftanilidů se zabývají **publikace č. 1, 2, 3, a 15**.

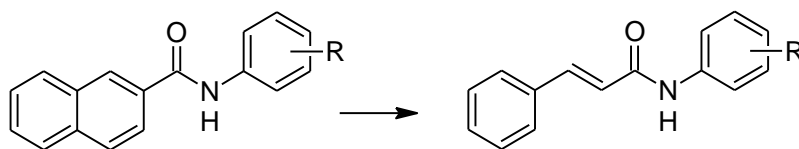
U série 3-hydroxynaftalen-2-karboxanilidů se substituovaným anilinovým kruhem kruhem se testovala jejich *in vitro* antitrypanosomální aktivita proti *Trypanosoma brucei brucei* (forma krevního řečiště S427). Výsledky jsou diskutovány v **publikaci č. 8**.

U látek tohoto typu se rovněž potvrdil antineoplastický potenciál. **Publikace č. 6** diskutuje vliv nitrovaných derivátů 3-hydroxynaftalen-2-karboxanilidu a 2-hydroxynaftalen-1-karboxanilidu na proliferaci a apoptózu s využitím THP-1 a MCF-7 nádorových linií. Halogenované deriváty 1-hydroxynaftalen-2-karboxanilidu, 2-hydroxynaftalen-1-karboxanilidu a 6-hydroxynaftalen-2-karboxanilidu byly součástí studií (**publikace č. 13 a 17**) věnované hledáním nových BRAF inhibitorů.

V rámci hodnocení herbicidní aktivity byla v **publikacích č. 1, 4, 5 a 18** testována schopnost látek inhibovat elektronový transport v chloroplastech špenátu (*Spinacia oleracea*).

Na základě dřívějších zkušeností s antivirotickými působícími chinoliny^{46,47,48,49}, byla proti viru ptačí chřipky H5N1 testována a v **publikaci č. 12** popsána série substituovaných derivátů 8-hydroxychinolin-2-karboxanilidu.

Častou nevýhodnou vlastností napříč všechny série připravených hydroxy(aza)naftanilidů byla jejich špatná rozpustnost ve vodě, kvůli které jsme naráželi na limity v screeningu biologické aktivity. Při optimalizaci struktury byl odstraněn jeden ze dvou kruhů naftalenového segmentu (Obrázek 2) za vzniku derivátů přírodní látky kyseliny skořicové. U série arylcinnamidů pak byly zjišťována antistafylokoková a antimykobakteriální aktivita a také schopnost inhibovat elektronový transport v chloroplastech listu špenátu (*Spinacia oleracea* L.) (**publikace č. 11 a 16**).



Obrázek 2

Po nástupu na místo vědeckého pracovníka na půdě Regionálního centra pokročilých technologií a materiálů University Palackého v Olomouci se náš tým začal věnovat také protizánětlivé aktivitě derivátů přírodních látek. Právě tato vlastnost arylcinnamidů je popisována v **publikaci č. 14**.

3. ZÁVĚR

Předkládaná habilitační práce obsahuje soubor sedmnácti komentovaných experimentálních publikací. Ty jsou zaměřené na syntézu a následné hodnocení vztahu struktury a účinku (SAR), které vychází ze zjištěných fyzikálně-chemických vlastností. Tato práce navazuje na mou práci dizertační a rozvíjí diskutovaná témata do dalších souvislostí. Společným znakem většiny uvedených studií je rychlá syntéza nových molekul stylem „click chemistry“. Pro tyto účely bylo využito mikrovlnné syntézy, která splňuje požadavky na rychlou, ekonomickou a energii šetřící přípravu rozsáhlých sérií nových látek. Cíleno bylo na jednoduché amidy typu hydroxy(aza)naftanilidů a cinnamanilidů. Následný rozsáhlý *in vitro* screening biologické aktivity připravených látek byl umožněn díky značné mezinárodní spolupráci. Byla tak hodnocena aktivita antimikrobiální, antitrypanosomální, antivirotická, protinádorová, protizánětlivá. Většina látek byla rovněž testována na schopnost inhibovat fotosyntézu. Veškerá získaná biologická a fyzikálně chemická data byla pak posuzována pro jednotlivé struktury molekul a na základě nalezených zákonitostí z nich byla vyvozena závislost mezi strukturou a biologickou aktivitou vybraných skupin diskutovaných látek.

V současné době pokračuji ve studiu vlastností biologicky aktivních anilidů. Další oblastí zájmu je příprava potenciálních inhibitorů acetylcholinesterasy a butyrylcholinesterasy, dvou důležitých cílů pro léčiva Alzheimerovy choroby. V reakci na světovou pandemii koronavirové choroby covid-19 se v mezinárodní spolupráci podílím na hledání nových antivirotik a molekul účinných proti zoonózám.

4. SEZNAM KOMENTOVANÝCH PUBLIKACÍ

č.	citace	ISSN
1	KOS, J , I ZADRAZILOVA, M PESKO, S KELTOSOVA, J TENGLER, T GONEC, P BOBAL, T KAUEROVA, M ORAVEC, P KOLLAR, A CIZEK, K KRALOVA a J JAMPILEK. Antibacterial and Herbicidal Activity of Ring-Substituted 3-Hydroxynaphthalene-2-carboxanilides. <i>MOLECULES</i> [online]. 2013, 18 (7), 7977–7997. Dostupné z: doi: 10.3390/molecules18077977	1420-3049
2	KOS, J , E NEVIN, M SORAL, I KUSHKEVYCH, T GONEC, P BOBAL, P KOLLAR, A COFFEY, J O'MAHONY, T LIPTAJ, K KRALOVA a J JAMPILEK. Synthesis and antimycobacterial properties of ring-substituted 6-hydroxynaphthalene-2-carboxanilides. <i>BIOORGANIC & MEDICINAL CHEMISTRY</i> [online]. 2015, 23 (9), 2035–2043. Dostupné z: doi: 10.1016/j.bmc.2015.03.018	0968-0896
3	KOS, J , I ZADRAZILOVA, E NEVIN, M SORAL, T GONEC, P KOLLAR, M ORAVEC, A COFFEY, J O'MAHONY, T LIPTAJ, K KRALOVA a J JAMPILEK. Ring-substituted 8-hydroxyquinoline-2-carboxanilides as potential antimycobacterial agents. <i>BIOORGANIC & MEDICINAL CHEMISTRY</i> [online]. 2015, 23 (15), 4188–4196. Dostupné z: doi: 10.1016/j.bmc.2015.06.047	0968-0896
4	PESKO, M, J KOS , K KRALOVA a J JAMPILEK. Inhibition of photosynthetic electron transport by 6-hydroxynaphthalene-2-carboxanilides. <i>INDIAN JOURNAL OF CHEMISTRY SECTION B-ORGANIC CHEMISTRY INCLUDING MEDICINAL CHEMISTRY</i> . 2015, 54 (12), 1511–1517.	0376-4699
5	JAMPILEK, J, K KRALOVA, M PESKO a J KOS . Ring-substituted 8-hydroxyquinoline-2-carboxanilides as photosystem II inhibitors. <i>BIOORGANIC & MEDICINAL CHEMISTRY LETTERS</i> [online]. 2016, 26 (16), 3862–3865. Dostupné z: doi: 10.1016/j.bmcl.2016.07.021	0960-894X
6	KAUEROVA, T, J KOS , T GONEC, J JAMPILEK a P KOLLAR. Antiproliferative and Pro-Apoptotic Effect of Novel Nitro-Substituted Hydroxynaphthanilides on Human Cancer Cell Lines. <i>INTERNATIONAL JOURNAL OF MOLECULAR SCIENCES</i> [online]. 2016, 17 (8). Dostupné z: doi: 10.3390/ijms17081219	1422-0067
7	KUSHKEVYCH, I, J KOS , P KOLLAR, K KRALOVA a J JAMPILEK. Activity of ring-substituted 8-hydroxyquinoline-2-carboxanilides against intestinal sulfate-reducing bacteria <i>Desulfovibrio piger</i> . <i>MEDICINAL CHEMISTRY RESEARCH</i> [online]. 2018, 27 (1), 278–284. Dostupné z: doi: 10.1007/s00044-017-2067-7	1054-2523

8	KOS, J , I KAPUSTIKOVA, C CLEMENTS, AI GRAY a J JAMPILEK. 3-Hydroxynaphthalene-2-carboxanilides and their antitrypanosomal activity. <i>MONATSHEFTE FUR CHEMIE</i> [online]. 2018, 149 (5), 887–892. Dostupné z: doi: 10.1007/s00706-017-2099-1	0026-9247
9	DOLAB, JG, B LIMA, E SPACZYNSKA, J KOS , NH CANO, G FERESIN, A TAPIA, F GARIBOTTO, E PETENATTI, M OLIVELLA, R MUSIOL, J JAMPILEK a RD ENRIZ. The Antimicrobial Activity of Annona emarginata (Schltdl.) H. Rainer and Most Active Isolated Compounds against Clinically Important Bacteria. <i>MOLECULES</i> [online]. 2018, 23 (5). Dostupné z: doi: 10.3390/molecules23051187	1420-3049
10	KUSHKEVYCH, I, M VITEZOVA, J KOS , P KOLLAR a J JAMPILEK. Effect of selected 8-hydroxyquinoline-2-carboxanilides on viability and sulfate metabolism of <i>Desulfovibrio piger</i> . <i>JOURNAL OF APPLIED BIOMEDICINE</i> [online]. 2018, 16 (3), 241–246. Dostupné z: doi: 10.1016/j.jab.2018.01.004	1214-021X
11	POSPISILOVA, S, J KOS*(corresponding author)* , H MICHNOVA, I KAPUSTIKOVA, T STRHARSKY, M ORAVEC, AM MORICZ, J BAKONYI, T KAUEKOVA, P KOLLAR, A CIZEK a J JAMPILEK. Synthesis and Spectrum of Biological Activities of Novel N-arylcinnamamides. <i>INTERNATIONAL JOURNAL OF MOLECULAR SCIENCES</i> [online]. 2018, 19 (8). Dostupné z: doi: 10.3390/ijms19082318	1422-0067
12	KOS, J , CF KU, I KAPUSTIKOVA, M ORAVEC, HJ ZHANG a J JAMPILEK. 8-Hydroxyquinoline-2-Carboxanilides as Antiviral Agents Against Avian Influenza Virus. <i>CHEMISTRYSELECT</i> [online]. 2019, 4 (15), 4582–4587. Dostupné z: doi: 10.1002/slct.201900873	2365-6549
13	CAMPOS, LE, FM GARIBOTTO, E ANGELINA, J KOS , T TOMASIC, N ZIDER, D KIKELJ, T GONEC, P MARVANNOVA, P MOKRY, J JAMPILEK, SE ALVAREZ a RD ENRIZ. Searching new structural scaffolds for BRAF inhibitors. An integrative study using theoretical and experimental techniques. <i>BIOORGANIC CHEMISTRY</i> [online]. 2019, 91 . Dostupné z: doi: 10.1016/j.bioorg.2019.103125	0045-2068
14	HOSEK, J, J KOS , T STRHARSKY, L CERNA, P STARHA, J VANCO, Z TRAVNICEK, F DEVINSKY a J JAMPILEK. Investigation of Anti-Inflammatory Potential of N-Arylcinnamamide Derivatives. <i>MOLECULES</i> [online]. 2019, 24 (24). Dostupné z: doi: 10.3390/molecules24244531	1420-3049
15	BAK, A, J KOS*(corresponding author)* , H MICHNOVA, T GONEC, S POSPISILOVA, V KOZIK, A CIZEK, A SMOLINSKI a J JAMPILEK. Consensus-Based Pharmacophore Mapping for New Set of N-(disubstituted-phenyl)-3-hydroxyl-naphthalene-2-carboxamides. <i>INTERNATIONAL JOURNAL OF MOLECULAR SCIENCES</i> [online]. 2020, 21 (18). Dostupné z: doi: 10.3390/ijms21186583	1422-0067
16	KOS, J , A BAK, V KOZIK, T JANKECH, T STRHARSKY, A SWIETLICKA, H MICHNOVA, J HOSEK, A SMOLINSKI, M ORAVEC, F DEVINSKY, M HUTTA a J JAMPILEK. Biological Activities and ADMET-Related Properties of Novel Set of Cinnamanilides. <i>MOLECULES</i> [online]. 2020, 25 (18). Dostupné z: doi: 10.3390/molecules25184121	1420-3049

17	CAMPOS, LE, F GARIBOTTO, E ANGELINA, J KOS , T GONEC, P MARVANOVA, M VETTORAZZI, M ORAVEC, I JENDRZEJEWSKA, J JAMPILEK, SE ALVAREZ a RD ENRIZ. Hydroxynaphthalenecarboxamides and substituted piperazinylpropandiols, two new series of BRAF inhibitors. A theoretical and experimental study. <i>BIOORGANIC CHEMISTRY</i> [online]. 2020, 103 . Dostupné z: doi: 10.1016/j.bioorg.2020.104145	0045-2068
18	KOS, J*(corresponding author)* , T GONEC, M ORAVEC, I JENDRZEJEWSKA a J JAMPILEK. Photosynthesis-Inhibiting Activity of N-(Disubstituted-phenyl)-3-hydroxynaphthalene-2-carboxamides. <i>MOLECULES</i> [online]. 2021, 26(14) . Dostupné z: doi: 10.3390/molecules26144336	1420-3049

5. SEZNAM POUŽITÉ LITERATURY

- ¹ Jampílek, J.; Oktábec, Z.; Řezáčová, A.; Plaček, L.; Kos, J.; Havelková, L.; Dohnal, J.; Král V. Preparation and properties of new co-crystals of ibandronate. Proceedings: *The 13th International Electronic Conference on Synthetic Organic Chemistry (ECSOC-13)*, November 1-30, 2009, c001, <http://www.sciforum.net/presentation/201>.
- ² Jampílek, J.; Kos, J.; Oktábec, Z.; Mandelová, Z.; Pekárek, T.; Tkadlecová, M.; Havlíček, J.; Dohnal, J.; Král V. Co-crystal screening study of risedronate and unsubstituted hexoses. Proceedings: *The 14th International Electronic Conference on Synthetic Organic Chemistry (ECSOC-14)*, November 1-30, 2010, A421, <http://www.sciforum.net/conference/ecsoc-14/paper/421>.
- ³ Šujan, J.; Peško, M.; Goněk, T.; Kos, J.; Bobál, P.; Imramovský, A.; Plaček, L.; Kráľová, K.; Jampílek, J.; Preparation and herbicidal properties of substituted quinoline-2-carboxanilides. Proceedings: *The 15th International Electronic Conference on Synthetic Organic Chemistry (ECSOC-15)*, November 1-30, 2011, B588, <http://www.sciforum.net/conference/ecsoc-15/paper/588>.
- ⁴ Kos, J.; Zdražilová, I.; Peško, M.; Pavlica, J.; Goněk, T.; Bobál, P.; Oravec, M.; Čížek, A.; Kráľová, K.; Jampílek, J. Preparation and biological properties of ring-substituted 3-hydroxynaphthalene-2-carboxanilides. Proceedings: *The 16th International Electronic Conference on Synthetic Organic Chemistry (ECSOC-16)*, November 1-30, 2012, B1009, <http://www.sciforum.net/conference/ecsoc-16/paper/1009>.
- ⁵ Kos, J.; Machalová, P.; Peško, M.; Goněk, T.; Bobál, P.; Oravec, M.; Liptaj, T.; Kráľová, K.; JAMPÍLEK, J. Preparation and herbicidal activity of halogenated 8-hydroxyquinoline-2-carboxanilides. Proceedings: *The 17th International Electronic Conference on Synthetic Organic Chemistry (ECSOC-17)*, November 1-30, 2013, B013, <http://sciforum.net/conference/ecsoc-17/paper/2261>.
- ⁶ Goněk, T.; Kos, J.; Šoral, M.; Peško, M.; Oravec, M.; Liptaj, T.; Kráľová, K.; Jampílek, J.; Preparation and photosynthesis-inhibiting activity of N-(n-alkoxy)phenylamides of 2-hydroxynaphthalene-1-carboxylic acid. Proceedings: *The 18th International Electronic Conference on Synthetic Organic Chemistry (ECSOC-18)*, November 1-30, 2014, b010, <http://www.sciforum.net/conference/ecsoc-18/paper/2538>.
- ⁷ Goněk, T.; Stráník, J.; Peško, M.; Kos, J.; Oravec, M.; Kráľová, K.; Jampílek, J. Preparation and photosynthesis-inhibiting activity of 1-[(2-chlorophenyl)carbonyl]naphthalen-2-yl alkylcarbamates. Proceedings: *The 19th International Electronic Conference on Synthetic Organic Chemistry (ECSOC-19)*, November 1-30, 2015, b006, <http://sciforum.net/conference/80/paper/3079>.
- ⁸ Goněk, T.; Stráník, J.; Peško, M.; Kos, J.; Oravec, M.; Kráľová, K.; Jampílek, J. Preparation and photosynthesis-inhibiting activity of 1-[(2-chlorophenyl)carbonyl]naphthalen-2-yl alkylcarbamates. Proceedings: *The 20th International Electronic Conference on Synthetic Organic Chemistry (ECSOC-20)*, November 1-30, 2016, b004, <http://sciforum.net/conference/94/paper/3535>.
- ⁹ Pospíšilová, Š.; Kos, J.; Michnová, Hana Strhářský, T.; Čížek, A.; Jampílek, J.; N-arylcinnamamides as antistaphylococcal agents. Proceedings: *The 4th International Electronic Conference on Medicinal Chemistry (ECMC-4)*, November 1–30, 2018, 5576, <https://sciforum.net/manuscripts/5576/slides.pdf>.
- ¹⁰ Kapustíková, I.; Goněk, T.; Kos, J.; Jampílek, J. Chromatographic and computational study of hydro-lipophilic properties of N-alkoxyphenylhydroxy-naphthalenecarboxamides.

-
- Proceedings: *The 21st International Electronic Conference on Synthetic Organic Chemistry (ECSOC-21)*, November 1–30, 2017, 4719, <http://sciforum.net/conference/ecsoc-21/paper/4719>.
- ¹¹ Kapustíková, I.; Goněc, T.; Kos, J.; Spaczyńska, E.; Oravec, M.; Doháňošová, J.; Iptaj, T.; and Musioł, R.; JAMPÍLEK, J. Preparation and hydro-lipophilic properties of methoxylated and methylated 1-hydroxynaphthalene-2-carboxanilides. Proceedings: *The 22nd International Electronic Conference on Synthetic Organic Chemistry (ECSOC-22)*, November 15 – December 15, 2018, 5660. *Proceedings* 2019, vol. 9, 43, <https://www.mdpi.com/2504-3900/9/1/43/pdf>.
- ¹² Strhářsky, T.; Jankech, T.; Kos, J.; Maričáková, K.; Pramuková, A.; Hutta, M.; Devínský, F.; Jampílek, J. Preparation and hydro-lipophilic properties of selected novel chlorinated and brominated *n*-arylcinnamamides. Proceedings: *The 23rd International Electronic Conference on Synthetic Organic Chemistry (ECSOC-23)*, November 15 – December 15, 2019, 6595. *Proceedings* **2019**, *41*, 11, <https://www.mdpi.com/2504-3900/41/1/11/pdf>.
- ¹³ Kos, J.; Goněc, T.; Strhářsky, T.; Oravec, M.; Jampílek, J. Preparation and photosynthesis-inhibiting activity of novel dihalogenated 3-hydroxynaphthalene-2-carboxanilides. Proceedings: *The 23rd International Electronic Conference on Synthetic Organic Chemistry (ECSOC-23)*, November 15 – December 15, 2019, 6596. *Proceedings* **2019**, *41*, 30, <https://www.mdpi.com/2504-3900/41/1/30/pdf>.
- ¹⁴ Jampílek, J.; Goněc, T.; Pospíšilová, Š.; Čížek, A.; Enriz, R. D.; Feresin, G. E.; Andujar, S. A.; Gutierrez, L. J. Kapustíková, I.; Kos, J. Utilization of novel multisubstituted naphthalene derivatives as broad-spectrum antibacterial compounds. Applicant: Comenius University in Bratislava, Faculty of Pharmacy. Slovak Patent Application PP 65-2017, July 17, 2017.
- ¹⁵ Jampílek, J.; Goněc, T.; Kos, J.; Pospíšilová, Š.; Michnová, H.; Čížek, A.; Coffey, A.; Utilization of novel multisubstituted hydroxynaphthalenes derivatives as antimycobacterial compounds. Applicant: Comenius University in Bratislava, Faculty of Pharmacy. Slovak Patent Application PP 71-2017, July 28, 2017.
- ¹⁶ Kos, J.; Goněc, T.; Jampílek, J. Investigating the spectrum of biological activity of ring-substituted 3-hydroxynaphthalene-2-carboxanilides. Book of Abstracts: *The 49th International Conference on Medicinal Chemistry (RICT 2013)*, Nice, France, July 3-5, 2013, p. 229 (HT-053).
- ¹⁷ Liu, C.; Bayer, A.; Cosgrove, S.E.; Daum, R.S.; Fridkin, S.K.; Gorwitz, R.J. Kaplan, S.L.; Karchmer, A.W.; Levine, D.P.; Murray, B.E.; Rybak, M.J.; Talan, D.A.; Chambers, H.F. Clinical practice guidelines by the infectious Diseases Society of America for the treatment of methicillin-resistant *Staphylococcus aureus* infections in adults and children: Executive Summary. *Clinical Infectious Diseases* **2011**, *52* (3), 285–292.
- ¹⁸ Kallen, A.J.; Mu, Y.; Bulens, S.; Reingold, A.; Petit, S.; Gershman, K.; Ray, S.M.; Harrison, L.H.; Lynfield, R.; Dumyati, G.; Townes, J.M.; Schaffner, W.; Patel, P.R.; Fridkin, S.K. Health care-associated invasive MRSA infections, 2005–2008. *The Journal of the American Medicinal Association* **2010**, *304* (6), 641–647.
- ¹⁹ Siddiqui, A.H.; Koirala, J. Methicillin Resistant *Staphylococcus Aureus* (MRSA) [Updated 2020 Jun 29]. In: *StatPearls*. Treasure Island (FL): StatPearls Publishing. Available from: <https://www.ncbi.nlm.nih.gov/books/NBK482221>.
- ²⁰ WHO – Global tuberculosis report 2019. Dostupné na: https://www.who.int/tb/publications/global_report/en.
- ²¹ Lincová, D.; Farghali, H. *Základní a aplikovaná farmakologie*. Praha: Galén, 2002. ISBN 8072621688.

-
- ²² Švihovec, J.; Bultas, J.; Anzenbacher, P.; Chládek, J.; Příborský, J.; Slíva, J.; Votava, M. *Farmakologie*. Praha: Grada Publishing, 2018.
- ²³ Ingen, J.; Beoree, M. J.; Soolingen, D.; Mouton, J. Resistance mechanism and drug susceptibility testing of nontuberculous mycobacteria. *Drug Resistance Updates* **2012**, *15* (3), 149–161.
- ²⁴ Griffith, D.E.; Aksamit T.; Brown-Elliott, B.A.; Catanzaro, A.; Daley, Ch.; Gordin, F.; Holland, S.M.; Horsburgh, R.; Huitt, G.; Iademarco, M.F.; Iseman, M.; Olivier, K.; Ruoss, S.; Fordham von Reyn, C.; Wallace, R.J.Jr.; Winthrop, K. An official ATS/IDSA statement: diagnosis, treatment, and prevention of nontuberculous mycobacterial diseases. *American Journal of Respiratory and Critical Care Medicine* **2007**, *175* (4), 367–416.
- ²⁵ Kos, J.; Zadražilová, I.; Nevin, E.; Šoral, M.; Goněc, T.; Kollár, P.; Oravec, M.; Coffey, A.; O'Mahony, J.; Liptaj, T.; Kráľová, K.; Jampílek, J. Ring-substituted 8-hydroxyquinoline-2-carboxanilides as potential antimycobacterial agents. *Bioorganic and Medicinal Chemistry* **2015**, *23* (15), 4188-4196.
- ²⁶ Fyfe, J.; Piccozi, K.; Waiswa, Ch.; Bardosh, K.L.; Welburn, S.Ch. Impact of mass chemotherapy in domestic livestock for control of zoonotic *T. b. rhodesiense* human African trypanosomiasis in Eastern Uganda. *Acta Tropica* **2017**, *165*, 216-229.
- ²⁷ WHO - Trypanosomiasis, human African (sleeping sickness). Dostupné na: https://www.who.int/gho/neglected_diseases/human_african_trypanosomiasis/en
- ²⁸ Kos, J.; Kapustíková, I.; Clements, C.; Gray, A. I.; Jampílek, J. 3-Hydroxynaphthalene-2-carboxanilides and their antitrypanosomal activity. *Monatshefte fur Chemie* **2018**, *149* (5), 887-892.
- ²⁹ Pinger, J.; Chowdhury, S.; Papavasiliou, F. Variant surface glycoprotein density defines an immune evasion threshold for African trypanosomes undergoing antigenic variation. *Nature Communication* **2017**, *8* (828), 1-9.
- ³⁰ Jacobs, R.T.; Nare, B.; Phillips, M.A. State of the art in african trypanosome drug discovery. *Current Topics in Medicinal Chemistry* **2011**, *11* (10), 1255-1274.
- ³¹ Kennedy, P. *The Fatal Sleep: Africa's killer disease that went undiscovered for centuries*. Edinburgh: Luath Press Limited, 2007.
- ³² Balasegaram, M.; Young, H.; Chappuis, F.; Priotto, G.; Raguenaud, M.E.; Checchi, F. Effectiveness of melarsoprol and eflornithine as first-line regimens for gambiense sleeping sickness in nine Médecins Sans Frontières programmes. *Transactions of the Royal Society of Tropical Medicine and Hygiene* **2009**, *103* (3), 280-290.
- ³³ Drugbank – Eflornithine. Dostupné na: <https://www.drugbank.ca/drugs/DB06243>.
- ³⁴ Drugbank – Pentamidine. Dostupné na: <https://www.drugbank.ca/drugs/DB00738>.
- ³⁵ Drugbank – Suramin. Dostupné na: <https://www.drugbank.ca/drugs/DB04786>.
- ³⁶ Kos, J.; Zadražilová, I.; Peško, M.; Keltošová, S.; Tengler, J.; Goněc, T.; Bobál, P.; Kauerová, T.; Oravec, M.; Kollár, P.; Čížek, A.; Kráľová, K.; Jampílek, J. Antibacterial and herbicidal activity of ring-substituted 3-hydroxynaphthalene-2-carboxanilides. *Molecules* **2013**, *18* (8), 7977-7997.
- ³⁷ Goněc, T.; Zadražilová, I.; Nevin, E.; Kauerová, T.; Peško, M.; Kos, J.; Oravec, M.; Kollár, P.; Coffey, A.; O'Mahony, J.; Čížek, A.; Kráľová, K.; Jampílek, J. Synthesis and biological evaluation of N-alkoxyphenyl-3-hydroxynaphthalene-2-carboxanilides. *Molecules* **2015**, *20* (6), 9767-9787.
- ³⁸ Krátky, M.; Vinšová, J. Salicylanilide ester prodrugs as potential antimicrobial agents - a review. *Current Pharmaceutical Design* **2011**, *17* (32), 3494-3505.

-
- ³⁹ Zdražilová, I.; Pospíšilová, S.; Masaříková, M.; Imramovský, A.; Monreal-Ferriz, J.; Vinšová, J.; Čížek, A.; Jampílek, J. Salicylanilide carbamates: Promising antibacterial agents with high in vitro activity against methicillin-resistant *Staphylococcus aureus* (MRSA). *European Journal of Pharmaceutical Sciences* **2015**, *77*, 197-207.
- ⁴⁰ Ferrins, L.; Gazdik, M.; Rahmani, R.; Varghese, S.; Sykes, M.L.; Jones, A.J.; Avery, V.M.; White, K.L.; Ryan, E.; Charman, S.A.; Kaiser, M.; Bergström, C.A.; Baell, J.B. Pyridyl benzamides as a novel class of potent inhibitors for the kinetoplastid *Trypanosoma brucei*. *Journal of Medicinal Chemistry* **2014**, *57* (15), 6393-6402.
- ⁴¹ Masand, V.H.; El-Sayed, N.N.E.; Mahajan, D.T.; Rastija, V. QSAR analysis for 6-arylpyrazine-2-carboxamides as *Trypanosoma brucei* inhibitors. *SAR and QSAR in Environmental Research* **2017**, *28* (2), 165-177.
- ⁴² Poovorawan, Y.; Pyungporn, S.; Prachayangprecha, S.; Makkoch, J. Global alert to avian influenza virus infection: from H5N1 to H7N9. *Pathogens and Global Health* **2013**, *107* (5), 217-223.
- ⁴³ Shen, Z.; Lou, K.; Wang, W. New small-molecule drug design strategies for fighting resistant influenza A. *Acta Pharmaceutica Sinica B* **2015**, *5* (5), 419-430.
- ⁴⁴ Drugbank – Oseltamivir. Dostupné na: <https://www.drugbank.ca/drugs/DB00198>.
- ⁴⁵ Tsang, N.Y.; Zhao, L.H.; Tsang, S.W.; Zhang, H.J. Antiviral activity and molecular targets of plant natural products against avian influenza virus. *Current Organic Chemistry* **2017**, *21*, 1777-1804.
- ⁴⁶ Song, Y.; Xu, H.; Chen, W.; Zhan, P.; Liu, X. 8-Hydroxyquinoline: A privileged structure with a broad-ranging pharmacological potential. *MedChemComm* **2015**, *6* (1), 61-74.
- ⁴⁷ Yeh, J.Y.; Coumar, M.S.; Shiao, H.Y.; Lin, T.J.; Lee, Y.C.; Hung, H.C.; Ko, S.; Kuo, F.M.; Fang, M.Y.; Huang, Y.L.; Hsu, J.T.; Yeh, T.K.; Shih, S.R.; Chao, Y.S.; Horng, J.T.; Hsieh, H.P. Anti-influenza drug discovery: Identification of an orally bioavailable quinoline derivative through activity- and property-guided lead optimization. *ChemMedChem* **2012**, *7* (9), 1546-1550.
- ⁴⁸ Wang, W.; Yin, R.; Zhang, M.; Yu, R.; Hao, C.; Zhang, L.; Jiang, T. Boronic acid modifications enhance the anti-influenza virus activities of novel quinoline derivatives. *Journal of Medicinal Chemistry* **2017**, *60* (7), 2840-2852.
- ⁴⁹ Guardia, C.; Stephens, D.E.; Dang, H.T.; Quijada, M.; Larionov, O.V.; Leonart, R. Antiviral activity of novel quinoline derivatives against dengue virus serotype 2. *Molecules* **2018**, *23* (3), 672.
- ⁵⁰ Medzhitov, R. Origin and physiological roles of inflammation. *Nature* **2008**, *454*, 428-435.
- ⁵¹ Libby, P. Inflammation in atherosclerosis. *Nature* **2002**, *420*, 868-874.
- ⁵² McInnes, I.B.; Schett, G. Cytokines in the pathogenesis of rheumatoid arthritis. *Nature Reviews. Immunology*. **2007**, *7* (8), 429-442.
- ⁵³ Nickoloff, B.J.; Nestle, F.O. Recent insights into the immunopathogenesis of psoriasis provide new therapeutic opportunities. *Journal of Clinical Investigation* **2004**, *113* (12), 1664-1675.
- ⁵⁴ Grivennikov, S.I.; Greten, F.R.; Karin, M. Immunity, inflammation, and cancer. *Cell* **2010**, *140* (6), 883-899.
- ⁵⁵ Barnes, P.J. Immunology of asthma and chronic obstructive pulmonary disease. *Nature Reviews. Immunology* **2008**, *8* (3), 183-192.
- ⁵⁶ Shoelson, S.E.; Herrero, L.; Naaz, A. Obesity, inflammation, and insulin resistance. *Gastroenterology* **2007**, *132* (6), 2169-2180.

-
- ⁵⁷ Scherer, H.U.; Häupl, T.; Burmester, G.R. The Etiology of rheumatoid arthritis. *Journal of Autoimmunity* **2020**, *110*, 102400.
- ⁵⁸ Ferenčík, M.; Štvrtinová, V. Endogenous control and modulation of inflammation. *Folia Biologica* **1996**, *42* (1-2), 47–55.
- ⁵⁹ Olejárová, M. *Biologická léčba v revmatologii*, 1. vyd. Praha: Mladá fronta, 2012, pp. 9–11.
- ⁶⁰ Pavelka, K.; Arenberger, P.; Lukáš, M.; Zima, T.; Doležal, T.; Olejárová, M.; Cetkovská, P. *Biologická léčba zánětlivých autoimunitních onemocnění*, 1. vyd. Praha: Grada, 2014, pp. 125-150.
- ⁶¹ Pavelka, K. *Farmakoterapie revmatických onemocnění*, 1. vyd. Praha: Maxdorf Jessenius, 2017, pp. 125-136.
- ⁶² Pavelková, A. *Revmatoidní artritida a biologická léčba*, 1. vyd. Praha: Maxdorf Jessenius, 2009, pp. 14-25.
- ⁶³ Newman, D.J.; Cragg, G.M. Natural products as sources of new drugs from 1981 to 2014. *Journal of Natural Products* **2016**, *79* (3), 629–661.
- ⁶⁴ Guzman, J.D. Natural cinnamic acids, synthetic derivatives and hybrids with antimicrobial activity. *Molecules* **2014**, *19* (12), 19292–19349.
- ⁶⁵ Sova, M. Antioxidant and antimicrobial activities of cinnamic acid derivatives. *Mini Reviews in Medicinal Chemistry* **2012**, *12* (8), 749–767.
- ⁶⁶ De, P.; Baltas, M.; Bedos-Belval, F. Cinnamic acid derivatives as anticancer agents – a review. *Current Medicinal Chemistry*. **2011**, *18*, 11, 1672–1703.
- ⁶⁷ Liao, J.C.; Deng, J.S.; Chiu, C.S.; Hou, W.C.; Huang, S.S.; Shie, P.H.; Huang, G.J. Anti-inflammatory activities of cinnamomum cassia constituents in vitro and in vivo. *Evidence-Based Complementary and Alternative* **2012**, *2012*, 429320.
- ⁶⁸ Choudhary, A.; Raines, R.T. An evaluation of peptide-bond isosteres. *ChemBioChem* **2011**, *12* (12), 1801–1807.
- ⁶⁹ Mahesh, S.; Tang, K.C.; Raj, M. Amide bond activation of biological molecules. *Molecules* **2018**, *23* (10), 2615–2658.
- ⁷⁰ Chen, G.Z.; Zhang, Y.L.; Liu, X.; Fang, Q.L.; Wang, Z.; Fu, L.L.; Liu, Z.G.; Wang, Y.; Zhao, Y.J.; Li, X.K.; Liang, G. Discovery of a new inhibitor of myeloid differentiation 2 from cinnamamide derivatives with anti-inflammatory activity in sepsis and acute lung injury. *Journal of Medicinal Chemistry* **2016**, *59* (6), 2436–2451.
- ⁷¹ Gaikwad, N.; Nanduri, S.; Madhavi, Y.V. Cinnamamide: An insight into the pharmacological advances and structure-activity relationships. *European Journal of Medicinal Chemistry* **2019**, *181*, 111561.
- ⁷² Meegan, M.J.; O’Boyle, N.M. Special Issue “Anticancer Drugs”. *Pharmaceuticals* **2019**, *12* (134), 1–6.
- ⁷³ The International Agency for Research on Cancer. Dostupné na: <https://www.who.int/cancer/PRGlobocanFinal.pdf>.
- ⁷⁴ Chanput, W.; Mes, J. J.; Wichers J.H. THP-1 cell line: An in vitro cell model for immune modulation approach. *International Immunopharmacology* **2014**, *23* (1), 37-45.
- ⁷⁵ Lee, A.V.; Oesterreich, S, Davidson, N.E. MCF-7 Cells—changing the course of breast cancer research and care for 45 years. *Journal of the National Cancer Institute* **2015**, *107* (7), 1-4.
- ⁷⁶ Campos, L.E.; Garibotto, F.; Angelina, E.; Kos, J.; Goněc, T.; Marvanová, P.; Vettorazzi, M.; Oravec, M.; Jendrzewska, I.; Jampílek, J.; Alvarez, S.; Enriz, R.D. Hydroxynaphthalenecarboxamides and substituted piperazinypropandiols, two new

-
- series of BRAF inhibitors. A theoretical and experimental study. *Bioorganic Chemistry* **2020**, *103*, 104145.
- ⁷⁷ Shaner, D.L. Herbicide safety relative to common targets in plants and mammal. *Pest Management Science* **2004**, *60* (1), 17–24.
- ⁷⁸ Duke, S.O. Herbicide and pharmaceutical relationships. *Weed Science* **2010**, *58* (3), 334–339.
- ⁷⁹ Delaney, J.; Clarke, E.; Hughes, D.; Rice, M. Modern agrochemical research: a missed opportunity for drug discovery? *Drug Discovery Today* **2006**, *11* (17-18), 839–845.
- ⁸⁰ Jampílek, J. Potential of agricultural fungicides for antifungal drug discovery. *Expert Opinion on Drug Discovery* **2016**, *11* (1), 1-9.
- ⁸¹ Kurenbach, B.; Hill, A. M.; Godsoe, W.; van Hamelsveld, S.; Heinmann, J.A. Agrichemicals and antibiotics in combination increase antibiotic resistance evolution. *Peer J* **2018**, *6*, e5801.
- ⁸² Laursen, J.S.; Engel-Andreasen, J.; Fristrup, P.; Harris, P.; Olsen, C.A. Cis-trans amide bond rotamers in β -peptoids and peptoids: Evaluation of stereoelectronic effects in backbone and side chains. *Journal of the American Chemical Society* **2013**, *135* (7), 2835–2844.
- ⁸³ Pattabiraman, V.R.; Bode, J.W. Rethinking amide bond synthesis. *Nature* **2011**, *480*, 471–479.
- ⁸⁴ Draber, W.; Tietjen, K.; Kluth, J.F.; Trebst, A. Herbicides in photosynthesis research. *Angewandte Chemie* **1991**, *30* (12), 1621–1633.
- ⁸⁵ Jampílek, J.; Kráľová, K.; Peško, M.; Kos, J. Ring-substituted 8-Hydroxyquinoline-2-carboxanilides as photosystem II inhibitors. *Bioorganic and Medicinal Chemistry Letters* **2016**, *26* (16), 3862-3865.
- ⁸⁶ Fuerst, E.P.; Norman, M.A. Interactions of herbicides with photosynthetic electron transport. *Weed Science* **1991**, *3* (39), 458–464.
- ⁸⁷ Duke, S.O. Overview of herbicide mechanism of action. *Environmental Health Perspectives* **1990**, *87*, 263–271.
- ⁸⁸ Dayan, E.F., Zaccaro de M.M.L. Chlorophyll fluorescence as a marker for herbicide mechanism of action. *Pesticide Biochemistry and Physiology* **2012**, *3* (102), 189–197.
- ⁸⁹ Norsworthy, J.K.; Ward, S.M.; Shaw, D.R.; Llewellyn, R.S.; Nichols, R.L.; Webster, T.; Bradley, K.W.; Frisvold, G.; Powles, S.B.; Burgos, N.R.; Witt, W.W.; Barret, M. Reducing the risks of herbicide resistance: Best management practices and recommendations. *Weed Science* **2012**, *60* (1), 31–62.
- ⁹⁰ Heap, J. International Survey of Herbicide-Resistant Weeds. 2020. Dostupné na: <http://www.weedscience.org>.
- ⁹¹ Lipinski, C.A.; Lombardo, F.; Dominy, B.W.; Feeney, P.J. Experimental and computational approaches to estimate solubility and permeability in drug discovery and development settings. *Advanced Drug Delivery Reviews* **1997**, *23* (1-3), 3–25.
- ⁹² Khan, M.T.H.; Sylte, I. Predictive QSAR modeling for the successful predictions of the ADMET properties of candidate drug molecules. *Current Drug Discovery Technologies* **2007**, *4* (3), 141–149.
- ⁹³ Adriamainty, F.; Malík, I. Farmaceutická chémia Vybrané liečiva - ich príprava a štúdium fyzikálno-chemických parametrů. Univerzita Komenského v Bratislavě, 2011.
- ⁹⁴ Hansch, C.; Mahoney, P.P.; Fujita, T.; Muir, R.M. Correlation of biological activity of phenoxyacetic acids with Hammett substituent constants and partition coefficients. *Nature* **1962**, *194*, 178–180.
- ⁹⁵ Hansch, C.; Fujita, T. ρ - σ - π analysis. a method for the correlation of biological activity and chemical structure. *Journal of the American Chemical Society* **1964**, *86* (8), 1616–1626.

-
- ⁹⁶ Leo, A.; Hansch, C.; Elkins, D. Partition coefficients and their uses. *Chemical Reviews* **1971**, *71* (6), 525–616.
- ⁹⁷ Valko, K. Application of high-performance liquid chromatography based measurements of lipophilicity to model biological distribution. *Journal of Chromatography A* **2004**, *1037* (1-2), 299–310.
- ⁹⁸ Valko, K.; Du, C.M.; Bevan, C.; Reynolds, D.P.; Abraham, M.H. Rapid method for the estimation of octanol/water partition coefficient (log P(oct)) from gradient RP-HPLC retention and a hydrogen bond acidity term ($\zeta\alpha(2)(H)$). *Current Medicinal Chemistry* **2001**, *8* (9), 1137–1146.
- ⁹⁹ Gocan, S.; Cimpan, G.; Comer, J. Lipophilicity measurements by liquid chromatography. *Advances in Chromatography* **2006**, *44*, 79–176.
- ¹⁰⁰ Meylan, W.M.; Howard, P.H. Atom/fragment contribution method for estimating octanol–water partition coefficients. *Journal of Pharmaceutical Science* **1995**, *84* (1), 83–92.
- ¹⁰¹ Oktábec, Z.; Kos, J.; Mandelová, Z.; Havelková, L.; Pekárek, T.; Řezáčová, A.; Plaček, L.; Tkadlecová, M.; Havlíček, J.; Dohnal, J.; Jampílek, Josef. Preparation and properties of new co-crystals of ibandronate with gluco- or galactopyranoside derivatives. *Molecules* **2010**, *15* (12), 8973–8987.
- ¹⁰² Kos, J.; Pěntáková, M.; Oktábec, Z.; Krejčík, L.; Mandelová, Z.; Haroková, P.; Hrušková, J.; Pekárek, T.; Dammer, O.; Tkadlecová, M.; Havlíček, J.; Král, V.; Vinšová, J.; Dohnal, J.; Jampílek, J. Crystallization products of risedronate with carbohydrates and their substituted derivatives. *Molecules* **2011**, *16* (5), 3740–3760.
- ¹⁰³ Vinšová, J.; Imramovský, A.; Buchta, V.; Čečková, M.; Doležal, M.; Štaud, F.; Jampílek, J.; Kaustová, J. Salicylanilide acetates: Synthesis and antibacterial evaluation. *Molecules* **2007**, *12*, 1–12.
- ¹⁰⁴ Imramovský, A.; Vinšová, J.; Monreal-Ferriz, J.; Doležal, R.; Jampílek, J.; Kaustová, J.; Kunc, F. New antituberculotics originated from salicylanilides with promising in vitro activity against atypical mycobacterial strains. *Bioorganic and Medicinal Chemistry* **2009**, *17*, 3572–3579.
- ¹⁰⁵ Krátký, M.; Vinšová, J.; Novotná, E.; Mandíková, J.; Wsól, V.; Trejtnar, F.; Ulmann, V.; Stolaříková, J.; Fernandes, S.; Bhat, S.; Liu, J.O. Salicylanilide derivatives block *Mycobacterium tuberculosis* through inhibition of isocitrate lyase and methionine aminopeptidase. *Tuberculosis* **2012**, *92*, 434–439.
- ¹⁰⁶ Krátký, M.; Vinšová, J. Salicylanilide ester prodrugs as potential antimicrobial agents – a review. *Current Pharmaceutical Design* **2011**, *17*, 3494–3505.
- ¹⁰⁷ Brown, E.M.; Fitzner, N.J.; Stevens, T.; Chin, W.; Wright, D.C.; Boyce P.J. Salicylanilides: Selective inhibitors of interleukin-12p40 production. *Bioorganic and Medicinal Chemistry* **2008**, *16*, 8760–8764.
- ¹⁰⁸ Pauk, K.; Zdražilová, I.; Imramovský, A.; Vinšová, J.; Pokorná, M.; Masaříková, M.; Čížek, A.; Jampílek, J. New derivatives of salicylamides: Preparation and antimicrobial activity against various bacterial species. *Bioorganic and Medicinal Chemistry* **2013**, *21*, 6574–6581.
- ¹⁰⁹ Musiol, R.; Tabak, D.; Niedbala, H.; Podeszwa, B.; Jampílek, J.; Králová, K.; Dohnal, J.; Finster, J.; Mencil, A.; Polanski, J. Investigating biological activity spectrum for novel quinoline analogues 2: Hydroxyquinolinecarboxamides with photosynthesis inhibiting activity. *Bioorganic and Medicinal Chemistry* **2008**, *16*, 4490–4499.
- ¹¹⁰ Musiol, R.; Jampílek, J.; Buchta, V.; Niedbala, H.; Podeszwa, B.; Palka, A.; MajerzManiecka, K.; Oleksyn, B.; Polanski, J. Antifungal properties of new series of quinoline derivatives. *Bioorganic and Medicinal Chemistry* **2006**, *14*, 3592–3598.

-
- ¹¹¹ Musiol, R.; Jampílek, J.; Kráľová, K.; Richardson, D.R.; Kalinowski, D.; Podeszwa, B.; Finster, J.; Niedbala, H.; Palka, A.; Polanski, J. Investigating biological activity spectrum for novel quinoline analogues. *Bioorganic and Medicinal Chemistry* **2007**, *15*, 1280–1288.
- ¹¹² Podeszwa, B.; Niedbala, H.; Polanski, J.; Musiol, R.; Tabak, D.; Finster, J.; Serafin, K.; Wietrzyk, J.; Boryczka, S.; Mol, W.; Jampílek, J.; Dohnal, J.; Kalinowski, D.; Richardson, D.R. Investigating the antiproliferative activity of quinoline-5,8-dione analogues on tumour cell lines. *Bioorganic and Medicinal Chemistry Letters* **2007**, *17*, 6138–6141.
- ¹¹³ Jampílek, J.; Musiol, R.; Finster, J.; Peško, M.; Carroll, J.; Kráľová, K.; Vejsová, M.; Coffey, A.; Polanski, J. Investigating biological activity spectrum for novel styrylquinazoline analogues. *Molecules* **2009**, *14*, 4246–4265.
- ¹¹⁴ Mrozek-Wilczkiewicz, A.; Kalinowski, D.; Musiol, R.; Finster, J.; Kovacevic, Z.; Jampílek, J.; Rzeszowska-Wolny, J.; Richardson, D.R.; Polanski, J. Investigating anti-proliferative activity of styrylzanaphthalenes and azanaphthalenediones. *Bioorganic and Medicinal Chemistry* **2010**, *18*, 2664–2671.
- ¹¹⁵ Goněc, T.; Bobál, P.; Šujan, J.; Peško, M.; Guo, J.; Kráľová, K.; Pavlacká, L.; Veselý, L.; Křečková, E.; Kos, J.; Coffey, A.; Kollár, P.; Imramovský, A.; Plaček, L.; Jampílek, J. Investigating the spectrum of biological activity of substituted quinoline-2-carboxamides and their isosteres. *Molecules* **2012**, *17* (1), 613–644.
- ¹¹⁶ Goněc, T.; Kos, J.; Zdražilová, Iveta Peško, M.; Govender, R.; Keltošová, S.; Chambel, B.; Pereira, D.; Kollár, P.; Imramovský, A.; O'Mahony, J.; Coffey, A.; Čížek, A.; Kráľová, K.; Jampílek, J. Antibacterial and herbicidal activity of ring-substituted 2-hydroxynaphthalene-1-carboxanilides. *Molecules* **2013**, *18* (8), 9397–9419.
- ¹¹⁷ Goněc, T.; Kos, J.; Zdražilová, I.; Peško, M.; Keltošová, S.; Tengler, J.; Bobál, P.; Kollár, P.; Čížek, A.; Kráľová, K.; Jampílek, J. Antimycobacterial and herbicidal activity of ring-substituted 1-hydroxynaphthalene-2-carboxanilides. *Bioorganic and Medicinal Chemistry* **2013**, *21* (21), 6531–6541.
- ¹¹⁸ Goněc, T.; Kos, J.; Nevin, E.; Govender, R.; Peško, M.; Tengler, J.; Kushkevych, I.; Šťastná, V.; Oravec, M.; Kollár, P.; O'Mahony, J.; Kráľová, K.; Coffey, A.; Jampílek, J. Preparation and biological properties of ring-substituted naphthalene-1-carboxanilides. *Molecules* **2014**, *19* (7), 10386–10409.
- ¹¹⁹ Kos, J.; Nevin, E.; Šoral, M.; Kushkevych, I.; Goněc, T.; Bobál, P.; Kollár, P.; Coffey, A.; O'Mahony, J.; Liptaj, T.; Kráľová, K.; Jampílek, J. Synthesis and antimycobacterial properties of ring-substituted 6-hydroxynaphthalene-2-carboxanilides. *Bioorganic and Medicinal Chemistry* **2015**, *23* (9), 2035–2043.
- ¹²⁰ Peško, M.; Kos, J.; Kráľová, K.; Jampílek, J. Inhibition of photosynthetic electron transport by 6-hydroxynaphthalene-2-carboxanilides. *Indian Journal of Chemistry - Section B* **2015**, *54B* (12), 1511–1517.
- ¹²¹ Jampílek, J.; Kráľová, K.; Peško, M.; Kos, J. Ring-substituted 8-hydroxyquinoline-2-carboxanilides as photosystem II inhibitors. *Bioorganic and Medicinal Chemistry Letters* **2016**, *26* (16), 3862–3865.
- ¹²² Kauerová, T.; Kos, J.; Goněc, T.; Jampílek, J.; Kollár, P. Antiproliferative and pro-apoptotic effect of novel nitro-substituted hydroxynaphthanilides on human cancer cell lines. *International Journal of Molecular Sciences* **2016**, *17* (8), 1219.
- ¹²³ Goněc, T.; Pospíšilová, Š.; Kauerová, T.; Kos, J.; Doháňošová, J.; Oravec, M.; Kollár, P.; Coffey, A.; Liptaj, T.; Čížek, A.; Jampílek, J. *N*-alkoxyphenylhydroxynaphthalene-carboxamides and their antimycobacterial activity. *Molecules* **2016**, *21* (8), 1068.

-
- ¹²⁴ Goněk, T.; Pospíšilová, Š.; Holaňová, L.; Stráník, J.; Černíková, Aneta Púdelková, V.; Kos, J.; Oravec, M.; Kollár, P.; Čížek, A.; Jampílek, J. Synthesis and antimicrobial evaluation of 1-[(2-substituted phenyl)carbamoyl]naphthalen-2-yl carbamates. *Molecules* **2016**, *21* (9), 1189.
- ¹²⁵ Goněk, T.; Stráník, J.; Peško, M.; Kos, J.; Oravec, M.; Kráľová, K.; Jampílek, J. Photosynthesis-inhibiting activity of 1-[(2-chlorophenyl)carbamoyl]- and 1-[(2-nitrophenyl)carbamoyl]naphthalen-2-yl alkylcarbamates. *Molecules* **2017**, *22* (7), 1199.
- ¹²⁶ Goněk, T.; Kos, J.; Peško, M.; Doháňošová, J.; Oravec, M.; Liptaj, T.; Kráľová, K.; Jampílek, J. Halogenated 1-hydroxynaphthalene-2-carboxanilides affecting photosynthetic electron transport in photosystem II. *Molecules* **2017**, *22* (10), 1709.
- ¹²⁷ Kushkevych, I.; Kos, J.; Kollár, P.; Kráľová, K.; Jampílek, J. Activity of ring-substituted 8-hydroxyquinoline-2-carboxanilides against intestinal sulfate-reducing bacteria *Desulfovibrio piger*. *Medicinal Chemistry Research* **2018**, *27* (1), 278–284.
- ¹²⁸ Dolab, J.G.; Beatriz, L.; Spaczyńska, E.; Kos, J.; Cano, N.H.; Feresin, G.; Tapia, A.; Garibotto, F.; Petenatti, E.; Olivella, M.; Musioł, R.; Jampílek, J.; Enriz, R.D. Antimicrobial activity of *Annona emarginata* (Schltdl.) H. Rainer and most active isolated compound against clinically important bacteria. *Molecules* **2018**, *23* (5), 1187.
- ¹²⁹ Kapustíková, I.; Bąk, A.; Goněk, T.; Kos, J.; Kozik, V.; Jampílek, J. Investigation of hydro-lipophilic properties of *N*-alkoxyphenylhydroxynaphthalenecarboxamides. *Molecules* **2018**, *23* (7), 1635.
- ¹³⁰ Kushkevych, I.; Vítězová, M.; Kos, J.; Kollár, P.; Jampílek, J. Effect of selected 8-hydroxyquinoline-2-carboxanilides on viability and sulfate metabolism of *Desulfovibrio piger*. *Journal of Applied Biomedicine* **2018**, *16* (3), 241–246.
- ¹³¹ Kos, J.; and Ku, Ch.F.; Kapustíková, I.; Oravec, M.; Zhang, H-J. Jampílek, J. 8-hydroxyquinoline-2-carboxanilides as antiviral agents against avian influenza virus. *ChemistrySelect* **2019**, *4* (15), 4582–4587.
- ¹³² Bąk, A.; Kos, J.; Michnová, H.; Goněk, T.; Pospíšilová, Š.; Kozik, V.; Čížek, A.; Smoliński, A.; Jampílek, J. Similarity-driven pharmacophore mapping for series of *N*-(disubstituted-phenyl)-3-hydroxynaphthalene-2-carboxamides. *International Journal of Molecular Sciences* **2020**, *21* (18), 6583.
- ¹³³ Spaczyńska, E.; Mrozek-Wilczkiewicz, A.; Malarz, K.; Kos, J.; Goněk, T.; Oravec, M.; Gawecki, R.; Bąk, A.; Doháňošová, J.; Kapustíková, I.; Liptaj, T.; Jampílek, J.; Musioł, R. Design and synthesis of anticancer 1-hydroxynaphthalene-2-carboxanilides with p53 independent mechanism of action. *Scientific Reports* **2019**, *9*, 6387.
- ¹³⁴ Kos, J.; Bąk, A.; Kozik, V.; Jankech, T.; Strhářsky, T.; Świetlicka, A.; Michnová, H.; Hošek, J.; Smoliński, A.; Oravec, M.; Devínsky, F.; Hutta, M.; Jampílek, J. Biological activities and ADMET-related properties of novel set of cinnamanilides. *Molecules* **2020**, *25* (18), 4121.
- ¹³⁵ Cummings, J.H.; Macfarlane, G.T.; Macfarlane, S. Intestinal bacteria and ulcerative colitis. *Current Issues in Intestinal Microbiology* **2003**, *4* (1), 9–20.

6. KOMENTOVANÉ PUBLIKACE

č.	citace	ISSN
1	KOS, J , I ZADRAZILOVA, M PESKO, S KELTOSOVA, J TENGLER, T GONEC, P BOBAL, T KAUEROVA, M ORAVEC, P KOLLAR, A CIZEK, K KRALOVA a J JAMPILEK. Antibacterial and Herbicidal Activity of Ring-Substituted 3-Hydroxynaphthalene-2-carboxanilides. <i>MOLECULES</i> [online]. 2013, 18 (7), 7977–7997. Dostupné z: doi: 10.3390/molecules18077977	1420-3049

Article

Antibacterial and Herbicidal Activity of Ring-Substituted 3-Hydroxynaphthalene-2-carboxanilides †

Jiri Kos ¹, Iveta Zadrazilova ^{1,2,3}, Matus Pesko ⁴, Stanislava Keltosova ⁵, Jan Tengler ¹, Tomas Gonec ¹, Pavel Bobal ¹, Tereza Kauerova ⁵, Michal Oravec ⁶, Peter Kollar ⁵, Alois Cizek ^{2,3}, Katarina Kralova ⁴ and Josef Jampilek ^{1,*}

¹ Department of Chemical Drugs, Faculty of Pharmacy, University of Veterinary and Pharmaceutical Sciences, Palackeho 1/3, 612 42 Brno, Czech Republic

² Department of Infectious Diseases and Microbiology, Faculty of Veterinary Medicine, University of Veterinary and Pharmaceutical Sciences, Palackeho 1/3, 612 42 Brno, Czech Republic

³ CEITEC VFU, University of Veterinary and Pharmaceutical Sciences, Palackeho 1/3, 612 42 Brno, Czech Republic

⁴ Institute of Chemistry, Faculty of Natural Sciences, Comenius University, Mlynska dolina Ch-2, 842 15 Bratislava, Slovakia

⁵ Department of Human Pharmacology and Toxicology, Faculty of Pharmacy, University of Veterinary and Pharmaceutical Sciences, Palackeho 1/3, 612 42 Brno, Czech Republic

⁶ Global Change Research Centre AS CR, Belidla 986/4a, 603 00 Brno, Czech Republic

† Preliminary results were presented at The Sixteenth Electronic Conference on Synthetic Organic Chemistry (ECSOC-16, <http://www.sciforum.net/presentation/1009>), 1–30 November 2012 (paper B1009).

* Author to whom correspondence should be addressed; E-Mail: josef.jampilek@gmail.com; Tel.: +420-54-156-2926.

Received: 23 May 2013; in revised form: 17 June 2013 / Accepted: 4 July 2013 /

Published: 8 July 2013

Abstract: In this study, a series of twenty-two ring-substituted 3-hydroxy-*N*-phenylnaphthalene-2-carboxanilides were prepared and characterized. The compounds were tested for their activity related to inhibition of photosynthetic electron transport (PET) in spinach (*Spinacia oleracea* L.) chloroplasts. Primary *in vitro* screening of the synthesized compounds was also performed against four *Staphylococcus* strains and against two mycobacterial species. 3-Hydroxy-*N*-(2-methoxyphenyl)naphthalene-2-carboxamide showed

high biological activity (MIC = 55.0 $\mu\text{mol/L}$) against *S. aureus* as well as methicillin-resistant strains. *N*-(2-Fluorophenyl)-3-hydroxynaphthalene-2-carboxamide showed higher activity (MIC = 28.4 $\mu\text{mol/L}$) against *M. marinum* than the standard isoniazid and 3-hydroxy-*N*-(4-nitrophenyl)naphthalene-2-carboxamide expressed higher activity (MIC = 13.0 $\mu\text{mol/L}$) against *M. kansasii* than the standard isoniazid. Cytotoxicity assay of effective antimicrobial compounds was performed using the human monocytic leukemia THP-1 cell line. The PET-inhibiting activity expressed by IC_{50} value of the most active compound 3-hydroxy-*N*-(3-nitrophenyl)naphthalene-2-carboxamide was 16.9 $\mu\text{mol/L}$. The structure-activity relationships of all compounds are discussed.

Keywords: hydroxynaphthalene-2-carboxanilides; lipophilicity; photosynthetic electron transport inhibition; spinach chloroplasts; *in vitro* antibacterial activity; *in vitro* antimycobacterial activity; *in vitro* cytotoxicity; structure-activity relationships

1. Introduction

The increasing number of bacterial, mycobacterial and associated fungal infections underlines the importance of searching for new antimicrobial chemotherapeutics [1]. Tuberculosis and other mycobacterial diseases are common, and in many cases lethal, infectious illnesses caused by various strains of pathogenic mycobacteria. The genus *Mycobacterium* consists of a closely related group of fast and slow-growing species. *Mycobacterium tuberculosis* causes one of the most serious human infections, tuberculosis. Difficulties should be considered while studying *M. tuberculosis*, especially a slow growth rate and the requirement to work in high containment biosafety facilities. To lower risks and make manipulation in the laboratory easier, surrogate model pathogens for *M. tuberculosis* can be used in laboratory studies. *M. marinum* is very closely related to the *M. tuberculosis*; it is the cause of TB-like infections in poikilothermic organisms, especially frogs and fish. *M. marinum* is a good model for studying because of the lower risk for laboratory workers, genetic relatedness and similar pathology to human TB [2,3]. However, because of *M. tuberculosis*, the pathogenic role of nontuberculous mycobacteria (NTM) in humans was overshadowed for a long time. *M. kansasii*, the most virulent of the NTM, causes nontuberculous mycobacterial lung infections which are very common nowadays and can be indistinguishable from tuberculosis [4]. That is the reason why *M. marinum* and *M. kansasii* are often chosen as model species for screening of prospective antimycobacterial drugs to control mycobacterial diseases.

The treatment of tuberculosis and nontuberculous diseases is mediated by administration of various antimicrobial chemotherapeutics, however massive using of these drugs is considered to be the main reason for increased antibiotic resistance among bacteria [5,6]. The antibiotic resistance of important Gram-positive pathogen, *Staphylococcus aureus*, has become one of the most challenging and persistent worldwide health problems. Methicillin-resistant *S. aureus* (MRSA) was first described in 1961 and since then has become one of the most common clinically relevant bacterial pathogens isolated almost all over the World. Even though originally limited to hospitals, nowadays MRSA is an increasing cause of infections in the community. Recent studies have shown that, despite antibacterial

therapy, MRSA infections are still associated with serious clinical consequences (treatment failure, higher morbidity and mortality, prolonged hospitalization, *etc.*). Because of the changing features of MRSA, it is one of the most difficult bacteria for clinicians to treat. The emergence of resistance to currently available drugs, their toxicity and general lack of oral agents justify an urgent need for new anti-MRSA agents [7,8].

Both pharmaceuticals and pesticides are designed to target particular biological functions, and in some cases these functions overlap in their molecular target sites, or they target similar processes or molecules. Taking into consideration that herbicides may also have molecular sites of action in mammals, until recently most pharmaceutical companies had pesticide divisions, sometimes with a different name. All compounds generated by either division of the company were evaluated for both pesticide and pharmaceutical uses. In the past, some leading pesticides have become pharmaceuticals and *vice versa* [9–11]. Moreover, good correlation between microbiological activities and herbicidal effects was found [12–15].

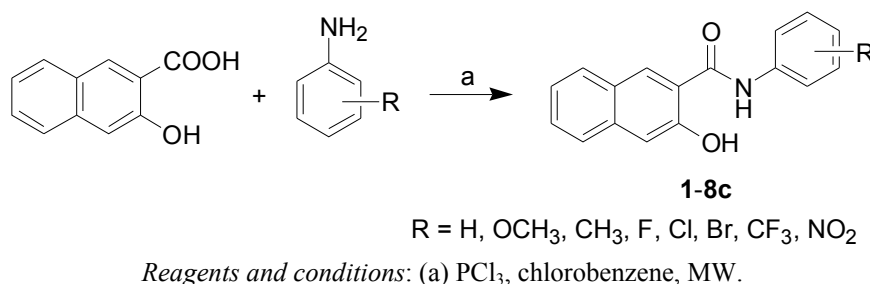
The presence of an amide (-NHCO-) group [16–20] is characteristic of a number of herbicides acting as photosynthesis inhibitors. Over 50% of commercially available herbicides act by reversibly binding to photosystem II (PS II), a membrane-protein complex in the thylakoid membranes, which catalyses the oxidation of water and the reduction of plastoquinone [21], and thereby inhibit photosynthesis [22–24].

Promising results of biological screening of some salicylanilides (their antimicrobial, antimycobacterial, antifungal, molluscicidal and herbicidal action) [17–19,25–33] inspired us to prepare and evaluate ring-substituted 3-hydroxynaphthalene-2-carboxanilides. The design of these 3-hydroxy-*N*-phenylnaphthalene-2-carboxanilides is based on ring analogy with salicylanilides (2-hydroxy-*N*-phenylbenzamide). Thus in the context of the previously-published results [16–20,25–33], primary *in vitro* screening of the synthesized compounds was also performed against four *Staphylococcus* strains, three of which were methicillin-resistant *Staphylococcus aureus* strains, and against two mycobacterial species, such as *Mycobacterium marinum* and *M. kansasii*.

2. Results and Discussion

2.1. Chemistry

All the studied compounds were prepared according to Scheme 1. Modified microwave-assisted synthesis [29] facilitated the process of obtaining 3-hydroxynaphthalene-2-carboxanilides, thus synthesis of the target compounds was carried out only by one step. At first the carboxyl group was activated with phosphorus trichloride. The final amide was immediately formed by aminolysis of the acyl chloride by ring-substituted aniline in dry chlorobenzene. All the compounds were recrystallized from ethanol; their HPLC purity exceeded 97%. By microwave-assisted synthesis reaction times were shortened from hours [34–37] to minutes, and yields of most compounds (except 2-NO₂ derivative **8a**) were more than 65%, for details see Section 3.2.

Scheme 1. Synthesis of ring-substituted 3-hydroxynaphthalene-2-carboxanilides **1–8c**.**2.2. Lipophilicities**

Lipophilicity is a property that has a major effect on solubility, absorption, distribution and biotransformation as well as pharmacological activity, because drugs cross biological membranes through passive transport, which strongly depends on their lipophilicity. Lipophilicity has been studied and applied as an important drug property for decades. Lipophilicity of the studied compounds was determined by RP-HPLC as capacity factor logarithm ($\log k$) and calculated as $\log P$ using ACD/Percepta software. The results of ring-substituted 3-hydroxynaphthalene-2-carboxanilides **1–8c** are shown in Table 1 and illustrated in Figure 1. The highest experimental lipophilicity was found for 3-hydroxy-*N*-(4-trifluoromethylphenyl)naphthalene-2-carboxamide (**7c**), while 3-hydroxy-*N*-phenylnaphthalene-2-carboxamide (**1**) showed the lowest $\log k$ value. It is important to note that lipophilicity also has a great impact on target and off-target interactions, as mentioned below.

The results obtained with the discussed compounds show that the experimentally-determined lipophilicities ($\log k$) of the *meta*- and *para*-substituted compounds are in accordance with the calculated $\log P$ values as shown in Figure 1B, while *ortho*-substituted derivatives showed poor match, see Figure 1A. The most significant deviations within the dependence illustrated in Figure 1B can be observed for 4-CF₃ (**7c**) and 4-NO₂ (**8c**). The influence of R substituents on lipophilicity is as follows: H < OCH₃ < CH₃ < F < NO₂ < Cl < Br ≤ CF₃. Within the individual series the lipophilicity determined by $\log k$ values increases for halogens and methyl substituents as follows: *ortho* < *para* < *meta*; for methoxy substituent as follows: *para* < *ortho* < *meta*, and for CF₃ and NO₂ as follows: *ortho* < *meta* < *para*. Generally, it could be concluded that the prediction power of the used experimental $\log k$ or calculated $\log P$ values, especially for *meta*- and *para*-substituted derivatives, may be a good tool for searching potential drugs. It can be assumed that $\log k$ values specify lipophilicity within individual series of the studied compounds.

2.3. Inhibition of Photosynthetic Electron Transport (PET) in Spinach Chloroplasts

The activity of the evaluated naphthanilide derivatives related to inhibition of photosynthetic electron transport (PET) in spinach (*Spinacia oleracea* L.) chloroplasts was moderate or low relative to the standard, see Table 1. Generally compounds showed poor aqueous solubility. Only seven compounds from twenty-two tested compounds could be evaluated. PET inhibition by **1**, **2c–5c**, **6b**, **6c** and **7b**, **7c** could not be determined due to precipitation of the compounds during the experiments. With respect to these small but specifically substituted groups of compounds some structure-activity relationships (SAR) can be proposed. Compound **8b** (R = 3-NO₂) expressed the highest PET-inhibiting

activity

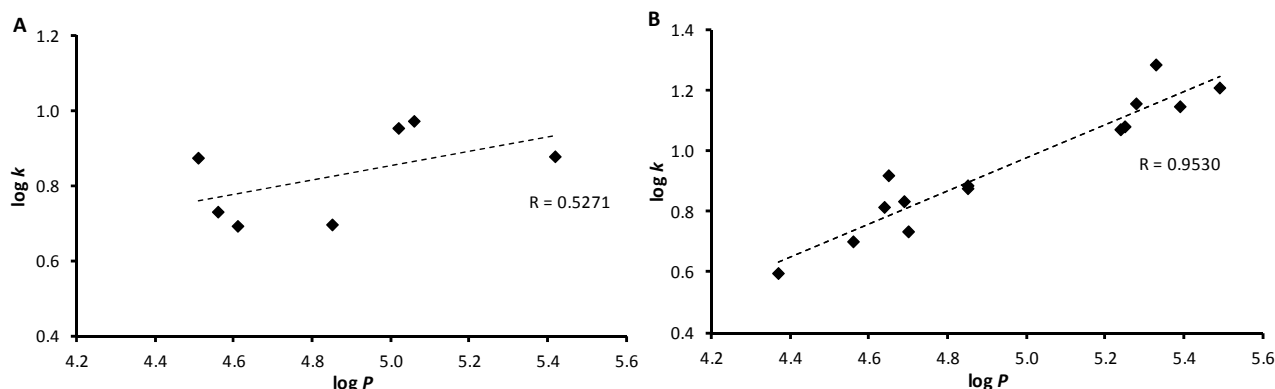
($IC_{50} = 16.9 \mu\text{mol/L}$), while compound **8c** ($R = 4\text{-NO}_2$) expressed the lowest PET-inhibiting activity ($IC_{50} = 187.5 \mu\text{mol/L}$).

Table 1. Structure of ring-substituted 3-hydroxynaphthalene-2-carboxanilides **1–8c**, experimentally determined values of lipophilicity $\log k$, calculated values of $\log P$ and electronic Hammett's σ parameters, IC_{50} [$\mu\text{mol/L}$] values related to PET inhibition in spinach chloroplasts in comparison with 3-(3,4-dichlorophenyl)-1,1-dimethylurea (DCMU) standard, *in vitro* anti-*Staphylococcus* activities [MIC ($\mu\text{mol/L}$)] in comparison with standards ampicillin (APC), *in vitro* antimycobacterial activity [MIC ($\mu\text{mol/L}$)] of compounds **1–8c** compared to isoniazid (INH) standard and *in vitro* cytotoxicity assay (LD_{50}) of selected compounds.

Comp.	R	$\log k$	$\log P^a$	σ^a	[$\mu\text{mol/L}$]							LD_{50}	
					PET IC_{50}	MIC					MM		MK
						SA	MRSA 63718	MRSA 630	MRSA 3202				
1	H	0.6310	4.52	0	<i>b</i>	>972	>972	>972	>972	122	972	–	
2a	2-OCH ₃	0.6916	4.61	–0.28	59.5	55.0	55.0	55.0	55.0	873	218	>30	
2b	3-OCH ₃	0.6971	4.56	0.12	53.4	>873	>873	>873	>873	>873	54.6	>30	
2c	4-OCH ₃	0.5951	4.37	–0.27	<i>b</i>	>873	>873	>873	>873	>873	873	–	
3a	2-CH ₃	0.6936	4.85	–0.17	<i>b</i>	>923	>923	>923	462	462	115	–	
3b	3-CH ₃	0.8831	4.85	–0.07	<i>b</i>	>923	>923	>923	462	923	57.7	>30	
3c	4-CH ₃	0.8753	4.85	–0.17	<i>b</i>	>923	>923	462	231	>923	923	–	
4a	2-F	0.7303	4.56	0.06	<i>b</i>	>910	>910	455	228	28.4	56.9	>30	
4b	3-F	0.8296	4.69	0.34	<i>b</i>	>910	>910	455	228	114	114	–	
4c	4-F	0.7317	4.70	0.06	<i>b</i>	>910	>910	455	228	910	114	–	
5a	2-Cl	0.9509	5.02	0.22	<i>b</i>	>860	>860	>860	215	860	860	–	
5b	3-Cl	1.0796	5.25	0.37	<i>b</i>	>860	>860	430	215	>860	860	–	
5c	4-Cl	1.0687	5.24	0.23	<i>b</i>	>860	>860	>860	>860	>860	430	–	
6a	2-Br	0.9715	5.06	0.22	43.2	>748	>748	>748	>748	>748	748	–	
6b	3-Br	1.1536	5.39	0.39	<i>b</i>	>748	>748	>748	187	>748	748	–	
6c	4-Br	1.1459	5.28	0.23	<i>b</i>	>748	>748	>748	187	>748	374	–	
7a	2-CF ₃	0.8762	5.42	0.51	105.2	>773	>773	>773	97	193	193	28.6 ± 0.5	
7b	3-CF ₃	1.2053	5.49	0.43	<i>b</i>	>748	>748	374	187	>748	748	–	
7c	4-CF ₃	1.2835	5.33	0.51	<i>b</i>	>748	>748	374	187	>748	187	–	
8a	2-NO ₂	0.8710	4.51	0.77	106.6	>830	>830	415	415	830	830	–	
8b	3-NO ₂	0.8143	4.64	0.71	16.9	>830	>830	>830	>830	>830	415	2.5 ± 0.9	
8c	4-NO ₂	0.9175	4.65	0.78	187.5	>830	>830	>830	>830	>830	13.0	<0.37	
DCMU	–	–	–	–	1.9	–	–	–	–	–	–	–	
APC	–	–	–	–	–	5.7	>45.8	>45.8	>45.8	–	–	–	
INH	–	–	–	–	–	–	–	–	–	467	29.2	–	

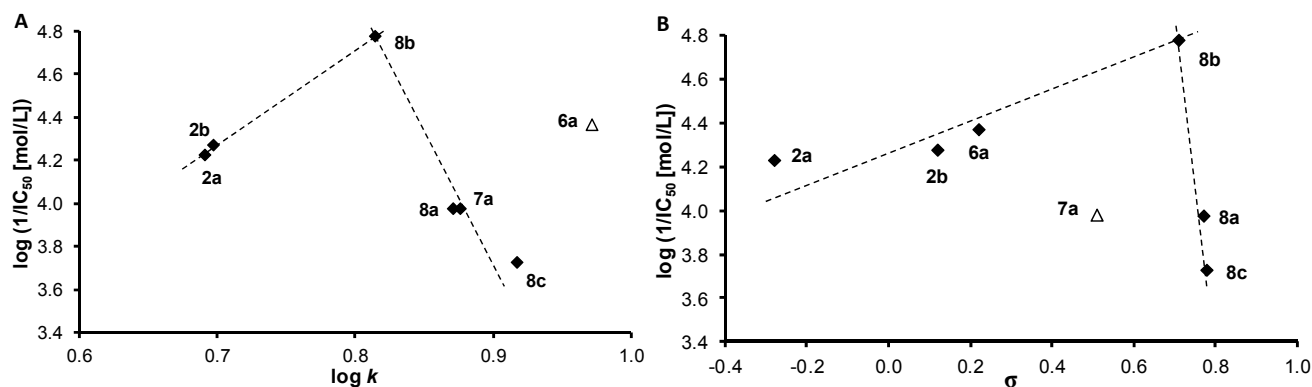
^a calculated using sw. ACD/Percepta ver. 2012; ^b precipitation during experiment; SA = *Staphylococcus aureus* ATCC 29213; MRSA = clinical isolates of methicillin-resistant *S. aureus* 63718, SA 630 and SA 3202 (National Institute of Public Health, Prague, Czech Republic); MM = *Mycobacterium marinum* CAMP 5644, MK = *M. kansasii* DSM 44162.

Figure 1. Comparison of experimentally found $\log k$ values with calculated $\log P$ of *ortho*-substituted (A) and *meta*- and *para*-substituted derivatives (B).



The PET-inhibiting activity was expressed by negative logarithm of IC_{50} value (compound concentration in mol/L causing 50% inhibition of PET). Despite the relatively low inhibitory activity of the studied compounds, correlations between $\log(1/IC_{50}$ [mol/L]) and the lipophilicity of compounds expressed as $\log k$ or electronic properties of individual anilide substituents expressed as Hammett's σ parameters were performed, see Figure 2. Based on the obtained results it is not possible to decide, whether some of *ortho*-, *meta*- or *para*-positions are preferred from the point of view of PET-inhibiting activity.

Figure 2. Relationships between PET inhibition $\log(1/IC_{50})$ [mol/L] in spinach chloroplasts and lipophilicity expressed as $\log k$ (A) or *N*-substituent electronic Hammett's σ parameters (B) of selected studied compounds.



The biological activity is affected by lipophilicity (see Table 1 and Figure 2A). In general, when the inactive anilide, *i.e.*, **6a**, was eliminated; the dependence of $\log(1/IC_{50}$ [mol/L]) on $\log k$ is bilinear with the optimum $\log k$ ca. 0.81 ($R = 3\text{-NO}_2$, compound **8b**). The corresponding correlation coefficients were $r = 0.9993$ and $r = -0.9673$. On the other hand, PET inhibition also increases with electron-withdrawing substituent to $\sigma = 0.71$ ($R = 3\text{-NO}_2$, compound **8b**), where the optimum can be found, and then decreases with a subsequent increase of electron-withdrawing properties of substituents ($\sigma = 0.78$, $R = 4\text{-NO}_2$, compound **8c** and $\sigma = 0.77$, $R = 2\text{-NO}_2$, compound **8a**). Thus, when the activity of compound **7a** is not considered, the dependence of PET-inhibiting activity on the electronic σ properties of substituents (Figure 2B) shows a similar bilinear trend as in case of $\log k$

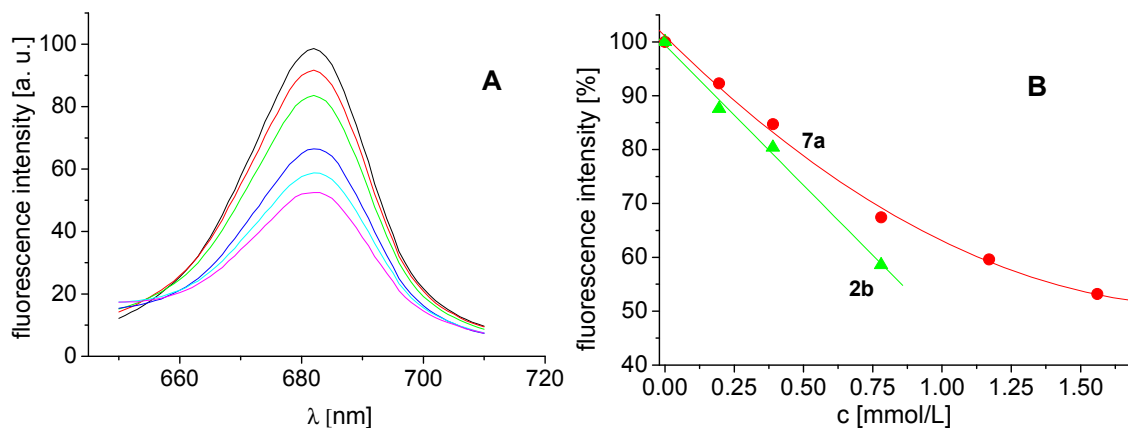
(Figure 2A), with correlations coefficients $r = 0.9313$ (for the σ range from -0.28 to 0.71) and $r = -0.9956$ for $\sigma > 0.71$).

Using artificial electron donors with the known site of action can help in the determination of inhibitory site of action of the studied compound in photosynthetic apparatus. For example, the artificial electron donor 1,5-diphenylcarbazide (DPC) acts in Z^{\bullet}/D^{\bullet} intermediate [38] and by supply of electrons it can restore PET in chloroplasts which was inhibited on the donor side of PS II in the section from the oxygen evolving complex to the Z^{\bullet}/D^{\bullet} intermediate. However, if PET is inhibited at the acceptor side of PS II, PET will not be restored. Application of the artificial electron donor 1,5-diphenylcarbazide acting in Z^{\bullet}/D^{\bullet} intermediate [38] to chloroplasts the activity of which was inhibited by the studied compounds (75% inhibition related to the control) practically completely restored PET (up to 97.8% of the control), indicating that PET on the acceptor side of PS II between the core of PS II (P680) and the secondary plastoquinone molecules/acceptor Q_B was not inhibited by the tested compounds. Consequently, it can be assumed that the site of action of the studied compounds is situated on the donor side of PS II in the section between the primary electron donor of PS II (H_2O) and Z^{\bullet}/D^{\bullet} intermediate.

The bilinear course of the dependence of $\log(1/IC_{50})$ on σ indicates that for the PET-inhibiting activity not only sufficient lipophilicity (enabling easier penetration of the compounds into the lipids of photosynthetic membranes) but also sufficient electronegativity of the R substituent (enabling interactions with proteins located near oxygen evolving complex present at the luminal side of thylakoid membrane) is necessary. 3-Hydroxy-*N*-(3-nitrophenyl)naphthalene-2-carboxamide (**8b**) was the most active compound from the series, and this result can indicate that PET inhibition can be associated with additional interaction of the nitro moiety with photosynthetic proteins, nevertheless the role of the nitro group in the *meta*-position might originate also from its electron withdrawing properties that influence electron distribution in the aromatic ring. A strong dependence of PET-inhibiting activity on σ was also found for 2-benzylsulphonylbenzimidazoles [39]. The site of action situated on the donor side of PS II was found also for 2-alkylthio-6-R-benzothiazoles (R = 6-formamido-, 6-acetamido-, and 6-benzoylamino-) [40], anilides of 2-alkylpyridine-4-carboxylic acids acting in intermediates Z^{\bullet}/D^{\bullet} [41], 5-bromo-*N*-phenylbenzamides [42] and 2-alkylsulphonyl-4-pyridinecarbothioamides acting in the D^{\bullet} intermediate [43].

The effects of the studied compounds on the photosynthetic apparatus of spinach chloroplasts were investigated by studying chlorophyll *a* (Chl*a*) fluorescence. The decreased intensity of the emission band at 686 nm belonging to the pigment-protein complexes in photosystem II [44] (Figure 3A) suggested PS II as the site of action of the studied inhibitors. Lower solubility of compound **2b** did not allow to record fluorescence emission spectra of chloroplasts treated with compound concentration higher than 0.780 mmol/L. The extent of perturbation of chlorophyll *a*-protein complexes in the thylakoid membrane reflected as decreased fluorescence (Figure 3B) correlated with PET inhibiting activity of compounds **2b** and **7a** ($IC_{50} = 53.4$ and $105.2 \mu\text{mol/L}$, respectively). A similar decrease of Chl*a* fluorescence in plant chloroplasts was observed after treatment with $HgCl_2$ [45], non-ionic surfactant Triton X 100 [46] as well as substituted benzanilides [47] and salicylanilides [48].

Figure 3. Fluorescence emission spectra of chlorophyll *a* in untreated spinach chloroplasts in presence of compound **7a**: 0, 0.195, 0.390, 0.780, 1.170 and 1.560 mmol/L (curves from top to bottom; $\lambda_{\text{ex}} = 436$ nm) (A) and dependence of fluorescence intensity of chlorophyll *a* on concentration of compounds **2b** (triangles) and **7a** (circles) (B).



2.4. In Vitro Antibacterial Susceptibility Testing

Although salicylanilides seem to be promising candidates of antibacterial agents [31,32], all the compounds showed only moderate activity, except for 3-hydroxy-*N*-(2-methoxyphenyl)naphthalene-2-carboxamide (**2a**). As MIC = 55 $\mu\text{mol/L}$ of compound **2a** was the same for all four strains, it can be speculated about specific effectivity against *Staphylococcus* sp. From Table 1 it is obvious that compound **2a** exhibited activity comparable with the standards. 3-Hydroxy-*N*-(2-trifluoromethylphenyl)naphthalene-2-carboxamide (**7a**) seems to be another noteworthy compound. Nevertheless due to moderate activity of the rest of the compounds, no thorough SAR could be established.

2.5. In Vitro Antimycobacterial Evaluation

Although all the compounds were evaluated for their *in vitro* antimycobacterial activity against both mycobacterial strains, most of compounds showed only moderate or no activity, see Table 1. Nevertheless *N*-(2-fluorophenyl)-3-hydroxynaphthalene-2-carboxamide (**4a**) expressed the activity comparable with or higher than the used standard isoniazid against both strains, and 3-hydroxy-*N*-(4-nitrophenyl)naphthalene-2-carboxamide (**8c**) showed relatively high activity against *M. kansasii*.

According to the results, it can be generally concluded that activity against *M. marinum* can be observed especially for *ortho*-substituted anilides. When the least active anilides **3b** and **4c** are eliminated, the dependences of activity on $\log k$ and on electronic σ properties are bilinear with the optima $\log k$ ca. 0.73 and $\sigma = 0.06$ ($R = 2\text{-F}$, compound **4a**). After the optima the antimycobacterial activity against *M. marinum* decreases with an increase of lipophilicity and/or electron-withdrawing properties of the R substituent.

Within activity against *M. kansasii*, it can be generally concluded that for anilides substituted in *meta*- or *para*-position by methyl and halogens (except the fluoro moiety) the activity slightly increases with increasing lipophilicity and electron-withdrawing properties. For *ortho*-substituted anilides similar bilinear relationships can be found, as discussed above, with the optima $\log k$ ca. 0.73 and $\sigma = 0.06$ ($R = 2\text{-F}$, compound **4a**).

2.6. In Vitro Cytotoxicity Assay

The most effective compounds **2a**, **2b**, **3b**, **4a**, **7a**, **8b** and **8c** were tested for their *in vitro* cytotoxicity LD₅₀ (μmol/L) using human monocytic leukemia THP-1 cells. These cells were used, because they represent human cell line [49]. In the past several works were published, where the toxicity of tested compounds (including antibacterial agents [20,50]) was assessed on THP-1 cells. The highest dose of compounds **2a,b** (R = 2-, 3-OCH₃), **3b** (R = 3-CH₃) and **4a** (R = 2-F) in the medium (30 μmol/L, it was not possible to solve higher amount) did not lead to significant lethal effect on THP-1 cells, *i.e.*, LD₅₀ > 30 μmol/L. Compound **7a** (2-CF₃) demonstrated low toxicity (LD₅₀ = 28.6 ± 0.5 μmol/L) against the human monocytic leukemia THP-1 cell line. Compounds containing 3-NO₂ (**8b**) and 4-NO₂ (**8c**) exerted fairly high toxicity LD₅₀ = 2.5 ± 0.9 μmol/L for **8b** and LD₅₀ < 0.37 μmol/L for **8c** (for example, LD₅₀ of oxaliplatin and camptothecin assessed in this line formerly were much lower: 1.7 ± 0.6 μmol/L and 0.20 ± 0.07 μmol/L respectively), which correlates with the positions of these substituents: toxicity increased with the shift of NO₂ moiety from *ortho* to *para* position (**8b** is less toxic than **8c**). Based on these observations it can be concluded that the discussed amides **2a**, **2b**, **3b** and **4a** can be considered as promising agents for subsequent design of novel antibacterial and antimycobacterial agents, respectively.

3. Experimental

3.1. General

All reagents were purchased from Aldrich (Sigma-Aldrich, St. Louis, MO, USA). TLC experiments were performed on alumina-backed silica gel 40 F254 plates (Merck, Darmstadt, Germany). The plates were illuminated under UV (254 nm) and evaluated in iodine vapour. The melting points were determined on Kofler hot-plate apparatus HMK (Franz Kustner Nacht KG, Dresden, Germany) and are uncorrected. Infrared (IR) spectra were recorded on a Smart MIRacle™ ATR ZnSe for Nicolet™ Impact 410 FT-IR spectrometer (Thermo Electron Corporation, West Palm Beach, FL, USA). The spectra were obtained by accumulation of 256 scans with 2 cm⁻¹ resolution in the region of 4000–600 cm⁻¹. All ¹H- and ¹³C-NMR spectra were recorded on a Bruker Avance III 400 MHz FT-NMR spectrometer (400 MHz for ¹H and 100 MHz for ¹³C, Bruker Comp., Karlsruhe, Germany). Chemical shifts are reported in ppm (δ) using internal Si(CH₃)₄ as the reference with diffuse, easily exchangeable signals being omitted. Mass spectra were measured using a LTQ Orbitrap Hybrid Mass Spectrometer (Thermo Electron Corporation) with direct injection into an APCI source (400 °C) in the positive mode. The purity of the compounds was checked by the HPLC method using the same conditions as described in Section 3.3. The detection wavelength of 210 nm was chosen. The peaks in the chromatogram of the solvent (blank) were deducted from the peaks in the chromatogram of the sample solution. A purity of individual compounds was determined from area peaks in the chromatogram of the sample solution.

3.2. Synthesis

3.2.1. General Procedure for Synthesis of Carboxamide Derivatives 1–8c

3-Hydroxynaphthalene-2-carboxylic acid (1.0 g, 5.3 mmol) was suspended in dry chlorobenzene (30 mL) at ambient temperature and phosphorus trichloride (0.23 mL, 2.7 mmol, 0.5 eq.), and the corresponding substituted aniline (5.3 mmol, 1 eq.) was added dropwise. The reaction mixture was transferred to the microwave reactor, where the synthesis was performed (1st phase: 10 min, 100 °C, 100 W; 2nd phase: 15 min, 120 °C, 500 W; 3rd phase: 20 min, 130 °C, 500 W). Then the mixture was cooled to 60 °C, and then the solvent was removed to dryness under reduced pressure. The residue was washed with hydrochloride acid and water. The crude product was recrystallized from EtOH. Studied compounds 1–8c are presented in Table 1.

3-Hydroxy-N-phenylnaphthalene-2-carboxamide (1). Yield 76%; Mp. 245–246 °C (Mp. 242–243 °C [34]); HPLC purity 99.41%; IR (Zn/Se ATR, cm^{-1}): 3291w, 1620m, 1556m, 1494w, 1448w, 1396w, 1344m, 1250w, 1209m, 1173m, 1064w, 950w, 915w, 870m, 842m, 771w, 739s, 712m, 687m; $^1\text{H-NMR}$ (DMSO- d_6), δ : 11.36 (s, 1H), 10.60 (s, 1H), 8.53 (s, 1H), 7.93 (d $J = 8.1$ Hz, 1H), 7.78 (m, 3H), 7.51 (ddd, $J = 8.1$ Hz, $J = 6.8$ Hz, $J = 1.3$ Hz, 1H), 7.44–7.33 (m, 4H), 7.15 (t, $J = 7.26$ Hz, 1H); $^{13}\text{C-NMR}$ (DMSO- d_6), δ : 165.67, 153.79, 138.37, 135.76, 130.42, 128.72, 128.66, 128.08, 126.83, 125.72, 124.03, 123.69, 121.55, 120.55, 110.57; HR-MS: for $\text{C}_{17}\text{H}_{14}\text{NO}_2[\text{M}+\text{H}]^+$ calculated 264.1019 m/z , found 264.1023 m/z .

3-Hydroxy-N-(2-methoxyphenyl)naphthalene-2-carboxamide (2a). Yield 80%; Mp. 165–166 °C (Mp. 164–166 °C [34]); HPLC purity 99.28%; IR (Zn/Se ATR, cm^{-1}): 3191w, 1624m, 1593s, 1549m, 1487w, 1435m, 1393w, 1393w, 1342m, 1284m, 1248w, 1227m, 1173m, 1115m, 1067m, 1031w, 922w, 864m, 837m, 801w, 771m, 735s, 685m; $^1\text{H-NMR}$ (DMSO- d_6), δ : 11.78 (s, 1H), 11.08 (s, 1H), 8.72 (s, 1H), 8.51 (d, $J = 7.7$ Hz, 1H), 7.98 (d, $J = 8.1$ Hz, 1H), 7.77 (d, $J = 8.1$ Hz, 1H), 7.51 (ddd, $J = 8.1$ Hz, $J = 6.8$ Hz, $J = 0.9$ Hz, 1H), 7.40–7.32 (m, 2H), 7.11–6.92 (m, 3H), 3.92 (s, 3H); $^{13}\text{C-NMR}$ (DMSO- d_6), δ : 162.27, 152.61, 148.64, 135.82, 132.50, 128.94, 128.22, 127.91, 127.19, 125.58, 123.94, 123.79, 121.29, 120.62, 120.19, 111.01, 110.71, 56.05; HR-MS: for $\text{C}_{18}\text{H}_{16}\text{NO}_3[\text{M}+\text{H}]^+$ calculated 294.1124 m/z , found 294.1130 m/z .

3-Hydroxy-N-(3-methoxyphenyl)naphthalene-2-carboxamide (2b). Yield 75%; Mp. 194–195 °C; HPLC purity 99.05%; IR (Zn/Se ATR, cm^{-1}): 3316w, 3047w, 1642m, 1622s, 1593s, 1556s, 1456m, 1398w, 1365w, 1346w, 1266m, 1225m, 1157m, 1134w, 1067m, 1046s, 962w, 913m, 873s, 799w, 770m, 752m, 682m; $^1\text{H-NMR}$ (DMSO- d_6), δ : 11.30 (s, 1H), 10.56 (s, 1H), 8.51 (s, 1H), 7.93 (d, $J = 8.1$ Hz, 1H), 7.77 (d, $J = 8.1$ Hz, 1H), 7.55–7.47 (m, 2H), 7.40–7.24 (m, 4H), 6.76–6.70 (m, 1H), 3.78 (s, 3H); $^{13}\text{C-NMR}$ (DMSO- d_6), δ : 165.64, 159.52, 153.67, 139.58, 135.73, 130.42, 129.50, 128.64, 128.06, 126.83, 125.72, 123.69, 121.75, 112.72, 110.54, 109.50, 106.28, 55.03; HR-MS: for $\text{C}_{18}\text{H}_{16}\text{NO}_3[\text{M}+\text{H}]^+$ calculated 294.1124 m/z , found 294.1131 m/z .

3-Hydroxy-N-(4-methoxyphenyl)naphthalene-2-carboxamide (2c). Yield 66%; Mp. 235–236 °C; HPLC purity 99.53%; IR (Zn/Se ATR, cm^{-1}): 3283w, 3013w, 1636m, 1618s, 1564m, 1510m, 1393w, 1357m, 1303w, 1247m, 1170m, 1146w, 1116w, 1070m, 1030m, 950m, 878m, 856m, 830s, 795w, 775w, 737m; $^1\text{H-NMR}$ (DMSO- d_6), δ : 11.47 (s, 1H), 10.50 (s, 1H), 8.56 (s, 1H), 7.92 (d, $J = 7.7$ Hz,

1H), 7.76 (d, $J = 8.6$ Hz, 1H), 7.71–7.64 (m, 2H), 7.51 (ddd, $J = 8.1$ Hz, $J = 6.8$ Hz, $J = 1.3$ Hz, 1H), 7.40–7.33 (m, 2H), 7.01–6.93 (m, 2H), 3.77 (s, 3H); $^{13}\text{C-NMR}$ (DMSO- d_6), δ : 165.65, 155.91, 154.18, 135.78, 131.25, 130.12, 128.62, 128.06, 126.75, 125.70, 123.64, 122.31, 120.87, 113.87, 110.59, 55.16; HR-MS: for $\text{C}_{18}\text{H}_{16}\text{NO}_3$ $[\text{M}+\text{H}]^+$ calculated 294.1124 m/z , found 294.1130 m/z .

3-Hydroxy-N-(2-methylphenyl)naphthalene-2-carboxamide (3a). Yield 74%; Mp. 195–196 °C (Mp. 194–196 °C [34]); HPLC purity 98.84%; IR (Zn/Se ATR, cm^{-1}): 3325w, 3115w, 1622s, 1586m, 1548m, 1456m, 1385w, 1355w, 1356w, 1248w, 1173m, 1065m, 954w, 915w, 873m, 844w, 803w, 773w, 742s, 679m; $^1\text{H-NMR}$ (DMSO- d_6), δ : 11.80 (s, 1H), 10.53 (s, 1H), 8.69 (s, 1H), 7.96 (d, $J = 7.7$ Hz, 2H), 7.78 (d, $J = 8.1$ Hz, 1H), 7.52 (ddd, $J = 8.1$ Hz, $J = 6.8$ Hz, $J = 1.3$ Hz, 1H), 7.41–7.36 (m, 2H), 7.33–7.22 (m, 2H), 7.16–7.08 (m, 1H), 2.34 (s, 3H); $^{13}\text{C-NMR}$ (DMSO- d_6), δ : 164.58, 153.57, 136.36, 135.87, 131.45, 130.29, 129.99, 128.82, 128.22, 126.99, 126.24, 125.67, 124.86, 123.76, 123.36, 120.60, 110.72, 17.73; HR-MS: for $\text{C}_{18}\text{H}_{16}\text{NO}_2$ $[\text{M}+\text{H}]^+$ calculated 278.1176 m/z , found 278.1182 m/z .

3-Hydroxy-N-(3-methylphenyl)naphthalene-2-carboxamide (3b). Yield 73%; Mp. 207–208 °C; HPLC purity 98.73%; IR (Zn/Se ATR, cm^{-1}): 3297w, 3048w, 1607s, 1557 m, 1489m, 1451w, 1397w, 1357w, 1344w, 1259m, 1210m, 1173w, 1076w, 951m, 923m, 859s, 836m, 783s, 744s, 689s; $^1\text{H-NMR}$ (DMSO- d_6), δ : 11.38 (s, 1H), 10.53 (s, 1H), 8.54 (s, 1H), 7.93 (d, $J = 8.6$ Hz, 1H), 7.77 (d, $J = 8.1$ Hz, 1H), 7.60–7.47 (m, 3H), 7.40–7.32 (m, 2H), 7.27 (t, $J = 7.7$ Hz, 1H), 6.97 (d, $J = 7.3$ Hz, 1H), 2.34 (s, 3H); $^{13}\text{C-NMR}$ (DMSO- d_6), δ : 165.62, 153.84, 138.26, 137.96, 135.77, 130.42, 128.66, 128.56, 128.08, 126.82, 125.71, 124.74, 123.69, 121.40, 121.06, 117.73, 110.59; 21.11; HR-MS: for $\text{C}_{18}\text{H}_{16}\text{NO}_2$ $[\text{M}+\text{H}]^+$ calculated 278.1176 m/z , found 278.1181 m/z .

3-Hydroxy-N-(4-methylphenyl)naphthalene-2-carboxamide (3c). Yield 68%; Mp. 220–221 °C (Mp. 221 °C [35]); HPLC purity 99.56%; IR (Zn/Se ATR, cm^{-1}): 3290w, 3008w, 1619s, 1556m, 1516w, 1450w, 1357m, 1252m, 1208m, 1175m, 1121w, 1070m, 951m, 913m, 869s, 832m, 810s, 761w, 741s, 716s; $^1\text{H-NMR}$ (DMSO- d_6), δ : 11.46 (s, 1H), 10.57 (s, 1H), 8.55 (s, 1H), 7.93 (d, $J = 8.1$ Hz, 1H), 7.77 (d, $J = 8.1$ Hz, 1H), 7.67 (d, $J = 8.6$ Hz, 2H), 7.51 (ddd, $J = 8.1$ Hz, $J = 6.8$ Hz, $J = 1.3$ Hz, 1H), 7.40–7.32 (m, 2H), 7.19 (d, $J = 8.6$ Hz, 2H), 2.29 (s, 3H); $^{13}\text{C-NMR}$ (DMSO- d_6), δ : 165.64, 154.01, 135.78, 133.12, 130.32, 129.10, 128.64, 128.06, 126.80, 125.70, 123.66, 121.16, 120.62, 110.60, 20.42; HR-MS: for $\text{C}_{18}\text{H}_{16}\text{NO}_2$ $[\text{M}+\text{H}]^+$ calculated 278.1176 m/z , found 278.1182 m/z .

N-(2-Fluorophenyl)-3-hydroxynaphthalene-2-carboxamide (4a). Yield 65%; Mp. 222–223 °C (Mp. 226–228 °C [36]); HPLC purity 97.21%; IR (Zn/Se ATR, cm^{-1}): 2981w, 1625s, 1605s, 1556m, 1488w, 1458m, 1345m, 1262m, 1219m, 1206w, 1191w, 1102w, 1065m, 1033m, 951w, 916e, 867m, 838w, 811m, 774w, 740s, 693w; $^1\text{H-NMR}$ (DMSO- d_6), δ : 11.86 (s, 1H), 10.95 (s, 1H), 8.69 (s, 1H), 8.36 (dt, $J = 7.7$ Hz, $J = 2.2$ Hz, 1H), 7.98 (d, $J = 8.1$ Hz, 1H), 7.78 (d, $J = 7.7$ Hz, 1H), 7.52 (ddd, $J = 8.1$ Hz, $J = 6.8$ Hz, $J = 1.3$ Hz, 1H), 7.41–7.33 (m, 2H), 7.30–7.25 (m, 1H), 7.24–7.16 (m, 2H); $^{13}\text{C-NMR}$ (DMSO- d_6), δ : 163.90, 153.08, (d, $J = 243.8$ Hz), 152.88, 135.97, 132.17, 128.93, 128.03, 127.08, 126.27 (d, $J = 10.7$ Hz), 125.66, 124.98 (d, $J = 6.9$ Hz), 124.62 (d, $J = 3.4$ Hz), 123.88, 122.87 (d, $J = 0.8$ Hz), 120.46, 115.18 (d, $J = 19.1$ Hz), 110.81; HR-MS: for $\text{C}_{17}\text{H}_{13}\text{FNO}_2$ $[\text{M}+\text{H}]^+$ calculated 282.0925 m/z , found 282.0931 m/z .

N-(3-Fluorophenyl)-3-hydroxynaphthalene-2-carboxamide (4b). Yield 67%; Mp. 248–249 °C; HPLC purity 97.78%; IR (Zn/Se ATR, cm^{-1}): 3305w, 3033w, 1622s, 1557w, 1516w, 1489w, 1449w, 1401w,

1361w, 1334w, 1253m, 1212s, 1178m, 952m, 915m, 872m, 840s 771m, 742s, 715m, 685m; $^1\text{H-NMR}$ (DMSO- d_6), δ : 11.19(s, 1H), 10.73 (s, 1H), 8.45 (s, 1H), 7.93 (d, $J = 7.7$ Hz, 1H), 7.82 (t, $J = 2.1$ Hz, 1H), 7.79–7.75 (m, 1H), 7.51 (t, $J = 7.1$ Hz, 2H), 7.44–7.32 (m, 3H), 7.02–6.92 (m, 1H); $^{13}\text{C-NMR}$ (DMSO- d_6), δ : 165.70, 162.09 (d, $J = 241.5$ Hz), 153.38, 140.24 (d, $J = 11.1$ Hz), 135.73, 130.54, 130.48, 130.30 (d, $J = 9.5$ Hz), 128.63, 128.08, 126.84, 125.73, 123.71, 122.09, 116.06 (d, $J = 2.7$ Hz), 110.32 (d, $J = 18.7$ Hz), 107.10 (d, $J = 25.9$ Hz); HR-MS: for $\text{C}_{17}\text{H}_{13}\text{FNO}_2$ $[\text{M}+\text{H}]^+$ calculated 282.0925 m/z , found 282.0932 m/z .

N-(4-Fluorophenyl)-3-hydroxynaphthalene-2-carboxamide (**4c**). Yield 69%; Mp. 264–265 °C (Mp. 264.5–265.5 °C [36]); HPLC purity 98.03%; IR (Zn/Se ATR, cm^{-1}): 3289w, 2994w, 1615s, 1569m, 1505m, 1445w, 1409w, 1357m, 1250w, 1206m, 1171w, 1100m, 1068m, 1011w, 952w, 915m, 871m, 829s, 799m, 766m, 739m, 706m; $^1\text{H-NMR}$ (DMSO- d_6), δ : 11.31 (s, 1H), 10.64 (s, 1H), 8.49 (s, 1H), 7.93 (d, $J = 8.12$ Hz, 1H), 7.83–7.75 (m, 3H), 7.51 (ddd, $J = 8.1$ Hz, $J = 6.8$ Hz, $J = 1.3$ Hz, 1H), 7.40–7.32 (m, 2H), 7.23 (t, $J = 9.0$ Hz, 2H); $^{13}\text{C-NMR}$ (DMSO- d_6), δ : 165.71, 158.50 (d, $J = 240.7$ Hz), 153.79, 135.76, 134.72 (d, $J = 2.7$ Hz), 130.29, 128.62, 128.06, 126.79, 125.72, 123.68, 122.44 (d, $J = 8.0$ Hz), 121.47, 115.28 (d, $J = 22.1$ Hz), 110.55; HR-MS: for $\text{C}_{17}\text{H}_{13}\text{FNO}_2$ $[\text{M}+\text{H}]^+$ calculated 282.0925 m/z , found 282.0930 m/z .

N-(2-Chlorophenyl)-3-hydroxynaphthalene-2-carboxamide (**5a**). Yield 50%; Mp. 226–227 °C (Mp. 225 °C [35]); HPLC purity 98.70%; IR (Zn/Se ATR, cm^{-1}): 3164w, 1625m, 1591s, 1546s, 1439m, 1345m, 1293w, 1243w, 1192m, 1171m, 1034m, 840m, 740s, 668m; $^1\text{H-NMR}$ (DMSO- d_6), δ : 11.91 (s, 1H), 11.13 (s, 1H), 8.73 (s, 1H), 8.51 (dd, $J = 8.1$ Hz, $J = 1.3$ Hz, 1H), 7.99 (d, $J = 7.69$ Hz, 1H), 7.78 (d, $J = 8.12$ Hz, 1H), 7.59–7.52 (m, 2H), 7.49–7.45 (m, 1H), 7.41–7.33 (m, 2H), 7.22–7.14 (m, 1H); $^{13}\text{C-NMR}$ (DMSO- d_6), δ : 163.49, 152.65, 135.99, 135.29, 132.62, 129.29, 128.99, 128.42, 127.77, 127.13, 125.62, 125.12, 123.88, 123.35, 122.69, 120.55, 110.78; HR-MS: for $\text{C}_{17}\text{H}_{13}\text{ClNO}_2$ $[\text{M}+\text{H}]^+$ calculated 298.0629 m/z , found 298.0637 m/z .

N-(3-Chlorophenyl)-3-hydroxynaphthalene-2-carboxamide (**5b**). Yield 69%; Mp. 257–258 °C (Mp. 258–261 °C [37]); HPLC purity 98.82%; IR (Zn/Se ATR, cm^{-1}): 3299w, 3054w, 1623s, 1545m, 1476w, 1426m 1364m, 1278w, 1248m, 1214m, 1174w, 1065w, 913w, 866m, 776m, 744m, 708m, 680m; $^1\text{H-NMR}$ (DMSO- d_6), δ : 11.16 (s, 1H); 10.68 (s, 1H), 8.46 (s, 1H), 7.99 (t, $J = 1.9$ Hz, 1H), 7.93 (d, $J = 8.1$ Hz, 1H), 7.76 (d, $J = 7.7$ Hz, 1H), 7.67 (d, $J = 8.1$ Hz, 1H), 7.51 (ddd, $J = 8.1$ Hz, $J = 6.8$ Hz, $J = 1.3$ Hz, 1H), 7.47–7.34 (m, 3H), 7.2 (d, $J = 8.1$ Hz, 1H); $^{13}\text{C-NMR}$ (DMSO- d_6), δ : 165.77, 153.42, 139.95, 135.73, 133.06, 130.45, 130.35, 128.61, 128.09, 126.81, 125.73, 123.71, 123.60, 122.03, 119.80, 118.73, 110.52; HR-MS: for $\text{C}_{17}\text{H}_{13}\text{ClNO}_2$ $[\text{M}+\text{H}]^+$ calculated 298.0629 m/z , found 298.0637 m/z .

N-(4-Chlorophenyl)-3-hydroxynaphthalene-2-carboxamide (**5c**). Yield 71%; Mp. 263–264 °C (Mp. 260 °C [34]); HPLC purity 99.35%; IR (Zn/Se ATR, cm^{-1}): 3283w, 3052w, 1612s, 1549m, 1488m, 1400m, 1359w, 1334w, 1252w, 1209m, 1170m, 1116w, 1068w, 1012m, 749s, 711m, 680m; $^1\text{H-NMR}$ (DMSO- d_6), δ : 11.24 (s, 1H), 10.68 (s, 1H), 8.47 (s, 1H), 7.93 (d, $J = 7.7$ Hz, 1H), 7.8 (t, $J = 9.6$ Hz, 2H), 7.54–7.46 (m, 2H), 7.42–7.32 (m, 4H); $^{13}\text{C-NMR}$ (DMSO- d_6), δ : 165.69, 153.56, 137.42, 135.74, 130.45, 130.40, 128.61, 128.08, 127.61, 126.81, 125.73, 123.70, 121.97, 121.83, 110.53; HR-MS: for $\text{C}_{17}\text{H}_{13}\text{ClNO}_2$ $[\text{M}+\text{H}]^+$ calculated 298.0629 m/z , found 298.0636 m/z .

N-(2-Bromophenyl)-3-hydroxynaphthalene-2-carboxamide (**6a**). Yield 61%; Mp. 215–216 °C; HPLC purity 97.75%; IR (Zn/Se ATR, cm^{-1}): 3158w, 1623s, 1582s, 1537s, 1446w, 1434m, 1388w, 1343m, 1312w, 1291w, 1193w, 1071w, 1047w, 1024m, 916m, 873m, 845m, 750s, 698m; $^1\text{H-NMR}$ (DMSO- d_6), δ : 11.88 (s, 1H), 11.00 (s, 1H), 8.72 (s, 1H), 8.42 (dd, $J = 8.1$ Hz, $J = 1.3$ Hz, 1H), 7.98 (d, $J = 8.1$ Hz, 1H), 7.80–7.70 (m, 2H), 7.57–7.50 (m, 2H), 7.45–7.34 (m, 2H), 7.13 (dt $J = 7.7$ Hz, $J = 1.7$ Hz, 1H); $^{13}\text{C-NMR}$ (DMSO- d_6), δ : 163.67, 152.77, 136.53, 136.02, 132.59, 132.54, 128.99, 128.45, 128.28, 127.10, 125.82, 125.64, 123.88, 123.50, 120.47, 114.35, 110.76; HR-MS: for $\text{C}_{17}\text{H}_{13}\text{BrNO}_2$ $[\text{M}+\text{H}]^+$ calculated 342.0124 m/z , found 342.0133 m/z .

N-(3-Bromophenyl)-3-hydroxynaphthalene-2-carboxamide (**6b**). Yield 73%; Mp. 251–252 °C; HPLC purity 98.67%; IR (Zn/Se ATR, cm^{-1}): 3295w, 3075w, 1622m, 1583m, 1553w, 1479m, 1403w, 1239w, 1209m, 1095w, 1073w, 992w, 953w, 923w, 867m, 852s, 837m, 780s, 745s, 667m; $^1\text{H-NMR}$ (DMSO- d_6), δ : 11.16 (s, 1H), 10.00 (s, 1H), 8.46 (s, 1H), 8.13 (s, 1H), 7.92 (d, $J = 7.69$ Hz, 1H), 7.78–7.68 (m, 2H), 7.51 (ddd, $J = 8.1$ Hz, $J = 6.8$ Hz, $J = 1.3$ Hz, 1H), 7.40–7.33 (m, 4H); $^{13}\text{C-NMR}$ (DMSO- d_6), δ : 165.79, 153.44, 140.08, 135.74, 130.66, 130.43, 128.62, 128.09, 126.80, 126.51, 125.74, 123.72, 122.66, 122.00, 121.48, 119.14, 110.52; HR-MS: for $\text{C}_{17}\text{H}_{13}\text{BrNO}_2$ $[\text{M}+\text{H}]^+$ calculated 342.0124 m/z , found 342.0130 m/z .

N-(4-Bromophenyl)-3-hydroxynaphthalene-2-carboxamide (**6c**). Yield 69%; Mp. 253–254 °C (Mp. 248–249 °C [35]); HPLC purity 99.02%; IR (Zn/Se ATR, cm^{-1}): 3288w, 3052w, 1605s, 1544m, 1486s, 1447w, 1394m, 1360w, 1251w, 1209m, 1169w, 1075m, 1010m, 955w, 915w, 871m, 828s, 810s, 785m, 749s, 712m; $^1\text{H-NMR}$ (DMSO- d_6), δ : 11.22 (s, 1H), 10.67 (s, 1H), 8.46 (s, 1H), 7.92 (d, $J = 7.7$ Hz, 1H), 7.76 (d, $J = 8.6$ Hz, 3H), 7.59–7.46 (m, 3H), 7.39–7.32 (m, 2H); $^{13}\text{C-NMR}$ (DMSO- d_6), δ : 165.66, 153.51, 137.83, 135.72, 131.52, 130.39, 128.60, 128.06, 126.80, 125.70, 123.69, 122.30, 121.87, 115.63, 110.52; HR-MS: for $\text{C}_{17}\text{H}_{13}\text{BrNO}_2$ $[\text{M}+\text{H}]^+$ calculated 342.0124 m/z , found 342.0132 m/z .

3-Hydroxy-*N*-(2-trifluoromethylphenyl)naphthalene-2-carboxamide (**7a**). Yield 49%; Mp. 209–210 °C; HPLC purity 99.66%; IR (Zn/Se ATR, cm^{-1}): 3274w, 1660w, 1626w, 1597w, 1515m, 1466s, 1352w, 1278s, 1217w, 1198w, 1146m, 1071w, 956m, 874m, 833m, 788m, 748w, 722m; $^1\text{H-NMR}$ (DMSO- d_6), δ : 11.67 (s, 1H), 10.43 (s, 1H), 8.72 (s, 1H), 7.99 (d, $J = 8.1$ Hz, 1H), 7.86 (d, $J = 7.8$ Hz, 1H), 7.83–7.77 (m, 2H), 7.70–7.66 (m, 1H), 7.62–7.57 (m, 1H), 7.53 (ddd, $J = 7.0$ Hz, $J = 5.5$ Hz, $J = 1.1$ Hz, 1H), 7.40 (s, 1H), 7.36 (ddd, $J = 8.4$ Hz, $J = 7.0$ Hz, $J = 1.1$ Hz); $^{13}\text{C-NMR}$ (DMSO- d_6), δ : 167.12, 153.35, 135.78, 135.47 (q, $J = 3.9$ Hz), 133.15, 131.16, 130.42, 128.63, 128.12, 126.86, 126.45 (q, $J = 4.6$ Hz), 126.16 (q, $J = 29.6$ Hz), 125.75, 123.75, 123.70, (q, $J = 276.2$ Hz), 122.11, 120.19, 110.55; HR-MS: for $\text{C}_{18}\text{H}_{13}\text{NO}_2\text{F}_3$ $[\text{M}+\text{H}]^+$ calculated 332.0893 m/z , found 332.0898 m/z .

3-Hydroxy-*N*-(3-trifluoromethylphenyl)naphthalene-2-carboxamide (**7b**). Yield 64%; Mp. 239–240 °C; HPLC purity 98.81%; IR (Zn/Se ATR, cm^{-1}): 3296w, 3108w, 1626s, 1575m, 1494m, 1428w, 1399w, 1361w, 1327s, 1207m, 1178s, 1148m, 1118s, 1100m, 1076m, 925w, 893m, 867s, 840m, 803s, 771m, 750s, 696s, 680m; $^1\text{H-NMR}$ (DMSO- d_6), δ : 11.16 (s, 1H), 10.83 (s, 1H), 8.45 (s, 1H), 8.29 (s, 1H), 7.96 (t, $J = 8.1$ Hz, 2H), 7.97 (d, $J = 8.1$ Hz, 1H), 7.62 (t, $J = 7.9$ Hz, 1H), 7.55–7.47 (m, 2H), 7.40–7.32 (m, 2H); $^{13}\text{C-NMR}$ (DMSO- d_6), δ : 166.06, 153.46, 139.32, 135.79, 130.45, 129.93, 129.51 (q, $J = 31.3$ Hz), 128.63, 128.13, 126.84, 125.76, 124.11 (q, $J = 277.7$ Hz), 123.94, 123.76, 122.09,

120.21 (q, $J = 3.8$ Hz), 116.47 (q, $J = 3.8$ Hz), 110.54; HR-MS: for $C_{18}H_{13}NO_2F_3$ $[M+H]^+$ calculated 332.0893 m/z , found 332.0900 m/z .

3-Hydroxy-N-(4-trifluoromethylphenyl)naphthalene-2-carboxamide (7c). Yield 58%; Mp. 281–282 °C; HPLC purity 99.46%; IR (Zn/Se ATR, cm^{-1}): 3292w, 3021w, 1623s, 1548m, 1450m, 1410m, 1324m, 1255w, 1212m, 1175m, 1112s, 1065s, 1016m, 960w, 916w, 873m, 841s, 822m, 791w, 752s, 707m; 1H -NMR (DMSO- d_6), δ : 11.17 (s, 1H), 10.85 (s, 1H), 8.45 (s, 1H), 8.03–7.91 (m, 3H), 7.79–7.72 (m, 3H), 7.51 (ddd, $J = 8.1$ Hz, $J = 6.8$ Hz, $J = 1.3$ Hz, 1H), 7.40–7.32 (m, 2H); ^{13}C -NMR (DMSO- d_6), δ : 165.87, 153.28, 142.15 (q, $J = 1.5$ Hz), 135.76, 130.61, 128.64, 128.12, 126.86, 125.98 (q, $J = 3.8$ Hz), 125.74, 124.30 (q, $J = 271.2$ Hz), 123.88 (q, $J = 32.0$ Hz), 123.74, 122.28, 120.18, 110.53; HR-MS: for $C_{18}H_{13}NO_2F_3$ $[M+H]^+$ calculated 332.0893 m/z , found 332.0899 m/z .

3-Hydroxy-N-(2-nitrophenyl)naphthalene-2-carboxamide (8a). Yield 29%; Mp. 174–175 °C; HPLC purity 97.17%; IR (Zn/Se ATR, cm^{-1}): 3240w, 1627m, 1581m, 1557w, 1494m, 1450w, 1434w, 1393w, 1341m, 1270m, 1203w, 1147m, 870w, 840m, 771w, 736s, 691w; 1H -NMR (DMSO- d_6), δ : 12.05 (s, 1H), 11.79 (s, 1H), 8.73 (s, 1H), 8.60 (dd, $J = 7.2$ Hz, $J = 1.2$ Hz, 1H), 8.16 (dd, $J = 8.2$ Hz, $J = 1.5$ Hz, 1H), 7.97 (t, $J = 8.0$ Hz, 2H), 7.82–7.78 (m, 1H), 7.51 (ddd, $J = 8.1$ Hz, $J = 6.8$ Hz, $J = 1.3$ Hz, 1H), 7.39–7.34 (m, 3H); ^{13}C -NMR (DMSO- d_6), δ : 164.21, 155.98, 152.85, 137.18, 136.17, 132.97, 132.43, 129.16, 128.94, 127.04, 126.62, 125.89, 125.63, 123.75, 120.74, 115.27, 110.75; HR-MS: for $C_{17}H_{13}N_2O_4$ $[M+H]^+$ calculated 309.0870 m/z , found 309.0875 m/z .

3-Hydroxy-N-(3-nitrophenyl)naphthalene-2-carboxamide (8b). Yield 58%; Mp. 250–251 °C; (Mp. 242–244 °C [34]); HPLC purity 97.62%; IR (Zn/Se ATR, cm^{-1}): 3394w, 1658m, 1586m, 1525m, 1463m, 1345s, 1297s, 1230m, 1209m, 1145m, 1033w, 911w, 876m, 808m, 747m, 738s, 668m; 1H -NMR (DMSO- d_6), δ : 11.12 (s, 1H), 10.93 (s, 1H), 8.83 (t, $J = 2.14$ Hz, 1H), 8.45 (s, 1H), 8.11 (dd, $J = 8.12$ Hz, $J = 1.28$ Hz, 1H), 8.01–7.91 (m, 2H), 7.77 (d, $J = 8.1$ Hz, 1H), 7.66 (t, $J = 8.1$ Hz, 1H), 7.51 (ddd, $J = 8.1$ Hz, $J = 6.8$ Hz, $J = 1.3$ Hz, 1H), 7.40–7.32 (m, 2H); ^{13}C -NMR (DMSO- d_6), δ : 166.08, 153.30, 147.95, 139.72, 135.76, 130.48, 130.08, 128.61, 128.12, 126.80, 126.24, 125.76, 123.76, 122.22, 118.32, 114.35, 110.50; HR-MS: for $C_{17}H_{13}N_2O_4$ $[M+H]^+$ calculated 309.0870 m/z , found 309.0876 m/z .

3-Hydroxy-N-(4-nitrophenyl)naphthalene-2-carboxamide (8c). Yield 72%; Mp. 265–266 °C; HPLC purity 99.03%; IR (Zn/Se ATR, cm^{-1}): 3285w, 2981w, 1618s, 1599m, 1568w, 1513s, 1449w, 1407w, 1337s, 1260w, 1210m, 1171m, 1147w, 1112m, 1033m, 916w, 851s, 772w, 747s, 704w; 1H -NMR (DMSO- d_6), δ : 11.10 (s, 1H), 11.03 (s, 1H), 8.41 (s, 1H), 8.28 (d, $J = 9.4$ Hz, 2H), 8.03 (d, $J = 9.0$ Hz, 2H), 7.93 (d, $J = 8.1$ Hz, 1H), 7.77 (d, $J = 8.6$ Hz, 1H), 7.51 (ddd, $J = 8.1$ Hz, $J = 6.8$ Hz, $J = 1.3$ Hz, 1H), 7.39–7.32 (m, 2H); ^{13}C -NMR (DMSO- d_6), δ : 165.89, 152.98, 144.80, 142.58, 135.76, 130.73, 128.63, 128.15, 126.85, 125.75, 124.82, 123.76, 122.68, 119.79, 110.49; HR-MS: for $C_{17}H_{13}N_2O_4$ $[M+H]^+$ calculated 309.0870 m/z , found 309.0875 m/z .

3.3. Lipophilicity Determination by HPLC (Capacity Factor k /Calculated $\log k$)

A HPLC system Agilent 1200 equipped with DAD detector (Agilent, Santa Clara, CA, USA) was used. A chromatographic column Symmetry[®] C_{18} 5 μm , 4.6×250 mm, Part No. WAT054275, (Waters Corp., Milford, MA, USA) was used. The HPLC separation process was monitored and evaluated by

EZChrom Elite software ver. 3.3.2 (Agilent). Isocratic elution by a mixture of MeOH p.a. (60%) and H₂O-HPLC Mili-Q grade (40%) as a mobile phase was used. The total flow of the column was 1.0 mL/min, injection 20 µL, column temperature 40 °C and sample temperature 10 °C. The detection wavelength 210 nm was chosen. The KI methanolic solution was used for the dead time (t_D) determination. Retention times (t_R) were measured in minutes. The capacity factors k were calculated according to formula $k = (t_R - t_D)/t_D$, where t_R is the retention time of the solute, whereas t_D denotes the dead time obtained using an unretained analyte. Log k , calculated from the capacity factor k , is used as the lipophilicity index converted to log P scale. The log k values of the individual compounds are shown in Table 1.

3.4. Study of Inhibition of Photosynthetic Electron Transport (PET) in Spinach Chloroplasts

Chloroplasts were prepared from spinach (*Spinacia oleracea* L.) according to Masarovicova and Kralova [51]. The inhibition of photosynthetic electron transport (PET) in spinach chloroplasts was determined spectrophotometrically (Genesys 6, Thermo Scientific), using an artificial electron acceptor 2,6-dichlorophenol-indophenol (DCIPP) according to Kralova *et al.* [52], and the rate of photosynthetic electron transport was monitored as a photoreduction of DCPIP. The measurements were carried out in phosphate buffer (0.02 mol/L, pH 7.2) containing sucrose (0.4 mol/L), MgCl₂ (0.005 mol/L) and NaCl (0.015 mol/L). The chlorophyll content was 30 mg/L in these experiments and the samples were irradiated (~100 W/m² with 10 cm distance) with a halogen lamp (250 W) using a 4 cm water filter to prevent warming of the samples (suspension temperature 22 °C). The studied compounds were dissolved in DMSO due to their limited water solubility. The applied DMSO concentration (up to 4%) did not affect the photochemical activity in spinach chloroplasts. The inhibitory efficiency of the studied compounds was expressed by IC₅₀ values, *i.e.*, by molar concentration of the compounds causing 50% decrease in the oxygen evolution rate relative to the untreated control. The comparable IC₅₀ value for a selective herbicide 3-(3,4-dichlorophenyl)-1,1-dimethylurea, DCMU (Diurone[®]) was about 1.9 µmol/L. The results are summarized in Table 1.

3.5. Study of Chlorophyll *a* Fluorescence in Spinach Chloroplasts

The fluorescence emission spectra of chlorophyll *a* (Chl*a*) in spinach chloroplasts were recorded on fluorescence spectrophotometer F-2000 (Hitachi, Tokyo, Japan) using excitation wavelength $\lambda_{ex} = 436$ nm for monitoring fluorescence of Chl*a*, excitation slit 20 nm and emission slit 10 nm. The samples were kept in the dark for 2 min before measuring. The phosphate buffer used for dilution of the chloroplast suspension was the same as described above. Due to low aqueous solubility the compounds were added to chloroplast suspension in DMSO solution. The DMSO concentration in all samples was the same as in the control (10%). The chlorophyll concentration in chloroplast suspension was 10 mg/L.

3.6. In Vitro Antibacterial Susceptibility Testing

The synthesized compounds were evaluated for *in vitro* antibacterial activity against representatives of multidrug-resistant bacteria, clinical isolates of methicillin-resistant *Staphylococcus aureus* (MRSA) 63718, SA 630 and SA 3202 that were obtained from the National Institute of Public Health,

Prague, Czech Republic. *Staphylococcus aureus* ATCC 29213 was used as a reference and quality control strain. Ampicillin (Sigma-Aldrich) was used as the standard. Prior to testing, each strain was passaged onto nutrient agar (Oxoid, Hampshire, UK) with 5% of bovine blood, and bacterial inocula were prepared by suspending a small portion of bacterial colony in sterile phosphate buffered saline (pH 7.2–7.3). The cell density was adjusted to 0.5 McFarland units using a densitometer (Densi-La-Meter, LIAP, Riga, Latvia). The final inoculum was made by 1:20 dilution of the suspension with the Mueller-Hinton broth (MH broth). The compounds were dissolved in DMSO (Sigma), and the final concentration of DMSO in the MH broth (Oxoid) did not exceed 2.5% of the total solution composition. The broth dilution micro-method modified according to NCCLS guidelines [53,54] in MH broth was used to determine the minimum inhibitory concentration (MIC). Drug-free controls, sterility controls and controls consisted of MH broth and DMSO alone were included. The determination of results was performed visually after 24 h of static incubation in the darkness at 37 °C in an aerobic atmosphere. The MICs were defined as the lowest concentration of the compound at which no visible bacterial growth was observed. The results are summarized in Table 1.

3.7. In Vitro Antimycobacterial Evaluation

The evaluation of *in vitro* antimycobacterial activity of the compounds was performed against *Mycobacterium marinum* CAMP 5644 and *M. kansasii* DSM 44162. The broth dilution micro-method in Middlebrook 7H9 medium (Difco, Lawrence, KS, USA) supplemented with ADC Enrichment (BBL, USA) was used to determine the minimum inhibitory concentration (MIC) as previously described [55]. The tested compounds were dissolved as described above in chapter 3.6. Isoniazid (Sigma-Aldrich) was used as reference antibacterial drug. Bacterial inocula were prepared by transferring colonies from culture to sterile water. The cell density was adjusted to 0.5 McFarland units using a densitometer (Densi-La-Meter, LIAP). The final inoculum was made by 1:1,000 dilution of the suspension with sterile water. Drug-free controls, sterility controls and controls consisted of medium and DMSO alone were included. The determination of results was performed visually after 7 days of static incubation in the darkness at 37 °C in an aerobic atmosphere for *M. kansasii* and after 21 days of static incubation in the darkness at 28 °C in an aerobic atmosphere for *M. marinum*. The MICs were defined as the lowest concentration of the compound at which no visible bacterial growth was observed. The results are summarized in Table 1.

3.8. In Vitro Cytotoxicity Assay

Human monocytic leukemia THP-1 cells were used for *in vitro* toxicity assay. Cells were obtained from the European Collection of Cell Cultures (ECACC, Salisbury, UK) and routinely cultured in RPMI medium supplemented with 10% fetal bovine serum, 2% L-glutamine, 1% penicillin and streptomycin at 37 °C with 5% CO₂. Cytotoxicity was determined using a WST-1 assay kit (Roche Diagnostics, Mannheim, Germany) according to the manufacturer's instructions. The tested compounds were dissolved in DMSO and added in five increasing concentrations (0.37, 1.1, 3.3, 10, and 30 µmol/L) to the cell suspension in the culture medium. Subsequently, the cells were incubated for 24 h at 37 °C with 5% CO₂. WST-1 assays conducted in triplicates were performed as previously described [49]. The median lethal dose values, LD₅₀, were deduced through the production of a dose-

response curve. All data were evaluated using GraphPad Prism 5.00 software (GraphPad Software, San Diego, CA, USA). The results are summarized in Table 1.

4. Conclusions

A series of twenty-two ring-substituted 3-hydroxynaphthalene-2-carboxanilides were prepared and characterized. The prepared compounds were tested for their ability to inhibit photosynthetic electron transport (PET) in spinach chloroplasts (*Spinacia oleracea* L.) and for their antibacterial and antimycobacterial activity against four *Staphylococcus* strains, *Mycobacterium marinum* and *M. kansasii*. 3-Hydroxy-*N*-(3-nitrophenyl)naphthalene-2-carboxamide (**8b**) showed relatively high PET inhibition. 3-Hydroxy-*N*-(2-methoxyphenyl)naphthalene-2-carboxamide (**2a**) showed the high biological activity against *S. aureus* as well as methicillin-resistant strains. *N*-(2-Fluorophenyl)-3-hydroxynaphthalene-2-carboxamide (**4a**) and *N*-(3-fluorophenyl)-3-hydroxynaphthalene-2-carboxamide (**4b**) expressed high activity against *M. marinum*. 3-Hydroxy-*N*-(4-nitrophenyl)naphthalene-2-carboxamide (**8c**) showed high activity against *M. kansasii*. All the above-mentioned compounds exhibited activity comparable with or higher than the standards ampicillin or isoniazid. Lipophilicity and electronic properties of anilide substituents influenced the biological activities of compounds in all biological assays. It can be stated that the dependences of activities on lipophilicity and on electronic properties show bilinear trends. The most effective compounds **2a**, **4a**, **7a**, **8b** and **8c** were tested for their *in vitro* cytotoxicity against THP-1 cells. It can be concluded that the discussed anilides **2a** and **4a** can be considered as promising agents for subsequent design of novel antibacterial and antimycobacterial agents.

Acknowledgements

This study was supported by the IGA VFU Brno 96/2012/FaF and 65/2012/FVL, the Slovak Grant Agency VEGA, Grant No. 1/0612/11, by the Project APVV-0061-11, by Sanofi-Aventis Pharma Slovakia, by the Project CzechGlobe (Centre for Global Climate Change Impacts Studies), Reg. No. CZ.1.05/1.1.00/02.0073, and by the project CEITEC (Central European Institute of Technology), Reg. No. CZ.1.05/1.1.00/02.0068 from the European Regional Development Fund.

Conflict of Interest

The authors declare no conflict of interest.

References

1. Baquero, F.; Coque, T.M.; de la Cruz, F. Ecology and evolution as targets: the need for novel eco-evo drugs and strategies to fight antibiotic resistance. *Antimicrob. Agents Chemother.* **2011**, *55*, 3649–3660.
2. Acharya, N.; Varshney, U. Biochemical properties of single-stranded DNA-binding protein from *Mycobacterium smegmatis*, a fast-growing *Mycobacterium* and its physical and functional interaction with uracil DNA glycosylases. *J. Mol. Biol.* **2002**, *318*, 1251–1264.

3. Broussard, G.W.; Ennis, D.G. *Mycobacterium marinum* produces long-term chronic infections in medaka: A new animal model for studying human tuberculosis. *Comp. Biochem. Phys. C* **2007**, *145*, 45–54.
4. Matveychuk, A.; Fuks, L.; Priess, R.; Hahim, I.; Shitrit, D. Clinical and radiological features of *Mycobacterium kansasii* and other NTM infections. *Resp. Med.* **2012**, *106*, 1472–1477.
5. Laughon, E.L. New tuberculosis drugs in development. *Curr. Top. Med. Chem.* **2007**, *7*, 463–473.
6. Levy, S.B. Antibiotic resistance—the problem intensifies. *Adv. Drug. Delivery Rev.* **2005**, *57*, 1446–1450.
7. Kallen, A.J.; Mu, Y.; Bulens, S.; Reingold, A.; Petit, S.; Gershman, K.; Ray, S.M.; Harrison, L.H.; Lynfield, R.; Dumyati, G.; *et al.* Health care-associated invasive MRSA infections, 2005–2008. *JAMA* **2010**, *304*, 641–647.
8. Liu, C.; Bayer, A.; Cosgrove, S.E.; Daum, R.S.; Fridkin, S.K.; Gorwitz, R.J.; Kaplan, S.L.; Karchmer, A.W.; Levine, D.P.; Murray, B.E.; *et al.* Clinical practice guidelines by the Infectious Diseases Society of America for the treatment of methicillin-resistant *Staphylococcus aureus* infections in adults and children. *Clin. Infect. Dis.* **2011**, *52*, 285–292.
9. Shaner, D.L. Herbicide safety relative to common targets in plants and mammals. *Pest. Manag. Sci.* **2004**, *60*, 17–24.
10. Delaney, J.; Clarke, E.; Hughes, D.; Rice, M. Modern agrochemical research: A missed opportunity for drug discovery? *Drug Discov. Today* **2006**, *11*, 839–845.
11. Duke, S.O. Herbicide and pharmaceutical relationships. *Weed Sci.* **2010**, *58*, 334–339.
12. Kralova, K.; Sersen, F.; Cizmarik, J. Inhibitory effect of piperidinoethylesters of alkoxyphenylcarbamic acids on photosynthesis. *Gen. Physiol. Biophys.* **1992**, *11*, 261–267.
13. Kralova, K.; Bujdakova, H.; Kuchta, T.; Loos, D. Correlation between biological activity and the structure of 6-amino-2-R-thiobenzothiazoles. Anti-yeast activity and inhibition of photochemical activity of chloroplasts. *Pharmazie* **1994**, *49*, 460–461.
14. Kralova, K.; Kallova, J.; Loos, D.; Devinsky, F. Correlation between biological activity and the structure of *N,N'*-bis(alkyldimethyl)-1,6-hexanediammonium dibromides. Antibacterial activity and inhibition of photochemical activity of chloroplasts. *Pharmazie* **1994**, *49*, 857–858.
15. Kralova, K.; Bujdakova, H.; Cizmarik, J. Antifungal and antialgal activity of piperidinopropyl esters of alkoxy substituted phenylcarbamic acids. *Pharmazie* **1995**, *50*, 440–441.
16. Musiol, R.; Tabak, D.; Niedbala, H.; Podeszwa, B.; Jampilek, J.; Kralova, K.; Dohnal, J.; Finster, J.; Mencil, A.; Polanski, J. Investigating biological activity spectrum for novel quinoline analogues 2: Hydroxyquinolinecarboxamides with photosynthesis inhibiting activity. *Bioorg. Med. Chem.* **2008**, *16*, 4490–4499.
17. Imramovsky, A.; Vinsova, J.; Monreal-Ferriz, J.; Buchta, V.; Jampilek, J. Salicylanilide esters of *N*-protected amino acids as novel antimicrobial agents. *Bioorg. Med. Chem. Lett.* **2009**, *19*, 348–351.
18. Otevrel, J.; Mandelova, Z.; Pesko, M.; Guo, J.; Kralova, K.; Sersen, F.; Vejsova, M.; Kalinowski, D.; Kovacevic, Z.; Coffey, A.; *et al.* Investigating the spectrum of biological activity of ring-substituted salicylanilides and carbamoylphenylcarbamates. *Molecules* **2010**, *15*, 8122–8142.

19. Imramovsky, A.; Pesko, M.; Kralova, K.; Vejsova, M.; Stolarikova, J.; Vinsova, J.; Jampilek, J. Investigating spectrum of biological activity of 4- and 5-chloro-2-hydroxy-*N*-[2-(arylamino)-1-alkyl-2-oxoethyl]benzamides. *Molecules* **2011**, *16*, 2414–2430.
20. Gonec, T.; Bobal, P.; Suján, J.; Pesko, M.; Guo, J.; Kralova, K.; Pavlacka, L.; Vesely, L.; Kreckova, E.; Kos, J.; *et al.* Investigating the spectrum of biological activity of substituted quinoline-2-carboxamides and their isosteres. *Molecules* **2012**, *17*, 613–644.
21. Draber, W.; Tietjen, K.; Kluth, J.F.; Trebst, A. Herbicides in photosynthesis research. *Angew. Chem.* **1991**, *3*, 1621–1633.
22. Tischer, W.; Strotmann, H. Relationship between inhibitor binding by chloroplasts and inhibition of photosynthetic electron-transport. *Biochim. Biophys. Acta* **1977**, *460*, 113–125.
23. Trebst, A.; Draber, W. Structure activity correlations of recent herbicides in photosynthetic reactions. In *Advances in Pesticide Science*; Greissbuehler, H., Ed.; Pergamon Press: Oxford, UK, 1979; pp. 223–234.
24. Bowyer, J.R.; Camilleri, P.; Vermaas, W.F.J. Photosystem II and its interaction with herbicides. In *Herbicides, Topics in Photosynthesis*; Baker, N.R., Percival, M.P., Eds.; Elsevier: Amsterdam, The Netherlands, 1991; Volume 10, pp. 27–85.
25. Koreyoshi, S.; Masato, M.; Tetsuji, I. (Yoshitomi Pharmaceutical Industries) Hydroxynaphthoic acid anilides, microbicides and slimicides. Japan. Kokai JP 52 076 430, 27 June 1977.
26. Macielag, M.J.; Demers, J.P.; Fraga-Spano, S.A.; Hlasta, J.D.; Johnson, G.S.; Kanojia, M.R.; Russell, K.R.; Sui, Z.; Weidner-Wells, A.M.; Werblood, H.; *et al.* Substituted salicylanilides as inhibitors of two-component regulatory systems in bacteria. *J. Med. Chem.* **1998**, *41*, 2939–2945.
27. Kauppi, A.M.; Nordfelth, R.; Uvell, H.; Wolf-Watz, H.; Elofsson, M. Targeting bacterial virulence: Inhibitors of type III secretion in *Yersinia*. *Chem. Biol.* **2003**, *10*, 241–249.
28. Vinsova, J.; Imramovsky, A.; Buchta, V.; Ceckova, M.; Dolezal, M.; Staud, F.; Jampilek, J.; Kaustova, J. Salicylanilide acetates: Synthesis and antibacterial evaluation. *Molecules* **2007**, *12*, 1–12.
29. Imramovsky, A.; Vinsova, J.; Monreal-Ferriz, J.; Dolezal, R.; Jampilek, J.; Kaustova, J.; Kunc, F. New antituberculotics originated from salicylanilides with promising *in vitro* activity against atypical mycobacterial strains. *Bioorg. Med. Chem.* **2009**, *17*, 3572–3579.
30. Imramovsky, A.; Pesko, M.; Monreal-Ferriz, J.; Kralova, K.; Vinsova, J.; Jampilek, J. Photosynthesis-Inhibiting efficiency of 4-chloro-2-(chlorophenylcarbamoyl)phenyl alkylcarbamates. *Bioorg. Med. Chem. Lett.* **2011**, *21*, 4564–4567.
31. Kratky, M.; Vinsova, J. Salicylanilide ester prodrugs as potential antimicrobial agents – a review. *Curr. Pharm. Des.* **2011**, *17*, 3494–3505.
32. Kratky, M.; Vinsova, J.; Buchta, V. *In vitro* antibacterial and antifungal activity of salicylanilide benzoates. *Sci. World J.* **2012**, *2012*, 290628.
33. Kratky, M.; Vinsova, J.; Novotna, E.; Mandikova, J.; Wsol, V.; Trejtnar, F.; Ulmann, V.; Stolarikova, J.; Fernandes, S.; Bhat, S.; *et al.* Salicylanilide derivatives block *Mycobacterium tuberculosis* through inhibition of isocitrate lyase and methionine aminopeptidase. *Tuberculosis* **2012**, *92*, 434–439.
34. Hartrodt, V.W.; Woohsmann, H. Ein Beitrag zur Darstellung von Alkalisalzen saurer Schwefelsäureester verschiedener Naphthol AS-Verbindungen. *J. Prakt. Chem.* **1965**, *27*, 99–107.

35. Tripathy, H.; Pradhan, D.G.; Dash, B.C.; Mahapatra, G.N. Synthesis of some new halogenated *N*-thiazolyl substituted hydroxy acid amides and their use as possible fungicides. *Agric. Biol. Chem.* **1973**, *6*, 1375–1383.
36. Hitch, F.E.; Dahlen, A.M.; Friedrich, M.E. (E.I. du Pont de Nemours & Company). Fluorinated arylamides. US 1982661, 4 December 1934.
37. Liechty, C.H.; Sequin, U.; Bold, G.; Furet, P.; Meyer, T.; Traxler, P. Salicylanilides as inhibitors of the protein tyrosine kinase epidermal growth factor receptor. *Eur. J. Med. Chem.* **2004**, *39*, 11–26.
38. Izawa, S. Acceptors and donors for chloroplast electron transport. In *Methods in Enzymology*; Colowick, P., Kaplan, N.O., Eds.; Academic Press: London, UK, 1980; Volume 69, Part C, pp. 413–434.
39. Kralova, K.; Sersen, F.; Pesko, M.; Klimesova, V.; Waisser, K. Photosynthesis-inhibiting effects of 2-benzylsulphonylbenzimidazoles in spinach chloroplasts. *Chem. Pap.* **2012**, *66*, 795–799.
40. Kralova, K.; Sersen, F.; Sidoova, E. Effect of 2-alkylthio-6-aminobenzothiazoles and their 6-*N*-substituted derivatives on photosynthesis inhibition in spinach chloroplasts. *Gen. Phys. Biophys.* **1993**, *12*, 421–427.
41. Kralova, K.; Sersen, F.; Miletin, M.; Hartl, J. Inhibition of photosynthetic electron transport by some anilides of 2-alkylpyridine-4-carboxylic acids in spinach chloroplasts. *Chem. Pap.* **1998**, *52*, 52–55.
42. Kralova, K.; Sersen, F.; Pesko, M.; Waisser, K.; Kubicova, L. 5-Bromo- and 3,5-dibromo-2-hydroxy-*N*-phenylbenzamides—Inhibitors of photosynthesis. *Chem. Pap.* **2013**, *67*, in press
43. Kralova, K.; Sersen, F.; Klimesova, V.; Waisser, K. 2-Alkylsulphonyl-4-pyridine-carbothioamides—Inhibitors of oxygen evolution in freshwater alga *Chlorella vulgaris*. *Chem. Pap.* **2011**, *65*, 909–912.
44. Atal, N.; Saradhi, P.P.; Mohanty, P. Inhibition of the chloroplast photochemical reactions by treatment of wheat seedlings with low concentrations of cadmium: Analysis of electron transport activities and changes in fluorescence yields. *Plant Cell Physiol.* **1995**, *32*, 943–951.
45. Sersen, F.; Kralova, K.; Bumbalova, A. Action of mercury on the photosynthetic apparatus of spinach chloroplasts. *Photosynthetica* **1998**, *35*, 551–559.
46. Apostolova, E.L.; Ivanov, A.G. Influence of Triton X-100 on the structure and functions of pea thylakoid membranes. *J. Plant Physiol.* **1995**, *145*, 239–244.
47. Kralova, K.; Sersen, F.; Kubicova, L.; Waisser, K. Inhibitory effects of substituted benzanilides on photosynthetic electron transport in spinach chloroplasts. *Chem. Pap.* **1999**, *53*, 328–331.
48. Kubicova, L.; Kralova, K.; Sersen, F.; Gregor, J.; Waisser, K. Effects of substituted salicylanilides on the photosynthetic apparatus of spinach chloroplasts. *Folia Pharm. Univ. Carol.* **2000**, *25*, 89–96.
49. Kollar, P.; Zavalova, V.; Barta, T.; Smejkal, K.; Hampl, A. Geranylated flavanone tomentodiplacone B inhibits proliferation of human monocytic leukaemia (THP-1) cells. *Br. J. Pharmacol.* **2011**, *162*, 1534–1541.
50. Fajkusova, D.; Pesko, M.; Keltosova, S.; Guo, J.; Oktabec, Z.; Vejsova, M.; Kollar, P.; Coffey, A.; Csollei, J.; Kralova, K.; Jampilek, J.: Anti-infective and herbicidal activity of *N*-substituted 2-aminobenzothiazoles. *Bioorg. Med. Chem.* **2012**, *20*, 7059–7068.

51. Masarovicova, E.; Kralova, K. Approaches to Measuring Plant Photosynthesis Activity. In *Handbook of Photosynthesis*, 2nd ed.; Pessaraki, M., Ed.; Taylor & Francis Group: Boca Raton, FL, USA, 2005; pp. 617–656.
52. Kralova, K.; Sersen, F.; Sidoova, E. Photosynthesis inhibition produced by 2-alkylthio-6-R-benzothiazoles. *Chem. Pap.* **1992**, *46*, 348–350.
53. National Committee for Clinical Laboratory Standards. *Methods for Dilution Antimicrobial Susceptibility Tests for Bacteria that Grow Aerobically*, 5th Edition; Approved Standard M7-A5. NCCLS: Wayne, PA, USA, 2000.
54. National Committee for Clinical Laboratory Standards. *Performance Standards for Antimicrobial Susceptibility Testing*; 12th Informational Supplement M100-S12. NCCLS: Wayne, PA, USA, 2002.
55. Schwalbe, R.; Steele-Moore, L.; Goodwin, A.C. *Antimicrobial Susceptibility Testing Protocols*. CRC Press: Boca Raton, FL, USA, 2007.

Sample Availability: Samples of the compounds are available from the authors.

© 2013 by the authors; licensee MDPI, Basel, Switzerland. This article is an open access article distributed under the terms and conditions of the Creative Commons Attribution license (<http://creativecommons.org/licenses/by/3.0/>).

č.	citace	ISSN
2	KOS, J , E NEVIN, M SORAL, I KUSHKEVYCH, T GONEC, P BOBAL, P KOLLAR, A COFFEY, J O'MAHONY, T LIPTAJ, K KRALOVA a J JAMPILEK. Synthesis and antimycobacterial properties of ring-substituted 6-hydroxynaphthalene-2-carboxanilides. <i>BIOORGANIC & MEDICINAL CHEMISTRY</i> [online]. 2015, 23 (9), 2035–2043. Dostupné z: doi: 10.1016/j.bmc.2015.03.018	0968-0896



Synthesis and antimycobacterial properties of ring-substituted 6-hydroxynaphthalene-2-carboxanilides



Jiri Kos^a, Eoghan Nevin^b, Michal Soral^c, Ivan Kushkevych^d, Tomas Gonec^a, Pavel Bobal^a, Peter Kollar^d, Aidan Coffey^b, Jim O'Mahony^b, Tibor Liptaj^c, Katarina Kralova^e, Josef Jampilek^{a,*}

^a Department of Chemical Drugs, Faculty of Pharmacy, University of Veterinary and Pharmaceutical Sciences, Palackeho 1/3, 612 42 Brno, Czech Republic

^b Department of Biological Sciences, Cork Institute of Technology, Bishopstown, Cork, Ireland

^c Department of NMR Spectroscopy and Mass Spectrometry, Faculty of Chemical and Food Technology, Slovak University of Technology in Bratislava, Radlinskeho 9, 812 37 Bratislava, Slovakia

^d Department of Human Pharmacology and Toxicology, Faculty of Pharmacy, University of Veterinary and Pharmaceutical Sciences, Palackeho 1/3, 612 42 Brno, Czech Republic

^e Institute of Chemistry, Faculty of Natural Sciences, Comenius University, Mlynska dolina Ch-2, 842 15 Bratislava, Slovakia

ARTICLE INFO

Article history:

Received 3 January 2015

Revised 2 March 2015

Accepted 5 March 2015

Available online 12 March 2015

Keywords:

Hydroxynaphthalene-2-carboxanilides

In vitro antimycobacterial activity

MTT assay

In vitro cytotoxicity

Structure–activity relationships

ABSTRACT

In this study, a series of twenty-two ring-substituted 6-hydroxynaphthalene-2-carboxanilides was prepared and characterized. Primary in vitro screening of the synthesized compounds was performed against *Mycobacterium tuberculosis* H37Ra, *Mycobacterium avium* complex and *M. avium* subsp. *paratuberculosis*. Derivatives substituted by trifluoromethyl, bromo, methyl and methoxy moieties in C₍₃₎ and C₍₄₎ positions of the anilide ring showed 2-fold higher activity against *M. tuberculosis* than isoniazid and 4.5-fold higher activity against *M. avium* subsp. *paratuberculosis* than rifampicin. 6-Hydroxy-*N*-(2-methylphenyl)naphthalene-2-carboxamide had MIC = 29 μM against *M. avium* complex. A significant decrease of mycobacterial cell metabolism (viability of *M. tuberculosis* H37Ra) was observed using MTT assay. Screening of the cytotoxicity of the most effective antimycobacterial compounds was performed using the THP-1 cells, and no significant lethal effect was observed. The structure–activity relationships are discussed.

© 2015 Elsevier Ltd. All rights reserved.

1. Introduction

Bacterial infections represent an increasing worldwide threat. The number of untreatable diseases decreased after the 1950s due to the introduction of antibacterial/antituberculous agents. However, since the 1980s morbidity has risen again, and mortality due to respiratory infections, AIDS and tuberculosis now represents about 85% of world mortality from infections. The resistance of common pathogens to first-choice drugs increased up to 100% during the last decade, and the resistance of some strains to second- or third-choice drugs is a great problem. Tuberculosis (TB) has again become a major bacterial cause of worldwide mortality. In 2013, an estimated 9.0 million people developed TB, and 1.5 million died from the disease, 360,000 of whom were HIV-positive. The rate of successful treatment has also decreased due to the emergence of cross-resistant, multidrug and extensively drug resistant strains. Multidrug-resistant TB strains (MDR-TB) are a worldwide problem; drug resistance surveillance data indicate that in 2013 approximately 480,000 people developed MDR-TB

worldwide. Among TB patients reported by national TB programmes in 2013, there were estimated 300,000 cases of MDR-TB. Extensively drug-resistant TB (XDR-TB, defined as MDR-TB plus resistance to any fluoroquinolone and any second-line injectable drugs) was identified in 100 countries globally in 2013, and the average proportion of MDR-TB cases with XDR-TB was 9.0%. Occurrences of lethal complications associated with immunocompromised populations are more frequent. These complications include systemic infections caused by common, initially non-pathogenic mycobacterial strains (e.g., *Mycobacterium avium*, *Mycobacterium kansasii*, *Mycobacterium abscessus*, *Mycobacterium fortuitum*, *Mycobacterium chelonae*, *Mycobacterium smegmatis*, etc.), which became difficult-to-treat or incurable diseases due to suppressed immunity. These non-tuberculous mycobacteria (NTM) are now recognized as significant human pathogens and cause diseases (such as pulmonary disease, lymphadenitis, skin and soft tissue disease, gastrointestinal and skeletal infections) representing a significant morbidity, especially in HIV-infected or immunocompromised patients. The emergence of MDR-TB and NTM makes the discovery of new molecular scaffolds a priority to achieve effective control of both TB and NTM.^{1–4}

* Corresponding author.

E-mail address: josef.jampilek@gmail.com (J. Jampilek).

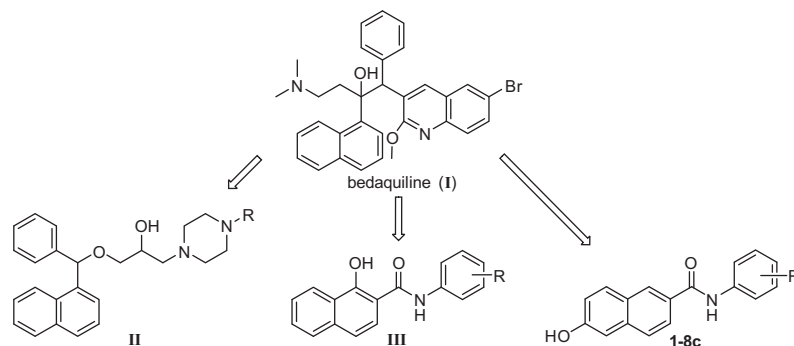


Figure 1. Structure of bedaquiline (I), its effective naphthalene analogues (II),²⁴ 1-hydroxynaphthalene-2-carboxanilides (III)¹⁵ and 6-hydroxynaphthalene-2-carboxanilides (1-8c) discussed herein.

The presence of an amide (–NHCO–) group with hydrophobic residue in its close vicinity is characteristic of a number of biologically active compounds. The amide is an important functional group that is able, due to its electron properties, to interact and bind with a number of enzymes/receptors and by means of these target sites affect the biological response. Therefore, the reason for widespread occurrence of amides in modern pharmaceuticals and biologically active compounds is obvious.^{5–11} The properties of the amide moiety can be easily modified by various substitutions. Thus the presence of an amide-like moiety is characteristic for various antibacterial, antimycobacterial or antiparasitic agents.^{12–18}

Synthesis and investigation of biological activity of 6-hydroxynaphthalene-2-carboxanilides is a follow-up contribution to understanding of the structure–activity relationships within a series of recently designed ring-substituted (aza)naphthalenes.^{15,19–23} All these compounds were designed to bear structural features of bedaquiline (I) and its naphthalene analogues (II), see Figure 1, which are potent mycobacterial ATP synthase inhibitors. ATP synthase is a ubiquitous key enzyme in respiratory energy metabolism that drives the synthesis of ADP from ADP and phosphate, which is a process that is essential to all cells.²⁴ Recently it was confirmed that ring-substituted naphthalene-1-carboxanilides caused a decrease of mycobacterial cell metabolism.²³ In the light of these facts, primary in vitro antimycobacterial screening of a series of twenty-two 6-hydroxynaphthalene-2-carboxanilides was performed. The structure–activity relationships of all the compounds are discussed.

2. Results and discussion

2.1. Chemistry and physicochemical properties

All studied compounds 1-8c were prepared according to Scheme 1 by modified microwave-assisted synthesis;^{21–23} thus synthesis of the target compounds was carried out in only one step with excellent yields (73–91%). At first the carboxyl group was activated with phosphorus trichloride. The final amide was immediately formed by aminolysis of the acyl chloride with ring-substituted

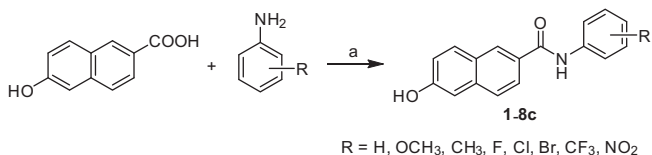
aniline in dry chlorobenzene. All the crude target compounds were recrystallized from ethanol.

Within structure–activity relationship investigations various parameters describing physicochemical properties are used. Lipophilicity is a property that has a major effect on solubility, absorption, distribution and biotransformation as well as pharmacological activity, because drugs cross biological membranes through passive transport, which strongly depends on their lipophilicity. Lipophilicity of the studied compounds was determined by RP-HPLC as capacity factor logarithm ($\log k$). The results of ring-substituted 6-hydroxynaphthalene-2-carboxanilides 1-8c are listed in Table 1. The highest experimental lipophilicity was found for 6-hydroxy-*N*-(4-trifluoromethylphenyl)naphthalene-2-carboxamide (7c), while 6-hydroxy-*N*-(4-methoxyphenyl)naphthalene-2-carboxamide (2c) showed the lowest $\log k$ value. Within the individual series the lipophilicity values increase for methyl, halogens and trifluoromethyl substituents as follows: *ortho* < *meta* < *para*; for methoxy substituent as follows: *para* < *meta* < *ortho*, and for NO₂ as follows: *ortho* ≈ *meta* > *para*. The presence of phenolic and carbonyl moieties can apparently cause intermolecular interactions.²⁵

The presence of different substituents in the anilide part of the discussed compounds results in a wide range of electronic properties. Electronic parameters (expressed as Hammett's σ parameters) of compounds 1-8c were predicted using ACD/Percepta ver. 2012 (Advanced Chemistry Development, Inc., Toronto, ON, Canada, 2012), see Table 1; they ranged from –0.28/–0.27 (compound 2a,c 2-OCH₃, 4-OCH₃) to 0.77/0.78 (compound 8a,c 2-NO₂, 4-NO₂).

2.2. In vitro antimycobacterial evaluation

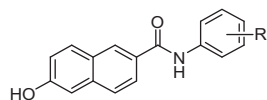
The evaluation of the in vitro antimycobacterial activity of the compounds was performed against *Mycobacterium tuberculosis* H37Ra ATCC 25177 (MT) and clinical isolates of *M. avium* complex CIT19/06 (MAC) and *M. avium* subsp. *paratuberculosis* CIT03 (MAP), see Table 1. To lower risk and make manipulation in the laboratory easier, surrogate model pathogens for *M. tuberculosis* can be used in laboratory studies. Avirulent *M. tuberculosis* strain H37Ra is very closely related to and has similar pathology to human-infecting *M. tuberculosis* strains, making it a good model for study especially because of the lower risk for laboratory workers.²⁶ Because of *M. tuberculosis*, the pathogenic role of NTM in humans was overshadowed for a long time. *Mycobacterium avium* complex includes ubiquitous atypical mycobacteria, found in the environment, that can easily infect immunosuppressed patients and cause disseminated disease, producing fever, sweats, weight loss and anaemia.²⁷ *M. avium* subsp. *paratuberculosis* is suspected to be a causative agent in gastrointestinal diseases; it is resistant to standard antimycobacterial therapy, but may be susceptible to some



Scheme 1. Synthesis of ring-substituted 6-hydroxynaphthalene-2-carboxanilides 1-8c: (a) PCl₃, chlorobenzene, microwave irradiation (MW).

Table 1

Structure of discussed ring-substituted 6-hydroxynaphthalene-2-carboxanilides **1–8c**, experimentally determined values of lipophilicity $\log k$, predicted values of electronic Hammett's σ parameters of R substituents, in vitro antimycobacterial activity (MIC) of compounds in comparison with isoniazid (INH) and rifampicin (RIF) and in vitro cytotoxicity assay (IC_{50}) of selected compounds



Compd	R	Logk	σ^a	MIC (μ M)			IC ₅₀ (μ M)
				MT	MAC	MAP	
1	H	0.6612	0	30	57	30	>30
2a	2-OCH ₃	0.6039	-0.28	27	51	27	>30
2b	3-OCH ₃	0.4463	0.12	27	102	27	>30
2c	4-OCH ₃	0.3313	-0.27	27	852	27	>30
3a	2-CH ₃	0.3690	-0.17	29	29	29	>30
3b	3-CH ₃	0.6086	-0.07	29	54	29	>30
3c	4-CH ₃	0.6227	-0.17	29	451	29	>30
4a	2-F	0.4921	0.06	107	107	53	—
4b	3-F	0.5766	0.34	28	53	53	—
4c	4-F	0.6726	0.06	28	213	53	—
5a	2-Cl	0.6777	0.22	27	50	840	>30
5b	3-Cl	0.7684	0.37	27	101	840	—
5c	4-Cl	0.7947	0.23	27	202	50	>30
6a	2-Br	0.7486	0.22	175	88	23	>30
6b	3-Br	0.8767	0.39	23	175	23	>30
6c	4-Br	0.8884	0.23	23	1461	731	—
7a	2-CF ₃	0.5623	0.51	91	181	377	—
7b	3-CF ₃	0.9558	0.43	24	91	24	>30
7c	4-CF ₃	1.0133	0.51	24	91	91	>30
8a	2-NO ₂	0.8553	0.77	97	195	26	>30
8b	3-NO ₂	0.8533	0.71	26	97	26	>30
8c	4-NO ₂	0.5911	0.78	26	49	97	—
INH	—	—	—	58	3646	1823	—
RIF	—	—	—	10	10	109	—

^a Calculated using ACD/Percepta ver. 2012 (Advanced Chemistry Development, Inc., Toronto, ON, Canada, 2012); MT = *M. tuberculosis* H37Ra ATCC 25177, MAC = *M. avium* complex CIT19/06 (clinical isolate) and MAP = *M. avium* subsp. *paratuberculosis* CIT03 (clinical isolate).

standard antibiotics. However, the resistance to these antibiotics develops quickly.²⁸ The potency of the compounds was expressed as the minimum inhibitory concentration (MIC) that is defined for mycobacteria as 90% or greater (IC_{90}) reduction of growth in comparison with the control. The MIC/ IC_{90} value is routinely and widely used in bacterial assays and is a standard detection limit according to the Clinical and Laboratory Standards Institute (CLSI).

Most compounds demonstrated good potency against *M. tuberculosis*. In most cases, *ortho*-substituted derivatives were less effective than *meta*- and *para*-derivatives. *N*-(3-Bromophenyl)-, *N*-(4-bromophenyl)-6-hydroxynaphthalene-2-carboxamides (**6b,c**)

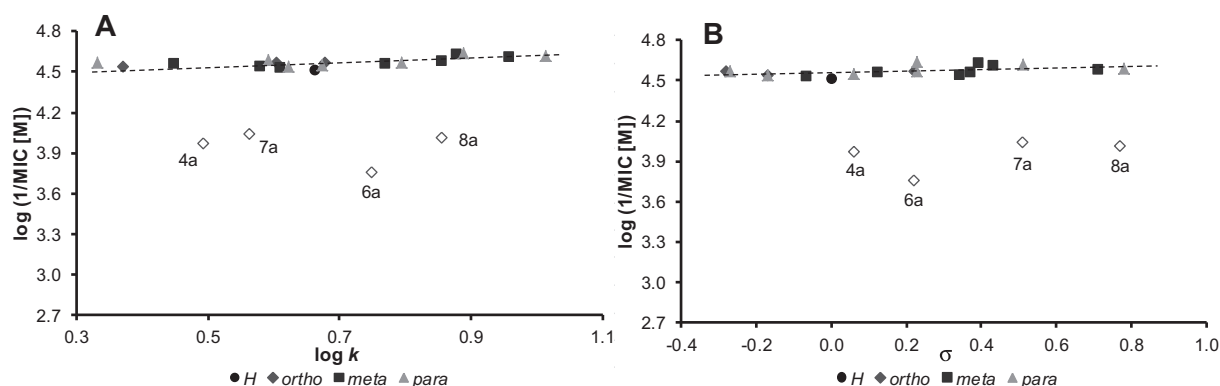


Figure 2. Dependence of antitubercular activity against *M. tuberculosis* expressed as $\log(1/MIC [M])$ of tested compounds on experimentally determined lipophilicity expressed as $\log k$ (A) and on Hammett's σ constants of R substituent (B). (Inactive compounds are marked by empty symbols.)

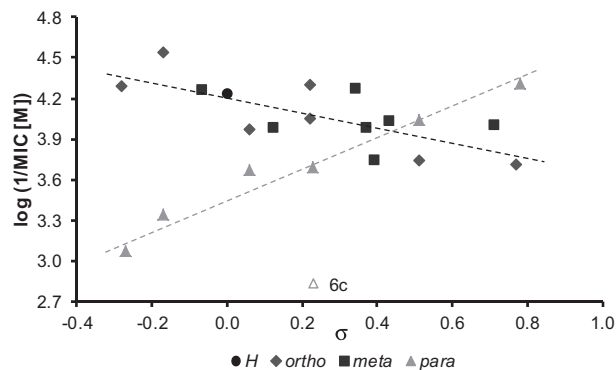


Figure 3. Dependence of antimycobacterial activity against *M. avium* complex expressed as $\log(1/MIC [M])$ of tested compounds on Hammett's σ constants of R substituent. (Eliminated compound **6c** is marked by empty symbol.)

and 6-hydroxy-*N*-(3-(trifluoromethyl)phenyl)-, 6-hydroxy-*N*-(4-(trifluoromethyl)-phenyl)naphthalene-2-carboxamides (**7b,c**) showed the highest activity (2-fold higher than that of isoniazid). The antitubercular activity of the compounds against *M. tuberculosis* expressed as $\log(1/MIC [M])$, the dependence on lipophilicity expressed as $\log k$ and the electronic properties expressed as Hammett's σ constants are illustrated in Figure 2A and B. When really inactive *ortho*-substituted compounds **4a**, **6a**, **7a** and **8a** ($R = 2-F$, $2-Br$, $2-CF_3$ and $2-NO_2$) are eliminated (marked by empty symbols), the activity of especially *meta*- and *para*-derivatives remains practically constant independently on lipophilicity or on electronic properties.

6-Hydroxy-*N*-(2-methylphenyl)naphthalene-2-carboxamide (**3a**) demonstrated the highest potency against *M. avium* complex ($MIC = 29 \mu M$). Generally it can be stated that *ortho*- and *meta*-substituted compounds showed higher potency against *M. avium* complex than *para* derivatives. The lowest measured effect was found for compound **6c** (4-Br), thus this compound was excluded from SAR study. Figure 3 shows the dependence of antimycobacterial activities against *M. avium* complex expressed as $\log(1/MIC [M])$ on electronic properties expressed as Hammett's σ constants. From the dependences illustrated in this figure it can be concluded that for *ortho*- and *meta*-substituted compounds the activity decreases with increasing electron-withdrawing properties of substituents (correlation coefficient $r_{o+m} = -0.7242$), while for *para*-substituted compounds the activity increases with increasing electron-withdrawing properties of substituents (correlation coefficient $r_p = 0.9832$). On the other hand it seems that lipophilicity plays only a secondary role. For *para*-substituted compounds the activity increases linearly with lipophilicity increase in the

following order: 4-OCH₃ (**2c**) < 4-CH₃ (**3c**) < 4-F (**4c**) < 4-Cl (**5c**) < 4-CF₃ (**7c**) with correlation coefficient $r = 0.9692$. Within *ortho*- and *meta*-substituted derivatives the activity decreases with increasing lipophilicity, nevertheless the activity of these compounds is primarily determined by electronic properties of substituents.

Most of compounds are more effective than rifampicin against *M. avium* subsp. *paratuberculosis*; twelve compounds expressed 3–4.5-fold higher activity than rifampicin, see Table 1. *N*-(2-Bromophenyl)-, *N*-(3-bromophenyl)-6-hydroxynaphthalene-2-carboxamide (**6a,b**) and 6-hydroxy-*N*-[3-(trifluoromethyl)phenyl]naphthalene-2-carboxamide (**7b**) showed the highest potency, followed by nitro, methoxy and methyl substituted derivatives. The lowest measured effect was found again for compound **6c** (4-Br) and this compound was excluded from SAR study, similarly as in the case of the activity against *M. avium* complex. The dependence of the antimycobacterial activity against *M. avium* subsp. *paratuberculosis* on lipophilicity remains practically constant and for *ortho*- and *meta*-derivatives no significant dependence on electronic properties of individual substituents was observed. For *para*-substituted compounds, a linear activity decrease was observed with increasing electron-withdrawing properties of individual substituents in the whole range of σ from -0.27 to 0.78 (4-OCH₃ (**2c**) > 4-CH₃ (**3c**) > 4-F (**4c**) > 4-Cl (**5c**) > 4-CF₃ (**7c**) > 4-NO₂ (**8c**)) with correlation coefficient $r = 0.9652$.

The antimycobacterial activity of the tested compounds can be affected by differences in permeability of the cell walls of *M. tuberculosis* and *M. avium*, and there are also some differences in the pathways of mycolic acid biosynthesis of these two species, because both species can synthesize α -mycolic and ketomycolic acids, but methoxymycolic acids are synthesized only by *M. tuberculosis*, and wax esters are synthesized only by *M. avium*.²⁹ In general, it can be stated that from the tested compounds *meta*- and *para*-substituted derivatives influenced *M. tuberculosis* more effectively than *ortho*-substituted derivatives. On the other hand, *ortho*- and *meta*-substituted derivatives expressed higher antimycobacterial activity against both NTM strains than *para*-substituted compounds. Due to the proximity of the *ortho*-substituent on the aniline ring to the carboxamide group, the twist of the aniline ring plain towards the carboxamide group, that is, towards the whole naphthalene core, occurs.³⁰ The described process results in the violation of the molecule planarity, implying subsequent conjugation of the π -bonds of the phenyl ring through the NH fragment to the carbonyl group.³¹ Consequently, the different electronic density (charge) at the carbonyl moiety appears, which can influence the potential of binding of the carboxamide group to possible binding sites in a mycobacterial cell. In the case of *meta*- and *para*-derivatives, the described secondary steric effect did not manifest. *para*-Substituted derivatives should have practically a linear/planar structure as was, for example, described for a similar type of molecule, where the X-ray analysis displayed a planar structure.^{19,32}

When these compounds are compared with other recently prepared antimycobacterially active anilides, it can be stated that especially *meta*- or *para*-positions of the anilide ring substituted by electron-withdrawing moieties are favourable (halogen, CF₃),^{13–16,33–36} and in the case of salicylanilide (4-arylcarbamoyl)benzoates also 4-Me can be an advantageous substituent in addition to the CF₃ moiety.³⁶

Additionally, a standard MTT assay was performed on the selected most effective compounds, the MICs of which were previously determined through alamarBlue assays, see Table 1. The MTT assay is a well-characterized method of assessing cell growth through measurement of respiration. For the purpose of this assay, a measured viability of *M. tuberculosis* H37Ra of less than 70%, as determined by MTT, after exposure to the MIC of each test compound (as determined by alamarBlue) was considered a

positive result. As such, a low level of cell viability may suggest inhibition of cell growth through respiratory inhibition.³⁷ All the selected compounds, i.e. 3-methoxy (**2b**, 62.2%), 4-methoxy (**2c**, 69.0%), 2-chloro (**5a**, 38.0%), 3-chloro (**5b**, 46.5%), 4-chloro (**5c**, 43.8%), 3-bromo (**6b**, 41.2%) and 3-trifluoromethyl (**7b**, 42.9%) derivatives showed less than 70% viability of *M. tuberculosis* H37Ra at the lowest tested concentration (8 μ g/mL, i.e., ca. 25 μ M).

Janin discusses a similar type of carboxamides in his review and suggests the hypothesis that all these compounds can interfere with the mycobacterial proton pump F₀F₁H⁺ATPase or inhibit biosynthesis of amino acids.³⁸ As mentioned above, bedaquiline (**I**) and its naphthalene analogues (**II**) inhibit the respiratory chain of mycobacteria.^{4,24,39} Based on the structure analogy, the discussed ring-substituted 6-hydroxynaphthalene-2-carboxanilides can be considered as simplified derivatives of bedaquiline-like compounds, see Figure 1. Since the change in colour of alamarBlue is caused by a decrease of mycobacterial cell metabolism, it is possible that also these compounds bind to the mycobacterial respiratory chain components. Also it may be hypothesized that differences between *M. tuberculosis* and the two clinical isolates of *M. avium* strains could be connected with more/less preferable spatial twist and the electron density of the molecule for binding to the respiratory chain components of individual mycobacterial strains. However, another possible site of action of the studied compounds in the mycobacteria cannot be excluded, for example, for structurally similar salicylanilides, inhibition of isocitrate lyase and methionine aminopeptidase⁴⁰ and destruction of the cellular proton gradient due to their function as proton shuttles, which results in cell death⁴¹, were reported.

2.3. In vitro cytotoxicity assay

The preliminary in vitro screening of the cytotoxicity of the most effective antimycobacterial compounds was performed using the human monocytic leukemia THP-1 cell line. The cytotoxicity was evaluated as the IC₅₀ value (compound concentration causing 50% inhibition of cell population proliferation), see Table 1. A compound is considered as cytotoxic when it demonstrates a toxic effect on cells at the concentration up to 10 μ M,⁴² and the highest tested concentration that was used for the toxicity assay was three times this value. Treatment with 30 μ M of the discussed compounds did not lead to significant lethal effect on THP-1 cells. Based on these observations it can be concluded that the discussed amides can be considered as non-toxic agents for subsequent design of novel potential antimycobacterial agents.

3. Conclusions

A series of twenty-two ring-substituted 6-hydroxynaphthalene-2-carboxanilides was prepared by means of microwave synthesis and subsequently characterized. All the compounds were tested for their in vitro antimycobacterial activity against *M. tuberculosis* and clinical isolates of *M. avium* complex and *M. avium* subsp. *paratuberculosis*. 6-Hydroxy-*N*-(3-trifluoromethylphenyl)naphthalene-2-carboxamide (**7b**), *N*-(2-bromophenyl)-6-hydroxynaphthalene-2-carboxamide (**6a**) and *N*-(3-bromophenyl)-6-hydroxynaphthalene-2-carboxamide (**6b**) demonstrated 4.5-fold higher activity than rifampicin against *M. avium* subsp. *paratuberculosis*. 3-Bromo-, 4-bromo-, 3-(trifluoromethyl)phenyl and 4-(trifluoromethyl)phenyl derivatives **6b,c** and **7b,c** had MICs of 23 or 24 μ M against *M. tuberculosis*, and 2-methylphenyl derivative **3a** expressed the highest potency against *M. avium* complex. Compounds substituted in C₍₃₎ and C₍₄₎ preferentially inhibited growth of *M. tuberculosis* contrary to C₍₂₎ and C₍₃₎ substituted ones that showed potency against both clinical isolates of *M. avium*

complex and *M. avium* subsp. *paratuberculosis*. The performed MTT assay of the selected most efficient compounds shows that they cause a decrease of mycobacterial cell metabolism; it seems that they could influence the mycobacterial respiratory chain. The most effective compounds were also tested for their *in vitro* cytotoxicity against the THP-1 cells, and within this preliminary screening they demonstrated insignificant toxicity. Based on the presented results it can be concluded that the discussed anilides can be considered as promising agents for subsequent design of novel antimycobacterial agents.

4. Experimental

4.1. Chemistry

All reagents were purchased from Aldrich (Sigma–Aldrich, St. Louis, MO, USA). TLC experiments were performed on alumina-backed silica gel 40 F254 plates (Merck, Darmstadt, Germany). The plates were illuminated under UV (254 nm) and evaluated in iodine vapour. The melting points were determined on Kofler hot-plate apparatus HMK (Franz Kustner Nacht KG, Dresden, Germany) and are uncorrected. Infrared (IR) spectra were recorded on a Smart MIRacle™ ATR ZnSe for Nicolet™ Impact 410 FT-IR spectrometer (Thermo Electron Corporation, West Palm Beach, FL, USA). The spectra were obtained by accumulation of 256 scans with 2 cm⁻¹ resolution in the region of 4000–600 cm⁻¹. All ¹H and ¹³C NMR spectra were recorded on an Agilent VNMR5 600 MHz system (Agilent Technologies, Santa Clara, CA, USA) equipped with a triple resonance HCN probe at 25 °C in DMSO-*d*₆. ¹H and ¹³C chemical shifts and ¹³C–¹⁹F coupling constants were determined from the standard ¹H and ¹³C spectra with digital resolution 0.3 Hz or better. Chemical shifts (δ) are reported in ppm. When necessary, additional experiments were done: ¹³C-APT (Attached Proton Test) for discrimination between CH and quaternary carbons; DQF COSY, HSQC and HMBC for through-bond ¹H–¹H and one- and multiple-bond ¹H–¹³C correlations. Mass spectra were measured using a LTQ Orbitrap Hybrid Mass Spectrometer (Thermo Electron Corporation) with direct injection into an APCI source (400 °C) in the negative mode.

4.1.1. General procedure for synthesis of *N*-(substituted phenyl)-6-hydroxynaphthalene-2-carboxamides 1–8c

6-Hydroxynaphthalene-2-carboxylic acid (1.0 g, 5.3 mM) was suspended in dry chlorobenzene (30 mL) at ambient temperature and phosphorus trichloride (0.23 mL, 2.7 mM, 0.5 equiv), and the corresponding substituted aniline (5.3 mM, 1 equiv) was added dropwise. The reaction mixture was transferred to the microwave reactor, where the synthesis was performed (1st phase: 10 min, 100 °C, 100 W; 2nd phase: 15 min, 120 °C, 500 W; 3rd phase: 20 min, 130 °C, 500 W). Then the mixture was cooled to 50 °C, and then the solvent was removed to dryness under reduced pressure. The residue was washed with hydrochloric acid and water. The crude product was recrystallized from EtOH. Studied compounds 1–8c are presented in Table 1.

4.1.1.1. 6-Hydroxy-*N*-phenylnaphthalene-2-carboxamide (1). Yield 73%; mp 165 °C; IR (cm⁻¹): 3376, 3299, 1625, 1550, 1490, 1440, 1394, 1344, 1220, 1117, 1060, 965, 915, 867, 816, 794, 770, 684; ¹H NMR (DMSO-*d*₆), δ : 7.14 (m, 3H), 7.20 (m, 1H), 7.23 (d, 1H, *J* = 2.2 Hz), 7.75 (m, 2H), 7.89 (m, 1H), 8.03 (m, 2H), 8.25 (s, 1H), 9.96 (s, 1H), 10.09 (s, 1H); ¹³C NMR (DMSO-*d*₆), δ : 110.77, 118.22, 120.66, 124.55, 124.62, 127.12, 127.95, 129.63, 130.27, 131.14, 132.21, 134.08, 138.33, 154.86, 166.22; HR-MS: for C₁₇H₁₂NO₂ [M–H]⁻ calculated 262.0874 *m/z*, found 262.0877 *m/z*.

4.1.1.2. 6-Hydroxy-*N*-(2-methoxyphenyl)naphthalene-2-carboxamide (2a). Yield 91%; mp 170–173 °C; IR (cm⁻¹): 3376, 3278, 1640, 1601, 1531, 1488, 1460, 1425, 1392, 1337, 1288, 1252, 1199, 1118, 1049, 1021, 876, 832, 744; ¹H NMR (DMSO-*d*₆), δ : 3.86 (s, 3H), 6.99 (td, 1H, *J* = 7.9, 1.2 Hz), 7.10 (dd, 1H, *J* = 7.9, 1.2 Hz), 7.18 (td, 1H, *J* = 7.9, 1.3 Hz), 7.19 (dd, 1H, *J* = 8.7, 2.4 Hz), 7.21 (d, 1H, *J* = 2.4 Hz), 7.80 (d, 1H, *J* = 8.6 Hz), 7.86 (dd, 1H, *J* = 7.9, 1.3 Hz), 7.92 (dd, 1H, *J* = 8.6, 1.5 Hz), 7.94 (d, 1H, *J* = 8.7 Hz), 8.48 (d, 1H, *J* = 1.5 Hz), 9.44 (s, 1H), 10.09 (br s, 1H); ¹³C NMR (DMSO-*d*₆), δ : 55.75, 108.66, 111.34, 119.52, 120.24, 124.02, 124.43, 125.45, 126.21, 126.67, 127.09, 127.90, 128.58, 130.84, 136.26, 151.27, 157.10, 165.10; HR-MS: for C₁₈H₁₄NO₃ [M–H]⁻ calculated 292.0979 *m/z*, found 292.0973 *m/z*.

4.1.1.3. 6-Hydroxy-*N*-(3-methoxyphenyl)naphthalene-2-carboxamide (2b). Yield 85%; mp 225–226 °C; IR (cm⁻¹): 3282, 1712, 1643, 1596, 1531, 1478, 1450, 1428, 1392, 1277, 1189, 1155, 1037, 864, 768, 744, 685; ¹H NMR (DMSO-*d*₆), δ : 3.77 (s, 3H), 6.68 (dd, 1H, *J* = 8.2, 2.2 Hz), 7.19 (dd, 1H, *J* = 8.7, 1.9 Hz), 7.21 (d, 1H, *J* = 1.9 Hz), 7.26 (t, 1H, *J* = 8.2 Hz), 7.43 (dd, 1H, *J* = 8.2, 2.2 Hz), 7.52 (t, 1H, *J* = 2.2 Hz), 7.79 (d, 1H, *J* = 8.6), 7.92 (dd, 1H, *J* = 8.6, 1.4 Hz), 7.93 (d, 1H, *J* = 8.7 Hz), 8.46 (d, 1H, *J* = 1.4 Hz), 10.09 (br s, 1H), 10.26 (s, 1H); ¹³C NMR (DMSO-*d*₆), δ : 55.01, 105.98, 108.68, 108.99, 112.51, 119.53, 124.69, 126.09, 126.57, 128.00, 128.98, 129.37, 130.76, 136.24, 140.60, 157.09, 159.44, 165.70; HR-MS: for C₁₈H₁₄NO₃ [M–H]⁻ calculated 292.0979 *m/z*, found 292.0975 *m/z*.

4.1.1.4. 6-Hydroxy-*N*-(4-methoxyphenyl)naphthalene-2-carboxamide (2c). Yield 77%; mp 182–183 °C; IR (cm⁻¹): 3315, 3255, 1651, 1626, 1597, 1511, 1479, 1394, 1354, 1147, 1030, 998, 911, 867, 816, 794; ¹H NMR (DMSO-*d*₆), δ : 3.75 (s, 3H), 6.939 (m, 2H), 7.18 (dd, 1H, *J* = 8.8, 2.3 Hz), 7.20 (d, 1H, *J* = 2.3 Hz), 7.72 (m, 2H), 7.79 (d, 1H, *J* = 8.6 Hz), 7.92 (d, 1H, *J* = 8.8 Hz), 7.93 (dd, 1H, *J* = 8.6, 1.3 Hz), 8.45 (d, 1H, *J* = 1.3 Hz), 10.10 (br s, 1H), 10.18 (s, 1H); ¹³C NMR (DMSO-*d*₆), δ : 55.19, 108.68, 113.75(2C), 119.50, 121.95(2C), 124.69, 126.04, 126.63, 127.84, 129.11, 130.72, 132.48, 136.15, 155.45, 157.01, 165.26; HR-MS: for C₁₈H₁₄NO₃ [M–H]⁻ calculated 292.0979 *m/z*, found 292.0974 *m/z*.

4.1.1.5. 6-Hydroxy-*N*-(2-methylphenyl)naphthalene-2-carboxamide (3a). Yield 75%; mp 118–121 °C; IR (cm⁻¹): 3213, 1699, 1652, 1616, 1575, 1505, 1436, 1394, 1271, 1184, 1052, 937, 860, 803; ¹H NMR (DMSO-*d*₆), δ : 2.27 (s, 3H), 7.17 (t, 1H, *J* = 7.7 Hz), 7.19 (dd, 1H, *J* = 8.8, 1.9 Hz), 7.21 (d, 1H, *J* = 1.9 Hz), 7.23 (t, 1H, *J* = 7.7 Hz), 7.28 (d, 1H, *J* = 7.7 Hz), 7.38 (d, 1H, *J* = 7.7 Hz), 7.79 (d, 1H, *J* = 8.6 Hz), 7.92 (d, 1H, *J* = 8.8 Hz), 7.96 (dd, 1H, *J* = 8.6, 1.2 Hz), 8.50 (d, 1H, *J* = 1.2 Hz), 9.93 (s, 1H), 10.10 (br s, 1H); ¹³C NMR (DMSO-*d*₆), δ : 18.01, 108.68, 119.51, 124.70, 125.85, 126.00, 126.08, 126.58, 126.66, 128.05, 128.64, 130.31, 130.74, 133.70, 136.23, 136.68, 157.03, 166.47; HR-MS: for C₁₈H₁₄NO₂ [M–H]⁻ calculated 276.1030 *m/z*, found 276.1025 *m/z*.

4.1.1.6. 6-Hydroxy-*N*-(3-methylphenyl)naphthalene-2-carboxamide (3b). Yield 74%; mp 155–156 °C; IR (cm⁻¹): 3238, 2989, 2900, 1639, 1597, 1549, 1505, 1423, 1316, 1250, 1211, 1155, 1066, 960, 909, 864, 812, 779, 716, 690; ¹H NMR (DMSO-*d*₆), δ : 2.32 (s, 3H), 6.92 (d, 1H, *J* = 7.7 Hz), 7.18 (dd, 1H, *J* = 8.8, 2.1 Hz), 7.20 (d, 1H, *J* = 2.1 Hz), 7.24 (t, 1H, *J* = 7.7 Hz), 7.62 (d, 1H, *J* = 7.7 Hz), 7.66 (s, 1H), 7.79 (d, 1H, *J* = 8.6 Hz), 7.92 (m, 2H), 8.46 (s, 1H), 10.08 (br s, 1H), 10.20 (s, 1H); ¹³C NMR (DMSO-*d*₆), δ : 21.24, 108.66, 117.49, 119.50, 120.85, 124.17, 124.70, 126.05, 126.57, 127.94, 128.42, 129.03, 130.72, 136.19, 137.70, 139.30, 157.04, 165.58; HR-MS: for C₁₈H₁₄NO₂ [M–H]⁻ calculated 276.1030 *m/z*, found 276.1025 *m/z*.

4.1.1.7. 6-Hydroxy-N-(4-methylphenyl)naphthalene-2-carboxamide (3c). Yield 78%; mp 195–198 °C; IR (cm⁻¹): 3235, 2989, 2900, 1634, 1599, 1538, 1511, 1476, 1436, 1394, 1329, 1272, 1234, 1201, 957, 911, 864, 818, 764; ¹H NMR (DMSO-*d*₆), δ: 2.284 (s, 3H), 7.162 (m, 2H), 7.18 (dd, 1H, *J* = 8.8, 2.2 Hz), 7.20 (d, 1H, *J* = 2.2 Hz), 7.70 (m, 2H), 7.79 (d, 1H, *J* = 8.6 Hz), 7.92 (m, 2H), 8.45 (s, 1H), 10.08 (br s, 1H), 10.21 (s, 1H); ¹³C NMR (DMSO-*d*₆), δ: 20.51, 108.66, 119.49, 120.34(2C), 124.70, 126.04, 126.59, 127.90, 128.99(2C), 129.08, 130.72, 132.40, 136.17, 136.86, 157.02, 165.46; HR-MS: for C₁₈H₁₄NO₂ [M–H]⁻ calculated 276.1030 *m/z*, found 276.1027 *m/z*.

4.1.1.8. N-(2-Fluorophenyl)-6-hydroxynaphthalene-2-carboxamide (4a). Yield 81%; mp 161 °C; IR (cm⁻¹): 3370, 3177, 1661, 1615, 1595, 1538, 1454, 1426, 1387, 1327, 1266, 1187, 1130, 1088, 1035, 914, 850, 814, 769; ¹H NMR (DMSO-*d*₆), δ: 7.19 (dd, 1H, *J* = 8.7, 2.2 Hz), 7.21 (d, 1H, *J* = 2.2 Hz), 7.23 (td, 1H, *J* = 7.5, 1.3 Hz), 7.27 (m, 1H), 7.30 (m, 1H), 7.65 (td, 1H, *J* = 7.5, 1.3 Hz), 7.80 (d, 1H, *J* = 8.7), 7.93 (d, 1H, *J* = 8.7), 7.94 (dd, 1H, *J* = 8.7, 1.5 Hz), 8.50 (d, 1H, *J* = 1.5 Hz), 10.10 (s, 1H), 10.14 (s, 1H); ¹³C NMR (DMSO-*d*₆), δ: 108.68, 115.80 (d, *J* = 19.9 Hz), 119.55, 124.27 (d, *J* = 3.5 Hz), 124.65, 126.00 (d, *J* = 12.3 Hz), 126.13, 126.59, 126.71 (d, *J* = 7.5 Hz), 127.07 (d, *J* = 1.8 Hz), 127.99, 128.35, 130.82, 136.36, 155.77 (d, *J* = 246.8 Hz), 157.17, 166.55; HR-MS: for C₁₇H₁₁NO₂F [M–H]⁻ calculated 280.0779 *m/z*, found 280.0776 *m/z*.

4.1.1.9. N-(3-Fluorophenyl)-6-hydroxynaphthalene-2-carboxamide (4b). Yield 76%; mp 230–232 °C; IR (cm⁻¹): 3362, 3180, 1661, 1617, 1598, 1547, 1491, 1415, 1392, 1324, 1255, 1205, 1168, 1140, 1072, 961, 925, 847, 779, 754, 676; ¹H NMR (DMSO-*d*₆), δ: 6.93 (td, 1H, *J* = 8.5, 2.4 Hz), 7.19 (dd, 1H, *J* = 8.7, 2.3 Hz), 7.21 (d, 1H, *J* = 2.3 Hz), 7.40 (m, 1H), 7.61 (ddd, 1H, *J* = 8.3, 1.8, 0.8 Hz), 7.81 (m, 2H), 7.92 (dd, 1H, *J* = 8.6, 1.6 Hz), 7.94 (d, 1H, *J* = 8.7 Hz), 8.47 (d, 1H, *J* = 1.6 Hz), 10.11 (s, 1H), 10.47 (s, 1H); ¹³C NMR (DMSO-*d*₆), δ: 106.89 (d, *J* = 26.2 Hz), 108.70, 109.89 (d, *J* = 21.1 Hz), 115.91 (d, *J* = 2.9 Hz), 119.60, 124.64, 126.17, 126.54, 128.17, 128.63, 130.21 (d, *J* = 9.7 Hz), 130.81, 136.35, 141.20 (d, *J* = 11.0), 157.20, 162.10 (d, *J* = 240.7), 165.95; HR-MS: for C₁₇H₁₁NO₂F [M–H]⁻ calculated 280.0779 *m/z*, found 280.0776 *m/z*.

4.1.1.10. N-(4-Fluorophenyl)-6-hydroxynaphthalene-2-carboxamide (4c). Yield 74%; mp 222–225 °C; IR (cm⁻¹): 3405, 3338, 1652, 1623, 1603, 1575, 1511, 1479, 1393, 1348, 1283, 1182, 916, 862, 838; ¹H NMR (DMSO-*d*₆), δ: 7.18 (dd, 1H, *J* = 8.8, 2.5 Hz), 7.20 (d, 1H, *J* = 2.5 Hz), 7.20 (m, 2H), 7.80 (d, 1H, *J* = 8.6 Hz), 7.83 (m, 2H), 7.92 (dd, 1H, *J* = 8.6, 1.5 Hz), 7.93 (d, 1H, *J* = 8.8 Hz), 8.46 (d, 1H, *J* = 1.5 Hz), 10.35 (s, 1H), 10.13 (br s, 1H); ¹³C NMR (DMSO-*d*₆), δ: 108.71, 115.19 (d, 2C, *J* = 22.1 Hz), 119.57, 122.13 (d, 2C, *J* = 7.8 Hz), 124.67, 126.13, 126.60, 128.03, 128.84, 130.77, 135.77 (d, *J* = 2.6 Hz), 136.27, 157.12, 158.22 (d, *J* = 240.1 Hz), 165.62; HR-MS: for C₁₇H₁₁NO₂F [M–H]⁻ calculated 280.0779 *m/z*, found 280.0775 *m/z*.

4.1.1.11. N-(2-Chlorophenyl)-6-hydroxynaphthalene-2-carboxamide (5a). Yield 88%; mp 158–159 °C; IR (cm⁻¹): 3271, 1666, 1622, 1603, 1593, 1520, 1481, 1436, 1398, 1311, 1269, 1236, 1205, 1159, 1033, 935, 885, 853, 804, 744, 687; ¹H NMR (DMSO-*d*₆), δ: 7.19 (dd, 1H, *J* = 8.7, 2.2 Hz), 7.21 (d, 1H, *J* = 2.2 Hz), 7.30 (td, 1H, *J* = 7.7, 1.0 Hz), 7.40 (td, 1H, *J* = 7.7, 0.8 Hz), 7.57 (dd, 1H, *J* = 7.7, 0.8 Hz), 7.65 (dd, 1H, *J* = 7.7, 1.0 Hz), 7.81 (d, 1H, 8.5 Hz), 7.93 (d, 1H, 8.7 Hz), 7.95 (dd, 1H, 8.5, 1.4 Hz), 8.51 (d, 1H, 1.4 Hz), 10.07 (s, 1H), 10.12 (br s, 1H); ¹³C NMR (DMSO-*d*₆), δ: 108.70, 119.58, 124.57, 126.19, 126.62, 127.27, 127.46, 128.02, 128.27, 128.33, 129.37, 129.55, 130.83,

135.32, 136.38, 157.18, 165.52; HR-MS: for C₁₇H₁₁NO₂Cl [M–H]⁻ calculated 296.0484 *m/z*, found 296.0483 *m/z*.

4.1.1.12. N-(3-Chlorophenyl)-6-hydroxynaphthalene-2-carboxamide (5b). Yield 76%; mp 196 °C; IR (cm⁻¹): 3362, 3252, 1659, 1616, 1590, 1575, 1533, 1475, 1456, 1394, 1354, 1311, 1201, 1094, 996, 915, 860, 780, 674; ¹H NMR (DMSO-*d*₆), δ: 7.15 (dt, 1H, *J* = 8.2, 0.9 Hz), 7.20 (dd, 1H, *J* = 8.7, 2.0 Hz), 7.21 (d, 1H, *J* = 2.0 Hz), 7.39 (t, 1H, *J* = 8.2 Hz), 7.77 (dt, 1H, *J* = 8.2, 0.9 Hz), 7.80 (d, 1H, *J* = 8.6 Hz), 7.92 (dd, 1H, *J* = 8.6, 1.1 Hz), 7.93 (d, 1H, *J* = 8.7 Hz), 8.03 (t, 1H, *J* = 0.9 Hz), 8.48 (d, 1H, *J* = 1.1 Hz), 10.16 (br s, 1H), 10.48 (s, 1H); ¹³C NMR (DMSO-*d*₆), δ: 108.73, 118.59, 119.64, 119.67, 123.15, 124.66, 126.18, 126.54, 128.24, 128.53, 130.32, 130.82, 132.96, 136.38, 140.94, 157.27, 165.95; HR-MS: for C₁₇H₁₁NO₂Cl [M–H]⁻ calculated 296.0484 *m/z*, found 296.0479 *m/z*.

4.1.1.13. N-(4-Chlorophenyl)-6-hydroxynaphthalene-2-carboxamide (5c). Yield 89%; mp 170 °C; IR (cm⁻¹): 3252, 1657, 1637, 1596, 1533, 1489, 1397, 1320, 1275, 1197, 1146, 1092, 997, 912, 890, 826, 810, 723, 677; ¹H NMR (DMSO-*d*₆), δ: 7.20 (dd, 1H, *J* = 8.8 Hz, 2.0 Hz), 7.22 (d, 1H, *J* = 2.0 Hz), 7.41 (m, 2H), 7.80 (d, 1H, *J* = 8.7 Hz), 7.88 (m, 2H), 7.93 (d, 1H, *J* = 8.8 Hz), 7.93 (dd, 1H, *J* = 8.7, *J* = 2.0 Hz), 8.48 (d, 1H, *J* = 2.0 Hz), 10.01 (br s, 1H), 10.45 (s, 1H); ¹³C NMR (DMSO-*d*₆), δ: 108.75, 119.63, 121.84(2C), 124.71, 126.15, 126.59, 127.11, 128.19, 128.53(2C), 128.72, 130.80, 136.35, 138.44, 157.24, 165.83; HR-MS: for C₁₇H₁₁NO₂Cl [M–H]⁻ calculated 296.0484 *m/z*, found 296.0480 *m/z*.

4.1.1.14. N-(2-Bromophenyl)-6-hydroxynaphthalene-2-carboxamide (6a). Yield 82%; mp 185–186 °C; IR (cm⁻¹): 3424, 3288, 1658, 1621, 1604, 1575, 1511, 1479, 1463, 1397, 1348, 1304, 1264, 1202, 1022, 875, 858, 802, 754; ¹H NMR (DMSO-*d*₆), δ: 7.19 (dd, 1H, *J* = 8.9, 2.1 Hz), 7.21 (d, 1H, *J* = 2.1 Hz), 7.23 (td, 1H, *J* = 7.7, 1.1 Hz), 7.44 (td, 1H, *J* = 7.7, 0.9 Hz), 7.61 (dd, 1H, *J* = 7.7, 1.1 Hz), 7.73 (dd, 1H, *J* = 7.7, 0.9 Hz), 7.81 (d, 1H, *J* = 8.6 Hz), 7.93 (d, 1H, *J* = 8.9 Hz), 7.95 (dd, 1H, *J* = 8.6 Hz, 1.4 Hz), 8.51 (d, 1H, *J* = 1.4 Hz), 10.05 (s, 1H), 10.12 (br s, 1H); ¹³C NMR (DMSO-*d*₆), δ: 108.71, 119.60, 120.49, 124.56, 126.20, 126.63, 127.76, 128.09, 128.10, 128.24, 128.76, 130.83, 132.68, 136.39, 136.76, 157.18, 165.47; HR-MS: for C₁₇H₁₁NO₂Br [M–H]⁻ calculated 339.9979 *m/z*, found 339.9972 *m/z*.

4.1.1.15. N-(3-Bromophenyl)-6-hydroxynaphthalene-2-carboxamide (6b). Yield 86%; mp 218 °C; IR (cm⁻¹): 3252, 1639, 1593, 1536, 1504, 1472, 1444, 1420, 1316, 1270, 1204, 1157, 1071, 996, 912, 903, 865, 812, 780, 767, 715, 685; ¹H NMR (DMSO-*d*₆), δ: 7.191 (dd, 1H, *J* = 8.7, 2.2 Hz), 7.208 (d, 1H, *J* = 2.2 Hz), 7.287 (dt, 1H, *J* = 8.0, 1.8 Hz), 7.331 (t, 1H, *J* = 8.0 Hz), 7.807 (m, 2H), 7.918 (dd, 1H, *J* = 8.7, 1.4 Hz), 7.934 (d, 1H, *J* = 8.7 Hz), 8.155 (t, 1H, *J* = 1.8 Hz), 8.469 (d, 1H, *J* = 1.4 Hz), 10.114 (br s, 1H), 10.432 (s, 1H); ¹³C NMR (DMSO-*d*₆), δ: 108.70, 118.92, 119.61, 121.43, 122.48, 124.62, 126.03, 126.17, 126.53, 128.19, 128.53, 130.61, 130.81, 136.35, 141.04, 157.21, 165.89; HR-MS: for C₁₇H₁₁NO₂Br [M–H]⁻ calculated 339.9979 *m/z*, found 339.9974 *m/z*.

4.1.1.16. N-(4-Bromophenyl)-6-hydroxynaphthalene-2-carboxamide (6c). Yield 83%; mp 222 °C; IR (cm⁻¹): 3366, 3247, 1658, 1622, 1589, 1506, 1393, 1311, 1274, 1226, 1195, 1144, 1072, 994, 911, 890, 865, 822, 776; ¹H NMR (DMSO-*d*₆), δ: 7.19 (dd, 1H, *J* = 8.8, 2.2 Hz), 7.20 (d, 1H, *J* = 2.2 Hz), 7.55 (m, 2H), 7.80 (d, 1H, 8.7 Hz), 7.81 (m, 2H), 7.92 (dd, 1H, *J* = 8.7, 1.3 Hz), 7.93 (d, 1H, *J* = 8.8 Hz), 8.46 (d, 1H, 1.3 Hz), 10.09 (br s, 1H), 10.41 (s, 1H); ¹³C NMR (DMSO-*d*₆), δ: 108.69, 115.12, 119.57, 122.16(2C),

124.64, 126.13, 126.54, 128.12, 128.70, 130.78, 131.42(2C), 136.30, 138.81, 157.16, 165.77; HR-MS: for $C_{17}H_{11}NO_2Br$ $[M-H]^-$ calculated 339.9979 m/z , found 339.9977 m/z .

4.1.1.17. 6-Hydroxy-N-(2-trifluoromethylphenyl)naphthalene-2-carboxamide (7a). Yield 76%; mp 222 °C; IR (cm^{-1}): 3233, 1652, 1622, 1588, 1520, 1471, 1453, 1394, 1356, 1310, 1268, 1236, 1203, 1170, 1110, 904, 861, 766; 1H NMR (DMSO- d_6), δ : 7.19 (dd, 1H, $J = 8.6, 2.3$ Hz), 7.21 (d, 1H, $J = 2.3$ Hz), 7.54 (t, 1H, $J = 7.8$ Hz), 7.57 (d, 1H, $J = 7.8$ Hz), 7.75 (t, 1H, $J = 7.8$ Hz), 7.81 (m, 2H), 7.923 (m, 2H), 8.47 (d, 1H, $J = 1.7$ Hz), 10.12 (br s, 1H), 10.16 (1H, s); ^{13}C NMR (DMSO- d_6), δ : 108.73, 119.65, 123.76 (q, $J = 273.8$ Hz), 124.57, 126.24, 126.45–126.60 (m, 2C), 126.65, 127.36, 128.03, 128.24, 130.84, 131.32, 133.12, 136.10, 136.41, 157.20, 166.51; HR-MS: for $C_{18}H_{11}NO_2F_3$ $[M-H]^-$ calculated 330.0747 m/z , found 330.0742 m/z .

4.1.1.18. 6-Hydroxy-N-(3-trifluoromethylphenyl)naphthalene-2-carboxamide (7b). Yield 78%; mp 179 °C; IR (cm^{-1}): 3277, 1663, 1646, 1619, 1539, 1492, 1438, 1394, 1329, 1309, 1264, 1199, 1162, 1110, 1066, 858, 796, 693; 1H NMR (DMSO- d_6), δ : 7.20 (dd, 1H, $J = 8.6, 2.5$ Hz), 7.22 (d, 1H, $J = 2.5$ Hz), 7.45 (d, 1H, $J = 7.9$ Hz), 7.60 (t, 1H, $J = 7.9$ Hz), 7.82 (d, 1H, $J = 8.7$ Hz), 7.94 (d, 1H, $J = 8.8$ Hz), 7.94 (dd, 1H, $J = 8.7, 1.3$ Hz), 8.11 (d, 1H, $J = 7.9$ Hz), 8.30 (s, 1H), 8.50 (d, 1H, $J = 1.3$ Hz), 10.13 (br s, 1H), 10.60 (s, 1H); ^{13}C NMR (DMSO- d_6), δ : 108.75, 116.32 (q, $J = 4.0$ Hz), 119.67, 119.76 (q, $J = 3.3$ Hz), 124.24 (q, $J = 272.4$ Hz), 123.71, 124.65, 126.23, 126.56, 128.28, 128.45, 129.40 (q, $J = 31.7$ Hz), 129.87, 130.85, 136.4, 140.2, 157.29, 166.1; HR-MS: for $C_{18}H_{11}NO_2F_3$ $[M-H]^-$ calculated 330.0747 m/z , found 330.0743 m/z .

4.1.1.19. 6-Hydroxy-N-(4-trifluoromethylphenyl)naphthalene-2-carboxamide (7c). Yield 88%; mp 191 °C; IR (cm^{-1}): 3369, 1661, 1621, 1598, 1527, 1481, 1433, 1394, 1356, 1318, 1229, 1195, 1159, 1126, 1066, 1018, 913, 863, 835, 746; 1H NMR (DMSO- d_6), δ : 7.20 (dd, 1H, $J = 8.7, 2.1$ Hz), 7.21 (d, 1H, $J = 2.1$ Hz), 7.73 (m, 2H), 7.82 (d, 1H, $J = 8.6$ Hz), 7.94 (dd, 1H, $J = 8.6, 1.5$ Hz), 7.95 (d, 1H, $J = 8.7$ Hz), 8.06 (m, 2H), 8.50 (d, 1H, $J = 1.5$ Hz), 10.14 (br s, 1H), 10.63 (s, 1H); ^{13}C NMR (DMSO- d_6), δ : 108.74, 119.65, 120.06(2C), 123.44 (q, $J = 32.1$ Hz), 124.49 (q, 272.1 Hz), 124.70, 125.93 (q, $J = 3.9$ Hz), 126.22, 126.54, 128.37, 128.49, 130.87, 136.44, 143.08, 157.29, 166.19; HR-MS: for $C_{18}H_{11}NO_2F_3$ $[M-H]^-$ calculated 330.0747 m/z , found 330.0741 m/z .

4.1.1.20. 6-Hydroxy-N-(2-nitrophenyl)naphthalene-2-carboxamide (8a). Yield 83%; mp 183–185 °C; IR (cm^{-1}): 3357, 2989, 2900, 1668, 1622, 1603, 1585, 1549, 1495, 1450, 1429, 1394, 1336, 1257, 1219, 1193, 1163, 966, 886, 857, 784, 741; 1H NMR (DMSO- d_6), δ : 7.20 (dd, 1H, $J = 8.8, 2.2$ Hz), 7.22 (d, 1H, $J = 2.2$ Hz), 7.42 (t, 1H, $J = 7.8$ Hz), 7.76 (t, 1H, $J = 7.8$ Hz), 7.83 (d, 1H, $J = 8.7$ Hz), 7.85 (d, 1H, $J = 7.8$ Hz), 7.90 (dd, 1H, $J = 8.7, 1.3$ Hz), 7.96 (d, 1H, $J = 8.8$ Hz), 8.03 (d, 1H, $J = 7.8$ Hz), 8.48 (d, 1H, $J = 1.3$ Hz), 10.17 (br s, 1H), 10.83 (s, 1H); ^{13}C NMR (DMSO- d_6), δ : 108.75, 119.75, 124.34, 125.00, 125.30, 125.74, 126.39, 126.57, 127.56, 128.54, 130.94, 131.90, 134.04, 136.60, 142.70, 157.44, 165.49; HR-MS: for $C_{17}H_{11}N_2O_4$ $[M-H]^-$ calculated 307.0724 m/z , found 307.0720 m/z .

4.1.1.21. 6-Hydroxy-N-(3-nitrophenyl)naphthalene-2-carboxamide (8b). Yield 74%; mp 250–252 °C; IR (cm^{-1}): 3374, 3291, 1666, 1616, 1590, 1533, 1475, 1436, 1410, 1394, 1346, 1318, 1295, 1264, 1199, 1156, 908, 879, 856, 830, 803, 735; 1H NMR (DMSO- d_6), δ : 7.20 (dd, 1H, $J = 8.7, 2.1$ Hz), 7.22 (d, 1H, $J = 2.1$ Hz), 7.65 (t, 1H, $J = 8.2$ Hz), 7.82 (d, 1H, $J = 8.6$ Hz), 7.95 (d,

1H, $J = 8.7$ Hz), 7.95 (m, 2H), 8.24 (d, 1H, $J = 8.2$), 8.51 (s, 1H), 8.84 (s, 1H), 10.15 (br s, 1H), 10.74 (s, 1H); ^{13}C NMR (DMSO- d_6), δ : 108.76, 114.30, 117.93, 119.69, 124.62, 126.10, 126.26, 126.54, 128.22, 128.38, 130.04, 130.88, 136.50, 140.64, 147.95, 157.35, 166.17; HR-MS: for $C_{17}H_{11}N_2O_4$ $[M-H]^-$ calculated 307.0724 m/z , found 307.0719 m/z .

4.1.1.22. 6-Hydroxy-N-(4-nitrophenyl)naphthalene-2-carboxamide (8c). Yield 73%; mp 232–234 °C; IR (cm^{-1}): 3324, 3055, 2834, 1678, 1622, 1584, 1498, 1475, 1426, 1393, 1338, 1275, 1191, 1143, 948, 860, 803, 765, 739; 1H NMR (DMSO- d_6), δ : 7.20 (dd, 1H, $J = 8.7, 2.1$ Hz), 7.22 (d, 1H, $J = 2.1$ Hz), 7.82 (d, 1H, $J = 8.7$ Hz), 7.94 (d, 1H, $J = 8.7$ Hz), 7.95 (d, 1H, $J = 8.7$ Hz), 8.11 (m, 2H), 8.28 (m, 2H), 8.51 (s, 1H), 10.15 (br s, 1H), 10.86 (s, 1H); ^{13}C NMR (DMSO- d_6), δ : 108.76, 119.72, 119.77(2C), 124.69, 124.85(2C), 126.29, 126.49, 128.18, 128.62, 130.95, 136.57, 142.33, 145.79, 157.43, 166.40; HR-MS: for $C_{17}H_{11}N_2O_4$ $[M-H]^-$ calculated 307.0724 m/z , found 307.0719 m/z .

4.2. Lipophilicity determination by HPLC (capacity factor k' calculated $\log k'$)

A HPLC system Agilent 1200 equipped with DAD detector (Agilent, Santa Clara, CA, USA) was used. A chromatographic column Symmetry[®]C₁₈ 5 μm , 4.6×250 mm, Part No. WAT054275, (Waters Corp., Milford, MA, USA) was used. The HPLC separation process was monitored and evaluated by EZChrom Elite software ver. 3.3.2 (Agilent). Isocratic elution by a mixture of MeOH p.a. (60%) and H₂O-HPLC Mili-Q grade (40%) as a mobile phase was used. The total flow of the column was 1.0 mL/min, injection 20 μL , column temperature 40 °C and sample temperature 10 °C. The detection wavelength 210 nm was chosen. The KI methanolic solution was used for the dead time (t_D) determination. Retention times (t_R) were measured in minutes. The capacity factors k were calculated according to formula $k = (t_R - t_D)/t_D$, where t_R is the retention time of the solute, whereas t_D denotes the dead time obtained using an unretained analyte. $\log k$, calculated from the capacity factor k , is used as the lipophilicity index converted to $\log P$ scale. The $\log k$ values of the individual compounds are shown in Table 1.

4.3. In vitro antimycobacterial evaluation

Mycobacterium tuberculosis H37Ra ATCC 25177 and well characterized clinical isolate isolates of *M. avium* complex CIT19/06, and *M. avium* subsp. *paratuberculosis* CIT03 were grown in Middlebrook broth (MB), supplemented with Oleic-Albumin-Dextrose-Catalase supplement (OADC, Becton Dickinson, UK) and mycobactin J (2 $\mu g/mL$). Identification of these isolates was performed using biochemical and molecular protocols. At log phase growth, a culture sample (10 mL) was centrifuged at 15,000 rpm/20 min using a bench top centrifuge (Model CR 4-12, Jouan Inc., UK). Following removal of the supernatant, the pellet was washed in fresh Middlebrook 7H9GC broth and re-suspended in fresh supplemented MB (10 mL). The turbidity was adjusted to match McFarland standard No. 1 (3×10^8 cfu) with MB broth. A further 1:20 dilution of the culture was then performed in MB broth. The antimicrobial susceptibility of all three mycobacterial species was investigated in a 96-well plate format. In these experiments, sterile deionised water (300 μL) was added to all outer-perimeter wells of the plates to minimize evaporation of the medium in the test wells during incubation. Each evaluated compound (100 μL) was incubated with each of the mycobacterial species (100 μL). Dilutions of each compound were prepared in duplicate. For all synthesized compounds, final concentrations ranged from 1000 $\mu g/mL$ to 8 $\mu g/mL$. All compounds were prepared in DMSO

and subsequent dilutions were made in supplemented MB. The plates were sealed with parafilm and incubated at 37 °C, for 5 days in the case of *M. avium complex*, 7 days in the case of *M. tuberculosis* and 11 days in the case of *M. avium paratuberculosis*. Following incubation, a 10% addition of alamarBlue (AbD Serotec, Kidlington, UK) was mixed into each well and readings at 570 nm and 600 nm were taken, initially for background subtraction and subsequently after 24 h re-incubation. The background subtraction is necessary for strongly coloured compounds, where the colour may interfere with the interpretation of any colour change. For non-interfering compounds, a blue colour in the well was interpreted as an absence of growth and a pink colour was scored as growth. The minimum inhibitory concentration (MIC) was defined as the lowest concentration of the compound at which no visible bacterial growth was observed, that is, the MIC is the lowest concentration that prevented a visual colour change from blue to pink. The MIC value is routinely and widely used in bacterial assays and is a standard detection limit according to the Clinical and Laboratory Standards Institute (CLSI, www.clsi.org). Rifampicin and isoniazid (Sigma-Aldrich) were used as the standards as they are clinically used antimycobacterial drugs. The results are summarized in Table 1.

4.4. MTT assay

For the MTT assay, the outer wells of a 96-well plate were filled with 200 µL of sterile water, and the inner wells were filled with 100 µL of the tested compound at the concentration to be examined. Compounds were prepared as previously stated and diluted in Middlebrook media to achieve the desired concentration. *Mycobacterium tuberculosis* H37Ra ATCC 25177 was suspended in ODAC supplemented Middlebrook broth at a MacFarland standard of 1.0 and then diluted through a 1:20, using Middlebrook broth as a diluent. The diluted mycobacteria (100 µL) were added to each well containing the compound to be tested. A negative growth control was composed of 100 µL of DMSO and 100 µL of media, and the diluted mycobacteria in broth absent of inhibiting compounds were used as a positive growth control. All compounds and controls were prepared in triplicate. Plates were incubated at 37 °C for 7 days. After the incubation period, 10% well volume of MTT reagent was mixed into each well and incubated at 37 °C for 24 h. The reagent and media were then aspirated from the wells, to which 50 µL 99% isopropanol was then added, and plates were read at 570 nm. The absorbance readings from the cells, grown in the presence of the tested compounds, were compared with uninhibited cell growth (using DMSO as the blank) to determine the relative percent viability. The percent viability was determined through the MTT assay. The percent viability is calculated through comparison of a measured value against that of the uninhibited control: %viability = $OD_{570E}/OD_{570P} \times 100$, where OD_{570E} is the reading from the compound-exposed cells, while OD_{570P} is the reading from the uninhibited cells (positive control). Cytotoxic potential is determined by a percent viability of <70%.

4.5. In vitro cytotoxicity assay

Human monocytic leukemia THP-1 cells were used for in vitro toxicity assay. Cells were obtained from the European Collection of Cell Cultures (ECACC, Salisbury, UK) and routinely cultured in RPMI 1640 medium supplemented with 10% fetal bovine serum, 2% L-glutamine, 1% penicillin and streptomycin at 37 °C with 5% CO₂. Cells were passaged at approximately one week intervals. Cytotoxicity of the compounds was determined using a WST-1 assay kit (Roche Diagnostics, Mannheim, Germany) according to the manufacturer's instructions. The tested compounds were dissolved in DMSO and added in five increasing concentrations

(0.37, 1.1, 3.3, 10, and 30 µM) to the cell suspension in the culture RPMI 1640 medium. The maximum concentration of DMSO in the assays never exceeded 0.1%. Subsequently, the cells were incubated for 24 h at 37 °C with 5% CO₂. For WST-1 assays, cells were seeded into 96-well plates (5 × 10⁴ cells/well in 100 µL culture medium) in triplicate in serum-free RPMI 1640 medium and measurements were taken 24 h after the treatment with the compounds. The median inhibition concentration values, IC₅₀, were deduced through the production of a dose-response curve. All data were evaluated using GraphPad Prism 5.00 software (GraphPad Software, San Diego, CA, USA). The results are summarized in Table 1.

Acknowledgments

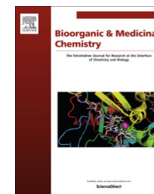
This study was supported by the IGA VFU Brno 304/2015/FaF, 322/2015/FaF, 37/2014/FaF, 108/2013/FaF, the Slovak Grant Agency VEGA 1/0972/12, by the Projects APVV-0061-11, CZ.1.07/2.3.00/30.0053 and by the Irish Department of Agriculture Fisheries and Food (FIRM): Refs 08RDCIT601 & 08RDCIT617.

References and notes

- World Health Organization *Global Strategy for Containment of Antimicrobial Resistance 2001, up-date 2013*; WHO Press: Geneva, Switzerland, 2013.
- World Health Organization *Global tuberculosis report 2014*; WHO Press: Geneva, Switzerland, 2014.
- Wagner, D.; Young, L. S. *Infection* **2004**, *32*, 257.
- Koul, A.; Arnoult, E.; Lounis, N.; Guillemont, J.; Andries, K. *Nature* **2011**, *469*, 483.
- Good, N. E. *Plant Physiol.* **1961**, *36*, 788.
- Roth, H. J.; Fenner, H. *Arzneistoffe*, 3rd ed.; Deutscher Apotheker Verlag: Stuttgart Germany, 2000.
- Kamat, S.; Buolamwini, J. K. *Med. Res. Rev.* **2006**, *26*, 569.
- Sinning, C.; Watzer, B.; De Petrocellis, L.; Di Marzo, V.; Imming, P. *ChemMedChem* **1956**, *2008*, 3.
- Pattabiraman, V. R.; Bode, J. W. *Nature* **2011**, *480*, 471.
- Jampilek, J.; Brychtova, K. *Med. Res. Rev.* **2012**, *32*, 907.
- Jampilek, J. *Curr. Med. Chem.* **2014**, *21*, 4347.
- Vinsova, J.; Cermakova, K.; Tomeckova, A.; Ceckova, M.; Jampilek, J.; Cermak, P.; Kunes, J.; Dolezal, M.; Staud, F. *Bioorg. Med. Chem.* **2006**, *14*, 5850.
- Dolezal, M.; Cmedlova, P.; Palek, L.; Vinsova, J.; Kunes, J.; Buchta, V.; Jampilek, J.; Kralova, K. *Eur. J. Med. Chem.* **2008**, *43*, 1105.
- Imramovsky, A.; Vinsova, J.; Monreal-Ferriz, J.; Dolezal, R.; Jampilek, J.; Kaustova, J.; Kunc, F. *Bioorg. Med. Chem.* **2009**, *17*, 3572.
- Gonec, T.; Kos, J.; Zadrzilova, I.; Pesko, M.; Keltosova, S.; Tengler, J.; Bobal, P.; Kollar, P.; Cizek, A.; Kralova, K.; Jampilek, J. *Bioorg. Med. Chem.* **2013**, *21*, 6531.
- Pauk, K.; Zadrzilova, I.; Imramovsky, A.; Vinsova, J.; Pokorna, M.; Masarikova, M.; Cizek, A.; Jampilek, J. *Bioorg. Med. Chem.* **2013**, *21*, 6574.
- Zumla, A.; Nahid, P.; Cole, S. T. *Nat. Rev. Drug Disc.* **2013**, *12*, 388.
- Zucca, M.; Scutera, S.; Savoia, D. *Curr. Med. Chem.* **2013**, *20*, 502.
- Musiol, R.; Jampilek, J.; Buchta, V.; Niedbala, H.; Podeszwa, B.; Palka, A.; Majerz-Maniecka, K.; Oleksyn, B.; Polanski, J. *Bioorg. Med. Chem.* **2006**, *14*, 3592.
- Cieslik, W.; Musiol, R.; Nycz, J.; Jampilek, J.; Vejsova, M.; Wolff, M.; Machura, B.; Polanski, J. *Bioorg. Med. Chem.* **2012**, *20*, 6960.
- Kos, J.; Zadrzilova, I.; Pesko, M.; Keltosova, S.; Tengler, J.; Gonec, T.; Bobal, P.; Kauerova, T.; Oravec, M.; Kollar, P.; Cizek, A.; Kralova, K.; Jampilek, J. *Molecules* **2013**, *18*, 7977.
- Gonec, T.; Kos, J.; Zadrzilova, I.; Pesko, M.; Govender, R.; Keltosova, S.; Chambel, B.; Pereira, D.; O'Mahony, J.; Kollar, P.; Coffey, A.; Cizek, A.; Kralova, K.; Jampilek, J. *Molecules* **2013**, *18*, 9397.
- Gonec, T.; Kos, J.; Nevin, E.; Govender, R.; Pesko, M.; Kushkevych, I.; Oravec, M.; Kollar, P.; O'Mahony, J.; Kralova, K.; Coffey, A.; Jampilek, J. *Molecules* **2014**, *19*, 10386.
- Bueno, R. V.; Braga, R. C.; Segretti, N. D.; Ferreir, E. I.; Trossini, G. H.; Andrade, C. H. *Curr. Pharm. Des.* **2014**, *20*, 4474.
- Karabulut, S.; Namli, H.; Kurtaran, R.; Yildirim, L. T.; Leszczynski, J. J. *Mol. Graph. Model.* **2014**, *48*, 1.
- Zheng, H.; Lu, L.; Wang, B.; Pu, S.; Zhang, X.; Zhu, G.; Shi, W.; Zhang, L.; Wang, H.; Wang, S.; Zhao, G.; Zhang, Y. *PLoS ONE* **2008**, *3*, e2375.
- Havlik, J. A.; Horsburgh, C. R.; Metchock, B.; Williams, P.; Fann, S. A.; Thompson, S. E. *J. Infect. Dis.* **1992**, *165*, 577.
- Rath, T.; Roderfeld, M.; Blocher, S.; Rhode, A.; Basler, T.; Akineden, O.; Abdulmawjood, A.; Halwe, J. M.; Goethe, R.; Bulte, M.; Roeb, E. *BMC Gastroenterology* **2011**, *11*, 34 (19 pages).
- Heifest, L. B. *Antituberculous drugs: Antimycobacterial activity in vitro*. In *Drug Susceptibility in the Chemotherapy of Mycobacterial Infections*; Heifest, L. B., Ed.; CRC Press, Boca Raton, FL: USA, 1991; pp 13–58.

30. Arjunan, V.; Santhanam, R.; Rani, T.; Rosi, H.; Mohan, S. *Spectrochim. Acta A Mol. Biomol. Spectrosc.* **2013**, *104*, 182.
31. Waisser, K.; Dolezal, R.; Cizmarik, J.; Malik, I.; Kaustova, J. *Folia Pharm. Univ. Carol.* **2007**, *35/36*, 45.
32. Bobal, P.; Sujan, J.; Otevrel, J.; Imramovsky, A.; Padelkova, Z.; Jampilek, J. *Molecules* **2012**, *17*, 1292.
33. Servusova, B.; Vobickova, J.; Paterova, P.; Kubicek, V.; Kunes, J.; Dolezal, M.; Zitko, J. *Bioorg. Med. Chem. Lett.* **2013**, *23*, 3589.
34. Zitko, J.; Servusova, B.; Paterova, P.; Mandikova, J.; Kubicek, V.; Kucera, R.; Hrabcova, V.; Kunes, J.; Soukup, O.; Dolezal, M. *Molecules* **2013**, *18*, 14807.
35. Kratky, M.; Vinsova, J.; Novotna, E.; Stolarikova, J. *Eur. J. Pharm. Sci.* **2014**, *53*, 1.
36. Kratky, M.; Bosze, S.; Baranyai, Z.; Szabo, I.; Stolarikova, J.; Paraskevopoulos, G.; Vinsova, J. *Bioorg. Med. Chem.* **2015**, *23*, 868.
37. Bueno, J. Antitubercular in vitro drug discovery: Tools for begin the search. In *Understanding Tuberculosis-New Approaches to Fighting against Drug Resistance*; Cardona, P. J., Ed.; InTech: Rijeka, Croatia, 2012; pp 147–168.
38. Janin, Y. L. *Bioorg. Med. Chem.* **2007**, *15*, 2479.
39. Koul, A.; Vranckx, L.; Dhar, N.; Gohlmann, H. W. H.; Ozdemir, E.; Neefs, J. M.; Schulz, M.; Lu, P.; Mortz, E.; McKinney, J. D.; Andries, K.; Bald, D. *Nat. Commun.* **2014**, *5*. <http://dx.doi.org/10.1038/ncomms4369>. Article No. 3369.
40. Kratky, M.; Vinsova, J.; Novotna, E.; Mandikova, J.; Wsol, V.; Trejtnar, F.; Ulmann, V.; Stolarikova, J.; Fernandes, S.; Bhat, S.; Liu, J. O. *Tuberculosis* **2012**, *92*, 434.
41. Lee, I. Y.; Gruber, T. D.; Samuels, A.; Yun, M.; Nam, B.; Kang, M.; Crowley, K.; Winterroth, B.; Boshoff, H. I.; Barry, C. E. *Bioorg. Med. Chem.* **2013**, *21*, 114.
42. Suffness, M.; Douros, J. J. *Nat. Prod.* **1982**, *45*, 1.

č.	citace	ISSN
3	<p>KOS, J, I ZADRAZILOVA, E NEVIN, M SORAL, T GONEC, P KOLLAR, M ORAVEC, A COFFEY, J O'MAHONY, T LIPTAJ, K KRALOVA a J JAMPILEK. Ring-substituted 8-hydroxyquinoline-2-carboxanilides as potential antimycobacterial agents. <i>BIOORGANIC & MEDICINAL CHEMISTRY</i> [online]. 2015, 23(15), 4188–4196. Dostupné z: doi:10.1016/j.bmc.2015.06.047</p>	0968-0896



Ring-substituted 8-hydroxyquinoline-2-carboxanilides as potential antimycobacterial agents



Jiri Kos^a, Iveta Zadrazilova^a, Eoghan Nevin^b, Michal Soral^c, Tomas Gonec^a, Peter Kollar^d, Michal Oravec^e, Aidan Coffey^b, Jim O'Mahony^b, Tibor Liptaj^c, Katarina Kralova^f, Josef Jampilek^{a,*}

^a Department of Chemical Drugs, Faculty of Pharmacy, University of Veterinary and Pharmaceutical Sciences, Palackeho 1/3, 612 42 Brno, Czech Republic

^b Department of Biological Sciences, Cork Institute of Technology, Bishopstown, Cork, Ireland

^c Department of NMR Spectroscopy and Mass Spectrometry, Faculty of Chemical and Food Technology, Slovak University of Technology in Bratislava, Radlinskeho 9, 812 37 Bratislava, Slovakia

^d Department of Human Pharmacology and Toxicology, Faculty of Pharmacy, University of Veterinary and Pharmaceutical Sciences, Palackeho 1/3, 612 42 Brno, Czech Republic

^e Global Change Research Centre AS CR, Belidla 986/4a, 603 00 Brno, Czech Republic

^f Institute of Chemistry, Faculty of Natural Sciences, Comenius University, Mlynska dolina Ch-2, 842 15 Bratislava, Slovakia

ARTICLE INFO

Article history:

Received 16 April 2015

Revised 13 June 2015

Accepted 18 June 2015

Available online 29 June 2015

Keywords:

8-Hydroxyquinolines

In vitro antimycobacterial activity

MTT assay

In vitro cytotoxicity

Structure–activity relationships

ABSTRACT

In this study, a series of twenty-two ring-substituted 8-hydroxyquinoline-2-carboxanilides was prepared and characterized. Primary in vitro screening of the synthesized compounds was performed against *Mycobacterium tuberculosis* H37Ra, *Mycobacterium avium* complex and *M. avium* subsp. *paratuberculosis*. Some of the tested compounds showed the antimycobacterial activity against *M. avium* subsp. *paratuberculosis* comparable with or higher than that of rifampicin. 8-Hydroxy-*N*-[3-(trifluoromethyl)phenyl]- and 8-hydroxy-*N*-[4-(trifluoromethyl)phenyl]quinoline-2-carboxamide showed MIC = 24 μ M against all tested mycobacterial strains. 3-Methoxyphenyl- and 3-methylphenyl derivatives expressed MIC = 27 or 29 μ M also against all the tested strains. Their activity against *M. avium* subsp. *paratuberculosis* was 4-fold higher than that of rifampicin. 2-Bromophenyl- and 2-(trifluoromethyl)phenyl derivatives had MIC = 23 or 24 μ M against *M. tuberculosis*. A significant decrease of mycobacterial cell metabolism (viability of *M. tuberculosis* H37Ra) was observed using MTT assay. Screening of cytotoxicity of the compounds was performed using the THP-1 cells, and no significant lethal effect was observed up to tested concentration 30 μ M. The structure–activity relationships are discussed.

© 2015 Elsevier Ltd. All rights reserved.

1. Introduction

Tuberculosis (TB) remains one of the world's deadliest communicable diseases. *Mycobacterium tuberculosis*, the pathogen responsible for TB, uses diverse strategies to survive in a variety of host lesions and to evade immune surveillance. In 2013, an estimated 9.0 million people developed TB and 1.5 million died from the disease, 360,000 of whom were HIV-positive. Multidrug-resistant TB strains (MDR-TB) are a great worldwide problem. Drug resistance surveillance data indicate that in 2013 approximately 480,000 people developed MDR-TB worldwide. Among TB patients reported by national TB programmes in 2013, there were an estimated 300,000 cases of MDR-TB. Extensively drug-resistant TB (XDR-TB, defined as MDR-TB plus resistance to any fluoroquinolone and any second-line injectable drugs) has been identified in 100 countries globally in

2013, and the average proportion of MDR-TB cases with XDR-TB was 9.0%. Also non-tuberculous mycobacteria (NTM), for example, *Mycobacterium avium*, *Mycobacterium kansasii*, *Mycobacterium abscessus*, *Mycobacterium fortuitum*, *Mycobacterium chelonae*, *Mycobacterium smegmatis*, which become the main human pathogens and cause difficult-to-treat or incurable diseases ending in death of mainly HIV-positive patients, are a threat. NTM can cause a broad spectrum of diseases, such as pulmonary disease, lymphadenitis, skin and soft tissue disease, gastrointestinal and skeletal infections. The number of infections that can be associated with specific species as well as the number of new species as etiological agents has exploded in the last few years due to the increase in the number of immunocompromised patients. The emergence of MDR-TB and NTM makes the discovery of new molecular scaffolds a priority to achieve effective control of both TB and NTM.^{1–4}

The quinoline nucleus can be considered as a privileged structure;⁵ quinoline-based compounds exhibit various activities such as anti-inflammatory, cardiovascular, anticonvulsant, antiproliferative, antiprotozoan, antifungal and antibacterial.^{6–12} Quinoline

* Corresponding author.

E-mail address: josef.jampilek@gmail.com (J. Jampilek).

analogues^{6–8,13,14} and especially 8-hydroxyquinolines have been also recognized as promising antimycobacterial agents.^{15–18} The best known quinoline anti-TB derivative, bedaquiline (Sirturo™) belonging to diarylquinolines, a new class of antitubercular drugs, was approved by FDA for treatment of MDR-TB.¹⁹ Structural modifications of quinolines by various groups have led to the identification of potent anti-TB compounds exhibiting significant activity especially against strains of *M. tuberculosis*.^{13,14,20–29} It was found that these anti-TB quinolines exhibit various mechanisms of action; for example, they inhibit mycobacterial ATP synthase,^{23,30} mycobacterial FtsZ protein,³¹ glutathione S-transferase,³² enoyl-ACP reductase^{20,21,33} or decaprenylphosphoryl- β -D-ribose-2'-epimerase;²⁴ also other sites of actions of 8-hydroxyquinolines can be found due to the bidentate metal-chelating property of 8-hydroxyquinolines.^{15–18}

The aim of this contribution is synthesis and antimycobacterial screening of 8-hydroxyquinoline-2-carboxanilides with following analysis of the structure–activity relationships as a continuation of the investigation of recently designed ring-substituted quinoline analogues.^{9–11,34–37} Based on the above mentioned facts all the presented compounds were designed to bear an 8-hydroxyquinoline fragment and an amide moiety. Both structural features are important functional groups that are able to interact with a number of enzymes/receptors via hydrogen bonds and in this manner to affect the biological response.^{38–40}

2. Results and discussion

2.1. Chemistry and physicochemical properties

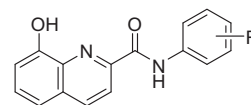
All studied compounds **1–8c** were prepared according to Scheme 1 by modified microwave-assisted (MW) synthesis;^{41,42} thus the synthesis of the target compounds was carried out in only one step with yields 66–76%. At first the carboxyl group was activated with phosphorus trichloride. The final amide was immediately formed by aminolysis of the acyl chloride by ring-substituted aniline in dry chlorobenzene. All the crude target compounds were recrystallized from ethanol.

Within structure–activity relationship studies various parameters describing physicochemical properties are investigated. Lipophilicity is a property that has a major effect on solubility, absorption, distribution and biotransformation as well as pharmacological activity, because drugs cross biological membranes through passive transport, which strongly depends on their lipophilicity. Lipophilicity of the studied compounds was determined by RP-HPLC as capacity factor logarithm ($\log k$) and calculated as $\log P$ using ACD/Percepta ver. 2012 (Advanced Chemistry Development, Inc., Toronto, ON, Canada, 2012). The corresponding values of ring-substituted 8-hydroxyquinoline-2-carboxanilides **1–8c** are shown in Table 1.

The highest experimental lipophilicity was found for 8-hydroxy-*N*-(4-trifluoromethylphenyl)quinoline-2-carboxamide (**7c**), while *N*-(2-fluorophenyl)-8-hydroxyquinoline-2-carboxamide (**4a**) showed the lowest $\log k$ value. The results obtained with the discussed compounds show that the experimentally-determined lipophilicities ($\log k$) of the *ortho*-substituted derivatives showed poor match, while the *meta*- and *para*-substituted compounds

Table 1

Structure of discussed 8-hydroxyquinoline-2-carboxanilides **1–8c**, experimentally determined values of lipophilicity $\log k$, predicted values of compound lipophilicity $\log P$ and electronic Hammett's σ parameters of R substituents, in vitro antimycobacterial activity (MIC) of compounds in comparison with rifampicin (RIF) standard and in vitro cytotoxicity assay (IC_{50}) of selected compounds

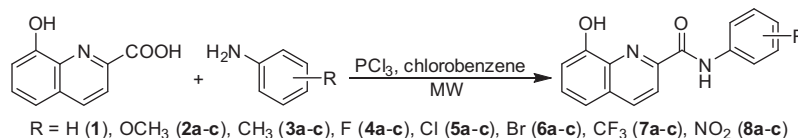


Compd	R	Log <i>k</i>	Log <i>P</i> ^a	σ^a	MIC [μ M]			IC ₅₀ [μ M]
					MT	MAC	MAP	
1	H	0.7600	2.55	0	30	30	30	>30
2a	2-OCH ₃	0.7935	2.67	−0.28	27	51	51	>30
2b	3-OCH ₃	0.8164	2.61	0.12	27	27	27	>30
2c	4-OCH ₃	0.7129	2.51	−0.27	849	425	849	>30
3a	2-CH ₃	0.6944	2.90	−0.17	29	54	29	>30
3b	3-CH ₃	0.9686	2.90	−0.07	29	29	29	>30
3c	4-CH ₃	0.9521	2.90	−0.17	29	54	29	>30
4a	2-F	0.6806	2.59	0.06	28	53	28	>30
4b	3-F	0.9420	2.76	0.34	53	53	53	>30
4c	4-F	0.8598	2.59	0.06	53	53	53	>30
5a	2-Cl	0.9566	3.07	0.22	27	837	27	>30
5b	3-Cl	1.1718	3.28	0.37	50	50	50	>30
5c	4-Cl	1.1543	3.05	0.23	837	50	837	>30
6a	2-Br	1.0536	3.16	0.22	23	729	23	>30
6b	3-Br	1.2357	3.31	0.39	44	44	44	>30
6c	4-Br	1.2347	3.19	0.23	729	44	729	>30
7a	2-CF ₃	0.9147	3.36	0.51	24	752	24	>30
7b	3-CF ₃	1.3206	3.44	0.43	24	24	24	>30
7c	4-CF ₃	1.3653	3.27	0.51	24	24	24	>30
8a	2-NO ₂	1.1277	2.73	0.77	97	808	97	>30
8b	3-NO ₂	0.9845	2.56	0.71	26	808	808	>30
8c	4-NO ₂	1.0495	2.45	0.78	26	808	404	>30
RIF	–	–	–	–	10	10	109	–

^a Calculated using ACD/Percepta ver. 2012 (Advanced Chemistry Development, Inc., Toronto, ON, Canada, 2012); MT = *M. tuberculosis* H37Ra ATCC 25177, MAC = *M. avium* complex CIT19/06 (clinical isolate) and MAP = *M. avium* subsp. *paratuberculosis* CIT03 (clinical isolate).

showed higher match with the predicted $\log P$ values. In this case the most significant deviations can be observed for nitro substituted derivatives; when 2-NO₂ (**8a**) is eliminated, correlation coefficient of the dependence of $\log k$ on $\log P$ values improves to $r = 0.7502$ ($n = 6$) and after elimination of 3-NO₂ (**8b**) and 4-NO₂ (**8c**) correlation coefficient of the dependence of $\log k$ on $\log P$ values improves to $r = 0.9759$ ($n = 13$), which reflects intra/intermolecular interactions of the nitro moiety. The influence of R substituents on lipophilicity of *ortho*-substituted derivatives is as follows: F < CH₃ < H < OCH₃ < CF₃ < Cl < Br < NO₂; for *meta*- and *para*-substituted derivatives it is as follows: OCH₃/H < F < CH₃ < NO₂ < Cl < Br < CF₃. Within the individual series the lipophilicity determined by $\log k$ values increases for halogens, methyl and trifluoromethyl substituents as follows: *ortho* < *para* < *meta*; for methoxy substituent as follows: *para* < *ortho* < *meta*, and for NO₂ as follows: *meta* < *para* < *ortho*.

Similarly poor correlation between experimental and calculated lipophilicity values was found also for different derivatives of 8-hydroxyquinolines.^{9–11,35,36,43} This is probably caused by the fact that between the hydroxyl moiety in C₍₈₎ of the quinoline nucleus



Scheme 1. Synthesis of ring-substituted 8-hydroxyquinoline-2-carboxanilides **1–8c**.

and nitrogen of quinoline intramolecular H-bond affecting lipophilicity, solubility and basicity/acidity is formed.⁴⁴ Based on the presented results, it can be stated that $\log k$ values specify lipophilicity within individual series of the studied compounds better than $\log P$ values.

The presence of different substituents in the anilide part of the discussed compounds results in a wide range of electronic properties. Electronic parameters (expressed as Hammett's σ parameters) of compounds **1–8c** were predicted using ACD/Percepta software, see Table 1; they ranged from $-0.28/-0.27$ (compound **2a,c** 2-OCH₃, 4-OCH₃) to $0.77/0.78$ (compound **8a,c** 2-NO₂, 4-NO₂).

2.2. In vitro antimycobacterial evaluation

The evaluation of the in vitro antimycobacterial activity of the compounds was performed against *Mycobacterium tuberculosis* H37Ra ATCC 25177 (MT) and clinical isolates of *M. avium* complex CIT19/06 (MAC) and *M. avium* subsp. *paratuberculosis* CIT03 (MAP), see Table 1. To reduce risk and make manipulation in the laboratory easier, surrogate model pathogens for *M. tuberculosis* can be used in laboratory studies. Avirulent *M. tuberculosis* strain H37Ra is very closely related to human-infecting *M. tuberculosis* strains (e.g., H37Rv), making it a good model for study especially because of the lower risk for laboratory workers.⁴⁵ Because of *M. tuberculosis*, the pathogenic role of NTM in humans was overshadowed for a long time. *Mycobacterium avium* complex includes ubiquitous atypical mycobacteria found in the environment that can easily infect immunosuppressed patients and cause disseminated disease, producing fever, sweats, weight loss and anaemia.⁴⁶ *M. avium* subsp. *paratuberculosis* is suspected to be a causative agent in gastrointestinal diseases; it is resistant to standard antimycobacterial therapy, but may be susceptible to some standard antibiotics, however, resistance to these antibiotics develops quickly.⁴⁷ The activity of compounds was expressed as the minimum inhibitory concentration (MIC), that is, defined for mycobacteria as a 90% or greater (IC₉₀) reduction of growth in comparison with the control. The MIC/IC₉₀ value is routinely and widely used in bacterial assays and is a standard detection limit according to the Clinical and Laboratory Standards Institute (CLSI).

Most of the target compounds showed activity against all three tested mycobacterial strains. With respect to *M. tuberculosis* a greater number of more efficient compounds showing higher effect than *para*-substituted compounds can be found among *ortho*- and *meta*-substituted derivatives, except for C₍₄₎ substituted derivatives **3c** (R = 4-CH₃), **7c** (R = 4-CF₃) and **8c** (R = 4-NO₂), which activity was comparable with that of *ortho*- and *meta*-substituted compounds. Compounds **6a** (R = 2-Br, MIC = 23 μ M), **7a** (R = 2-CF₃, MIC = 24 μ M), **7b** (3-CF₃, MIC = 24 μ M) and **7c** (4-CF₃, MIC = 24 μ M) exhibited the highest activity. The antimycobacterial

activity of the compounds against *M. tuberculosis* was expressed as $\log(1/\text{MIC} [\text{M}])$, and the dependences of the activity on lipophilicity expressed as $\log k$ and electronic properties expressed as Hammett's σ constants are illustrated in Figure 1A and B. When really inactive *para*-substituted compounds **2c**, **5c** and **6c** (R = 4-OCH₃, 4-Cl, 4-Br) are eliminated (marked by empty symbols), it is evident that neither lipophilicity nor electronic properties possess any significant effect on the antitubercular activity. Compounds **4b,c** (R = 3-, 4-F), **5b** (R = 3-Cl) and **6b** (R = 3-Br) had slightly lower activity than other 14 illustrated compounds. Similar trends can be found for the dependences of the activity against *M. avium* subsp. *paratuberculosis* on physicochemical parameters, therefore these dependences are not illustrated. It is important to note that nitro substituted derivatives **8a–c** expressed different activity than it could be expected. As mentioned in Section 2.1, all nitro derivatives **8a–c** showed poor correlation between experimental and calculated lipophilicity values. Especially C₍₂₎ substituted derivative **8a** has the highest experimentally determined lipophilicity ($\log k = 1.1277$) along with the strongest electron-withdrawing properties but the lowest antitubercular activity within the series. Probably the above mentioned interactions of the nitro moiety with the amide bond limited binding of the nitro substituted derivatives to target sites in mycobacterial cells. These interactions are most evident for compound **8a**, therefore this compound is also eliminated (marked by empty symbols in Fig. 1A and B) from SAR discussion. Similar observations for compound **8a** were made in respect to *M. avium* subsp. *paratuberculosis*.

Compounds **6a** (R = 2-Br, MIC = 23 μ M), **7b** (R = 3-CF₃, MIC = 24 μ M) and **7c** (R = 4-CF₃, MIC = 24 μ M) showed the highest activity against *M. avium* subsp. *paratuberculosis*. Based on the results it can be stated that *ortho*- and especially *meta*-substituted derivatives expressed higher activity than *para*-substituted ones. Only **7c** showed high effect within the C₍₄₎ substituted compounds. Similarly as for the previous strain, electronic properties show that the character of individual substituents R does not influence the antimycobacterial activity significantly.

Compounds **7b** (3-CF₃, MIC = 24 μ M) and **7c** (4-CF₃, MIC = 24 μ M) showed the highest activity against *M. avium* complex. The nitro moiety in all three positions (compounds **8a–c**) is the least favoured substituent, therefore these compounds are not considered for SAR discussion. Most effective compounds can be found among *meta*-substituted derivatives. The antimycobacterial activity of the compounds against *M. avium* complex was expressed as $\log(1/\text{MIC} [\text{M}])$, and the dependences of the activity on lipophilicity expressed as $\log k$ and electronic properties expressed as Hammett's σ constants are illustrated in Figure 2A and B. Generally, it seems that within the whole discussed series of compounds dependences of antimycobacterial activity against *M. avium* complex on lipophilicity and electronic

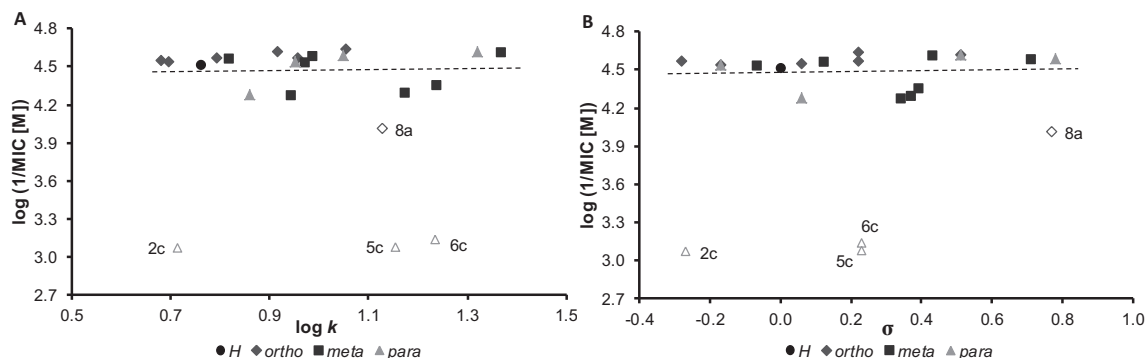


Figure 1. Dependence of antitubercular activity against *M. tuberculosis* expressed as $\log(1/\text{MIC} [\text{M}])$ of tested compounds on lipophilicity expressed as $\log k$ (A) and on Hammett's σ constants of R substituent (B). (Inactive compounds are marked by empty symbols.)

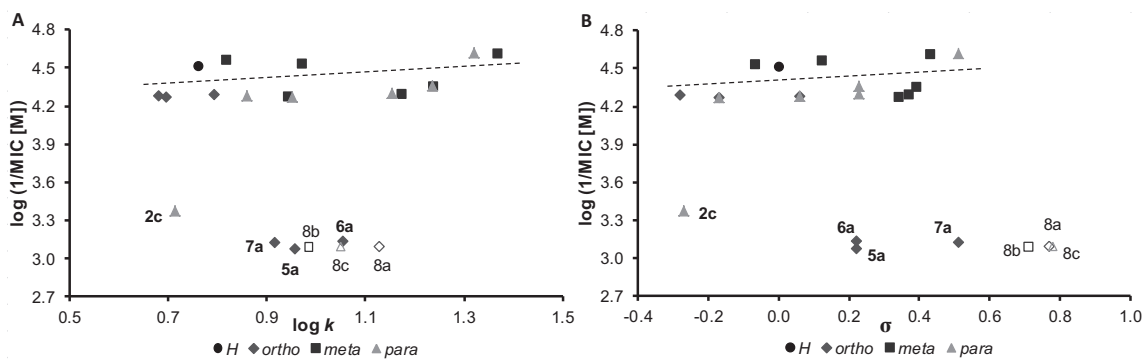


Figure 2. Dependence of antimycobacterial activity against *M. avium* complex expressed as $\log 1/\text{MIC}$ [M] of tested compounds on lipophilicity expressed as $\log k$ (A) and on Hammett's σ constants of R substituent (B). (Compounds **8a–c** not included in SAR discussion are marked by empty symbols.)

properties increase slightly with increasing of lipophilicity values and electron-withdrawing effect of substituents; although for the *meta*-substituted compounds this dependence is very slight, see Figure 2A and B. The significant dependence of antimycobacterial activity on lipophilicity and electronic properties of the *ortho*- and *para*-substituents can be observed. The *ortho*-substituted derivatives are completely ineffective when lipophilicity ($\log k$) is >0.8 along with Hammett's σ constants of R substituents >0.1 (see compounds **5a**, **6a**, **7a**), contrary to the properties of the *para*-substituted compounds that are ineffective when $\log k < 0.8$ and $\sigma < -0.2$ (compound **2c**), see Figure 2A and B.

Generally all the prepared compounds showed relatively high lipophilicity ($\log P = 2.5\text{--}3.4$ or $\log k = 0.68\text{--}1.36$) that enables the compounds to permeate through hydrophobic mycobacterial cell wall. Compound **2c** (R = 4-OCH₃) was completely inactive against all three mycobacterial strains; compounds **5c**, **6c**, **8b** and **8c** (R = 4-Cl, 4-Br, 3-NO₂, 4-NO₂) were ineffective against two of the tested mycobacterial strains. It can be stated that there is no any significant difference between antimycobacterial activities against *M. tuberculosis* and *M. avium* subsp. *paratuberculosis*, nevertheless *ortho*-substituted derivatives seem to be favourable, see **4a** $>$ **4b** = **4c**, **5a** $>$ **5b** \gg **5c**, **6a** $>$ **6b** \gg **6c**, except **7a** (2-CF₃) and **8a** (2-NO₂) substituted derivatives. On the other hand, the *meta*-substituted derivatives showed the highest potency against *M. avium* complex. When the compounds showed potency against *M. avium* complex, they were effective also against *M. tuberculosis* and *M. avium* subsp. *paratuberculosis*. Thus, it can be postulated that compounds with potency against all three strains were received by the substitution of C₍₃₎ position of aniline. On the other hand also the hydroxyl moiety in C₍₈₎ of quinoline seems to play a significant role for activity, because its absence in quinoline-2-carboxanilides led to a decrease of antimycobacterial effect.³⁷ Similar essential contribution of the hydroxyl moiety amplifying antimycobacterial potency was also observed for 1-hydroxynaphthalene-2-carboxanilides⁴¹ and 6-hydroxynaphthalene-2-carboxanilides⁴² versus naphthalene-2-carboxanilides.³⁷

2.3. MTT assay

Additionally, a standard MTT assay was performed for the selected most effective compounds, the MICs of which were previously determined through alamarBlue assays, see Table 1. The MTT assay is a well-characterized method of assessing cell growth through measurement of respiration. For the purpose of this assay, a measured viability of *M. tuberculosis* H37Ra of less than 70%, as determined by MTT, after exposure to the MIC of each test compound (as determined by the alamarBlue assay) was considered a positive result. As such, a low level of cell viability may suggest inhibition of cell growth through respiratory inhibition.⁴⁸ Model

compounds selected from 14 derivatives with the highest antitubercular activity, namely 3-methoxy (**2b**, 30.9%), 3-methyl (**3b**, 66.4%), 2-fluoro (**4a**, 26.9%), 2-chloro (**5a**, 21.4%), 2-bromo (**6a**, 26.9%), 2-trifluoromethyl (**7a**, 53.4%), 3-trifluoromethyl (**7b**, 18.8%), 4-trifluoromethyl (**7c**, 33.1%), 3-nitro (**8b**, 7.0%) and 4-nitro (**8c**, 17.3%) derivatives, showed less than 70% viability of *M. tuberculosis* H37Ra at the lowest tested concentration (8 $\mu\text{g}/\text{mL}$, i.e., ca. 26 μM). Similar effect was observed previously with ring-substituted naphthalene-1-carboxanilides⁴⁹ where 3-methoxy and 4-methyl derivatives showed more than 80% reduction in activity at the lowest tested concentration (8 $\mu\text{g}/\text{mL}$, i.e., ca. 30 μM) after 4 h of incubation, similar to the reduction observed in the rifampicin and ciprofloxacin standards and 2-methoxy and 3-fluoro derivatives achieved similar levels of inhibition at 16 $\mu\text{g}/\text{mL}$ (ca. 60 μM) concentration.^{20,33}

Based on the fact that the change in colour of alamarBlue is caused by a decrease of mycobacterial cell metabolism, it may be hypothesized that the mechanism of action of these ring-substituted 8-hydroxyquinoline-2-carboxanilides could be connected with affection of mycobacterial energy metabolism;³⁸ nevertheless, another possible site of action of the studied compounds in the mycobacteria cannot be excluded.^{15–18}

2.4. In vitro cytotoxicity assay

The preliminary in vitro screening of the cytotoxicity of the compounds was performed using the human monocytic leukemia THP-1 cell line. The cytotoxicity was evaluated as the IC₅₀ value (compound concentration causing 50% inhibition of cell population proliferation), see Table 1. A compound is considered as cytotoxic when it demonstrates a toxic effect on cells at the concentration up to 10 μM ,⁵⁰ and the highest tested concentration that was used for the toxicity assay was three times this value. Treatment with 30 μM of the discussed compounds did not lead to significant lethal effect on THP-1 cells. Based on these observations it can be concluded that the discussed amides can be considered as non-toxic agents for subsequent design of novel antimycobacterial agents.

3. Conclusions

A series of twenty-two ring-substituted 8-hydroxyquinoline-2-carboxanilides were prepared by means of microwave-assisted synthesis and subsequently characterized. All the compounds were tested for their in vitro antimycobacterial activity against *M. tuberculosis* and clinical isolates of *M. avium* complex and *M. avium* subsp. *paratuberculosis*. Some of the tested compounds showed the antimycobacterial activity against *M. avium* subsp. *paratuberculosis* comparable with or higher than that of rifampicin.

8-Hydroxy-*N*-[3-(trifluoromethyl)phenyl]- (7b) and 8-hydroxy-*N*-[4-(trifluoromethyl)phenyl]quinoline-2-carboxamide (7c) showed MIC = 24 μ M against all three tested mycobacterial strains. 3-Methoxyphenyl- (2b) and 3-methylphenyl (3b) derivatives expressed MIC = 27 or 29 μ M also against all the tested strains. 2-Bromophenyl- (6a) and 2-(trifluoromethyl)phenyl (7a) derivatives showed MIC = 23 or 24 μ M against *M. tuberculosis*. All the compounds possess high lipophilicity; they can permeate through hydrophobic mycobacterial cell wall. Based on the results it can be postulated that compounds with potency against all three strains were received by the substitution of C₍₃₎ position of aniline. The performed MTT assay of the selected compounds shows that they cause a decrease of mycobacterial cell metabolism; probably they influence the mycobacterial respiratory chain. All the compounds were tested for their in vitro cytotoxicity against the THP-1 cells and within this preliminary screening they demonstrated insignificant toxicity up to tested concentration 30 μ M, therefore it can be concluded that the discussed anilides can be considered as promising agents for subsequent design of novel antimycobacterial agents.

4. Experimental

4.1. Chemistry

All reagents were purchased from Aldrich (Sigma–Aldrich, St. Louis, MO, USA). TLC experiments were performed on alumina-backed silica gel 60 F254 plates (Merck, Darmstadt, Germany). The plates were illuminated under UV (254 nm) and evaluated in iodine vapour. The melting points were determined on Kofler hot-plate apparatus HMK (Franz Kustner Nacht KG, Dresden, Germany) and are uncorrected. Infrared (IR) spectra were recorded on a Smart MIRacle™ ATR ZnSe for Nicolet™ Impact 410 FT-IR spectrometer (Thermo Electron Corporation, West Palm Beach, FL, USA). The spectra were obtained by accumulation of 256 scans with 2 cm⁻¹ resolution in the region of 4000–600 cm⁻¹. All ¹H and ¹³C NMR spectra were recorded on an Agilent VNMRS 600 MHz system (Agilent Technologies, Santa Clara, CA, USA) equipped with a triple resonance HCN probe at 25 °C in DMSO-*d*₆. ¹H and ¹³C chemical shifts and ¹³C–¹⁹F coupling constants were determined from the standard ¹H and ¹³C spectra with digital resolution 0.3 Hz or better. Chemical shifts (δ) are reported in ppm. When necessary, additional experiments were done: ¹³C-APT (Attached Proton Test) for discrimination between CH and quaternary carbons; DQF COSY, HSQC and HMBC for through-bond ¹H–¹H and one- and multiple-bond ¹H–¹³C correlations. Mass spectra were measured using a LTQ Orbitrap Hybrid Mass Spectrometer (Thermo Electron Corporation) with direct injection into an APCI source (400 °C) in the negative mode.

4.1.1. General procedure for synthesis of 8-hydroxy-*N*-(substituted-phenyl)quinoline-2-carboxamides 1–8c

8-Hydroxyquinoline-2-carboxylic acid (5.3 mM) was suspended in dry chlorobenzene (30 mL) at ambient temperature and phosphorus trichloride (2.7 mM, 0.5 equiv), and the corresponding substituted aniline (5.3 mM, 1 equiv) was added dropwise. The reaction mixture was transferred to the microwave reactor, where the synthesis was performed (1st phase: 10 min, 100 °C, 100 W; 2nd phase: 15 min, 120 °C, 500 W; 3rd phase: 20 min, 130 °C, 500 W). Then the mixture was cooled to 50 °C, and then the solvent was removed to dryness under reduced pressure. The residue was washed with hydrochloric acid and water. The crude product was recrystallized from isopropanol. Studied compounds 1–8c are presented in Table 1.

4.1.2. 8-Hydroxy-*N*-phenylquinoline-2-carboxamide (1)

Yield 78%; mp 197 °C; IR (cm⁻¹): 3336, 3046, 1679, 1600, 1575, 1527, 1505, 1461, 1444, 1429, 1389, 1366, 1310, 1287, 1235, 1197, 1129, 1117, 1082, 931, 906, 879, 847, 814, 802, 761, 752, 722, 692; ¹H NMR (DMSO-*d*₆), δ : 7.183 (tt, 1H, *J* = 7.4, 1.1 Hz), 7.228 (dd, 1H, *J* = 7.6, 1.2 Hz), 7.447 (m, 2H), 7.524 (dd, 1H, *J* = 8.1, 1.2 Hz), 7.608 (t, 1H, *J* = 7.9 Hz), 7.901 (m, 2H), 8.272 (d, 1H, *J* = 8.5 Hz), 8.571 (d, 1H, *J* = 8.5 Hz), 10.404 (s, 1H), 11.171 (s, 1H); ¹³C NMR (DMSO-*d*₆), δ : 112.03, 117.64, 118.95, 120.70 (2C), 124.13, 128.77 (2C), 129.69, 129.72, 136.36, 138.10, 138.25, 147.28, 153.70, 162.09; HR-MS: C₁₆H₁₁N₂O₂ [M–H]⁻ calcd 263.0826 *m/z*, found 263.0822 *m/z*.

4.1.3. 8-Hydroxy-*N*-(2-methoxyphenyl)quinoline-2-carboxamide (2a)

Yield 71%; mp 187–189 °C; IR (cm⁻¹): 3446, 3372, 1679, 1601, 1538, 1505, 1485, 1456, 1432, 1326, 1289, 1236, 1198, 1135, 1105, 1083, 1046, 1030, 929, 888, 848, 813, 744, 722, 680; ¹H NMR (DMSO-*d*₆), δ : 3.349 (s, 3H), 7.027 (td, 1H, *J* = 7.7, 1.3 Hz), 7.151 (dd, 1H, *J* = 8.3, 1.3 Hz), 7.211 (dd, 1H, *J* = 7.6, 1.2 Hz), 7.243 (ddd, 1H, *J* = 9.1, 7.5, 1.6 Hz), 7.510 (dd, 1H, *J* = 8.2, 1.2 Hz), 7.587 (t, 1H, *J* = 7.9 Hz), 7.800 (dd, 1H, *J* = 7.8, 1.6 Hz), 8.221 (d, 1H, *J* = 8.5 Hz), 8.544 (d, 1H, *J* = 8.5 Hz), 10.374 (s, 1H), 10.885 (s, 1H); ¹³C NMR (DMSO-*d*₆), δ : 55.66, 111.50, 112.13, 117.65, 118.84, 120.26, 124.95, 126.14, 126.22, 129.56, 129.77, 136.64, 137.95, 147.44, 152.05, 153.78, 162.28; HR-MS: C₁₇H₁₃N₂O₃ [M–H]⁻ calcd 293.0932 *m/z*, found 293.0928 *m/z*.

4.1.4. 8-Hydroxy-*N*-(3-methoxyphenyl)quinoline-2-carboxamide (2b)

Yield 69%; mp 199–201 °C; IR (cm⁻¹): 3331, 3307, 1684, 1657, 1605, 1592, 1525, 1504, 1456, 1416, 1391, 1358, 1328, 1286, 1265, 1247, 1224, 1201, 1159, 1081, 1053, 1033, 994, 874, 843, 822, 774, 765, 758, 736, 723, 702, 688; ¹H NMR (DMSO-*d*₆), δ : 3.813 (s, 3H), 6.768 (dd, 1H, *J* = 8.3, 2.5 Hz), 7.230 (dd, 1H, *J* = 7.6, 1.3 Hz), 7.349 (t, 1H, *J* = 8.2 Hz), 7.499 (dm, 1H, *J* = 8.1 Hz), 7.524 (d, 1H, *J* = 8.2 Hz), 7.577 (t, 1H, *J* = 2.2 Hz), 7.609 (t, 1H, *J* = 7.9 Hz), 8.269 (d, 1H, *J* = 8.5 Hz), 8.572 (d, 1H, *J* = 8.5 Hz), 10.413 (s, 1H), 11.133 (s, 1H); ¹³C NMR (DMSO-*d*₆), δ : 55.12, 106.38, 109.60, 112.08, 112.91, 117.66, 118.96, 129.59, 129.71, 129.76, 136.36, 138.13, 139.44, 147.24, 153.71, 159.58, 162.13; HR-MS: C₁₇H₁₃N₂O₃ [M–H]⁻ calcd 293.0932 *m/z*, found 293.0927 *m/z*.

4.1.5. 8-Hydroxy-*N*-(4-methoxyphenyl)quinoline-2-carboxamide (2c)

Yield 66%, mp 209 °C; IR (cm⁻¹): 3334w, 3208w, 1675m, 1627m, 1593m, 1528s, 1510s, 1464s, 1410w, 1302w, 1287w, 1230s, 1174m, 1163m, 1110m, 1086m, 1036s, 937w, 855m, 828s, 815s, 762s, 748s, 723s, 677w; ¹H NMR (DMSO-*d*₆), δ : 3.779 (s, 3H), 7.017 (m, 2H), 7.217 (dd, 1H, *J* = 7.6, 1.2 Hz), 7.511 (dd, 1H, *J* = 8.2, 1.2 Hz), 7.594 (t, 1H, *J* = 7.9 Hz), 7.795 (m, 2H), 8.253 (d, 1H, *J* = 8.5 Hz), 8.553 (d, 1H, *J* = 8.5 Hz), 10.357 (s, 1H), 11.605 (s, 1H); ¹³C NMR (DMSO-*d*₆), δ : 55.22, 111.94, 113.93 (2C), 117.63, 118.92, 122.26 (2C), 129.61 (2C), 131.30, 136.36, 138.04, 147.46, 153.66, 155.89, 161.74; HR-MS: C₁₇H₁₃N₂O₃ [M–H]⁻ calcd 293.0932 *m/z*; found 293.0925 *m/z*.

4.1.6. 8-Hydroxy-*N*-(2-methylphenyl)quinoline-2-carboxamide (3a)

Yield 73%; mp 139–140 °C; IR (cm⁻¹): 3177, 3043, 2960, 1661, 1615, 1587, 1538, 1523, 1456, 1428, 1367, 1325, 1247, 1208, 1144, 1106, 1083, 1067, 1050, 933, 882, 846, 814, 758, 710; ¹H NMR (DMSO-*d*₆), δ : 2.303 (s, 3H), 7.211 (dd, 1H, *J* = 7.6, 1.0 Hz), 7.232 (td, 1H, *J* = 7.3, 1.2 Hz), 7.291 (t, 1H, *J* = 7.5 Hz), 7.347 (d, 1H,

$J = 7.5$ Hz), 7.451 (d, 1H, $J = 7.7$ Hz), 7.525 (d, 1H, $J = 8.3$ Hz), 7.602 (t, 1H, $J = 7.9$ Hz), 8.230 (d, 1H, $J = 8.5$ Hz), 8.562 (d, 1H, $J = 8.5$ Hz), 10.240 (s, 1H), 11.055 (s, 1H); ^{13}C NMR (DMSO- d_6), δ : 17.96, 111.84, 117.61, 118.91, 126.16, 126.25, 126.49, 129.63, 129.65, 130.43, 133.72, 135.81, 136.44, 137.99, 147.28, 153.64, 162.27; HR-MS: $\text{C}_{17}\text{H}_{13}\text{N}_2\text{O}_2$ [M-H] $^-$ calcd 277.0983 m/z , found 277.0977 m/z .

4.1.7. 8-Hydroxy-*N*-(3-methylphenyl)quinoline-2-carboxamide (3b)

Yield 75%; mp 203–204 °C; IR (cm $^{-1}$): 3342, 3312, 3049, 1686, 1656, 1612, 1538, 1505, 1489, 1462, 1392, 1358, 1327, 1308, 1289, 1224, 1181, 1163, 1117, 1084, 1046, 940, 897, 881, 853, 779, 758, 741, 724, 692; ^1H NMR (DMSO- d_6), δ : 2.368 (s, 3H), 7.000 (dm, 1H, $J = 7.5$ Hz), 7.226 (dd, 1H, $J = 7.6, 1.2$ Hz), 7.321 (t, 1H, $J = 7.7$ Hz), 7.520 (dd, 1H, $J = 8.1, 1.2$ Hz), 7.606 (t, 1H, $J = 7.9$ Hz), 7.720 (s, 1H), 7.729 (d, 1H, $J = 7.7$ Hz), 8.265 (d, 1H, $J = 8.5$ Hz), 8.568 (d, 1H, $J = 8.5$ Hz), 10.407 (s, 1H), 11.107 (s, 1H); ^{13}C NMR (DMSO- d_6), δ : 21.17, 112.04, 117.64, 117.81, 118.94, 121.17, 124.81, 128.62, 129.68, 129.71, 136.37, 137.99, 138.10, 138.18, 147.33, 153.72, 162.02; HR-MS: $\text{C}_{17}\text{H}_{13}\text{N}_2\text{O}_2$ [M-H] $^-$ calcd 277.0983 m/z , found 277.0980 m/z .

4.1.8. 8-Hydroxy-*N*-(4-methylphenyl)quinoline-2-carboxamide (3c)

Yield 68%; mp 208 °C; IR (cm $^{-1}$): 3457, 3204, 2917, 1683, 1630, 1590, 1527, 1501, 1464, 1404, 1319, 1297, 1260, 1230, 1185, 1163, 1086, 1047, 1019, 980, 931, 889, 851, 809, 761, 749, 724; ^1H NMR (DMSO- d_6), δ : 2.321 (s, 3H), 7.221 (dd, 1H, $J = 7.6, 1.3$ Hz), 7.248 (m, 2H), 7.521 (dd, 1H, $J = 8.2, 1.2$ Hz), 7.604 (t, 1H, $J = 7.9$ Hz), 7.779 (m, 2H), 8.259 (d, 1H, $J = 8.5$ Hz), 8.556 (d, 1H, $J = 8.5$ Hz), 10.382 (s, 1H), 11.110 (s, 1H); ^{13}C NMR (DMSO- d_6), δ : 20.530, 112.00, 117.64, 118.94, 120.67 (2C), 129.18 (2C), 129.66, 129.67, 133.16, 135.73, 136.36, 138.08, 147.38, 153.69, 162.92; HR-MS: $\text{C}_{17}\text{H}_{13}\text{N}_2\text{O}_2$ [M-H] $^-$ calcd 277.0983 m/z ; found 277.0988 m/z .

4.1.9. *N*-(2-Fluorophenyl)-8-hydroxyquinoline-2-carboxamide (4a)

Yield 68%; mp 145 °C; IR (cm $^{-1}$): 3489, 3376, 1689, 1618, 1594, 1537, 1505, 1455, 1359, 1327, 1290, 1252, 1232, 1194, 1169, 1121, 1083, 1031, 887, 848, 757, 722; ^1H NMR (DMSO- d_6), δ : 11.168 (s, 1H), 10.352 (s, 1H), 8.576 (d, 1H, $J = 8.5$ Hz), 8.230 (d, 1H, $J = 8.5$ Hz), 7.745 (td, 1H, $J = 7.8, 1.8$ Hz), 7.608 (dd, 1H, $J = 7.7, 8.1$ Hz), 7.523 (dd, 1H, $J = 8.2, 1.2$ Hz), 7.40–7.28 (m, 3H), 7.219 (dd, 1H, $J = 7.7, 1.2$ Hz); ^{13}C NMR (DMSO- d_6), δ : 162.54, 155.81 ($J = 247.4$ Hz), 153.74, 146.76, 138.06, 136.46, 129.82, 129.73, 127.22 ($J = 9.2$ Hz), 127.20, 125.05 ($J = 12.2$ Hz), 124.45 ($J = 3.6$ Hz), 118.92, 115.95 ($J = 19.8$ Hz), 117.60, 111.93; HR-MS: $\text{C}_{16}\text{H}_{10}\text{FN}_2\text{O}_2$ [M-H] $^-$ calcd 281.0732 m/z , found 281.0737 m/z .

4.1.10. *N*-(3-Fluorophenyl)-8-hydroxyquinoline-2-carboxamide (4b)

Yield 72%; mp 197 °C; IR (cm $^{-1}$): 3333, 1686, 1612, 1599, 1528, 1504, 1463, 1443, 1391, 1365, 1325, 1295, 1276, 1237, 1200, 1174, 1145, 1111, 1083, 965, 872, 846, 775, 760, 748, 722, 684; ^1H NMR (DMSO- d_6), δ : 11.265 (s, 1H), 10.376 (s, 1H), 8.572 (d, 1H, $J = 8.5$ Hz), 8.263 (d, 1H, $J = 8.5$ Hz), 7.866 (dt, 1H, $J = 11.6, 2.2$ Hz), 7.698 (ddd, 1H, $J = 8.1, 1.9, 0.9$ Hz), 7.611 (t, 1H, $J = 7.9$ Hz), 7.522 (dd, 1H, $J = 8.2, 1.2$ Hz), 7.484 (dt, 1H, $J = 6.8, 8.2$ Hz), 7.233 (dd, 1H, $J = 7.6, 1.2$ Hz), 7.012 (td, 1H, $J = 8.4, 2.5$ Hz); ^{13}C NMR (DMSO- d_6), δ : 162.35, 162.33 ($J = 241.6$ Hz), 153.67, 146.87, 140.01 ($J = 11.0$ Hz), 138.20, 136.32, 130.43 ($J = 9.5$ Hz), 129.87, 129.77, 118.95, 117.68, 116.33 ($J = 2.6$ Hz), 112.10, 110.61 ($J = 20.9$ Hz), 107.30 ($J = 26.1$ Hz); HR-MS: $\text{C}_{16}\text{H}_{10}\text{FN}_2\text{O}_2$ [M-H] $^-$ calcd 281.0732 m/z , found 281.0736 m/z .

4.1.11. *N*-(4-Fluorophenyl)-8-hydroxyquinoline-2-carboxamide (4c)

Yield 71%; mp 200 °C; IR (cm $^{-1}$): 3318, 1677, 1655, 1609, 1528, 1528, 1504, 1464, 1405, 1359, 1309, 1286, 1225, 1189, 1156, 1133, 1089, 1083, 932, 886, 854, 827, 760, 723, 678; ^1H NMR (DMSO- d_6), δ : 11.206 (s, 1H), 10.349 (s, 1H), 8.565 (d, 1H, $J = 8.5$ Hz), 8.260 (d, 1H, $J = 8.5$ Hz), 7.909 (m, 2H), 7.604 (dd, 1H, $J = 8.1, 7.7$ Hz), 7.519 (dd, 1H, $J = 8.2, 1.2$ Hz), 7.290 (m, 2H), 7.226 (dd, 1H, $J = 7.6, 1.2$ Hz); ^{13}C NMR (DMSO- d_6), δ : 162.05, 158.57 ($J = 240.9$ Hz), 153.64, 147.12, 138.12, 136.33, 134.60 ($J = 2.7$ Hz), 129.74, 129.68, 122.56 (2C, $J = 8.0$ Hz), 118.93, 117.65, 115.41 (2C, $J = 22.4$ Hz), 111.99; HR-MS: $\text{C}_{16}\text{H}_{10}\text{FN}_2\text{O}_2$ [M-H] $^-$ calcd 281.0732 m/z , found 281.0728 m/z .

4.1.12. *N*-(2-Chlorophenyl)-8-hydroxyquinoline-2-carboxamide (5a)

Yield 71%; mp 151–152 °C; IR (cm $^{-1}$): 3355, 1695, 1595, 1581, 1535, 1505, 1461, 1433, 1362, 1328, 1310, 1290, 1237, 1198, 1136, 1115, 1088, 1052, 1032, 885, 848, 743, 724, 668; ^1H NMR (DMSO- d_6), δ : 11.224 (s, 1H), 10.322 (s, 1H), 8.571 (d, 1H, $J = 8.5$ Hz), 8.229 (d, 1H, $J = 8.5$ Hz), 7.746 (dd, 1H, $J = 7.9, 1.6$ Hz), 7.630 (dd, 1H, $J = 8.0, 1.4$ Hz), 7.610 (t, 1H, $J = 7.9$ Hz), 7.528 (dd, 1H, $J = 8.2, 1.1$ Hz), 7.458 (td, 1H, $J = 7.6, 1.5$ Hz), 7.352 (td, 1H, $J = 7.8, 1.6$ Hz), 7.233 (dd, 1H, $J = 7.6, 1.2$ Hz); ^{13}C NMR (DMSO- d_6), δ : 162.57, 153.72, 146.77, 138.07, 136.50, 134.58, 129.80, 129.79, 129.67, 129.14, 128.09, 127.63, 127.59, 118.86, 117.62, 111.97; HR-MS: $\text{C}_{16}\text{H}_{10}\text{ClN}_2\text{O}_2$ [M-H] $^-$ calcd 297.0436 m/z , found 297.0437 m/z .

4.1.13. *N*-(3-Chlorophenyl)-8-hydroxyquinoline-2-carboxamide (5b)

Yield 75%; mp 227 °C; IR (cm $^{-1}$): 3342, 1689, 1589, 1524, 1502, 1481, 1464, 1405, 1324, 1296, 1222, 1191, 1169, 1118, 1097, 1078, 977, 881, 855, 817, 786, 765, 722, 685; ^1H NMR (DMSO- d_6), δ : 11.243 (s, 1H), 10.354 (s, 1H), 8.573 (d, 1H, $J = 8.5$ Hz), 8.261 (d, 1H, $J = 8.5$ Hz), 8.060 (t, 1H, $J = 2.1$ Hz), 7.874 (ddd, 1H, $J = 8.2, 2.0, 0.9$ Hz), 7.614 (dd, 1H, $J = 7.7, 8.1$ Hz), 7.524 (dd, 1H, $J = 8.2, 1.1$ Hz), 7.478 (t, 1H, $J = 8.1$ Hz), 7.240 (ddd, 1H, $J = 8.0, 2.1, 0.9$ Hz), 7.236 (dd, 1H, $J = 7.6, 1.2$ Hz); ^{13}C NMR (DMSO- d_6), δ : 162.33, 153.65, 146.82, 139.74, 138.20, 136.30, 133.11, 130.50, 129.88, 129.76, 123.80, 119.98, 118.93, 118.90, 117.67, 112.07; HR-MS: $\text{C}_{16}\text{H}_{10}\text{ClN}_2\text{O}_2$ [M-H] $^-$ calcd 297.0436 m/z , found 297.0432 m/z .

4.1.14. *N*-(4-Chlorophenyl)-8-hydroxyquinoline-2-carboxamide (5c)

Yield 75%; mp 272–273 °C; IR (cm $^{-1}$): 3390, 3316, 1686, 1651, 1589, 1528, 1502, 1466, 1399, 1362, 1307, 1283, 1226, 1187, 1090, 1008, 889, 839, 804, 748, 722, 671; ^1H NMR (DMSO- d_6), δ : 11.229 (s, 1H), 10.356 (s, 1H), 8.563 (d, 1H, $J = 8.5$ Hz), 8.255 (d, 1H, $J = 8.5$ Hz), 7.938 (m, 2H), 7.605 (dd, 1H, $J = 8.1, 7.7$ Hz), 7.515 (dd, 1H, $J = 8.1, 1.2$ Hz), 7.502 (m, 2H, $J = 7.9$ Hz), 7.226 (dd, 1H, $J = 7.6, 1.2$ Hz); ^{13}C NMR (DMSO- d_6), δ : 162.19, 153.66, 146.98, 138.16, 137.22, 136.32, 129.81, 129.72, 128.71 (2C), 127.79, 122.17 (2C), 118.93, 117.66, 112.04; HR-MS: $\text{C}_{16}\text{H}_{10}\text{ClN}_2\text{O}_2$ [M-H] $^-$ calcd 297.0436 m/z , found 297.0433 m/z .

4.1.15. *N*-(2-Bromophenyl)-8-hydroxyquinoline-2-carboxamide (6a)

Yield 76%; mp 176–177 °C; IR (cm $^{-1}$): 3452, 3336, 1696, 1592, 1575, 1532, 1504, 1460, 1431, 1362, 1328, 1305, 1235, 1196, 1134, 1109, 1087, 1045, 1021, 848, 814, 758, 723, 668; ^1H NMR (DMSO- d_6), δ : 11.208 (s, 1H), 10.306 (s, 1H), 8.571 (d, 1H, $J = 8.5$ Hz), 8.223 (d, 1H, $J = 8.5$ Hz), 7.786 (dd, 1H, $J = 8.0, 1.4$ Hz), 7.700 (dd, 1H, $J = 7.9, 1.6$ Hz), 7.610 (t, 1H, $J = 7.9$ Hz), 7.528 (dd,

1H, $J = 8.2, 1.1$ Hz), 7.499 (td, 1H, $J = 7.7, 1.4$ Hz), 7.283 (td, 1H, $J = 7.7, 1.7$ Hz), 7.219 (dd, 1H, $J = 7.7, 1.2$ Hz); ^{13}C NMR (DMSO- d_6), δ : 162.56, 153.72, 146.80, 138.07, 136.50, 136.10, 132.80, 129.80, 129.78, 128.50, 128.24, 128.05, 120.10, 118.86, 117.62, 111.95; HR-MS: $\text{C}_{16}\text{H}_{10}\text{BrN}_2\text{O}_2$ [M-H] $^-$ calcd 340.9931 m/z , found 340.9935 m/z .

4.1.16. N-(3-Bromophenyl)-8-hydroxyquinoline-2-carboxamide (6b)

Yield 75%; mp 235 °C; IR (cm $^{-1}$): 3445, 3279, 3057, 1626, 1584, 1536, 1504, 1504, 1478, 1409, 1329, 1306, 1230, 1190, 1163, 1123, 1072, 994, 881, 850, 722, 747, 725, 677; ^1H NMR (DMSO- d_6), δ : 11.228 (s, 1H), 10.347 (s, 1H), 8.572 (d, 1H, $J = 8.5$ Hz), 8.257 (d, 1H, $J = 8.5$ Hz), 8.183 (t, 1H, $J = 2.0$ Hz), 7.924 (ddd, 1H, $J = 8.1, 1.9, 1.0$ Hz), 7.612 (dd, 1H, $J = 7.8, 8.1$ Hz), 7.522 (dd, 1H, $J = 8.3, 1.2$ Hz), 7.415 (t, 1H, $J = 8.0$ Hz), 7.368 (ddd, 1H, $J = 7.9, 1.9, 1.1$ Hz), 7.233 (dd, 1H, $J = 7.7, 1.2$ Hz); ^{13}C NMR (DMSO- d_6), δ : 162.31, 153.65, 146.82, 139.88, 138.21, 136.30, 130.81, 129.88, 129.76, 126.70, 122.81, 121.54, 119.28, 118.94, 117.68, 112.08; HR-MS: for $\text{C}_{16}\text{H}_{10}\text{BrN}_2\text{O}_2$ [M-H] $^-$ calcd 340.9931 m/z , found 340.9937 m/z .

4.1.17. N-(4-Bromophenyl)-8-hydroxyquinoline-2-carboxamide (6c)

Yield 75%; mp 283–284 °C; IR (cm $^{-1}$): 3386, 3316, 1686, 1650, 1585, 1524, 1500, 1393, 1305, 1280, 1224, 1179, 1161, 1111, 1072, 1005, 933, 887, 837, 822, 811, 801, 720; ^1H NMR (DMSO- d_6), δ : 11.221 (s, 1H), 10.356 (s, 1H), 8.565 (d, 1H, $J = 8.5$ Hz), 8.255 (d, 1H, $J = 8.5$ Hz), 7.888 (m, 2H), 7.631 (m, 2H), 7.607 (t, 1H, $J = 7.9$ Hz), 7.519 (dd, 1H, $J = 8.2, 1.2$ Hz), 7.227 (dd, 1H, $J = 7.6, 1.2$ Hz); ^{13}C NMR (DMSO- d_6), δ : 162.19, 153.65, 146.96, 138.16, 137.63, 136.32, 131.62 (2C), 129.82, 129.72, 122.51 (2C), 118.93, 117.66, 115.87, 112.04; HR-MS: $\text{C}_{16}\text{H}_{10}\text{BrN}_2\text{O}_2$ [M-H] $^-$ calcd 340.9931 m/z , found 340.9932 m/z .

4.1.18. 8-Hydroxy-N-(2-trifluoromethylphenyl)quinoline-2-carboxamide (7a)

Yield 71%; mp 142–143 °C; IR (cm $^{-1}$): 3312, 1666, 1590, 1524, 1505, 1483, 1459, 1365, 1315, 1280, 1240, 1202, 1170, 1117, 1056, 1032, 935, 894, 857, 817, 754, 733, 668; ^1H NMR (DMSO- d_6), δ : 11.221 (s, 1H), 10.269 (s, 1H), 8.569 (d, 1H, $J = 8.5$ Hz), 8.208 (d, 1H, $J = 8.5$ Hz), 7.867 (dm, 1H, $J = 7.9$ Hz), 7.807 (t, 1H, $J = 7.8$ Hz), 7.706 (dm, 1H, $J = 7.8$ Hz), 7.612 (dd, 1H, $J = 7.7, 8.2$ Hz), 7.592 (tm, 1H, $J = 7.7$ Hz), 7.529 (dd, 1H, $J = 8.2, 1.2$ Hz), 7.218 (dd, 1H, $J = 7.6, 1.2$ Hz); ^{13}C NMR (DMSO- d_6), δ : 163.49, 153.69, 146.62, 138.07, 136.49, 135.36 (q, $J = 2.9$ Hz), 133.32, 130.53, 129.83, 129.78, 127.49, 126.61 (q, $J = 4.9$ Hz), 126.03 (q, $J = 29.4$ Hz), 123.60 (q, $J = 273.5$ Hz), 118.80, 117.60, 111.91; HR-MS: $\text{C}_{17}\text{H}_{10}\text{F}_3\text{N}_2\text{O}_2$ [M-H] $^-$ calcd 331.0699 m/z , found 331.0703 m/z .

4.1.19. 8-Hydroxy-N-(3-trifluoromethylphenyl)quinoline-2-carboxamide (7b)

Yield 68%; mp 213–214 °C; IR (cm $^{-1}$): 3293, 1691, 1657, 1614, 1541, 1493, 1393, 1329, 1224, 1161, 1111, 1096, 880, 854, 794, 754, 724, 694; ^1H NMR (DMSO- d_6), δ : 11.373 (s, 1H), 10.343 (s, 1H), 8.575 (d, 1H, $J = 8.5$ Hz), 8.267 (d, 1H, $J = 8.5$ Hz), 8.321 (t, 1H, $J = 2.2$ Hz), 8.199 (dm, 1H, $J = 8.1$ Hz), 7.689 (t, 1H, $J = 8.0$ Hz), 7.613 (t, 1H, $J = 7.9$ Hz), 7.527 (dm, 1H, $J = 7.6$ Hz), 7.522 (dd, 1H, $J = 8.3, 1.2$ Hz), 7.237 (dd, 1H, $J = 7.6, 1.1$ Hz); ^{13}C NMR (DMSO- d_6), δ : 162.54, 153.66, 146.75, 139.08, 138.22, 136.31, 130.05, 129.91, 129.79, 129.54 (q, $J = 31.5$ Hz), 124.11 (q, $J = 272.2$ Hz), 124.08, 120.40 (q, $J = 3.9$ Hz), 118.94, 117.69, 116.57 (q, $J = 4.0$ Hz), 112.08; HR-MS: $\text{C}_{17}\text{H}_{10}\text{F}_3\text{N}_2\text{O}_2$ [M-H] $^-$ calcd 331.0699 m/z , found 331.0698 m/z .

4.1.20. 8-Hydroxy-N-(4-trifluoromethylphenyl)quinoline-2-carboxamide (7c)

Yield 72%; mp 253 °C; IR (cm $^{-1}$): 3315, 1692, 1662, 1614, 1595, 1530, 1501, 1464, 1409, 1360, 1318, 1228, 1183, 1108, 1063, 1016, 933, 852, 837, 755, 722; ^1H NMR (DMSO- d_6), δ : 11.378 (s, 1H), 10.398 (s, 1H), 8.577 (d, 1H, $J = 8.5$ Hz), 8.273 (d, 1H, $J = 8.5$ Hz), 8.146 (m, 2H), 7.818 (m, 2H), 7.617 (t, 1H, $J = 7.9$ Hz), 7.526 (dd, 1H, $J = 8.2, 1.3$ Hz), 7.238 (dd, 1H, $J = 7.6, 1.3$ Hz); ^{13}C NMR (DMSO- d_6), δ : 162.57, 153.69, 146.75, 141.89, 138.23, 136.32, 129.95, 129.81, 126.07 (q, 2C, $J = 3.8$ Hz), 124.34 (q, $J = 271.3$ Hz), 124.05 (q, $J = 32.2$ Hz), 120.45 (2C), 118.98, 117.69, 112.13; HR-MS: $\text{C}_{17}\text{H}_{10}\text{F}_3\text{N}_2\text{O}_2$ [M-H] $^-$ calcd 331.0699 m/z , found 331.0704 m/z .

4.1.21. 8-Hydroxy-N-(2-nitrophenyl)quinoline-2-carboxamide (8a)

Yield 79%; mp 239–241 °C; IR (cm $^{-1}$): 3462, 3287, 1697, 1606, 1581, 1548, 1499, 1464, 1447, 1427, 1363, 1338, 1292, 1271, 1234, 1198, 1143, 1132, 1115, 1088, 935, 862, 847, 809, 783, 753, 736, 724, 668; ^1H NMR (DMSO- d_6), δ : 7.247 (d, 1H, $J = 7.7$ Hz), 7.502 (t, 1H, $J = 7.7$ Hz), 7.545 (d, 1H, $J = 8.2$ Hz), 7.632 (t, 1H, $J = 7.8$ Hz), 7.845 (t, 1H, $J = 7.7$ Hz), 7.934 (d, 1H, $J = 8.1$ Hz), 8.101 (d, 1H, $J = 8.1$ Hz), 8.206 (d, 1H, $J = 8.5$ Hz), 8.590 (d, 1H, $J = 8.5$ Hz), 10.219 (s, 1H), 11.826 (s, 1H); ^{13}C NMR (DMSO- d_6), δ : 112.08, 117.73, 118.92, 125.23, 126.01, 126.21, 129.92, 130.07, 130.84, 134.21, 136.45, 138.30, 142.99, 146.20, 153.69, 162.46; HR-MS: $\text{C}_{16}\text{H}_{10}\text{N}_3\text{O}_4$ [M-H] $^-$ calcd 308.0677 m/z , found 308.0673 m/z .

4.1.22. 8-Hydroxy-N-(3-nitrophenyl)quinoline-2-carboxamide (8b)

Yield 73%; mp 273–276 °C; IR (cm $^{-1}$): 3463, 3276, 1680, 1594, 1525, 1502, 1456, 1429, 1347, 1295, 1275, 1230, 1186, 1164, 1124, 1076, 946, 894, 882, 833, 803, 755, 735, 724, 668; ^1H NMR (DMSO- d_6), δ : 7.244 (dd, 1H, $J = 7.6, 1.2$ Hz), 7.538 (dd, 1H, $J = 8.1, 1.0$ Hz), 7.627 (t, 1H, $J = 8.0$ Hz), 7.746 (t, 1H, $J = 8.1$ Hz), 8.030 (dd, 1H, $J = 8.2, 2.1$ Hz), 8.278 (d, 1H, $J = 8.5$ Hz), 8.350 (dd, 1H, $J = 8.2, 1.8$ Hz), 8.594 (d, 1H, $J = 8.5$ Hz), 8.854 (t, 1H, $J = 2.1$ Hz), 10.360 (s, 1H), 11.469 (s, 1H); ^{13}C NMR (DMSO- d_6), δ : 112.10, 114.55, 117.70, 118.53, 118.95, 126.37, 129.82, 130.00, 130.25, 136.29, 138.26, 139.47, 146.53, 147.99, 153.66, 162.66; HR-MS: $\text{C}_{16}\text{H}_{10}\text{N}_3\text{O}_4$ [M-H] $^-$ calcd 308.0677 m/z , found 308.0672 m/z .

4.1.23. 8-Hydroxy-N-(4-nitrophenyl)quinoline-2-carboxamide (8c)

Yield 75%; mp 297–300 °C; IR (cm $^{-1}$): 3253, 3116, 1690, 1595, 1567, 1535, 1501, 1464, 1409, 1328, 1303, 1244, 1177, 1113, 1083, 977, 942, 914, 847, 802, 748, 690; ^1H NMR (DMSO- d_6), δ : 7.242 (dd, 1H, $J = 7.7, 1.2$ Hz), 7.537 (dd, 1H, $J = 8.2, 1.2$ Hz), 7.631 (t, 1H, $J = 7.9$ Hz), 8.189 (m, 2H), 8.273 (d, 1H, $J = 8.5$ Hz), 8.347 (m, 2H), 8.593 (d, 1H, $J = 8.5$ Hz), 10.442 (s, 1H), 11.531 (s, 1H); ^{13}C NMR (DMSO- d_6), δ : 112.51, 117.99, 119.23, 120.48 (2C), 125.08 (2C), 130.11, 130.37, 136.55, 138.55, 143.03, 144.62, 146.65, 153.85, 163.05; HR-MS: $\text{C}_{16}\text{H}_{10}\text{N}_3\text{O}_4$ [M-H] $^-$ calcd 308.0677 m/z , found 308.0675 m/z .

4.2. Lipophilicity determination by HPLC (Capacity factor k /calculated $\log k$)

A HPLC system Agilent 1200 equipped with DAD detector (Agilent, Santa Clara, CA, USA) was used. A chromatographic column Symmetry[®] C₁₈ 5 μm , 4.6 \times 250 mm, Part No. WAT054275, (Waters Corp., Milford, MA, USA) was used. The HPLC separation process was monitored and evaluated by EZChrom Elite software ver. 3.3.2 (Agilent). Isocratic elution by a mixture of MeOH p.a.

(60%) and H₂O-HPLC Mili-Q grade (40%) as a mobile phase was used. The total flow of the column was 1.0 mL/min, injection 20 µL, column temperature 40 °C and sample temperature 10 °C. The detection wavelength 210 nm was chosen. The KI methanolic solution was used for the dead time (t_D) determination. Retention times (t_R) were measured in minutes. The capacity factors k were calculated according to formula $k = (t_R - t_D)/t_D$, where t_R is the retention time of the solute, whereas t_D denotes the dead time obtained using an unretained analyte. Log k , calculated from the capacity factor k , is used as the lipophilicity index converted to log P scale. The log k values of the individual compounds are shown in Table 1.

4.3. In vitro antimycobacterial evaluation

Mycobacterium tuberculosis H37Ra ATCC 25177 and well characterised clinical isolates of *M. avium* complex CIT19/06, and *M. avium* subsp. *paratuberculosis* CIT03 were grown in Middlebrook broth (MB), supplemented with Oleic-Albumin-Dextrose-Catalase supplement (OADC, Becton Dickinson, UK) and mycobactin J (2 µg/mL). Identification of these isolates was performed using biochemical and molecular protocols. At log phase growth, a culture sample (10 mL) was centrifuged at 15,000 rpm/20 min using a bench top centrifuge (Model CR 4-12, Jouan Inc., UK). Following removal of the supernatant, the pellet was washed in fresh Middlebrook 7H9GC broth and re-suspended in fresh supplemented MB (10 mL). The turbidity was adjusted to match McFarland standard No. 1 (3×10^8 cfu) with MB broth. A further 1:20 dilution of the culture was then performed in MB broth. The antimicrobial susceptibility of all three mycobacterial species was investigated in a 96-well plate format. In these experiments, sterile deionised water (300 µL) was added to all outer-perimeter wells of the plates to minimize evaporation of the medium in the test wells during incubation. Each evaluated compound (100 µL) was incubated with each of the mycobacterial species (100 µL). Dilutions of each compound were prepared in duplicate. For all synthesized compounds, final concentrations ranged from 1000 µg/mL to 8 µg/mL. All compounds were prepared in DMSO and subsequent dilutions were made in supplemented MB. The plates were sealed with parafilm and incubated at 37 °C, for 5 days in the case of *M. avium* complex, 7 days in the case of *M. tuberculosis* and 11 days in the case of *M. avium paratuberculosis*. Following incubation, a 10% addition of alamarBlue (AbD Serotec, Kidlington, UK) was mixed into each well and readings at 570 nm and 600 nm were taken, initially for background subtraction and subsequently after 24 h re-incubation. The background subtraction is necessary for strongly coloured compounds, where the colour may interfere with the interpretation of any colour change. For non-interfering compounds, a blue colour in the well was interpreted as an absence of growth and a pink colour was scored as growth. The minimum inhibitory concentration (MIC) was defined as the lowest concentration of the compound at which no visible bacterial growth was observed, that is, the MIC is the lowest concentration that prevented a visual colour change from blue to pink. The MIC value is routinely and widely used in bacterial assays and is a standard detection limit according to the Clinical and Laboratory Standards Institute (CLSI, www.clsi.org). Rifampicin (Sigma-Aldrich) was used as the standard, as it is a clinically used antimycobacterial drug. The results are summarized in Table 1.

4.4. MTT assay

For the MTT assay, the outer wells of a 96-well plate were filled with 200 µL of sterile water, and the inner wells were filled with 100 µL of the tested compound at the concentration to be examined. Compounds were prepared as previously stated and diluted

in Middlebrook media to achieve the desired concentration. *Mycobacterium tuberculosis* H37Ra ATCC 25177 was suspended in ODAC supplemented Middlebrook broth at a MacFarland standard of 1.0 and then diluted through a 1:20 dilution using Middlebrook broth as a diluent. The diluted mycobacteria (100 µL) were added to each well containing the compound to be tested. A negative growth control was composed of 100 µL of DMSO and 100 µL of media, and the diluted mycobacteria in broth absent of inhibiting compounds were used as a positive growth control. All compounds and controls were prepared in triplicate. Plates were incubated at 37 °C for 7 days. After the incubation period, 10% well volume of MTT reagent was mixed into each well and incubated at 37 °C for 24 h. The reagent and media were then aspirated from the wells, to which 50 µL 99% propan-2-ol was then added, and plates were read at 570 nm. The absorbance readings from the cells, grown in the presence of the tested compounds, were compared with uninhibited cell growth (using DMSO as the blank) to determine the relative percent viability. The percent viability was determined through the MTT assay. The percent viability is calculated through comparison of a measured value against that of the uninhibited control: %viability = $OD_{570E}/OD_{570P} \times 100$, where OD_{570E} is the reading from the compound-exposed cells, while OD_{570P} is the reading from the uninhibited cells (positive control). Cytotoxic potential is determined by a percent viability of <70%.

4.5. In vitro cytotoxicity assay

Human monocytic leukemia THP-1 cells were used for in vitro toxicity assay. Cells were obtained from the European Collection of Cell Cultures (ECACC, Salisbury, UK) and routinely cultured in RPMI 1640 medium supplemented with 10% fetal bovine serum, 2% L-glutamine, 1% penicillin and streptomycin at 37 °C with 5% CO₂. Cells were passaged at approximately 1 week intervals. Cytotoxicity of the compounds was determined using a WST-1 assay kit (Roche Diagnostics, Mannheim, Germany) according to the manufacturer's instructions. The tested compounds were dissolved in DMSO and added in five increasing concentrations (0.37, 1.1, 3.3, 10, and 30 µM) to the cell suspension in the culture RPMI 1640 medium. The maximum concentration of DMSO in the assays never exceeded 0.1%. Subsequently, the cells were incubated for 24 h at 37 °C with 5% CO₂. For WST-1 assays, cells were seeded into 96-well plates (5×10^4 cells/well in 100 µL culture medium) in triplicate in serum-free RPMI 1640 medium and measurements were taken 24 h after the treatment with the compounds. The median inhibition concentration values, IC₅₀, were deduced through the production of a dose-response curve. All data were evaluated using GraphPad Prism 5.00 software (GraphPad Software, San Diego, CA, USA). The results are summarized in Table 1.

Acknowledgments

This study was supported by IGA VFU Brno 37/2014/FaF, 304/2015/FaF, 320/2015/FaF, 322/2015/FaF, Slovak Grant Agency VEGA 1/0770/15, by Project APVV-0061-11 and by the Irish Department of Agriculture Fisheries and Food (FIRM): Refs. 08RDCIT601 and 08RDCIT617. The system of high-performance liquid chromatography coupled to an LTQ Orbitrap XL high-resolution mass spectrometer forms a part of the National Infrastructure CzeCos/ICOS (LM2010007).

References and notes

1. World Health Organization *Global Tuberculosis Report 2014*; WHO Press: Geneva, Switzerland, 2014.
2. Wagner, D.; Young, L. S. *Infection* **2004**, *32*, 257.

3. Koul, A.; Arnoult, E.; Lounis, N.; Guillemont, J.; Andries, K. *Nature* **2011**, *469*, 483.
4. Baquero, F.; Coque, T. M.; de la Cruz, F. *Antimicrob. Agents Chemother.* **2011**, *55*, 3649.
5. Polanski, J.; Kurczyk, A.; Bak, A.; Musiol, R. *Curr. Med. Chem.* **2012**, *19*, 1921.
6. Kumar, S.; Bawa, S.; Gupta, H. *Mini-Rev. Med. Chem.* **2009**, *9*, 1648.
7. Pati, B.; Banerjee, S. *J. PharmaSciTech.* **2014**, *3*, 59.
8. Marella, A.; Tanwar, O. P.; Saha, R.; Ali, M. R.; Srivastava, S.; Akhter, M.; Shaquiquzzaman, M.; Alam, M. M. *Saudi Pharm. J.* **2013**, *21*, 1.
9. Musiol, R.; Jampilek, J.; Buchta, V.; Niedbala, H.; Podeszwa, B.; Palka, A.; Majerz-Maniecka, K.; Oleksyn, B.; Polanski, J. *Bioorg. Med. Chem.* **2006**, *14*, 3592.
10. Musiol, R.; Serda, M.; Hensel-Bielowka, S.; Polanski, J. *Curr. Med. Chem.* **2010**, *17*, 1960.
11. Cieslik, W.; Musiol, R.; Nycz, J.; Jampilek, J.; Vejsova, M.; Wolff, M.; Machura, B.; Polanski, J. *Bioorg. Med. Chem.* **2012**, *20*, 6960.
12. Sahu, K. B.; Ghosh, S.; Banerjee, M.; Maity, A.; Mondal, S.; Paira, R.; Saha, P.; Naskar, S.; Hazra, A.; Banerjee, S.; Samanta, A.; Mondal, N. B. *Med. Chem. Res.* **2013**, *22*, 94.
13. Beena; Rawat, D. S. *Med. Res. Rev.* **2013**, *33*, 693.
14. Keri, R. S.; Patil, S. A. *Biomed. Pharmacother.* **2014**, *68*, 1161.
15. Fraser, S. S. R.; Creanor, J. *Biochem. J.* **1975**, *147*, 401.
16. Hongmanee, P.; Rukseree, K.; Buabut, B.; Somsri, B.; Palittapongarnpim, P. *Antimicrob. Agents Chemother.* **2007**, *51*, 1105.
17. Darby, C. M.; Nathan, C. F. *J. Antimicrob. Chemother.* **2010**, *65*, 1424.
18. Prachayasittikul, V.; Prachayasittikul, S.; Ruchirawat, S.; Prachayasittikul, V. *Drug Des. Devel. Ther.* **2013**, *7*, 1157.
19. Sirturo. <http://www.sirturo.com/>. (April 9, 2015).
20. Gratraud, P.; Surolia, N.; Besra, G. S.; Surolia, A.; Kremer, L. *Antimicrob. Agents Chemother.* **2008**, *52*, 1162.
21. Thomas, K. D.; Adhikari, A. V.; Chowdhury, I. H.; Sumesh, E.; Pal, N. K. *Eur. J. Med. Chem.* **2011**, *46*, 2503.
22. Thomas, K. D.; Adhikari, A. V.; Telkar, S.; Chowdhury, I. H.; Mahmood, R.; Pal, N. K.; Row, G.; Sumesh, E. *Eur. J. Med. Chem.* **2011**, *46*, 5283.
23. Khan, S. R.; Singh, S.; Roy, K. K.; Akhtar, M. S.; Saxena, A. K.; Krishnan, M. Y. *Int. J. Antimicrob. Agents* **2013**, *41*, 41.
24. Naik, M.; Humnabadkar, V.; Tantry, S. J.; Panda, M.; Narayan, A.; Guptha, S.; Panduga, V.; Manjrekar, P.; Jena, L. K.; Koushik, K.; Shanbhag, G.; Jatheendranath, S.; Manjunatha, M. R.; Gorai, G.; Bathula, C.; Rudrapatna, S.; Achar, V.; Sharma, S.; Ambady, A.; Hegde, N.; Mahadevaswamy, J.; Kaur, P.; Sambandamurthy, V. K.; Awasthy, D.; Narayan, C.; Ravishankar, S.; Madhavapeddi, P.; Reddy, J.; Prabhakar, K.; Saralaya, R.; Chatterji, M.; Whiteaker, J.; McLaughlin, B.; Chiarelli, L. R.; Riccardi, G.; Pasca, M. R.; Binda, C.; Neres, J.; Dhar, N.; Signorino-Gelo, F.; McKinney, J. D.; Ramachandran, V.; Shandil, R.; Tommasi, R.; Iyer, P. S.; Narayanan, S.; Hosagrahara, V.; Kavanagh, S.; Dinesh, N.; Ghorpade, S. R. *J. Med. Chem.* **2014**, *57*, 5419.
25. Marriner, G. A.; Nayyar, A.; Uh, E.; Wong, S. Y.; Mukherjee, T.; Via, L. E.; Carroll, M.; Edwards, R. L.; Grubber, T. D.; Choi, I.; Lee, J.; Arora, K.; England, K. D.; Boshoff, H. I. M.; Barry, C. E. *Top. Med. Chem.* **2011**, *7*, 47.
26. Balcells, L.; Bates, R. H.; Young, R. J.; Alvarez-Gomez, D.; Alvarez-Ruiz, E.; Barroso, V.; Blanco, D.; Crespo, B.; Escribano, J.; Gonzalez, R.; Lozano, S.; Huss, S.; Santos-Villarejo, A.; Martin-Plaza, J. J.; Mendoza, A.; Rebollo-Lopez, M. J.; Remuinan-Blanco, M.; Lavandera, J. L.; Perez-Herran, E.; Gamo-Benito, F. J.; Garcia-Bustos, J. F.; Barros, D.; Castro, J. P.; Cammack, N. *ChemMedChem* **2013**, *8*, 313.
27. Upadhyaya, R. S.; Vandavasi, J. K.; Kardile, R. A.; Lahore, S. V.; Dixit, S. S.; Deokar, H. S.; Shinde, P. D.; Sarmah, M. P.; Chattopadhyaya, J. *Eur. J. Med. Chem.* **2010**, *45*, 1854.
28. Nayyar, A.; Monga, V.; Malde, A.; Coutinho, E.; Jain, R. *Bioorg. Med. Chem.* **2007**, *15*, 626.
29. Nayyar, A.; Jain, R. *Ind. J. Chem.* **2008**, *47B*, 117.
30. Bueno, R. V.; Braga, R. C.; Segretti, N. D.; Ferreir, E. I.; Trossini, G. H.; Andrade, C. H. *Curr. Pharm. Des.* **2014**, *20*, 4474.
31. Mathew, B.; Ross, L.; Reynolds, R. C. *Tuberculosis* **2013**, *93*, 398.
32. Paritala, H.; Carroll, K. S. *Infect. Disord. Drug Targets* **2013**, *13*, 85.
33. Joshi, S. D.; More, U. A.; Dixit, S. R.; Dubey, D.; Tripathi, A.; Kulkarni, V. H. *Ind. Am. J. Pharm. Res.* **2014**, *4*, 864.
34. Jampilek, J.; Dolezal, M.; Kunes, J.; Buchta, V.; Silva, L.; Kralova, K. *Med. Chem.* **2005**, *1*, 591.
35. Musiol, R.; Jampilek, J.; Kralova, K.; Richardson, D. R.; Kalinowski, D.; Podeszwa, B.; Finster, J.; Niedbala, H.; Palka, A.; Polanski, J. *Bioorg. Med. Chem.* **2007**, *15*, 1280.
36. Musiol, R.; Tabak, D.; Niedbala, H.; Podeszwa, B.; Jampilek, J.; Kralova, K.; Dohnal, J.; Finster, J.; Mencil, A.; Polanski, J. *Bioorg. Med. Chem.* **2008**, *16*, 4490.
37. Gonec, T.; Bobal, P.; Pesko, M.; Guo, J. H.; Kralova, K.; Kos, J.; Coffey, A.; Kollar, P.; Imramovsky, A.; Jampilek, J. *Molecules* **2012**, *17*, 613.
38. Zumla, A.; Nahid, P.; Cole, S. T. *Nat. Rev. Drug Disc.* **2013**, *12*, 388.
39. Pattabiraman, V. R.; Bode, J. W. *Nature* **2011**, *480*, 471.
40. Lavecchia, A.; Di Giovanni, C. *Curr. Med. Chem.* **2013**, *20*, 2839.
41. Gonec, T.; Kos, J.; Zadrazilova, I.; Pesko, M.; Keltosova, S.; Tengler, J.; Bobal, P.; Kollar, P.; Cizek, A.; Kralova, K.; Jampilek, J. *Bioorg. Med. Chem.* **2013**, *21*, 6531.
42. Kos, J.; Nevin, E.; Soral, M.; Kushkevych, I.; Gonec, T.; Bobal, P.; Kollar, P.; Coffey, A.; O'Mahony, J.; Liptaj, T.; Kralova, K.; Jampilek, J. *Bioorg. Med. Chem.* **2015**, *23*, 2035.
43. Musiol, R.; Jampilek, J.; Podeszwa, B.; Finster, J.; Tabak, D.; Dohnal, J.; Polanski, J. *Cent. Eur. J. Chem.* **2009**, *7*, 586.
44. Palmer, M. H. *The Structure and Reactions of Heterocyclic Compounds*; Edward Arnold: London, UK, 1967; pp 105–144.
45. Zheng, H.; Lu, L.; Wang, B.; Pu, S.; Zhang, X.; Zhu, G.; Shi, W.; Zhang, L.; Wang, H.; Wang, S.; Zhao, G.; Zhang, Y. *PLoS One* **2008**, *3*, e2375.
46. Havlik, J. A.; Horsburgh, C. R.; Metchock, B.; Williams, P.; Fann, S. A.; Thompson, S. E. *J. Infect. Dis.* **1992**, *165*, 577.
47. Rath, T.; Roderfeld, M.; Blocher, S.; Rhode, A.; Basler, T.; Akineden, O.; Abdulmawjood, A.; Halwe, J. M.; Goethe, R.; Bulte, M.; Roeb, E. *BMC Gastroenterol.* **2011**, *11*, 34.
48. Bueno, J. Antitubercular in vitro drug discovery: tools for begin the search. In *Understanding Tuberculosis – New Approaches to Fighting against Drug Resistance*; Cardona, P. J., Ed.; InTech: Rijeka, Croatia, 2012; pp 147–168.
49. Gonec, T.; Kos, J.; Nevin, E.; Govender, R.; Pesko, M.; Kushkevych, I.; Oravec, M.; Kollar, P.; O'Mahony, J.; Kralova, K.; Coffey, A.; Jampilek, J. *Molecules* **2014**, *19*, 10386.
50. Suffness, M.; Douros, J. J. *Nat. Prod.* **1982**, *45*, 1.

č.	citace	ISSN
4	PESKO, M, J KOS , K KRALOVA a J JAMPILEK. Inhibition of photosynthetic electron transport by 6-hydroxynaphthalene-2-carboxanilides. <i>INDIAN JOURNAL OF CHEMISTRY SECTION B-ORGANIC CHEMISTRY INCLUDING MEDICINAL CHEMISTRY</i> . 2015, 54 (12), 1511–1517.	0376-4699

Inhibition of photosynthetic electron transport by 6-hydroxynaphthalene-2-carboxanilides

Matus Pesko^a, Jiri Kos^b, Katarina Kralova^c & Josef Jampilek^{*b}

^aDepartment of Environmental Ecology, Faculty of Natural Sciences, Comenius University, Mlynska dolina Ch-2, 842 15 Bratislava, Slovakia

^bDepartment of Chemical Drugs, Faculty of Pharmacy, University of Veterinary and Pharmaceutical Sciences, Palackeho 1/3, 612 42 Brno, Czech Republic

^cInstitute of Chemistry, Faculty of Natural Sciences, Comenius University, Mlynska dolina Ch-2, 842 15 Bratislava, Slovakia
E-mail: josef.jampilek@gmail.com

Received 31 March 2015; accepted (revised) 8 August 2015

Inhibition of photosynthetic electron transport (PET) in spinach chloroplasts by 6-hydroxynaphthalene-2-carboxanilides has been investigated. The PET inhibiting activity of the studied compounds depends on compound lipophilicity, on the position of substituents on the anilide moiety as well as on electron-accepting and electron-donating properties of these substituents. The most active PET inhibitors are *m*-substituted derivatives; the lowest activity is shown by the *o*-substituted ones. The most potent PET inhibitor is 6-hydroxy-*N*-(3-trifluoromethylphenyl)naphthalene-2-carboxamide (IC₅₀ = 10.8 μmol/L). Study of chlorophyll *a* fluorescence in the suspension of spinach chloroplasts in the presence of studied compounds confirms their site of action in PS II, and it can be assumed that the inhibitory site of action of the studied compounds is situated on the acceptor side of PS II at Q_B site.

Keywords: Chlorophyll *a* fluorescence, chloroplasts, hydroxynaphthalene carboxanilides, inhibition, photosynthetic electron transport, *Spinacia oleracea* L.

Herbicides are used routinely to control noxious plants. Urea- and triazine-based herbicides, with a common chemical structure of *sp*² hybrid bound to N, O, or =CH and attached to a lipophilic substituent, belong to the class of herbicides interacting with photosystem (PS) II. They have the same site of action but their activity is affected by the various side chains¹. Shipman suggested that polar components of the herbicides bind *via* coulombic interactions at or near a highly polar protein site, probably a protein salt bridge or the terminus of an α -helix on Q_B protein (denoted also as D₁ protein)². Herbicides that target PS II compete with the native electron acceptor plastoquinone (PQ) for binding at the Q_B site in the D₁ subunit and thus block the electron transfer from Q_A to Q_B. Thus, the mechanism of action of these herbicides is displacement of Q_B from its binding site on Q_B protein, which is situated on the acceptor side of PS II. Binding sites of herbicides to Q_B protein were described^{1,3}. On the other hand, some compounds could inhibit photosynthetic electron transport (PET) also on the donor side of PS II acting in D[•] or Z[•]/D[•] intermediates⁴⁻⁶. For several herbicides

acting as PET inhibitors by reversible binding to PS II (a membrane-protein complex in the thylakoid membranes) that catalyses the oxidation of water and the reduction of PQ (Ref 7) and thereby inhibit photosynthesis^{1,8,9}, the presence of an amide-like moiety is characteristic¹⁰⁻¹⁶. The –NHCO– group is an important functional group that is able, due to its electronic properties, to interact and bind with a number of enzymes/receptors and affect the biological response by means of these target sites.

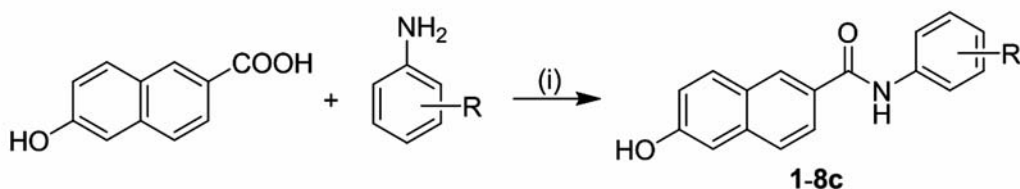
Recently it was found that ring-substituted 1-hydroxynaphthalene-2-carboxanilides¹⁶, 2-hydroxynaphthalene-2-carboxanilides¹⁷ and 3-hydroxynaphthalene-2-carboxanilides¹⁸ showing antibacterial activity inhibited PET in PS II, and their PET-inhibiting activity depended on the position of the substituent on the anilide ring, its electronic parameters as well as on the compound lipophilicity. Structurally similar 6-hydroxynaphthalene-2-carboxanilides exhibited activity against *Mycobacterium tuberculosis* H37Ra, *M. avium* complex and *M. avium* subsp. *paratuberculosis*, whereby compounds substituted in C'(3) and C'(4)

preferentially inhibited growth of *M. tuberculosis* contrary to C'(2) and C'(3) substituted ones that showed potency against both nontuberculous mycobacteria. A significant decrease of mycobacterial cell metabolism (monitored as a viability of *M. tuberculosis* H37Ra) was also observed¹⁹.

The goal of the present work is to investigate the inhibitory effect of twenty two 6-hydroxynaphthalene-2-carboxanilides on the photosynthetic electron transport in spinach (*Spinacia oleracea* L.) chloroplasts using the Hill reaction and fluorescence spectroscopy and to discuss the structure-activity relationships between the chemical structure, physical properties and PET-inhibiting activities of the tested compounds, the anilide moiety of which was modified by groups with electron-accepting and electron-donating properties. A good correlation between microbiological activity and herbicidal effect was described in previous studies^{15-17,20-24}. This idea is based on the fact that both pharmaceuticals and pesticides are designed to target particular biological functions, and in some cases these functions overlap in their molecular target sites, or they target similar processes or molecules. Taking into the consideration that herbicides may also have molecular sites of action in mammals, until recently most pharmaceutical companies had pesticide divisions. All compounds generated by either division of the company were evaluated for both pesticide and pharmaceutical uses. In the past, some leading pesticides have become pharmaceuticals and *vice versa*²⁵⁻²⁸.

Results and Discussion

Ring-substituted 6-hydroxynaphthalene-2-carboxanilides **1-8c** were prepared by microwave-assisted synthesis in one step, see **Scheme I**. At first the carboxyl group was activated with phosphorus trichloride and the final amide was immediately formed by aminolysis of the acyl chloride with ring-substituted aniline in dry chlorobenzene¹⁹.



R = H, OCH₃, CH₃, F, Cl, Br, CF₃, NO₂

(i) PCl₃, chlorobenzene, microwave irradiation (MW)

Scheme I

Lipophilicity is a property that has a major effect on activity, because bioactive compounds mostly cross biological membranes through passive transport, which strongly depends on their lipophilicity. Lipophilicity has been studied and applied as an important drug property for decades. This parameter was measured by means of RP-HPLC and expressed as logarithm of capacity factor *k* (Ref 19). The experimentally estimated log *k* values of ring-substituted 6-hydroxynaphthalene-2-carboxanilides **1-8c** as well as log *P* values calculated using ACD/Percepta ver. 2012 (Advanced Chemistry Development, Inc., Toronto, ON, Canada, 2012) are listed in **Table I**.

The highest experimentally-determined lipophilicity was found for 6-hydroxy-*N*-(4-trifluoromethylphenyl)naphthalene-2-carboxamide (log *k* = 1.0133; **7c**), while 6-hydroxy-*N*-(4-methoxyphenyl)naphthalene-2-carboxamide (log *k* = 0.3313; **2c**) showed the lowest log *k* value. It could be noted that the experimentally-determined lipophilicity (log *k*) of the discussed compounds poorly correlates with the calculated values of compounds **1-8c**, nevertheless these proven poor match between the experimentally-determined and calculated values of lipophilicity corresponds to observations described recently by Karabulut *et al.*²⁹ Based on these facts it can be supposed that the differences between the predicted and the experimentally-determined lipophilicity values within the series of 6-hydroxynaphthalene-2-carboxanilides are caused by intermolecular interactions between phenolic and carbonyl moieties in individual molecules in a polar environment²⁹. Strong intramolecular interactions of spatially close phenolic and carbonyl moieties were reported previously for structurally similar compounds^{12,17}. It can be stated that the log *k* values better specify lipophilicity within the series of the studied compounds than the predicted log *P* values.

Table I — Calculated values of lipophilicity $\log P$, experimentally determined values of lipophilicity $\log k$, predicted values of electronic Hammett's σ parameters of R substituents and IC_{50} values related to PET inhibition in spinach chloroplasts in comparison with 3-(3,4-dichlorophenyl)-1,1-dimethylurea (DCMU) standard

Compd	R	$\log P^a$	$\log k^{19}$	σ^a	IC_{50} [$\mu\text{mol/L}$]
1	H	3.33	0.6612	0	108
2a	2-OCH ₃	3.36	0.6039	-0.28	154
2b	3-OCH ₃	3.37	0.4463	0.12	164
2c	4-OCH ₃	3.29	0.3313	-0.27	ND
3a	2-CH ₃	3.63	0.3690	-0.17	470
3b	3-CH ₃	3.63	0.6086	-0.07	216
3c	4-CH ₃	3.63	0.6227	-0.17	226
4a	2-F	3.36	0.4921	0.06	ND
4b	3-F	3.54	0.5766	0.34	25.7
4c	4-F	3.32	0.6726	0.06	234.5
5a	2-Cl	3.81	0.6777	0.22	184
5b	3-Cl	4.44	0.7684	0.37	37.6
5c	4-Cl	3.89	0.7947	0.23	62.3
6a	2-Br	4.10	0.7486	0.22	160
6b	3-Br	4.46	0.8767	0.39	21.0
6c	4-Br	4.22	0.8884	0.23	118
7a	2-CF ₃	4.06	0.5623	0.51	353
7b	3-CF ₃	4.17	0.9558	0.43	10.8
7c	4-CF ₃	4.05	1.0133	0.51	55.0
8a	2-NO ₂	3.44	0.8553	0.77	151
8b	3-NO ₂	3.48	0.8533	0.71	41.2
8c	4-NO ₂	3.34	0.5911	0.78	385
DCMU	-	-	-	-	1.9

^aCalculated using ACD/Percepta ver. 2012; ND = not determined

Electronic parameters expressed as Hammett's σ parameters of substituents in the anilide part of compounds **1–8c** were predicted using ACD/Percepta ver. 2012, see **Table I**; they ranged from -0.28/-0.27 (compounds **2a,c** 2-OCH₃, 4-OCH₃) to 0.77/0.78 (compounds **8a,c** 2-NO₂, 4-NO₂).

Biological Evaluation (Inhibition of photosynthetic electron transport)

The PET inhibiting activity of the studied 6-hydroxynaphthalene-2-carboxanilides was evaluated and has been expressed by IC_{50} values, *i.e.*, molar concentration of the compounds causing 50% inhibition relative to the untreated control. Due to low activity IC_{50} values could not be determined for compounds **2c** (R = 4-OCH₃) and **4a** (R = 2-F). The IC_{50} values of the rest of the tested compounds varied

in wide concentration range, from 10.8 $\mu\text{mol/L}$ (**7b**, R = 3-CF₃) to 470 $\mu\text{mol/L}$ (**3a**, R = 2-CH₃), see **Table I**. The solubility of studied compounds in testing medium was satisfactory and the activity strongly depended on the position of the substituent on the phenyl ring. The most active compounds were *m*-substituted; the less active were *o*-substituted. The reduced activity of *o*-substituted derivatives could be connected with intramolecular interactions of the substituent in position 2 with the amide group, which could adversely affect its possible interaction with constituents of the photosynthetic apparatus.

The dependence of the PET-inhibiting activity expressed as $\log(1/IC_{50})$ on the lipophilicity of the compounds expressed as $\log P$ is illustrated in **Figure 1a**. The PET-inhibiting activity of *o*-substituted derivatives was characterized by great variance, and no correlation between corresponding IC_{50} values and $\log P$ was observed. On the other hand, the IC_{50} values of *m*- and *p*-substituted derivatives were significantly affected by compound lipophilicity and the dependences of $\log(1/IC_{50})$ on $\log P$ were bilinear (**Figure 1a**). The optimal lipophilicity for *p*-substituted derivatives was found to be $\log P$ approx. 4.0 and for *m*-substituted approx. 3.8. Further lipophilicity increase was reflected in declined PET inhibiting activity (**Figure 1a**). However, it could be noted that the PET-inhibiting activity of **3b** (R = 3-CH₃) was lower than expected. On the other hand, the PET inhibition linearly increases with increasing $\log k$ not only for *o*- and *p*-substituted compounds ($r = 0.8571$, $n = 6$ and $r = 0.8769$, $n = 6$), but also for more active *m*-substituted ones ($r = 0.7603$, $n = 7$), see **Figure 1b**. The discrepancies between the presented dependences of $\log(1/IC_{50})$ on $\log P$ and $\log(1/IC_{50})$ on $\log k$ are likely due to intermolecular interactions of the studied compounds, which could modify the resulting compound lipophilicity and which are reflected only in experimentally-determined $\log k$ values. Such interactions were reported previously for structurally similar compounds^{12,17}.

The dependence of PET-inhibiting activity on the values of R substituent was found to be bilinear for the *m*-substituted ($r = 0.9447$, $n = 6$) and the *p*-substituted ($r = 0.7967$, $n = 5$) compounds (similarly as the above-discussed dependence of $\log(1/IC_{50})$ on $\log P$), while no correlation between the corresponding IC_{50} values and $\log k$ was observed for

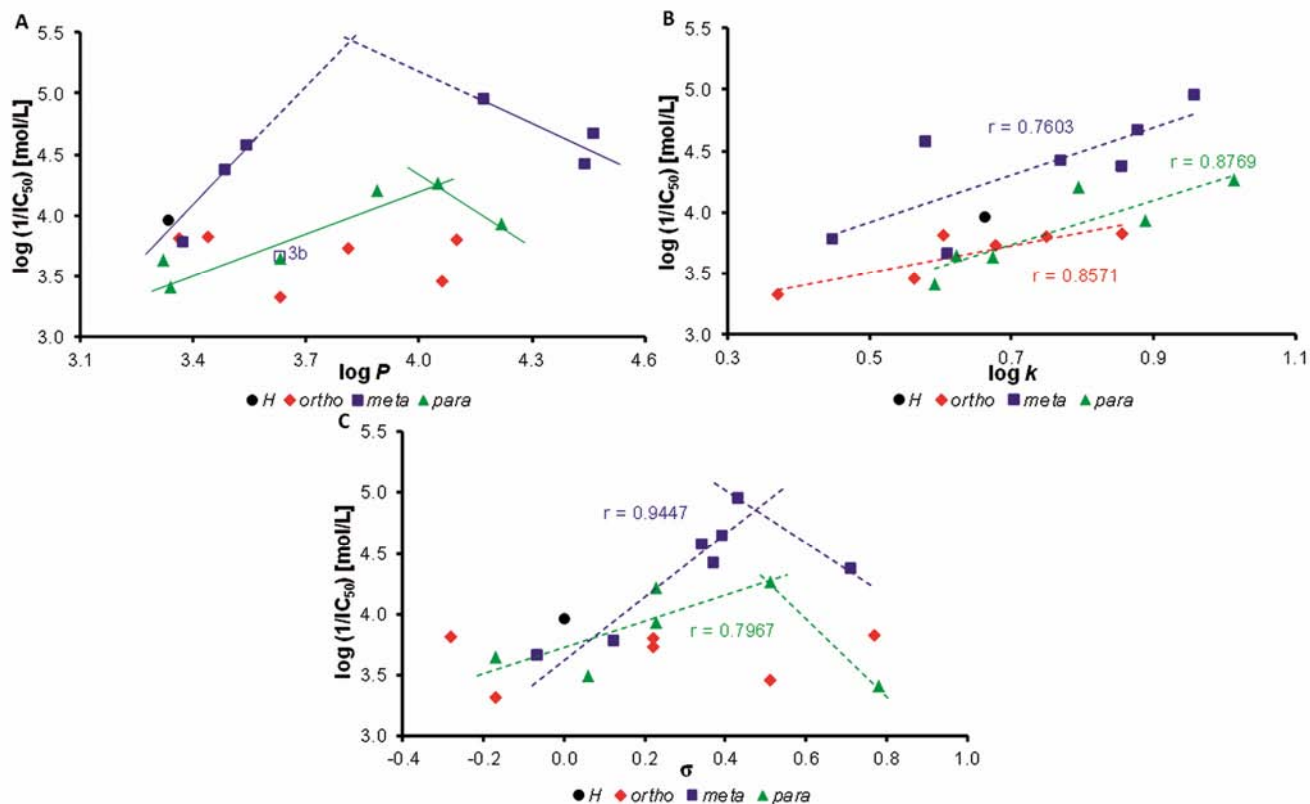


Figure 1 — Dependence of PET inhibiting activity $\log(1/IC_{50})$ [mol/L] of tested compounds on lipophilicity expressed as $\log P$ (A) or $\log k$ (B) and on Hammett's σ constants of R substituent (C); (Eliminated compound 3-CH₃ (3b) in A is marked by empty square)

the *o*-substituted ones, see **Figure 1c**. The optimal value for *m*- and *p*-substituted derivatives was similar, approximately 0.5; the activity decreased with further increase in values.

In the studied 6-hydroxynaphthalene-2-carboxanilides, due to the proximity of the *o*-substituent on the aniline ring to the carboxamide group, the twist of the aniline ring plane towards the carboxamide group, *i.e.* towards the whole naphthalene core, occurs³⁰. The described process results in the violation of the molecule planarity, implying subsequent conjugation of the π -bonds of the phenyl ring through the NH fragment to the carbonyl group³¹. Consequently, the different electronic density (charge) at the carbonyl moiety appears, which can influence the potential binding of the carboxamide group to possible binding sites in the photosynthetic apparatus. In the case of *m*- and *p*-substituted derivatives, the described secondary steric effect did not manifest. *p*-Substituted derivatives should have practically a linear/planar structure as was, for example, described for a similar

type of molecule, where the X-ray analysis displayed a planar structure^{32,33}. The lower PET-inhibiting activity of *o*-substituted derivatives as compared to *m*- and *p*-substituted ones was also observed for several esters of 2-, 3- and 4-substituted alkoxyphenyl-carbamic acids^{20,34} as well as for previously studied 1-hydroxynaphthalene-2-carboxanilides¹⁶, while for ring-substituted 2-hydroxynaphthalene-1-carboxanilides the PET-inhibiting activity was not affected by the position of the substituent on the phenyl ring¹⁷. On the other hand, the dependence of PET-inhibiting activity on σ was found to be bilinear with the optimum $\sigma = 0.51$ for *o*-, *m*- and *p*-substituted 2-hydroxynaphthalene-1-carboxanilides¹⁷, $\sigma = 0.43$ for *m*- and *p*-substituted 1-hydroxynaphthalene-2-carboxanilides¹⁶ and $\sigma = 0.71$ for *o*-, *m*- and *p*-substituted 3-hydroxynaphthalene-2-carboxanilides¹⁸.

By the addition of 1,5-diphenylcarbazide (DPC), an artificial electron donor acting in Z^*/D^* intermediate on the donor side of PS II (Ref 35), to chloroplasts treated with the studied compounds, in which PET

was inhibited by about 90-93%, PET was practically completely restored, however only in the presence of very high DPC concentration, approximately 2 mmol/L. Based on the fact that DPC can alter the binding of compounds with herbicidal activity, *e.g.*, atrazin or metribuzin, presumably because of overlapping of the binding domain in the Q_B pocket, but its effect on the Q_B site can affect PQ reduction only at relatively high concentrations (>2 mol/L)^{36,37}, it could be assumed that the inhibitory site of action of the studied compounds is situated on the acceptor side of PS II, in the section at Q_B site. However, for PS II herbicides such are DCMU or atrazin also a second binding site situated on the donor side of PS II near Z^*/D^* intermediates and the high-affinity Mn-binding sites was reported³⁸⁻⁴⁰. Similarly, using EPR spectroscopy it was found that the site of action of 5-bromo- and 3,5-dibromo-2-hydroxy-*N*-phenylbenzamides⁶, phenylcarbamates and phenylthiocarbamates⁴¹ and *N*-phenylpyrazine-2-carboxamides⁵ in the photosynthetic apparatus is also situated on the donor side of PS 2, in D^* or in the Z^*/D^* intermediates. Therefore the second site of action of the studied 6-hydroxynaphthalene-2-carboxanilides situated on the donor side of PS II could not be excluded.

The studied compounds affected chlorophyll *a* (Chla) fluorescence in spinach chloroplasts indicating their interactions with constituents of the photosynthetic apparatus. The fluorescence emission spectra of Chla in spinach chloroplasts treated with compound **7b** are shown in **Figure 2a**. The decreased intensity of the emission band at 686 nm belonging to the Chla-protein complexes occurring mainly in photosystem II (Ref 42) suggested PS II as the site of action of the studied inhibitors. The extent of perturbation of Chla-protein complexes in the thylakoid membrane is reflected in the sharpness of the decreased fluorescence of the pigment (see **Figure 2b**). As shown in **Figure 2b**, the rate of the decline of Chla fluorescence with increasing concentration of the compound correlated with its PET inhibiting activity expressed by IC_{50} value. Perturbation of Chla-protein complexes increased in the following order: **3b** ($IC_{50} = 289$ mol/L) < **5a** ($IC_{50} = 80.4$ mol/L) < **7b** ($IC_{50} = 10.8$ mol/L). A similar decrease of Chla fluorescence in plant chloroplasts was also observed previously after treatment with ring-substituted 1-hydroxynaphthalene-2-carboxanilides¹⁶ and 2-hydroxynaphthalene-1-carboxanilides¹⁷, 5-bromo-

and 3,5-dibromo-2-hydroxy-*N*-phenylbenzamides⁶ or ring-substituted 4-arylamino-7-chloroquinolinium chlorides⁴³. Hsu and Lee who examined the effect of DCMU on the fluorescence of PS II preparations reported that the lowering of the fluorescence yield was not due to an inhibition on the donor side of PS II but to a non-photochemical quenching by oxidized PQ (Ref 44). The ability of the PQ pool in the oxidized form to quench the fluorescence of isolated thylakoids was described by Vernotte *et al.*⁴⁵ and Thielen and van Gorkom⁴⁶; however PQ acts more effectively as a deexcitation trap only for certain chlorophyll species responsible for fluorescence emission, such as those emitting at 687, 665 and 650 nm⁴⁴.

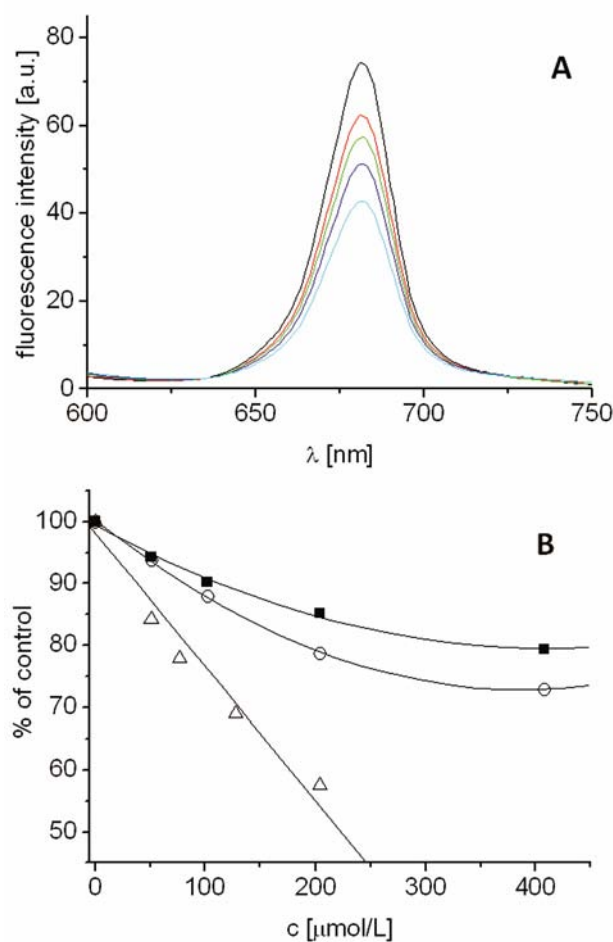


Figure 2 — Fluorescence emission spectra of chlorophyll *a* in untreated spinach chloroplasts in presence of compound **7b**: 0 μmol/L (black line), 51 μmol/L (red line), 76.5 μmol/L (green line), 127.5 μmol/L (blue line) and 204 μmol/L (cyan line) (ex = 436 nm) (A) and dependence of fluorescence intensity of chlorophyll *a* expressed as % of control on concentration of compounds **3b** (squares), **5a** (circles) and **7b** (triangles) (B)

The above presented results indicate a significant effect of lipophilicity and the electron properties of the R substituent on the biological activity of the tested compounds. It is important to note that a correlation between the antitubercular (*M. tuberculosis* H37Ra ATCC 25177)¹⁹ and the PET-inhibiting activity (expressed by MIC and IC₅₀ [μmol/L], respectively) of compounds substituted in *m*-position of aniline ring, *i.e.* compounds showing the highest activity in both tests, was found, for example: **7b** (R = 3-CF₃, MIC = 24 mol/L, IC₅₀ = 10.8 mol/L), **6b** (R = 3-Br, MIC = 23 mol/L, IC₅₀ = 21.0 mol/L) and **4b** (R = 3-F, MIC = 28 mol/L, IC₅₀ = 25.7 mol/L). This fact supports the hypothesis that for high activity of the discussed compounds transport through the mycobacterial or thylakoid membrane and suitable distribution of electron charge in the molecule, *i.e.* rather an electron-deficiency system, are preferable.

Experimental Section

Chemistry

The detailed synthetic pathway and complete characterization of compounds **1–8c** as well as lipophilicity determination using HPLC (capacity factor *k* /calculated log *k*) are provided in Kos *et al.*¹⁹ All the studied compounds are presented in **Table I**.

Study of inhibition of photosynthetic electron transport (PET) in spinach chloroplasts

Chloroplasts were prepared from spinach (*Spinacia oleracea* L.) according to Masarovicova and Kralova⁴⁷. The inhibition of photosynthetic electron transport (PET) in spinach chloroplasts was determined spectrophotometrically (Genesys 6, Thermo Scientific, USA), using an artificial electron acceptor 2,6-dichlorophenol-indophenol (DCIPP) according to Kralova *et al.*⁴⁸, and the rate of photosynthetic electron transport was monitored as a photoreduction of DCIPP. The measurements were carried out in phosphate buffer (0.02 mol/L, pH 7.2) containing sucrose (0.4 mol/L), MgCl₂ (0.005 mol/L) and NaCl (0.015 mol/L). The chlorophyll content was 30 mg/L in these experiments and the samples were irradiated (~100 W/m² with 10 cm distance) with a halogen lamp (250 W) using a 4 cm water filter to prevent warming of the samples (suspension temperature 22°C). The studied compounds were dissolved in DMSO due to their limited aqueous solubility. The applied DMSO concentration (up to

4%) did not affect the photochemical activity in spinach chloroplasts. The inhibitory efficiency of the studied compounds was expressed by IC₅₀ values, *i.e.*, by molar concentration of the compounds causing 50% inhibition relative to the untreated control. The comparable IC₅₀ value for a selective herbicide 3-(3,4-dichlorophenyl)-1,1-dimethylurea, DCMU (Diuron[®]) was about 1.9 μmol/L. The results are summarized in **Table I**.

The emission fluorescence spectra were recorded on a fluorescence spectrophotometer F-2000 (Hitachi, Tokyo, Japan) at RT (24°C). The samples of chloroplast suspension (10 mg chlorophyll/L) with and without the studied inhibitor were excited at 436 nm using a slit width of 10 nm and were kept in the dark for 2 min prior to the measurement. Due to low aqueous solubility the compounds were added to a chloroplast suspension in DMSO solution. The DMSO concentration in all samples was the same as in the control (10%).

Conclusion

Twenty-two new antimycobacterially effective ring-substituted 6-hydroxynaphthalene-2-carboxanilides were investigated for their ability to inhibit photosynthetic electron transport (PET) in spinach (*Spinacia oleracea* L.) chloroplasts. The most active PET inhibitors were *m*-substituted derivatives, the lowest activity was shown by the *o*-substituted ones. The most potent PET inhibitor was 6-hydroxy-*N*-(3-trifluoromethylphenyl)naphthalene-2-carboxamide (**7b**, IC₅₀ = 10.8 μmol/L). The PET inhibiting activity of the studied compounds depended on the position of substituents on the anilide moiety, on compound lipophilicity (linear increase with increasing lipophilicity expressed as log *k*), as well as on electron-accepting and electron-donating properties of these substituents (bilinear for *m*- and *p*-substituted compounds with optimum approx. ≈ 0.5). The study of chlorophyll *a* fluorescence in the suspension of spinach chloroplasts in the presence of the studied compounds confirmed their site of action in PS II, and it could be assumed that the inhibitory site of action of the studied compounds is situated on the acceptor side of PS II at Q_B site.

Acknowledgments

This study was supported by IGA VFU Brno 37/2014/Fa and 322/2015/FaF and by Project APVV-0061-11.

References

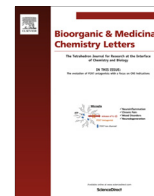
- 1 Trebst A & Draber W, "Structure activity correlations of recent herbicides in photosynthetic reactions" in, *Advances in Pesticide Science*, edited by Greissbuehler H (Pergamon Press, Oxford), **1979**, pp.223–234.
- 2 Shipman L L, *J Theor Biol*, **90**, **1981**, 123.
- 3 Pfister K & Arntzen C J, *Z Naturforsch*, **34c**, **1979**, 996.
- 4 Kralova K, Sersen F, Kubicova L & Waisser K, *Chem Pap*, **53**, **1999**, 328.
- 5 Dolezal M, Kralova K, Sersen F & Miletin M, *Folia Pharm Univ Carol*, **26**, **2001**, 13.
- 6 Kralova K, Sersen F, Pesko M, Waisser K & Kubicova L, *Chem Pap*, **68**, **2014**, 46.
- 7 Draber W, Tietjen K, Kluth J F & Trebst A, *Angew Chem*, **3**, **1991**, 1621.
- 8 Tischer W & Strotmann H, *Biochim Biophys Acta*, **460**, **1977**, 113.
- 9 Bowyer J R, Camilleri P & Vermaas W F J, "Photosystem II and its interaction with herbicides" in, *Herbicides, Topics in Photosynthesis*, Volume 10, edited by Baker N R and Percival M P (Elsevier, Amsterdam), **1991**, pp.27–85.
- 10 Good N E, *Plant Physiol*, **36**, **1961**, 788.
- 11 Dolezal M, Cmedlova P, Palek L, Vinsova J, Kunes J, Buchta V, Jampilek J & Kralova K, *Eur J Med Chem*, **43**, **2008**, 1105.
- 12 Musiol R, Tabak D, Niedbala H, Podeszwa B, Jampilek J, Kralova K, Dohnal J, Finster J, Mencil A & Polanski J, *Bioorg Med Chem*, **16**, **2008**, 4490.
- 13 Otevrel J, Mandelova Z, Pesko M, Guo J, Kralova K, Sersen F, Vejsova M, Kalinowski D, Kovacevic Z, Coffey A, Csollei J, Richardson D R & Jampilek J, *Molecules*, **15**, **2010**, 8122.
- 14 Imramovsky A, Pesko M, Kralova K, Vejsova M, Stolarikova J, Vinsova J & Jampilek J, *Molecules*, **16**, **2011**, 2414.
- 15 Imramovsky A, Pesko M, Monreal-Ferriz J, Kralova K, Vinsova J & Jampilek J, *Bioorg Med Chem Lett*, **21**, **2011**, 4564.
- 16 Gonec T, Kos J, Zadrazilova I, Pesko M, Keltosova S, Tengler J, Bobal P, Kollar P, Cizek A, Kralova K & Jampilek J, *Bioorg Med Chem*, **21**, **2013**, 6531.
- 17 Gonec T, Kos J, Zadrazilova I, Pesko M, Govender R, Keltosova S, Chambel B, Pereira D, Kollar P, Imramovsky A, O'Mahony J, Coffey A, Cizek A, Kralova K & Jampilek J, *Molecules*, **18**, **2013**, 9397.
- 18 Kos J, Zadrazilova I, Pesko M, Keltosova S, Tengler J, Gonec T, Bobal P, Kauerova T, Oravec M, Kollar P, Cizek A, Kralova K & Jampilek J, *Molecules*, **18**, **2013**, 7977.
- 19 Kos J, Nevin E, Soral M, Kushkevych I, Gonec T, Bobal P, Kollar P, Coffey A, O'Mahony J, Liptaj T, Kralova K & Jampilek J, *Bioorg Med Chem*, **23**, **2015**, 2035.
- 20 Kralova K, Sersen F & Cizmarik J, *Gen Physiol Biophys*, **11**, **1992**, 261.
- 21 Kralova K, Bujdakova H, Kuchta T & Loos D, *Pharmazie*, **49**, **1994**, 460.
- 22 Kralova K, Kallova J, Loos D & Devinsky F, *Pharmazie*, **49**, **1994**, 857.
- 23 Kralova K, Bujdakova H & Cizmarik J, *Pharmazie*, **50**, **1995**, 440.
- 24 Kralova K, Perina M, Waisser K & Jampilek J, *Med Chem*, **11**, **2015**, 156.
- 25 Shaner D L, *Pest Manag Sci*, **2004**, **60**, 17.
- 26 Delaney J, Clarke E, Hughes D & Rice M, *Drug Discov Today*, **11**, **2006**, 839.
- 27 Duke S O, *Weed Sci*, **58**, **2010**, 334.
- 28 Myung K & Klittich C J, *Drug Discov Today*, **20**, **2015**, 7.
- 29 Karabulut S, Namli H, Kurtaran R, Yildirim L T & Leszczynski J, *J Mol Graph Model*, **48**, **2014**, 1.
- 30 Arjunan V, Santhanam R, Rani T, Rosi H & Mohan S, *Spectrochim Acta A*, **104**, **2013**, 182.
- 31 Waisser K, Dolezal R, Cizmarik J, Malik I & Kaustova J, *Folia Pharm Univ Carol*, **35/36**, **2007**, 45.
- 32 Majerz-Maniecka K A, Musiol R, Nitek W, Oleksyn B J & Polanski J, *Bioorg Med Chem Lett*, **16**, **2006**, 1005.
- 33 Bobal P, Suján J, Otevrel J, Imramovsky A, Padelkova Z & Jampilek J, *Molecules*, **17**, **2012**, 1292.
- 34 Kralova K, Sersen F & Cizmarik J, *Chem Pap*, **46**, **1992**, 266.
- 35 Izawa S, "Acceptors and donors for chloroplast electron transport" in, *Methods Enzymol*, Volume 69, Part C, edited by Colowick P and Kaplan N O (Academic Press, London), **1980**, pp.413–434.
- 36 Purcell M, Leroux G & Carpentier R, *Biochim Biophys Acta*, **1058**, **1991**, 374.
- 37 Borse T H, Maheswarim V L & Baviskar M P, *J Plant Biochem Biotechnol*, **9**, **2000**, 119.
- 38 Renger G, *Biochim Biophys Acta*, **314**, **1973**, 113.
- 39 Carpentier R, Fuerst E P, Nakatani H Y & Arntzen C J, *Biochim Biophys Acta*, **808**, **1985**, 293.
- 40 Kamachi H, Tamura N & Inoue H, *Plant Cell Physiol*, **33**, **1992**, 437.
- 41 Sersen F, Kralova K & Macho V, *Pest Biochem Physiol*, **68**, **2000**, 113.
- 42 Govindjee, *Aust J Plant Physiol*, **22**, **1995**, 131.
- 43 Otevrel J, Bobal P, Zadrazilova I, Govender R, Pesko M, Keltosova S, Koleckarova P, Marsalek P, Imramovsky A, Coffey A, O'Mahony J, Kollar P, Cizek A, Kralova K & Jampilek J, *Molecules*, **18**, **2013**, 10648.
- 44 Hsu B D & Lee J Y, *J Photochem Photobiol B*, **30**, **1995**, 57.
- 45 Vernotte C, Etienne A L & Briantais J M, *Biochim Biophys Acta*, **545**, **1979**, 519.
- 46 Thielen A P G M & van Gorkom H J, *FEBS Lett*, **129**, **1981**, 205.
- 47 Masarovicova E & Kralova K, "Approaches to measuring plant photosynthesis activity" in, *Handbook of Photosynthesis*, 2nd edn., edited by Pessaraki M (Taylor and Francis Group, Boca Raton), **2005**, pp. 617–656.
- 48 Kralova K, Sersen F & Sidoova E, *Chem Pap*, **46**, **1992**, 348.

č.	citace	ISSN
5	JAMPILEK, J, K KRALOVA, M PESKO a J KOS. Ring-substituted 8-hydroxyquinoline-2-carboxanilides as photosystem II inhibitors. <i>BIOORGANIC & MEDICINAL CHEMISTRY LETTERS</i> [online]. 2016, 26 (16), 3862–3865. Dostupné z: doi: 10.1016/j.bmcl.2016.07.021	0960-894X



Contents lists available at ScienceDirect

Bioorganic & Medicinal Chemistry Letters

journal homepage: www.elsevier.com/locate/bmcl

Ring-substituted 8-hydroxyquinoline-2-carboxanilides as photosystem II inhibitors

Josef Jampilek^{a,*}, Katarina Kralova^b, Matus Pesko^c, Jiri Kos^d^a Department of Pharmaceutical Chemistry, Faculty of Pharmacy, Comenius University, Odbojarov 10, 832 32 Bratislava, Slovakia^b Institute of Chemistry, Faculty of Natural Sciences, Comenius University, Mlynska dolina Ch-2, 842 15 Bratislava, Slovakia^c Department of Environmental Ecology, Faculty of Natural Sciences, Comenius University, Mlynska dolina Ch-2, 842 15 Bratislava, Slovakia^d Department of Chemical Drugs, Faculty of Pharmacy, University of Veterinary and Pharmaceutical Sciences, Palackeho 1/3, 612 42 Brno, Czech Republic

ARTICLE INFO

Article history:

Received 2 June 2016

Revised 6 July 2016

Accepted 7 July 2016

Available online 7 July 2016

Keywords:

8-Hydroxyquinolines

Hill reaction

Photosystem II

Structure–activity relationships

ABSTRACT

Ring-substituted 8-hydroxyquinoline-2-carboxanilides inhibited photosynthetic electron transport (PET) through photosystem (PS) II. Their inhibitory efficiency depended on the compound lipophilicity, the electronic properties of the substituent R and the position of the substituent R on the benzene ring. The most effective inhibitors showing IC₅₀ values in the range 2.3–3.6 μM were substituted in C₍₃₎ by F, CH₃, Cl and Br. The dependence of the PET-inhibiting activity on the lipophilicity of the compounds was quasi-parabolic for 3-substituted derivatives, while for C₍₂₎ ones a slight increase and for C₍₄₎ derivatives a sharp decrease of the activity were observed with increasing lipophilicity. In addition, the dependence of PET-inhibiting activity on electronic Hammett's σ parameter of the substituent R was observed with optimum σ value 0.06 for C₍₄₎ and 0.34 for C₍₃₎ substituted derivatives, while the value of σ parameter did not significantly influence the PET-inhibiting activity of C₍₂₎ substituted compounds. Interactions of the studied compounds with chlorophyll *a* and aromatic amino acids present in the pigment–protein complexes mainly in PS II were documented by fluorescence spectroscopy. The section between P680 and plastoquinone Q_B occurring on the acceptor side of PS II can be suggested as the site of action of the compounds.

© 2016 Elsevier Ltd. All rights reserved.

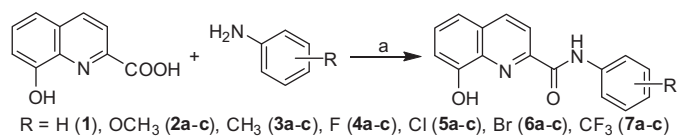
8-Hydroxyquinoline scaffold represents an important type of 'privileged structure' possessing a rich diversity of biological properties.¹ Some quinoline derivatives and their analogues/isosteres also show noteworthy herbicidal activities. Quinclorac belongs to the class of highly selective auxin herbicides and is used primarily to control weeds in rice crops.² Some other quinoline derivatives could be used to control undesirable plant growth.^{3–5} Also several recently described hydroxyquinoline-carboxamides reduced chlorophyll content in *Chlorella vulgaris* with IC₅₀ values about 5.9–10.9 μM.⁶ On the other hand, some quinoline derivatives originating from anthropogenic activities are environmental contaminants that are toxic to living organisms.^{7–9}

Quinoline derivatives were found to inhibit photosynthetic electron transport (PET) in plant chloroplasts. 2-Heptyl-1-hydroxy-4(1*H*)-quinolone and 4-hydroxy-2-nonylquinoline-*N*-oxide are potent inhibitors of PET in isolated thylakoids acting in photosystem (PS) II at the Q_B-site before the site of diuron and, in addition, at the cytochrome b₆f-complex.^{10,11} Also quinolone-*N*-oxides inhibited PET in PS II and in the cytochrome b₆f-complex.

The most potent inhibitors were found to be 2-methyl-3-alkyl-, 1-hydroxy-2-methyl-3-alkyl- and 1-hydroxy-2-alkyl-(1*H*)-quinolones with *n*-alkyl side chains varying from C₅ to C₁₇.¹² Displacement experiments with [¹⁴C]atrazine indicated that the quinolones share an identical binding site with other PS II commercial herbicides. Maximal inhibitory potency was achieved at the carbon chain length of 12–14 Å, and a further increase of the chain length resulted in a decreased activity. PET inhibition in spinach chloroplasts was also observed for several other quinoline derivatives.^{6,13–15}

Ring-substituted 8-hydroxyquinoline-2-carboxanilides were prepared according to Scheme 1 and published recently.¹⁶ Based on the above-mentioned observations,^{6,13–15} they were tested for their PET-inhibiting activity in spinach (*Spinacia oleracea* L.) chloroplasts, where PET through PS II, from H₂O to plastoquinone Q_B, was monitored spectrophotometrically as photoreduction of the artificial electron acceptor 2,6-dichlorophenol indophenol (DCPIP) according to Kralova et al.¹⁷ The studied compounds strongly inhibited photoreduction of DCPIP in spinach chloroplasts, and their activity was compared with the commercial PET inhibitor diuron. DMSO solutions of the studied compounds were added to

* Corresponding author.



Scheme 1. Synthesis of ring-substituted 8-hydroxyquinoline-2-carboxanilides **1–7c**: (a) PCl_3 , chlorobenzene, microwave-assisted synthesis.¹⁶

chloroplasts due to the limited solubility of the compounds in water. The applied DMSO concentration (up to 4 vol %) did not affect the photochemical activity of spinach chloroplasts. Relationships between the structure and the PET inhibition of the studied compounds are discussed.

The PET-inhibiting activity was expressed by the negative logarithm of IC_{50} value (compound concentration in mol/L causing 50% inhibition of PET). The activity of the most potent compound **4b** ($R = 3\text{-F}$; $\text{IC}_{50} = 2.3 \mu\text{M}$) was comparable with that of the standard DCMU ($\text{IC}_{50} = 1.9 \mu\text{M}$). However, also other 3-substituted compounds **3b** ($R = 3\text{-CH}_3$; $\text{IC}_{50} = 2.7 \mu\text{M}$), **6b** ($R = 3\text{-Br}$; $\text{IC}_{50} = 3.4 \mu\text{M}$) and **5b** ($R = 3\text{-Cl}$; $\text{IC}_{50} = 3.6 \mu\text{M}$) were very effective PET inhibitors. The dependences of $\log(1/\text{IC}_{50})$ on the lipophilicity of the compounds expressed as $\log k$ ¹⁶ are presented in Figure 1. The lipophilicity of the compounds is additionally expressed and listed in Table 1 as $\log P$ values predicted by sw. ACD/Percepta ver. 2012 for comparison. Below discussed relationships are valid both for $\log k$ and $\log P$ values, therefore the dependence of $\log(1/\text{IC}_{50})$ on $\log P$ values is not illustrated. Based on the obtained results it can be stated that the $C'_{(3)}$ substituted compounds expressed the highest PET-inhibiting activity, and the dependence of their PET-inhibiting activity on lipophilicity was quasi-parabolic (Fig 1). The lipophilicity of the most active compounds (IC_{50} range 2.3–3.6 μM) varied in the range from 0.9420 to 1.2357 for $\log k$ (from 2.76 to 3.31 for $\log P$). On the other hand, while the PET-inhibiting activity of $C'_{(2)}$ substituted compounds increased slightly with increasing compound lipophilicity, the activity of $C'_{(4)}$ substituted compounds showed a strong decrease (Fig. 1).

Electronic properties of individual anilide substituents expressed as Hammett's σ constants (predicted by sw. ACD/Percepta ver. 2012, see Table 1) were determined as another parameter that could influence PET-inhibiting activity. For $C'_{(3)}$ and $C'_{(4)}$ substituted derivatives increasing σ values of halogen substituents caused a gradual decrease of activity expressed as IC_{50} , namely from 2.3 μM (**4b**, $R = 3\text{-F}$; $\sigma = 0.34$) to 21.3 μM (**7b**, $R = 3\text{-CF}_3$; $\sigma = 0.43$) and from 5.6 μM (**4c**, $R = 4\text{-F}$; $\sigma = 0.06$) to 477.6 μM (**7c**, $R = 4\text{-CF}_3$; $\sigma = 0.51$), respectively, whereby anilides

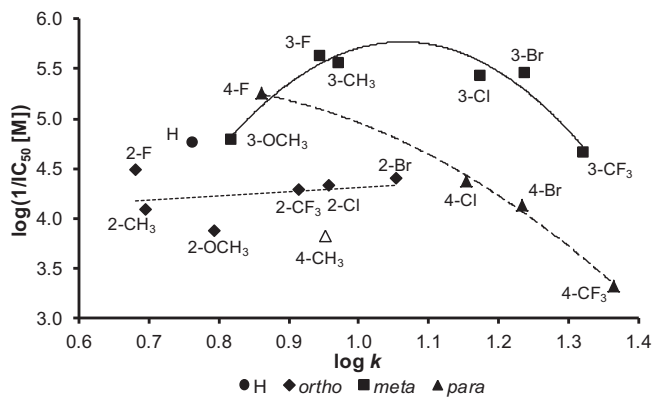


Figure 1. Relationships between PET inhibition $\log(1/\text{IC}_{50})$ [M] in isolated spinach chloroplasts and lipophilicity expressed as $\log k$. (Compound **3c** (4-CH_3) not included in SAR discussion is marked by empty symbol.).

Table 1

Predicted values of lipophilicity $\log P$, experimentally determined values of lipophilicity $\log k$ and electronic Hammett's σ parameters of substituents R, IC_{50} values related to PET inhibition in spinach chloroplasts in comparison with diuron (DCMU, 3-(3,4-dichlorophenyl)-1,1-dimethylurea) standard

Compd	R ¹	$\log k$	$\log P^a$	σ^b	PET IC_{50} [μM]
1	H	0.7600	2.55	0	16.6
2a	2-OCH ₃	0.7935	2.67	-0.28	134.6
2b	3-OCH ₃	0.8164	2.61	0.12	16.0
2c	4-OCH ₃	0.7129	2.51	-0.27	b
3a	2-CH ₃	0.6944	2.90	-0.17	81.6
3b	3-CH ₃	0.9686	2.90	-0.07	2.7
3c	4-CH ₃	0.9521	2.90	-0.17	150.0
4a	2-F	0.6806	2.59	0.06	32.1
4b	3-F	0.9420	2.76	0.34	2.3
4c	4-F	0.8598	2.59	0.06	5.6
5a	2-Cl	0.9566	3.07	0.22	46.0
5b	3-Cl	1.1718	3.28	0.37	3.6
5c	4-Cl	1.1543	3.05	0.23	42.5
6a	2-Br	1.0536	3.16	0.22	38.9
6b	3-Br	1.2357	3.31	0.39	3.4
6c	4-Br	1.2347	3.19	0.23	72.7
7a	2-CF ₃	0.9147	3.36	0.51	51.2
7b	3-CF ₃	1.3206	3.44	0.43	21.3
7c	4-CF ₃	1.3653	3.27	0.51	477.6
DCMU	—	—	—	—	1.9

^a Predicted using sw. ACD/Percepta ver. 2012.

^b Not determined due to precipitation during experiment.

4b and **7c** were the most active compounds among $C'_{(3)}$ and $C'_{(4)}$ substituted derivatives. On the other hand, the value of σ parameter did not significantly influence the PET-inhibiting activity of $C'_{(2)}$ substituted compounds.

From the above-mentioned results it is evident that beside lipophilicity and electronic properties, the PET-inhibiting activity of the studied compounds is significantly affected by the position of substituents R on the phenyl ring. For example, the lower PET-inhibiting activity of $C'_{(2)}$ substituted derivatives as compared to $C'_{(3)}$ and $C'_{(4)}$ substituted ones was observed previously for several esters of 2-, 3- and 4-substituted alkoxyphenylcarbamic acids.^{18,19} In these series, the lower inhibitory activity of 2-alkoxy substituted derivatives in comparison with their 3- and 4-substituted analogues can be explained by a secondary steric effect, which is induced due to interactions between the alkoxy substituent and the carbamate group.²⁰ The lower activity of the tested $C'_{(2)}$ substituted 8-hydroxyquinoline-2-carboxanilides could be connected with intramolecular interactions of the substituent R with the NH group resulting in reduced interaction of these compounds with photosynthetic proteins embedded in thylakoid membranes. On the other hand, the strong activity decrease with increasing lipophilicity of 4-substituted compounds could be caused by the limited solubility of more lipophilic compounds. Summarizing, it could be concluded that for PET-inhibiting activity, sufficient (but not too high) lipophilicity enabling easier penetration of the compounds into the lipids of photosynthetic membranes is necessary. On the other hand, the increasing electronegativity of halogen substituents in positions $C'_{(3)}$ and $C'_{(4)}$ was reflected in a gradual activity decrease.

The detection of PET through PS II (from the intermediate Z' situated on the donor side of PS II to Q_B located on the acceptor side of PS II) was performed according to Xiao et al.²¹ and Sersen et al.²² using the artificial electron donor 1,5-diphenylcarbazide (DPC) acting in the Z'/D' intermediate.²³ The application of DPC to chloroplasts, the activity of which was inhibited by compounds **4b** ($R = 3\text{-F}$) or **6b** ($R = 3\text{-Br}$) to 85%, resulted in a gradual restoration of PET with increasing DPC concentration. The complete restoration of PET occurred only when the concentration of DPC was higher by more than one order of magnitude than the concentration of the applied inhibitor. Therefore it could be assumed that

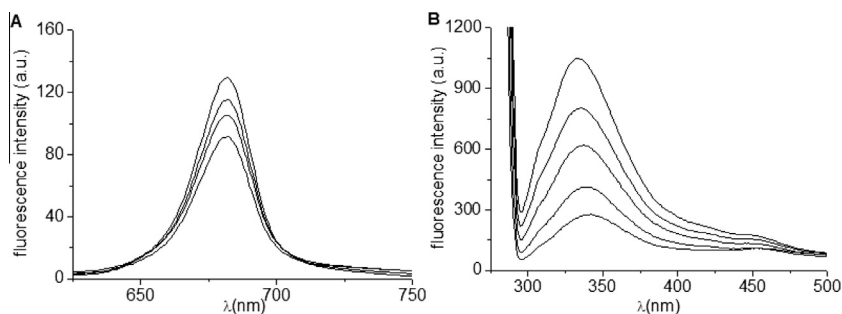


Figure 2. Fluorescence emission spectra of chlorophyll *a* in suspension of spinach chloroplasts without and with compound **4b** ($R = 3\text{-F}$; $c = 0, 55, 110$ and $220 \mu\text{M}$, the curves from top to bottom; excitation wave length $\lambda = 436 \text{ nm}$) (A) and fluorescence emission spectra of aromatic amino acids in suspension of spinach chloroplasts without and with compound **4b** ($c = 0, 11, 22, 44$ and $66 \mu\text{M}$, the curves from top to bottom; excitation wave length $\lambda = 275 \text{ nm}$) (B). Chlorophyll concentration in chloroplast suspension: 10 mg/L .

the section between P680 (primary donor of PS II) and plastoquinone Q_B occurring on the acceptor side of PS II was damaged by these PET inhibitors. The complete restoration of the photochemical activity of chloroplasts treated with **4b** or **6b** at higher DPC concentrations could be connected with the replacement of these inhibitors from their binding site by *sym*-diphenylcarbazine due to their direct interaction with the herbicide-binding niche, similarly as it was demonstrated for atrazine²⁴ or metribuzin.²⁵ Inhibition of electron transport in PS II at the Q_B site before the site of diuron by 4-hydroxyquinoline-*N*-oxides¹⁰ or quinolones and quinolone *N*-oxides¹² was reported previously.

The effect of the studied compounds on the fluorescence of chlorophyll *a* (Chla) and aromatic amino acids (AAA) in spinach chloroplasts was investigated as well, applying a published method.²⁶ The DMSO concentration in all samples was the same as in the control (10% (v/v)). The studied 8-hydroxyquinoline-2-carboxanilides affected the chlorophyll *a* (Chla) fluorescence in spinach chloroplasts. As shown in Figure 2A, the intensity of the Chla emission band at 686 nm belonging to the pigment–protein complexes in PS II decreased in the presence of compound **4b**, indicating a perturbation of the Chla–protein complexes in the thylakoid membrane²⁷ caused by the this compound. A similar Chla fluorescence decrease in spinach chloroplasts was observed previously for several PET inhibitors, namely ring-substituted 3-hydroxynaphthalene-2-carboxanilides,²⁸ 1-hydroxynaphthalene-2-carboxanilides,²⁹ 2-hydroxynaphthalene-1-carboxanilides³⁰ and ring-substituted 4-arylamino-7-chloroquinolinium chlorides.¹⁵ The tested 8-hydroxyquinoline-2-carboxanilides also interacted with residues of AAA, mainly tryptophan and tyrosine occurring in photosynthetic proteins situated mainly in PS II. This was documented by the quenching of AAA fluorescence at 334 nm. Figure 2B presents fluorescence emission spectra of AAA of untreated spinach chloroplasts and of chloroplasts treated with increasing concentrations of compound **4b**. As shown in Figure 2B, the quenching of the fluorescence of aromatic amino acids at 334 nm increased with the increasing concentration of the tested compound. The quenching of the fluorescence of Chla as well as of aromatic amino acids in the presence of 5-bromo- and 3,5-dibromo-2-hydroxy-*N*-phenylbenzamides and ring-substituted 2-hydroxynaphthalene-1-carboxanilides was observed previously.^{30,31}

The studied ring-substituted 8-hydroxyquinoline-2-carboxanilides were tested previously for their *in vitro* antimycobacterial activity against *Mycobacterium tuberculosis* and clinical isolates of *Mycobacterium avium* complex and *M. avium* subsp. *paratuberculosis*, and some of them showed the antimycobacterial activity against *M. avium* subsp. *paratuberculosis* comparable with or higher than that of rifampicin. However, it could be noted that with the exception of some compounds with lower solubility, the

antitubercular activity of compounds mainly against *M. tuberculosis* was comparable, independently of compound lipophilicity, electronic properties of R substituent or its position of substitution.¹⁶ Similarly to the present results in relation to PET-inhibiting activity, compounds with potency against all three mycobacterial strains were obtained by the substitution of $C_{(3)}$ position of aniline; however, also the hydroxyl moiety in $C_{(8)}$ of quinoline seems to play a significant role in antimycobacterial activity, because its absence in quinoline-2-carboxanilides led to an activity decrease.³² An essential contribution of the hydroxyl moiety for amplifying antimycobacterial potency was observed previously also for 1-hydroxynaphthalene-2-carboxanilides²⁹ and 6-hydroxynaphthalene-2-carboxanilides³³ contrary to naphthalene-2-carboxanilides.³²

Acknowledgment

This study was supported by IGA VFU Brno 322/2015/FaF.

References and notes

- Song, Y.; Xu, H.; Chen, W. M.; Zhan, P.; Liu, X. Y. *Med. Chem. Commun.* **2015**, *6*, 61.
- Grossmann, K. *Weed Sci.* **1998**, *46*, 707.
- Hagen, H.; Eichenauer, U.; Plath, P.; Meyer, N.; Wuerzer, B. US Pat. 4797148, 1989.
- Ryu, E. K.; Chung, K. H.; Lee, W. H.; Kim, J. N.; Hong, K. S. US Pat. 5489687, 1996.
- Liu, Y. X.; Zhao, H. P.; Wang, Z. W.; Li, Y. H.; Song, H. B.; Riches, H.; Beattie, D.; Gu, Y. C.; Wang, Q. M. *Mol. Divers.* **2013**, *17*, 701.
- Musiol, R.; Tabak, D.; Niedbala, H.; Podeszwa, B.; Jampilek, J.; Kralova, K.; Finster, J.; Mencil, A.; Polanski, J. *Bioorg. Med. Chem.* **2008**, *16*, 4490.
- Johansen, S. S.; Hansen, A. B.; Mosbæk, H.; Arvin, E. *Ground Water Monit. Rem.* **1997**, *17*, 106.
- Pereira, W. E.; Rostad, C. E.; Garbarino, J. R.; Hult, M. F. *Environ. Toxicol. Chem.* **1983**, *21*, 283.
- Pereira, W. E.; Rostad, C. E.; Updegraff, D. M.; Bennett, J. L. *Environ. Toxicol. Chem.* **1987**, *6*, 163.
- Avron, M. *Biochem. J.* **1961**, *78*, 735.
- Barton, J. R.; MacPeck, W. A.; Cohen, W. S. J. *Bioenerg. Biomembr.* **1983**, *5*, 93.
- Reil, E.; Hofle, G.; Draber, W.; Oettmeier, W. *Biochim. Biophys. Acta* **2001**, *1506*, 127.
- Musiol, R.; Jampilek, J.; Kralova, K.; Richardson, D. R.; Kalinowski, D.; Podeszwa, B.; Finster, J.; Niedbala, H.; Palka, A.; Polanski, J. *Bioorg. Med. Chem.* **2007**, *15*, 1280.
- Musiol, R.; Jampilek, J.; Nycz, J. E.; Pesko, M.; Carroll, J.; Kralova, K.; Vejsova, M.; O'Mahony, J.; Coffey, A.; Mrozek, A.; Polanski, J. *Molecules* **2010**, *15*, 288.
- Otevre, J.; Bobal, P.; Zadrzilova, I.; Govender, R.; Pesko, M.; Imramovsky, A.; Coffey, A.; O'Mahony, J.; Kollar, P.; Cizek, A.; Kralova, K.; Jampilek, J. *Molecules* **2013**, *18*, 10648.
- Kos, J.; Zadrzilova, I.; Nevin, E.; Soral, M.; Gonec, T.; Kollar, P.; Oravec, M.; Coffey, A.; O'Mahony, J.; Liptaj, T.; Kralova, K.; Jampilek, J. *Bioorg. Med. Chem.* **2015**, *23*, 4188.
- Kralova, K.; Sersen, F.; Sidoova, E. *Chem. Pap.* **1992**, *46*, 348.
- Kralova, K.; Sersen, F.; Cizmarik, J. *Gen. Physiol. Biophys.* **1992**, *11*, 26.
- Kralova, K.; Sersen, F.; Cizmarik, J. *Chem. Pap.* **1992**, *46*, 266.
- Cizmarik, J.; Borovansky, A.; Svec, P. *Acta Fac. Pharm. Univ. Comenianae* **1976**, *29*, 53.

21. Xiao, R.; Ghosh, S.; Tanaka, A. R.; Greenberg, B. M.; Dumbroff, E. B. *Plant Physiol. Biochem.* **1997**, *35*, 411.
22. Sersen, F.; Kralova, K.; Macho, V. *Pest. Biochem. Physiol.* **2000**, *68*, 113.
23. Izawa, S. Acceptors and Donors for Chloroplast Electron Transport In *Methods in Enzymology*; Colowick, P., Kaplan, N. O., Eds.; Academic Press: New York – London, 1980; Vol. 69, pp 413–434. Part C.
24. Purcell, M.; Leroux, G.; Carpentier, R. *Biochim. Biophys. Acta Int. J. Biochem. Biophys.* **1991**, *1058*, 374.
25. Borse, T. H.; Maheswarim, V. L.; Baviskar, M. P. *J. Plant Biochem. Biotechnol.* **2000**, *9*, 119.
26. Servusova, B.; Eibinova, D.; Dolezal, M.; Kubicek, V.; Paterova, P.; Pesko, M.; Kralova, K. *Molecules* **2012**, *17*, 13183.
27. Govindjee *Aust. J. Plant. Physiol.* **1995**, *22*, 131.
28. Kos, J.; Zadrazilova, I.; Pesko, M.; Keltosova, S.; Gonec, T.; Bobal, P.; Oravec, M.; Kollar, P.; Cizek, A.; Kralova, K.; Jampilek, J. *Molecules* **2013**, *18*, 7977.
29. Gonec, T.; Kos, J.; Zadrazilova, I.; Pesko, M.; Keltosova, S.; Bobal, P.; Kollar, P.; Cizek, A.; Kralova, K.; Jampilek, J. *Bioorg. Med. Chem.* **2013**, *21*, 6531.
30. Gonec, T.; Kos, J.; Zadrazilova, I.; Pesko, M.; Govender, R.; Kollar, P.; Imramovsky, A.; O'Mahony, J.; Coffey, A.; Cizek, A.; Kralova, K.; Jampilek, J. *Molecules* **2013**, *18*, 9397.
31. Kralova, K.; Sersen, F.; Pesko, M.; Waisser, K.; Kubicova, L. *Chem. Pap.* **2014**, *68*, 46.
32. Gonec, T.; Bobal, P.; Pesko, M.; Guo, J. H.; Kralova, K.; Kos, J.; Coffey, A.; Kollar, P.; Imramovsky, A.; Jampilek, J. *Molecules* **2012**, *17*, 613.
33. Kos, J.; Nevin, E.; Soral, M.; Kushkevych, I.; Gonec, T.; Bobal, P.; Kollar, P.; Coffey, A.; O'Mahony, J.; Liptaj, T.; Kralova, K.; Jampilek, J. *Bioorg. Med. Chem.* **2015**, *23*, 2035.

č.	citace	ISSN
6	KAUEROVA, T, J KOS , T GONEC, J JAMPILEK a P KOLLAR. Antiproliferative and Pro-Apoptotic Effect of Novel Nitro-Substituted Hydroxynaphthanilides on Human Cancer Cell Lines. <i>INTERNATIONAL JOURNAL OF MOLECULAR SCIENCES</i> [online]. 2016, 17 (8). Dostupné z: doi: 10.3390/ijms17081219	1422-0067



Article

Antiproliferative and Pro-Apoptotic Effect of Novel Nitro-Substituted Hydroxynaphthanilides on Human Cancer Cell Lines

Tereza Kauerova ¹, Jiri Kos ², Tomas Gonec ², Josef Jampilek ³ and Peter Kollar ^{1,*}

¹ Department of Human Pharmacology and Toxicology, Faculty of Pharmacy, University of Veterinary and Pharmaceutical Sciences Brno, Palackeho 1946/1, 612 42 Brno, Czech Republic; tereza.kauerova@gmail.com

² Department of Chemical Drugs, Faculty of Pharmacy, University of Veterinary and Pharmaceutical Sciences Brno, Palackeho 1946/1, 612 42 Brno, Czech Republic; kosj@vfu.cz (J.K.); t.gonec@seznam.cz (T.G.)

³ Department of Pharmaceutical Chemistry, Faculty of Pharmacy, Comenius University, Odbojarov 10, 832 32 Bratislava, Slovakia; josef.jampilek@gmail.com

* Correspondence: kollarp@vfu.cz; Tel.: +420-541-562-892

Academic Editor: Maurizio Battino

Received: 22 June 2016; Accepted: 21 July 2016; Published: 28 July 2016

Abstract: Ring-substituted hydroxynaphthanilides are considered as cyclic analogues of salicylanilides, compounds possessing a wide range of pharmacological activities, including promising anticancer properties. The aim of this study was to evaluate the potential anticancer effect of novel nitro-substituted hydroxynaphthanilides with a special focus on structure-activity relationships. The antiproliferative effect was assessed by Water Soluble Tetrazolium Salts-1 (WST-1) assay, and cytotoxicity was evaluated via dye exclusion test. Flow cytometry was used for cell cycle analysis and detection of apoptosis using Annexin V-FITC/PI assay. Protein expression was estimated by Western blotting. Our data indicate that the potential to cause the antiproliferative effect increases with the shift of the nitro substituent from the *ortho*- to the *para*-position. The most potent compounds, 3-hydroxy-*N*-(3-nitrophenyl)naphthalene-2-carboxamide (**2**), and 2-hydroxy-*N*-(4-nitrophenyl)-naphthalene-1-carboxamide (**6**) showed antiproliferative activity against THP-1 and MCF-7 cancer cells without affecting the proliferation of 3T3-L1 non-tumour cells. Compounds **2** and **6** induced the accumulation of THP-1 and MCF-7 cells in G1 phase associated with the downregulation of cyclin E1 protein levels, while the levels of cyclin B1 were not affected. Moreover, compound **2** was found to exert the pro-apoptotic effect on the THP-1 cells. These results suggest that hydroxynaphthanilides might represent a potential model structure for the development of novel anticancer agents.

Keywords: hydroxynaphthanilides; salicylanilides; cell proliferation; apoptosis; anticancer effect

1. Introduction

Salicylanilide derivatives (*N*-substituted hydroxybenzamides) are known as multitarget agents that possess a wide spectrum of pharmacological activities. These compounds are largely investigated for their promising antibacterial and antimycobacterial effects [1–5]. Some salicylanilides, such as niclosamide or closantel, belong to the class of broad-spectrum anthelmintic agents [6]. Recently, using high-throughput screening, several studies uncovered an antitumor activity of niclosamide, thereby becoming widely studied as a potential anticancer agent [7]. It was proved to effectively induce growth inhibition in a broad spectrum of tumour cell lines together with a minimal toxicity on non-tumour cells [8,9]. On the molecular level, niclosamide inhibited multiple key oncogenic signalling pathways (e.g., Wnt/ β -catenin, mTORC1, and NF- κ B) [9–12]. In general, salicylanilide derivatives are presumed to share the structure similarity with the pharmacophore of 4-arylaminoquinazoline

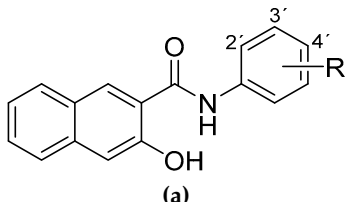
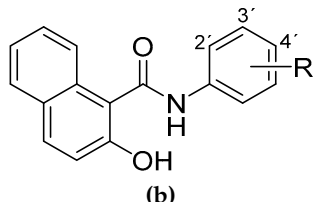
derivatives (e.g., gefitinib and erlotinib) that belong to the class of small molecule inhibitors of the protein kinase epidermal growth factor receptor (EGFR PTK) [13–15]. This fact led to the intensive research of salicylanilides anticancer properties, as their structure became an attractive model for the design of potent antitumor agents. Several studies were published, in which a series of newly-prepared salicylanilides showed antiproliferative activity against a spectrum of human cancer cell lines, such as promyelocytic leukaemia cells HL-60, chronic myelogenous leukaemia cells K562, human epithelial carcinoma cells A431, or breast carcinoma cells MCF-7. In addition, some salicylanilides have been recently reported to elicit cell cycle arrest or to induce apoptosis in human cancer cell lines [13,16–18].

Recently, several series of various ring-substituted hydroxynaphthanilides were designed and prepared as ring analogues of salicylanilides. Based on the principle of bioisosterism with quinoline-like compounds, the aromatic ring in the salicylanilide pharmacophore was extended by another to obtain the naphthalene scaffold in the structure [3,5]. Compounds containing a quinoline moiety exhibit various pharmacological effects, including anticancer activity [19], hence the hydroxynaphthanilides may possess promising pharmacological properties due to the connection of these two pharmacophores.

The biological activity of salicylanilide pharmacophore could be modified by introducing appropriate substituents in the structure. In addition to a substitution pattern on the salicylic scaffold, SAR studies were focused also on substituents located on the aromatic ring of the anilide part in the structure. It was proved that the biological effects of salicylanilide derivatives are related to both the nature and the position of substituents. The electron parameters of anilide substituents could modify the conformational equilibrium between the closed-ring and open-ring forms of the structure and thus affect the biological activity of the whole molecule. That activity is usually referred to the presence of electron-withdrawing substituents on the anilide moiety [14,20]. In accordance with these findings, our previous results revealed the same relation between the toxicity of ring-substituted hydroxynaphthanilides to the THP-1 cancer cells and the presence of substituents with electron-withdrawing properties [3–5]. The SAR studies also found the presence of an electron-withdrawing nitro group to be one of the essential requirements for the anticancer effect of niclosamide [21]. Based on these findings, the substitution by a nitro moiety was determined to be appropriate for the potent anticancer effect of newly-designed hydroxynaphthanilides.

Therefore, we have selected six newly-designed hydroxynaphthanilides, nitro-substituted in different positions on the anilide ring (Table 1), to evaluate their potential anticancer effects in the context of these structural differences. The aim of this work was to assess their antiproliferative activity in two cancer cell lines, THP-1 and MCF-7. Moreover, we also examined the effect on the growth of non-tumour cells 3T3-L1. In addition, changes in cell cycle distribution were evaluated, as well as their pro-apoptotic effect.

Table 1. Structures of tested compounds: (a) 3-hydroxy-*N*-(nitrophenyl)naphthalene-2-carboxamides; and (b) 2-hydroxy-*N*-(nitrophenyl)naphthalene-1-carboxamide.

 (a)		 (b)	
Compound	R	Compound	R
1	2-NO ₂	4	2-NO ₂
2	3-NO ₂	5	3-NO ₂
3	4-NO ₂	6	4-NO ₂

2. Results

2.1. Effect on Cell Proliferation and Viability

Initially, we examined the effect of six nitro-substituted hydroxynaphthanilides on the proliferation of human leukaemia and breast carcinoma cell lines, using Water Soluble Tetrazolium Salts-1 (WST-1) assay. For such analyses, THP-1 and MCF-7 cells were treated with the compounds at concentrations ranging from 0.5 to 20 μM for 24 h. As shown in Figure 1a, compounds 2, 3, and 6 inhibit cell growth in both cell lines in a dose-dependent manner. The inhibitory effect of 2 and 6 was statistically significant ($p < 0.001$) starting from the concentration of 2.5 and 5 μM in THP-1 and MCF-7 cells, respectively. From the concentration-response curves, the IC_{50} values were determined. As summarized in Table 2, the IC_{50} values were found to be 3.06 μM in THP-1 and 4.61 μM in MCF-7 cells for compound 2, and 5.80 and 5.23 μM in THP-1 and MCF-7 cells, respectively, for compound 6. The strongest antiproliferative effect was observed in both THP-1 and MCF-7 cell lines after the treatment with compound 3 (IC_{50} 1.05 and 1.65 μM , respectively). In contrast, neither compound 1 nor 4 (both *ortho*-substituted derivatives) was able to induce the inhibition of cell growth in THP-1 or MCF-7 cells at concentrations used in the assay. Compound 5 demonstrated antiproliferative activity only in MCF-7 cells, significant ($p < 0.001$) at concentrations of 10 and 20 μM (data not shown), however, a 50% reduction in cell growth was not achieved. The proliferation of THP-1 cells was not affected by this compound.

Table 2. Antiproliferative and cytotoxic effects of tested compounds 1–6. IC_{50} and LC_{50} values were calculated using concentration-response curves generated from the results of WST-1 analysis and erythrosin B exclusion test, respectively. The values represent means \pm SD of three independent experiments, each performed in triplicate.

Compound	THP-1		MCF-7		3T3-L1
	IC_{50} (μM)	LC_{50} (μM)	IC_{50} (μM)	LC_{50} (μM)	IC_{50} (μM)
1	>20	>20	>20	>20	>20
2	3.06 \pm 0.206	7.91 \pm 0.240	4.61 \pm 0.068	>20	>20
3	1.05 \pm 0.199	3.44 \pm 1.209	1.65 \pm 0.938	12.91 \pm 1.984	4.41 \pm 0.293
4	>20	>20	>20	>20	>20
5	>20	>20	>20	>20	>20
6	5.80 \pm 0.370	9.98 \pm 0.349	5.23 \pm 0.802	>20	>20

After we found that compounds 2, 3, and 6 effectively inhibit the growth of both THP-1 and MCF-7 cancer cells at micromolar concentrations, we assessed additionally their effect on proliferation of non-tumour cell line, 3T3-L1, using WST-1 assay. While compounds 2 and 6 did not decrease cell growth at any of concentrations used, compound 3 affected the proliferation of 3T3-L1 cells in a dose-dependent manner (IC_{50} 4.41 μM) (Figure 1b and Table 2).

Subsequently, for the comparison of the antiproliferative and cytotoxic effects we assessed the cell viability after 24 h treatment with compounds 1–6 in both tumour cell lines using the dye exclusion test. In THP-1 cells, we obtained lower LC_{50} values: 7.91, 3.44, and 9.98 μM for compounds 2, 3, and 6, respectively. In general, less sensitivity towards the cytotoxic effect of tested compounds was observed in MCF-7 cells. Neither compound 2 nor 6 reduced cell viability under 50% in comparison with the control, while the strongest effect was induced by compound 3 (LC_{50} 12.91 μM).

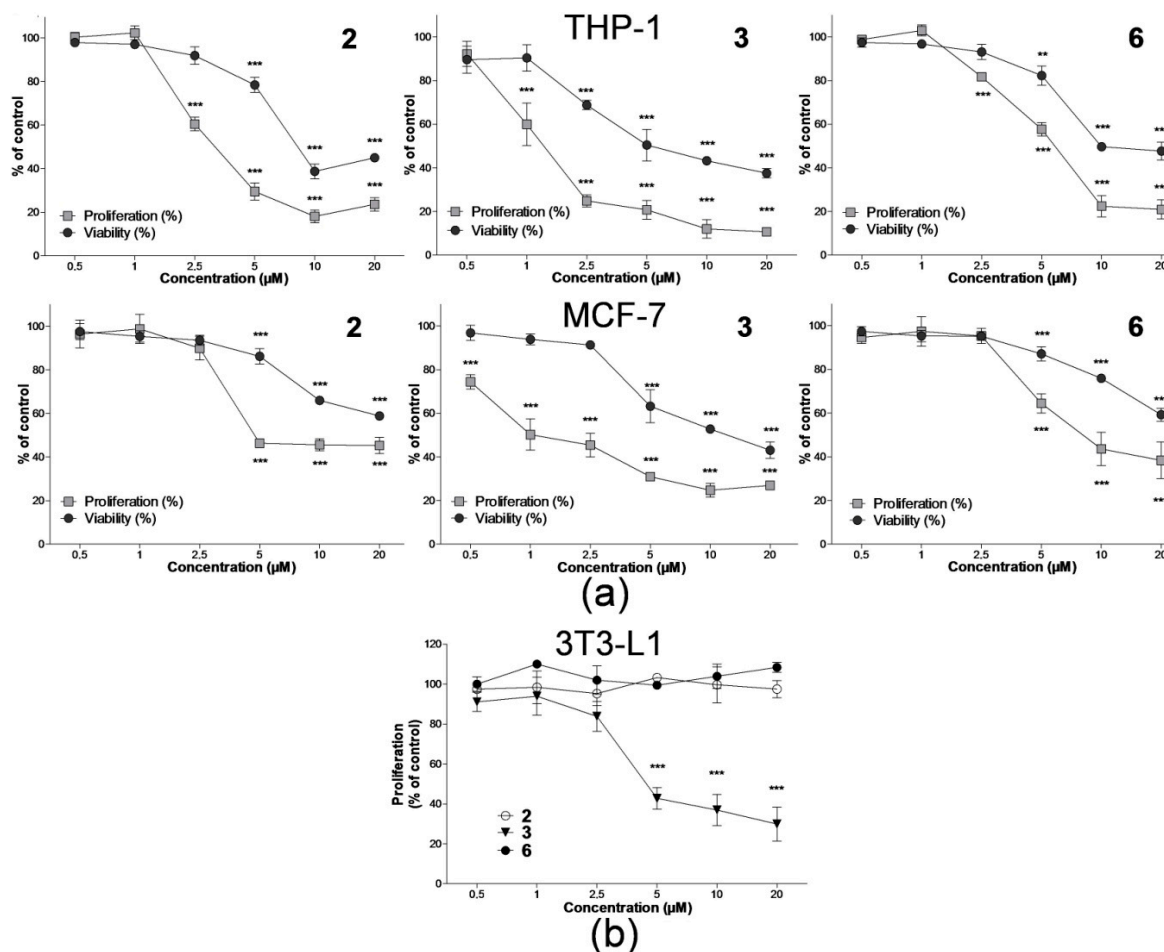


Figure 1. Effect of compounds 2, 3, and 6 on cell proliferation and viability in THP-1, MCF-7 and 3T3-L1 cell lines. Cells were cultured with indicated concentrations of compounds 2, 3, and 6 for 24 h. (a) Proliferation of THP-1 and MCF-7 cells was determined using WST-1 assay; cell viability was assessed by erythrosin B exclusion test; (b) Proliferation of 3T3-L1 cells was determined using WST-1 assay. The results are shown as the means \pm standard deviation (SD) of three independent experiments, each performed in triplicate. ** $p < 0.01$, *** $p < 0.001$, statistically significant difference in comparison with drug-free control (CTRL).

2.2. Effect on Distribution of Cells in Cell Cycle Phases

The cell proliferation assays showed us the ability of selected compounds 2 and 6 to inhibit cancer cell growth. In order to determine at which stage of the cell cycle these compounds induce cell growth inhibition, flow cytometric analyses of cell cycle profiles in THP-1 and MCF-7 cell lines were performed. Cells were exposed to compounds 2 and 6 for 24 h at concentrations exerting significant inhibition of cell proliferation with no or very little concurrent effect on the cell viability. Therefore, THP-1 and MCF-7 cells were treated for 24 h with the compounds at concentrations of 2.5, 5, and 10 μM , respectively. In general, we detected a qualitatively similar effect on the distribution of cells in cell cycle phases following the treatment with compounds 2 and 6 in both leukaemia and breast carcinoma cells. Compounds 2 and 6 induced accumulation of cells in G1 phase in both THP-1 (Figure 2) and MCF-7 (Figure 3) cell lines. This was in concert with a simultaneous decrease in the number of cells observed in the S phase compared to the drug-free control, while the percentage of cells in the G2/M phase remained unchanged.

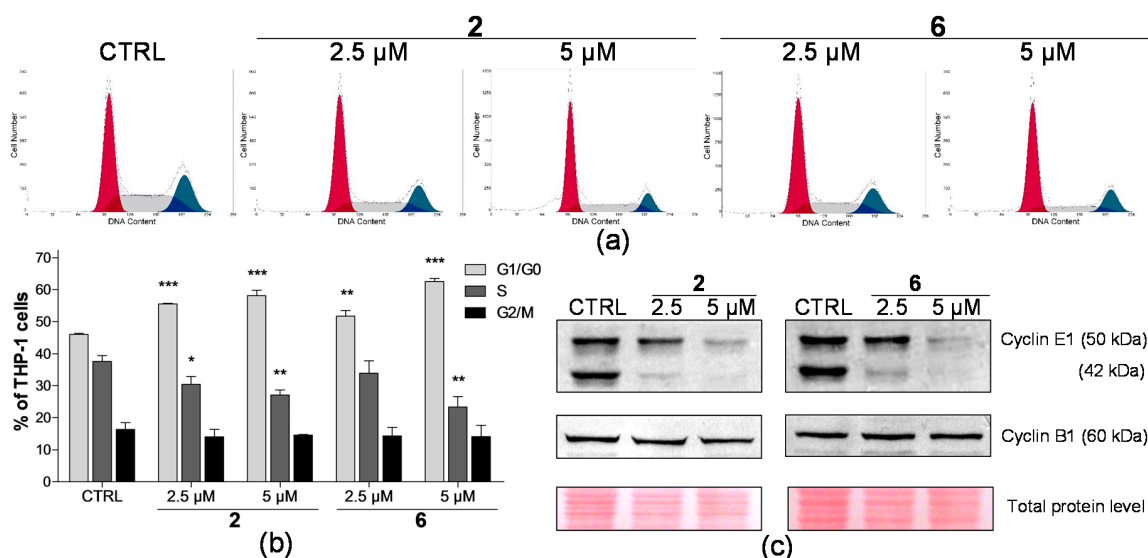


Figure 2. Compounds 2 and 6 induce accumulation of THP-1 cells in the G1 phase. (a) Representative histograms of flow cytometric analysis of the DNA content in THP-1 cells after the incubation with indicated concentrations of compounds 2 and 6 for 24 h; (b) The distribution of THP-1 cells in the phases of the cell cycle upon the treatment with compounds 2 and 6 at 24 h. The results are expressed as the means \pm SD of three independent experiments. * $p < 0.05$, ** $p < 0.01$, *** $p < 0.001$, statistically significant difference in comparison with control sample; (c) Expression of cell cycle regulators cyclin E1 and B1 in THP-1 cells treated by compounds 2 and 6 for 24 h, as determined by Western blot analysis. Protein levels of the samples were normalized according to the total protein stains. CTRL, control cells treated by the drug-free medium.

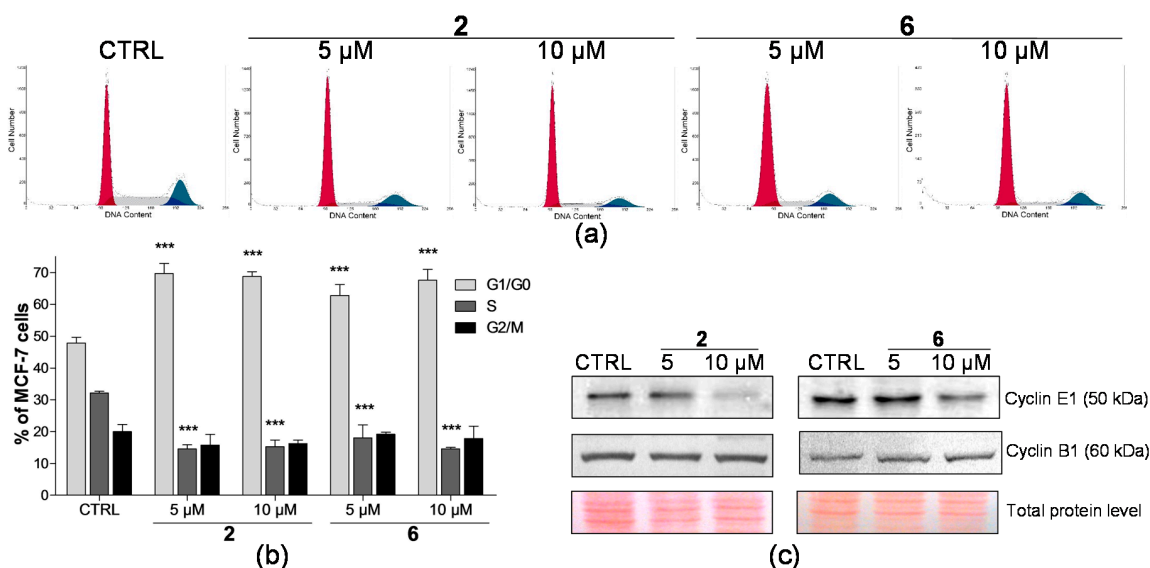


Figure 3. Compounds 2 and 6 induce accumulation of MCF-7 cells in the G1 phase. (a) Representative histograms of flow cytometric analysis of the DNA content in MCF-7 cells after the incubation with indicated concentrations of compounds 2 and 6 for 24 h; (b) The distribution of MCF-7 cells in phases of the cell cycle upon the treatment with compounds 2 and 6 at 24 h. The results are expressed as the means \pm SD of three independent experiments. *** $p < 0.001$, statistically significant difference in comparison with control sample; (c) Expression of cell cycle regulators cyclin E1 and B1 in MCF-7 cells treated by compounds 2 and 6 for 24 h, as determined by Western blot analysis. Protein levels of the samples were normalized according to the total protein stains. CTRL, control cells treated by the drug-free medium.

Additionally, the cell cycle analysis allows determining the presence of a subdiploid cell population as a characteristic marker of cells with fractional DNA content. A significant increase ($p < 0.001$) of the sub-G1 peak was found only after the treatment with 5 μM of compound **2** in THP-1 cells, where an approximately eight-fold increase was observed compared to the drug-free control (Figure 4). In contrast, compound **2** did not induce any elevation of the sub-G1 peak in breast carcinoma cells. Similarly, no significant increase of sub-diploid population of THP-1 or MCF-7 cells caused by 24 h treatment with compound **6** in comparison with the control sample was detected. Next, based on the flow cytometric data that showed the accumulation of cells in the G1 phase upon the treatment with compounds **2** and **6**, we examined their effect on the expression of regulatory proteins controlling G1/S and G2/M progression. Whereas total protein levels of cyclin B1 were not changed in THP-1 or MCF-7 cells, the treatment with both compounds **2** and **6** led to the dose-dependent decrease in expression of cyclin E1 (Figures 2c and 3c). Importantly, the levels of cyclin E1 low molecular weight (LMW E1) isoform (42 kDa) were found to be significantly decreased in THP-1 cells.

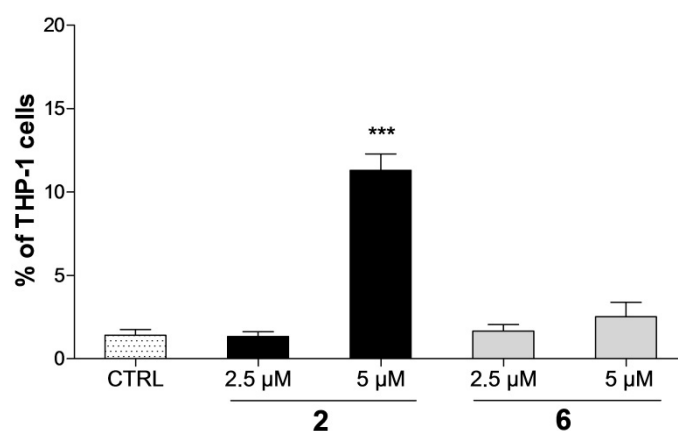


Figure 4. Compound **2** causes a significant increase of hypodiploid sub-G1 peak in THP-1 cells. Quantification of the sub-G1 peak in THP-1 cells after the treatment by compounds **2** and **6** for 24 h. The results are expressed as the means \pm SD of three independent experiments. *** $p < 0.001$, statistically significant difference in comparison with the drug-free control (CTRL).

2.3. Detection of Apoptosis by Annexin V-FITC/PI Assay

To further examine possible pro-apoptotic effect of compound **2** on THP-1 cells, Annexin V-FITC/PI assay was performed using flow cytometry for the quantification of the early and late stages of apoptosis. Staining of cells by Annexin V-FITC conjugate reflects the externalization of phosphatidylserine on the outer surface of the cell membrane as one of the early indicators of apoptosis [22]. In order to obtain further insight into the mechanism of cell death induced by compound **2**, we exposed THP-1 cells to a wider concentration range of 2.5, 5, and 10 μM and subsequently analysed the effect at three time-points of incubation (12, 18, and 24 h).

The assay revealed that compound **2** induced a dose-dependent increase of the percentage of early apoptotic as well as late apoptotic/secondary necrotic leukaemia THP-1 cells. In correspondence with the previous detection of a subdiploid cell population compound **2**, at concentrations of 2.5 μM , 5 μM , and 10 μM , elicited elevations of Annexin V/FITC-stained cell populations. As shown in Figure 5, this effect was observed even after 12 h of incubation; 10 μM of compound **2** increased significantly ($p < 0.01$) the proportion of early apoptotic cells to 9.37% in comparison to the percentage of control cells, 2.41%. The same concentration of compound **2** induced the elevation of the number of double-stained cells with incubation time, from 22.48% after 12 h to 41.88% after 24 h incubation. In general, the percentage of late apoptotic/secondary necrotic cells at higher concentrations of compound **2** (5 and 10 μM) prevailed over the early apoptotic cell population at all determined time points.

Nevertheless, the different effect was observed after the treatment with two model compounds exerting the pro-apoptotic effect in THP-1 cells. As summarized in Figure 5, cisplatin was found to most effectively increase the rate of early apoptotic cells in a time-dependent manner up to 44.38% after 24 h exposure. While camptothecin increased significantly ($p < 0.001$) the percentage of both early and late apoptotic cells up to 21.28% and 24.10%, respectively, after 12 h, 24 h treatment led to a decrease of the early apoptotic population to 9.65%; in contrast, late apoptosis increased to 33.08%.

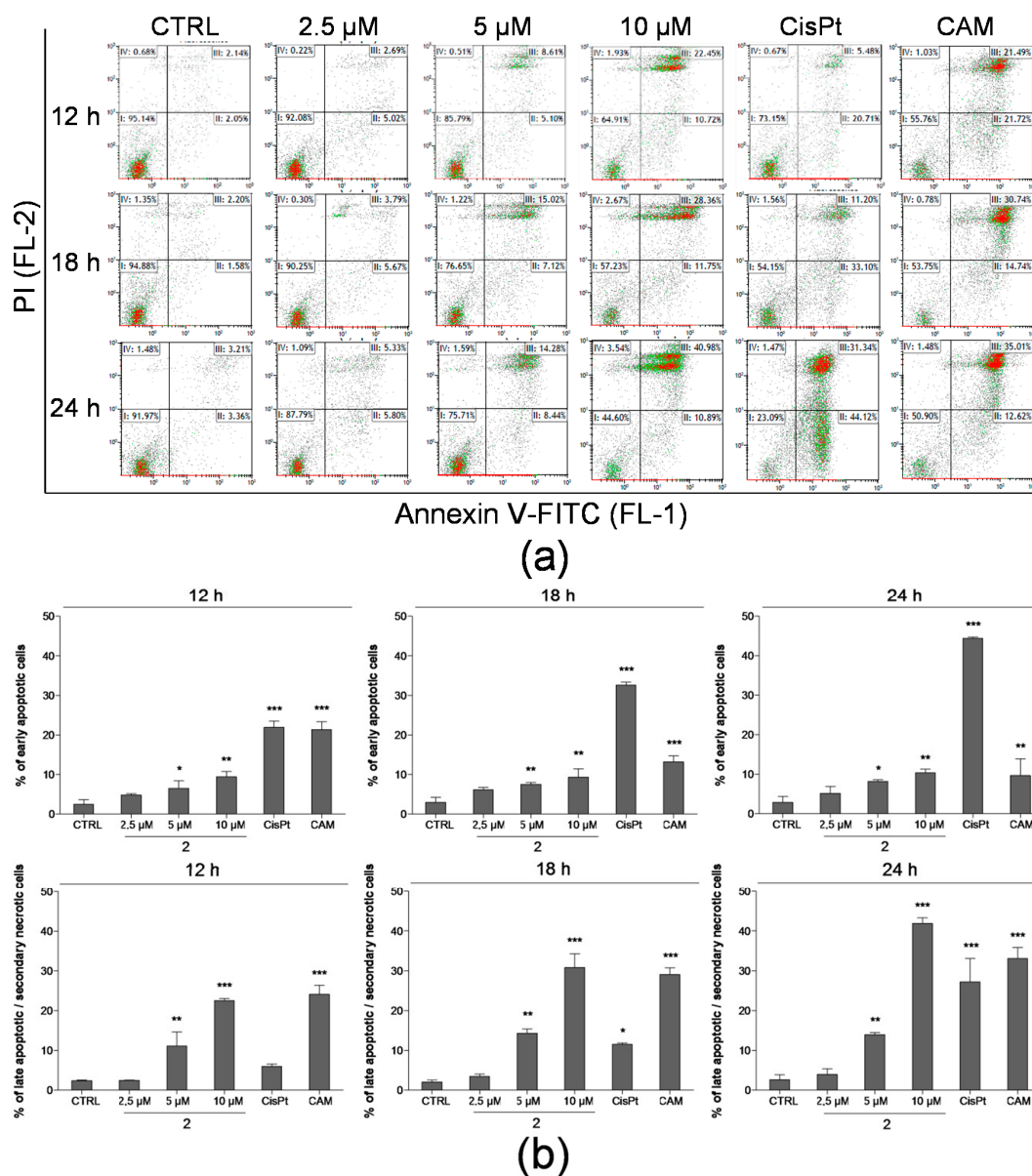


Figure 5. Detection of apoptosis after treatment with compound 2 in THP-1 cells at three points of incubation (12, 18, and 24 h). Cells were stained by Annexin V-FITC conjugate and PI; subsequent analysis was performed by flow cytometry. Cisplatin (10 $\mu\text{g}/\text{mL}$) and camptothecin (5 μM) were used as model compounds. (a) Representative dot plots of Annexin V-FITC/PI assay are shown. The particular quadrants represent proportion of cells that are I: viable; II: early apoptotic; III: late apoptotic/secondary necrotic; IV: necrotic; (b) Proportion of early apoptotic and late apoptotic/secondary necrotic THP-1 cells after the treatment by compound 2 and model compounds. The results are expressed as the means \pm SD of three independent experiments. * $p < 0.05$, ** $p < 0.01$, *** $p < 0.001$, statistically significant difference in comparison with the drug-free control (CTRL).

2.4. Analysis of Proteins Levels Involved in Apoptotic Pathways

Most of the apoptotic signalling pathways are controlled by caspases that belong to a group of cysteine proteases [23]. To assess whether compound **2** affects these signalling cascades and which pathway is activated (intrinsic or extrinsic), the activities of caspase 3, caspase 9, and caspase 8 were evaluated using Western blot analysis. As summarized in Figure 6, after 24 h incubation, compound **2** induced cleavage of pro-caspase 3 dose-dependently; an approximately two-fold decrease of the inactive form upon the treatment with 10 μM compared to the control was detected. Similarly, a comparable two-fold increase of active caspase 3 level was observed after the exposure to the 10 μM concentration of compound **2** in comparison to the control. Additionally, a significant increase of cleaved caspase 9 levels was detected with the most pronounced effects at 10 μM . On the contrary, the level of active caspase 8 was not altered after the treatment with compound **2** in comparison to the control.

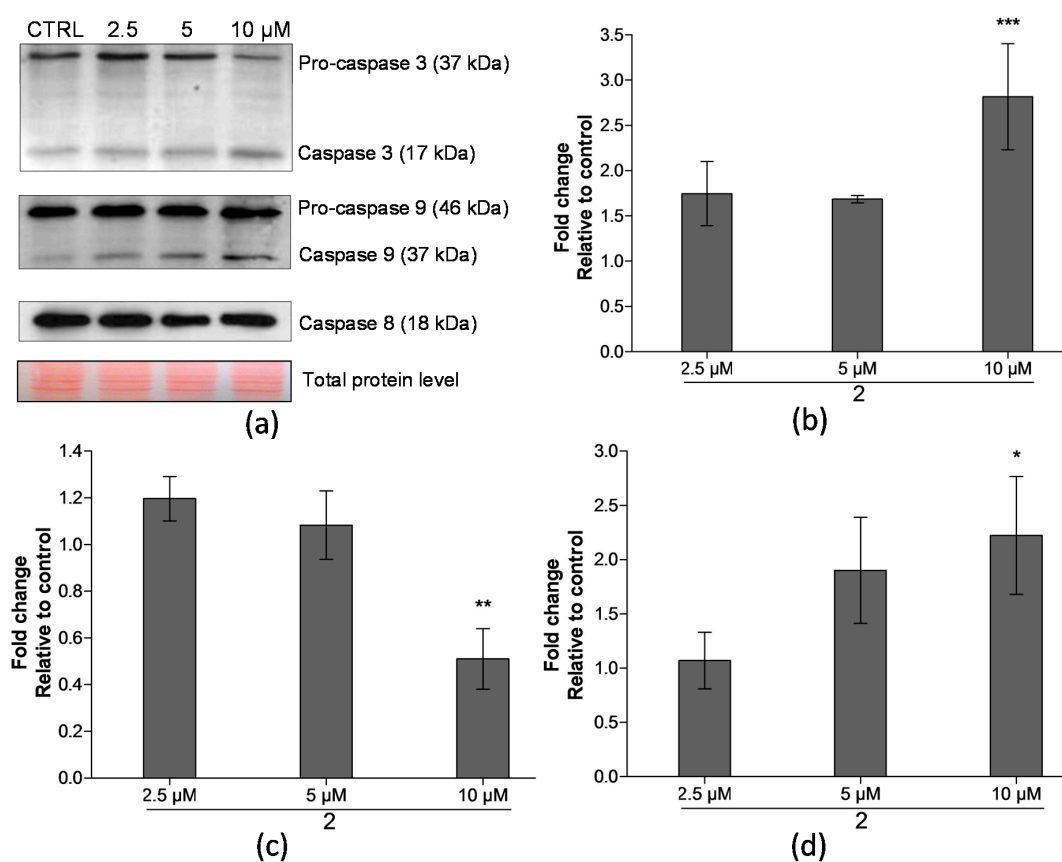


Figure 6. Levels of proteins involved in apoptotic pathways in THP-1 cells after 24 h treatment by compound **2**. (a) Levels of caspase 3, caspase 8, and caspase 9 in THP-1 cells treated by compound **2** for 24 h, as determined by Western blot analysis. Data of typical immunoblot are reported; (b) Summary data of cleaved caspase 9 levels in THP-1 cells; (c) Summary data of pro-caspase 3 levels in THP-1 cells; (d) Summary data of cleaved caspase 3 levels in THP-1 cells. Protein levels of the samples were normalized according to the total protein stains. The results are expressed as the means \pm SD of three independent experiments. * $p < 0.05$, ** $p < 0.01$, *** $p < 0.001$, statistically significant difference in comparison with the drug-free control (CTRL).

3. Discussion

In the present study, we examined the anticancer effects of a series of newly-synthesized nitro-substituted hydroxynaphthanilide derivatives through the assessment of their antiproliferative activity and cytotoxicity.

Our results showed the difference among the tested compounds in the antiproliferative activity. We found that the potency of cell growth inhibition correlates with the position of the electron-withdrawing nitro group on the anilide ring of the tested compounds. While *ortho*-substituted derivatives did not elicit any antiproliferative effect in both THP-1 and MCF-7 cancer cells, the shift of the nitro group to the *meta*- or *para*-position in compounds **2**, **3**, and **6**, led to the cell growth inhibition. Thus, it can be assumed that, most likely, the antiproliferative activity of 3-hydroxynaphthalene-2-carboxanilide and 2-hydroxynaphthalene-1-carboxanilide derivatives increase depending on the position of the nitro group as follows: *ortho* < *meta* < *para*. This different activity could be possibly related to the steric effect of the anilide substituents. Recently, it was described that the presence of a substituent in the *ortho* position causes the twist of the whole aniline ring plane towards the naphthalene scaffold, while *meta*- and, especially, *para*-substituted derivatives have a practically linear molecule [24]. Moreover, not only the location of the substituent on the anilide moiety but also the position of the β -ring of naphthalene towards the phenolic and carboxanilide moieties affected the intensity of the antiproliferative effect of these compounds. In our study, stronger antiproliferative activity was observed in substituted 3-hydroxynaphthalene-2-carboxanilides when comparing the IC₅₀ values of *meta*-substituted compounds **2** and **4** or *para*-substituted **3** and **6**. The similar structure-activity relationship was determined for the cytotoxicity of the tested compounds. Nevertheless, compounds **2**, **3**, and **6** exerted stronger antiproliferative rather than cytotoxic effect in cancer cells; approximately 2–3-fold higher LC₅₀ values compared to IC₅₀ values were obtained in the assays on THP-1 cells. Even more pronounced difference was observed in MCF-7 cells, where the LC₅₀ values were achieved only upon the treatment with compound **3**, with an approximately seven-fold higher dose in comparison with IC₅₀.

To assess whether tested compounds also influence the growth of other than cancer cells, we have extended our antiproliferative analysis and employed non-tumour fibroblast cell line 3T3-L1. Compound **3** that exerted the most substantial antiproliferative and cytotoxic effects towards both cancer cell lines was also capable of inhibiting the growth of the non-tumour line. Interestingly, a different effect was observed upon the treatment with compounds **2** and **6**, where such antiproliferative activity in non-tumour cells was not detected. Results of antiproliferative effects showed us that among all tested compounds, compounds **2** and **6** were the most potent and, thus, were chosen for further, more detailed analyses.

One characteristic feature of cancer cells is the deregulation of the cell cycle, which leads to their uncontrolled proliferation. Therefore, the inhibition of cell cycle progression represents a common target of anticancer agents [25]. We performed the cell cycle analysis to reveal whether the antiproliferative effect of compounds **2** and **6** is reflected in the modification of cell cycle progression. Our results showed that both compounds were able to accumulate THP-1 and MCF-7 cancer cells in the G1 phase and to inhibit the transition of cells to the synthetic phase. We assume that this most likely reflects the antiproliferative effect observed in both cell lines (Figure 1a). The progression through the cell cycle is mediated by a family of cyclin-dependent kinases, the activity of which depends on the binding of the regulatory proteins, cyclins [26]. The observed accumulation of THP-1 and MCF-7 cells in the G1 phase after the treatment with compounds **2** and **6** was accompanied by a reduction of cyclin E1 level in a dose-dependent manner (Figure 2c). As the activator of CDK2, cyclin E1 is responsible for the G1/S phase progression and, thus, it is involved in surpassing the restriction point [27]. Many cancers typically overexpress cyclin E1, which is also proved in the MCF-7 cell line [28]. This might support our finding of only slight downregulation of cyclin E1 caused by the treatment of MCF-7 cells with compounds **2** and **6**, although these compounds effectively inhibited the G1/S transition. Interestingly, besides the downregulation of cyclin E1 full-length form, we also detected a more pronounced reduction of LMW E1 isoform levels in THP-1 cells treated with compounds **2** and **6**. LMW E1 isoforms are generated primarily in cancer cells, where they still remain fully functional. They have even higher potency to increase CDK2/E1 activity than the full-length form and, thus, they move the cells through the cell cycle more effectively than the full-length form [29,30].

Our previous study reported a similar detection of the decreased levels of cyclin E1 isoforms in THP-1 cells treated with geranylated flavanone tomentodiplacone B that coincided with an induced accumulation of cells in G1 phase [31]. While cyclin B1 is involved in the G2/M transition associated with CDK1 [26], we did not observe any change in the levels of cyclin B1 in THP-1 or MCF-7 cells after the exposure to compounds 2 and 6. These findings are supported by our flow cytometric data that did not indicate any significant difference in the proportion of cells in G2/M cell cycle phase upon the treatment with these compounds (Figures 2b and 3b). Based on those results, we could suggest that compounds 2 and 6 most likely affect G1/S rather than the G2/M transition.

The presence of cell nuclei with hypodiploid DNA content during the cell cycle analysis could indicate a possible presence of apoptotic cells [32]. The assessment of sub-G1 peak levels revealed different effects among the tested compounds; a significant increase was detected only in THP-1 cells upon the treatment with compound 2 (Figure 4). Based on these findings, we performed further analysis to prove its possible pro-apoptotic effect in the THP-1 cell line. Results of Annexin V-FITC/PI assay showed us that compound 2 induced the THP-1 cells to undergo an early stage of apoptosis even after 12 h exposure (Figure 5). Nevertheless, compound 2 accumulated more effectively (dose and time-dependently) in cells in the late apoptotic stage. These results correlate with the data obtained from the viability staining assay. In addition, two already known anticancer agents of a different mode of action, cisplatin, which is able to crosslink with the DNA and, thus, cause DNA damage [33], and camptothecin as the S-phase-specific inhibitor of the enzyme DNA topoisomerase-I [34], were added to the assay as model compounds with proved pro-apoptotic effects in THP-1 cells [35,36]. Although our results found all three compounds to significantly increase the number of cells positive for Annexin V-FITC staining, their effect led to different proportions of early and late apoptotic/secondary necrotic cells. While cisplatin induced a time-dependent substantial increase in the fraction of early apoptotic cells, camptothecin most likely elicited the time-dependent transfer of cells from early apoptotic to late apoptotic stages. These differences observed in the effect of three tested compounds enable us to presume a different mechanism of action of compound 2 in comparison with one of the two model anticancer agents.

These findings prompted us to further investigate the involvement of compound 2 in the apoptotic pathways. The caspases regulate the process of apoptosis in a different manner. The activation of caspase 8 is realized through the extrinsic apoptotic pathway after the binding of a ligand to an appropriate death receptor. Subsequently, the active form interacts with effector caspase 3 and that results in its cleavage and activation. On the other hand, initiator caspase 9 is involved in the intrinsic, also known as the mitochondrial apoptosis pathway, and is activated after the leakage of the mitochondrial cytochrome c. This also leads to proteolytic cleavage of inactive procaspase 3 and to its activation. Therefore, it denotes the essential role of caspase 3 in both extrinsic and intrinsic pathways, as it also comprises a link between them [37,38]. After 24 h treatment, compound 2 was found to be capable of inducing an increase of active caspase 3 level, including the decreased level of inactive pro-caspase 3, both significantly at a concentration of 10 μ M (Figure 6). At the same time, compound 2 caused also the cleavage of pro-caspase 9. On the contrary, no change in the level of the active form of caspase 8 was observed in comparison with the control, non-treated cells. These results indicate that compound 2 induces apoptosis in THP-1 cells by activating a caspase cascade. In addition, we could hypothesize that this compound might be preferably involved in the intrinsic apoptotic pathway. However, such specificity needs to be proved by additional analyses, and the mechanism of targeting apoptotic pathway remains unknown.

4. Materials and Methods

4.1. Chemicals and Reagents

The tested nitro-substituted hydroxynaphthanilides 1–6 were prepared and supplied by the Department of Chemical Drugs, Faculty of Pharmacy, University of Veterinary and Pharmaceutical

Sciences Brno, Czech Republic. The synthesis and structural characterization of these compounds have been described previously [3,5]. Due to poor solubility in water, the compounds were dissolved in dimethyl sulfoxide (DMSO) (Sigma-Aldrich, St. Louis, MO, USA), while the stock solutions were prepared freshly before each experiment. The final concentration of DMSO in the assays never exceeded 0.1% (*v/v*). Cisplatin and camptothecin were purchased from Sigma-Aldrich. RPMI 1640 and DMEM culture media, phosphate-buffered saline (PBS), foetal bovine serum (FBS) and antibiotics (penicillin and streptomycin) were obtained from HyClone Laboratories, Inc. (GE Healthcare, Logan, UT, USA). Mouse monoclonal antibodies against cyclin E1 (sc-247), caspase 3 (sc-7272) and caspase 9 (sc-17784) were purchased from Santa Cruz Biotechnology (Santa Cruz, CA, USA). Rabbit polyclonal antibodies against cyclin B1 (ab2949) and caspase 8 (ab-25901) were purchased from Abcam (Cambridge, UK). All other reagents, unless specified elsewhere, were purchased from Sigma-Aldrich.

4.2. Cell Culture

THP-1 human monocytic leukemia cell line, MCF-7 human breast adenocarcinoma cells and 3T3-L1 mouse embryonic fibroblast were purchased from the European Collection of Cell Cultures (ECACC, Salisbury, UK). Cells were routinely tested for the absence of mycoplasma (Hoechst 33258 staining method). THP-1 cells were maintained in RPMI 1640 culture medium containing 2 mM L-glutamine; MCF-7 and 3T3-L1 cells were cultured in DMEM medium. All of the culture media were supplemented with 10% heat-inactivated FBS and antibiotics (100 U/mL penicillin and 100 µg/mL streptomycin). Cells were maintained at 37 °C in a humidified atmosphere containing 5% CO₂.

4.3. Analysis of Cell Proliferation and Viability

Cell proliferation was evaluated using Cell Proliferation Reagent WST-1 (2-(4-iodophenyl)-3-(4-nitrophenyl)-5-(2,4-disulfophenyl)-2H-tetrazolium) (Roche Diagnostics, Mannheim, Germany) according to the manufacturer's instructions. THP-1 (5×10^4 cells/100 µL culture medium per well), MCF-7 cells (1×10^4 cells/100 µL per well), and 3T3-L1 (2.5×10^3 cells/100 µL per well) were cultured in 96-well plates in triplicate. The measurement was performed using Synergy 2 Multi-Mode Microplate Reader (BioTek, Winooski, VT, USA) after 24 h incubation of cells with tested compounds dissolved in DMSO and subsequently in RPMI 1640 to final concentration ranging 0.5–20 µM in the assays. Cell viability was assessed by dye exclusion test. THP-1 (2×10^5 cells/mL per well) and MCF-7 cells (8×10^4 cells/mL per well) were incubated in 24-well plates with the indicated concentrations of compounds for 24 h. The number of viable cells was determined using hemocytometer after their staining with a solution of erythrosin B (0.1% erythrosin B (*w/v*) in PBS). The assays were conducted in triplicate. The IC₅₀ and LC₅₀ values were calculated from fitted concentration-response curves using GraphPad Prism 5.00 software (GraphPad Software, San Diego, CA, USA).

4.4. Cell Cycle Analysis

THP-1 and sub-confluent MCF-7 cells were treated and subsequently incubated with indicated concentrations of compounds **2** and **6** for 24 h. After the incubation, cells were washed twice in PBS (pH 7.4), fixed in 70% ethanol and stored at –20 °C overnight. Fixed cells were collected by centrifugation, and supernatant was discarded. The cell pellet was washed twice with PBS and incubated with RNaseA (0.02 mg/mL) and 0.05% (*v/v*) Triton X-100 in PBS for 30 min at 37 °C. After the nuclei staining with propidium iodide (PI) (0.04 mg/mL), the cell cycle distribution was analysed using a flow cytometer Cell Lab Quanta SC (Beckman Coulter, Brea, CA, USA). The quantification of cell cycle distribution was carried out using software MultiCycle AV (Phoenix Flow System, San Diego, CA, USA). A total number of 2×10^4 cells was analysed per sample.

4.5. Detection of Apoptosis Using Annexin V-FITC/PI Assay

Early and late stages of apoptosis were detected using Annexin V-FITC Kit—Apoptosis Detection Kit according to the manufacturer's instructions. THP-1 cells were treated with increasing

concentrations of compound **2** (2.5, 5, and 10 μM), cisplatin (10 $\mu\text{g}/\text{mL}$) and camptothecin (5 μM). At each time-point of incubation (12, 18, and 24 h) the cells were washed with ice-cold PBS prior to being resuspended at a concentration of 5×10^6 cells/mL in a total volume of 100 μL of $1 \times$ binding buffer. Annexin V-FITC solution (final concentration 0.25 $\mu\text{g}/\text{mL}$) and PI (final concentration 12.5 $\mu\text{g}/\text{mL}$) were added to each sample; the cell suspension was kept on ice and incubated for 15 min in the dark. After that, the analysis was carried out by flow cytometry. The data were evaluated using Kaluza Flow Cytometry Analysis 1.2. Per sample, a total number of 2×10^4 cells were analysed.

4.6. Western Blotting

For Western blotting, cells were washed with PBS and lysed in lysis buffer (100 mM Tris-HCl, pH = 6.8; 20% glycerol; 1% SDS) containing protease and phosphatase inhibitor cocktails. Protein concentration was measured using Roti[®]-Quant universal (Carl Roth, Karsruhe, Germany) according to the manufacturer's instructions. Cell lysates were supplemented with bromophenol blue (final concentration 0.01% (*w/v*)) and β -mercaptoethanol (final concentration 1% (*v/v*)) prior to being heated for 5 min at 95 °C. Equal amounts of protein (10 μg) were loaded into a 12% polyacrylamide gel, separated by SDS-polyacrylamide gel electrophoresis and subsequently electrotransferred onto nitrocellulose membranes. Reversible Ponceau S. staining was performed to assess equal sample loading. Then, the membranes were blocked with 5% non-fat dry milk in TBST (10 mM Tris-HCl pH = 7.5, 150 mM NaCl, 0.1% (*v/v*) Tween-20) and appropriate primary and secondary antibodies were used for immunodetection. The proteins were visualized by ECL Plus reagent according to the manufacturer's instructions. The intensity of bands was semi-quantitatively analysed using the ImageJ software (National Institute of Mental Health, Bethesda, MD, USA).

4.7. Statistical Analysis

All experimental data were expressed as the arithmetical mean \pm standard deviation (SD). Statistical analysis was performed using one-way analysis of variance (ANOVA) followed by the Dunnett's post test using GraphPad Prism 5.00 software. Statistical significance was assessed at levels of $p < 0.05$, $p < 0.01$ and $p < 0.001$.

5. Conclusions

The present study provides the first description of the antiproliferative activity of nitro-substituted hydroxynaphthanilides in the context of structure-activity relationships. Our results indicate that the potency of ring-substituted hydroxynaphthanilides towards cell growth inhibition increases with positioning of the nitro group as follows: *ortho* < *meta* < *para*. The most promising compounds **2** and **6** exerted antiproliferative activity in THP-1 and MCF-7 cancer cells with single-digit micromolar IC_{50} values, while they had a minimal effect on the growth of 3T3-L1 non-tumour cells. Compounds **2** and **6** accumulated cancer cells THP-1 and MCF-7 in G1 cell cycle phase, which was accompanied by the observed down-regulation of cyclin E1 levels. Moreover, compound **2** was found to induce apoptosis in THP-1 cells via a caspase-mediated cascade. The results also indicate that apoptosis was probably induced through the intrinsic apoptotic pathway, although further analysis is still required to verify such assumption. According to the results, nitro-substituted hydroxynaphthanilides **2** and **6** can be considered as potential anticancer agents, and the structure of hydroxynaphthanilides is an appropriate model moiety for further design of compounds with potential anticancer properties.

Acknowledgments: This work was supported by the Internal Grant Agency of the University of Veterinary and Pharmaceutical Sciences Brno (323/2015/FaF).

Author Contributions: Peter Kollar conceived and designed the experiments; Tereza Kauerova performed the experiments and analyzed the data; Jiri Kos, Tomas Gonec and Josef Jampilek contributed reagents/materials/analysis tools; Tereza Kauerova and Peter Kollar wrote the paper.

Conflicts of Interest: The authors declare no conflict of interest.

References

1. Kratky, M.; Vinsova, J.; Novotna, E.; Mandikova, J.; Wsol, V.; Trejtnar, F.; Ulmann, V.; Stolarikova, J.; Fernandes, S.; Bhat, S.; et al. Salicylanilide derivatives block mycobacterium tuberculosis through inhibition of isocitrate lyase and methionine aminopeptidase. *Tuberculosis (Edinburgh)* **2012**, *92*, 434–439. [[CrossRef](#)] [[PubMed](#)]
2. Zadrazilova, I.; Pospisilova, S.; Masarikova, M.; Imramovsky, A.; Ferriz, J.M.; Vinsova, J.; Cizek, A.; Jampilek, J. Salicylanilide carbamates: Promising antibacterial agents with high in vitro activity against methicillin-resistant staphylococcus aureus (MRSA). *Eur. J. Pharm. Sci.* **2015**, *77*, 197–207. [[CrossRef](#)] [[PubMed](#)]
3. Gonec, T.; Kos, J.; Zadrazilova, I.; Pesko, M.; Govender, R.; Keltosova, S.; Chambel, B.; Pereira, D.; Kollar, P.; Imramovsky, A.; et al. Antibacterial and herbicidal activity of ring-substituted 2-hydroxynaphthalene-1-carboxanilides. *Molecules* **2013**, *18*, 9397–9419. [[CrossRef](#)] [[PubMed](#)]
4. Gonec, T.; Kos, J.; Zadrazilova, I.; Pesko, M.; Keltosova, S.; Tengler, J.; Bobal, P.; Kollar, P.; Cizek, A.; Kralova, K.; et al. Antimycobacterial and herbicidal activity of ring-substituted 1-hydroxynaphthalene-2-carboxanilides. *Bioorg. Med. Chem.* **2013**, *21*, 6531–6541. [[CrossRef](#)] [[PubMed](#)]
5. Kos, J.; Zadrazilova, I.; Pesko, M.; Keltosova, S.; Tengler, J.; Gonec, T.; Bobal, P.; Kauerova, T.; Oravec, M.; Kollar, P.; et al. Antibacterial and herbicidal activity of ring-substituted 3-hydroxynaphthalene-2-carboxanilides. *Molecules* **2013**, *18*, 7977–7997. [[CrossRef](#)] [[PubMed](#)]
6. Olliaro, P.; Seiler, J.; Kuesel, A.; Horton, J.; Clark, J.N.; Don, R.; Keiser, J. Potential drug development candidates for human soil-transmitted helminthiasis. *PLoS Negl. Trop. Dis.* **2011**, *5*, e1138. [[CrossRef](#)] [[PubMed](#)]
7. Mudduluru, G.; Walther, W.; Kobelt, D.; Dahlmann, M.; Treese, C.; Assaraf, Y.G.; Stein, U. Repositioning of drugs for intervention in tumor progression and metastasis: Old drugs for new targets. *Drug Resist. Updat.* **2016**, *26*, 10–27. [[CrossRef](#)] [[PubMed](#)]
8. Osada, T.; Chen, M.; Yang, X.Y.; Spasojevic, I.; Vandeusen, J.B.; Hsu, D.; Clary, B.M.; Clay, T.M.; Chen, W.; Morse, M.A.; et al. Antihelminth compound niclosamide downregulates Wnt signaling and elicits antitumor responses in tumors with activating APC mutations. *Cancer Res.* **2011**, *71*, 4172–4182. [[CrossRef](#)] [[PubMed](#)]
9. Li, Y.; Li, P.K.; Roberts, M.J.; Arend, R.C.; Samant, R.S.; Buchsbaum, D.J. Multi-targeted therapy of cancer by niclosamide: A new application for an old drug. *Cancer Lett.* **2014**, *349*, 8–14. [[CrossRef](#)] [[PubMed](#)]
10. Fonseca, B.D.; Diering, G.H.; Bidinosti, M.A.; Dalal, K.; Alain, T.; Balgi, A.D.; Forestieri, R.; Nodwell, M.; Rajadurai, C.V.; Gunaratnam, C.; et al. Structure-activity analysis of niclosamide reveals potential role for cytoplasmic pH in control of mammalian target of rapamycin complex 1 (mTORC1) signaling. *J. Biol. Chem.* **2012**, *287*, 17530–17545. [[CrossRef](#)] [[PubMed](#)]
11. Lu, W.; Lin, C.; Roberts, M.J.; Waud, W.R.; Piazza, G.A.; Li, Y. Niclosamide suppresses cancer cell growth by inducing Wnt co-receptor LRP6 degradation and inhibiting the Wnt/ β -catenin pathway. *PLoS ONE* **2011**, *6*, e29290. [[CrossRef](#)] [[PubMed](#)]
12. Jin, Y.; Lu, Z.; Ding, K.; Li, J.; Du, X.; Chen, C.; Sun, X.; Wu, Y.; Zhou, J.; Pan, J. Antineoplastic mechanisms of niclosamide in acute myelogenous leukemia stem cells: Inactivation of the NF-kappaB pathway and generation of reactive oxygen species. *Cancer Res.* **2010**, *70*, 2516–2527. [[CrossRef](#)] [[PubMed](#)]
13. Kang, B.-R.; Shan, A.-L.; Li, Y.-P.; Xu, J.; Lu, S.-M.; Zhang, S.-Q. Discovery of 2-aryl-8-hydroxy (or methoxy)-isoquinolin-1(2H)-ones as novel EGFR inhibitor by scaffold hopping. *Bioorg. Med. Chem.* **2013**, *21*, 6956–6964. [[CrossRef](#)] [[PubMed](#)]
14. Liechti, C.; Sequin, U.; Bold, G.; Furet, P.; Meyer, T.; Traxler, P. Salicylanilides as inhibitors of the protein tyrosine kinase epidermal growth factor receptor. *Eur. J. Med. Chem.* **2004**, *39*, 11–26. [[CrossRef](#)] [[PubMed](#)]
15. Deng, W.; Guo, Z.; Guo, Y.; Feng, Z.; Jiang, Y.; Chu, F. Acryloylamino-salicylanilides as EGFR PTK inhibitors. *Bioorg. Med. Chem. Lett.* **2016**, *16*, 469–472. [[CrossRef](#)] [[PubMed](#)]
16. Zhu, X.F.; Wang, J.S.; Cai, L.L.; Zeng, Y.X.; Yang, D. SUCI02 inhibits the erbb-2 tyrosine kinase receptor signaling pathway and arrests the cell cycle in G1 phase in breast cancer cells. *Cancer Sci.* **2006**, *97*, 84–89. [[CrossRef](#)] [[PubMed](#)]
17. Imramovsky, A.; Jorda, R.; Pauk, K.; Reznickova, E.; Dusek, J.; Hanusek, J.; Krystof, V. Substituted 2-hydroxy-N-(arylalkyl)benzamides induce apoptosis in cancer cell lines. *Eur. J. Med. Chem.* **2016**, *68*, 253–259. [[CrossRef](#)] [[PubMed](#)]

18. Zuo, M.; Zheng, Y.W.; Lu, S.M.; Li, Y.; Zhang, S.Q. Synthesis and biological evaluation of *N*-aryl salicylamides with a hydroxamic acid moiety at 5-position as novel HDAC-EGFR dual inhibitors. *Bioorg. Med. Chem.* **2012**, *20*, 4405–4412. [[CrossRef](#)] [[PubMed](#)]
19. Solomon, V.R.; Lee, H. Quinoline as a privileged scaffold in cancer drug discovery. *Curr. Med. Chem.* **2011**, *18*, 1488–1508. [[CrossRef](#)] [[PubMed](#)]
20. Guo, L.; Wang, Q.L.; Jiang, Q.Q.; Jiang, Q.J.; Jiang, Y.B. Anion-triggered substituent-dependent conformational switching of salicylanilides. New hints for understanding the inhibitory mechanism of salicylanilides. *J. Org. Chem.* **2007**, *72*, 9947–9953. [[CrossRef](#)] [[PubMed](#)]
21. Walters Haygood, C.L.; Arend, R.C.; Gangrade, A.; Chettiar, S.; Regan, N.; Hassmann, C.J., 2nd; Li, P.K.; Hidalgo, B.; Straughn, J.M., Jr.; Buchsbaum, D.J. Niclosamide analogs for treatment of ovarian cancer. *Int. J. Gynecol. Cancer* **2015**, *25*, 1377–1385. [[CrossRef](#)] [[PubMed](#)]
22. Brumatti, G.; Sheridan, C.; Martin, S.J. Expression and purification of recombinant annexin V for the detection of membrane alterations on apoptotic cells. *Methods* **2008**, *44*, 235–240. [[CrossRef](#)] [[PubMed](#)]
23. Kumar, S. Caspase function in programmed cell death. *Cell Death Differ.* **2007**, *14*, 32–43. [[CrossRef](#)] [[PubMed](#)]
24. Malik, I.; Bukovsky, M.; Andriamainty, F.; Galisinova, J. Antimicrobial activity of meta-alkoxyphenylcarbamates containing substituted *N*-phenylpiperazine fragment. *Braz. J. Microbiol.* **2012**, *3*, 959–965.
25. Williams, G.H.; Stoeber, K. The cell cycle and cancer. *J. Pathol.* **2012**, *226*, 352–364. [[CrossRef](#)] [[PubMed](#)]
26. Malumbres, M.; Barbacid, M. Cell cycle, CDKs and cancer: A changing paradigm. *Nat. Rev. Cancer* **2009**, *9*, 153–166. [[CrossRef](#)] [[PubMed](#)]
27. Diaz-Moralli, S.; Tarrado-Castellarnau, M.; Miranda, A.; Cascante, M. Targeting cell cycle regulation in cancer therapy. *Pharmacol. Ther.* **2013**, *138*, 255–271. [[CrossRef](#)] [[PubMed](#)]
28. Guo, X.; Hartley, R.S. Hur contributes to cyclin E1 deregulation in MCF-7 breast cancer cells. *Cancer Res.* **2006**, *66*, 7948–7956. [[CrossRef](#)] [[PubMed](#)]
29. Wingate, H.; Bedrosian, I.; Akli, S.; Keyomarsi, K. The low molecular weight (LMW) isoforms of cyclin E deregulate the cell cycle of mammary epithelial cells. *Cell Cycle* **2003**, *2*, 461–466. [[CrossRef](#)] [[PubMed](#)]
30. Akli, S.; Keyomarsi, K. Cyclin E and its low molecular weight forms in human cancer and as targets for cancer therapy. *Cancer Biol. Ther.* **2003**, *2*, S38–S47. [[CrossRef](#)] [[PubMed](#)]
31. Kollar, P.; Barta, T.; Zavalova, V.; Smejkal, K.; Hampl, A. Geranylated flavanone tomentodiplacone B inhibits proliferation of human monocytic leukaemia (THP-1) cells. *Br. J. Pharmacol.* **2011**, *162*, 1534–1541. [[CrossRef](#)] [[PubMed](#)]
32. Kajstura, M.; Halicka, H.D.; Pryjma, J.; Darzynkiewicz, Z. Discontinuous fragmentation of nuclear DNA during apoptosis revealed by discrete “sub-G1” peaks on DNA content histograms. *Cytom. A* **2007**, *71*, 125–131. [[CrossRef](#)] [[PubMed](#)]
33. Dasari, S.; Tchounwou, P.B. Cisplatin in cancer therapy: Molecular mechanisms of action. *Eur. J. Pharmacol.* **2014**, *740*, 364–378. [[CrossRef](#)] [[PubMed](#)]
34. Liu, L.F.; Desai, S.D.; Li, T.K.; Mao, Y.; Sun, M.; Sim, S.P. Mechanism of action of camptothecin. *Ann. N. Y. Acad. Sci.* **2000**, *922*, 1–10. [[CrossRef](#)] [[PubMed](#)]
35. Stephenson, D.A.; Toltl, L.J.; Beaudin, S.; Liaw, P.C. Modulation of monocyte function by activated protein C, a natural anticoagulant. *J. Immunol.* **2006**, *177*, 2115–2122. [[CrossRef](#)] [[PubMed](#)]
36. Amran, D.; Sancho, P.; Fernandez, C.; Esteban, D.; Ramos, A.M.; de Blas, E.; Gomez, M.; Palacios, M.A.; Aller, P. Pharmacological inhibitors of extracellular signal-regulated protein kinases attenuate the apoptotic action of cisplatin in human myeloid leukemia cells via glutathione-independent reduction in intracellular drug accumulation. *Biochim. Biophys. Acta* **2005**, *1743*, 269–279. [[CrossRef](#)] [[PubMed](#)]
37. McIlwain, D.R.; Berger, T.; Mak, T.W. Caspase functions in cell death and disease. *Cold Spring Harb. Perspect. Biol.* **2013**, *5*, a008656. [[CrossRef](#)] [[PubMed](#)]
38. Degterev, A.; Boyce, M.; Yuan, J. A decade of caspases. *Oncogene* **2003**, *22*, 8543–8567. [[CrossRef](#)] [[PubMed](#)]



č.	citace	ISSN
7	KUSHKEVYCH, I, J KOS , P KOLLAR, K KRALOVA a J JAMPILEK. Activity of ring-substituted 8-hydroxyquinoline-2-carboxanilides against intestinal sulfate-reducing bacteria <i>Desulfovibrio piger</i> . <i>MEDICINAL CHEMISTRY RESEARCH</i> [online]. 2018, 27 (1), 278–284. Dostupné z: doi: 10.1007/s00044-017-2067-7	1054-2523

Activity of ring-substituted 8-hydroxyquinoline-2-carboxanilides against intestinal sulfate-reducing bacteria *Desulfovibrio piger*

Ivan Kushkevych¹ · Jiri Kos² · Peter Kollar³ · Katarina Kralova⁴ · Josef Jampilek^{1,2} 

Received: 30 June 2017 / Accepted: 5 September 2017 / Published online: 15 September 2017
© Springer Science+Business Media, LLC 2017

Abstract *Desulfovibrio* genus is dominant among sulfate-reducing bacteria (SRB) in the large intestine of healthy people and animals. It is mostly isolated from patients with inflammatory bowel disease (IBD) and can be involved in the disease initiation. Primary in vitro screening of 8-hydroxyquinoline-2-carboxanilides was performed against *Desulfovibrio piger* Vib-7 representing SRB. The most effective compounds with MIC₉₀/MBC values in the range of 17–23 μM/20–23 μM, respectively, were substituted in C' (3) by CF₃, OCH₃, CH₃ and in C' (4) by CF₃. Their activity was twofold higher than that of ciprofloxacin. These compounds did not express any significant cytotoxic effect on THP-1 cells up to the tested concentration of 30 μM. The antibacterial efficacy of the most active C' (3)-substituted compounds practically did not change with increasing compound lipophilicity, indicating that this position of substitution is favorable for significant antimicrobial effect, while the antibacterial activity of most of C' (2) and C' (4)-substituted derivatives decreased linearly with increasing

compound lipophilicity. In addition, the dependence of activity on electronic Hammett's σ parameter of the substituent R was quasi-parabolic for the most effective C' (3)-substituted compounds.

Keywords 8-Hydroxyquinolines · Sulfate-reducing bacteria · Lipophilicity · Electronic parameter · Structure–activity relationships

Introduction

The species of *Desulfovibrio* genus are dominant among sulfate-reducing bacteria (SRB) and common inhabitants of the human and animal large intestine, capable of dissimilatory sulfate reduction (Gibson et al. 1991, 1993; Kushkevych 2015a, b; Kushkevych et al. 2015a, b; Wegmann et al. 2017). These microorganisms are the most isolated from patients with inflammatory bowel disease (IBD) and can be involved in the disease initiation caused by their main metabolite hydrogen sulfide, which is an inhibitor of butyrate oxidation in colonocytes. In addition, it is cytotoxic, mutagenic and cancerogenic to epithelial intestinal cells, which leads to the damage of the epithelial barrier function, resulting in inflammatory responses characteristic for IBD (Kushkevych et al. 2014; Pitcher and Cummings 1996; Zinkevich and Beech 2000). Therefore, the association between SRB and IBD, such as ulcerative colitis (UC), was hypothesized (Zinkevich and Beech 2000; Rowan et al. 2009; Loubinoux et al. 2002; Kushkevych 2014; Cummings et al. 2003). Over 1 million residents in the USA and 2.5 million in Europe are estimated to have IBD, with substantial costs for health care, whereas these estimates do not

✉ Ivan Kushkevych
ivan.kushkevych@gmail.com

✉ Josef Jampilek
josef.jampilek@gmail.com

¹ Department of Experimental Biology, Faculty of Science, Masaryk University, Kamenice 753/5, 625 00 Brno, Czech Republic

² Department of Pharmaceutical Chemistry, Faculty of Pharmacy, Comenius University, Odbojarov 10, 832 32 Bratislava, Slovakia

³ Department of Human Pharmacology and Toxicology, Faculty of Pharmacy, University of Veterinary and Pharmaceutical Sciences, Palackeho 1, 612 42 Brno, Czech Republic

⁴ Institute of Chemistry, Faculty of Natural Sciences, Comenius University, Ilkovicova 6, 842 15 Bratislava, Slovakia

factor in the ‘real’ price of IBD, which can impede career aspirations, instil social stigma and impair quality of life in patients (Kaplan 2015). Unlike Crohn’s disease, UC occurs only in the large bowel, where bacteria amount is greater than in the rest of the gut and also where the rate of passage of material is characterized by slow movement of digestive materials. Both acute and chronic forms of UC affect the colon and rectum and can be a highly uncomfortable condition (Cummings et al. 2003). UC usually has a relapsing/remitting pattern and current medical approaches focus on treating active disease to address symptoms, to improve the quality of life and thereafter to maintain remission. Diarrhea accompanied with blood, an urgent need to defecate and abdominal pain are the main symptoms of active disease or relapse. The reported incidence is 1.2 to 20.3 cases per 100,000 persons per year, and the prevalence is 7.6 to 245 cases per 100,000 per year (Feuerstein and Cheifetz 2014; Cesar da Silva et al. 2014).

The benefits of antibiotic therapy in UC are mediated by different mechanisms, such as decreasing the concentration of luminal bacteria, altering the composition of gut microflora, decreasing bacterial tissue invasion and decreasing bacterial translocation and systemic dissemination. Antibiotics have been prescribed for UC, however, they have been largely ineffective (Cummings et al. 2003; Garud and Peppercorn 2009). For example, the study of the in vitro activities of rifaximin and comparator agents against 536 anaerobic intestinal bacteria performed by Finegold et al. showed that the overall MIC₉₀ of rifaximin for 90% the tested strains were 338 µM, an activity equivalent to those of teicoplanin and vancomycin (Finegold et al. 2009). Nakao et al. (2009) tested the antimicrobial susceptibilities of 23 strains of *Desulfovibrio* spp. and found that they were susceptible to sulbactam-ampicillin, meropenem, clindamycin, and metronidazole with MIC₉₀ corresponding to 17, 10, 0.45, and 1.46 µM, respectively. On the other hand, Lozniewski et al. (2001) tested the antimicrobial susceptibilities of 16 clinical isolates of *Desulfovibrio* spp. and found that these isolates were resistant to piperacillin-tazobactam, cefoxitin and cefotetan with MIC₉₀ corresponding to 495, >600 and 111 µM, respectively. Therefore, it is necessary to study new antibacterial agents in order to improve the treatment and discover alternative therapeutics.

This paper follows our recently published articles dealing with the spectrum of biological activities of hydroxyquinoline-based compounds (Jampilek et al. 2005; Musiol et al. 2006, 2007, 2008, 2010; Mrozek-Wilczkiewicz et al. 2010; Gonec et al. 2012; Cieslik et al. 2012, 2015; Kos et al. 2015a; Jampilek et al. 2016). This study is focused on the investigation of the efficacy and searching for the structure–activity relationships within a series of 8-hydroxyquinoline-2-carboxanilides (Kos et al. 2015a)

against *Desulfovibrio piger* Vib-7 representing SRB. *D. piger* is a Gram-negative strict anaerobe that is usually considered as a commensal bacterium in humans. More recently, it has attracted more interest as it was found to be the most prevalent species of SRB in feces of patients with IBDs (Kushkevych 2014; Barton and Hamilton 2010; Holt et al. 1994).

Material and methods

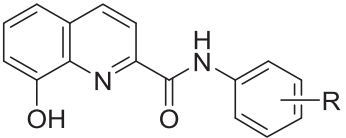
Synthesis

The discussed 8-hydroxyquinoline-2-carboxanilides **1–8c** (see Table 1) were synthesized previously (Kos et al. 2015a) by means of microwave-assisted synthesis. The compounds were fully characterized by melting point, infrared, nuclear magnetic resonance, and high-resolution mass spectrometry (Kos et al. 2015a).

In vitro antibacterial susceptibility testing

The synthesized compounds were evaluated for in vitro antibacterial activity against the intestinal SRB *Desulfovibrio piger* Vib-7 (Genbank: KT881309.1) that were isolated from the healthy human large intestine as described previously (Kushkevych 2013; Kushkevych et al. 2014). The strain has been kept in the collection of microorganisms at the Department of Molecular Biology and Pharmaceutical Biotechnology of the Faculty of Pharmacy at the University of Veterinary and Pharmaceutical Sciences Brno (Czech Republic). Ciprofloxacin (Sigma-Aldrich) was used as the standard. Prior to testing, the strain at exponential phase growth was passaged onto nutrition modified Kravtsov-Sorokin’s (KS) agar medium (Kushkevych and Moroz 2012). Bacterial inocula were prepared by suspending a small portion of bacterial colony in sterile KS liquid medium (pH 7.5). Before bacterial passage in the medium, 10 mL/L of sterile Mohr’s salt solution [(NH₄)SO₄Fe(SO₄)₂·6H₂O] (10%) for visual detecting colonies of the SRB was added. A culture sample (10 mL) was centrifuged at 15,000 rpm/20 min using a bench top centrifuge (Model CR 4-12, Jouan Inc., Winchester, VA, USA). Following removal of the supernatant, the pellet was washed in fresh liquid KS and re-suspended in fresh supplemented KS (10 mL). The turbidity was adjusted to match McFarland standard No. 1 (5 × 10⁶ cfu) with KS using a densitometer (Densi-La-Meter, LIAP, Latvia). The final inoculum was made to a 1:20 dilution of the suspension with KS liquid medium. The antimicrobial susceptibility of SRB was investigated in a 96-well plate format. In these experiments, sterile KS (300 µL) was added to all outer-perimeter wells of the plates to minimize evaporation of the medium in the

Table 1 Experimentally determined values of lipophilicity $\log k$, predicted electronic Hammett's σ parameters of substituents R, in vitro antibacterial activity against *Desulfovibrio piger* Vib-7 (MIC, IC₅₀, MBC) of the compounds in comparison with ciprofloxacin (CPX) standard



Compounds	R ¹	$\log k^a$	σ^b	MIC ₉₀ [μ M]	IC ₅₀ [μ M]	MBC [μ M]
1	H	0.7600	0	23	12	25
2a	2-OCH ₃	0.7935	-0.28	28	17	28
2b	3-OCH ₃	0.8164	0.12	17	11	20
2c	4-OCH ₃	0.7129	-0.27	557	380	557
3a	2-CH ₃	0.6944	-0.17	44	15	48
3b	3-CH ₃	0.9686	-0.07	23	10	23
3c	4-CH ₃	0.9521	-0.17	75	40	80
4a	2-F	0.6806	0.06	90	50	95
4b	3-F	0.9420	0.34	45	20	50
4c	4-F	0.8598	0.06	60	28	60
5a	2-Cl	0.9566	0.22	120	95	123
5b	3-Cl	1.1718	0.37	50	20	55
5c	4-Cl	1.1543	0.23	480	330	486
6a	2-Br	1.0536	0.22	150	103	150
6b	3-Br	1.2357	0.39	33	18	35
6c	4-Br	1.2347	0.23	337	225	340
7a	2-CF ₃	0.9147	0.51	48	35	50
7b	3-CF ₃	1.3206	0.43	17	10	20
7c	4-CF ₃	1.3653	0.51	20	10	22
8a	2-NO ₂	1.1277	0.77	197	134	202
8b	3-NO ₂	0.9845	0.71	237	218	240
8c	4-NO ₂	1.0495	0.78	223	165	225
CPX	-	-	-	45	28	45

^a Experimental procedure described in Kos et al. (2015a)

^b Predicted using sw. ACD/Percepta ver. 2012

test wells during incubation. Sample wells were composed of 100 μ L of test compound dilution and 100 μ L of the bacterial stock being tested against. The compounds were dissolved in dimethyl sulfoxide (DMSO, Sigma), and the final concentration of DMSO in the KS liquid medium did not exceed 0.1% of the total solution composition. Dilutions of each compound were prepared in triplicate. The final concentrations of the evaluated compounds ranged from 100 to 0.05 μ M. Plates were sealed with parafilm, introduced into an anaerobic box with oxygen uptake generators (GENbox anaer, France) for anaerobiosis. The determination of results was performed visually after

72 h of static incubation in the darkness at 37 °C under anaerobic conditions. In the process of bacterial growth, hydrogen sulfide was formed and interacted with Fe²⁺ from Mohr's salt. As a result, FeS was formed by the bacterial cells that caused black colored colonies that was interpreted as a presence of bacterial growth. The medium dilution micro-method modified according to NCCLS guidelines (CLSI 2012, 2014) in KS medium was used to determine the minimum inhibitory concentration (MIC₉₀), the inhibitory concentration (IC₅₀) and minimum bactericidal concentration (MBC). Drug-free controls, sterility controls and controls consisted of KS medium and DMSO alone were included. The MICs were defined as the lowest concentration of the compound at which no visible bacterial growth was observed. The IC₅₀ values were defined as the compound concentration causing 50% inhibition of bacterial growth and the MBCs were defined as the lowest concentration of the compound at which an antimicrobial agent kills a bacteria (CLSI 2012, 2014). The results are summarized in Table 1.

Results and discussion

In the previous studies it was confirmed that 2-substituted 8-hydroxyquinolines are promising antimicrobial agents (Jampilek et al. 2005; Musiol et al. 2006, 2010; Darby and Nathan 2010; Gonec et al. 2012; Cieslik et al. 2012; 2015; Kos et al. 2015a). Based on these observations, 8-hydroxyquinoline-2-carboxanilides prepared according to Scheme 1 and described recently (Kos et al. 2015a) were tested against *Desulfovibrio piger* Vib-7. The testing was performed according to Kushkevych et al. (2016).

The antibacterial potency of ring-substituted 8-hydroxyquinoline-2-carboxanilides was expressed as the MICs, IC₅₀ values and MBCs, see Table 1. The activity of the most potent compounds **7b** (R = 3-CF₃; MIC = 17 μ M, IC₅₀ = 10 μ M, MBC = 20 μ M), **7c** (R = 4-CF₃; MIC = 20 μ M, IC₅₀ = 10 μ M, MBC = 22 μ M) and **2b** (R = 3-OCH₃; MIC = 17 μ M, IC₅₀ = 11 μ M, MBC = 20 μ M) was twofold higher than that of the clinically used drug ciprofloxacin (MIC = MBC = 45 μ M) that was used as the standard. Also other compounds such as **3b** (R = 3-CH₃; MBC = 23 μ M), **1** (R = H; MBC = 25 μ M), **2a** (R = 2-OCH₃; MBC = 28 μ M), and **5b** (R = 3-Br; MBC = 35 μ M) were effective in killing *D. piger* Vib-7. It is also important to note that no significant cytotoxic effect of these compounds on THP-1 cells up to tested concentration 30 μ M was observed (Kos et al. 2015a).

The dependence of $\log(1/IC_{50})$ on compound lipophilicity expressed by $\log k$ (Kos et al. 2015a) is shown in Fig. 1a. After exclusion of three derivatives: 4-OCH₃ (**2c**), which precipitated from testing solution due to limited

Scheme 1 Synthesis of ring-substituted 8-hydroxyquinoline-2-carboxanilides **1–8c**: Reagents and conditions: **a** PCl_3 , chlorobenzene, microwave-assisted synthesis (Kos et al. 2015a)

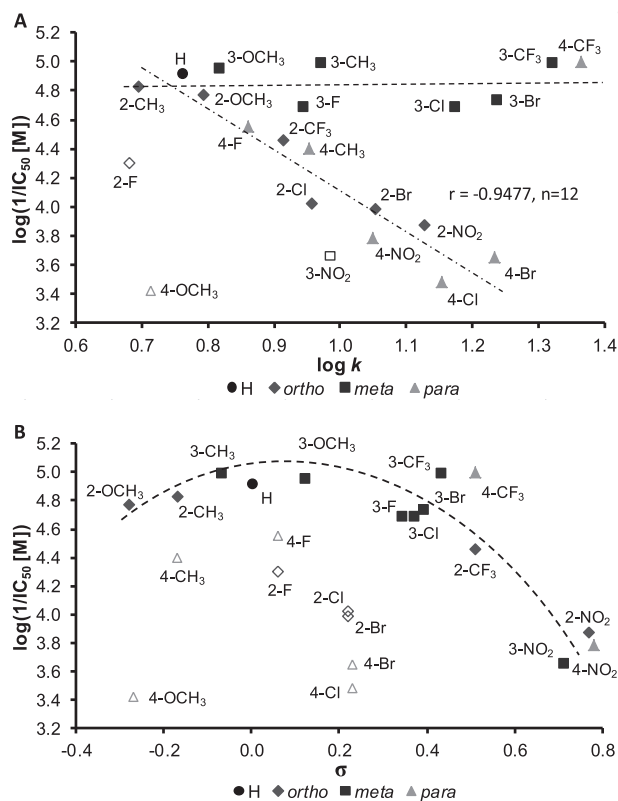
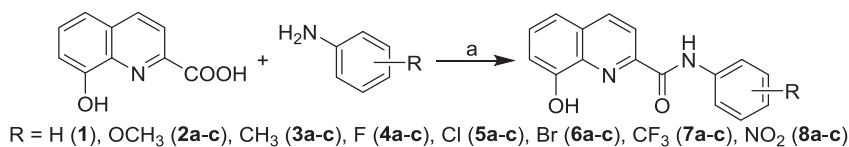


Fig. 1 Dependence of antibacterial activity against *Desulfovibrio piger* Vib-7 expressed as $\log(1/IC_{50})$ [M] of tested compounds on lipophilicity expressed as $\log k$ (**a**) and on Hammett's σ constants of R substituent (**b**). (Compounds not included in individual SAR discussions are marked by empty symbol.)

aqueous solubility, and 2-F (**4a**) and 3-NO₂ (**8b**), showing lower activity than expected, the compounds can be divided into two groups. The antibacterial activity of nine derivatives with R = 2-CH₃ (**3a**), 2-OCH₃ (**2a**), 3-OCH₃ (**2a**), 3-F (**4b**), 3-CH₃ (**3b**), 3-Cl (**5b**), 3-Br (**6b**), 3-CF₃ (**7b**), and 4-CF₃ (**7c**) expressed by IC₅₀ value was comparable with that of unsubstituted derivative **1** (R = H; IC₅₀ = 12 μM) and varied in the range from 10 μM (3-CF₃ and 4-CF₃, 3-CH₃) to 20 μM (3-F and 3-Cl), while the antibacterial activity of other 12 tested (C'₍₂₎, C'₍₄₎-substituted derivatives and **1**) compounds decreased linearly with increasing compound lipophilicity from $\log k = 0.6944$ (2-CH₃, **3a**; IC₅₀ = 15 μM) to $\log k = 1.2347$ (4-Br, **6c**; IC₅₀ = 225 μM) ($r = -0.9477$, $n = 12$). Thus, from seven C'₍₃₎-substituted

compounds, six derivatives belonged to the set of the above-mentioned most active compounds, the antibacterial activity of which practically did not change with increasing compound lipophilicity, indicating that this position of substitution is favorable for significant antimicrobial effect.

The dependence of $\log(1/IC_{50})$ on the Hammett's σ constants of the R substituent is shown in Fig. 1b. Except for derivatives with R = 4-OCH₃ (**2c**) and 4-CH₃ (**3c**) as well as derivatives with F, Cl, and Br substituents in positions C'₍₂₎ and C'₍₄₎, i.e., **4a**, **4c**, **5a**, **5c**, **6a**, and **6c**, for the remaining 14 compounds quasi-parabolic dependence of $\log(1/IC_{50})$ on σ constants was estimated. However, it could be mentioned that within a narrow range of σ from 0.06 to 0.22/0.23, the activity of C'₍₄₎ halogen-substituted compounds decreased more sharply with increasing σ values than that of C'₍₂₎-substituted ones.

Similar trends as for the dependence of $\log(1/IC_{50})$ on lipophilicity or on Hammett's σ constants can be found also for the dependences of the activity expressed as MIC or MBC values on both parameters; therefore, these dependences are not illustrated.

Summarizing, it can be concluded that generally for high antibacterial activity against *D. piger*, halogen substituent in the C'₍₃₎ position is favorable, whereby the highest antibacterial activity was exhibited by derivatives with R = 3-CF₃ and 4-CF₃, i.e., substituents that are known to promote electrostatic interactions with targets and improve the cellular membrane permeability of small molecules but also compounds with low lipophilicity (2-CH₃, 3-CH₃, 2-OCH₃, 3-OCH₃).

The estimated MIC values for *D. piger* (Table 1) are comparable with those estimated for the antimycobacterial activity of the tested compounds against *Mycobacterium tuberculosis* H37Ra ATCC 25177, *M. avium* complex CIT19/06 (clinical isolate) and *M. avium* subsp. *paratuberculosis* CIT03 (clinical isolate) (Kos et al. 2015a). It was found that with the exception of compounds with R = 4-OCH₃ (**2c**), 4-Cl (**5c**), 4-Br (**6c**), neither lipophilicity nor electronic properties of the R substituent nor the position of substitution exhibited any significant effect on the anti-tubercular activity against *M. tuberculosis*, and the 2-, 3- and 4-CF₃ (**7a-c**)-substituted derivatives belonged to the most active compounds with MIC = 24 μM . There were no any significant differences between antimycobacterial activities against *M. tuberculosis* and *M. avium* subsp. *paratuberculosis*. On the other hand, C'₍₂₎ and especially C'₍₃₎-

substituted derivatives expressed higher antimycobacterial activity against *M. avium* complex than C'₍₄₎-substituted ones, and antimycobacterial activity slightly increased with increasing lipophilicity (log *k* values) and electron-withdrawing effect of R substituents; the C'₍₂₎-substituted compounds with log *k* > 0.8 and Hammett's σ constants of R substituents > 0.1 and C'₍₄₎-substituted compounds with log *k* < 0.8 were found to be completely ineffective. However, the activity of compounds with potency against all three strains was achieved by the substitution of the C'₍₃₎ position of aniline. The significant bacterial/antimycobacterial activity of the studied compounds bearing an 8-hydroxyquinoline fragment and an amide moiety in their molecule is caused by the fact that these function groups are able to interact with a number of enzymes/receptors via hydrogen bonds and in this manner to affect the biological response (Pattabiraman and Bode 2011; Lavecchia and Di Giovanni 2013; Zumla et al. 2013). The significant contribution of the hydroxyl moiety in C₍₈₎ of quinoline to the antimycobacterial activity was reported by Gonec et al. (2012), who observed that its absence in quinoline-2-carboxanilides resulted in a decrease of antimycobacterial effect, while strengthening of antimycobacterial potency due to the presence of the hydroxyl moiety was observed with 1-hydroxy-naphthalene-2-carboxanilides (Gonec et al. 2013) and 6-hydroxy-naphthalene-2-carboxanilides (Kos et al. 2015b) as compared to naphthalene-2-carboxanilides (Gonec et al. 2012).

Ring-substituted 8-hydroxyquinoline-2-carboxanilides were previously tested also as photosystem II (PS II) inhibitors (Jampilek et al 2016). The inhibition of photosynthetic electron transport (PET) in spinach chloroplasts by these compounds significantly depended on the position of substitution, and the inhibitory activity of C'₍₃₎-substituted compounds was by one or two orders higher than that of C'₍₂₎ and C'₍₄₎-substituted derivatives. For the most active compounds, the following IC₅₀ values were observed: 2.7 μ M (3-CH₃, **3b**), 2.3 μ M (3-F, **4b**), 3.6 μ M (3-Cl, **5b**), and 3.4 μ M (3-Br, **6b**). However, it could be mentioned that the dependence of the PET-inhibiting activity on the lipophilicity of the compounds expressed by log *k* was quasi-parabolic for C'₍₃₎-substituted derivatives, while for C'₍₂₎ ones a slight increase and for C'₍₄₎ derivatives a sharp decrease of the activity were observed with increasing lipophilicity. Consequently, it could be assumed that for targeting the site of action in the photosynthetic apparatus suggested on the acceptor side of photosystem II between P680 and plastoquinone Q_B substitution in the C'₍₃₎ position is the most favorable.

Previously tested six 2-(phenylcarbamoyl)phenyl *N*-[(benzyloxy)carbonyl] alkanooates and three 2-hydroxy-*N*-[(2*S*)-1-oxo-1-(phenylamino)alkan-2-yl]benzamides showed

MIC values in the range from 0.22 to 0.35 μ M against *D. piper* Vib-7 and in the range from 0.27 to 8.52 μ M against *Desulfomicrobium* sp. Rod-9, while the MIC values of ciprofloxacin were 41.2 μ M and 39.3 μ M, respectively. Lipophilicity was recognized as a significant parameter affecting biological activities, and higher activity for both SRB was observed rather with electron-withdrawing R² substituent and less lipophilic (isopropyl or benzyl) R³ substituent, and it was supposed that these derivatives interact with enzymatic systems of the bacteria affecting vital cell functions (Kushkevych 2015a, b; Kushkevych et al. 2015a, b; Kushkevych et al. 2016). This is in agreement with the presented results concerning the antibacterial activity of ring-substituted 8-hydroxyquinoline-2-carboxanilides against *D. piper* Vib-7. Thus, these results confirmed that the investigated compounds showed high efficiency not only against the aerobic microorganisms, but also against the anaerobic microorganism.

Conclusion

Primary in vitro screening of a prepared series of ring-substituted 8-hydroxyquinoline-2-carboxanilides was performed against *Desulfovibrio piper* Vib-7. The most effective compounds with MIC/MBC values in the range of 17–23 μ M/20–23 μ M, respectively, were as follows: 8-hydroxy-*N*-(3-trifluoromethylphenyl)- (**7b**), 8-hydroxy-*N*-(3-methoxyphenyl)- (**2b**) 8-hydroxy-*N*-(3-methylphenyl)- (**3b**), and 8-hydroxy-*N*-(4-trifluoromethylphenyl)quinoline-2-carboxamide (**7c**). Their activity was twofold higher than that of ciprofloxacin. The antibacterial efficacy of the most active C'₍₃₎-substituted compounds practically did not change with increasing compound lipophilicity, indicating that this position of substitution is favorable for significant antimicrobial effect, while the antibacterial activity of most of C'₍₂₎ and C'₍₄₎-substituted derivatives decreased linearly with increasing compound lipophilicity. In addition, the dependence of activity on electronic Hammett's σ parameter of the substituent R was quasi-parabolic for the most effective C'₍₃₎-substituted compounds. The most potent compounds did not express any significant cytotoxic effect on THP-1 cells up to the tested concentration of 30 μ M.

Acknowledgements This study was supported by CZ.1.07/2.3.00/30.0053, APVV-0516-12, IGA VFU Brno 318/2017/FaF, and also by SANOFI-AVENTIS Pharma Slovakia, s.r.o.

Compliance with ethical standards

Conflict of interest The authors declare that they have no competing interests.

References

- Barton LL, Hamilton WA (2010) Sulphate-reducing bacteria. Environmental and engineered systems. Cambridge University Press, Cambridge
- Cesar da Silva B, Lyra AC, Rocha R, Santana GO (2014) Epidemiology, demographic characteristics and prognostic predictors of ulcerative colitis. *World J Gastroenterol* 20:9458–9467
- Cieslik W, Musiol R, Nycz J, Jampilek J, Vejsova M, Wolff M, Machura B, Polanski J (2012) Contribution to investigation of antimicrobial activity of styrylquinolines. *Bioorg Med Chem* 20:6960–6968
- Cieslik W, Spaczynska E, Malarz K, Tabak D, Nevin E, O'Mahony J, Coffey A, Mrozek-Wilczkiewicz A, Jampilek J, Musiol R (2015) Investigation of the antimycobacterial activity of 8-hydroxyquinoline. *Med Chem* 11:771–779
- Clinical and Laboratory Standards Institute (CLSI) (2012). Methods for antimicrobial susceptibility testing of anaerobic bacteria; Approved standard, 8th edn. CLSI Document M11-A8. CLSI, Wayne
- Clinical and Laboratory Standards Institute (CLSI) (2014). performance standards for antimicrobial susceptibility testing, 24th Informational Supplement M100-S24. CLSI, Wayne
- Cummings JH, MacFarlane GT, MacFarlane S (2003) Intestinal bacteria and ulcerative colitis. *Curr Issues Intest Microbiol* 4:9–20
- Darby CM, Nathan CF (2010) Killing of non-replicating *Mycobacterium tuberculosis* by 8-hydroxyquinoline. *J Antimicrob Chemother* 65:1424–1427
- Feuerstein JD, Cheifetz AS (2014) Ulcerative colitis: Epidemiology, diagnosis, and management. *Mayo Clinic Proc* 89:1553–1563
- Finegold SM, Molitoris D, Vaaisanen ML (2009) Study of the *in vitro* activities of rifaximin and comparator agents against 536 anaerobic intestinal bacteria from the perspective of potential utility in pathology involving bowel flora. *Antimicrob Agents Chemother* 53:281–286
- Garud S, Peppercorn MA (2009) Ulcerative colitis: Current treatment strategies and future prospects. *Therap Adv Gastroenterol* 2:99–108
- Gibson GR, Cummings JH, MacFarlane GT (1991) Growth and activities of sulphate-reducing bacteria in gut contents of health subjects and patients with ulcerative colitis. *FEMS Microbiol Ecol* 86:103–112
- Gibson GR, MacFarlane S, MacFarlane GT (1993) Metabolic interactions involving sulphate-reducing and methanogenic bacteria in the human large intestine. *FEMS Microbiol Ecol* 12:117–125
- Gonec T, Bobal P, Suján J, Pesko M, Guo J, Kralova K, Pavlacka L, Vesely L, Kreckova E, Kos J, Coffey A, Kollar P, Imramovsky A, Placek L, Jampilek J (2012) Investigating the spectrum of biological activity of substituted quinoline-2-carboxamides and their isosteres. *Molecules* 17:613–644
- Gonec T, Kos J, Zadrazilova I, Pesko M, Keltsova S, Tengler J, Bobal P, Kollar P, Cizek A, Kralova K, Jampilek J (2013) Antimycobacterial and herbicidal activity of ring-substituted 1-hydroxynaphthalene-2-carboxanilides. *Bioorg Med Chem* 21:6531–6541
- Holt JG, Krieg NR, Sneath PH (1994) *Bergey's manual of determinative bacteriology*, 9th edn. Williams & Wilkins, Philadelphia, PA
- Jampilek J, Dolezal M, Kunes J, Buchta V, Silva L, Kralova K (2005) Quinaldine derivatives: Preparation and biological activity. *Med Chem* 1:591–599
- Jampilek J, Kralova K, Pesko M, Kos J (2016) Ring-Substituted 8-hydroxyquinoline-2-carboxanilides as photosystem II inhibitors. *Bioorg Med Chem Lett* 26:3862–3865
- Kaplan GG (2015) The global burden of IBD: from 2015 to 2025. *Nat Rev Gastroenterol Hepatol* 12:720–727
- Kos J, Zadrazilova I, Nevin E, Soral M, Gonec T, Kollar P, Oravec M, Coffey A, O'Mahony J, Liptaj T, Kralova K, Jampilek J (2015a) Ring-substituted 8-hydroxyquinoline-2-carboxanilides as potential antimycobacterial agents. *Bioorg Med Chem* 23:4188–4196
- Kos J, Nevin E, Soral M, Kushkevych I, Gonec T, Bobal P, Kollar P, Coffey A, O'Mahony J, Liptaj T, Kralova K, Jampilek J (2015b) Synthesis and antimycobacterial properties of ring-substituted 6-hydroxynaphthalene-2-carboxanilides. *Bioorg Med Chem* 23:2035–2043
- Kushkevych I, Moroz OM (2012) Growth of various strains of sulfate-reducing bacteria of human large intestine. *Stud Biol* 6:115–124
- Kushkevych I (2013) Identification of sulfate-reducing bacteria strains of human large intestine. *Stud Biol* 7:115–124
- Kushkevych I (2014) Etiological role of sulfate-reducing bacteria in the development of inflammatory bowel diseases and ulcerative colitis. *Am J Infect Dis Microbiol* 2:63–73
- Kushkevych I, Bartos M, Bartosova L (2014) Sequence analysis of the 16S rRNA gene of sulfate-reducing bacteria isolated from human intestine. *Int J Curr Microbiol Appl Sci* 3:239–248
- Kushkevych I (2015a) Kinetic properties of pyruvate ferredoxin oxidoreductase of intestinal sulfate-reducing bacteria *Desulfovibrio piger* Vib-7 and *Desulfomicrobium* sp. Rod-9. *Polish J Microbiol* 64:107–114
- Kushkevych I (2015b) Activity and kinetic properties of phosphotransacetylase from intestinal sulfate-reducing bacteria. *Acta Bioch Pol* 62:1037–108
- Kushkevych I, Fafula R, Parak T, Bartos M (2015a) Activity of Na⁺/K⁺-activated Mg²⁺-dependent ATP hydrolase in the cell-free extracts of the sulfate-reducing bacteria *Desulfovibrio piger* Vib-7 and *Desulfomicrobium* sp. Rod-9. *Acta Vet Brno* 84:3–12
- Kushkevych I, Kollar P, Ferreira AL, Palma D, Duarte A, Lopes MM, Bartos M, Pauk K, Imramovsky A, Jampilek J (2016) Antimicrobial effect of salicylamide derivatives against intestinal sulfate-reducing bacteria. *J Appl Biomed* 14:125–130
- Kushkevych I, Kollar P, Suchy P, Parak T, Pauk K, Imramovsky A (2015b) Activity of selected salicylamides against intestinal sulfate-reducing bacteria. *Neuroendocrinol Lett* 36:106–113
- Lavecchia A, Di Giovanni C (2013) Virtual screening strategies in drug discovery: A critical review. *Curr Med Chem* 20:2839–2860
- Loubinoux J, Valente FMA, Pereira IAC (2002) Reclassification of the only species of the genus *Desulfomonas*, *Desulfomonas pigra*, as *Desulfovibrio piger* comb. nov. *Int J Syst Evol Microbiol* 52:1305–1308
- Lozniewski A, Labia R, Haristoy X, Mory F (2001) Antimicrobial susceptibilities of clinical *Desulfovibrio* isolates. *Antimicrob Agents Chemother* 45:2933–2935
- Mrozek-Wilczkiewicz A, Kalinowski D, Musiol R, Finster J, Szurko A, Serafin K, Knas M, Kamalapuram SK, Kovacevic Z, Jampilek J, Ratuszna A, Rzeszowska-Wolny J, Richardson DR, Polanski J (2010) Investigating anti-proliferative activity of styrylanaphthalenes and azanaphthalenediones. *Bioorg Med Chem* 18:2664–2671
- Musiol R, Jampilek J, Buchta V, Niedbala H, Podeszwa B, Palka A, Majerz-Maniecka K, Oleksyn B, Polanski J (2006) Antifungal properties of new series of quinoline derivatives. *Bioorg Med Chem* 14:3592–3598
- Musiol R, Jampilek J, Kralova K, Richardson DR, Kalinowski D, Podeszwa B, Finster J, Niedbala H, Palka A, Polanski J (2007) Investigating biological activity spectrum for novel quinoline analogues. *Bioorg Med Chem* 15:1280–1288
- Musiol R, Tabak D, Niedbala H, Podeszwa B, Jampilek J, Kralova K, Dohnal J, Finster J, Mencil A, Polanski J (2008) Investigating biological activity spectrum for novel quinoline analogues 2:

- Hydroxyquinolinecarboxamides with photosynthesis inhibiting activity. *Bioorg Med Chem* 16:4490–4499
- Musiol R, Jampilek J, Nycz JE, Pesko M, Carroll J, Kralova K, Vejsova M, O'Mahony J, Coffey A, Mrozek A, Polanski J (2010) Investigating the activity spectrum for ring-substituted 8-hydroxyquinolines. *Molecules* 15:288–304
- Nakao K, Tanaka K, Ichiishi S, Mikamo H, Shibata T, Watanabe K (2009) Susceptibilities of 23 *Desulfovibrio* isolates from humans. *Antimicrob Agents Chemother* 53:5308–5311
- Pattabiraman VR, Bode JW (2011) Rethinking amide bond synthesis. *Nature* 480:471–479
- Pitcher MC, Cummings JH (1996) Hydrogen sulphide: A bacterial toxin in ulcerative colitis? *Gut* 39:1–4
- Rowan FE, Docherty NG, Coffey JC, O'Connell PR (2009) Sulphate-reducing bacteria and hydrogen sulphide in the aetiology of ulcerative colitis. *Br J Surg* 96:151–158
- Wegmann U, Nueno-Palop C, Mayer MJ, Crost E, Narbad A (2017) Complete genome sequence of *Desulfovibrio piger* FII1049. *Genome Announc* 5:e01528–16
- Zinkevich V, Beech IB (2000) Screening of sulfate-reducing bacteria in colonoscopy samples from healthy and colitic human gut mucosa. *FEMS Microbiol Ecol* 34:147–155
- Zumla A, Nahid P, Cole ST (2013) Advances in the development of new tuberculosis drugs and treatment regimens. *Nat Rev Drug Discov* 12:388–404

č.	citace	ISSN
8	KOS, J, I KAPUSTIKOVA, C CLEMENTS, AI GRAY a J JAMPILEK. 3-Hydroxynaphthalene-2-carboxanilides and their antitrypanosomal activity. <i>MONATSCHEFTE FUR CHEMIE</i> [online]. 2018, 149 (5), 887–892. Dostupné z: doi: 10.1007/s00706-017-2099-1	0026-9247



3-Hydroxynaphthalene-2-carboxanilides and their antitrypanosomal activity

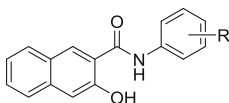
Jiri Kos¹ · Iva Kapustikova¹ · Carol Clements² · Alexander I. Gray² · Josef Jampilek¹

Received: 17 October 2017 / Accepted: 13 November 2017 / Published online: 6 February 2018
© Springer-Verlag GmbH Austria, part of Springer Nature 2018

Abstract

Series of ring-substituted 3-hydroxynaphthalene-2-carboxanilides were screened for their in vitro activity against wild-type S427 (bloodstream form) of *Trypanosoma brucei brucei*. 3-Hydroxy-*N*-(3-trifluoromethylphenyl)- and 3-hydroxy-*N*-(4-trifluoromethylphenyl)naphthalene-2-carboxamides showed the highest biological activity (MIC = 1.56 and 2.08 $\mu\text{mol}/\text{dm}^3$, respectively). Antitrypanosomal activity was correlated with the experimentally determined lipophilicity and acid–base dissociation constants of the compounds as well as with the calculated electronic properties of individual anilide substituents expressed as Hammett's σ parameters. The substitution in the *meta*- or *para*-position of anilide of derivatives with higher lipophilicity by an electron-withdrawing moiety is favourable for higher activity. The optimum thermodynamic $\text{p}K_{\text{a}}^{\text{T}}$ value was found to be ca. 7.5. The structure–activity relationships of all compounds are discussed.

Graphical abstract



Library 22 compounds: R = H, OCH₃, CH₃, F, Cl, Br, CF₃, NO₂

Optimal: R = 3-, 4-CF₃, 3-, 4-Br, 3-, 4-OCH₃

MIC = 1.56–6.25 $\mu\text{mol}/\text{dm}^3$ (*Trypanosoma brucei brucei* wild-type S427, bloodstream form)

Keywords Carbonyl compounds · Antitrypanosomal activity · Bioorganic chemistry · Structure–activity relationships

Introduction

Sleeping sickness, human African trypanosomiasis, is caused by protozoan parasites *Trypanosoma brucei* that have traditionally been grouped into three subspecies: *T. b. brucei*, *T. b. gambiense*, and *T. b. rhodesiense*. *T. b. gambiense* is found in the West and Central Africa region and currently accounts for 97% of cases and causes a chronic infection. *T. b. rhodesiense* is found in the Eastern and Southern Africa, represents < 3% of cases, and causes an acute infection. Currently, the estimated number of actual cases is 20,000, and the estimated population at risk is 65 million people. Only five drugs have been used for the

✉ Carol Clements
c.j.clements@strath.ac.uk

✉ Josef Jampilek
josef.jampilek@gmail.com

¹ Department of Pharmaceutical Chemistry, Faculty of Pharmacy, Comenius University, Bratislava, Slovakia

² Strathclyde Institute of Pharmacy and Biomedical Sciences, University of Strathclyde, Glasgow, Scotland, UK

treatment of sleeping sickness: pentamidine (against *T. b. gambiense*) and suramin (against *T. b. rhodesiense*) are used for the first stage treatment and melarsoprol (used for the treatment of both types), eflornithine, and nifurtimox (against *T. b. gambiense*) are used for the second stage treatment. Four from these five drugs approved for the treatment of sleeping sickness show non-negligible undesirable effects [1, 2]. These facts underline the urgency of searching for new and inexpensive structure types of drugs to achieve the effective control of African trypanosomes [1, 3, 4].

3-Hydroxynaphthalene-2-carboxanilides, cyclic analogues of salicylanilides, were recently prepared and published as compounds with noteworthy biological activities [5, 6] based on the presence of an amide group [3, 7, 8] and a spatially close hydroxy moiety [6, 9–14] in the naphthalene scaffold. Salicylanilides are known as multitarget agents with a broad spectrum of biological activities [15, 16]. The properties of the amide moiety can be easily modified by various substitutions [17]. The amide moiety also occurs in many antiprotozoan drugs [2–4, 18–20]. Due to the formation of hydrogen bonds between the CONH group of amides and target proteins, changes in protein conformation may occur, which results in killing protozoans [21].

Thus, in the context of the above-mentioned facts, the recently prepared series of ring-substituted 3-hydroxynaphthalene-2-carboxanilides [5] were additionally tested on their *in vitro* antitrypanosomal activity against *T. b. brucei*.

Results and discussion

Chemistry

All the studied compounds were prepared according to Scheme 1 by means of microwave-assisted synthesis in one step. Briefly, the carboxyl group was activated with phosphorus trichloride, and then, aminolysis of acyl chloride by ring-substituted aniline in dry chlorobenzene yielded a final

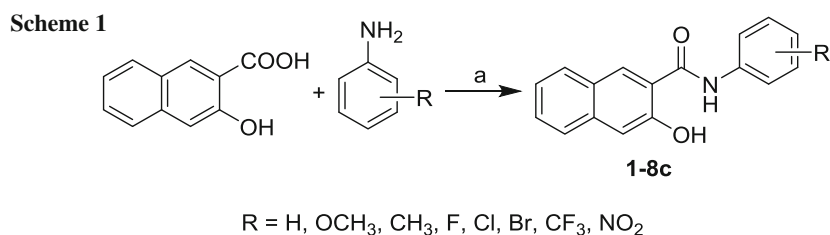
amide. All the compounds were purified by recrystallization from ethanol [5].

The structures of the investigated compounds are mentioned in Table 1 together with the physicochemical parameters: electronic properties of individual anilide substituents expressed as Hammett's σ constants predicted using sw. ACD/Percepta ver. 2012; lipophilicity values of the anilides expressed as logarithm of capacity factor $\log k$ experimentally determined by RP-HPLC [5]; and acid–base dissociation constants expressed as pK_a^T experimentally determined using capillary electrophoresis. Lipophilicity and acid–base dissociation constants are fundamental and most important physicochemical parameters that influence the bioavailability of drugs, i.e., their transport through biological membranes to their active site [22, 23].

The determination of acid–base dissociation constant (pK_a) using capillary zone electrophoresis is based on the measurement of the effective electrophoretic mobility of the studied compound as a function of separation electrolyte pHs. This relationship is then fitted by a sigmoidal curve, where pK_a is the value of pH in the sigmoid inflection point. Then, pK_a value obtained in buffer solutions is recalculated to thermodynamic pK_a^T , which correspond to water medium with zero ionic strength [23–25]. The pK_a and pK_a^T values of individual compounds are given in Table 1.

In vitro antitrypanosomal activity

3-Hydroxynaphthalene-2-carboxanilides showed the highest potency against wild-type S427 (bloodstream form) of *T. b. brucei* compared to other positional isomers, e.g., 2-hydroxynaphthalene-1-carboxanilides or 1-hydroxynaphthalene-2-carboxanilides [26]. The potency of the compounds was expressed as the minimum inhibitory concentration (MIC). Activity was primarily associated with *meta*- and *para*-substituted derivatives. 3-Hydroxy-*N*-(3-trifluoromethylphenyl)-(7b), 3-hydroxy-*N*-(4-trifluoromethylphenyl)-(7c), 3-hydroxy-*N*-(3-nitrophenyl)-(8b),



a) PCl₃, anhydrous chlorobenzene, MW: 1st phase: 10 min, 100 °C, 100 W; 2nd phase: 15 min, 120 °C, 500 W; 3rd phase: 20 min, 130 °C, 500 W

Table 1 Structure of 3-hydroxynaphthalene-2-carboxanilides **1–8c**, experimentally determined values of lipophilicity $\log k$ [5], predicted values of electronic Hammett's σ parameters of substituents R , experimentally determined values of pK_a expressed as mean \pm SD $(n = 3$ experiments), coefficients of determination (R^2), calculated thermodynamic acid–base dissociation constants pK_a^{T} and in vitro antitrypanosomal activity against *T. b. brucei* (MIC/ $\mu\text{mol}/\text{dm}^3$) in comparison with suramin (SUR) standard

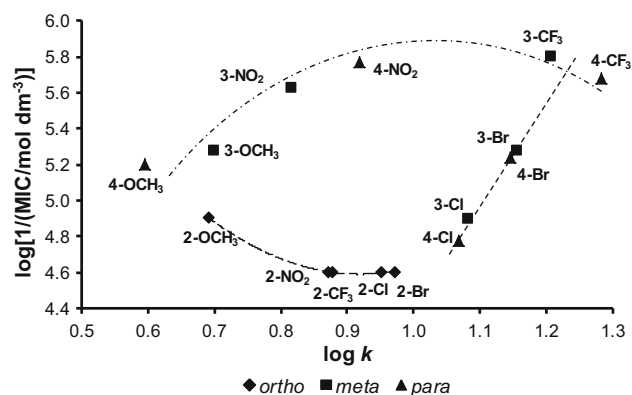
Comp.	R	$\log k$ [5]	σ^a	$pK_a \pm \text{SD}$	R^2	pK_a^T	MIC/ $\mu\text{mol}/\text{dm}^3$
1	H	0.6310	0	7.551 \pm 0.012	0.9994	7.594	NA
2a	2-OCH ₃	0.6916	– 0.28	7.802 \pm 0.034	0.9930	7.846	12.50
2b	3-OCH ₃	0.6971	0.12	7.344 \pm 0.034	0.9936	7.387	5.21
2c	4-OCH ₃	0.5951	– 0.27	7.743 \pm 0.041	0.9962	7.787	6.25
3a	2-CH ₃	0.6936	– 0.17	7.587 \pm 0.028	0.9947	7.630	NA
3b	3-CH ₃	0.8831	– 0.07	7.484 \pm 0.012	0.9994	7.527	NA
3c	4-CH ₃	0.8753	– 0.17	7.646 \pm 0.040	0.9867	7.689	NA
4a	2-F	0.7303	0.06	7.422 \pm 0.017	0.9980	7.465	NA
4b	3-F	0.8296	0.34	7.455 \pm 0.010	0.9992	7.499	NA
4c	4-F	0.7317	0.06	7.506 \pm 0.017	0.9987	7.550	NA
5a	2-Cl	0.9509	0.22	7.455 \pm 0.016	0.9994	7.499	25.00
5b	3-Cl	1.0796	0.37	7.638 \pm 0.036	0.9979	7.682	12.50
5c	4-Cl	1.0687	0.23	7.563 \pm 0.030	0.9977	7.606	16.67
6a	2-Br	0.9715	0.22	7.638 \pm 0.041	0.9972	7.681	25.00
6b	3-Br	1.1536	0.39	7.592 \pm 0.032	0.9983	7.636	5.21
6c	4-Br	1.1459	0.23	7.614 \pm 0.052	0.9933	7.658	5.73
7a	2-CF ₃	0.8762	0.51	7.638 \pm 0.022	0.9986	7.681	25.00
7b	3-CF ₃	1.2053	0.43	7.445 \pm 0.000	0.9976	7.489	1.56
7c	4-CF ₃	1.2835	0.51	7.937 \pm 0.176	0.9735	7.981	2.08
8a	2-NO ₂	0.8710	0.77	7.633 \pm 0.036	0.9921	7.677	25.00
8b	3-NO ₂	0.8143	0.71	7.529 \pm 0.051	0.9822	7.573	2.34
8c	4-NO ₂	0.9175	0.78	7.509 \pm 0.054	0.9789	7.553	1.69
SUR	–	–	–	–	–	–	0.13

NA no activity

^aCalculated using the ACD/Percepta ver. 2012 (Advanced Chemistry Development, Inc., Toronto, ON, Canada)

and 3-hydroxy-*N*-(4-nitrophenyl)naphthalene-2-carboxamides (**8c**) demonstrated the highest activity within the series with MIC = 1.56, 2.08, 2.34, and 1.69 $\mu\text{mol}/\text{dm}^3$, respectively. Unfortunately, as was published recently by Kos et al. [5], both nitro derivatives **8b** and **8c** showed significant cytotoxic effect against human monocytic leukemia THP-1 cells [$\text{LD}_{50} = 2.5 \pm 0.9 \mu\text{mol}/\text{dm}^3$ (**8b**) and $\text{LD}_{50} < 0.37 \mu\text{mol}/\text{dm}^3$ (**8c**)]. For example, LD_{50} of oxaliplatin is $1.7 \pm 0.6 \mu\text{mol}/\text{dm}^3$ and camptothecin LD_{50} is $0.20 \pm 0.07 \mu\text{mol}/\text{dm}^3$ [5, 27]. The toxicity of nitro derivatives correlates with the position of the substituents on the aniline moiety, where the toxicity increases with the nitro group shift from the *ortho*- to *para*-position. The highest dose of other effective compounds in the medium (30 $\mu\text{mol}/\text{dm}^3$) did not lead to significant lethal effect on THP-1 cells, i.e., $\text{LD}_{50} > 30 \mu\text{mol}/\text{dm}^3$ [5].

The dependence of antitrypanosomal activity on lipophilicity, expressed as $\log k$, is shown in Fig. 1. There are three separate trends in the chart. The activity decreases with increasing lipophilicity for the least effective *ortho*-

**Fig. 1** Dependence of antitrypanosomal activity expressed as $\log[1/(\text{MIC}/\text{mol}/\text{dm}^3)]$ of investigated compounds on lipophilicity expressed as $\log k$

substituted derivatives. In general, for *meta*- and *para*-substituted compounds, it can be stated that the activity increases with increasing lipophilicity; however, for methoxy, nitro, and trifluoromethyl derivatives, i.e.,

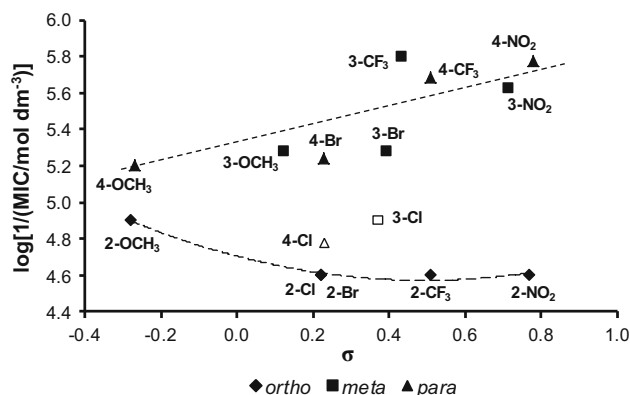


Fig. 2 Dependence of antitrypanosomal activity expressed as $\log[1/(\text{MIC}/\text{mol}/\text{dm}^3)]$ of the tested compounds on Hammett σ constants of individual substituents R . Excluded compounds are marked by an empty symbol

substituents with an ability to form hydrogen bonds and other weak intermolecular interactions, the dependence of the activity on $\log k$ seems to be as quasi-parabolic, while for chlorinated, brominated (and also trifluoromethyl substituted) compounds, the efficiency increases with increasing lipophilicity. Thus, it seems that $\log k$ about 1.2 can be considered as a lipophilicity optimum. It should be noted that compounds **5b** ($R = 3\text{-Cl}$) and **5c** ($R = 4\text{-Cl}$) showed worse solubility in the testing medium than the corresponding bromo (compounds **6b**, **6c**) and trifluoromethyl (compounds **7b**, **7c**) substituted derivatives.

From the distribution of the individual substituents in Fig. 1, it is evident that the antitrypanosomal activity is also dependent on the electron properties of individual substituents R that are expressed as Hammett σ constants. This dependence is illustrated in Fig. 2. In general, less active *ortho*-substituted isomers show again a clear trend, where the activity decreases with the electron-withdrawing character of the substituent R . When the least effective compounds **5b** (3-Cl) and **5c** (4-Cl) from *meta*- and *para*-substituted derivatives are excluded, the opposite trend can be observed for *meta*- and *para*-derivatives; activity increases with electron-withdrawing properties.

A phenolic moiety in position 3 of the naphthalene scaffold of the discussed compounds is important for their biological activity [5, 9]. As mentioned above, acid–base properties also play an important role in biological activity of many drugs; therefore, the $\text{p}K_{\text{a}}$ values of this phenolic moiety were determined by capillary electrophoresis. Figure 3 illustrates the dependence of antitrypanosomal activity on acid–base properties expressed as thermodynamic $\text{p}K_{\text{a}}^{\text{T}}$ values. It seems that $\text{p}K_{\text{a}}^{\text{T}}$ values of the phenolic moiety in the $\text{C}_{(3)}$ position are important for effective *meta*- and *para*-substituted derivatives. Compound **7c** (4-CF_3) showed limited solubility in the electrophoretic system (SD was higher than for other compounds); therefore, it was excluded from the

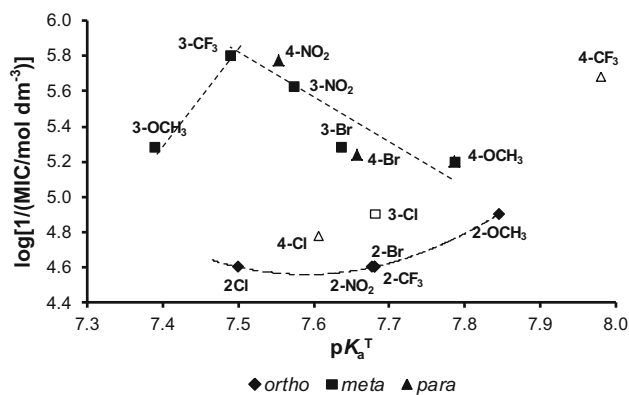


Fig. 3 Dependence of antitrypanosomal activity expressed as $\log[1/(\text{MIC}/\text{mol}/\text{dm}^3)]$ of investigated compounds on acid–base properties of $\text{C}_{(3)}$ phenolic moiety expressed as thermodynamic $\text{p}K_{\text{a}}^{\text{T}}$ values. Excluded compounds are marked by an empty symbol

evaluation. For poorly active *ortho*-substituted derivatives, it can be stated that the activity increases with the increasing $\text{p}K_{\text{a}}^{\text{T}}$ value, i.e., with the decrease of the acidity and ionizability of phenolic hydroxyl. For effective *meta*- and *para*-substituted derivatives, a bilinear trend with the optimal $\text{p}K_{\text{a}}^{\text{T}}$ value between 7.49 compound **7b** (3-CF_3) and 7.55 **8b** (4-NO_2) can be observed in Fig. 3.

Conclusion

A recently synthesised series of 22 ring-substituted 3-hydroxynaphthalene-2-carboxanilides were screened for their in vitro activity against wild-type S427 (bloodstream form) of *Trypanosoma b. brucei*. 3-Hydroxy-*N*-(3-trifluoromethylphenyl)- (7b) and 3-hydroxy-*N*-(4-trifluoromethylphenyl)naphthalene-2-carboxamides (7c) showed the highest biological activity ($\text{MIC} = 1.56$ and $2.08 \mu\text{mol}/\text{dm}^3$, respectively). It can be stated that higher potency is connected with the *meta*- and *para*-positions of anilide substituents, while *ortho*-substituted derivatives showed much less efficiency, and their activity is not significantly influenced by neither lipophilicity, electron properties nor acid–base properties. On the other hand, the antitrypanosomal activity of the *meta*- and *para*-substituted 3-hydroxynaphthalene-2-carboxanilides is positively affected by increasing lipophilicity and electron-withdrawing properties of anilide substituents. The optimum $\text{p}K_{\text{a}}^{\text{T}}$ value seems to be 7.5.

Experimental

Synthesis

The detailed synthetic pathway and full analytical characterization (m.p., HPLC purity, IR, NMR, HR-MS) of

discussed compounds **1–8a** are provided in Kos et al. [5]. All the studied compounds are presented in Table 1.

Acid–base dissociation constant determination

All chemicals and solvents were of analytical-reagent grade. MES, TAPS, CAPS, TES, and methanol were purchased from Sigma-Aldrich (Germany). Sodium hydroxide was from Fluka (Switzerland), and calibration buffers were from WTW (Weilheim in Oberbayern, Germany). Experiments were carried out using an Agilent 3D CE system (Agilent Technologies, Waldbronn, Germany) equipped with a diode array detector. Results were enregistered by a system Agilent ChemStation and processed in the program SigmaPlot v. 10.0 (San Rafael, CA, USA). The pH values of used background electrolytes were measured with a pH meter WTW InoLab pH Level 2 equipped with a combined electrode WTW SenTix 41[®] (Germany). Electrophoretic measurements were performed in a fused-silica capillary of 33.0 cm total length, 24.5 cm effective length (from injection to detector), and 50 μm internal diameter. Before first using and when background electrolyte was changed, capillary was rinsed with 0.1 mol/dm³ NaOH for 15 min, then deionised water for 15 min, and background electrolyte for 15 min. Between consecutive runs, capillary was rinsed for 30 s with water and 30 s with background electrolyte. The sample was injected by pressure of 30–50 mbar for 3–5 s. A constant voltage of 15 kV was applied at 25 °C. Detection was at wavelength 200 and 254 nm.

Stock solutions of tested substances were prepared in methanol (0.5 mg/cm³). Working solution was prepared by diluting stock solution of analytes in methanol to the final concentration of 0.1 mg/cm³. Measurements were performed in the system of seven or eight buffer solutions with constant ionic strength 0.01 mol/dm³ within pH range 5.50–11.20. The online program Buffer Calculator was employed to calculate the composition of the series of background electrolytes with various pH values [28]. The pH range of background electrolyte solutions was chosen to guarantee the practically full deprotonation (A[−]) of analytes at the highest pH and the absence of their ionisation (HA) at the lowest pH. An increase of the absolute value of effective mobility with increasing pH was observed. At the highest pH, the mobility of analyte is maximal, which indicates the predominance of anionic species. As pH decreases, a new species with zero electric charge is formed by protonation of analyte, and its effective mobility goes to zero. Measurement of each compound in each of background electrolytes was repeated three times.

The effective electrophoretic mobilities μ_{eff} (m²/V/s) of analytes were calculated from the observed migration times

of each analyte and the migration time of methanol as electroosmotic flow marker according to the equation:

$$\mu_{\text{eff}} = \left(\frac{1}{t_{\text{mig}}} - \frac{1}{t_{\text{EOF}}} \right) \frac{L_d L_t}{U}, \quad (1)$$

where L_t is the total length of capillary (m), L_d is the effective length (m), U is the applied voltage (V), t_{mig} is the migration time of analyte (s), and t_{EOF} is the migration time of electroosmotic flow marker(s) [24, 29, 30].

The dependence of experimentally obtained effective mobilities on background electrolyte pH was fitted by the sigmoid curve, which is described by the following equation for monoprotic weak acid:

$$\mu_{\text{eff}} = \frac{\mu_{\text{A}^-}}{1 + 10^{(\text{p}K_a - \text{pH})}}, \quad (2)$$

where μ_{A^-} is the ionic mobility of fully deprotonated acid. This relationship was fitted by a sigmoidal mobility curve, where $\text{p}K_a$ is the value of pH in the sigmoid inflection point [24, 25].

As the measurements were carried out in the system of buffer solutions with the ionic strength of 0.01 mol/dm³, the obtained values of $\text{p}K_a$ had to be converted to the thermodynamic dissociation constants ($\text{p}K_a^{\text{T}}$), which correspond to aquatic environment of the zero ionic strength:

$$\text{p}K_a^{\text{T}} = \text{p}K_a - \log \gamma_{\text{A}^-}, \quad (3)$$

where the following formula was used for the calculation of the activity coefficients:

$$\log \gamma = - \frac{0.5084z^2\sqrt{I}}{1 + 0.3281a\sqrt{I}}. \quad (4)$$

For the ionic strength of 0.01 mol/dm³ and $a = 5 \text{ \AA}$, $\log \gamma$ has the value of -0.0437 [29, 30]. The $\text{p}K_a$ and $\text{p}K_a^{\text{T}}$ values of individual compounds are given in Table 1.

In vitro antitrypanosomal activity

The biological activity of the prepared compounds against African trypanosome was performed using a modified alamarBlue assay according to Raz et al. [31]. Biological assays were performed in 96-well microtiter plates using the alamarBlue reduction indicator. Resazurin (blue), which is reduced to light pink fluorescence resorufin in the presence of live parasite, is the active ingredient. *Trypanosoma brucei brucei* S427 (a bloodstream form) was cultivated at an optimal density of 3×10^4 trypanosome/cm³ in HMI-9 medium (Invitrogen, USA) supplemented with 10% fetal calf serum at 37 °C and 5% CO₂. The tested compounds were dissolved in DMSO, the concentration of which did not exceed 1% in the total sample. The final concentration of the discussed compounds in the range of 10–0.08 $\mu\text{mol/dm}^3$ was obtained from a 200 $\mu\text{mol/dm}^3$

stock solution by repeated dilution with the medium. Prior to the addition of alamarBlue (20 mm³/well, 0.49 mmol/dm³ in 1× PBS, pH 7.4), the plates were incubated at 37 °C, 5% CO₂ for 48 h. Then, an additional 24 h of incubation followed. Fluorescence values were measured using a Wallac Victor 2 microplate reader (Perkin Elmer, USA) (excitation 560 nm, 590 nm emission) giving control values in %. MIC values were obtained for compounds showing less than 20% control values against *T. brucei brucei*. The experiment was performed in duplicate three times according to the previously described studies [32, 33]. Suramin sulfate (Sigma) was used as a standard. The results are summarized in Table 1.

Acknowledgements This study was supported by Grants FaF UK/13/2016 and FaF UK/4/2017 and by SANOFI-AVENTIS Pharma Slovakia.

References

- WHO (2017) Trypanosomiasis, human African (sleeping sickness). Fact sheets. <http://www.who.int/mediacentre/factsheets/fs259/en/>. Accessed 3 Nov
- Steinhilber D, Schubert-Zsilavec M, Roth HJ (2010) Antiprotozoische Wirkstoffe. In: Medizinische Chemie: Targets, Arzneistoffe, Chemische Biologie. Deutscher Apotheker Verlag, Stuttgart, p 586
- Jampilek J (2014) *Curr Med Chem* 21:4347
- Cullen DR, Mocerino M (2017) *Curr Med Chem* 24:701
- Kos J, Zadrazilova I, Pesko M, Keltosova S, Tengler J, Gonec T, Bobal P, Kauerova T, Oravec M, Kollar P, Cizek A, Kralova K, Jampilek J (2013) *Molecules* 18:7977
- Gonec T, Zadrazilova I, Nevin E, Kauerova T, Pesko M, Kos J, Oravec M, Kollar P, Coffey A, O'Mahony J, Cizek A, Kralova K, Jampilek J (2015) *Molecules* 20:9767
- Asif M (2016) *Mod Chem Appl* 4:194
- Jampilek J, Brychtova K (2012) *Med Res Rev* 32:907
- Gonec T, Bobal P, Suján J, Pesko M, Guo J, Kralova K, Pavlacka L, Vesely L, Kreckova E, Kos J, Coffey A, Kollar P, Imramovsky A, Placek L, Jampilek J (2012) *Molecules* 17:613
- Gonec T, Kos J, Nevin E, Govender R, Pesko M, Tengler J, Kushkevych I, Stastna V, Oravec M, Kollar P, O'Mahony J, Kralova K, Coffey A, Jampilek J (2014) *Molecules* 19:10386
- Gonec T, Kos J, Zadrazilova I, Pesko M, Govender R, Keltosova S, Chambel B, Pereira D, Kollar P, Imramovsky A, O'Mahony J, Coffey A, Cizek A, Kralova K, Jampilek J (2013) *Molecules* 18:9397
- Gonec T, Kos J, Zadrazilova I, Pesko M, Keltosova S, Tengler J, Bobal P, Kollar P, Cizek A, Kralova K, Jampilek J (2013) *Bioorg Med Chem* 21:6531
- Gonec T, Pospisilova S, Holanova L, Stranik J, Cernikova A, Pudelkova V, Kos J, Oravec M, Kollar P, Cizek A, Jampilek J (2016) *Molecules* 21:1189
- Kos J, Nevin E, Soral M, Kushkevych I, Gonec T, Bobal P, Kollar P, Coffey A, O'Mahony J, Liptaj T, Kralova K, Jampilek J (2015) *Bioorg Med Chem* 23:2035
- Kratky M, Vinsova J (2011) *Curr Pharm Des* 17:3494
- Zadrazilova I, Pospisilova S, Masarikova M, Imramovsky A, Monreal-Ferriz J, Vinsova J, Cizek A, Jampilek J (2015) *Eur J Pharm Sci* 77:197
- Pattabiraman VR, Bode JW (2011) *Nature* 480:471
- Ferrins L, Gazdik M, Rahmani R, Varghese S, Sykes ML, Jones AJ, Avery VM, White KL, Ryan E, Charman SA, Kaiser M, Bergström CA, Baell JB (2014) *J Med Chem* 57:6393
- Russell S, Rahmani R, Jones AJ, Newson HL, Neilde K, Cotillo I, Rahmani Khajouei M, Ferrins L, Qureishi S, Nguyen N, Martinez-Martinez MS, Weaver DF, Kaiser M, Riley J, Thomas J, De Rycker M, Read KD, Flematti GR, Ryan E, Tanghe S, Rodriguez A, Charman SA, Kessler A, Avery VM, Baell JB, Piggott MJ (2016) *J Med Chem* 59:9686
- Masand VH, El-Sayed NNE, Mahajan DT, Rastija V (2017) *Environ Res* 28:165
- Jacobs RT, Nare B, Phillips MA (2011) *Curr Top Med Chem* 11:1255
- Testa B, van de Waterbeemd H, Folkers G, Guy R (2001) Pharmacokinetic optimization in drug research. Wiley, Weinheim
- Babic S, Horvat AJM, Mutavdzic Pavlovic D, Kastelan-Macan M (2007) *Trends Anal Chem* 26:1043
- Fuguet E, Reta M, Gibert C, Roses M, Bosch E, Rafols C (2008) *Electrophoresis* 29:2841
- Slampova A, Krivankova L, Gebauer P, Bocek PJ (2008) *J Chromatogr A* 1213:25
- Jampilek J, Clements C, Kos J, Gonec T, Gray AI (2014) Book of abstracts: the 6th conversatory on medicinal chemistry, Lublin, Poland, Sept 18–20, p 24 (K5)
- Kauerova T, Kos J, Gonec T, Jampilek J, Kollar P (2016) *Int J Mol Sci* 17:1219
- Robinson D (2017) Buffer calculator. <http://dbr.csoft.net/chem/bufcalc.php>. Accessed 30 Sept
- Poole SK, Patel S, Dehring K, Workman H, Poole CF (2014) *J Chromatogr A* 1037:445
- Ornskov E, Linusson A, Folestad S (2003) *J Pharm Biomed Anal* 33:379
- Raz B, Iten M, Grether-Buhler Y, Kaminsky R, Brun R (1997) *Acta Trop* 68:139
- Spencer J, Rathnam RP, Harvey AL, Clements CJ, Clark RL, Barrett MP, Wong PE, Male L, Coles SJ, MacKay SP (2011) *Bioorg Med Chem* 19:1802
- Lang S, Khalaf AI, Breen D, Huggan JK, Clements CJ, MacKay SP, Suckling CJ (2014) *Med Chem Res* 23:1170

č.	citace	ISSN
9	DOLAB, JG, B LIMA, E SPACZYNSKA, J KOS , NH CANO, G FERESIN, A TAPIA, F GARIBOTTO, E PETENATTI, M OLIVELLA, R MUSIOL, J JAMPILEK a RD ENRIZ. The Antimicrobial Activity of Annona emarginata (Schltdl.) H. Rainer and Most Active Isolated Compounds against Clinically Important Bacteria. <i>MOLECULES</i> [online]. 2018, 23 (5). Dostupné z: doi: 10.3390/molecules23051187	1420-3049

Article

The Antimicrobial Activity of *Annona emarginata* (Schltdl.) H. Rainer and Most Active Isolated Compounds against Clinically Important Bacteria

Juan G. Dolab ¹ , Beatriz Lima ², Ewelina Spaczynska ³, Jiri Kos ⁴, Natividad H. Cano ², Gabriela Feresin ², Alejandro Tapia ², Francisco Garibotto ^{1,5}, Elisa Petenatti ¹ , Monica Olivella ¹, Robert Musiol ³, Josef Jampilek ^{4,*}  and Ricardo D. Enriz ^{1,5,*}

¹ Faculty of Chemistry Biochemistry and Pharmacy, National University of San Luis, Chacabuco 917, 5700 San Luis, Argentina; juandolab@gmail.com (J.G.D.); fgaribotto@gmail.com (F.G.); elipete@unsl.edu.ar (E.P.); olivellamonica@gmail.com (M.O.)

² Institute of Biotechnology-Institute of Basic Sciences, National University of San Juan, Av. Libertador General San Martin 1109, 5400 San Juan, Argentina; blima@unsj.edu.ar (B.L.); natividadhc17@hotmail.com (N.H.C.); gferesin@unsj.edu.ar (G.F.); atapia@unsj.edu.ar (A.T.)

³ Institute of Chemistry, University of Silesia, 75 Pulku Piechoty 1, 41500 Chorzow, Poland; ewelina.spaczynska@gmail.com (E.S.); robert.musiol@us.edu.pl (R.M.)

⁴ Department of Pharmaceutical Chemistry, Faculty of Pharmacy, Comenius University, Odbojarov 10, 83232 Bratislava, Slovakia; jirikos85@gmail.com

⁵ Multidisciplinary Institute of Biological Research IMIBIO-CONICET, Chacabuco 917, 5700 San Luis, Argentina

* Correspondence: josef.jampilek@gmail.com (J.J.); denriz@unsl.edu.ar (R.D.E.); Tel.: +421-250-117-229 (J.J.); +54-0266-4520300 (R.D.E.)

Received: 24 April 2018; Accepted: 10 May 2018; Published: 16 May 2018



Abstract: *Annona emarginata* (Schltdl.) H. Rainer, commonly known as “arachichú”, “araticú”, “aratigú”, and “yerba mora”, is a plant that grows in Argentina. Infusions and decoctions are used in folk medicine as a gargle against throat pain and for calming toothache; another way to use the plant for these purposes is chewing its leaves. Extracts from bark, flowers, leaves, and fruits from *A. emarginata* were subjected to antibacterial assays against a panel of Gram (+) and Gram (−) pathogenic bacteria according to Clinical and Laboratory Standards Institute protocols. Extracts from the stem bark and leaves showed moderate activity against the bacteria tested with values between 250–1000 µg/mL. Regarding flower extracts, less polar extracts (hexane, dichloromethane) showed very strong antibacterial activity against methicillin-sensitive *Staphylococcus aureus* ATCC 25923 and methicillin-resistant *S. aureus* ATCC 43300 with values between 16–125 µg/mL. Additionally, hexane extract showed activity against *Klebsiella pneumoniae* (MIC = 250 µg/mL). The global methanolic extract of the fruits (MeOHGEF) was also active against the three strains mentioned above, with MICs values 250–500 µg/mL. Bioassay-guided fractionation of MeOHGEF led to the isolation of a new main compound—(R)-2-(4-methylcyclohex-3-en-1-yl)propan-2-yl (E)-3-(4-hydroxyphenyl)acrylate (**1**). The structure and relative configurations have been determined by means of 1D and 2D NMR techniques, including COSY, HMQC, HMBC, and NOESY correlations. Compound **1** showed strong antimicrobial activity against all Gram (+) species tested (MICs = 3.12–6.25 µg/mL). In addition, the synthesis and antibacterial activity of some compounds structurally related to compound **1** (including four new compounds) are reported. A SAR study for these compounds was performed based on the results obtained by using molecular calculations.

Keywords: *Annona emarginata*; (R)-2-(4-methylcyclohex-3-en-1-yl)propan-2-yl (E)-3-(4-hydroxyphenyl)-acrylate; antibacterial activity; *Staphylococcus aureus*; structure-activity relationships

1. Introduction

Some genera from the family *Annonaceae* are an important natural source of products with antifungal [1], bactericidal [2], pesticidal [3], herbicidal [4], antimalarial [5], antiprotozoal [6], and cytostatic [7,8] activity, especially some chemically isolated components (primarily from seeds, leaves, and bark). These compounds include flavonoids, alkaloids, and acetogenins. This family is widely distributed in tropical and subtropical regions around the world in diversity of habitats (forests, scrub, and grassland), with higher prevalence in rain forests. In general, representatives of the family are shrubs, but it is also possible to find dwarf shrubs or small trees and, rarely, canopy trees or lianas among them. The *Annona* genus comprises ca. 160 species from the tropical and subtropical areas, from both hemispheres. Four species grow mainly in Argentina: *Annona emarginata* (Schltdl.) H. Rainer (= *Rollinia emarginata* Schltdl.), *A. neosalicifolia* H. Rainer (= *Rollinia salicifolia* Schltdl.), *A. nutans* (R.E. Fr.), and *A. rugulosa* (Schltdl.) H. Rainer. Previous studies related to ethnopharmacological use have shown that the infusions and decoctions of the leaves of *A. emarginata*, commonly known as “arachichú”, “araticú”, “aratigú”, and “yerba mora”, are used in folk medicine as a gargle against throat pain and for calming the toothache. Another way it is used is by absorbing juice produced by chewing the leaves [9,10]. Antiprotozoal [11] and antifeedant [12] properties have been reported. Regarding its chemical composition, rolliniastatin-1, sylvaticin, squamocin, rollidecin B, liriioresinol B, liriodenine [11]; vomifoliol, dehydrovomifoliol, blumenol C, loliolide, 7-epiloliolide, vanillin, dihydroactinolide [12]; ursolic acid, oleanolic acid, 8-*trans-p*-coumaroyloxy- α -terpineol, quercetin-3-*O*- α -L-arabinopyranosyl(1 \rightarrow 2)- α -L-rhamnopyranoside [13]; alkaloids including two aporphines (–)-anonaine, (–)-asimilobine and one benzyltetrahydroisoquinoline, (+)-reticuline [14], and cyanogenic glycosides [15] have been previously isolated from its aerial parts. Resistance to antimicrobials is a problem that increasingly threatens the world population [16]. The World Health Organization established as “priority pathogens” those resistant to antibiotics, which include 12 families of bacteria most dangerous to human health, the so-called “superbugs”. Among them, especially the threat posed by Gram (–) bacteria resistant to multiple antibiotics is highlighted. Among the Gram (+) bacteria, methicillin-resistant *Staphylococcus aureus* (MRSA) [17] is one of the most important. Thus, the development of new molecules, alternative strategies, and prevention and control measures is necessary to avoid this problem.

The main objective of this work is to determine the antibacterial effect of different extracts of *A. emarginata* (Schltdl.) H. Rainer, which is widely used in folk medicine in the northeast part of Argentina. Another goal is to try to determine which active compound is responsible for such activity. Thus, this work has been done in several stages. In the first step, the antimicrobial properties of extracts of *A. emarginata* were studied, and the bioassay-guided isolation of its most active compound was made. The compound was tested against an extended panel of both standardized and clinical opportunistic pathogenic bacteria. The species were selected to include Gram (+) and Gram (–) species of the most common human pathogens. Once the structure of the compound responsible for the antibacterial activity was determined, some structurally related compounds were synthesized. Finally, based on molecular calculations, we performed a study of the structure-activity relationships of antibacterial compounds of the different series reported here.

2. Results and Discussion

2.1. Antimicrobial Evaluation of *A. emarginata* Extracts and Its Active Ingredient

The extracts from the stem bark and leaves of *A. emarginata* showed moderate activity against the bacteria tested, with values between 250 and 1000 $\mu\text{g}/\text{mL}$ (Table 1). Regarding flower extracts, the less polar (hexane, dichloromethane) extracts, HFIE and DCMFIE, showed very strong antibacterial activity against methicillin-sensitive *S. aureus* (MSSA) ATCC 25923 and methicillin-resistant *S. aureus* (MRSA) ATCC 43300, with values between 16 and 125 $\mu\text{g}/\text{mL}$. Additionally, hexane extract showed activity against *Klebsiella pneumoniae* (MIC = 250 $\mu\text{g}/\text{mL}$). The global methanolic extract from the fruits

(MeOHGFE) was also active against the three strains mentioned above, with minimum inhibitory concentration (MIC) values between 250–500 µg/mL. In order to identify bioactive compounds, a bioassay-guided fractionation of the MeOHGFE was performed.

Table 1. Antibacterial activity (MIC (µg/mL)) of extracts of *A. emarginata* (Annonaceae).

Extracts	MIC (µg/mL)						
	MSSA	MRSA	<i>E. coli</i> ATCC 25922	<i>E. coli</i> LM2	<i>K. pneumoniae</i>	<i>Salmonella</i> sp.	
Stem bark	HBE	>1000	>1000	250	500	>1000	1000
	DCMBE	1000	>1000	500	>1000	1000	250
	EtAcOBE	500	1000	500	500	>1000	500
	MeOHBE	500	500	1000	1000	>1000	1000
Leaves	HLE	500	250	>1000	>1000	>1000	500
	DCMLE	500	500	>1000	1000	1000	500
	EtAcOLE	500	500	>1000	>1000	250	500
	MeOHLE	>1000	>1000	500	500	500	500
Flowers	HFIE	125	125	>1000	>1000	250	1000
	DCMFIE	62.5	16	>1000	>1000	1000	>1000
	EtAcOFIE	250	250	1000	>1000	500	>1000
	MeOHFIE	>1000	>1000	1000	1000	>1000	>1000
Fruits	MeOHGFE	500	500	>1000	>1000	250	>1000
	cefotaxime	0.5	0.5	1.9	0.5	15	12.5

HBE: hexane bark extract; DCMBE: dichloromethane bark extract; EtOAcBE: ethyl acetate bark extract; MeOHBE: methanol bark extract; HLE: hexane leaf extract; DCMLE: dichloromethane leaf extract; EtOAcLE: ethyl acetate leaf extract; MeOHLE: methanol leaf extract; HFIE: hexane flower extract; DCMFIE: dichloromethane flower extract; EtOAcFIE: ethyl acetate flower extract; MeOHFIE: methanol flower extract; MeOHGFE: methanol global fruit extract.

Tables 2 and 3 show the antimicrobial activity of fractions and subfractions of the MeOHGFE. Fraction F₃ displayed the strongest antibacterial activity (Table 2) against MSSA, MRSA, *Escherichia coli* ATCC 25922 (MIC = 500 µg/mL), and *K. pneumoniae* (MIC = 125 µg/mL). To gain further information about their activity spectrum against Gram (+) strains, we added a panel of clinical isolates obtained from human patients (coagulase negative *Staphylococcus aureus* 502, *Streptococcus pyogenes* and *Streptococcus agalactiae*) (Tables 3 and 4). Fraction F₃ was further percolated on Sephadex LH-20 affording 5 subfractions (I–V). One of them, subfraction F_{IV}, showed strong antibacterial activity with MIC = 16 µg/mL against all the Gram (+) bacteria tested, except for coagulase negative *S. aureus* 502 (MIC = 31.2 µg/mL), *Escherichia coli* LM2 (MIC = 125 µg/mL), and *K. pneumoniae* (MIC = 250 µg/mL, respectively). On the basis of the previous results, subfraction F_{IV} was successively purified by Sephadex LH-20 and silica gel column, affording the main antibacterial compound 1 (Figure 1). As we expected, compound 1 showed stronger antimicrobial activity against both Gram (+) ATCC strains with MICs = 3.12–6.25 µg/mL, and the expanded panel strains were also sensitive to this compound with MICs value equal 3.12 µg/mL (Table 4). In contrast, compound 2 (see below) was practically inactive.

Table 2. Antibacterial activity (MIC ($\mu\text{g/mL}$)) of fractions F₁-F₆ from MeOHGEF.

Extracts	MIC ($\mu\text{g/mL}$)					
	MSSA	MRSA	<i>E. coli</i> ATCC 25922	<i>E. coli</i> LM2	<i>K. pneumoniae</i>	<i>Salmonella</i> sp.
MeOHGEF	500	500	>1000	>1000	250	>1000
MeOHGEF Fractions	F ₁	>1000	>1000	>1000	>1000	>1000
	F ₂	500	250	>1000	>1000	>1000
	F ₃	500	500	500	>1000	125
	F ₄	1000	1000	1000	125	1000
	F ₅	500	500	1000	250	125
	F ₆	250	500	250	250	>1000
cefotaxime	0.5	0.5	1.9	0.5	15	12.5

MeOHGEF: methanol global extract fruit; F₁ (200 mg; hex 100%), F₂ (115 mg; 50:50% H:DCM), F₃ (1200 mg; 90:10% DCM:EtOAc), F₄ (187.7 mg 80:20% DCM:EtOAc), F₅ (155 mg; 70:30% DCM:EtOAc), and F₆ (137 mg; EtOAc100%).

Table 3. Antibacterial activity (MIC ($\mu\text{g/mL}$)) of subfractions F_{I-V} from F₃.

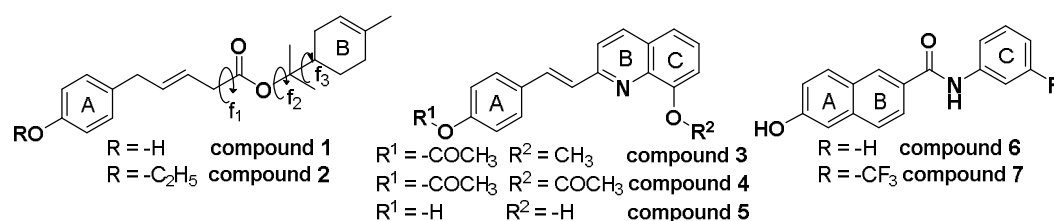
Extracts	MIC ($\mu\text{g/mL}$)									
	MSSA	MRSA	SA	SP	SAG	EC	ELM	KP	Ssp	
MeOHGEF Fraction F ₃	500	500	500	250	250	500	>1000	125	>1000	
F ₃ subfractions	Subfraction I	>250	>250	>250	>250	>250	>250	>250	>250	
	Subfraction II	>250	>250	>250	>250	>250	250	>250	>250	
	Subfraction III	>250	>250	>250	>250	>250	>250	250	>250	
	Subfraction IV	16	16	31.2	16	16	>250	125	250	
	Subfraction V	62.5	62.5	62.5	62.5	62.5	>250	>250	>250	
cefotaxime	0.5	0.5	0.5	0.25	0.25	1.9	0.5	15	12.5	

MSSA = methicillin-sensitive *Staphylococcus aureus* ATCC 25923, MRSA = methicillin-resistant *Staphylococcus aureus* ATCC 43300, SA = coagulase negative *Staphylococcus aureus* 502, SP = *Streptococcus pyogenes*, SAG = *Streptococcus agalactiae*, EC = *Escherichia coli* ATCC 25922, ELM = *Escherichia coli* LM2, KP = *Klebsiella pneumoniae*, Ssp = *Salmonella* sp.

Table 4. Antibacterial activity (MIC [$\mu\text{g/mL}$]) of compound 1 (isolated from subfraction F_{IV}) and compounds 2–7 obtained by synthesis.

Comp.	MIC ($\mu\text{g/mL}$)							
	MSSA	MRSA	SA	SP	SAG	EC	ELM	KP
1	4	6.25	3.12	3.12	3.12	>50	50	50
2	>50	>50	>50	>50	>50	>50	>50	>50
3	50	50	50	50	50	>50	>50	>50
4	>50	>50	>50	>50	>50	>50	>50	>50
5	50	>50	25	25	50	>50	>50	>50
6	25	50	50	50	50	>50	25	>50
7	12.5	50	12.5	25	12.5	>50	12.5	>50
CEF	0.5	0.5	0.5	0.25	0.25	1.9	0.5	15

MSSA = methicillin-sensitive *Staphylococcus aureus* ATCC 25923, MRSA = methicillin-resistant *Staphylococcus aureus* ATCC 43300, SA = coagulase negative *Staphylococcus aureus* 502, SP = *Streptococcus pyogenes*, SAG = *Streptococcus agalactiae*, EC = *Escherichia coli* ATCC 25922, ELM = *Escherichia coli* LM2, KP = *Klebsiella pneumoniae*, CEF = cefotaxime.

**Figure 1.** Structural features of compounds studied. Torsional angles are shown for compound 1.

2.2. Natural Lead Structure

The strongest antimicrobial subfraction IV was successively chromatographed on silica gel to afford pure compound **1**, which was identified by its spectroscopic data, including ^1H , ^{13}C -NMR, and HR-EIMS spectra as (*R*)-2-(4-methylcyclohex-3-en-1-yl)propan-2-yl (*E*)-3-(4-hydroxyphenyl)acrylate (**1**), see Figure 1 and spectra in Supplementary Material. The relevant NOESY correlations (Figure 2), a strong positive Cotton effect observed in the CD spectrum and spectroscopic data, which are in partial agreement with those previously published for the compound 9-*trans*-*p*-coumaroyloxy- α -terpineol, isolated from *Haplopappus taeda* [18], support the structure and absolute configuration proposed in Figure 2. In addition, (DFT) (B3LYP/6-31G (d)) calculations suggest that this structure is 0.46 Kcal/mol more stable than its isomeric form, giving additional support to the experimental data.

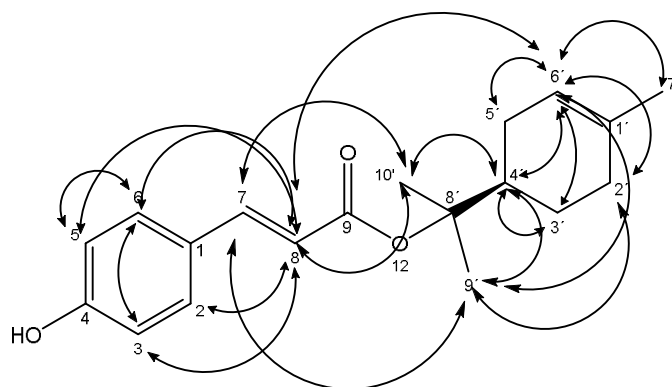
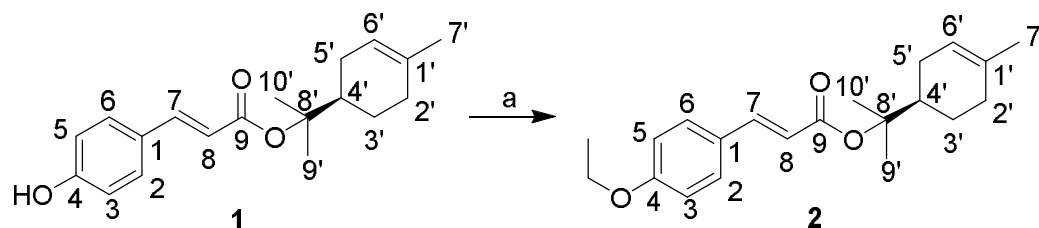


Figure 2. Key NOESY correlations of compound **1**.

2.3. Synthetic Analogues

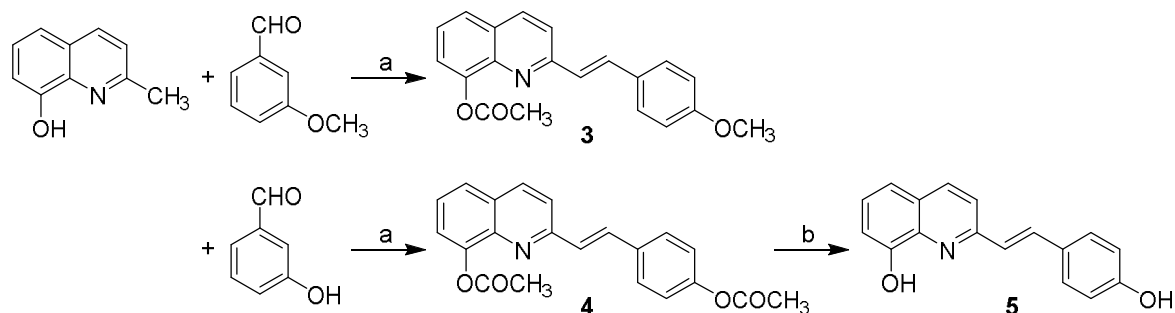
Observing the structure of compound **1**, it is interesting to note that the moiety having the aromatic ring corresponds to a structure very similar to that of *p*-coumaric and caffeic acids. Previously, it was reported that analogues of *p*-coumaric and caffeic acids have significant antibacterial and antifungal activities [19,20]. In fact, several phenolic compounds and derivatives possessing antifungal effects have been reported. For example, gallic acid has been reported to prevent aflatoxin biosynthesis by *Aspergillus flavus* [21]. Two compounds of natural origin, 1-(3'-methoxypropanoyl)-2,4,5-trimethoxybenzene and 2-(2*Z*)-(3-hydroxy-3,7-dimethylocta-2,6-dienyl)-1,4-benzenediol, isolated from the root bark of *Cordia alliodora*, have been also reported as antifungal and larvicidal compounds [22]. In turn, Kim et al. [23] reported antifungal effects of several phenolic compounds, including cinnamic, *m*-coumaric, *p*-coumaric, and caffeic acids; therefore, the significant antibacterial activity found for compound **1** should not be so surprising.

At this stage of the study, efforts were focused on finding new compounds structurally related to lead compound **1** that may have antibacterial activity. First, (*R*)-2-(4-methylcyclohex-3-en-1-yl)propan-2-yl (*E*)-3-(4-ethoxyphenyl)acrylate (**2**) was obtained by a simple modification of compound **1**, see Scheme 1. Interestingly, compound **2** was devoid of antibacterial activity displaying MICs values >50 $\mu\text{g}/\text{mL}$. It should be noted that the only structural difference between compounds **1** and **2** is the ethylation of the hydroxyl group of compound **1**.



Scheme 1. (R)-2-(4-Methylcyclohex-3-en-1-yl)propan-2-yl (E)-3-(4-ethoxyphenyl)acrylate (**2**)—etherified product of (R)-2-(4-methylcyclohex-3-en-1-yl)propan-2-yl (E)-3-(4-hydroxyphenyl)-acrylate (**1**). *Reagents and conditions:* (a) *t*-BuOK, DMSO, CH₃CH₂I, 30 min.

Then, compounds **3–5** were synthesized, in which the first moiety of compound **1** was maintained, while the second part (4-hydroxyphenyl) of the molecule was replaced by a fused ring (rings A and B) of the quinoline scaffold (see Figure 1). Styrylquinoline derivatives **3** and **4** were prepared by condensation of the quinoline derivative with an appropriate aldehyde in a mixture of acetic anhydride/acetic acid. 2-[2-(4-Hydroxyphenyl)vinyl]quinolin-8-ol (**5**) was hydrolysed in methanol with K₂CO₃, then precipitated by concentrated HCl and crystallized from ethanol, see Scheme 2.



Scheme 2. Synthesis of compound **3–5**. *Reagents and conditions:* (a) Ac₂O, 80% AcOH, 18 h at 130 °C, and N₂ atmosphere; (b) MeOH, K₂CO₃, and HCl.

After synthesis of compounds **3–5**, their potential antibacterial activities were evaluated. While compound **5** showed moderate antibacterial activity, compounds **3** and **4** were inactive. It is interesting to note that the only structural difference between compound **5** and compounds **3** and **4** is the replacement of the OH group by OAc and OCH₃, respectively. These results are in accord with those obtained for compounds **1** and **2**, since the ethylation of the OH group of **1** produced significant loss of antibacterial activity. From these results, it appears that the presence of a proton donor group in the ring A of these compounds could play an important role in the antibacterial effect, e.g., compare Gonce et al. [24] with Kos et al. [25,26]. In order to understand better this behaviour, a conformational and electronic study was performed for these compounds with the aim to determine their stereo-electronic characteristics. Details about the type of molecular calculations and the methodology used are explained in the Section 3.4. In addition, details about the conformational analysis of the compounds are also given in the same section. Knowledge of the stereo-electronic attributes and properties of these compounds will contribute significantly to the elucidation of the structural requirements to produce antibacterial activity. Molecular electrostatic potentials (MEP) are of particular value, because they allow the visualization and assessment of the capacity of a molecule to interact electrostatically with a putative-binding site [27–29]. Thus, once the conformational behaviours of compounds reported here had been analysed, an electronic study of their respective preferred conformations by using Electrostatic Potentials Maps (EPMs) was performed. Figure 3 gives the Molecular Electrostatic Potentials (MEP) obtained for compounds **1** and **3**. The MEP obtained for compound **1** (Figure 3a) exhibit three characteristic regions: a clear minimum value (deep red zone with V(r)_{min} ≈ −0.1559

el/au³) in the vicinity of the OH group of the ring A, a positive region (deep blue zone with $V(r)_{\max} \approx 0.20$ el/au³) located in the linker chain, and an extended hydrophobic zone (deep and light green zone with an almost neutral potential $V(r)_{\text{med}} \approx -0.0011$ el/au³) in the zone near to the ring B.

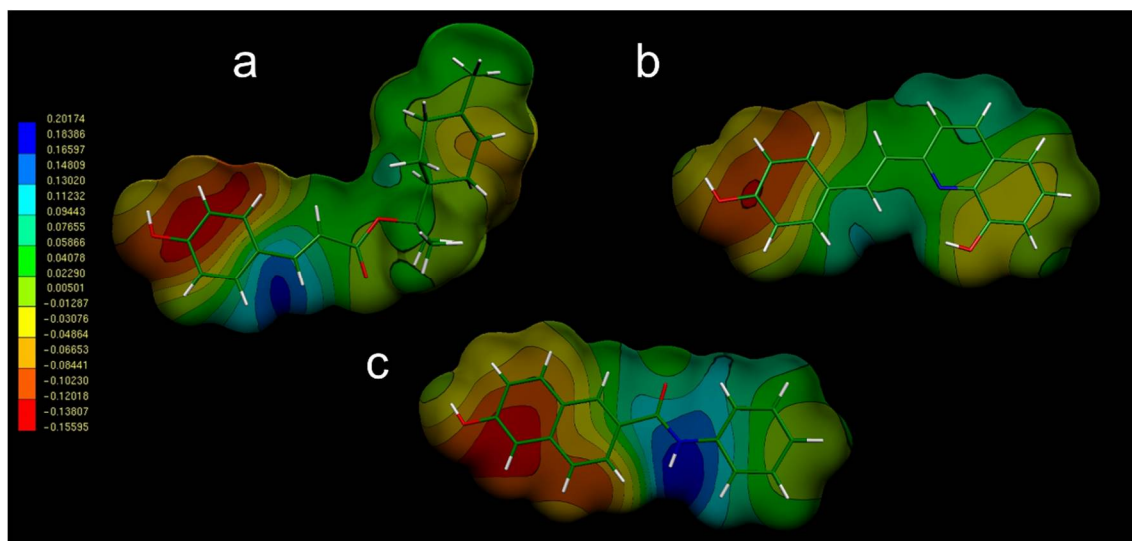
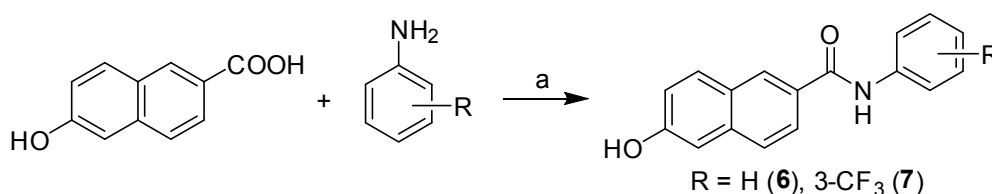


Figure 3. Electrostatic potential-encoded electron density surfaces of core structures of compounds **1** (a), **3** (b), and **6** (c). The colouring represents electrostatic potential, with red indicating the strongest attraction to a positive point charge and blue indicating the strongest repulsion. The electrostatic potential is the energy of interaction of the positive point charge with the nuclei and electrons of a molecule. It provides a representative measure of overall molecular charge distribution.

It is interesting to note that the MEP of compound **3** (Figure 3b) is similar to that obtained for **1**. However, for compound **3**, both the most electronegative zone (zone with red and orange tones) and the electropositive part of the molecule (area with bluish tonalities) are significantly more tenuous with values of $V(r)_{\min} \approx -0.120$ el/au³ and $V(r)_{\max} \approx 0.110$ el/au³, respectively. These results are in agreement with the experimental data, considering that compound **3** displayed lower antibacterial activity than compound **1**.

A series of carboxanilides with antimycobacterial properties, including 6-hydroxy-*N*-phenylnaphthalene-2-carboxamide (**6**) and 6-hydroxy-*N*-(3-trifluoromethylphenyl) naphthalene-2-carboxamide (**7**) (see Figure 1), was reported recently [25]. They were prepared according to Scheme 3 by modified microwave-assisted synthesis in one step with excellent yields. At first, the carboxyl group was activated with phosphorus trichloride. The final amide was immediately formed by aminolysis of acyl chloride by a ring-substituted aniline in dry chlorobenzene. All the crude target compounds were recrystallized from ethanol.



Scheme 3. Synthesis of ring-substituted 6-hydroxynaphthalene-2-carboxanilides **6** and **7**. *Reagents and conditions:* (a) PCl₃, chlorobenzene, and microwave irradiation (MW) [25].

It should be noted that these compounds are naphthalene analogues (carbon isosteres) of the quinoline scaffold, i.e., they also possess fused rings in their structure (rings A and B), which gives a

certain structural similarity to the first portion of compound **1**. Next, a conformational and electronic study of compounds **6** and **7** was performed, and the results were compared with those obtained for the rest of compounds studied here. Figure 3c indicates that compound **6** displays MEP that are very similar to those obtained for compound **1** (compare Figure 3a,c). In this case, the values obtained for $V(r)_{\max}$ and $V(r)_{\min}$ are very similar to those observed in compound **1**. A very similar result was obtained for compound **7**. Based on these results, it was decided to test these compounds as potential antibacterial agents. Compounds **6** and **7**, especially compound **7**, showed significant antibacterial effects against the different strains studied here (Table 4). These experimental results fully agree with the molecular calculations and give additional support to the proposed pharmacophoric pattern. Once again, the presence of a proton donor group at ring A appears to be an essential structural requirement for antibacterial effect.

3. Materials and Methods

3.1. Extractions and Isolation

3.1.1. General Methods

^1H and ^{13}C -NMR spectra were recorded on a High Resolution Spectrometer Advance 400 (working frequency 400 MHz and 100 MHz, respectively) at ambient temperature in CDCl_3 (Aldrich, St. Louis, MO, USA). Carbon spectra assignments are supported by DEPT-135 spectra, ^{13}C - ^1H (HMQC) and ^{13}C - ^1H (HMBC), and NOESY correlations. High-resolution mass spectrums were measured on Bruker Micro TOF Q II equipment (Bruker, Karlsruhe, Germany), operated with an ESI source in the positive mode. Optical rotations were measured with a Jasco polarimeter DIP-1000 P-1010 34 (Jasco, Easton, MD, USA). The CD (Circular Dichroism) and UV-VIS spectra of methanol solutions of **1** and **2** were recorded simultaneously using a Jasco J-810 spectropolarimeter, model J-810 150S and a 100 lm quartz cuvette with resolution 1 nm, time constant 1 s, scan speed 100 nm/min, and 3 accumulations, employing standard sensitivity and a measurement range of 700–190 nm.

3.1.2. Plant Material

The aerial parts (leaves, flowers, and fruits) of *A. emarginata* were collected in San Cosme, province of Corrientes (Argentina) at 27.36667 lat. S; 58.51667 long. W, in the summer of 2013 and were authenticated by Dra. Elisa Petenatti and L.A. Del Vitto. A voucher specimen (L.A. Del Vitto & E.M. Petenatti # 9490) has been deposited at the Herbarium, National University of San Luis, Argentina.

3.1.3. Preparation of Extracts

Finely ground *A. emarginata* fruits (100 g) were extracted at room temperature using methanol MeOH (200 mL \times 3-fold \times 96 h each), filtered and concentrated under reduced pressure to afford the corresponding crude global methanolic extract (MeOHGFE; 17.7 g, yield 17.7% *w/w*). Dried and finely ground *A. emarginata* flowers (100 g) were successively extracted at room temperature (200 mL \times 3-fold \times 96 h, each 3 \times 24 h) with hexane (H), dichloromethane (DCM), ethyl acetate (EtOAc), and methanol (MeOH). Then, solvents were evaporated under vacuum to give flower extracts HFIE, DCMFIE, EtOAcFIE, and MeOHFIE with yields (*w/w*) of 4.3%, 1.9%, 0.66%, and 5.9%, respectively. Finely ground dried *A. emarginata* stem bark (100 g) was successively extracted at room temperature (200 mL \times 3-fold \times 96 h, each 3 \times 24 h) with H, DCM, EtOAc, and MeOH. The solvents were evaporated under vacuum to afford bark extracts HBE, DCMBE, EtOAcBE, and MeOHBE with yields (*w/w*) of 0.92%, 0.27%, 0.34%, and 4.23%, respectively. Finely ground dried *A. emarginata* leaves (100 g) were successively extracted at room temperature (200 mL \times 3-fold \times 96 h, each 3 \times 24 h) with H, DCM, EtOAc, and MeOH. Then, solvents were evaporated under vacuum to produce leaf extracts HLE, DCMLE, EtOAcLE, and MeOHLE, affording 0.63%, 1.54%, 0.75%, and 1.02% yield (*w/w*), respectively.

3.1.4. Bioassay-Guided Fractionation of *Annona emarginata* Fruit Extracts (MeOHGFE)

MeOHGFE (11 g) was applied onto a column (column length 70 cm, i.d. 5 cm) containing silica gel (0.063–0.2 mesh, Merck 60, Merck, Darmstadt, Germany) and eluted with H, DCM, and EtOAc gradients (100% H to 100% EtOAc). Six fractions of 1 L each were obtained, which concentrated under reduced pressure to afford F₁ (200 mg; H 100%), F₂ (115 mg; 50:50% H/DCM), F₃ (1200 mg; 90:10% DCM/EtOAc), F₄ (187.7 mg 80:20% DCM/EtOAc), F₅ (155 mg; 70:30% DCM/EtOAc), and F₆ (137 mg; EtOAc 100%) fractions. Fractions F₁–F₆ were tested for antimicrobial activity. Fraction F₃ (1100 mg) permeated through Sephadex LH-20 (column length 23 cm, i.d. 4 cm; petroleum ether (PE)/MeOH/DCM 2:1:1). Some 21 fractions of 15 mL each were obtained. After TLC comparison (silica gel, PE/EtOAc 8:2) as the mobile phase, detection under UV light and spraying with *p*-anisaldehyde sulfuric acid, the fractions with similar TLC patterns were combined as follows: I (477 mg), II (142 mg), III (98 mg), IV (295 mg), and V (84 mg).

3.1.5. Isolation and Characterization of (R)-2-(4-Methylcyclohex-3-en-1-yl)propan-2-yl (E)-3-(4-hydroxyphenyl)acrylate (**1**)

Separation of the fraction IV (295 mg) using column chromatography on silica gel (column length 40 cm, internal diameter 2 cm; 50 g silica gel 0.063–0.2 mesh, Merck 60); (100% H to 100% EtOAc) provided 200 mg of pure compound **1**: oil; $[\alpha]_D^{23} + 29$ (c = 0.17 g/100 mL, CHCl₃), ¹H-NMR (400 MHz, CDCl₃) δ 1.50 (s, 3H, H-9'), 1.53 (s, 3H, H10'), 1.67 (s, 3H, H-7'), 1.85–1.35 (m, 2H, H-3'), 2.12 (m, 1H, H-4'), 2.16–1.86 (m, 4H, H-2', H-5'), 5.39 (s, 1H, H-6'), 6.22 (d, J = 16 Hz, 1H, H-8), 6.85 (d, J = 8 Hz, 2H, H-3 and H-5), 7.38 (d, J = 8 Hz, 2H, H-2 and H-6), 7.51 (d, J = 16 Hz, 1H, H-7); ¹³C-NMR (100 MHz, CDCl₃) δ 23.3 CH₃, δ 23.4 CH₃, 23.5 CH₃, 24.0 CH₂, 26.5 CH₂, 30.9 CH₂, 42.8 CH (C-4'), 85.2 C (C-8'), 115.9 CH × 2 (C-3 and C-5), 117.2 CH (C-8), 120.3 CH (C-6'), 127.0 (C-1), 129.9 CH × 2 (C-2 and C-6), 134.0 (C-1'), 143.8 (C-7), 158.4 (C-4), 167.8 C (C=O), HR-EIMS 323.1618, (calcd for C₁₉H₂₄O₃ (M + Na) 323.1618). (See spectra in Supplementary Material).

3.2. Synthesis

3.2.1. General Methods

All of the reagents were purchased from Aldrich. Kieselgel 60, 0.040–0.063 mm (Merck, Darmstadt, Germany) was used for the column chromatography. TLC experiments were performed on alumina-backed silica gel 40 F₂₅₄ plates (Merck, Darmstadt, Germany). The plates were illuminated under UV (254 nm) and evaluated in iodine vapour. The melting points were determined on an Optimelt MPA-100 apparatus (SRS, Stanford, CA, USA). The purity of the final compounds was checked using HPLC. Detection wavelengths of 210 and 250 nm were chosen for detection. The purity of individual compounds was determined from the area peaks in the chromatogram of the sample solution in order to ensure >95% purity. All ¹H-NMR spectra were recorded on a Bruker AM-400 (400 MHz for ¹H and 101/126 MHz for ¹³C), BrukerBioSpin Corp., Rheinstetten, Germany. Chemical shifts are reported in ppm (δ) against the internal standard, Si(CH₃)₄. Easily exchangeable signals were omitted when they were diffused. Signals are designated as follows: s, singlet; d, doublet; dd, doublet of doublets; m, multiplet. The high-resolution mass spectra of compounds 3–5 were measured using a high-performance liquid chromatograph Dionex UltiMate®3000 (Thermo Scientific, Waltham, MA, USA) coupled with a LTQ Orbitrap XLTM Hybrid Ion Trap-Orbitrap Fourier Transform Mass Spectrometer (Thermo Scientific) with injection into HESI II in the positive mode.

3.2.2. Synthesis of (R)-2-(4-Methylcyclohex-3-en-1-yl)propan-2-yl (E)-3-(4-ethoxyphenyl)acrylate (**2**)

In a Schlenk tube equipped with a magnetic stirrer, *t*-BuOK (0.118 mmol) was added to 2 mL of degassed DMSO under nitrogen atmosphere. After 10 min, when no more solid was present, compound **1** (0.098 mmol) was added. The reaction mixture was stirred for 30 min until the formation of the corresponding ions. The reaction was then quenched by adding excess ethyl iodide (0.196 mmol)

to obtain compound **2**. The solution was extracted with ethyl acetate and water. The organic extract was analysed by GC-MS. The reaction was then quenched by adding excess ethyl iodide (0.196 mmol) to obtain a brown oil that was purified by column chromatography on silica gel (column length 40 cm, internal diameter 2 cm; 50 g silica gel (0.063–0.2 mesh, Merck 60) using a solvent gradient (100% PE to 100% EtOAc) to afford 110 mg of pure compound **2**: oil (yield 95%); $[\alpha]_D^{23} + 23$ ($c = 0.11$ g/100 mL, CHCl_3), $^1\text{H-NMR}$ (400 MHz, CDCl_3) δ 1.42 (t, 3H, CH_3 ethyl), 1.50 (s, 3H, H-9'), 1.53 (s, 3H, H10'), 1.65 (s, 3H, H-7'), 1.85–1.35 (m, 2H, H-3'), 2.12 (m, 1H, H-4') 2.16–1.86 (m, 4H, H-2', H-5'), 4.05 (q, 2H, CH_2 ethyl), 5.39 (s, 1H, H-6'), 6.23 (d, $J = 16$ Hz, 1H, H-8), 6.87 (d, $J = 8$ Hz, 2H, H-3, H-5), 7.44 (d $J = 8$ Hz, 2H, H-2, H-6), 7.52 (d, $J = 16$ Hz, 1H, H-7); $^{13}\text{C-NMR}$ (100 MHz, CDCl_3) δ 14.7 CH_3 (ethyl) 23.3 CH_3 , 23.4 CH_3 , 23.5 CH_3 , 24.0 CH_2 , 26.5 CH_2 , 30.9 CH_2 , 42.7 CH (C-4'), 63.5 (s, 2 H, CH_2 ethyl), 84.9 C (C-8'), 114.7 CH (C-3, C-5), 117.6 CH (C-8), 120.4 CH (C-6'), 127.2 (C-1), 129.6 CH (C-2 and C-6), 134.0 (C-1'), 143.3 (C-7), 160.0 CH (C-4), 168.9 C (C=O), HREIMS 351.1935, (calcd for $\text{C}_{21}\text{H}_{28}\text{O}_3$ (M + Na) 351.1931). (See spectra in Supplementary Material).

3.2.3. General Synthesis of Styrylquinoline Derivatives 3–5

The appropriate quinoline derivative (2.5 mmol) in acetic anhydride with 80% acetic acid was thoroughly mixed with one equivalent aldehyde and heated in an inert gas atmosphere (N_2) at 130 °C for 18 h. Then, the mixture was evaporated to dryness, and a solid was recrystallized from ethanol. The appropriate styrylquinoline derivative (2.5 mmol) in methanol was thoroughly mixed with 2.5 equivalent K_2CO_3 at room temperature for 2 h. Then, concentrated HCl was added, and the resulting precipitate was filtered and washed with H_2O . The crude product was crystallized from ethanol.

2-[2-(4-Methoxyphenyl)vinyl]quinolin-8-yl acetate (**3**): yield 20%, light brown solid, m.p. 97–100 °C; HPLC purity 95.82%; $^1\text{H-NMR}$ (400 MHz, $\text{DMSO-}d_6$) δ 8.38 (d, $J = 8.6$ Hz, 1H), 7.90–7.82 (m, 2H), 7.78 (d, $J = 16.3$ Hz, 1H), 7.70 (d, $J = 8.5$ Hz, 2H), 7.57–7.47 (m, 2H), 7.30 (d, $J = 16.3$ Hz, 1H), 7.02 (d, $J = 8.5$ Hz, 2H), 3.82 (s, 3H), 2.50 (s, 3H); $^{13}\text{C-NMR}$ (126 MHz, $\text{DMSO-}d_6$) δ 172.49, 160.23, 154.26, 153.29, 138.60, 136.84, 134.57, 129.58, 129.39, 129.11, 127.97, 127.24, 126.14, 122.09, 121.25, 118.02, 114.87, 111.58, 55.69, 21.52. HR-MS: for $\text{C}_{20}\text{H}_{18}\text{NO}_3$ [M + H] $^+$ calculated 320.1281 m/z , found 320.1284 m/z .

2-[2-(4-Acetoxyphenyl)vinyl]quinolin-8-yl acetate (**4**): yield 67%, yellow solid, m.p. 157–159 °C; HPLC purity 95.83%; $^1\text{H-NMR}$ (400 MHz, CDCl_3) δ 8.15 (dd, $J = 8.5, 5.1$ Hz, 1H), 7.73–7.60 (m, 5H), 7.55–7.37 (m, 3H), 7.19–7.12 (m, 2H), 2.58 (s, 3H), 2.35 (s, 3H); $^{13}\text{C-NMR}$ (101 MHz, CDCl_3) δ 169.84, 169.33, 155.65, 150.91, 147.38, 140.94, 136.41, 134.25, 133.71, 131.21, 129.10, 128.60, 128.32, 125.75, 125.54, 121.95, 121.68, 120.19, 21.17, 21.03. HR-MS: for $\text{C}_{21}\text{H}_{18}\text{NO}_4$ [M + H] $^+$ calculated 348.1230 m/z , found 348.1239 m/z .

2-[2-(4-Hydroxyphenyl)vinyl]quinolin-8-ol (**5**): yield 63%, orange solid, m.p. 156–157 °C; HPLC purity 98.38%; $^1\text{H-NMR}$ (400 MHz, $\text{DMSO-}d_6$) δ 11.81 (s, 1H), 10.38 (s, 1H), 8.84 (d, $J = 8.9$ Hz, 1H), 8.42 (d, $J = 8.9$ Hz, 1H), 8.22 (d, $J = 16.2$ Hz, 1H), 7.79 (d, $J = 16.3$ Hz, 1H), 7.67–7.56 (m, 4H), 7.47 (dd, $J = 6.1, 2.6$ Hz, 1H), 6.95 (d, $J = 8.6$ Hz, 2H); $^{13}\text{C-NMR}$ (126 MHz, $\text{DMSO-}d_6$) δ 161.19, 153.30, 148.85, 144.14, 143.99, 143.72, 130.85, 129.57, 128.20, 126.55, 119.16, 118.74, 116.83, 116.50. HR-MS: for $\text{C}_{17}\text{H}_{13}\text{NO}_2$ [M + H] $^+$ calculated 264.1019 m/z , found 264.1028 m/z .

6-Hydroxy-*N*-phenyl-naphthalene-2-carboxamide (**6**) and 6-hydroxy-*N*-(3-trifluoromethylphenyl)-naphthalene-2-carboxamide (**7**) were synthesized and characterized recently [25].

3.3. Antibacterial Activity

For the antibacterial evaluation, methicillin-sensitive *Staphylococcus aureus* ATCC 25923, methicillin-resistant *S. aureus* ATCC 43300, *Escherichia coli* ATCC 25922, and clinical isolates from human patients—coagulase negative *Staphylococcus aureus* 502, *Streptococcus pyogenes*, *Streptococcus agalactiae*, *Escherichia coli* LM2, *Salmonella* sp. and *Klebsiella pneumoniae*—provided by Laboratorio de Microbiologia, Hospital Marcial Quiroga, San Juan, Argentina, were used.

Minimal inhibitory concentration (MIC) values were determined using the broth microdilution method according to the protocols of the Clinical and Laboratory Standards Institute [30]. The assay was executed in Mueller–Hinton broth (MHB), using strains 24 h old. The inoculum employed was $1\text{--}5 \times 10^5$ CFU/mL. Stock solutions of extracts in DMSO (50 mg/mL) were diluted to give serial 2-fold dilutions that were added to each medium to obtain final concentrations ranging from 1000 to 1 $\mu\text{g}/\text{mL}$. Stock solutions of compounds in DMSO (5 mg/mL) were diluted to give serial 2-fold dilutions that were added to each medium to obtain final concentrations ranging from 50 to 1 $\mu\text{g}/\text{mL}$. The final concentration of DMSO in the assay did not exceed 1%. Cefotaxime Argentia[®] (Bristol-Myers Squibb, Buenos Aires, Argentina) was included in the assays as a positive control, while MHB and DMSO (1%) were used as negative controls. The plates were incubated for 24 h at 37 °C. Activity was evaluated at 620 nm using a Multiskan[™] FC Microplate Photometer (Thermo Fisher Scientific, Vantaa, Finland). The MIC values were defined as the lowest extract concentrations showing no bacterial growth after the incubation time. Tests were done in triplicate.

3.4. Conformational and Electronic Study

All calculations were carried out using the Gaussian 09 program (Gaussian, Wallingford, CT, USA) [31]. The search for low-energy conformations on the potential energy surface for compounds 1, 3, 6, and 7 was carried out by using combined *ab initio* (RHF/3-21G) and density functional theory (DFT) (B3LYP/6-31G(d)) calculations. Final DFT geometries were obtained from the geometry optimisation jobs. Minima were characterized through harmonic frequency analysis calculated at DFT level. Correlations effects were included using DFT and the functional of Lee [32] as proposed and parameterized by Becke [33,34] (RB3LYP) and 6-31G (d) basis set. Compound 1 looks like a relatively simple conformational problem, in which three torsional angles (ϕ_1 , ϕ_2 , and ϕ_3 , Figure 1) are main rotations in this molecule. Our calculations predict that the torsional angle ϕ_1 possesses only two possible quasi-planar conformations: one of them near to 0°, and the opposite position giving values near to 180°. The energy barrier obtained for this rotation is more than 10 Kcal/mol, suggesting a significantly restricted torsional angle (see Figure S1 in Supplementary Material). It should be noted that the *cis* form possesses about 1 Kcal/mol above the *trans* form; therefore, the conformational analysis of compound 1 considering ϕ_1 near to 180° was performed. The orientations of the ring B are mainly described by the dihedral angles ϕ_2 and ϕ_3 , and probably the most comprehensive computational method to evaluate how the local energy minima and the transition states are linked together requires an exploration of the complete potential energy surface (PES) generated by ϕ_2 vs. ϕ_3 . This PES was calculated using a 12×12 grid generated by rotating through ϕ_2 and ϕ_3 in 30° increments from -180 to 180° . At each point, a complete geometry optimization was performed with ϕ_2 and ϕ_3 frozen at their respective grid values. The graphical presentation of the PES was generated using the program AXUN 5.0 (MathSoft, Cambridge, MA, USA), plotting the total energy values as a dependent variable generated by double scans over independent variables ϕ_2 and ϕ_3 . The optimum coordinates of ϕ_2 and ϕ_3 for all possible minima were then visually estimated from the level contours diagrams (Figure S2 in Supplementary Material). Five different conformations (conformations 1–5) were obtained for 1; such low-energy conformers might be well appreciated in this surface. The global minimum (conformer 1) corresponds to a partially extended form (see Table S1 in Supplementary Material). On the other hand, the conformational analysis suggests planar forms as energetically preferred structures for compounds 3, 6, and 7. This is an expected result, considering the structural characteristics of their connecting chains. In compound 3, it is a highly delocalized system, while in compounds 6 and 7, it is a peptide bond. The electronic study of compounds 1, 3, 6, and 7 was carried out using molecular electrostatic potentials (MEP) [27]. MEP have been shown to provide reliable information both on the interaction sites of the molecules with point charges and on the comparative reactivities of such sites [28,29]. These MEP were calculated using B3LYP/6-311G (d,p) wave functions from the MOLEKEL 4.0. program (CSCS, Manno, Switzerland) [35].

4. Conclusions

Strong antibacterial activities found for some of the extracts studied here fully justify the use of infusions and decoctions of *Annona emarginata* (Schltdl.) H. Rainer in folk medicine for the treatment of some infections. First, it is interesting to remark that the less polar flower extracts (hexane, dichloromethane) showed very strong antibacterial activity against methicillin-sensitive *S. aureus* ATCC 25923 and methicillin-sensitive *S. aureus* ATCC 43300. Additionally, the hexane extract showed activity against *K. pneumoniae*, while the methanol extract from the fruits was also active against the three strains mentioned above. Such activity might be explained at least in part by the content of the new main compound (*R*)-2-(4-methylcyclohex-3-en-1-yl)propan-2-yl (*E*)-3-(4-hydroxyphenyl)acrylate (**1**). This compound showed strong antimicrobial activity against all Gram (+) species tested. The demand for new antibacterial agents and the new trend towards the use of characterized natural extracts or compounds isolated as medicines instead of pure drugs might open an alternative way for the development of new antibacterial agents, trying to avoid the serious problem of resistance to the antibiotics in use today. On the other hand, the molecular calculations allowed for the establishment of structure-activity relationships between the antibacterial compounds reported here, which gives important information about a possible pharmacophoric pattern of these compounds. This information may be of great interest for the search and procurement of new structurally related antibacterial agents.

Supplementary Materials: The Supplementary materials are available online.

Author Contributions: Ricardo D. Enriz, Josef Jampilek, and Alejandro Tapia conceived and designed the experiments. Juan G. Dolab, Beatriz Lima, Natividad H. Cano, Gabriela Feresin, and Alejandro Tapia performed and analyzed the experiments, isolation, synthesis, the spectroscopic data of compounds **1** and **2**, and the antibacterial activity. Francisco Garibotto and Monica Olivella performed the molecular modelling. Ewelina Spaczynska and Robert Musiol performed synthesis and characterization of compounds **3–5**. Jiri Kos and Josef Jampilek performed synthesis and characterization of compounds **6** and **7**. Elisa Petenatti identified the plant. All authors wrote, read, and approved the final manuscript.

Acknowledgments: This research was partially supported by grants from Universidad Nacional de San Luis and PIP 444-CONICET. J.D. thanks a fellowship from CONICET. E.S. and R.M. appreciate National Science Centre grant No 2013/09/B/NZ7/00423. J.K. and J.J. were supported by the grant of the Faculty of Pharmacy of Comenius University in Bratislava No. FaF UK/37/2018 and by SANOFI-AVENTIS Pharma Slovakia, s.r.o. The authors thank Luis A. Del Vitto (UNSL) for his help in the botanical classification and Marcos Maiocchi (UNNE) for the help in the collection of the plant material. B.L., G.E.F. and A.T. thank CICITCA-UNSJ.

Conflicts of Interest: The authors declare no conflict of interest.

References

1. Moreira, I.C.; Lago, J.H.G.; Young, M.C.M.; Roque, N.F. Antifungal aromadendrane sesquiterpenoids from the leaves of *Xylopia brasiliensis*. *J. Braz. Chem. Soc.* **2003**, *14*, 828–831. [[CrossRef](#)]
2. Takahashi, J.A.; Pereira, C.R.; Pimenta, L.P.; Boaventura, M.A.; Silva, L.G. Antibacterial activity of eight Brazilian *Annonaceae* plants. *Nat. Prod. Res.* **2006**, *20*, 21–26. [[CrossRef](#)] [[PubMed](#)]
3. Santos Pimenta, L.P.; Pinto, G.B.; Takahashi, J.A.; Silva, L.G.F.; Boaventura, M.A.D. Biological screening of Annonaceous Brazilian Medicinal Plants using *Artemia salina* (Brine Shrimp Test). *Phytomedicine* **2003**, *10*, 209–212. [[CrossRef](#)] [[PubMed](#)]
4. Novaes, P.; Bezerra Torres, P.; Alves, D.Y.; dos Santos, C. Biological activities of *Annonaceae* species extracts from Cerrado. *Braz. J. Bot.* **2016**, *39*, 131–137. [[CrossRef](#)]
5. Frausin, G.; Lima, R.B.S.; Hidalgo, A.F.; Maas, P.; Pohlit, A.M. Plants of the *Annonaceae* traditionally used as antimalarials: A review. *Rev. Bras. Frutic.* **2014**, *36*, 315–337. [[CrossRef](#)]
6. Waechter, A.I.; Cave, A.; Hocquemiller, R.; Bories, C.; Munoz, V.; Fournet, A. Antiprotozoal activity of aporphine alkaloids isolated from *Unonopsis buchtienii* (*Annonaceae*). *Phytotherapy Res.* **1999**, *13*, 175–177. [[CrossRef](#)]
7. Chen, Y.; Xu, S.S.; Chen, J.W.; Wang, Y.; Xu, H.Q.; Fan, N.B.; Li, X. Anti-tumor activity of *Annona squamosa* seeds extract containing annonaceous acetogen in compounds. *J. Ethnopharmacol.* **2012**, *142*, 462–466. [[CrossRef](#)] [[PubMed](#)]

8. Monks, N.R.; Bordignon, S.A.L.; Ferraz, A.; Machado, K.R.; Faria, D.H.; Lopes, R.M.; Mondin, C.A.; Schwartzmann, G. Anti-tumour screening of Brazilian plants. *Pharm. Biol.* **2002**, *40*, 603–616. [[CrossRef](#)]
9. Barboza, G.E.; Cantero, J.J.; Nunez, C.; Pacciaroni, A.; Ariza Espinar, L. Medicinal plants: A general review and a phytochemical and ethnopharmacological screening of the native Argentine flora. *Kurtziana* **2009**, *34*, 7–365.
10. Martinez Crovetto, R. *Plantas Utilizadas en Medicina en el NO de Corrientes*; Ministry of Culture and Education, Miguel Lillo Foundation: Tucuman, Argentina, 1981.
11. Fevrier, A.; Ferreira, M.E.; Fournet, A.; Yaluff, G.; Inchausti, A.; Rojas de Arias, A.; Hocquemiller, R.; Waechter, A.I. Acetogenins and other compounds from *Rollinia emarginata* and their antiprotozoal activities. *Planta Med.* **1999**, *65*, 47–49. [[CrossRef](#)] [[PubMed](#)]
12. Colom, O.A.; Popich, S.; Bardon, A. Bioactive constituents from *Rollinia emarginata* (Annonaceae). *Nat. Prod. Res.* **2007**, *21*, 254–259. [[CrossRef](#)] [[PubMed](#)]
13. Roth, M.; Araya, J.J.; Timmermann, B.N.; Hagenbuch, B. Isolation of modulators of the liver-specific organic anion-transporting polypeptides (OATPs) 1B1 and 1B3 from *Rollinia emarginata* Schltdl. (Annonaceae). *J. Pharmacol. Exp. Ther.* **2011**, *339*, 624–632. [[CrossRef](#)] [[PubMed](#)]
14. Nieto, M. Alkaloids from *Rollinia emarginata*. *J. Nat. Prod.* **1986**, *49*, 717. [[CrossRef](#)] [[PubMed](#)]
15. Leboeuf, M.; Cave, A.; Bhaumik, P.K.; Mukherjee, B.; Mukherjee, R. The phytochemistry of the Annonaceae. *Phytochem* **1982**, *21*, 2783–2813. [[CrossRef](#)]
16. O'Neill, J. *Tackling Drug-Resistant Infections Globally: Final Report and Recommendations*; HM Government and the Wellcome Trust: London, UK, 2016.
17. Ggetti, P.; Corso, A. Actualización en *Staphylococcus aureus* resistente a metilicina de la comunidad. *Bol. Assoc. Argent. Microbiol.* **2011**, *193*, 7–8.
18. Faini, F.; Labbe, C.; Torres, R.; Rodilla, J.M.; Silva, L.; Delle Monache, F. New phenolic esters from the resinous exudate of *Haplopappus taeda*. *Fitoterapia* **2007**, *78*, 611–613. [[CrossRef](#)] [[PubMed](#)]
19. Feresin, G.E.; Tapia, A.; Gimenez, A.; Gutierrez Ravelo, A.; Zacchino, S.; Sortino, M.; Schmeda-Hirschman, G. Constituents of the Argentinean medicinal plant *Baccharis grisebachii* and their antimicrobial activity. *J. Ethnopharmacol.* **2003**, *89*, 73–80. [[CrossRef](#)]
20. Gianello, J.C.; Giordano, O.S. Constituents from *Baccharis grisebachii*. *An. Assoc. Quím. Argent.* **1987**, *75*, 1–3.
21. Bisogno, F.; Mascoti, L.; Sanchez, C.; Garibotto, F.; Giannini, F.; Kurina, M.; Enriz, R.D. Structure-antifungal activity relationship of related cinnamic acid derivatives. *J. Agric. Food Chem.* **2007**, *55*, 10635–10640. [[CrossRef](#)] [[PubMed](#)]
22. Ioset, J.R.; Marston, A.; Gupta, M.P.; Hostettmann, K. Antifungal and larvicidal compounds from the root bark of *Cordia alliodora*. *J. Nat. Prod.* **2000**, *63*, 424–426. [[CrossRef](#)] [[PubMed](#)]
23. Kim, J.H.; Campbell, B.C.; Mahomey, N.E.; Chan, K.L.; Molyneux, R.J. Identification of phenolics for control of *Aspergillus flavus* using *Saccharomyces cerevisiae* in a model target-gene bioassay. *J. Agric. Food Chem.* **2004**, *52*, 7814–7821. [[CrossRef](#)] [[PubMed](#)]
24. Gonec, T.; Bobal, P.; Suján, J.; Pesko, M.; Guo, J.; Kralova, K.; Pavlacka, L.; Vesely, L.; Kreckova, E.; Kos, J.; et al. Investigating the spectrum of biological activity of substituted quinoline-2-carboxamides and their isosteres. *Molecules* **2012**, *17*, 613–644. [[CrossRef](#)] [[PubMed](#)]
25. Kos, J.; Nevin, E.; Soral, M.; Kushkevych, I.; Gonec, T.; Bobal, P.; Kollar, P.; Coffey, A.; O'Mahony, J.; Liptaj, T.; et al. Synthesis and antimycobacterial properties of ring-substituted 6-hydroxynaphthalene-2-carboxanilides. *Bioorg. Med. Chem.* **2015**, *23*, 2035–2043. [[CrossRef](#)] [[PubMed](#)]
26. Kos, J.; Zadrazilova, I.; Nevin, E.; Soral, M.; Gonec, T.; Kollar, P.; Oravec, M.; Coffey, A.; O'Mahony, J.; Liptaj, T.; et al. Ring-substituted 8-Hydroxyquinoline-2-carboxanilides as potential antimycobacterial agents. *Bioorg. Med. Chem.* **2015**, *23*, 4188–4196. [[CrossRef](#)] [[PubMed](#)]
27. Politzer, P.; Truhlar, D.G. *Chemical Applications of Atomic and Molecular Electrostatic Potentials*; Plenum Publishing: New York, NY, USA, 1991.
28. Carrupt, P.A.; El Tayar, N.; Karlen, A.; Testa, B. Molecular electrostatic potentials for characterizing drug-biosystem interactions. *Methods Enzymol.* **1991**, *202*, 638–677.
29. Geerlings, P.; Langenaeker, W.; De Proft, F.; Baeten, A. Molecular electrostatic potentials vs. DFT descriptors of reactivity. In *Molecular Electrostatic Potentials: Concepts and Applications. Theoretical and Computational Chemistry*; Politzer, P., Maksic, Z.B., Eds.; Elsevier Science B.V.: Amsterdam, The Netherlands, 1996; Volume 3, pp. 587–617.

30. Clinical and Laboratory Standards Institute. *Performance Standards for Antimicrobial Susceptibility Testing*; M100-S22; CLSI: Wayne, PA, USA, 2012.
31. Frisch, M.J.; Trucks, G.W.; Schlegel, H.B.; Scuseria, G.E.; Robb, M.A.; Cheeseman, J.R.; Scalmani, G.; Barone, V.; Mennucci, B.; Petersson, G.A.; et al. *Gaussian 09*; Gaussian, Inc.: Wallingford, CT, USA, 2009.
32. Lee, C.; Yang, W.; Parr, R.G. Development of the Colle-Salvetti correlation-energy formula into a functional of the electron density. *Phys. Rev. B* **1998**, *37*, 785–789. [[CrossRef](#)]
33. Becke, A.D. Density-functional thermochemistry. III. The role of exact exchange. *J. Chem. Phys.* **1993**, *98*, 5618–5652. [[CrossRef](#)]
34. Becke, A.D. Density-functional exchange-energy approximation with correct asymptotic behavior. *Phys. Rev. A* **1998**, *38*, 3098–3100.
35. Flukiger, P.; Luthi, H.P.; Portmann, S.; Weber, J. *MOLEKEL 4.0*; Swiss Center for Scientific Computing: Manno, Switzerland, 2000.

Sample Availability: Samples of the compounds are available from the authors.



© 2018 by the authors. Licensee MDPI, Basel, Switzerland. This article is an open access article distributed under the terms and conditions of the Creative Commons Attribution (CC BY) license (<http://creativecommons.org/licenses/by/4.0/>).

č.	citace	ISSN
10	KUSHKEVYCH, I, M VITEZOVA, J KOS , P KOLLAR a J JAMPILEK. Effect of selected 8-hydroxyquinoline-2-carboxanilides on viability and sulfate metabolism of <i>Desulfovibrio piger</i> . <i>JOURNAL OF APPLIED BIOMEDICINE</i> [online]. 2018, 16 (3), 241–246. Dostupné z: doi:10.1016/j.jab.2018.01.004	1214-021X



Original research article

Effect of selected 8-hydroxyquinoline-2-carboxanilides on viability and sulfate metabolism of *Desulfovibrio piger*Ivan Kushkevych^{a,*}, Monika Vítězová^a, Jiří Kos^b, Peter Kollár^c, Josef Jampílek^{b,**}^a Masaryk University, Faculty of Science, Department of Experimental Biology, Brno, Czech Republic^b Comenius University, Faculty of Pharmacy, Department of Pharmaceutical Chemistry, Bratislava, Slovak Republic^c University of Veterinary and Pharmaceutical Sciences, Faculty of Pharmacy, Department of Human Pharmacology and Toxicology, Brno, Czech Republic

ARTICLE INFO

Article history:

Received 3 August 2017

Received in revised form 5 January 2018

Accepted 15 January 2018

Available online 10 February 2018

Keywords:

Sulfate-reducing bacteria
Dissimilatory sulfate reduction
Inflammatory bowel disease
8-hydroxyquinolines
Structure-activity relationships

ABSTRACT

An increased number of sulfate-reducing bacteria is often isolated from faeces of patients with gastrointestinal diseases, which can be the cause of the development of bowel inflammation. Frequent use of antibiotics causes the resistance of intestinal microorganisms and ineffective treatment of these diseases. The antimicrobial activity and biological properties of the selected ring-substituted 8-hydroxyquinoline-2-carboxanilides against *Desulfovibrio piger* Vib-7 were studied. The addition of these compounds in the cultivation medium inhibited the bacterial growth and the process of sulfate reduction dose-dependently. A significant cytotoxic activity under the influence of ring-substituted 8-hydroxyquinoline-2-carboxanilides was determined. The strongest cytotoxic effect of the derivatives was observed for compounds 8-hydroxy-*N*-(3-methoxyphenyl)quinoline-2-carboxamide and 8-hydroxy-*N*-(3-trifluoromethylphenyl)quinoline-2-carboxamide that caused a low survival of *D. piger* Vib-7 in concentration 17 μ M and high toxicity rates.

© 2018 Faculty of Health and Social Sciences, University of South Bohemia in Ceske Budejovice. Published by Elsevier Sp. z o.o. All rights reserved.

Introduction

A high number of sulfate-reducing bacteria (SRB) and the intense process of dissimilatory sulfate reduction in the gut are thought to be significant risk factors of inflammatory bowel diseases in both humans and animals (Gibson et al., 1991, 1993; Kushkevych, 2016, Kushkevych et al., 2016). These bacteria are often found in patients with rheumatic diseases, ankylosing spondylitis, etc. (Barton and Hamilton, 2010). The species of *Desulfovibrio* genus can cause bloody diarrhea, weight loss, anorexia, epithelial hyperplasia, abscesses and inflammatory infiltrates in animals and humans (Loubinoux et al., 2000, 2002a,b). There is also an assumption that SRB can be responsible for some forms of cancer of the rectum through the formation of hydrogen sulfide that affects the metabolism of intestinal cells.

An increased number of SRB was found in faeces from people with ulcerative colitis in comparison with healthy individuals (Cummings et al., 2003). The injection of these bacteria in hamster intestine caused an infection clinically similar to human colitis (Cummings et al., 2003; Pitcher and Cummings, 1996). Using the model of laboratory rats, the etiological role of the cultures of SRB, *Desulfovibrio piger* Vib-7 and *Desulfomicrobium* sp. Rod-9, in the development of inflammatory processes in the intestine was examined. It was found that the introduction of pure cultures of SRB led to a high production of hydrogen sulfide and acetate in the intestine, and clinical manifestations similar to non-specific intestinal inflammation in humans appeared (Kushkevych, 2014).

Ulcerative colitis (UC) is a chronic inflammatory disease of the colon that affects up to 12 per 100,000 people in Western countries, mostly between 15 and 30 years of age (Rowan et al., 2009). The treatment of mild to moderate UC includes, in the first instance, sulfasalazine and mainly 5-aminosalicylate containing drugs, the type and dosage of which depend on the location and severity of the disease. Other options of treatment include corticosteroids and immunosuppressants (for moderate to severe UC, with a high mortality) or probiotics (for improving the microbial balance) (Cummings et al., 2003; Kushkevych, 2016). Despite the bacterial nature of the disease, antibiotics have failed

* Author for correspondence: Masaryk University, Faculty of Science, Department of Experimental Biology, Kamenice 753/5, 625 00 Brno, Czech Republic.

** Author for correspondence: Comenius University, Faculty of Pharmacy, department of Pharmaceutical Chemistry, Odbojarov 10, 832 32 Bratislava, Slovak Republic.

E-mail addresses: kushkevych@mail.muni.cz (I. Kushkevych), josef.jampilek@gmail.com (J. Jampílek).

in the treatment of UC so far. However, new antibacterial compounds with high specific effect against SRB could yield better efficiency in the treatment of this disease.

Quinoline-based compounds have a wide range of promising biological properties (Cieslik et al., 2012; Jampilek, 2017; Jampilek et al., 2016; Kos et al., 2015; Mucaji et al., 2017; Musiol et al., 2006, 2007, 2008, 2010); therefore a special attention is paid to them at research and designing of new drugs (Cieslik et al., 2012; Jampilek et al., 2016; Kos et al., 2015; Musiol et al., 2006, 2007; Ranjith et al., 2017). This simple scaffold possesses unique physicochemical properties and provides a possibility of a great number of targeted modifications. Ring-substituted 8-hydroxyquinoline-2-carboxanilides were recently prepared (Kos et al., 2015) and published as compounds with noteworthy biological activities (Jampilek et al., 2016; Kos et al., 2015) based on the presence of an amide group and a hydroxy moiety in the quinoline scaffold (Gonec et al., 2012; Jampilek et al., 2016; Kos et al., 2015). Thus, in the context of the above-mentioned facts, the aim of this work was to evaluate viability of intestinal sulfate-reducing bacteria *Desulfovibrio piger* and parameters of their dissimilatory sulfate reduction (production of hydrogen sulfide and acetate as well as sulfate and lactate consumption) under effect of selected 8-hydroxyquinoline-2-carboxanilides (Kos et al., 2015).

Materials and methods

Tested compounds

The studied ring-substituted 8-hydroxyquinoline-2-carboxanilides were synthesized by means of microwave-assisted synthesis described recently. The compounds were isolated and fully characterized (melting point, elemental analysis, infrared as well as ^1H and ^{13}C NMR spectroscopy) (Kos et al., 2015). The compounds were kept in microtubes dissolved in dimethyl sulfoxide (DMSO) solution. The quantity of DMSO necessary to dissolve each compound was calculated previously to achieve the concentration of the component 30 mM. Afterwards it was diluted 4-fold in a proportion 1:3, and 5 different concentrations of the chemical compound – 5, 10, 15, 20, 25, 30 and 35 mM – were obtained. The maximum concentration of DMSO in the assays never exceeded 0.1%.

Bacterial culture and cultivation

The sulfate-reducing bacteria *D. piger* Vib-7 (GenBank: KT881309.1) were isolated from the healthy human large intestine as described previously (Kushkevych, 2013; Kushkevych et al., 2014). The strain has been kept in the collection of microorganisms at the Department of Experimental Biology, Faculty of Science at the Masaryk University (Brno, Czech Republic). The bacteria were grown for 36 h at 37 °C under anaerobic conditions in nutrition modified Postgate's liquid medium (Postgate, 1984). Before bacterial passage in the medium, 0.05 mM of sterile solution of $\text{Na}_2\text{S} \times 9\text{H}_2\text{O}$ (1%) was added. The sterile 10 ml solution of NaOH (0.9 mM) in the medium was used to provide the final pH 7.2. The medium was heated in boiling water for 30 min in order to obtain an oxygen-free medium and cooled to 30 °C. The tubes were brim-filled with medium and closed to provide anaerobic conditions.

Assay of bacterial cell concentration

The best concentration of *D. piger* Vib-7 was assessed to be 5×10^5 CFU/ml. Based on our previous work, the correlation between OD_{340} and the amount of cells in the solutions measured

in the biophotometer was determined as $y = 1.0 \times 10^9 \chi - 6.0 \times 10^6$, where y means the bacterial concentration and χ means the OD_{340} measured as was described in our previous paper (Kushkevych et al., 2015a).

Treatment of bacterial culture

The bacterial culture of the stationary phase of growth was centrifuged for 3 min at a rotation speed of 3500 rpm. Supernatant was removed and replaced by a fresh liquid medium, where the bacterial precipitate was diluted. The bacterial suspension was mixed, and OD_{340} was measured. Numbers and viabilities of the bacterial cells were determined by counting with a haemocytometer after staining with erythrosine B [0.1% erythrosine B (w/v) in phosphate-buffered saline (PBS), pH 7.2–7.4]. Unstained cells were considered to be viable.

The bacterial suspension (initial concentration 0.5 mg/ml) was poured in microtubes (350 μl) that contained samples + solvent control (DMSO) + sample control + blanks; each sample as well as the controls were prepared in triplicate, so that the average of the results did not had a great discrepancy from the results independently (except in 3 blanks). The sample controls contained only bacterial suspension and medium (free of tested compounds); and for the 3 blanks only medium. Calculations were made to assess how much bacterial solution should be in each, based on the OD. The determination of biomass and concentrations of sulfate, lactate, acetate and sulfide in the culture medium under the treatment of 5, 10, 15, 20, 25, 30 and 35 μM compounds after 36 h was carried out. During experiments, bacteria were grown at 37 °C under anaerobic conditions.

Analysis of viability of *D. piger* Vib-7 and cytotoxicity of compounds

The bacterial suspension (5×10^4 cells/well in 300 μl culture medium) was filled in 100-well plates in triplicate in the Postgate's liquid medium (without Mohr's salt), treated with 5, 10, 15, 20, 25, 30 and 35 μM compounds and incubated at +37 °C. The relative survival of *D. piger* Vib-7 cells and the cytotoxicity of the compounds were determined at the 36th hour of cultivation using a WST-1 assay kit (Roche Diagnostics, Mannheim, Germany) according to the manufacturer's instructions. The relative survival rate was calculated by the following equation: $(A_{\text{Sample}} - A_{\text{Blank}}) / (A_{\text{Control}} - A_{\text{Blank}})$, and multiplied by 100 for the result in percentage. The relative toxicity rate was determined as described previously (Kos et al., 2015). All data were evaluated using GraphPad Prism 5.00 software (GraphPad Software, San Diego, CA, USA, <http://www.graphpad.com>).

Assay of sulfate, lactate, sulfide and acetate in cultivation medium

The sulfate ion concentration in the medium was determined by the turbidimetric method after it had been precipitated by barium chloride. To stabilize the suspension, glycerol was used (Kolmert et al., 2000). Lactate concentration was measured through the dehydrogenation reaction using Lactate Assay Kit (Sigma-Aldrich, Catalog Number MAK064). Sulfide concentration in the culture medium was assayed by the spectrophotometric method as was described (Cline, 1969). Accumulation of acetate ions in the process of bacterial growth in the medium was determined using Acetate Assay Kit (Colorimetric, Catalog Number KA3764).

Statistical analysis

The statistical calculations of the results were carried out using the software MS Office and Origin program. The research results were treated by methods of variation statistics using Student t -test.

Statistical significance was tested using the one-way analysis of variance with Dunnett's test and Tukey post-test for comparisons between the means, and differences between two conditions were retained for $P \leq 0.05$. Statistical significance was determined at levels of $P < 0.05$, $P < 0.01$, and $P < 0.001$ (Bailey, 1995).

Results

The structures of the selected and discussed ring-substituted 8-hydroxyquinoline-2-carboxanilides are shown in Table 1. A synthetic pathway and characterization were published by Kos et al. (2015).

The relative survival of *D. piger* Vib-7 cells and cytotoxicity of ring-substituted 8-hydroxyquinoline-2-carboxanilides were studied. In this series of experiments, compounds **1–7** exerted cytotoxicity against these bacteria already in low (5–35 μM) concentrations (Fig. 1).

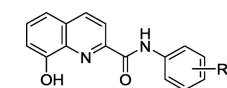
Treatment with all tested compounds led to a significant dose-dependent activity with the strongest effect observed in compounds **3** (R=3-OCH₃) and **6** (R=3-CF₃). Since some of ring-substituted 8-hydroxyquinoline-2-carboxanilides (such as **3** or **6**) have a pronounced antimicrobial effect against *D. piger* Vib-7 (combination of low survival and high toxicity rates), they could be considered as promising agents against the growth of this type of bacteria.

The effect of different concentrations of ring-substituted 8-hydroxyquinoline-2-carboxanilides on the process of dissimilatory sulfate reduction in *D. piger* Vib-7 cells at the 36th h of cultivation was studied. As shown in Figs. 2 and 3, the addition of the compounds in the culture medium inhibits the process of dissimilation of sulfate directly proportional to the increase in concentrations (5–35 μM). Under these conditions, the utilization of sulfate and lactate was inhibited; hence the level of accumulation of hydrogen sulfide and acetate was reduced. These data are consistent with our research in previous series of the experiments. The percentage inhibition of sulfate reduction process correlates with the percentage of bacterial growth inhibition under the ring-substituted 8-hydroxyquinoline-2-carboxanilides treatment.

Based on the obtained results, the MIC and IC₅₀ values of ring-substituted 8-hydroxyquinoline-2-carboxanilides against intestinal sulfate-reducing bacteria were established. As shown in Table 1, the MICs of all the compounds were $\leq 33 \mu\text{M}$. The

Table 1

Structures of ring-substituted 8-hydroxyquinoline-2-carboxanilides and *in vitro* antibacterial activity against *Desulfovibrio piger* Vib-7 (minimal inhibition concentration: MIC, half maximal inhibitory concentration: IC₅₀, minimal bactericidal concentration: MBC) of the compounds in comparison with ciprofloxacin (CPX).



Comp.	R	[μM]		
		MIC	IC ₅₀	MBC
1	H	23	12	25
2	2-OCH ₃	28	17	28
3	3-OCH ₃	17	11	20
4	3-CH ₃	23	10	23
5	3-Br	33	18	35
6	3-CF ₃	17	10	20
7	4-CF ₃	20	10	22
CPX	–	45	28	45

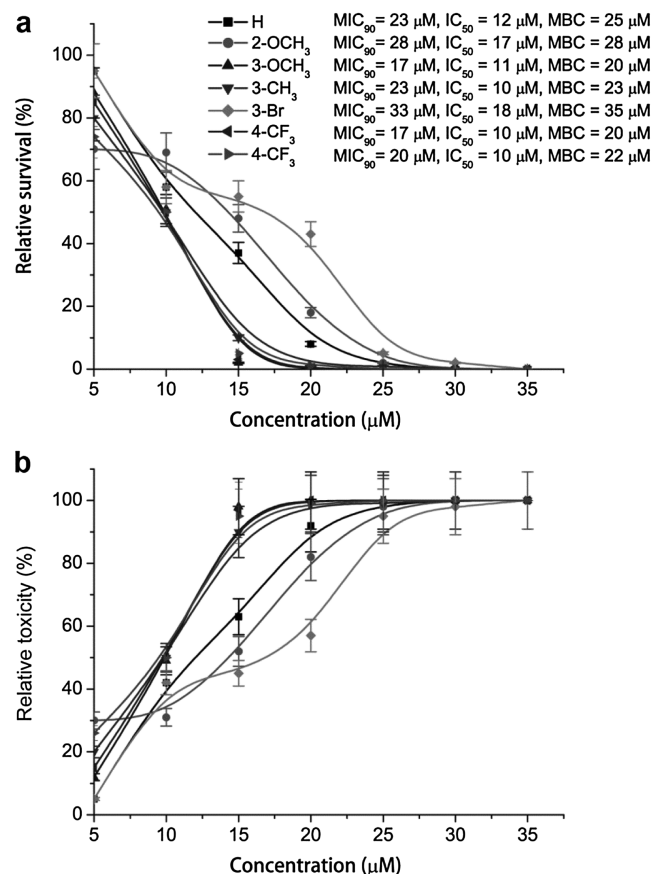


Fig. 1. Relative survival of *D. piger* Vib-7 cells (a) and toxicity (b) of ring-substituted 8-hydroxyquinoline-2-carboxanilides.

least potent compounds among the tested compounds for the bacterial strain were **2** (R=2-OCH₃) and **5** (R=3-Br), the MICs of which were 28 and 33 μM , respectively. The similar MICs were determined for compounds **1** (R=H) and **4** (R=3-CH₃). It can be supposed that these compounds show the same cytotoxicity effect on sulfate-reducing bacteria *D. piger* Vib-7 cells. IC₅₀ of compounds **4**, **6** and **7** was 10 μM . Compounds **2** and **5** had IC₅₀ only 17 and 18 μM , which is consistent with the MICs of these compounds.

Discussion and conclusion

Sulfate-reducing bacteria of *Desulfovibrio* genus belong to the intestinal microbiota of humans and animals (Kushkevych, 2012, 2013). They are anaerobic microorganisms, dissimilating sulfate as an electron acceptor and organic compounds as an electron donor and carbon source in the process of “dissimilatory sulfate reduction” (also known as “dissimilatory anaerobic sulfate respiration”) (Kushkevych, 2016). Lactate is the most common substrate used by the species belonging to the intestinal sulfate-reducing bacteria. The species of *Desulfovibrio* oxidize lactate incompletely to acetate. Lactate oxidation to acetate occurs together with the concurrent reduction of sulfate to sulfide (Barton and Hamilton, 2010). The presence of lactate and sulfate in the human intestine contributes to the intensive bacteria growth and the accumulation of their final metabolic products, acetate and hydrogen sulfide, that are toxic, mutagenic and cancerogenic to epithelial intestinal cells (Pitcher and Cummings, 1996; Rowan et al., 2009). There is also an assumption that sulfate-reducing bacteria can cause some forms of cancer of the rectum through the

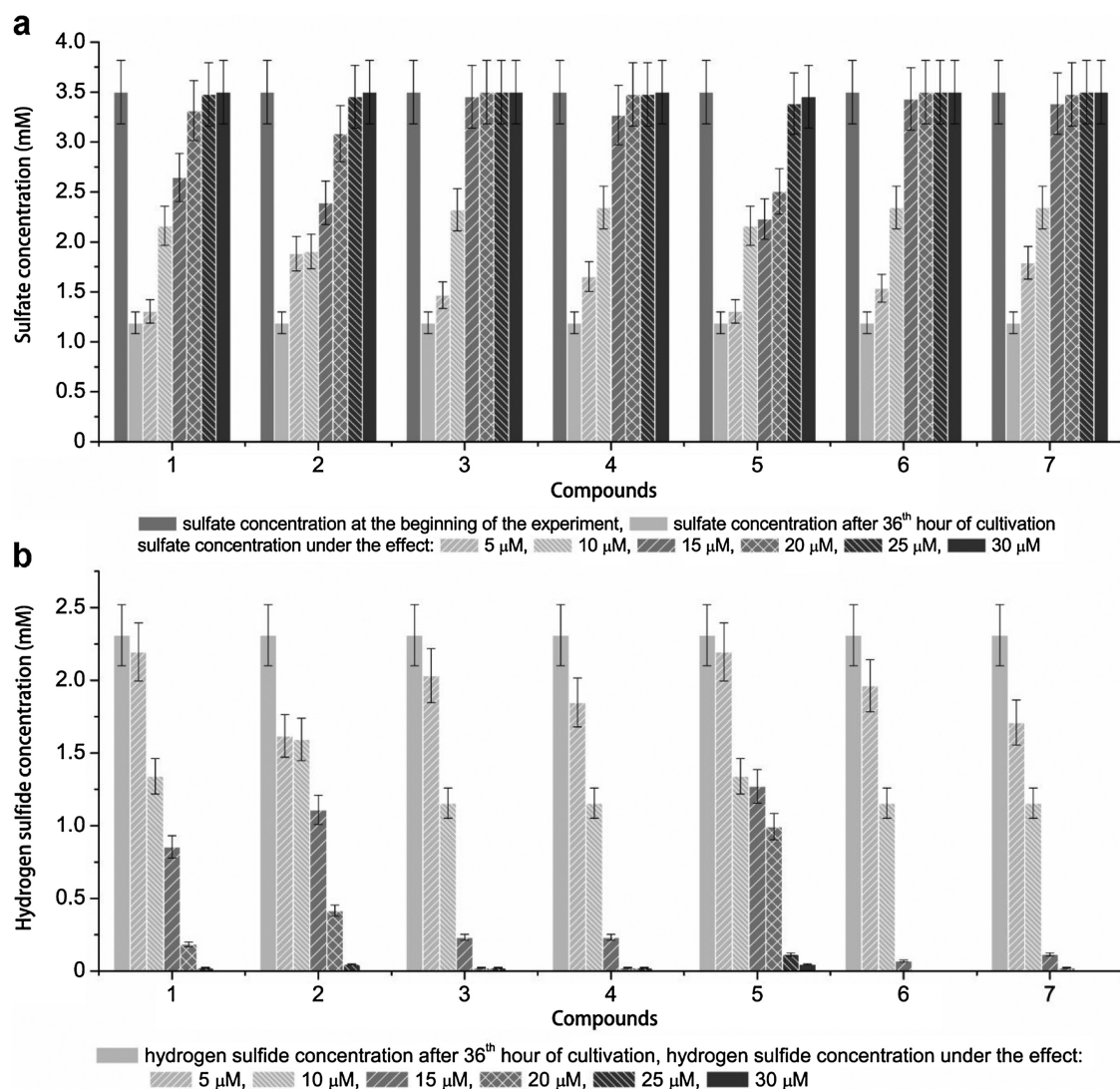


Fig. 2. Sulfate reduction of *D. piger* Vib-7 cells under the treatment of indicated doses of ring-substituted 8-hydroxyquinoline-2-carboxanilides: sulfate dissimilation (a), hydrogen sulfide production (b).

formation of hydrogen sulfide. In our previous studies, it was shown that bacteria *D. piger* Vib-7 consumed sulfate and accumulated hydrogen sulfide in concentration of 2.31 ± 0.21 mM (Kushkevych, 2013).

Based on all the obtained results in this study, it can be concluded that compounds **1–7** in concentrations 5–35 μ M inhibited the growth and, accordingly, the process of dissimilatory sulfate reduction. This antimicrobial activity was concentration-dependent, with the strongest effect in 30 μ M concentration. Similar effect was observed in our previous research for the activity of selected salicylamides against intestinal sulfate-reducing bacteria (Kushkevych et al., 2015a, 2016). Derivatives **1**, **2**, **4**, **5** and **7** showed cytotoxic affect at concentrations higher than 17 μ M. The highest level of inhibition of this process and high activity rates were observed at concentration 17 μ M of compounds **3** and **6** and thus are interesting for further studies. The cytotoxic effect of these compounds can be due to the inhibition of the enzymes of dissimilatory sulfate reduction (Kushkevych, 2015a,b; Kushkevych et al., 2015b), including sulfite reductase that is susceptible for various factors in intestinal sulfate-reducing bacteria *D. piger* Vib-7 (Kushkevych and Fafula, 2014). The tested

compounds can be considered good alternatives for the treatment of colitis or colorectal cancer although it should be taken in account that these compounds can be aggressive also to commensally bacteria and even to other parts of the human body. This should be a concern to be clarified in the near future with complementary assays.

Despite the fact that evaluated bacteria *Desulfovibrio* species are heterogeneous group of microorganisms which are widespread in anaerobic areas of soils, wetlands, marine and fresh water, they are available in microbiota of large intestine of humans and animals. It is known that intestinal *Desulfovibrio* species are different from other SRB by their biochemical and physiological properties (Barton and Hamilton, 2010; Brenner et al., 2005; Holt et al., 1994). So, the mechanisms of the effect of studied compounds on these bacteria can also differ. These compounds may influence the synthesis of the bacterial cell wall (peptidoglycan), ribosomes, enzymes or other phenotypic features such as inhibition the synthesis of desulfovibridin, cytochrome c3 and menaquinone MK-6. Effect of studied compounds may depend on their activity, structure and properties.

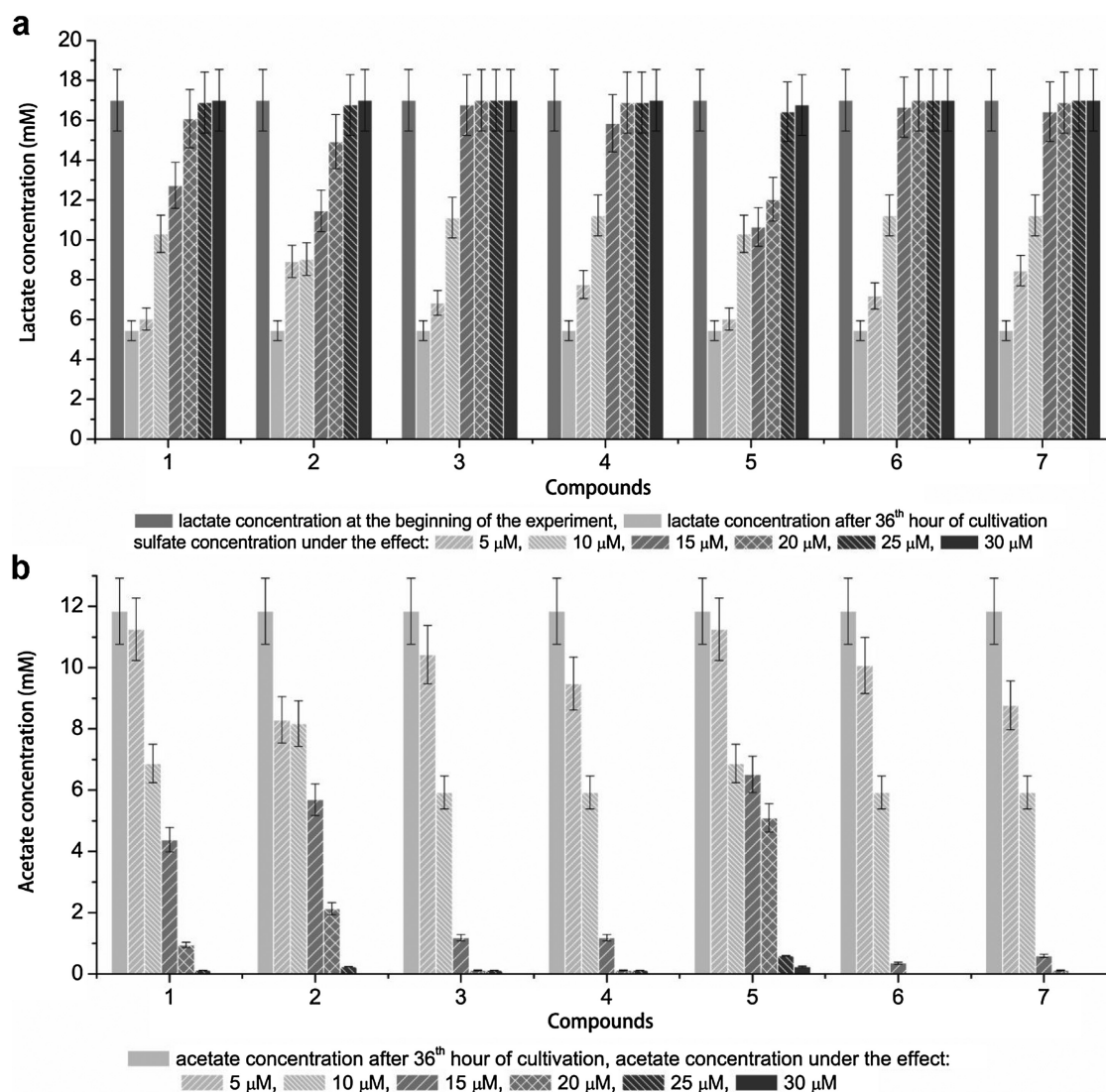


Fig. 3. The effect of ring-substituted 8-hydroxyquinoline-2-carboxanilides on lactate consumption (a) and acetate production (b) by *D. piger* Vib-7 cells.

The studied compounds are able to inhibit the number of sulfate-reducing bacteria and/or reduce the production of sulfide and acetate. This would help to clarify the factors influencing sulfide production in the human and animal colon.

Conflict of interests

The authors declare that they have no conflict of interests regarding the publication of this paper.

Acknowledgements

This study was supported by CZ.1.07/2.3.00/30.0053, APVV-0516-12 and by Sanofi-Aventis Pharma Slovakia, s.r.o.

References

Bailey, N.T.J., 1995. *Statistical Methods in Biology*. Cambridge University Press.

Barton, L.L., Hamilton, W.A., 2010. *Sulphate-reducing Bacteria*. Environmental and Engineered Systems. Cambridge University Press.

Brenner, D.J., Krieg, N.R., Staley, J.T., Garrity, G.M., 2005. *Bergey's Manual of Systematic Bacteriology*, second ed. The Proteobacteria, Part C: The Alpha-, Beta-, Delta-, and Epsilonproteobacteria, Vol. 2. Springer, New York.

Cieslik, W., Musiol, R., Nycz, J.E., Jampilek, J., Vejsova, M., Wolff, M., Machura, B., Polanski, J., 2012. Contribution to investigation of antimicrobial activity of styrylquinolines. *Bioorg. Med. Chem.* 20, 6960–6968.

Cline, J.D., 1969. Spectrophotometric determination of hydrogen sulfide in natural water. *Limnol. Ocean* 14, 454–458.

Cummings, J.H., Macfarlane, G.T., Macfarlane, S., 2003. Intestinal bacteria and ulcerative colitis. *Curr. Issues Intest. Microbiol.* 4, 9–20.

Gibson, G.R., Cummings, J.H., Macfarlane, G.T., 1991. Growth and activities of sulphate-reducing bacteria in gut contents of health subjects and patients with ulcerative colitis. *FEMS Microbiol. Ecol.* 86, 103–112.

Gibson, G.R., Macfarlane, S., Macfarlane, G.T., 1993. Metabolic interactions involving sulphate-reducing and methanogenic bacteria in the human large intestine. *FEMS Microbiol. Ecol.* 12, 117–125.

Gonec, T., Bobal, P., Suján, J., Pesko, M., Guo, J., Kralova, K., et al., 2012. Investigating the spectrum of biological activity of substituted quinoline-2-carboxamides and their isosteres. *Molecules* 17, 613–644.

Holt, J.G., Krieg, N.R., Sneath, P.H., 1994. *Bergey's Manual of Determinative Bacteriology*, ninth ed. Williams & Wilkins, Philadelphia.

Jampilek, J., Kralova, K., Pesko, M., Kos, J., 2016. Ring-substituted 8-hydroxyquinoline-2-carboxanilides as photosystem II inhibitors. *Bioorg. Med. Chem. Lett.* 26, 3862–3865.

Jampilek, J., 2017. Design of antimalarial agents based on natural products. *Curr. Org. Chem.* 21, 1824–1846.

Kolmert, A., Wikstrom, P., Hallberg, K.B., 2000. A fast and simple turbidimetric method for the determination of sulfate in sulfate-reducing bacterial cultures. *J. Microbiol. Methods* 41, 179–184.

Kos, J., Zadrzilova, I., Nevin, E., Soral, M., Gonec, T., Kollar, P., et al., 2015. Ring-substituted 8-hydroxyquinoline-2-carboxanilides as potential antimycobacterial agents. *J. Bioorg. Med. Chem.* 23 (15) 4188–4096.

- Kushkevych, I., Fafula, R.V., 2014. Dissimilatory sulfite reductase in cell-free extracts of intestinal sulfate-reducing bacteria. *Stud. Biol.* 8 (2), 101–112.
- Kushkevych, I., Bartos, M., Bartosova, L., 2014. Sequence analysis of the 16S rRNA gene of sulfate-reducing bacteria isolated from human intestine. *Int. J. Curr. Microbiol. Appl. Sci.* 3, 239–248.
- Kushkevych, I., Kollar, P., Suchy, P., 2015a. Activity of selected salicylamides against intestinal sulfate-reducing bacteria. *Neuroendocrinol. Lett.* 36, 106–113.
- Kushkevych, I., Fafula, R., Parak, T., Bartos, M., 2015b. Activity of Na⁺/K⁺-activated Mg²⁺-dependent ATP hydrolase in the cell-free extracts of the sulfate-reducing bacteria *Desulfovibrio piger* Vib-7 and *Desulfomicrobium* sp. Rod-9. *Acta Vet. Brno* 84 (1), 3–12.
- Kushkevych, I., Kollar, P., Ferreira, A.L., Palma, D., Duarte, A., Lopes, M.M., et al., 2016. Antimicrobial effect of salicylamide derivatives against intestinal sulfate-reducing bacteria. *J. Appl. Biomed.* 14 (2), 125–130.
- Kushkevych, I., 2012. Sulfate-reducing bacteria of the human intestine: I. Dissimilatory sulfate reduction. *Stud. Biol.* 6, 149–180.
- Kushkevych, I., 2013. Identification of sulfate-reducing bacteria strains of human large intestine. *Stud. Biol.* 7, 115–124.
- Kushkevych, I., 2014. Etiological role of sulfate-reducing bacteria in the development of inflammatory bowel diseases and ulcerative colitis. *Am. J. Inf. Dis. Microbiol.* 2 (3), 63–73.
- Kushkevych, I., 2015a. Kinetic properties of pyruvate ferredoxin oxidoreductase of intestinal sulfate-reducing bacteria *Desulfovibrio piger* Vib-7 and *Desulfomicrobium* sp. Rod-9. *Polish J. Microbiol.* 64 (2), 107–114.
- Kushkevych, I., 2015b. Activity and kinetic properties of phosphotransacetylase from intestinal sulfate-reducing bacteria. *Acta Bioch. Pol.* 62 (1), 1037–1108.
- Kushkevych, I., 2016. Dissimilatory sulfate reduction in the intestinal sulfate-reducing bacteria. *Stud. Biol.* 10 (1) 197–128.
- Loubinoux, J., Mory, F., Pereira, I.A., Le Faou, A.E., 2000. Bacteremia caused by a strain of *Desulfovibrio* related to the provisionally named *Desulfovibrio fairfieldensis*. *J. Clin. Microbiol.* 38, 931–934.
- Loubinoux, J., Bronowicji, J.P., Pereira, I.A., 2002a. Sulphate-reducing bacteria in human feces and their association with inflammatory diseases. *FEMS Microbiol. Ecol.* 40, 107–112.
- Loubinoux, J., Valente, F.M.A., Pereira, I.A.C., 2002b. Reclassification of the only species of the genus *Desulfomonas* *Desulfomonas pigra*, as *Desulfovibrio piger* comb. nov. *Int. J. Syst. Evol. Microbiol.* 52, 1305–1308.
- Mucaji, P., Atanasov, A.G., Bąk, A., Kozik, V., Sieron, K., Olsen, M., et al., 2017. The forty-sixth EuroCongress on drug synthesis and analysis: snapshot. *Molecules* 22, 1848.
- Musiol, R., Jampilek, J., Buchta, V., Silva, L., Niedbala, H., Podeszwa, B., et al., 2006. Antifungal properties of new series of quinoline derivatives. *Bioorg. Med. Chem.* 14, 3592–3598.
- Musiol, R., Jampilek, J., Kralova, K., Richardson, D.R., Kalinowski, D., Podeszwa, B., et al., 2007. Investigating biological activity spectrum for novel quinoline analogues. *Bioorg. Med. Chem.* 15, 1280–1288.
- Musiol, R., Tabak, D., Niedbala, H., Podeszwa, B., Jampilek, J., Kralova, K., et al., 2008. Investigating biological activity spectrum for novel quinoline analogues 2: Hydroxyquinolinecarboxamides with photosynthesis-inhibiting activity. *Bioorg. Med. Chem.* 16, 4490–4499.
- Musiol, R., Jampilek, J., Nycz, J.E., Pesko, M., Carroll, J., Kralova, K., et al., 2010. Investigating the activity spectrum for ring-substituted 8-hydroxyquinolines. *Molecules* 15, 288–304.
- Pitcher, M.C., Cummings, J.H., 1996. Hydrogen sulphide: a bacterial toxin in ulcerative colitis? *Gut* 39, 1–4.
- Postgate, J.R., 1984. *The Sulfate-Reducing Bacteria*. Cambridge University Press.
- Ranjith, P.K., Mary, S.Y., Panicker, Y.C., Anto, P.L., Armakovic, S., Armakovic, S.J., et al., 2017. New quinolone derivative: spectroscopic characterization and reactivity study by DFT and MD approaches. *J. Mol. Struct.* 1135, 1–14.
- Rowan, F.E., Docherty, N.G., Coffey, J.C., O'Connell, P.R., 2009. Sulphate-reducing bacteria and hydrogen sulphide in the aetiology of ulcerative colitis. *Br. J. Surg.* 96, 151–158.

č.	citace	ISSN
11	POSPISILOVA, S, <i>J KOS*(corresponding author)*</i> , H MICHNOVA, I KAPUSTIKOVA, T STRHARSKY, M ORAVEC, AM MORICZ, J BAKONYI, T KAUEROVA, P KOLLAR, A CIZEK a J JAMPILEK. Synthesis and Spectrum of Biological Activities of Novel N-arylcinnamamides. <i>INTERNATIONAL JOURNAL OF MOLECULAR SCIENCES</i> [online]. 2018, 19 (8). Dostupné z: doi:10.3390/ijms19082318	1422-0067



Article

Synthesis and Spectrum of Biological Activities of Novel *N*-arylcinnamamides

Sarka Pospisilova ^{1,2}, Jiri Kos ^{1,*}, Hana Michnova ^{1,2}, Iva Kapustikova ¹, Tomas Strharsky ¹, Michal Oravec ³, Agnes M. Moricz ⁴, Jozsef Bakonyi ⁴, Tereza Kauerova ⁵, Peter Kollar ⁵, Alois Cizek ² and Josef Jampilek ¹

¹ Department of Pharmaceutical Chemistry, Faculty of Pharmacy, Comenius University, Odbojarov 10, 83232 Bratislava, Slovakia; sharka.pospisilova@gmail.com (S.P.); michnova.hana@gmail.com (H.M.); kapustikova@fpharm.uniba.sk (I.K.); strharsky2@uniba.sk (T.S.); josef.jampilek@gmail.com (J.J.)

² Department of Infectious Diseases and Microbiology, Faculty of Veterinary Medicine, University of Veterinary and Pharmaceutical Sciences, Palackeho 1, 61242 Brno, Czech Republic; cizeka@vfu.cz

³ Global Change Research Institute CAS, Belidla 986/4a, 60300 Brno, Czech Republic; oravec.m@cezhglobe.cz

⁴ Plant Protection Institute, Centre for Agricultural Research, Hungarian Academy of Sciences, Herman Otto Str. 15, 1022 Budapest, Hungary; moricz.agnes@agrar.mta.hu (A.M.M.); bakonyi.jozsef@agrar.mta.hu (J.B.)

⁵ Department of Human Pharmacology and Toxicology, Faculty of Pharmacy, University of Veterinary and Pharmaceutical Sciences, Palackeho 1, 61242 Brno, Czech Republic; tereza.kauerova@gmail.com (T.K.); kollarp@vfu.cz (P.K.)

* Correspondence: jirikos85@gmail.com; Tel.: +421-2-5011-7224

Received: 9 July 2018; Accepted: 3 August 2018; Published: 7 August 2018



Abstract: A series of sixteen ring-substituted *N*-arylcinnamamides was prepared and characterized. Primary in vitro screening of all the synthesized compounds was performed against *Staphylococcus aureus*, three methicillin-resistant *S. aureus* strains, *Mycobacterium tuberculosis* H37Ra, *Fusarium avenaceum*, and *Bipolaris sorokiniana*. Several of the tested compounds showed antistaphylococcal, antitubercular, and antifungal activities comparable with or higher than those of ampicillin, isoniazid, and benomyl. (2*E*)-*N*-[3,5-bis(trifluoromethyl)phenyl]-3-phenylprop-2-enamide and (2*E*)-3-phenyl-*N*-[3-(trifluoromethyl)phenyl]prop-2-enamide showed the highest activities (MICs = 22.27 and 27.47 μ M, respectively) against all four staphylococcal strains and against *M. tuberculosis*. These compounds showed an activity against biofilm formation of *S. aureus* ATCC 29213 in concentrations close to MICs and an ability to increase the activity of clinically used antibiotics with different mechanisms of action (vancomycin, ciprofloxacin, and tetracycline). In time-kill studies, a decrease of CFU/mL of >99% after 8 h from the beginning of incubation was observed. (2*E*)-*N*-(3,5-Dichlorophenyl)- and (2*E*)-*N*-(3,4-dichlorophenyl)-3-phenylprop-2-enamide had a MIC = 27.38 μ M against *M. tuberculosis*, while a significant decrease (22.65%) of mycobacterial cell metabolism determined by the MTT assay was observed for the 3,5-dichlorophenyl derivative. (2*E*)-*N*-(3-Fluorophenyl)- and (2*E*)-*N*-(3-methylphenyl)-3-phenylprop-2-enamide exhibited MICs = 16.58 and 33.71 μ M, respectively, against *B. sorokiniana*. The screening of the cytotoxicity of the most effective antimicrobial compounds was performed using THP-1 cells, and these chosen compounds did not show any significant lethal effect. The compounds were also evaluated for their activity related to the inhibition of photosynthetic electron transport (PET) in spinach (*Spinacia oleracea* L.) chloroplasts. (2*E*)-*N*-(3,5-dichlorophenyl)-3-phenylprop-2-enamide (IC₅₀ = 5.1 μ M) was the most active PET inhibitor. Compounds with fungicide potency did not show any in vivo toxicity against *Nicotiana tabacum* var. Samsun. The structure–activity relationships are discussed.

Keywords: cinnamamides; antistaphylococcal activity; time-kill assay; biofilm; antitubercular activity; MTT assay; antifungal activity; PET inhibition; toxicity; structure–activity relationship

1. Introduction

Cinnamic acids and other hydroxy- or phenyl-substituted derivatives of cinnamic acids have been widely investigated by scientists due to their significant and varied biological effects. Cinnamic acids occur naturally in all plants [1]. They are formed in the biochemical pathway providing phenyl-propanoids, coumarins, lignans, isoflavonoids, flavonoids, stilbenes, aurones, anthocyanins, spermidines, and tannins [2]. The spectrum of their biological activities include anti-inflammatory, antioxidant, hepatoprotective, antidiabetic, antidepressant/anxiolytic, antifungal, antibacterial, antiviral, and anticancer effects [3–16]. Derivatives of cinnamic acids are used as agriculture fungicides as well [17].

The adaptation of microorganisms to external influences and, thus, the development of their resistance against antimicrobial agents is not a surprise; unfortunately, this process is faster and faster. Thus, the emerging resistance of microbial pathogens to clinically used drugs, including second- and third-choice drugs, and the development of cross-resistant or multidrug-resistant strains are alarming. Microbial pathogens have developed a number of mechanisms to adapt to the effects of the environment. In addition, the increase in the number of infections and the occurrence of new, especially opportunistic species are also caused by the general immunosuppression of patients, and this fact makes these diseases extremely serious. Since the 1990s, only an inconsiderable number of really new drugs for systemic administration have been marketed for the treatment of infections, although the discovery of new molecules has been a priority [18].

Thus, in the light of the above mentioned facts, new simple anilides of cinnamic acid were designed as antimicrobial multitarget agents, synthesized using a modern microwave-assisted method and screened against a battery of bacterial/mycobacterial and fungal pathogens. These compounds were designed based on the experience with naphthalenecarboxamides—simple molecules with a number of biological activities, and in fact, the new ring-substituted (2*E*)-*N*-phenyl-3-phenylprop-2-enamides can be considered as open analogues of recently described naphthalene-2-carboxanilides [19,20].

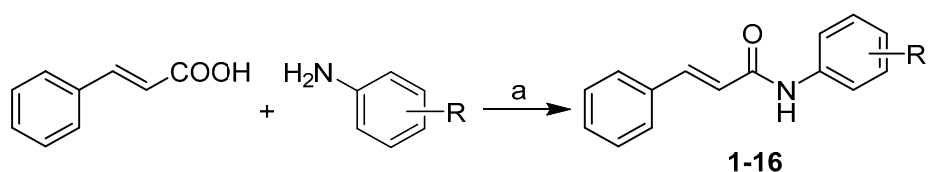
As an amide moiety is able to affect photosystem II (PS II) by reversible binding [21], resulting in the interruption of the photosynthetic electron transport (PET) [22–24], and can be found in many herbicides acting as photosynthesis inhibitors [25–30], these *N*-arylcinnamamides were additionally tested on the inhibition of PET in spinach (*Spinacia oleracea* L.) chloroplasts using the Hill reaction. The idea of this screening is based on the fact that both drugs and pesticides are designed to target particular biological functions. These functions/effects may overlap at the molecular level, which causes a considerable structural similarity between drugs and pesticides. Since different classes of herbicides are able to bind to different mammalian cellular receptors, the majority of pharmaceutical companies have pesticide divisions, and developed biologically active agents are investigated as both pesticides and drugs. Previously, several successful pesticides became pharmaceuticals and vice versa [31–35].

2. Results and Discussion

2.1. Chemistry and Physicochemical Properties

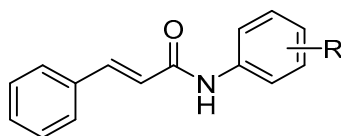
All the studied compounds 1–16 were prepared according to Scheme 1. The carboxyl group of starting cinnamic acid was activated with phosphorus trichloride. In the reaction with an appropriate ring-substituted aniline, the generated acyl chloride subsequently gave the final amide in dry chlorobenzene via microwave-assisted synthesis. All the compounds were recrystallized from ethanol.

Many different molecular parameters/descriptors are used to determine structure-activity relationships (SAR). Lipophilicity and electronic properties are among the most frequent ones. Hammett's σ parameters were used for the description of electronic properties. They were calculated for the whole substituted anilide ring using ACD/Percepta ver. 2012 (Advanced Chemistry Development Inc., Toronto, ON, Canada, 2012), see Table 1. The lipophilicity of the studied compounds was predicted as $\log P$ using ACD/Percepta software and $\text{Clog } P$ using ChemBioDraw Ultra 13.0 (CambridgeSoft, PerkinElmer Inc., Cambridge, MA, USA). $\log P$ is the logarithm of the partition coefficient for *n*-octanol/water. $\text{Clog } P$ is the logarithm of *n*-octanol/water partition coefficient based on the established chemical interactions. In addition, the lipophilicity of studied compounds 1–16 was investigated by means of reversed-phase high-performance liquid chromatography (RP-HPLC) determination of capacity factors k with the subsequent calculation of $\log k$ [36]. The analysis was made under isocratic conditions with methanol as an organic modifier in the mobile phase using an end-capped nonpolar C18 stationary RP column. The results are shown in Table 1.



Scheme 1. Synthesis of (2*E*)-*N*-aryl-3-phenylprop-2-enamides 1–16. Reagents and conditions: (a) PCl_3 , chlorobenzene, and MW.

Table 1. Structure of ring-substituted (2*E*)-*N*-aryl-3-phenylprop-2-enamides 1–16, experimentally determined values of lipophilicity $\log k$, calculated values of $\log P$ / $\text{Clog } P$, and electronic Hammett's σ parameters.



Comp.	R	$\log k$	$\text{Clog } P^a$	$\log P^b$	σ_{Ar}^b
1	H	0.1146	3.6640	3.18	0.60
2	3- CH_3	0.2729	4.1630	3.40	0.48
3	4- CH_3	0.2640	4.1630	3.40	0.46
4	2-F	0.1330	3.4646	3.17	1.02
5	3-F	0.2327	4.0646	3.32	0.82
6	3- CF_3	0.4859	4.9978	4.26	0.89
7	2,5- CH_3	0.2691	4.0120	3.57	0.59
8	2,5-Cl	0.5799	4.5878	4.65	1.22
9	2,6-Cl	0.0632	3.7378	4.56	1.33
10	3,4-Cl	0.6821	5.3178	4.70	1.19
11	3,5-Cl	0.8155	5.4378	4.79	1.11
12	2,6-Br	0.0992	3.9778	4.80	1.33
13	3,5- CF_3	0.9814	6.0386	5.68	1.05
14	2-F-5-Br	0.4875	4.4178	4.07	1.28
15	2-Br-5-F	0.4588	4.1378	4.12	1.19
16	2-Cl-5- CF_3	0.6178	4.9509	4.88	1.19

^a calculated using ChemBioDraw Ultra 13.0; ^b calculated using ACD/Percepta ver. 2012.

The results obtained with the discussed compounds show that the experimentally-determined lipophilicities ($\log k$) are in accordance with the calculated $\text{Clog } P$ values as illustrated in Figure 1A; correlation coefficient $r = 0.9513$, $n = 16$. On the other hand, $\log P$ values calculated by ACD/Percepta show differences for compounds 9 (2,6-Cl) and 12 (2,6-Br), see Figure 1B. When these two compounds

are excluded, $r = 0.9774$ ($n = 14$) is observed. This poor match for 2,6-disubstituted anilides **9** and **12** may be caused by intramolecular interactions that are probably caused by the steric effect of spatially-close moieties, which was not included in prediction by ACD/Percepta. The proximity of the di-*ortho*-substituents to the carboxamide group on the aniline ring leads to the twist of the aniline ring plane towards the carboxamide group, i.e., to the plane of the benzene ring of cinnamic acid. The described process resulted in the planarity violation of the molecule. Otherwise, (2*E*)-*N*-[3,5-bis(trifluoromethyl)phenyl]-3-phenylprop-2-enamide (**13**) is the most lipophilic, while compounds **9**, **12** and *N*-phenylcinnamamide (**1**) are characterized by the lowest lipophilicity. It can be stated that $\log k$ values specify lipophilicity within the series of the studied compounds.

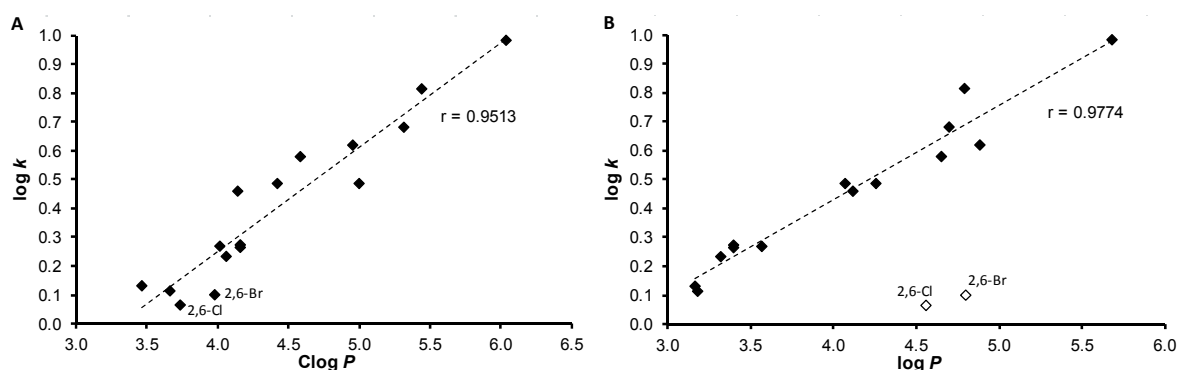


Figure 1. Comparison of experimentally found $\log k$ values of ring-substituted *N*-arylcinnamamides **1–16** with $\text{Clog } P$ calculated using ChemBioDraw Ultra (A) and $\log P$ calculated using ACD/Percepta (B).

2.2. In Vitro Antibacterial Susceptibility Testing

All the cinnamanilides were tested on their antistaphylococcal activity against three clinical isolates of methicillin-resistant *Staphylococcus aureus* (MRSA) [37,38] and *S. aureus* ATCC 29213 as the reference and quality control strain. Although various derivatives of cinnamic acid were described as promising antibacterial agents [4–6,8,9,14,15], the compounds showed only limited activity (MICs > 256 $\mu\text{g}/\text{mL}$), except for (2*E*)-3-phenyl-*N*-[3-(trifluoromethyl)phenyl]prop-2-enamide (**6**) and 3,5-bis(trifluoromethyl)phenyl derivative **13**, see Table 2. As minimum inhibitory concentrations (MICs) of these compounds are the same against the reference and the MRSA strains (27.47 and 22.27 μM , respectively), it can be speculated about the specific effectivity against *Staphylococcus* sp. These compounds were also tested against *Enterococcus faecalis* ATCC 29212 as the reference strain and three isolates from American crows of vanA-carrying vancomycin-resistant *E. faecalis* (VRE) [39] but without any effect in the tested concentrations, which may indicate a specific mechanism of action [37,40]. From Table 2 it is obvious that compounds **6** and **13** exhibited activities comparable with those of the standards. Due to the small number of active compounds, no SAR could be established.

2.2.1. Synergy Effect with Clinically Used Drugs against MRSA

The most effective compounds **6** and **13** were tested for their ability of synergic activity with clinically used antibacterial drugs tetracycline, ciprofloxacin, and vancomycin. These antibiotics have different mechanisms of actions and different mechanisms of resistance to them, thus the prospective synergism could give an idea of the mechanism of action of the cinnamic derivatives. The investigation of synergistic activity was performed according to the methodology [41]. The method of fractional inhibitory concentration (FIC) was used [42]. For all the wells of the microtitration plates that corresponded to a MIC value, the sum of the FICs (ΣFIC) was calculated for each well, using the equation $\Sigma\text{FIC} = \text{FIC}_A + \text{FIC}_B = (C_A/\text{MIC}_A) + (C_B/\text{MIC}_B)$, where MIC_A and MIC_B are the MICs of drugs A and B alone, respectively, and C_A and C_B are the concentrations of the drugs in the combination,

respectively [42]. Synergy was defined as $\Sigma\text{FIC} \leq 0.5$; additivity was defined as $0.5 < \Sigma\text{FIC} < 1$; indifference was defined as $1 \leq \Sigma\text{FIC} < 4$; and antagonism was defined as $\Sigma\text{FIC} \geq 4$ [41]. As the FIC index was evaluated for every single well corresponding to the MIC value, the results are presented as a range. The test was made with all 3 methicillin-resistant isolates, MRSA 63718, SA 3202, and SA 630. The isolates were also resistant to used antibiotics. Note that isolate MRSA SA 630 is susceptible to tetracycline. The results are mentioned in Table 3.

Table 2. Structure of ring-substituted (2E)-N-aryl-3-phenylprop-2-enamides 1–16, IC₅₀ (μM) values related to PET inhibition in spinach chloroplasts in comparison with 3-(3,4-dichlorophenyl)-1,1-dimethylurea (DCMU) standard, in vitro anti-*Staphylococcus* activities MIC (μM) in comparison with standard ampicillin (AMP), in vitro antitubercular activity MIC (μM (μg/mL)) in comparison with standard isoniazid (INH), in vitro antifungal activity MIC (μM (μg/mL)) of compounds 1–16 compared to standard benomyl (BNM), and in vitro antiproliferative (Tox) assay (IC₅₀ (μM)) of chosen compounds compared to standard camptothecin (CMP).

Comp.	R	MIC (μM (μg/mL))							Tox IC ₅₀ (μM)	PET IC ₅₀ (μM)
		SA	MRSA 63718	MRSA SA 630	MRSA SA 3202	Mtb	FA	BS		
1	H	>1146 (>256)	>1146 (>256)	>1146 (>256)	>1146 (>256)	286 (64)	1146 (256)	143 (32)	–	250
2	3-CH ₃	>1078 (>256)	>1078 (>256)	>1078 (>256)	>1078 (>256)	67.43 (16)	270 (64)	33.71 (8)	>30	343
3	4-CH ₃	>1078 (>256)	>1078 (>256)	>1078 (>256)	>1078 (>256)	134 (32)	1078 (256)	539 (128)	–	320
4	2-F	>1061 (>256)	>1061 (>256)	>1061 (>256)	>1061 (>256)	265 (64)	1061 (256)	66.32 (16)	–	223
5	3-F	>1061 (>256)	>1061 (>256)	>1061 (>256)	>1061 (>256)	66.31 (16)	531 (128)	16.58 (4)	>30	165
6	3-CF ₃	27.47 (8)	27.47 (8)	27.47 (8)	27.47 (8)	27.47 (8)	54.93 (16)	54.93 (16)	22.72 ± 1.73	189
7	2,5-CH ₃	>1018 (>256)	>1018 (>256)	>1018 (>256)	>1018 (>256)	254 (64)	1019 (256)	1019 (256)	–	338
8	2,5-Cl	>876 (>256)	>876 (>256)	>876 (>256)	>876 (>256)	876 (256)	876 (256)	876 (256)	–	67.1
9	2,6-Cl	>876 (>256)	>876 (>256)	>876 (>256)	>876 (>256)	876 (256)	876 (256)	876 (256)	–	1380
10	3,4-Cl	438 (128)	876 (256)	438 (128)	876 (256)	27.38 (8)	219 (64)	110 (32)	29.81 ± 0.31	54.9
11	3,5-Cl	438 (128)	876 (256)	109 (64)	438 (128)	27.38 (8)	219 (64)	110 (32)	29.44 ± 1.73	5.1
12	2,6-Br	>671 (256)	>671 (256)	>671 (256)	>671 (256)	167 (64)	671 (256)	671 (256)	–	732
13	3,5-CF ₃	22.27 (8)	22.27 (8)	22.27 (8)	22.27 (8)	22.27 (8)	713 (256)	356 (128)	22.59 ± 1.88	111
14	2-F-5-Br	>799 (>256)	>799 (>256)	>799 (>256)	>799 (>256)	199 (64)	799 (256)	49.98 (16)	–	188
15	2-Br-5-F	>799 (>256)	>799 (>256)	>799 (>256)	>799 (>256)	199 (64)	799 (256)	799 (256)	–	205
16	2-Cl-5-CF ₃	>785 (>256)	>785 (>256)	>785 (>256)	>785 (>256)	785 (256)	785 (256)	785 (256)	–	63.2
AMP	–	5.72 (2)	45.81 (16)	45.81 (16)	45.81 (16)	–	–	–	–	–
INH	–	–	–	–	–	36.55 (5)	–	–	–	–
BNM	–	–	–	–	–	–	1.94 (0.5)	17.22 (5)	–	–
CMP	–	–	–	–	–	–	–	–	0.16 ± 0.07	–
DCMU	–	–	–	–	–	–	–	–	–	2.1

SA = *Staphylococcus aureus* ATCC 29213; MRSA = clinical isolates of methicillin-resistant *S. aureus* 63718, SA 630, and SA 3202 (National Institute of Public Health, Prague, Czech Republic); Mtb = *Mycobacterium tuberculosis* H37Ra; FA = *Fusarium avenaceum* (Fr.) Sacc. IMI 319947; BS = *Bipolaris sorokiniana* (Sacc.) Shoemaker H-299 (NCBI GenBank accession No. MH697869).

Table 3. Combined effect of most potent *N*-arylcinnamamides and tetracycline (TET), ciprofloxacin (CPX), and vancomycin (VAN).

Isolate	Combination of Compds.	Separate MIC ($\mu\text{g/mL}$)	FIC Index	Concentration ($\mu\text{g/mL}$) Causing Synergistic Effect	Concentration ($\mu\text{g/mL}$) Causing Additive Effect
MRSA 63718	6/TET	8/128	1.004–2.250	–	2/64; 8/32
	6/CPX	16/16	0.75–1.125	–	8/4; 4/8
	6/VAN	32/2	1.000–1.250	–	–
MRSA SA 3202	6/TET	16/64	1.002–1.25	–	–
	6/CPX	8/8	1.000–1.250	–	–
	6/VAN	8/1	0.750–1.256	–	4/0.25
	13/TET	32/64	0.500–1.125	8/16	16/16; 4/32; 2/64
	13/CPX	32/8	0.375–1.250	8/1	2/4
	13/VAN	32/1	0.750–1.25	–	16/0.25
MRSA SA 630	6/CPX	8/256	0.625–1.125	–	4/64; 1/128
	6/VAN	8/1	0.750–1.250	–	2/0.5
	13/CPX	8/256	0.375–1.004	2/32; 1/64	4/8
	13/VAN	4/1	0.562–1.250	–	0.25/0.5

Although the activity of cinnamic acid derivatives is known for a long time, the exact mechanism of action is still unknown. The most reported mechanism of action is interaction with plasmatic membrane. The compounds can cause disruption of the membrane, damage the membrane proteins, etc. [43–46]. There are also specific targets for cinnamic acid derivatives [46]. Nevertheless, it is possible that the wide spectrum of effects to cells is caused by the primary activity of the compounds, which is membrane destabilization [46].

Both compounds 6 and 13 tested for synergy showed additivity with vancomycin against MRSA SA 630 and SA 3202. A similar effect was reported by Hemaiswarya et al. [47]; compound 13 had synergistic effect with ciprofloxacin against both tested strains. The effect of derivative 13 was also synergistic with tetracycline against MRSA SA 3202. The rest combinations with compound 13 had additive effect. Whereas compound 13 had a potential to increase the activity of all tested antibiotics, which have different mechanisms of actions and to which bacteria develop different resistance mechanisms, it can be expected that compound 13 acts by its own mechanism of action or increases the availability of the antibiotics by interaction with the membrane.

2.2.2. Dynamics of Antibacterial Activity

Within the pre-test subcultivation aliquots on agar, antistaphylococcal-effective compounds 6 and 13 showed bactericidal activity, i.e., minimal bactericidal concentrations were $\leq 4 \times \text{MIC}$. These facts were verified using the time-kill curve assay for testing the bactericidal effect. The dynamics of antibacterial activity was tested against *S. aureus* ATCC 29213 for the most active compounds 6 (Figure 2A) and 13 (Figure 2B). Both compounds showed concentration-dependent activity that was bactericidal in concentration $4 \times \text{MIC}$ in the case of compound 13 or very close to the bactericidal level for compound 6 after 8 h from the beginning of incubation. The increase of bacterial growth at 24 h could be caused by the selection of resistant mutants, as observed previously [37].

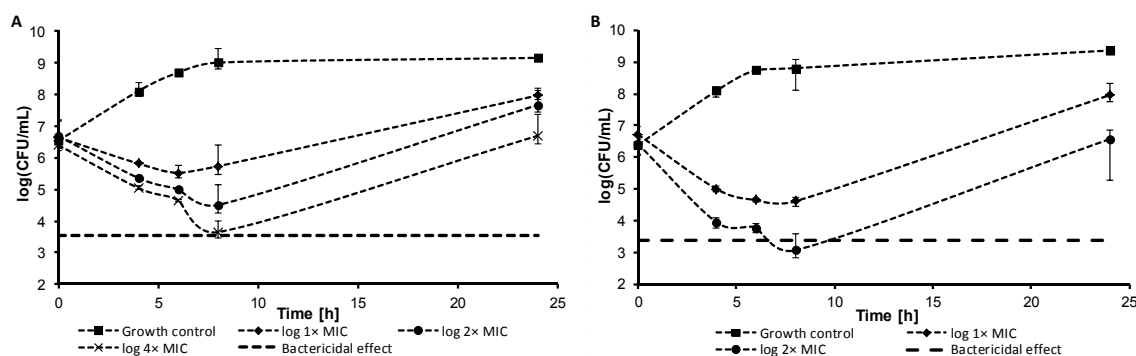


Figure 2. Time-kill curve of compound 6 (A) and compound 13 (B) against *S. aureus* ATCC 29213.

2.2.3. Inhibition of Biofilm Formation

There are many evidences in literature that cinnamic acid derivatives are inhibitors of biofilm formation [47–51]. The most studied derivate is cinnamaldehyde that interacts with quorum sensing system in bacterial biofilms [46,52,53]. Thus, selected compounds were also tested for their ability to inhibit biofilm formation. Compounds 6 and 13 were tested as inhibitors of biofilm formation against *S. aureus* ATCC 29213. MRSA strains were not producers of biofilm.

The activity of compound 6 does not depend on concentration in concentrations above 8 $\mu\text{g}/\text{mL}$; only the highest concentration showed lower inhibition effect. This could be caused the higher lipophilicity of the compound and potential formation of precipitates, which could decrease the antibacterial activity of the compound. The lowest concentration of the compound, which inhibited $\geq 80\%$ of biofilm formation, was 8 $\mu\text{g}/\text{mL}$, then the activity sharply decreased. Interestingly, on the other hand, concentrations of compound 13 close to MIC against planktonic cells had the lowest inhibition activities against biofilm forming, and the activity increased for sub-MIC values. These conditions could be potentially toxic for planktonic cells, but they can induce biofilm formation [54]. In general, the inhibition activity against biofilm formation was comparable with the activity against planktonic cells. Despite many studies reported a higher resistance of biofilm, there were also studies that proved a similar or only little lower antibiofilm activity of tested compounds compared to planktonic cells. [13,55]. Budzynska et al. [55] described high antibiofilm activity of plant essential oils compared to MICs. De Vita et al. [13] studied the activity of cinnamic acid derivatives against candida biofilm. These compounds had good effect against biofilm formation, and the effective concentrations were lower than $10\times$ MIC. Thus, the high activity of our compounds can be explained due to their structure, based on cinnamic acid.

Ampicillin (16–0.125 $\mu\text{g}/\text{mL}$), vancomycin (32–0.25 $\mu\text{g}/\text{mL}$), and ciprofloxacin (8–0.063 $\mu\text{g}/\text{mL}$) were used as positive controls. Ciprofloxacin and vancomycin caused the induction of biofilm formation in sub-MIC concentrations, which is in line with already published results [56,57]. All the results are shown in Figure 3.

2.3. In Vitro Antitubercular Activity

The evaluation of the in vitro antitubercular activity of the compounds was performed against *Mycobacterium tuberculosis* ATCC 25177/H37Ra, see Table 2. In order to reduce risks, a replacement of model pathogens is commonly used in basic laboratory screening. For *M. tuberculosis*, avirulent strain H37Ra is used that has a similar pathology as *M. tuberculosis* strains infecting humans and, thus, represents a good model for testing antitubercular agents [58]. The potency of the compounds was expressed as the MIC that is defined for mycobacteria as 90% or greater (IC_{90}) reduction of growth in comparison with the control.

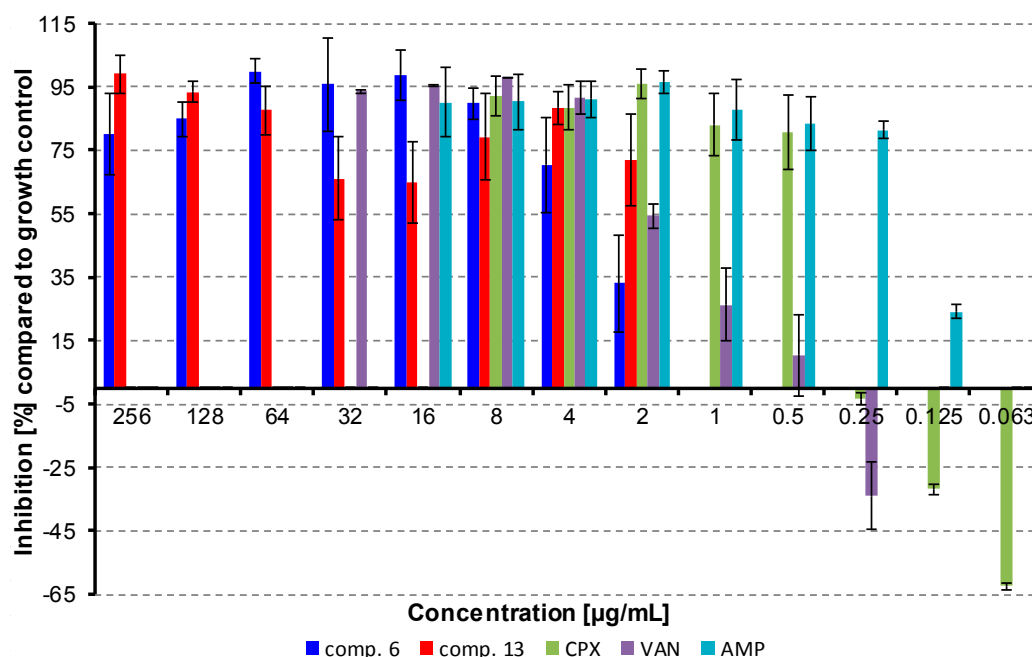


Figure 3. Inhibition of bacterial film formation. (CPX = ciprofloxacin, AMP = ampicillin, VAN = vancomycin).

In comparison with antibacterial activities, the investigated compounds exhibited much higher effect against *M. tuberculosis*. Compounds **13** (R = 3,5-CF₃), **10** (R = 3,4-Cl), **11** (R = 3,5-Cl), and **6** (R = 3-CF₃) were the most effective; their activity ranged from 22.27 to 27.47 µM. The dependences of the antitubercular activity of the compounds against *M. tuberculosis* expressed as log (1/MIC (M)) on lipophilicity expressed as log *k* are illustrated in Figure 4A. When inactive compounds **8** (R = 2,5-Cl), **9** (R = 2,6-Cl), and **16** (R = 2-Cl-5-CF₃) are eliminated from the SAR study (illustrated by empty symbols), two different dependences in relation to the position and the type of substituents can be observed. Based on Figure 4A, it can be stated that compounds substituted in positions C_{(3)'}, C_{(3,4)'}, C_{(3,5)'}, or C_{(2,6)'} showed an increasing trend of activity with the lipophilicity increase up to compound **6** (R = 3-CF₃), at which the activity achieved plateau and from approximately log *k* ≈ 0.5 had an insignificant increase. The second, in fact, a linear, insignificantly increasing dependence can be found for the compounds substituted in positions C_{(2)'} and C_{(2,5)'}. It is important to note that the antitubercular activity of the discussed cinnamanilides is also dependent on electronic σ parameters, see Figure 4B. As mentioned above, the linear insignificantly increasing dependence can be found for the derivatives substituted on the anilide in positions C_{(2)'} and C_{(2,5)'}, while a bilinear dependence of activity on σ (for derivatives substituted in positions C_{(3)'}, C_{(3,4)'}, C_{(3,5)'}, and C_{(2,6)'}) can be observed. The activity increases with the increasing electron-withdrawing effect with *r* = 0.8803 (*n* = 5) to optimum σ_{Ar} ca. 1 (compound **13**, R = 3,5-CF₃) and then decreases (*r* = 0.9162, *n* = 4) with increasing values of the electron-withdrawing parameter.

Additionally, a standard MTT (3-(4,5-dimethylthiazol-2-yl)-2,5-diphenyltetrazolium bromide) assay was performed on selected compounds that were the most effective against *M. tuberculosis* H37Ra and the MICs of which were previously determined, see Table 2. The MTT test can be used to assess cell growth by measuring respiration. The MTT measured viability of *M. tuberculosis* H37Ra less than 70% after exposure to the MIC values for each test agent is considered as a positive result of this assay. This low level of cell viability indicates inhibition of cell growth by inhibition of respiration [59]. All the selected compounds, i.e., **6** (R = 3-CF₃, 40.99%), **10** (R = 3,4-Cl, 59.65%), **11** (R = 3,5-Cl, 22.65%), and **13** (R = 3,5-CF₃, 66.09%) showed less than 70% viability of *M. tuberculosis* H37Ra at the tested concentration equal to MICs (i.e., 8 µg/mL or 22 and 27 µM). At MIC = 16 µg/mL (33 µM) compound

2 (R = 3-CH₃) showed inhibition of viability 13.23%, and compound **5** (R = 3-F) showed inhibition of viability 11.04% at MIC = 32 µg/mL (33 µM).

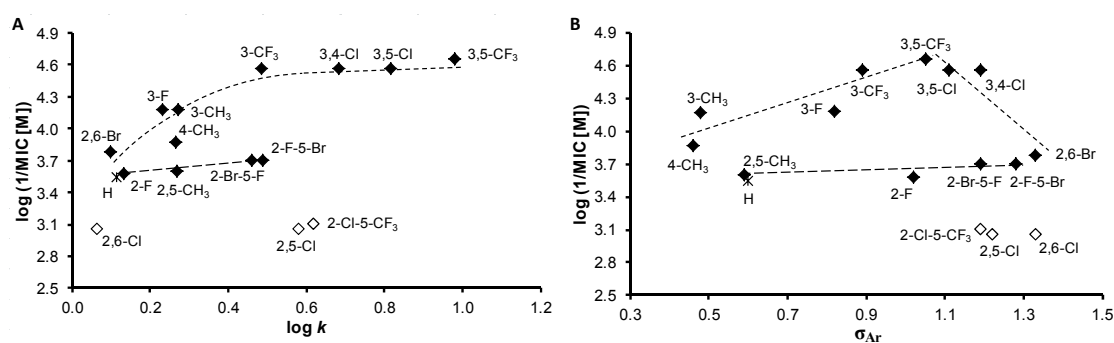


Figure 4. Relationships between in vitro antitubercular activity against *M. tuberculosis* log (1/MIC (M)) and lipophilicity expressed as log *k* (A) and electronic Hammett's σ parameters of ring-substituted anilide ring (B) of studied compounds. (Derivatives excluded from SAR are illustrated by empty symbols).

Similar effects were observed previously, for example, with ring-substituted 6-hydroxynaphthalene-2-carboxanilides, where 3-Cl, 4-Cl, 3-Br, and 3-CF₃ substituted derivatives decreased the viability of *M. tuberculosis* H37Ra in the range from 41.2% to 46.5% at the lowest tested concentration (MICs = 8 µg/mL) [20], with 8-hydroxy-*N*-(3-trifluoromethylphenyl)quinoline-2-carboxamide, where the decrease of the viability of *M. tuberculosis* H37Ra was to 18.8% at MIC = 8 µg/mL [60], and with *N*-alkoxyphenylhydroxynaphthalenecarboxanilides substituted in C_{(3)'} position of the anilide core by a longer alkoxy tail [61,62]. Since the MTT assay was positive, it can be stated that the tested compounds caused a decrease of mycobacterial cell metabolism. Thus, based on the structure analogy of (2*E*)-*N*-aryl-3-phenylprop-2-enamides with naphthalene-2-carboxanilides, it may be hypothesized that the mechanism of action of these ring-substituted anilides of cinnamic acid could be connected with the affection of mycobacterial energy metabolism [59,63–66]; nevertheless, another possible site of action of the studied compounds in the mycobacteria cannot be excluded [67–70].

2.4. In Vitro Activity against Plant Pathogenic Fungi

Fungal infections are not only a problem in human and veterinary medicine, but also an important problem in agriculture. Plants diseases in general are a major factor limiting the crop quality. Fungal pathogens cause production losses and also can produce mycotoxins, which are dangerous for consumers. The widespread use of fungicides increases food availability and safety, but it can lead to the selection of resistant pathogens and an increase of the production of mycotoxins [71]. As cinnamic acid and its derivatives do not have only antibacterial and antimycobacterial activity, but also activity against plant pathogens [7,72], all the prepared compounds were tested for their potency against *Fusarium avenaceum* (Fr.) Sacc. IMI 319947 and *Bipolaris sorokiniana* (Sacc.) Shoemaker H-299. *B. sorokiniana* is a wide-spread wheat and barley pathogen. It causes many diseases, such as head blight, seedling blight, common root rot, spot blotch, etc. [73]. The last one is a big problem, especially in Southern Asia, where 20% of crop yield is lost because of leaf blight disease [74]. *F. avenaceum* is one of the most common *Fusarium* species causing head blight disease of cereals. It can be isolated from cereal seeds and feed products [75]. *Fusarium* spp. produces a wide spectrum of mycotoxins. The most important are the trichothecenes, zearalenone, moniifromin, and the fumonisins. These compounds have a toxic effect on humans and animals [76].

Only compound **6** (R = 3-CF₃) showed moderate activity (MIC = 54.93 µM) against *F. avenaceum* within the series of compounds, see Table 2. On the other hand, the investigated compounds demonstrated higher effect against *B. sorokiniana*. (2*E*)-*N*-(3-Fluorophenyl)- (**5**) and (2*E*)-*N*-(3-methylphenyl)-3-phenylprop-2-enamide (**2**) had MICs = 16.58 and 33.71 µM, respectively,

which is comparable with the benomyl standard. Also compounds **6**, **4** (R = 2-F), and **14** (2-F-5-Br) demonstrated moderate activity (MIC range 49.98–66.32 μM) against *B. sorokiniana*. Surprising was the inactivity of compound **13** (R = 3,5-CF₃) against both fungal pathogens.

The dependences of the antifungal activity of the compounds against *B. sorokiniana* expressed as $\log(1/\text{MIC (M)})$ on lipophilicity expressed as $\log k$ are illustrated in Figure 5. In general, effective compounds are preferentially substituted in positions C₍₃₎', C_(3,5)', or C_(3,4)'. When inactive compounds (illustrated by empty symbols) substituted in C₍₄₎', C_(2,6)', or C_(2,5)' are eliminated from the SAR study, a bilinear dependence can be found. The activity increases with increasing lipophilicity from unsubstituted derivative **1** to compound **5** (R = 3-F) with the supposed lipophilicity optimum $\log k = 0.23$ and then decreases to derivative **13** (R = 3,5-CF₃); $r = 0.9678$, $n = 7$. It can be stated that it is an opposite trend in comparison with antitubercular findings, which can be caused by differences in the composition and structure of mycobacterial and fungal cell walls [77]. A similar trend can be found for electronic properties of substituents in individual derivatives. The activity increases with an increase of electron-withdrawing effect from compound **2** (R = 3-CH₃, $\sigma_{\text{Ar}} = 0.48$) to an optimum $\sigma_{\text{Ar}} = 0.82$ (compound **5**, R = 3-F) and then decreases with increasing electron-withdrawing effect as follows: $\sigma_{\text{Ar}} = 0.89$ (compound **6**, R = 3-CF₃), 1.02 (compound **4**, R = 2-F), 1.11 (compound **11**, R = 3,5-Cl), and 1.19 (compound **10**, R = 3,4-Cl).

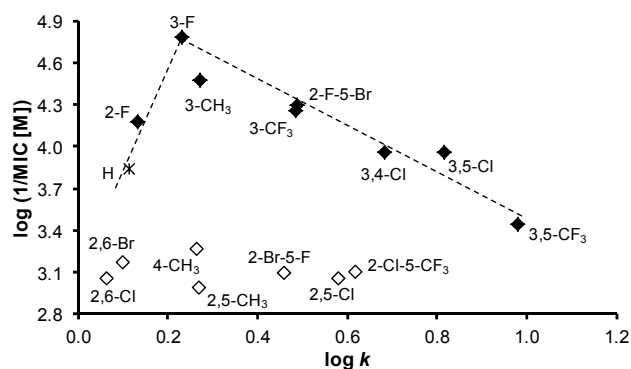


Figure 5. Relationships between in vitro antifungal activity against *B. sorokiniana* $\log(1/\text{MIC (M)})$ and lipophilicity expressed as $\log k$ of studied compounds. (Derivatives excluded from SAR are illustrated by empty symbols.)

Inhibition of *B. sorokiniana* Germination

All the compounds were additionally evaluated for the inhibition of *B. sorokiniana* conidium germination at two concentrations (128 and 256 $\mu\text{g/mL}$), see results in Table 4. It can be stated that at both concentrations, the compounds showed the inhibition of germination. The effect was concentration-dependent for compounds **7**, **10**, **15**, and **16**, and the rest of compounds had concentration-independent effect on the germination. Interestingly, compound **6** that was one of the most active against all bacterial cells including *M. tuberculosis* and displayed strong inhibition on the mycelial growth of both investigated fungi (*F. avenaceum* and *B. sorokiniana*) (Table 2), showed the weakest effect in the germination test. Apart from compound **6**, compounds **2**, **4**, **5**, and **14** exerted the highest *B. sorokiniana* mycelial growth inhibitory effect and had characteristic anti-germination activity. Moreover, compound **5** was the most effective in both assays ($\text{IC}_{50} = 16.58 \mu\text{M}$ in mycelial growth test and 95.4% germination inhibition at 128 $\mu\text{g/mL}$).

2.5. In Vitro Antiproliferative Assay

The preliminary in vitro screening of the antiproliferative activity of the most effective antimicrobial compounds was performed using a Water Soluble Tetrazolium salts-1 (WST-1) assay kit [78] and the human monocytic leukemia THP-1 cell line by means of the method described

recently [20,79]. The principle of the WST-1 assay kit is that antiproliferative compounds inhibit mitochondrial dehydrogenases. The activity of this enzyme directly correlates with the number of metabolically active cells in the culture. Antiproliferative effect was evaluated as IC₅₀ value (concentration of compound causing 50% inhibition of cell proliferation). It can be stated that a compound is considered cytotoxic if it shows a toxic effect on cells up to 10 μM [80]. The highest compound concentration used for the toxicity test was 3-fold higher than this.

IC₅₀ values of the most effective compounds **2** (R = 3-CH₃), **5** (R = 3-F), **6** (R = 3-CF₃), **10** (R = 3,4-Cl), **11** (R = 3,5-Cl), and **13** (R = 3,5-CF₃) ranged from ca. 22 to >30 μM, see Table 2. For comparison, the IC₅₀ of camptothecin was 0.16 ± 0.07 μM. Both compounds **5** and **2** effective against *B. sorokiniana* as well as compounds **10** and **11** potent against *M. tuberculosis* showed IC₅₀ approximately 30 μM and higher, and compounds **6** and **13** showed IC₅₀ = 22 μM, i.e., the treatment with these concentrations did not lead to significant antiproliferative effect on THP-1 cells, and these compounds inhibited selectively vital processes in *B. sorokiniana*, *M. tuberculosis*, or *Staphylococcus* strains. Based on these observations, it can be concluded that all the tested compounds can be considered as nontoxic agents for subsequent design of novel therapeutic agents.

Table 4. Inhibition (%) of *Bipolaris sorokiniana* conidium germination by compounds 1–16 in comparison to negative control. Benomyl (BNM) was used as positive control.

Comp.	Concentration (μg/mL)	Inhibition (%) Compared to Negative Control	Comp.	Concentration (μg/mL)	Inhibition (%) Compared to Negative Control
1	256	59.6	9	256	82.5
	128	74.2		128	76.3
2	256	64.7	10	256	84.3
	128	59.1		128	51.3
3	256	88.7	11	256	84.8
	128	89.1		128	82.6
4	256	60.8	12	256	91.3
	128	58.7		128	82.1
5	256	93.6	13	256	76.3
	128	95.4		128	75.5
6	256	18.4	14	256	81.8
	128	26.7		128	77.6
7	256	73.5	15	256	100
	128	35.1		128	60.9
8	256	92.7	16	256	86.2
	128	88.7		128	61.2
BNM	10	100	BNM	10	100
	5	100		5	100

2.6. Inhibition of Photosynthetic Electron Transport (PET) in Spinach Chloroplasts

The activity of the evaluated cinnamamides related to the inhibition of photosynthetic electron transport (PET) in spinach (*Spinacia oleracea* L.) chloroplasts was moderate or low relative to the standard, see Table 2, except for compound **11** (R = 3,5-Cl) that expressed the highest PET-inhibiting activity comparable with the Diuron[®] standard (IC₅₀ = 5.1 μM). With respect to these low activities, no detailed SAR study can be proposed; nevertheless, from the results listed in Table 2, bilinear trends for both PET inhibition vs. lipophilicity and PET inhibition vs. electronic properties of the anilide core can be suggested. Thus, PET inhibition activity increases with the lipophilicity (log *k*) increase as follows: 0.063 (**9**, R = 2,6-Cl) < 0.264 (**3**, R = 4-CH₃) < 0.487 (**14**, R = 2-F-5-Br) < 0.682 (**10**, R = 3,4-Cl) <<< 0.815 (**11**, R = 3,5-Cl) and then decreases to 0.981 (**13**, R = 3,5-CF₃). Also PET inhibition activity increases with the increase of electron-withdrawing (σ_{Ar}) properties as follows: 0.46 (**3**, R = 4-CH₃) < 1.05 (**13**, 3,5-CF₃) <<< 1.11 (**11**, R = 3,5-Cl) and decreases as follows: >>> 1.19 (**10**, R = 3,4-Cl) > 1.28 (**14**,

$R = 2\text{-F-5-Br} \gg 1.33$ (9 , $R = 2,6\text{-Cl}$). It can be concluded, as mentioned above, that the substitution of the anilide core in $C_{(3,5)}$ or $C_{(3,4)}$ positions is preferable for high PET-inhibiting activity.

The inhibition of electron transport in PS II at the Q_B site plastoquinone, i.e., at the acceptor side of PS II was observed for ring-substituted salicylanilides and carbamoylphenylcarbamates [26,28], ring-substituted hydroxynaphthalene-2-carboxanilides [27,30], *N*-alkoxyphenylhydroxynaphthalene-carboxamides [29], 8-hydroxyquinoline-2-carboxamides [81], and *N*-substituted 2-aminobenzothiazoles [82]. Based on the structural analogy and the presence of the amide bond, it can be hypothesized that the mechanism of action of the investigated compounds is not different from the mechanism of action of the above compounds. Moreover, as mentioned previously [26–29,83,87], a good correlation between antimycobacterial activity and herbicidal effect was found.

2.7. In Vivo Toxicity against Plant Cells

The most potent antifungal compounds **2**, **5**, **6**, and **14** were tested for in vivo toxicity against plant cells. *Nicotiana tabacum* var. Samsun was used for this test [88]. The results of treatment of plant leaves with injected water solutions of each compound as well as dimethyl sulfoxide (DMSO) are illustrated in Figure 6, where photographs of leaves are shown. The negative DMSO control did not have any toxic effect to the plant cells as well. On the other hand, the 5% aqueous solution of DMSO showed a significant toxic effect on the leaves demonstrated as a loss of chlorophyll in the injected area (Figure 6A). Based on Figure 6B,C, it can be concluded that the most effective antifungal compounds had no visible influence on the plant tissue.

These results correspond to above-mentioned PET-inhibiting activity, when all the tested compounds showed no PET inhibition, and thus, they will not be toxic for plants at their prospective application as a plant fungicide.

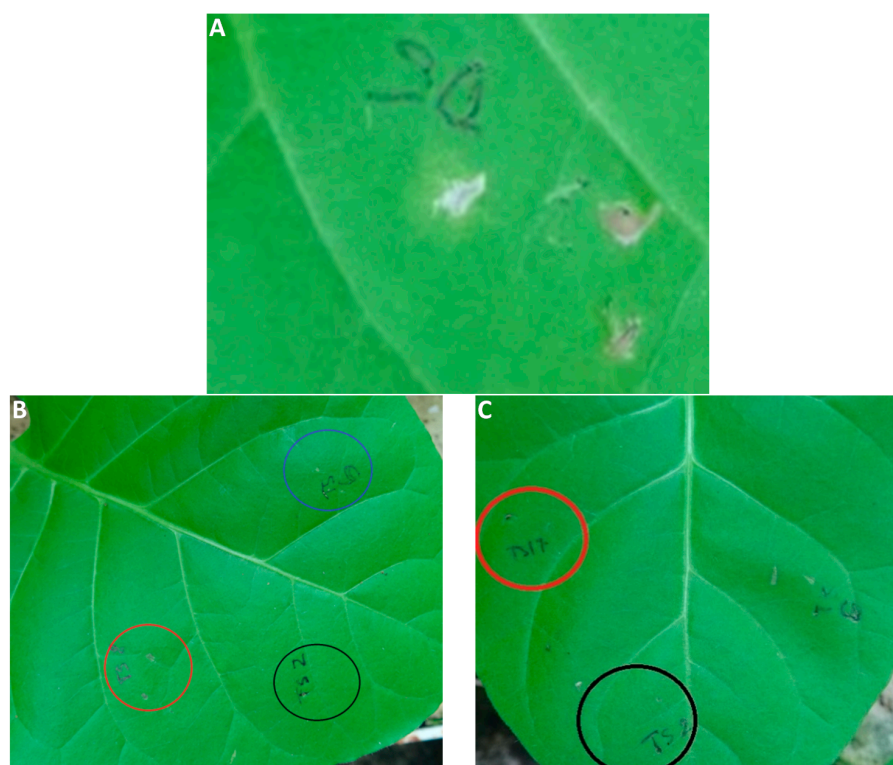


Figure 6. Toxic effect of 5% DMSO (A) to leaf of *Nicotiana tabacum* compared to nontoxic effect of compounds **2** (blue ring), **5** (red ring), and **6** (black ring) (B) and nontoxic effect of compounds **6** (black ring) and **14** (red ring) (C). The black spots in the injected area of compound **5** in Figure 6B are damages of the leaf tissue caused by a needle.

3. Materials and Methods

3.1. Chemistry—General Information

All reagents were purchased from Merck (Sigma-Aldrich, St. Louis, MO, USA) and Alfa (Alfa-Aesar, Ward Hill, MA, USA). Reactions were performed using a CEM Discover SP microwave reactor (CEM, Matthews, NC, USA). Melting points were determined on an apparatus Stuart SMP10 (Stone, UK) and are uncorrected. Infrared (IR) spectra were recorded on an UATR Zn/Se for a Spectrum Two™ Fourier-transform IR spectrometer (PerkinElmer, Waltham, MA, USA). The spectra were obtained by the accumulation of 32 scans with 4 cm⁻¹ resolution in the region of 4000–400 cm⁻¹. All ¹H- and ¹³C-NMR spectra were recorded on a JEOL ECZR 400 MHz NMR spectrometer (400 MHz for ¹H and 100 MHz for ¹³C, Jeol, Tokyo, Japan) in dimethyl sulfoxide-*d*₆ (DMSO-*d*₆). ¹H and ¹³C chemical shifts (δ) are reported in ppm. High-resolution mass spectra were measured using a high-performance liquid chromatograph Dionex UltiMate® 3000 (Thermo Scientific, West Palm Beach, FL, USA) coupled with an LTQ Orbitrap XL™ Hybrid Ion Trap-Orbitrap Fourier Transform Mass Spectrometer (Thermo Scientific) equipped with a HESI II (heated electrospray ionization) source in the positive mode.

Synthesis

Cinnamic acid (3.37 mM) was suspended at room temperature in dry chlorobenzene (20 mL) inside a microwave tube, where phosphorus trichloride (1.7 mM) and the corresponding aniline (3.37 mM) were added dropwise. Then a magnetic stirrer was used, and the reaction mixture was transferred to the microwave reactor at 120 °C for 20 min, where the synthesis at elevated pressure was performed. After the mixture was cooled to 60 °C, and solvent was evaporated in vacuum. A solid was washed with 2 M HCl, and a crude product was recrystallized, first using 96% ethanol and then using 50% ethanol.

(2*E*)-*N*-Phenyl-3-phenylprop-2-enamide (**1**) [89]. Yield 91%; Mp 116–118 °C; IR (cm⁻¹): 3062, 3028, 1661, 1626, 1594, 1578, 1543, 1493, 1442, 1347, 1288, 1248, 1188, 976, 904, 864, 759, 737, 704, 690, 676, 620, 592, 553, 512, 484, 454; ¹H-NMR (DMSO-*d*₆), δ: 10.22 (s, 1H), 7.72 (d, *J* = 7.3 Hz, 2H), 7.64–7.59 (m, 3H), 7.47–7.36 (m, 3H), 7.34 (t, *J* = 8 Hz, 2H), 7.09–7.05 (m, 1H), 6.85 (d, *J* = 16 Hz, 1H); ¹³C-NMR (DMSO-*d*₆), δ: 163.53, 140.16, 139.28, 134.73, 129.77, 129.03, 128.81, 127.72, 123.36, 122.29, 119.23; HR-MS: for C₁₅H₁₄NO [M + H]⁺ calculated 224.1070 *m/z*, found 224.1065 *m/z*.

(2*E*)-*N*-(3-Methylphenyl)-3-phenylprop-2-enamide (**2**) [89]. Yield 80%; Mp 113–115 °C; IR (cm⁻¹): 3259, 3136, 3082, 3064, 3028, 2918, 1658, 1620, 1541, 1488, 1447, 1408, 1342, 1292, 1201, 987, 978, 864, 775, 763, 729, 714, 685, 676, 556, 487; ¹H-NMR (DMSO-*d*₆), δ: 10.14 (s, 1H), 7.64–7.60 (m, 2H), 7.58 (d, *J* = 15.6 Hz, 1H), 7.53 (m, 1H), 7.5 (d, *J* = 8.2 Hz, 1H), 7.47–7.40 (m, 3H), 7.21 (t, *J* = 7.8 Hz, 1H), 6.89 (d, *J* = 7.8 Hz, 1H), 6.84 (d, *J* = 15.6 Hz, 1H), 2.3 (s, 3H); ¹³C-NMR (DMSO-*d*₆), δ: 163.48, 140.06, 139.23, 137.99, 134.75, 129.78, 129.04, 128.67, 127.73, 124.11, 122.38, 119.73, 116.45, 21.25; HR-MS: for C₁₆H₁₆NO [M + H]⁺ calculated 238.1226 *m/z*, found 238.1222 *m/z*.

(2*E*)-*N*-(4-Methylphenyl)-3-phenylprop-2-enamide (**3**) [89]. Yield 82%; Mp 166–168 °C; IR (cm⁻¹): 3240, 3187, 3128, 3085, 3028, 2954, 1660, 1622, 1597, 1538, 1493, 1448, 1405, 1342, 1252, 1187, 984, 973, 813, 781, 762, 720, 674, 533, 510, 485; ¹H-NMR (DMSO-*d*₆) δ: 10.14 (s, 1H), 7.63–7.55 (m, 5H), 7.47–7.40 (m, 3H), 7.15–7.13 (m, 2H), 6.83 (d, *J* = 16 Hz, 1H), 2.26 (s, 3H); ¹³C-NMR (DMSO-*d*₆) δ: 163.33, 139.90, 136.81, 134.79, 132.32, 129.73, 129.22, 129.03, 127.70, 122.40, 119.22, 20.51; HR-MS: for C₁₆H₁₆NO [M + H]⁺ calculated 238.1226 *m/z*, found 238.1222 *m/z*.

(2*E*)-*N*-(2-Fluorophenyl)-3-phenylprop-2-enamide (**4**) [89]. Yield 85%; Mp 114–116 °C; IR (cm⁻¹): 3238, 3182, 3126, 3085, 3059, 3020, 1661, 1627, 1539, 1491, 1448, 1342, 1257, 1188, 1105, 973, 760, 731, 719, 701, 687, 659, 557, 535, 495, 479; ¹H-NMR (DMSO-*d*₆) δ: 9.69 (s, 1H), 8.11 (td, *J* = 7.9 Hz, 2.1 Hz, 1H), 7.64–7.57 (m, 3H), 7.48–7.40 (m, 4H), 7.31–7.26 (m, 1H), 7.20–7.16 (m, 1H), 7.09 (d, *J* = 15.6 Hz, 1H);

^{13}C -NMR (DMSO- d_6) δ : 163.96, 153.34 (d, $J = 244.7$ Hz), 140.72, 134.74, 129.90, 129.05, 127.82, 126.41 (d, $J = 10.6$ Hz), 125.09 (d, $J = 7.7$ Hz), 124.44 (d, $J = 2.9$ Hz), 121.88, 119.23, 115.47 (d, $J = 19.3$ Hz); HR-MS: for $\text{C}_{15}\text{H}_{13}\text{FNO}$ $[\text{M} + \text{H}]^+$ calculated 242.0976 m/z , found 242.0971 m/z .

(2*E*)-*N*-(3-Fluorophenyl)-3-phenylprop-2-enamide (5). Yield 84%; Mp 112–114 °C; IR (cm^{-1}): 3298, 3061, 3031, 2979, 1625, 1596, 1529, 1489, 1420, 1334, 1186, 974, 943, 858, 777, 768, 756, 727, 714, 688, 679, 658, 556, 492; ^1H -NMR (DMSO- d_6) δ : 10.44 (s, 1H), 7.76–7.72 (m, 1H), 7.65–7.61 (m, 3H), 7.48–7.34 (m, 5H), 6.92–6.88 (m, 1H), 6.82 (d, $J = 15.6$ Hz, 1H); ^{13}C -NMR (DMSO- d_6) δ : 163.87, 162.23 (d, $J = 241.8$ Hz), 141.00 (d, $J = 10.6$ Hz), 140.80, 134.61, 130.44 (d, $J = 9.6$ Hz), 129.95, 129.06, 127.85, 121.87, 115.02 (d, $J = 2.9$ Hz), 109.83 (d, $J = 21.2$ Hz), 106.07 (d, $J = 27.3$ Hz); HR-MS: for $\text{C}_{15}\text{H}_{13}\text{FNO}$ $[\text{M} + \text{H}]^+$ calculated 242.0976 m/z , found 242.0972 m/z .

(2*E*)-3-Phenyl-*N*-[3-(trifluoromethyl)phenyl]prop-2-enamide (6) [90]. Yield 75%; Mp 109–111 °C; IR (cm^{-1}): 3400, 2905, 2360, 1678, 1630, 1526, 1491, 1331, 1154, 1112, 1100, 1072, 982, 886, 808; ^1H -NMR (DMSO- d_6) δ : 10.57 (s, 1H), 8.22 (s, 1H), 7.87 (d, $J = 8.2$ Hz, 1H), 7.66–7.62 (m, 3H), 7.58 (t, $J = 7.8$ Hz, 1H), 7.48–7.40 (m, 4H), 6.82 (d, $J = 15.6$ Hz, 1H); ^{13}C -NMR (DMSO- d_6) δ : 164.05, 140.98, 140.07, 134.54, 130.04, 129.99, 129.58 (q, $J = 30.8$ Hz), 129.05, 127.88, 124.16 (q, $J = 272.6$ Hz), 122.76, 121.72, 119.65 (q, $J = 3.9$ Hz), 115.29 (q, $J = 3.9$ Hz); HR-MS: for $\text{C}_{16}\text{H}_{13}\text{F}_3\text{NO}$ $[\text{M} + \text{H}]^+$ calculated 292.0944 m/z , found 292.0938 m/z .

(2*E*)-*N*-(2,5-Dimethylphenyl)-3-phenylprop-2-enamide (7). Yield 91%; Mp 174–176 °C; IR (cm^{-1}): 3242, 3056, 3028, 2977, 2918, 1657, 1621, 1579, 1544, 1494, 1449, 1417, 1343, 1286, 1266, 1199, 1159, 990, 978, 878, 780, 764, 746, 734, 724, 707, 681, 624, 560, 492; ^1H -NMR (DMSO- d_6) δ : 9.42 (s, 1H), 7.63 (d, $J = 6.9$ Hz, 2H), 7.58 (d, $J = 16$ Hz, 1H), 7.47–7.39 (m, 4H), 7.10 (d, $J = 7.8$ Hz, 1H), 6.99 (d, $J = 16$ Hz, 1H), 6.90 (d, $J = 7.3$ Hz, 1H), 2.26 (s, 3H), 2.20 (s, 3H); ^{13}C -NMR (DMSO- d_6) δ : 163.58, 139.88, 136.17, 134.97, 134.85, 130.15, 129.67, 128.99, 127.94, 127.68, 125.70, 124.97, 122.36, 20.67, 17.54; HR-MS: for $\text{C}_{17}\text{H}_{18}\text{NO}$ $[\text{M} + \text{H}]^+$ calculated 252.1383 m/z , found 252.1378 m/z .

(2*E*)-*N*-(2,5-Dichlorophenyl)-3-phenylprop-2-enamide (8). Yield 83%; Mp 173–175 °C; IR (cm^{-1}): 3234, 3108, 3062, 3026, 1662, 1622, 1582, 1463, 1449, 1406, 1341, 1261, 1182, 1093, 1055, 992, 979, 917, 872, 856, 806, 761, 718, 693, 675, 580, 559, 488; ^1H -NMR (DMSO- d_6) δ : 9.77 (s, 1H), 8.15 (d, $J = 2.3$ Hz, 1H), 7.66–7.62 (m, 3H), 7.54 (d, $J = 8.7$ Hz, 1H), 7.45–7.41 (m, 3H), 7.24 (dd, $J = 8.7$ Hz, 2.7 Hz, 1H), 7.18 (d, $J = 15.6$ Hz, 1H); ^{13}C -NMR (DMSO- d_6) δ : 164.20, 141.47, 136.28, 134.60, 131.61, 130.83, 130.05, 129.03, 127.94, 125.40, 124.11, 123.61, 121.51; HR-MS: for $\text{C}_{18}\text{H}_{12}\text{Cl}_2\text{NO}$ $[\text{M} + \text{H}]^+$ calculated 292.0290 m/z , found 292.0289 m/z .

(2*E*)-*N*-(2,6-Dichlorophenyl)-3-phenylprop-2-enamide (9). Yield 85%; Mp 212–214 °C; IR (cm^{-1}): 3256, 1661, 1630, 1569, 1522, 1449, 1428, 1338, 1183, 971, 782, 758, 712, 697, 508; ^1H -NMR (DMSO- d_6) δ : 10.09 (s, 1H), 7.67–7.62 (m, 3H), 7.58–7.56 (m, 2H), 7.48–7.41 (m, 3H), 7.39–7.35 (m, 1H), 6.89 (d, $J = 16$ Hz, 1H); ^{13}C -NMR (DMSO- d_6) δ : 163.67, 140.98, 134.51, 133.69, 133.03, 129.97, 129.19, 129.05, 128.56, 127.85, 120.72; HR-MS: for $\text{C}_{15}\text{H}_{12}\text{Cl}_2\text{NO}$ $[\text{M} + \text{H}]^+$ calculated 292.0290 m/z , found 292.0288 m/z .

(2*E*)-*N*-(3,4-Dichlorophenyl)-3-phenylprop-2-enamide (10). Yield 78%; Mp 173–175 °C; IR (cm^{-1}): 3269, 3095, 3025, 1663, 1627, 1585, 1526, 1474, 1378, 1339, 1289, 1229, 1182, 1126, 1025, 974, 863, 810, 761, 699, 677, 579, 564, 515, 484; ^1H -NMR (DMSO- d_6) δ : 10.52 (s, 1H), 8.12–8.11 (m, 1H), 7.64–7.61 (m, 3H), 7.58 (s, 2H), 7.46–7.40 (m, 3H), 6.79 (d, $J = 16$ Hz, 1H); ^{13}C -NMR (DMSO- d_6) δ : 163.63, 141.08, 139.38, 134.49, 131.09, 130.72, 130.03, 129.05, 127.88, 124.78, 121.55, 120.39, 119.25; HR-MS: for $\text{C}_{15}\text{H}_{12}\text{Cl}_2\text{NO}$ $[\text{M} + \text{H}]^+$ calculated 292.0290 m/z , found 292.0288 m/z .

(2*E*)-*N*-(3,5-Dichlorophenyl)-3-phenylprop-2-enamide (11) [89]. Yield 79%; Mp 139–141 °C; IR (cm^{-1}): 3246, 3177, 3085, 2967, 1663, 1622, 1584, 1532, 1442, 1408, 1338, 1180, 1109, 969, 937, 844, 802, 760, 717, 668, 556, 484; ^1H -NMR (DMSO- d_6) δ : 10.56 (s, 1H), 7.76 (d, $J = 1.8$ Hz, 2H), 7.65–7.61 (m, 3H), 7.48–7.40 (m, 3H), 7.29 (t, $J = 2.1$ Hz, 1H), 6.76 (d, $J = 15.6$ Hz, 1H); ^{13}C -NMR (DMSO- d_6) δ : 164.06, 141.60, 141.35, 134.41, 134.12, 130.06, 129.02, 127.90, 122.48, 121.37, 117.30; HR-MS: for $\text{C}_{15}\text{H}_{12}\text{Cl}_2\text{NO}$ $[\text{M} + \text{H}]^+$ calculated 292.0290 m/z , found 292.0288 m/z .

(2E)-N-(2,6-Dibromophenyl)-3-phenylprop-2-enamide (**12**). Yield 81%; Mp 240–242 °C; IR (cm⁻¹): 3251, 3180, 3028, 2902, 1660, 1627, 1558, 1516, 1441, 1422, 1337, 1263, 1180, 970, 781, 766, 759, 721, 710, 694, 686, 626, 561, 501; ¹H-NMR (DMSO-*d*₆) δ: 10.12 (s, 1H), 7.75 (d, *J* = 7.8 Hz, 2H), 7.67–7.64 (m, 2H), 7.60 (d, *J* = 16 Hz, 1H), 7.48–7.40 (m, 3H), 7.21 (t, *J* = 8 Hz, 1H), 6.87 (d, *J* = 15.6 Hz, 1H); ¹³C-NMR (DMSO-*d*₆) δ: 163.50, 140.85, 135.77, 134.50, 132.24, 130.19, 129.94, 129.05, 127.80, 124.33, 120.86; HR-MS: for C₁₅H₁₂Br₂NO [M + H]⁺ calculated 379.9280 *m/z*, found 379.9288 *m/z*.

(2E)-N-[3,5-bis(Trifluoromethyl)phenyl]-3-phenylprop-2-enamide (**13**). Yield 75%; Mp 143–145 °C; IR (cm⁻¹): 3272, 3085, 2967, 2938, 2879, 1663, 1622, 1575, 1472, 1440, 1377, 1276, 1168, 1129, 1110, 1096, 974, 937, 886, 859, 841, 728, 680, 627, 557, 486; ¹H-NMR (DMSO-*d*₆) δ: 10.89 (s, 1H), 8.36 (s, 2H), 7.77 (s, 1H), 7.70–7.65 (m, 3H), 7.48–7.40 (m, 3H), 6.78 (d, *J* = 16 Hz, 1H); ¹³C-NMR (DMSO-*d*₆) δ: 164.42, 141.78, 141.13, 134.28, 130.80 (q, *J* = 32.8 Hz), 130.22, 129.08, 127.98, 123.23 (q, *J* = 272.6 Hz), 121.07, 118.93–118.78 (m), 116.12–115.98 (m); HR-MS: for C₁₇H₁₂F₆NO [M + H]⁺ calculated 360.0818 *m/z*, found 360.0811 *m/z*.

(2E)-N-(2-Fluoro-5-bromophenyl)-3-phenylprop-2-enamide (**14**). Yield 83%; Mp 161–164 °C; IR (cm⁻¹): 3280, 2967, 2936, 2879, 1660, 1613, 1529, 1474, 1448, 1411, 1345, 1254, 1174, 985, 870, 800, 762, 722, 676, 617, 600, 564, 484; ¹H-NMR (DMSO-*d*₆) δ: 10.13 (s, 1H), 8.44 (dd, *J* = 7.1 Hz, 2.5 Hz, 1H), 7.65–7.60 (m, 3H), 7.48–7.40 (m, 3H), 7.35–7.27 (m, 2H), 7.11 (d, *J* = 15.6 Hz, 1H); ¹³C-NMR (DMSO-*d*₆) δ: 164.22, 152.03 (d, *J* = 245.6 Hz), 141.30, 134.60, 130.02, 129.04, 128.25 (d, *J* = 12.5 Hz), 127.88, 127.10 (d, *J* = 7.7 Hz), 125.10, 121.50, 117.41 (d, *J* = 21.2 Hz), 115.91 (d, *J* = 2.9 Hz); HR-MS: for C₁₅H₁₂FBrNO [M + H]⁺ calculated 320.0081 *m/z*, found 320.0077 *m/z*.

(2E)-N-(2-Bromo-5-fluorophenyl)-3-phenylprop-2-enamide (**15**). Yield 81%; Mp 164–166 °C; IR (cm⁻¹): 3230, 3072, 3045, 2967, 2937, 2880, 1661, 1623, 1591, 1538, 1420, 1342, 1198, 1155, 991, 977, 869, 854, 804, 761, 715, 668, 598, 589, 559, 482; ¹H-NMR (DMSO-*d*₆) δ: 9.64 (s, 1H), 7.83 (dd, *J* = 11 Hz, 3.2 Hz, 1H), 7.72 (dd, *J* = 8.7 Hz, 5.9 Hz, 1H), 7.67–7.62 (m, 3H), 7.48–7.42 (m, 3H), 7.15 (d, *J* = 15.6 Hz, 1H), 7.04 (ddd, *J* = 8.9 Hz, 8 Hz, 3.2 Hz, 1H); ¹³C-NMR (DMSO-*d*₆) δ: 164.12, 161.05 (d, *J* = 243.7 Hz), 141.44, 137.74 (d, *J* = 11.6 Hz), 134.61, 133.85 (d, *J* = 8.7 Hz), 130.05, 129.04, 127.95, 121.55, 113.41 (d, *J* = 23.1 Hz), 112.44 (d, *J* = 27 Hz), 110.6 (d, *J* = 2.9 Hz); HR-MS: for C₁₅H₁₂FBrNO [M + H]⁺ calculated 320.0081 *m/z*, found 320.0077 *m/z*.

(2E)-N-[2-Chloro-5-(trifluoromethyl)phenyl]-3-phenylprop-2-enamide (**16**). Yield 77%; Mp 144–146 °C; IR (cm⁻¹): 3280, 2967, 2936, 2879, 1528, 1329, 1262, 1165, 1116, 1080, 964, 892, 814, 758, 707, 686, 668, 644, 605, 560, 534, 490, 452; ¹H-NMR (DMSO-*d*₆) δ: 9.22 (s, 1H), 8.40 (d, *J* = 1.8 Hz, 1H), 7.79–7.77 (m, 1H), 7.68–7.64 (m, 3H), 7.55–7.53 (m, 1H), 7.49–7.40 (m, 3H), 7.19 (d, *J* = 15.6 Hz, 1H); ¹³C-NMR (DMSO-*d*₆) δ: 164.42, 141.66, 135.99, 134.60, 130.70, 130.06, 129.02, 128.98, 128.09 (q, *J* = 38.2 Hz), 127.96, 123.69 (q, *J* = 272.6 Hz), 121.98 (q, *J* = 3.9 Hz), 121.46, 120.95 (q, *J* = 3.9 Hz); HR-MS: for C₁₆H₁₂ClF₃NO [M + H]⁺ calculated 326.0554 *m/z*, found 326.0547 *m/z*.

3.2. Lipophilicity Determination by HPLC (Capacity Factor *k*/Calculated log *k*)

A HPLC separation module Waters® e2695 equipped with a Waters 2996 PDA Detector (Waters Corp., Milford, MA, USA) were used. A chromatographic column Symmetry® C₁₈ 5 μm, 4.6 × 250 mm, Part No. W21751W016 (Waters Corp.) was used. The HPLC separation process was monitored by the Empower™ 3 Chromatography Data Software (Waters Corp.). Isocratic elution by a mixture of MeOH p.a. (72%) and H₂O-HPLC Mili-Q grade (28%) as a mobile phase was used. The total flow of the column was 1.0 mL/min, injection 5 μL, column temperature 40 °C, and sample temperature 10 °C. The detection wavelength 214 nm was chosen. The KI methanolic solution was used for the determination of dead time (*t*_D). Retention times (*t*_R) were measured in minutes. The capacity factors *k* were calculated using the Empower™ 3 Chromatography Data Software according to the formula $k = (t_R - t_D)/t_D$, where *t*_R is the retention time of the solute, while *t*_D is the dead time obtained using an unretained analyte. Each experiment was repeated three times. Log *k*, calculated from the

capacity factor k , is used as the lipophilicity index converted to log P scale [36]. The log k values of individual compounds are shown in Table 1.

3.3. Biological Testing

3.3.1. In Vitro Antibacterial Evaluation

The synthesized compounds were evaluated for in vitro antibacterial activity against representatives of multidrug-resistant bacteria and clinical isolates of methicillin-resistant *Staphylococcus aureus* (MRSA) 63718, SA 630, and SA 3202 [37,38] that were obtained from the National Institute of Public Health (Prague, Czech Republic). *S. aureus* ATCC 29213 was used as a reference and quality control strain. In addition, all the compounds were tested for their activity against vancomycin-susceptible *Enterococcus faecalis* ATCC 29212 as a reference strain and three isolates from American crows of vanA-carrying vancomycin-resistant *E. faecalis* (VRE) 342B, 368, and 725B [39]. Ampicillin (Sigma) was used as the standard. Prior to testing, each strain was passaged onto nutrient agar (Oxoid, Basingstoke, UK) with 5% of bovine blood, and bacterial inocula were prepared by suspending a small portion of bacterial colony in sterile phosphate buffered saline (pH 7.2–7.3). The cell density was adjusted to 0.5 McFarland units using a densitometer (Densi-La-Meter, LIAP, Riga, Latvia). This inoculum was diluted to reach the final concentration of bacterial cells 5×10^5 CFU/mL in the wells. The compounds were dissolved in DMSO (Sigma), and the final concentration of DMSO in the Cation Adjusted Mueller-Hinton (CaMH) broth (Oxoid) or Brain-Heart Infusion for enterococci did not exceed 2.5% of the total solution composition. The final concentrations of the evaluated compounds ranged from 256 to 0.008 $\mu\text{g/mL}$. The broth dilution micro-method, modified according to the NCCLS (National Committee for Clinical Laboratory Standards) guidelines [91] in Mueller-Hinton (MH) broth, was used to determine the minimum inhibitory concentration (MIC). Drug-free controls, sterility controls, and controls consisting of MH broth and DMSO alone were included. The determination of results was performed visually after 24 h of static incubation in the darkness at 37 °C in an aerobic atmosphere. The results are shown in Table 2.

3.3.2. Synergy Effect with Clinically Used Drugs

For synergy effect study, a method of fractional inhibitory concentration was used. The tested compounds (A) and conventional used antibiotic (B) (tetracycline, ciprofloxacin, and vancomycin (purchased from Sigma)) were diluted in the microtitration plate in CaMH broth (Oxoid) to get an original combination of concentration in every well. The row H was used for evaluation of $\text{MIC}_{(A)}$; column 12 was used for evaluation of $\text{MIC}_{(B)}$. The plate was inoculated by the bacterial suspension to reach final concentration 5×10^5 CFU/mL in the wells. The fractional inhibitory concentration (FIC) index was calculated using the concentrations in the first nonturbid (clear) well found in each row and column along the turbidity/nonturbidity interface [42]. A $\Sigma\text{FIC} \leq 0.5$ means synergy; $0.5 < \Sigma\text{FIC} < 1$ is additivity; $1 \leq \Sigma\text{FIC} < 4$ is indifference; and $\Sigma\text{FIC} \geq 4$ is antagonism [41]. The tests were made in duplicate, and the results were averaged. The results are summarized in Table 3.

3.3.3. Dynamics of Antibacterial Effect

The most active antistaphylococcal compounds were studied for their dynamics of antibacterial effect. The method of time-kill curves were used [37,40]. Compound 6 was diluted in CaMH to reach the final concentration equal to $1 \times \text{MIC}$, $2 \times \text{MIC}$, and $4 \times \text{MIC}$. For the compound 13, only concentrations $1 \times \text{MIC}$ and $2 \times \text{MIC}$ were used, due to the higher MIC and dissolution problems in the concentration equal to $4 \times \text{MIC}$. The tubes were inoculated with the culture of *S. aureus* ATCC 29213 diluted to 1 McFarland in the exponential phase of growth. The final concentration of bacteria was 7.5×10^6 CFU/mL. Tubes were stored in an incubator at 37 °C without shaking. Immediately after 4, 6, 8, and 24 h of inoculation, 100 μL of sample was serially diluted 1:10 in phosphate buffered saline (PBS). From each dilution $2 \times 20 \mu\text{L}$ were put onto MH agar plates. The plates were incubated at 37 °C

for 24 h, and the colonies were counted. Bactericidal effect is defined as a $-3\log$ decrease of CFU/mL compared to the growth control in time 0. The test was made in duplicate on 2 separate occasions, and the results were averaged. The results are illustrated in Figure 2.

3.3.4. Biofilm Inhibition Assay

The most active antistaphylococcal compounds were studied for their ability to inhibit biofilm formation. The compounds were diluted in a 96-well plate in tryptic soy broth (TSB) containing 2% of glucose to reach concentrations 256–2 $\mu\text{g}/\text{mL}$. *S. aureus* ATCC 29213 cultivated overnight on blood agar was used for preparing the inoculum. A few colonies were put in a tube with 5 mL of TSB + 2% glucose and cultivated to reach the exponential phase of growth. The inoculum was diluted to 1 McFarland and then 1:1000 in TSB + 2% glucose. The final concentration of bacteria in each well was 1×10^5 . As positive controls, ampicillin, vancomycin, ciprofloxacin, and tetracycline (Sigma) were used. As the compounds were dissolved in DMSO (up to 5%), the growth control included 5% of DMSO for verification that the applied DMSO concentration did not possess bacterial growth-inhibiting activity. The plate was cultivated for 48 h at 37 °C without shaking. After incubation, the content of the wells was removed and the wells were washed 3-fold by PBS. After drying, 125 μL of 0.1% crystal violet was put to every well. The plate was stained for 20 min at room temperature, the content was removed, and the plate was again washed by PBS 3-fold. The coloured biofilm was taken off from the wells by 33% acetic acid, and absorbance in 595 nm was measured. As a blank, non-inoculated plate treated in the same way was used. The test was made in triplicates in 3 separated occasions. The ability to inhibit biofilm formation was evaluated as a percentage inhibition of growth compared to the growth control. The results are illustrated in Figure 3.

3.3.5. In Vitro Antimycobacterial Evaluation

Mycobacterium tuberculosis ATCC 25177/H37Ra was grown in Middlebrook broth (MB), supplemented with Oleic-Albumin-Dextrose-Catalase (ODAC) supplement (Difco, Lawrence, KS, USA). At log phase growth, a culture sample (10 mL) was centrifuged at 15,000 rpm/20 min using a bench top centrifuge (MPW-65R, MPW Med Instruments, Warszawa, Poland). Following the removal of the supernatant, the pellet was washed in fresh Middlebrook 7H9GC broth and resuspended in fresh, ODAC-supplemented MB (10 mL). The turbidity was adjusted to match McFarland standard No. 1 (3×10^8 CFU) with MB broth. A further 1:10 dilution of the culture was then performed in MB broth. The antimicrobial susceptibility of *M. tuberculosis* was investigated in a 96-well plate format. In these experiments, sterile deionised water (300 μL) was added to all outer-perimeter wells of the plates to minimize evaporation of the medium in the test wells during incubation. Each evaluated compound (100 μL) was incubated with *M. tuberculosis* (100 μL). Dilutions of each compound were prepared in duplicate. For all synthesized compounds, final concentrations ranged from 128 to 4 $\mu\text{g}/\text{mL}$. All compounds were dissolved in DMSO, and subsequent dilutions were made in supplemented MB. The plates were sealed with Parafilm and incubated at 37 °C for 14 days. Following incubation, a 10% addition of alamarBlue (Difco) was mixed into each well, and readings at 570 nm and 600 nm were taken, initially for background subtraction and subsequently after 24 h reincubation. The background subtraction is necessary for strongly coloured compounds, where the colour may interfere with the interpretation of any colour change. For noninterfering compounds, a blue colour in the well was interpreted as the absence of growth, and a pink colour was scored as growth. Isoniazid (Sigma) was used as the positive control, as it is a clinically used antitubercular drug. The results are shown in Table 2.

3.3.6. MTT Assay

Compounds were prepared as previously stated and diluted in Middlebrook media to achieve the desired final concentration 128–1 $\mu\text{g}/\text{mL}$. *Mycobacterium tuberculosis* ATCC 25177/H37Ra was suspended in ODAC supplemented Middlebrook broth at a MacFarland standard of 1.0 and

then diluted 1:10, using Middlebrook broth as a diluent. The diluted mycobacteria (50 μ L) were added to each well containing the compound to be tested. Diluted mycobacteria in broth free from inhibiting compounds were used as a growth control. As positive controls, ciprofloxacin and rifampicin were used. All compounds and controls were prepared in duplicate. Plates were incubated at 37 °C for 7 days. After the incubation period, 10% well volume of MTT (3-(4,5-dimethylthiazol-2-yl)-2,5-diphenyl-tetrazolium bromide) reagent (Sigma) was mixed into each well and incubated at 37 °C for 4 h in dark. Then 100 μ L of 17% Sodium dodecyl sulfate in 40% dimethylformamide was added to each well. The plates were read at 570 nm. The absorbance readings from the cells grown in the presence of the tested compounds were compared with uninhibited cell growth to determine the relative percent viability. The percent viability was determined through the MTT assay. The percent viability is calculated through comparison of a measured value against that of the uninhibited control: % viability = $OD_{570E}/OD_{570P} \times 100$, where OD_{570E} is the reading from the compound-exposed cells, while OD_{570P} is the reading from the uninhibited cells (positive control). Cytotoxic potential is determined by a percent viability of <70% [59,92]. Rifampicin a ciprofloxacin (Sigma) were used as positive controls.

3.3.7. In Vitro Antifungal Activity

96-Well microplates were used for testing the inhibitory effect of compounds against mycelial growth of *Fusarium avenaceum* (Fr.) Sacc. IMI 319947 and *Bipolaris sorokiniana* (Sacc.) Shoemaker H-299 (NCBI GenBank accession No. MH697869). The compounds were diluted in DMSO to reach the concentration of 10 mg/mL and then diluted in the microtiter plates in supplemented lysogeny broth (LB, 10 g/L tryptone (Microtrade, Budapest, Hungary), 5 g/L yeast extract (Scharlau, Barcelona, Spain), and 10 g/L NaCl (Reanal, Budapest, Hungary)) to get the final concentration of 256–2 μ g/mL. Positive (benomyl, Chinoin Fundazol 50WP[®], Chinoin, Budapest, Hungary) and negative (solvents of the compounds) controls were used. 50 mL LB medium was inoculated with the fungal culture grown in an agar plate and shaken at 100 rpm at 22 °C for 3 days in dark; then mycelium was cut with a sterile blender to small parts. The mycelium suspension was diluted to set $OD_{600} = 0.2$. This inoculum was diluted 2-fold with the content of the wells. The absorbance at 600 nm was measured by a spectrophotometer (Labsystems Multiscan MS 4.0, Thermo Scientific) immediately, and the plates were incubated at 22 °C. The absorbance was measured again after 24, 48, and 72 h. The MIC was counted in the time, when absorbance in the negative control tripled. The experiment was repeated on 3 separated occasions, and the results were averaged. The results are summarized in Table 2.

3.3.8. Inhibition of *Bipolaris sorokiniana* Germination

The inhibitory effect on the conidium germination was tested according to De Lucca et al. [93] with some modifications. The tested compounds were diluted in a 96-well microplate in 45 μ L sterile distilled water to reach the final concentrations of 256 and 128 μ g/mL. As a positive control, benomyl (10 and 5 μ g/mL) was used. As a negative control, nontreated wells with 5% DMSO were used. Conidium suspension was prepared from sporulating culture grown on an agar plate. 5 μ L of the aliquot was added to each well. The final concentration of conidia in each well was 3000 conidia in 1 mL. The plate was incubated at 22 °C for 48 h in dark. After the incubation, the aliquot from each well was observed microscopically (400 \times) for germination. A total of 50 conidia from each well were observed. Germination was defined as the development of germ tube(s) of any size from a conidium. The inhibition effect was counted as a ratio of nongerminated conidia compared to the negative control. The experiment was performed in duplicate. The results are summarized in Table 4.

3.3.9. In Vitro Antiproliferative Assay

Human monocytic leukemia THP-1 cells were used for in vitro antiproliferative assay. Cells were obtained from the European Collection of Cell Cultures (ECACC, Salisbury, UK) and routinely cultured in RPMI (Roswell Park Memorial Institute) 1640 medium supplemented

with 10% fetal bovine serum, 2% L-glutamine, 1% penicillin, and streptomycin at 37 °C with 5% CO₂. Cells were passaged at approximately one-week intervals. The antiproliferative activity of the compounds was determined using a Water Soluble Tetrazolium Salts-1 (WST-1, 2-(4-iodophenyl)-3-(4-nitrophenyl)-5-(2,4-disulfophenyl)-2H-tetrazolium) assay kit (Roche Diagnostics, Mannheim, Germany) according to the manufacturer's instructions. The tested compounds were dissolved in DMSO and added in five increasing concentrations (0.37, 1.1, 3.3, 10, and 30 μM) to the cell suspension in the culture RPMI 1640 medium. The maximum concentration of DMSO in the assays never exceeded 0.1%. Subsequently, the cells were incubated at 37 °C with 5% CO₂ for 24 h. For WST-1 assays, cells were seeded into 96-well plates (5 × 10⁴ cells/well in 100 μL culture medium) in triplicate in serum-free RPMI 1640 medium, and measurements were taken 24 h after the treatment with the compounds. The median inhibition concentration values, IC₅₀, were deduced through the production of a dose-response curve. All data were evaluated using GraphPad Prism 5.00 software (GraphPad Software, San Diego, CA, USA). The results are shown in Table 2.

3.3.10. Study of Inhibition of Photosynthetic Electron Transport (PET) in Spinach Chloroplasts

Chloroplasts were prepared from spinach (*Spinacia oleracea* L.) according to Masarovicova and Kralova [94]. The inhibition of photosynthetic electron transport (PET) in spinach chloroplasts was determined spectrophotometrically (Genesys 6, Thermo Scientific), using an artificial electron acceptor 2,6-dichlorophenol-indophenol (DCIPP) according to Kralova et al. [95], and the rate of photosynthetic electron transport was monitored as a photoreduction of DCPIP. The measurements were carried out in phosphate buffer (0.02 mol/L, pH 7.2) containing sucrose (0.4 mol/L), MgCl₂ (0.005 mol/L), and NaCl (0.015 mol/L). The chlorophyll content was 30 mg/L in these experiments, and the samples were irradiated (~100 W/m² with 10 cm distance) with a halogen lamp (250 W) using a 4 cm water filter to prevent warming of the samples (suspension temperature 22 °C). The studied compounds were dissolved in DMSO due to their limited water solubility. The applied DMSO concentration (up to 4%) did not affect the photochemical activity in spinach chloroplasts. The inhibitory efficiency of the studied compounds was expressed by IC₅₀ values, i.e., by molar concentration of the compounds causing a 50% decrease in the oxygen evolution rate relative to the untreated control. The comparable IC₅₀ value for the selective herbicide 3-(3,4-dichlorophenyl)-1,1-dimethylurea, DCMU (Diuron®) was about 2.1 μmol/L. The results are shown in Table 2.

3.3.11. In Vivo Toxicity against Plant Cells

Nicotiana tabacum var. Samsun was used for this test. The compounds were diluted in water to reach concentrations equal to 1 × MIC and 4 × MIC. As the negative control, solutions of DMSO in the same concentration were used. The positive control was 5% DMSO, which should be toxic to the plant cells. The aqueous solutions were injected into the plant leaves by a syringe (needle 27G × 3/4") to fill area approx. 1 cm² [88]. The test was made in triplicates in three different plants. The plants were kept in a greenhouse on direct sunlight. The effect of the compounds was visually checked every day for 5 weeks. In the presence of tested compounds, no visible changes in the plant tissues were observed. The results are illustrated in Figure 6.

4. Conclusions

A series of sixteen ring-substituted *N*-arylcinnamamides was prepared, characterized, and evaluated against *Staphylococcus aureus*, three methicillin-resistant *S. aureus* strains, *Mycobacterium tuberculosis* H37Ra, *Fusarium avenaceum*, and *Bipolaris sorokiniana*. Additionally, the compounds were tested for their activity related to the inhibition of photosynthetic electron transport in spinach chloroplasts. (2*E*)-3-Phenyl-*N*-[3-(trifluoromethyl)phenyl]prop-2-enamide (6) and (2*E*)-*N*-[3,5-bis(tri-fluoromethyl)phenyl]-3-phenylprop-2-enamide (13) showed the highest activity (MIC = 27.47 and 22.27 μM, respectively) against all four staphylococcal strains as well as against *M. tuberculosis*. These compounds also showed activity against bacterial

biofilm forming, the ability to increase the effect of clinically used antibiotics such as tetracycline, vancomycin, and ciprofloxacin and concentration-dependent antibacterial effect, which led to killing >99% of bacteria. On the other hand, (2*E*)-*N*-(3-fluorophenyl)- (5) and (2*E*)-*N*-(3-methylphenyl)-3-phenylprop-2-enamide (2) had MICs = 16.58 and 33.71 μ M, respectively, against *B. sorokiniana*, while both compounds did not show any in vivo toxicity against *Nicotiana tabacum* var. Samsun. (2*E*)-*N*-(3,5-dichlorophenyl)-3-phenylprop-2-enamide (11, IC₅₀ = 5.1 μ M) was the most active PET inhibitor. These compounds showed activities comparable with or higher than those of standards. A significant decrease of mycobacterial cell metabolism (viability of *M. tuberculosis* H37Ra) was observed using the MTT assay. The screening of the cytotoxicity of the selected compounds was performed using THP-1 cells, and no significant lethal effect was observed for the most potent compounds. The position of substituents on the anilide ring seems to be crucial for both antitubercular and antifungal activity; positions C_{(3)'}, C_{(3,4)'}, and C_{(3,5)'} are preferable. Lipophilicity is another important factor; antitubercular activity increases with increasing lipophilicity, while antifungal activity, to the contrary, decreases from the most effective compound 5 (R = 3-F) with lipophilicity log *k* = 0.23 with increasing lipophilicity. The activity is also dependent on the electronic parameters of substituents on the anilide core. Bilinear trends for effective compounds can be observed for both antitubercular and antifungal dependences; nevertheless, for antitubercular effectivity, rather more electron-withdrawing properties are preferred ($\sigma_{Ar} \approx 1$, compound 13, R = 3,5-CF₃), while for antifungal activity against *B. sorokiniana*, less electron-withdrawing properties are preferred ($\sigma_{Ar} = 0.82$, compound 5, R = 3-F). Also the dependences of PET-inhibiting activity on lipophilicity and electronic properties showed bilinear trends, as mentioned above, where C_{(3,5)'} or C_{(3,4)'} substitution of the anilide core is preferable.

Author Contributions: J.K. and T.S.—synthesis and characterization of the compounds and study of PET inhibition. I.K. and M.O.—analysis of the compounds. S.P., H.M., A.C., A.M.M., and J.B.—antimicrobial and pesticide evaluation and in vivo toxicity test. T.K. and P.K.—in vitro cytotoxicity assay. J.J.—conceived and designed the experiments, SAR, and the writing of the paper.

Acknowledgments: This contribution was supported by grant of the Comenius University in Bratislava No. UK/229/2018, grants of the Faculty of Pharmacy of Comenius University in Bratislava FaF UK/9/2018 and FaF UK/37/2018, VEGA project No.1/0040/17 and partially by SANOFI-AVENTIS Pharma Slovakia, s.r.o. and the National Research, Development, and Innovation Office (NKFIH) of Hungary (grant no. K119276). The HPLC/HRMS system forms a part of the National Infrastructure CzeCOŠ ProCES CZ.02.1.01/0.0/0.0/16_013/0001609; Michal Oravec was supported by the National Sustainability Program (NPU I; Grant No. LO1415).

Conflicts of Interest: The authors declare no conflicts of interest.

References

1. Lichtenthaler, H.K.; Schweiger, J. Cell wall bound ferulic acid, the major substance of the blue-green fluorescence emission of plants. *J. Plant Physiol.* **1998**, *152*, 272–282. [[CrossRef](#)]
2. Vogt, T. Phenylpropanoid biosynthesis. *Mol. Plant* **2010**, *3*, 2–20. [[CrossRef](#)] [[PubMed](#)]
3. Adisakwattana, S.; Chantarasinlapin, P.; Thammarat, H.; Yibchok-Anun, S. A series of cinnamic acid derivatives and their inhibitory activity on intestinal alpha-glucosidase. *J. Enzyme Inhib. Med. Chem.* **2009**, *24*, 1194–1200. [[CrossRef](#)] [[PubMed](#)]
4. Berrin, O.; Murat, K.; Ilkay, O. Cytotoxicity, antiviral and antimicrobial activities of alkaloids, flavonoids, and phenolic acids. *Pharm. Biol.* **2011**, *49*, 396–402.
5. Sharma, P. Cinnamic acid derivatives: A new chapter of various pharmacological activities. *J. Chem. Pharm. Res.* **2011**, *3*, 403–423.
6. Sova, M. Antioxidant and antimicrobial activities of cinnamic acid derivatives. *Mini Rev. Med. Chem.* **2012**, *12*, 749–767. [[CrossRef](#)] [[PubMed](#)]
7. Korosec, B.; Sova, M.; Turk, S.; Krasevec, N.; Novak, M.; Lah, L.; Stojan, J.; Podobnik, B.; Berne, S.; Zupanec, N.; et al. Antifungal activity of cinnamic acid derivatives involves inhibition of benzoate 4-hydroxylase (CYP53). *J. Appl. Microbiol.* **2014**, *116*, 955–966. [[CrossRef](#)] [[PubMed](#)]
8. Guzman, J.D. Natural cinnamic acids, synthetic derivatives and hybrids with antimicrobial activity. *Molecules* **2014**, *19*, 19292–19349. [[CrossRef](#)] [[PubMed](#)]

9. Peperidou, A.; Kapoukranidou, D.; Kontogiorgis, C.; Hadjipavlou-Litina, D. Multitarget molecular hybrids of cinnamic acids. *Molecules* **2014**, *19*, 20197–20226. [CrossRef] [PubMed]
10. Pontiki, E.; Hadjipavlou-Litina, D.; Litinas, K.; Geromichalos, G. Novel cinnamic acid derivatives as antioxidant and anticancer agents: Design, synthesis and modeling studies. *Molecules* **2014**, *19*, 9655–9674. [CrossRef] [PubMed]
11. Hadjipavlou-Litina, D.; Pontiki, E. Aryl-acetic and cinnamic acids as lipoxygenase inhibitors with antioxidant, anti-inflammatory, and anticancer activity. *Methods Mol. Biol.* **2015**, *1208*, 361–377. [PubMed]
12. Su, P.; Shi, Y.; Wang, J.; Shen, X.; Zhang, J. Anticancer agents derived from natural cinnamic acids. *Anticancer Agents Med. Chem.* **2015**, *15*, 980–987. [CrossRef] [PubMed]
13. De Vita, D.; Simonetti, G.; Pandolfi, F.; Costi, R.; Di Santo, R.; D'Auria, F.D.; Scipione, L. Exploring the anti-biofilm activity of cinnamic acid derivatives in *Candida albicans*. *Bioorg. Med. Chem. Lett.* **2016**, *26*, 5931–5935. [CrossRef] [PubMed]
14. Peperidou, A.; Pontiki, E.; Hadjipavlou-Litina, D.; Voulgari, E.; Avgoustakis, K. Multifunctional cinnamic acid derivatives. *Molecules* **2017**, *22*, 1247. [CrossRef] [PubMed]
15. Lima, T.C.; Ferreira, A.R.; Silva, D.F.; Lima, E.O.; de Sousa, D.P. Antifungal activity of cinnamic acid and benzoic acid esters against *Candida albicans* strains. *Nat. Prod. Res.* **2018**, *32*, 572–575. [CrossRef] [PubMed]
16. Dolab, J.G.; Lima, B.; Spaczynska, E.; Kos, J.; Cano, N.H.; Feresin, G.; Tapia, A.; Garibotto, F.; Petenatti, E.; Olivella, M.; et al. Antimicrobial activity of *Annona emarginata* (Schltdl.) H. Rainer and most active isolated compound against clinically important bacteria. *Molecules* **2018**, *23*, 1187. [CrossRef] [PubMed]
17. FRAC Code List 2018. Available online: http://www.frac.info/docs/default-source/publications/frac-code-list/frac_code_list_2018-final.pdf?sfvrsn=6144b9a_2 (accessed on 18 June 2018).
18. WHO. *Global Antimicrobial Resistance Surveillance System (GLASS) Report*; HO Press: Geneva, Switzerland, 2017.
19. Gonec, T.; Bobal, P.; Suján, J.; Pesko, M.; Guo, J.; Kralova, K.; Pavlacka, L.; Vesely, L.; Kreckova, E.; Kos, J.; et al. Investigating the spectrum of biological activity of substituted quinoline-2-carboxamides and their isosteres. *Molecules* **2012**, *17*, 613–644. [CrossRef] [PubMed]
20. Kos, J.; Nevin, E.; Soral, M.; Kushkevych, I.; Gonec, T.; Bobal, P.; Kollar, P.; Coffey, A.; O'Mahony, J.; Liptaj, T.; et al. Synthesis and antimycobacterial properties of ring-substituted 6-hydroxynaphthalene-2-carboxanilides. *Bioorg. Med. Chem.* **2015**, *23*, 2035–2043. [CrossRef] [PubMed]
21. Tischer, W.; Strotmann, H. Relationship between inhibitor binding by chloroplasts and inhibition of photosynthetic electron-transport. *Biochim. Biophys. Acta* **1977**, *460*, 113–125. [CrossRef]
22. Trebst, A.; Draber, W. Structure activity correlations of recent herbicides in photosynthetic reactions. In *Advances in Pesticide Science*; Greissbuehler, H., Ed.; Pergamon Press: Oxford, UK, 1979; pp. 223–234.
23. Bowyer, J.R.; Camilleri, P.; Vermaas, W.F.J. *Herbicides, Topics in Photosynthesis*; Baker, N.R., Percival, M.P., Eds.; Elsevier: Amsterdam, The Netherlands, 1991; Volume 10, pp. 27–85.
24. Izawa, S. Acceptors and donors for chloroplast electron transport. In *Methods in Enzymology*; Colowick, P., Kaplan, N.O., Eds.; Academic Press: New York, NY, USA; London, UK, 1980; Volume 69, Part C; pp. 413–434.
25. Good, N.E. Inhibitors of the Hill reaction. *Plant Physiol.* **1961**, *36*, 788–803. [CrossRef] [PubMed]
26. Otevrel, J.; Mandelova, Z.; Pesko, M.; Guo, J.; Kralova, K.; Sersen, F.; Vejsova, M.; Kalinowski, D.; Kovacevic, Z.; Coffey, A.; et al. Investigating the spectrum of biological activity of ring-substituted salicylanilides and carbamoylphenylcarbamates. *Molecules* **2010**, *15*, 8122–8142. [CrossRef] [PubMed]
27. Gonec, T.; Kos, J.; Zadrazilova, I.; Pesko, M.; Keltosova, S.; Tengler, J.; Bobal, P.; Kollar, P.; Cizek, A.; Kralova, K.; et al. Antimycobacterial and herbicidal activity of ring-substituted 1-hydroxynaphthalene-2-carboxanilides. *Bioorg. Med. Chem.* **2013**, *21*, 6531–6541. [CrossRef] [PubMed]
28. Kralova, K.; Perina, M.; Waisser, K.; Jampilek, J. Structure-activity relationships of *N*-benzylsalicylamides for inhibition of photosynthetic electron transport. *Med. Chem.* **2015**, *11*, 156–164. [CrossRef] [PubMed]
29. Gonec, T.; Kralova, K.; Pesko, M.; Jampilek, J. Antimycobacterial *N*-Alkoxyphenylhydroxynaphthalene-carboxamides Affecting Photosystem II. *Bioorg. Med. Chem. Lett.* **2017**, *27*, 1881–1885. [CrossRef] [PubMed]
30. Gonec, T.; Kos, J.; Pesko, M.; Dohanosova, J.; Oravec, M.; Liptaj, T.; Kralova, K.; Jampilek, J. Halogenated 1-Hydroxynaphthalene-2-carboxanilides Affecting Photosynthetic Electron Transport in Photosystem II. *Molecules* **2017**, *22*, 1709. [CrossRef] [PubMed]
31. Shaner, D.L. Herbicide safety relative to common targets in plants and mammals. *Pest. Manag. Sci.* **2004**, *60*, 17–24. [CrossRef] [PubMed]

32. Delaney, J.; Clarke, E.; Hughes, D.; Rice, M. Modern agrochemical research: A missed opportunity for drug discovery? *Drug Discov. Today* **2006**, *11*, 839–845. [[CrossRef](#)] [[PubMed](#)]
33. Duke, S.O. Herbicide and pharmaceutical relationships. *Weed Sci.* **2010**, *58*, 334–339. [[CrossRef](#)]
34. Myung, K.; Klittich, C.J. Can agricultural fungicides accelerate the discovery of human antifungal drugs? *Drug Discov. Today* **2015**, *20*, 7–10. [[CrossRef](#)] [[PubMed](#)]
35. Jampilek, J. Potential of agricultural fungicides for antifungal drug discovery. *Expert Opin. Drug Dis.* **2016**, *11*, 1–9. [[CrossRef](#)] [[PubMed](#)]
36. Pliska, V. Methods and Principles in Medicinal Chemistry. In *Lipophilicity in Drug Action and Toxicology*, 1st ed.; Pliska, V., Testa, B., van der Waterbeemd, H., Eds.; Wiley-VCH: Weinheim, Germany, 1996; Volume 4.
37. Zadrazilova, I.; Pospisilova, S.; Pauk, K.; Imramovsky, A.; Vinsova, J.; Cizek, A.; Jampilek, J. In vitro bactericidal activity of 4- and 5-chloro-2-hydroxy-N-[1-oxo-1-(phenylamino)alkan-2-yl]benzamides against MRSA. *Biomed Res. Int.* **2015**, *2015*, 349534. [[CrossRef](#)] [[PubMed](#)]
38. Zadrazilova, I.; Pospisilova, S.; Masarikova, M.; Imramovsky, A.; Monreal-Ferriz, J.; Vinsova, J.; Cizek, A.; Jampilek, J. Salicylanilide carbamates: Promising antibacterial agents with high in vitro activity against methicillin-resistant *Staphylococcus aureus*. *Eur. J. Pharm. Sci.* **2015**, *77*, 197–207. [[CrossRef](#)] [[PubMed](#)]
39. Oravcova, V.; Zurek, L.; Townsend, A.; Clark, A.B.; Ellis, J.C.; Cizek, A. American crows as carriers of vancomycin-resistant enterococci with vanA gene. *Environ. Microbiol.* **2014**, *16*, 939–949. [[CrossRef](#)] [[PubMed](#)]
40. Pospisilova, S.; Michnova, H.; Kauerova, T.; Pauk, K.; Kollar, P.; Vinsova, J.; Imramovsky, A.; Cizek, A.; Jampilek, J. In vitro activity of salicylamide derivatives against vancomycin-resistant enterococci. *Bioorg. Med. Chem. Lett.* **2018**, *28*, 2184–2188. [[CrossRef](#)] [[PubMed](#)]
41. Schwalbe, R.; Steele-Moore, L.; Goodwin, A.C. *Antimicrobial Susceptibility Testing Protocols*; CRC Press: Boca Raton, FL, USA, 2007.
42. Bonapace, C.R.; Bosso, J.A.; Friedrich, L.V.; White, R.L. Comparison of methods of interpretation of checkerboard synergy testing. *Diagn. Microbiol. Infect. Dis.* **2002**, *44*, 363–366. [[CrossRef](#)]
43. Helander, I.M.; Alakomi, H.L.; Latva-Kala, K.; Mattila-Sandholm, T.; Pol, I.; Smid, E.J.; Gorris, L.G.M.; von Wright, A. Characterization of the action of selected essential oil components on gram negative bacteria. *J. Agric. Food Chem.* **1998**, *46*, 3590–3595. [[CrossRef](#)]
44. Ultee, A.; Bennik, M.H.J.; Moezelaar, R. The phenolic hydroxyl group of carvacrol is essential for action against the food-borne pathogen *Bacillus cereus*. *Appl. Environ. Microbiol.* **2002**, *68*, 1561–1568. [[CrossRef](#)] [[PubMed](#)]
45. Gill, A.O.; Holley, R.A. Inhibition of membrane bound ATPases of *Escherichia coli* and *Listeria monocytogenes* by plant oil aromatics. *Int. J. Food Microbiol.* **2006**, *3*, 170–174. [[CrossRef](#)] [[PubMed](#)]
46. Langeveld, W.T.; Veldhuizen, E.J.; Burt, S.A. Synergy between essential oil components and antibiotics: A review. *Crit. Rev. Microbiol.* **2014**, *40*, 76–94. [[CrossRef](#)] [[PubMed](#)]
47. Hemaiswarya, S.; Doble, M. Synergistic interaction of phenylpropanoids with antibiotics against bacteria. *J. Med. Microbiol.* **2010**, *59*, 1469–1476. [[CrossRef](#)] [[PubMed](#)]
48. Kim, Y.G.; Lee, J.H.; Kim, S.I.; Baek, K.H.; Lee, J. Cinnamon bark oil and its components inhibit biofilm formation and toxin production. *Int. J. Food Microbiol.* **2015**, *195*, 30–39. [[CrossRef](#)] [[PubMed](#)]
49. Brackman, G.; Defoirdt, T.; Miyamoto, C.; Bossier, P.; Van Calenberg, S.; Nelis, H.; Coenye, T. Cinnamaldehyde and cinnamaldehyde derivatives reduce virulence in *Vibrio* spp. by decreasing the DNA-binding activity of the quorum sensing response regulator LuxR. *BMC Microbiol.* **2008**, *8*, 149. [[CrossRef](#)] [[PubMed](#)]
50. Zodrow, K.R.; Schiffman, J.D.; Elimelech, M. Biodegradable polymer (PLGA) coatings featuring cinnamaldehyde and carvacrol mitigate biofilm formation. *Langmuir* **2012**, *28*, 13993–13999. [[CrossRef](#)] [[PubMed](#)]
51. Jia, P.; Xue, Y.J.; Duan, X.J.; Shao, S.H. Effect of cinnamaldehyde on biofilm formation and sarA expression by methicillin-resistant *Staphylococcus aureus*. *Letts. Appl. Microbiol.* **2011**, *53*, 409–416. [[CrossRef](#)] [[PubMed](#)]
52. Brackman, G.; Coenye, T. Quorum sensing inhibitors as anti-biofilm agents. *Curr. Pharm. Des.* **2015**, *21*, 5–11. [[CrossRef](#)] [[PubMed](#)]
53. Niu, C.; Afre, S.; Gilbert, E.S. Subinhibitory concentrations of cinnamaldehyde interfere with quorum sensing. *Letts. Appl. Microbiol.* **2006**, *43*, 489–494. [[CrossRef](#)] [[PubMed](#)]

54. Nuryastuti, T.; van der Mei, H.C.; Busscher, H.J.; Iravati, S.; Aman, A.T.; Krom, B.P. Effect of cinnamon oil on icaA expression and biofilm formation by *Staphylococcus epidermidis*. *Appl. Environ. Microbiol.* **2009**, *75*, 6850–6855. [[CrossRef](#)] [[PubMed](#)]
55. Budzynska, A.; Wieckowska-Szakiel, M.; Sadowska, B.; Kalembe, D.; Rozalska, B. Antibiofilm activity of selected plant essential oils and their major components. *Pol. J. Microbiol.* **2011**, *60*, 35–41. [[PubMed](#)]
56. Kaplan, J.B. Antibiotic-induced biofilm formation. *Int. J. Artif. Organs* **2011**, *34*, 737–751. [[CrossRef](#)] [[PubMed](#)]
57. Mirani, Z.A.; Jamil, N. Effect of sub-lethal doses of vancomycin and oxacillin on biofilm formation by vancomycin intermediate resistant *Staphylococcus aureus*. *J. Basic Microbiol.* **2011**, *51*, 191–195. [[CrossRef](#)] [[PubMed](#)]
58. Zheng, H.; Lu, L.; Wang, B.; Pu, S.; Zhang, X.; Zhu, G.; Shi, W.; Zhang, L.; Wang, H.; Wang, S.; et al. Genetic basis of virulence attenuation revealed by comparative genomic analysis of *Mycobacterium tuberculosis* strain H37Ra versus H37Rv. *PLoS ONE* **2008**, *3*, e2375. [[CrossRef](#)] [[PubMed](#)]
59. Bueno, J. Antitubercular in vitro drug discovery: Tools for begin the search. In *Understanding Tuberculosis-New Approaches to Fighting against Drug Resistance*; Cardona, P.J., Ed.; InTech: Rijeka, Croatia, 2012; pp. 147–168.
60. Kos, J.; Zadrazilova, I.; Nevin, E.; Soral, M.; Gonec, T.; Kollar, P.; Oravec, M.; Coffey, A.; O'Mahony, J.; Liptaj, T.; et al. Ring-substituted 8-Hydroxyquinoline-2-carboxanilides as potential antimycobacterial agents. *Bioorg. Med. Chem.* **2015**, *23*, 4188–4196. [[CrossRef](#)] [[PubMed](#)]
61. Gonec, T.; Zadrazilova, I.; Nevin, E.; Kauerova, T.; Pesko, M.; Kos, J.; Oravec, M.; Kollar, P.; Coffey, A.; O'Mahony, J.; et al. Synthesis and biological evaluation of *N*-alkoxyphenyl-3-hydroxynaphthalene-2-carbox-anilides. *Molecules* **2015**, *20*, 9767–9787. [[CrossRef](#)] [[PubMed](#)]
62. Gonec, T.; Pospisilova, S.; Kauerova, T.; Kos, J.; Dohanosova, J.; Oravec, M.; Kollar, P.; Coffey, A.; Liptaj, T.; Cizek, A.; et al. *N*-Alkoxyphenylhydroxynaphthalenecarboxamides and their antimycobacterial activity. *Molecules* **2016**, *21*, 1068. [[CrossRef](#)] [[PubMed](#)]
63. Zumla, A.; Nahid, P.; Cole, S.T. Advances in the development of new tuberculosis drugs and treatment regimens. *Nat. Rev. Drug Discov.* **2013**, *12*, 388–404. [[CrossRef](#)] [[PubMed](#)]
64. Upadhayaya, R.S.; Vandavasi, J.K.; Kardile, R.A.; Lahore, S.V.; Dixit, S.S.; Deokar, H.S.; Shinde, P.D.; Sarmah, M.P.; Chattopadhyaya, J. Novel quinoline and naphthalene derivatives as potent antimycobacterial agents. *Eur. J. Med. Chem.* **2010**, *45*, 1854–1867. [[CrossRef](#)] [[PubMed](#)]
65. Wang, Z.; Li, L.; Zhou, Z.; Geng, Y.; Chen, Y.; Sun, T. Design, synthesis, configuration research, and in vitro antituberculosis activities of two chiral naphthylamine substituted analogs of bedaquiline. *J. Heterocycl. Chem.* **2017**, *54*, 1024–1030. [[CrossRef](#)]
66. Tong, A.S.T.; Choi, P.J.; Blaser, A.; Sutherland, H.S.; Tsang, S.K.Y.; Guillemont, J.; Motte, M.; Cooper, C.B.; Andries, K.; van den Broeck, W.; et al. 6-Cyano analogues of bedaquiline as less lipophilic and potentially safer diarylquinolines for tuberculosis. *ACS Med. Chem. Lett.* **2017**, *8*, 1019–1024. [[CrossRef](#)] [[PubMed](#)]
67. Chen, Y.L.; Huang, S.T.; Sun, F.M.; Chiang, Y.L.; Chiang, C.J.; Tsai, C.M.; Weng, C.J. Transformation of cinnamic acid from trans- to cis-form raises a notable bactericidal and synergistic activity against multiple-drug resistant *Mycobacterium tuberculosis*. *Eur. J. Pharm. Sci.* **2011**, *43*, 188–194. [[CrossRef](#)] [[PubMed](#)]
68. De, P.; Koumba, Y.G.; Constant, P.; Bedos-Belval, F.; Duran, H.; Saffon, N.; Daffe, M.; Baltas, M. Design, synthesis, and biological evaluation of new cinnamic derivatives as antituberculosis agents. *J. Med. Chem.* **2011**, *54*, 1449–1461. [[CrossRef](#)] [[PubMed](#)]
69. De, P.; Veau, D.; Bedos-Belval, F.; Chassaing, S.; Baltas, M. Cinnamic derivatives in tuberculosis. In *Understanding Tuberculosis-New Approaches to Fighting against Drug Resistance*; Cardona, P.J., Ed.; InTech: Rijeka, Croatia, 2012; pp. 337–362.
70. Adeniji, S.E.; Uba, S.; Uzairu, A. Quantitative structure–activity relationship and molecular docking of 4-alkoxy-cinnamic analogues as anti-mycobacterium tuberculosis. *J. King Saud Uni. Sci.* **2018**. [[CrossRef](#)]
71. Degola, F.; Morcia, C.; Bisceglie, F.; Mussi, F.; Tumino, G.; Ghizzoni, R.; Pelosi, G.; Terzi, V.; Buschini, A.; Restivo, F.M.; et al. In vitro evaluation of the activity of thiosemicarbazone derivatives against mycotoxigenic fungi affecting cereals. *Int. J. Food Microbiol.* **2015**, *200*, 104–111. [[CrossRef](#)] [[PubMed](#)]
72. Zhou, K.; Chen, D.; Li, B.; Zhang, B.; Miao, F.; Zhou, L. Bioactivity and structure-activity relationship of cinnamic acid esters and their derivatives as potential antifungal agents for plant protection. *PLoS ONE* **2017**, *12*, e0176189. [[CrossRef](#)] [[PubMed](#)]

73. Krishnendu, A.; Dutta, A.K.; Pradhan, P. Bipolaris sorokiniana'(Sacc.) Shoem.: The most destructive wheat fungal pathogen in the warmer areas. *Aust. J. Crop Sci.* **2011**, *5*, 1064–1071.
74. Saari, E.E. Leaf blight disease and associated soil borne fungal pathogens of wheat in South and Southeast Asia. In *Helminthosporium Blights of Wheat: Spot Blotch and Tan Spot*; Duveiller, E., Dubin, H.J., Reeves, J., McNab, A., Eds.; CIMMYT: Texcoco de Mora, Mexico, 1998; pp. 37–51.
75. Sundheim, L.; Brodal, G.; Hofgaard, I.S.; Rafoss, T. Temporal variation of mycotoxin producing fungi in norwegian cereals. *Microorganisms* **2013**, *1*, 188–198. [[CrossRef](#)] [[PubMed](#)]
76. Placinta, C.M.; D'Mello, J.P.F.; MacDonald, A.M.C. A review of worldwide contamination of cereal grains and animal feed with Fusarium mycotoxins. *Anim. Feed Sci. Technol.* **1999**, *78*, 21–37. [[CrossRef](#)]
77. Tortora, G.J.; Funke, B.R.; Case, C.L. *Microbiology: An introduction*, 10th ed.; Benjamin Cummings: San Francisco, CA, USA, 2010.
78. ROCHE. Cell proliferation reagent WST-1. Roche Diagnostics GmbH, Mannheim, Germany. 2011. Available online: <https://www.sigmaaldrich.com/content/dam/sigma-aldrich/docs/Roche/Bulletin/1/cellproprbul.pdf> (accessed on 26 June 2018).
79. Kauerova, T.; Kos, J.; Gonec, T.; Jampilek, J.; Kollar, P. Antiproliferative and pro-apoptotic effect of novel nitro-substituted hydroxynaphthanilides on human cancer cell lines. *Int. J. Mol. Sci.* **2016**, *17*, 1219. [[CrossRef](#)] [[PubMed](#)]
80. Suffness, M.; Douros, J. Current status of the NCI plant and animal product program. *J. Nat. Prod.* **1982**, *45*, 1–14. [[CrossRef](#)] [[PubMed](#)]
81. Jampilek, J.; Kralova, K.; Pesko, M.; Kos, J. Ring-substituted 8-hydroxyquinoline-2-carboxanilides as photosystem II inhibitors. *Bioorg. Med. Chem. Lett.* **2016**, *26*, 3862–3865. [[CrossRef](#)] [[PubMed](#)]
82. Fajkusova, D.; Pesko, M.; Keltosova, S.; Guo, J.; Oktabec, Z.; Vejsova, M.; Kollar, P.; Coffey, A.; Csollei, J.; Kralova, K.; et al. Anti-infective and herbicidal activity of N-substituted 2-aminobenzothiazoles. *Bioorg. Med. Chem.* **2012**, *20*, 7059–7068. [[CrossRef](#)] [[PubMed](#)]
83. Gonec, T.; Kos, J.; Zadrazilova, I.; Pesko, M.; Govender, R.; Keltosova, S.; Kollar, B.; Imramovsky, A.; O'Mahony, J.; Coffey, A.; et al. Antibacterial and herbicidal activity of ring-substituted 2-hydroxynaphthalene-1-carboxanilides. *Molecules* **2013**, *18*, 9397–9419. [[CrossRef](#)] [[PubMed](#)]
84. Kralova, K.; Sersen, F.; Cizmarik, J. Inhibitory effect of piperidinoethylesters of alkoxyphenylcarbamic acids on photosynthesis. *Gen. Physiol. Biophys.* **1992**, *11*, 261–267.
85. Kralova, K.; Bujdakova, H.; Kuchta, T.; Loos, D. Correlation between biological activity and the structure of 6-amino-2-R-thiobenzothiazoles. Anti-yeast activity and inhibition of photochemical activity of chloroplasts. *Pharmazie* **1994**, *49*, 460–461. [[PubMed](#)]
86. Kralova, K.; Kallova, J.; Loos, D.; Devinsky, F. Correlation between biological activity and the structure of N,N'-bis(alkyldimethyl)-1,6-hexanediammonium dibromides. Antibacterial activity and inhibition of photochemical activity of chloroplasts. *Pharmazie* **1994**, *49*, 857–858. [[PubMed](#)]
87. Kralova, K.; Bujdakova, H.; Cizmarik, J. Antifungal and antialgal activity of piperidinopropyl esters of alkoxy substituted phenylcarbamic acids. *Pharmazie* **1995**, *50*, 440–441. [[PubMed](#)]
88. Szabo, E. Isolation and characterization of EBR specific induced chitinases from tobacco (*Nicotiana tabacum*). *Acta Biol. Szeged.* **2008**, *52*, 251–252.
89. Zhang, M.; Lu, X.; Zhang, H.J.; Li, N.; Xiao, Y.; Zhu, H.L.; Ye, Y.H. Synthesis, structure, and biological assay of cinnamic amides as potential EGFR kinase inhibitors. *Med. Chem. Res.* **2013**, *22*, 986–994. [[CrossRef](#)]
90. Lee, C.C.; Lo, Y.; Ho, L.J.; Lai, J.H.; Lien, S.B.; Lin, L.C.; Chen, C.L.; Chen, T.C.; Liu, F.C.; Huang, H.S. A new application of parallel synthesis strategy for discovery of amide-linked small molecules as potent chondroprotective agents in TNF- α -stimulated chondrocytes. *PLoS ONE* **2016**, *11*, e0149317. [[CrossRef](#)] [[PubMed](#)]
91. Clinical and Laboratory Standards Institute. *Performance Standards for Antimicrobial Susceptibility Testing*; The 8th Informational Supplement Document; CLSI: Wayne, PA, USA, 2012; M100-S22.
92. Abate, G.; Mshana, R.N.; Miorner, H. Evaluation of a colorimetric assay based on 3-(4,5-dimethylthiazol-2-yl)-2,5-diphenyl tetrazolium bromide (MTT) for rapid detection of rifampicin resistance in *Mycobacterium tuberculosis*. *Int. J. Tuberc. Lung Dis.* **1998**, *2*, 1011–1016. [[PubMed](#)]
93. De Lucca, A.J.; Walsh, T.J.; Daigle, D.J. N-acetylcysteine inhibits germination of conidia and growth of *Aspergillus* spp. and *Fusarium* spp. *Antimicrob. Agents Chemother.* **1996**, *40*, 1274–1276. [[PubMed](#)]

94. Masarovicova, E.; Kralova, K. Approaches to Measuring Plant Photosynthesis Activity. In *Handbook of Photosynthesis*, 2nd ed.; Pessarakli, M., Ed.; Taylor & Francis Group: Boca Raton, FL, USA, 2005; pp. 617–656.
95. Kralova, K.; Sersen, F.; Sidoova, E. Photosynthesis inhibition produced by 2-alkylthio-6-R-benzothiazoles. *Chem. Pap.* **1992**, *46*, 348–350.



© 2018 by the authors. Licensee MDPI, Basel, Switzerland. This article is an open access article distributed under the terms and conditions of the Creative Commons Attribution (CC BY) license (<http://creativecommons.org/licenses/by/4.0/>).

č.	citace	ISSN
12	KOS, J , CF KU, I KAPUSTIKOVA, M ORAVEC, HJ ZHANG a J JAMPILEK. 8-Hydroxyquinoline-2-Carboxanilides as Antiviral Agents Against Avian Influenza Virus. <i>CHEMISTRYSELECT</i> [online]. 2019, 4 (15), 4582–4587. Dostupné z: doi: 10.1002/slct.201900873	2365-6549

Medicinal Chemistry & Drug Discovery

8-Hydroxyquinoline-2-Carboxanilides as Antiviral Agents Against Avian Influenza Virus

Jiri Kos⁺,^[a] Chuen Fai Ku⁺,^[b] Iva Kapustikova,^[a] Michal Oravec,^[c] Hong-Jie Zhang,^{*[b]} and Josef Jampilek^{*[d, e]}

Series of thirty-two mono-, di- and tri-substituted 8-hydroxyquinoline-2-carboxanilides were prepared by microwave-assisted synthesis. The compounds were characterized, and their lipophilicity was experimentally determined. Primary *in vitro* screening of the cytotoxicity of all the synthesized compounds was performed using adenocarcinomic human alveolar basal epithelial cells (A549), and determined nontoxic compounds were then tested for their activity against highly pathogenic H5N1 avian influenza virus. 8-Hydroxy-*N*-(3,4,5-trichlorophenyl)quinoline-2-carboxamide, *N*-(3-chloro-2-fluorophenyl)-8-hydroxyquinoline-2-carboxamide and *N*-(3,4-dichlorophenyl)-8-hydrox-

quinoline-2-carboxamide demonstrated the highest activity within the investigated series ($IC_{50} = 11.3, 21.2$ and $31.2 \mu\text{M}$, respectively), while *N*-(4-chloro-2-fluorophenyl)-8-hydroxyquinoline-2-carboxamide expressed the highest cytotoxic effect ($CC_{50} = 31.6 \mu\text{M}$). In general, the inhibitory activity of the compounds depends on the position of halogen substituents on the anilide ring and is also affected by the lipophilicity and electron properties of individual substituents of the anilide part of the molecule. The structure-activity relationships are discussed.

Introduction

The quinoline scaffold, especially the 8-hydroxyquinoline scaffold can be considered as a privileged structure,^[1–3] because quinoline-based compounds demonstrate a wide spectrum of biological activities such as anti-inflammatory, cardiovascular, anticonvulsant, antiproliferative, antiprotozoal, antifungal and antibacterial activities.^[2,5–15] They are able to affect specifically many different target structures in cells and are known metal chelators. Thus, their mechanisms of action can be considered as complex,^[2,4–6,13,14] which meets the modern definition of so-called multi-target agents.^[16] Within the investigation of simple derivatives of 8-hydroxyquinolines,^[17–19] 8-hydroxyquinoline-2-

carboxanilides were prepared, and their antimycobacterial and antibacterial activities were described.^[20–22] In addition, these compounds have also proven to be strong inhibitors of photosynthetic electron transport (PET) in photosystem II.^[23]

The influenza disease caused by infection with the highly pathogenic avian influenza H5N1 virus is one of the most devastating zoonotic viral infectious diseases affecting humans worldwide. At present, only two classes of antiviral drugs, M2 ion channel blockers and neuraminidase inhibitors, are approved for the prevention and treatment of influenza virus infections, but their utility has been limited by their low effectiveness in killing the virus, their side effects and the rapid emergence of drug-resistant viral strains.^[24] Although a number of different classes of natural compounds have been studied for their anti-H5N1 activity, no quinolone alkaloids have been investigated as agents against avian influenza.^[25] Recently, quinoline-based compounds were reported to show antiviral properties,^[2,26–29] and thus, in the context of the above-mentioned facts, 8-hydroxyquinoline-2-carboxanilides were subjected to the primary screening on anti-avian influenza activity.

This study is a follow-up contribution to previously published papers^[7,8,12,20–23] investigating a compound library comprising 8-hydroxyquinolinecarboxanilides to counteract the deadly H5N1 virus. Based on the results of the primary screening of a mono-substituted anilides as an original series, it was completed by specifically designed new di- and tri-substituted anilides, and the structure-activity relationships (SAR) of all the mentioned compounds have been investigated.

[a] Dr. J. Kos,⁺ Dr. I. Kapustikova

Department of Pharmaceutical Chemistry, Faculty of Pharmacy, Comenius University, Odbojarov 10, Bratislava 83232, Slovakia

[b] Dr. C. F. Ku,⁺ Prof. H.-J. ZhangSchool of Chinese Medicine, Hong Kong Baptist University, 7 Baptist University Road, Kowloon Tong, Kowloon, Hong Kong SAR China
E-mail: zhanghj@hkbu.edu.hk

[c] Dr. M. Oravec

Global Change Research Centre AS CR, Belidla 986/4a, 603 00 Brno, Czech Republic


[d] Prof. J. Jampilek

Department of Analytical Chemistry, Faculty of Natural Sciences, Comenius University, Ilkovicova 6, 842 15 Bratislava, Slovakia
E-mail: josef.jampilek@gmail.com

[e] Prof. J. Jampilek

Division of Biologically Active Complexes and Molecular Magnets, Regional Centre of Advanced Technologies and Materials, Faculty of Science, Palacky University Olomouc, Slechtitelu 27, 78371 Olomouc, Czech Republic

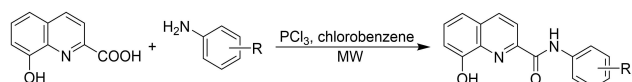
[†] These authors contributed equally to this work.

 Supporting information for this article is available on the WWW under <https://doi.org/10.1002/slct.201900873>

Results and Discussion

Chemistry and physicochemical properties

The discussed 8-hydroxyquinoline-2-carboxanilides were prepared via microwave-assisted synthesis in high yields in short reaction time based on the recently published study.^[20] The condensation of activated 8-hydroxyquinoline-2-carboxylic acid by phosphorus trichloride with ring-substituted aniline in chlorobenzene gave a series of target compounds 1–32, see Scheme 1.



Scheme 1. Synthesis of ring-substituted 8-hydroxyquinoline-2-carboxanilides 1–32.

Diverse molecular parameters are used to determine structure-activity relationships (SAR). Lipophilicity and electronic properties are among the most frequent ones. Therefore, the lipophilicity of studied compounds 1–32 was determined as $\log k$ value using reversed-phase high-performance liquid chromatography (RP-HPLC). The analysis was performed under isocratic conditions with methanol as an organic modifier in the mobile phase using an end-capped nonpolar C18 stationary RP column. The results are shown in Table 1. Hammett's σ parameters were used for the description of electronic properties of the whole anilide core, see Table 1. They were calculated using ACD/Percepta ver. 2012 (Advanced Chemistry Development Inc., Toronto, ON, Canada, 2012).

In vitro activity against avian influenza virus

At first, monosubstituted 8-hydroxyquinoline-2-carboxanilides 1–22, described recently by Kos et al.,^[20] were evaluated against H5N1 influenza virus. Anti-influenza activity was expressed as % of growth inhibition (GI) of H5N1 virus cultivated in the adenocarcinomic human alveolar basal epithelial cells (A549) at concentration 20 $\mu\text{g}/\text{mL}$. Based on the results presented in Table 1, it is evident that most compounds did not show any antiviral activity or demonstrated only moderate activity. In addition, some of the derivatives exhibiting an antiviral effect demonstrated simultaneously cytotoxicity expressed as % of GI of the A549 cells. For example, the following compounds expressed disadvantageous cytotoxicity/activity rate: **19** ($R = 4\text{-CF}_3$, $\text{GI} = 17.8/22.5\%$), **10** ($R = 4\text{-F}$, $\text{GI} = 34.9/35.0\%$) and **11** ($R = 2\text{-Cl}$, $\text{GI} = 33.5/20.0\%$). *N*-(3-fluorophenyl)-8-hydroxyquinoline-2-carboxamide (**9**) demonstrated the highest cytotoxic effect ($\text{GI} = 44.2\%$) among the monosubstituted derivatives. On the other hand, several compounds with noteworthy activity can be found among the monosubstituted derivatives, e.g., 8-hydroxy-*N*-(3-nitrophenyl)quinoline-2-carboxamide (**21**, $\text{GI} = 85.0\%$) and *N*-(4-chlorophenyl)-8-hydroxyquinoline-2-car-

Table 1. Structures of ring-substituted 8-hydroxyquinoline-2-carboxanilides 1–32, determined $\log k$ values, calculated values of electronic σ parameters of anilide (σ_{Ar}) ring and inhibition (%) of A549 cells growth as well as H5N1 virus growth cultivated in A549 at conc. 20 $\mu\text{g}/\text{mL}$.

Comp.	R	$\log k$	$\sigma_{\text{Ar}}^{[a]}$	% inhibition \pm SD	
				A549 tox.	H5N1 in A549
1 ^[b]	H	0.2389	0.6	1.1 \pm 3.8	-93.9 \pm 14.3
2 ^[b]	2-OCH ₃	0.2556	0.11	8.7 \pm 1.9	-20.0 \pm 0.0
3 ^[b]	3-OCH ₃	0.2729	0.66	28.5 \pm 4.2	-8.3 \pm 13.7
4 ^[b]	4-OCH ₃	0.1962	0.36	6.0 \pm 3.6	15.0 \pm 0.0
5 ^[b]	2-CH ₃	0.1877	0.59	21.1 \pm 5.5	-42.9 \pm 1.6
6 ^[b]	3-CH ₃	0.4106	0.48	28.2 \pm 6.9	2.5 \pm 10.6
7 ^[b]	4-CH ₃	0.2947	0.46	6.7 \pm 3.3	20.0 \pm 35.4
8 ^[b]	2-F	0.1708	1.02	17.7 \pm 2.5	-94.0 \pm 26.3
9 ^[b]	3-F	0.3826	0.82	44.2 \pm 1.6	17.5 \pm 10.6
10 ^[b]	4-F	0.3579	0.62	34.9 \pm 2.0	35.0 \pm 7.1
11 ^[b]	2-Cl	0.3998	1.05	33.5 \pm 5.4	20.0 \pm 21.2
12 ^[b]	3-Cl	0.5754	0.85	17.6 \pm 4.9	-52.5 \pm 53.0
13 ^[b]	4-Cl	0.5509	0.75	12.9 \pm 4.6	37.5 \pm 31.8
14 ^[b]	2-Br	0.4841	0.97	15.9 \pm 1.2	7.5 \pm 38.9
15 ^[b]	3-Br	0.6196	0.86	10.7 \pm 7.1	-17.5 \pm 10.6
16 ^[b]	4-Br	0.6185	0.74	5.0 \pm 6.8	0.0 \pm 7.1
17 ^[b]	2-CF ₃	0.3544	0.91	27.8 \pm 2.4	-7.5 \pm 10.6
18 ^[b]	3-CF ₃	0.6918	0.89	9.8 \pm 3.4	-70.0 \pm 56.6
19 ^[b]	4-CF ₃	0.7409	0.95	17.8 \pm 0.7	22.5 \pm 3.5
20 ^[b]	2-NO ₂	0.5684	1.12	26.7 \pm 2.8	-160.0 \pm 21.2
21 ^[b]	3-NO ₂	0.4140	1.09	4.0 \pm 7.0	85.0 \pm 3.8
22 ^[b]	4-NO ₂	0.4708	1.14	12.4 \pm 4.5	-120.0 \pm 99.0
23	2,4-Cl	0.7402	1.12	2.7 \pm 1.4	-82.0 \pm 34.1
24	3,4-Cl	0.8775	1.19	-11.0 \pm 8.6	62.6 \pm 2.7
25	3,5-Cl	1.0225	1.11	13.7 \pm 4.0	12.1 \pm 17.2
26	2,4,6-Cl	0.4652	1.48	-12.5 \pm 8.3	-151.9 \pm 30.6
27	3,4,5-Cl	1.2562	1.46	2.4 \pm 1.3	79.3 \pm 1.5
28	3-Cl-2-F	1.4382	1.27	9.7 \pm 3.3	91.2 \pm 2.1
29	3-Cl-4-F	0.6444	1.25	5.6 \pm 2.2	-140.8 \pm 36.0
30	5-Cl-2-F	0.4843	1.27	17.3 \pm 2.4	-11.5 \pm 3.9
31	4-Cl-2-F	0.4884	1.17	67.4 \pm 0.7 ^[c]	-
32	2,4-NO ₂	-0.2129	1.66	10.8 \pm 4.4	33.1 \pm 17.8

[a] calculated using ACD/Percepta ver. 2012 (Advanced Chemistry Development, Toronto, ON, Canada); [b] published in Kos et al.^[20]; [c] the compound is cytotoxic with CC_{50} value 31.6 \pm 1.2 μM .

boxamide (**13**, $\text{GI} = 37.5\%$), while their cytotoxicity was insignificant: $\text{GI} = 4.0$ and 12.9% , respectively.

Based on these data, the dependence of the H5N1 virus growth-inhibiting activity (expressed in %) on the experimentally determined lipophilicity (expressed as $\log k$) of the discussed mono-*N*-aryl substituted anilides is shown in Figure 1A, and the dependence on the electron σ parameters of the whole *N*-aryl part of individual anilides is illustrated in Figure 1B. Although only a limited number of derivatives may be taken into account, it can be stated that the antiviral activity is influenced by increasing electron-withdrawing properties of substituents on the anilide ring (correlation coefficient $r = 0.9795$, $n = 4$) (Figure 1B). On the other hand, the antiviral

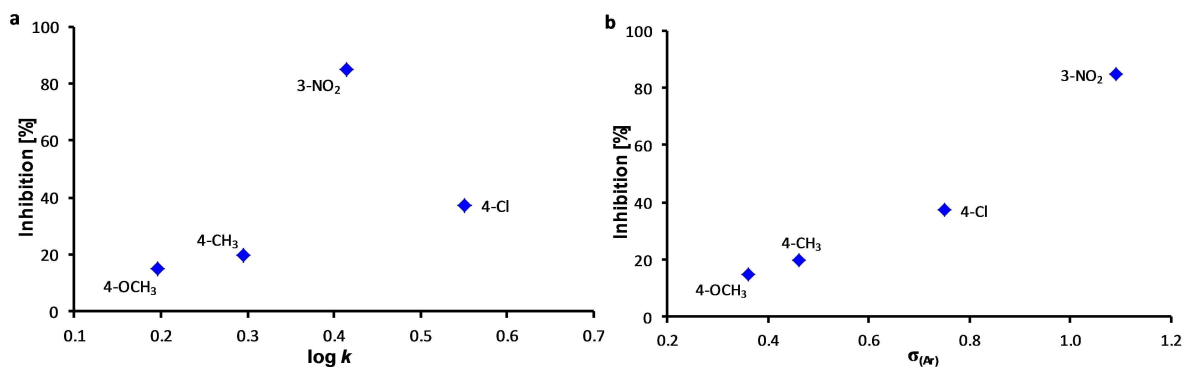


Figure 1. Dependence of H5N1 virus growth-inhibiting activity (%) on lipophilicity expressed as log k (a) and electronic σ parameters of whole N -aryl part of individual monosubstituted anilides (b).

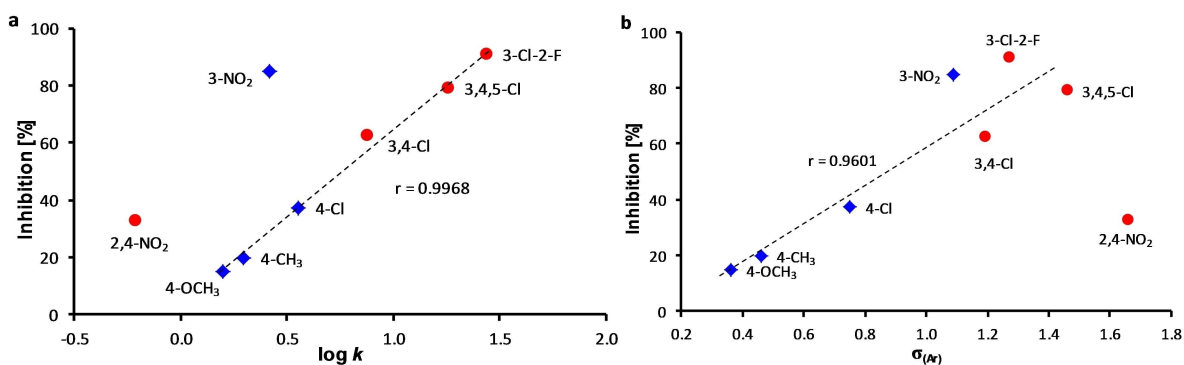


Figure 2. Dependence of H5N1 virus growth-inhibiting activity (%) on lipophilicity expressed as log k (a) and electronic σ parameters of whole N -aryl part of individual mono-, di- and tri-substituted anilides (b).

effect seems to be positively influenced by increasing lipophilicity; in this manner, compound **21** ($R = 3\text{-NO}_2$, log k ca. 0.41) showed maximum activity at insignificant cytotoxicity.

Based on the above-mentioned observations, new di- and tri-substituted derivatives were designed. The synthesis of derivatives with a chloro-substituent in *meta* and *para* positions of the anilide ring was more preferred than that of various *meta*-nitro substituted anilines due to the risk of the higher cytotoxicity of nitro-substituted derivatives.^[9,11,30–33] Thus, ten new compounds were prepared and tested, of which four, compounds **24** ($R = 3,4\text{-Cl}$), **27** ($3,4,5\text{-Cl}$), **28** (3-Cl-2-F), **32** ($2,4\text{-NO}_2$), showed high inhibition of H5N1 growth and simultaneously low cytotoxicity. It is interesting that compound **28** ($R = 3\text{-Cl-2-F}$) demonstrated 91.2% virus growth-inhibitory activity but only 9.7% inhibition against A549 cells, while the movement of the fluoro substituent to $C'_{(4)}$ position (compound **29**) caused a total loss of activity resulting in $\text{GI} = -140.8/5.6\%$ in addition to increased toxicity, similarly as the movement of the chloro-substituent to $C'_{(5)}$ position (compound **30**, $\text{GI} = -11.5/17.3\%$). Fluorine in $C'_{(2)}$ position and the change of the chloro-substituent from $C'_{(3)}$ to $C'_{(4)}$ position gave N -(4-chloro-2-fluorophenyl)-8-hydroxyquinoline-2-carboxamide (**31**), which had significantly increased toxicity. Compound **31** expressed the highest cytotoxic effect ($\text{CC}_{50} = 31.6 \mu\text{M}$) among all the screened derivatives. A similar situation was observed for

derivatives **23–25** and **26/27** that differed from each other only by the position of the chlorine atom on the anilide core. Compound **24** ($R = 3,4\text{-Cl}$, $\text{GI} = 62.6/-11.0\%$) is effective without toxic effect. Change of the position of one chlorine atom from $C'_{(3)}$ to $C'_{(2)}$ position (compound **23**) led again to a total loss of effect and a slight increase of toxicity ($\text{GI} = -82.0/2.7\%$), while two chlorine atoms in the *meta* positions of anilide caused an increase of activity but also toxicity (compound **25**, $\text{GI} = 12.1/13.7\%$). It was also observed that disadvantageous di-*ortho*-positions of two chlorine atoms resulted in the loss of activity (compound **26**, $\text{GI} = -151.9/-12.5\%$) contrary to di-*meta*- and *para*-positions (compound **27**, $\text{GI} = 79.3/2.4\%$). Based on these facts, it can be stated that the position of substituents seems to be a critical factor affecting the antiviral activity and cytotoxicity.

The dependences of the antiviral activity on the lipophilicity (log k) and the electron σ parameters of the whole N -aryl part of individual anilides are shown in Figures 2A and 2B, respectively. Compounds **24**, **27**, **28**, **32** were additionally plotted on the graphs for better lucidity and SAR interpretation. Based on the dependences, it is evident that the above-mentioned expectations were true. After the completion of the series of compounds, antiviral activity linearly increased with increasing lipophilicity ($r = 0.9968$, $n = 6$) from derivative **4** ($R = 4\text{-OCH}_3$) to compound **28** ($R = 3\text{-Cl-2-F}$). Both nitro

derivatives, **21** and **32**, lie out of this dependence due to different properties of the nitro moiety in comparison with halogen or alkyl moieties. In addition, the antiviral effect is positively influenced by increasing electron-withdrawing properties of anilide substituents ($r = 0.9601$, $n = 7$). Based on the results, it can be supposed that lipophilicity with $\log k$ ca.1.4 and electron properties with σ ca.1.3 seem to be advantageous for antiviral efficacy.

Consequently, the IC_{50} values (compound concentration causing 50% inhibition of H5N1 proliferation) were determined (Table 2) for the most effective compounds, and selectivity

Comp.	R	IC_{50} [μ M]	CC_{50} [μ M]	SI
21	3-NO ₂	26.3	>60	>2.5
24	3,4-Cl	31.2	>60	>1.9
27	3,4,5-Cl	11.3	>60	>4.8
28	3-Cl-2-F	21.2	>60	>3.0

indices of individual compounds were calculated as well. The dependences of the antiviral activity expressed as IC_{50} values on lipophilicity and electron parameters are illustrated in Figures 3A and 3B, respectively. These results include not only H5N1 antiproliferative activity but also cytotoxicity against A549 cells (contrary to the results illustrated in Figures 2A and 2B), which leads to a change in the "order" of compounds **28** and **27**, the latter of which possesses a preferable toxicology profile. Nevertheless, it is important that the main trends for antiviral efficacy, i.e. higher lipophilicity and strong electron-withdrawing properties are preserved and preferred.

To verify the anti-influenza (H5N1) specificity of effective compounds, they were screened with HIV/VSV pseudovirions, which have the same HIV backbone but expressed a different envelop protein, Vesicular stomatitis virus glycoprotein.^[34] These compounds did not inhibit the entry of HIV/VSV, while they displayed the inhibition of H5N1 glycoprotein-mediated entry, see Figure 4. The selected quinolines could directly target the H5N1 glycoprotein or critical host factors for viral entry. In

further investigation, the anti-influenza mechanism of the effective quinolines will be evaluated.

Conclusions

Series of twenty-two monosubstituted and ten di- and tri-substituted 8-hydroxyquinoline-2-carboxanilides were prepared and characterized. All the compounds were tested for their cytotoxicity against the A549 cell line and consequently were tested for their activity against pathogenic H5N1 influenza virus. *N*-(3-fluorophenyl)-8-hydroxyquinoline-2-carboxamide (**9**) demonstrated the highest cytotoxic effect (A549 growth inhibition 44.2%) among the monosubstituted derivatives. *N*-(4-chloro-2-fluorophenyl)-8-hydroxyquinoline-2-carboxamide (**31**) expressed the highest cytotoxic effect ($CC_{50} = 31.6 \mu$ M) among all the studied compounds, and thus, it has potential to be further investigated as an antineoplastic agent. 8-Hydroxy-*N*-(3-nitrophenyl)quinoline-2-carboxamide (**21**) and *N*-(4-chlorophenyl)-8-hydroxyquinoline-2-carboxamide (**13**) showed the highest H5N1-inhibiting activity among monosubstituted derivatives (85.0 and 37.5%, respectively). The IC_{50} values were determined for the most effective and insignificantly A549 toxic compounds: 8-hydroxy-*N*-(3,4,5-trichlorophenyl)quinoline-2-carboxamide (**27**, $IC_{50} = 11.3 \mu$ M), *N*-(3-chloro-2-fluorophenyl)-8-hydroxyquinoline-2-carboxamide (**28**, $IC_{50} = 21.2 \mu$ M) and *N*-(3,4-dichlorophenyl)-8-hydroxyquinoline-2-carboxamide (**24**, $IC_{50} = 31.2 \mu$ M). The position of substituents on the anilide ring is a critical factor influencing the antiviral efficacy and especially cytotoxicity. Particularly substitution by chlorine in both *meta* and at the same time in *para* positions is the most preferable. The antiviral activity increases with electron-withdrawing properties of anilide substituents as well as with increasing lipophilicity. The effective compounds were identified as avian influenza (H5N1) virus-specific entry inhibitors.

Supporting Information Summary

Detail information on synthesis, characterization and biological evaluation of the investigated compounds including used reagents, procedures and instruments is provided in Experimental Section.

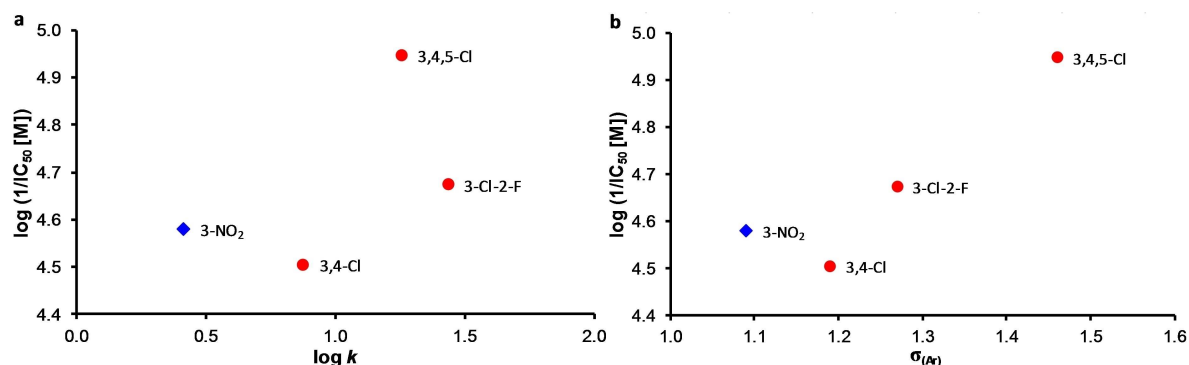


Figure 3. Dependence of antiviral activity against H5N1 expressed as $\log 1/IC_{50}$ [M] of selectively tested compounds on lipophilicity expressed as $\log k$ (a) and on electron σ constants of *N*-aryl part of individual mono- and di-substituted anilides (b).

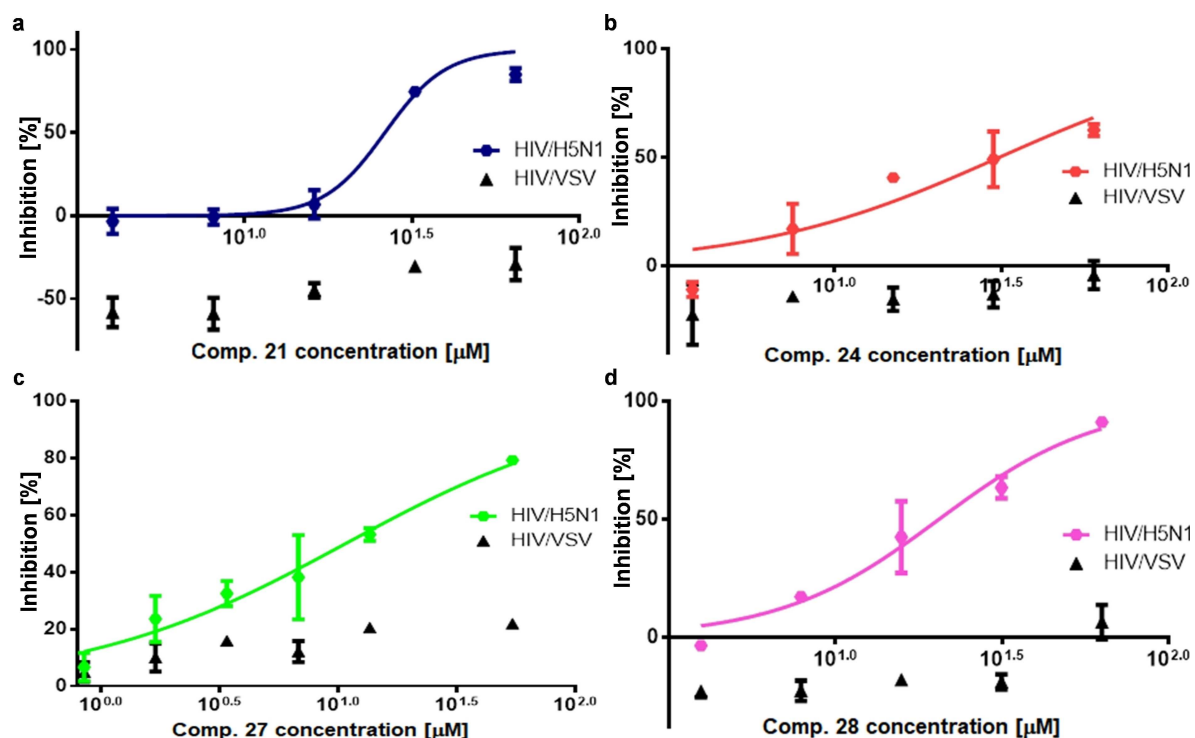


Figure 4. Inhibitory effect of most potent compounds on HIV/H5N1 and HIV/VSV infectivity investigated using A549 cells.

Acknowledgments

This study was supported by the Hong Kong Baptist University (HKBU) Interdisciplinary Research Matching Scheme (RC-IRMS/15-16/02) and the Research Grants Council of the Hong Kong Special Administrative Region, China (Project No. HKBU 12103917 and 12103618). In addition, the investigation was supported by VEGA 1/0770/15 and by APVV-17-0373. The HPLC/HRMS system forms a part of the National Infrastructure CzeCOS ProCES CZ.02.1.01/0.0/0.0/16_013/0001609; Michal Oravec was supported by the National Sustainability Program (NPU I; Grant No. LO1415). Josef Jampilek gratefully thanks the National Program of Sustainability I (LO1305) of the Ministry of Education, Youth and Sports of the Czech Republic for the financial support.

Conflict of Interest

The authors declare no conflict of interest.

Keywords: cytotoxicity · H5N1 influenza virus · hydroxyquinolinecarboxanilides · lipophilicity · microwave-assisted synthesis · structure-activity relationships

- [1] J. Polanski, A. Kurczyk, A. Bak, R. Musiol, *Curr. Med. Chem.* **2012**, *19*, 1921–1945.
- [2] Y. Song, H. Xu, W. Chen, P. Zhan, X. Liu, *Med. Chem. Commun.* **2015**, *6*, 61–74.
- [3] J. Jampilek, *Curr. Med. Chem.* **2014**, *21*, 4347–4373.
- [4] J. Jampilek, *Curr. Med. Chem.* **2018**, *25*, 4972–5006.
- [5] R. Musiol, *Expert Opin. Drug Discov.* **2017**, *12*, 583–597.
- [6] J. Jampilek, *Curr. Org. Chem.* **2017**, *21*, 1824–1846.

- [7] R. Musiol, J. Jampilek, V. Buchta, L. Silva, H. Niedbala, B. Podeszwa, A. Palka, K. Majerz-Maniecka, B. Oleksyn, J. Polanski, *Bioorg. Med. Chem.* **2006**, *14*, 3592–3598.
- [8] R. Musiol, J. Jampilek, K. Kralova, D. R. Richardson, D. Kalinowski, B. Podeszwa, J. Finster, H. Niedbala, A. Palka, J. Polanski, *Bioorg. Med. Chem.* **2007**, *15*, 1280–1288.
- [9] B. Podeszwa, H. Niedbala, J. Polanski, R. Musiol, D. Tabak, J. Finster, K. Serafin, J. Wietrzyk, S. Boryczka, W. Mol, J. Jampilek, J. Dohnal, D. S. Kalinowski, D. R. Richardson, *Bioorg. Med. Chem. Lett.* **2007**, *17*, 6138–6141.
- [10] J. Jampilek, R. Musiol, J. Finster, M. Pesko, J. Carroll, K. Kralova, M. Vejsova, J. O'Mahony, A. Coffey, J. Dohnal, J. Polanski, *Molecules* **2009**, *14*, 4246–4265.
- [11] A. Mrozek-Wilczkiewicz, D. Kalinowski, R. Musiol, J. Finster, A. Szurko, K. Serafin, M. Knas, S. K. Kamalapuram, Z. Kovacevic, J. Jampilek, A. Ratuszna, J. Rzeszowska-Wolny, D. R. Richardson, J. Polanski, *Bioorg. Med. Chem.* **2010**, *18*, 2664–2671.
- [12] W. Cieslik, R. Musiol, J. Nycz, J. Jampilek, M. Vejsova, M. Wolff, B. Machura, J. Polanski, *Bioorg. Med. Chem.* **2012**, *20*, 6960–6968.
- [13] R. Musiol, K. Malarz, J. Mularski, *Curr. Org. Chem.* **2017**, *21*, 1896–1906.
- [14] K. Pavic, I. Perkovic, S. Pospisilova, M. Machado, D. Fontinha, M. Prudencio, J. Jampilek, A. Coffey, L. Endersen, H. Rimac, B. Zorc, *Eur. J. Med. Chem.* **2018**, *143*, 769–779.
- [15] Z. Rajic, M. Beus, H. Michnova, J. Vlajnic, L. Persoons, I. Kosalec, J. Jampilek, D. Schols, T. Keser, *Zorc, B. Molecules* **2018**, *23*, 1724.
- [16] A. A. Mangoni, C. Guillou, J. J. Vanden Eynde, C. Hulme, J. Jampilek, W. Li, K. Prokai-Tatrai, J. Rautio, S. Collina, T. Tuccinardi, M. E. Sousa, J. M. Sabatier, S. Galdiero, Karaman, R. Kokotos, G. Torri, G. Luque, F. J. Vasconcelos, M. H. Hadjipavlou-D. Litina, C. Siciliano, M. Gutschow, R. Ragno, P. A. C. Gomes, L. A. Agrofoglio, D. Munoz-Torrero, *Molecules* **2019**, *24*, 130.
- [17] J. Jampilek, M. Dolezal, J. Kunes, V. Buchta, L. Silva, K. Kralova, *Med. Chem.* **2005**, *1*, 591–599.
- [18] R. Musiol, J. Jampilek, J. E. Nycz, M. Pesko, J. Carroll, K. Kralova, M. Vejsova, J. O'Mahony, A. Coffey, A. Mrozek, J. Polanski, *Molecules* **2010**, *15*, 288–304.

- [19] T. Gonec, P. Bobal, J. Sujan, M. Pesko, J. Guo, K. Kralova, L. Pavlacka, L. Vesely, E. Kreckova, J. Kos, A. Coffey, P. Kollar, A. Imramovsky, L. Placek, J. Jampilek, *Molecules* **2012**, *17*, 613–644.
- [20] J. Kos, I. Zadrazilova, E. Nevin, M. Soral, T. Gonec, P. Kollar, M. Oravec, A. Coffey, J. O'Mahony, T. Liptaj, K. Kralova, J. Jampilek, *Bioorg. Med. Chem.* **2015**, *23*, 4188–4196.
- [21] I. Kushkevych, J. Kos, P. Kollar, K. Kralova, J. Jampilek, *Med. Chem. Res.* **2018**, *27*, 278–284.
- [22] I. Kushkevych, M. Vitezova, J. Kos, P. Kollar, J. Jampilek, *J. Appl. Biomed.* **2018**, *16*, 241–246.
- [23] J. Jampilek, K. Kralova, M. Pesko, J. Kos, *Bioorg. Med. Chem. Lett.* **2016**, *26*, 3862–3865.
- [24] Z. Shen, K. Lou, W. Wang, *Acta Pharm. Sin. B* **2015**, *5*, 419–430.
- [25] N. Y. Tsang, L. H. Zhao, S. W. Tsang, H. J. Zhang, *Curr. Org. Chem.* **2017**, *21*, 1777–1804.
- [26] J. Y. Yeh, M. S. Coumar, H. Y. Shiao, T. J. Lin, Y. C. Lee, H. C. Hung, S. Ko, F. M. Kuo, M. Y. Fang, Y. L. Huang, J. T. Hsu, T. K. Yeh, S. R. Shih, Y. S. Chao, J. T. Horng, H. P. Hsieh, *ChemMedChem* **2012**, *7*, 1546–1550.
- [27] W. Wang, R. Yin, M. Zhang, R. Yu, C. Hao, L. Zhang, T. Jiang, *J. Med. Chem.* **2017**, *60*, 2840–2852.
- [28] V. A. Shibnev, P. G. Deryabin, E. Burtseva, T. M. Garaev, M. P. Finogenova, E. S. Kirillova, A. G. Botikov (Federal Research Center for Epidemiology and Microbiology of the Ministry of Health of the Russian Federation). 2-quinaldicarboxylic acid derivatives and their anti-influenza activity. RU2624906 C2, 07/10/2017.
- [29] C. de la Guardia, D. E. Stephens, H. T. Dang, M. Quijada, O. V. Larionov, R. Lleonart, *Molecules* **2018**, *23*, 672.
- [30] T. Gonec, J. Kos, I. Zadrazilova, M. Pesko, R. Govender, S. Keltosova, P. Kollar, A. Imramovsky, J. O'Mahony, A. Coffey, A. Cizek, K. Kralova, J. Jampilek, *Molecules* **2013**, *18*, 9397–9419.
- [31] J. Kos, I. Zadrazilova, M. Pesko, S. Keltosova, J. Tengler, T. Gonec, P. Bobal, T. Kauerova, M. Oravec, P. Kollar, A. Cizek, K. Kralova, J. Jampilek, *Molecules* **2013**, *18*, 7977–7997.
- [32] T. Kauerova, J. Kos, T. Gonec, J. Jampilek, P. Kollar, *Int. J. Mol. Sci.* **2016**, *17*, 1219.
- [33] J. Kos, I. Kapustikova, C. Clements, A. I. Gray, J. Jampilek, *Monatsh. Chem.* **2018**, *149*, 887–892.
- [34] H.J. Zhang, E. Rumschlag-Booms, Y.F. Guan, D.Y. Wang, K.L. Liu, W.F. Li, V.H. Nguyen, N.M. Cuong, D.D. Soejarto, H.H.S. Fong, L.J. Rong, *J. Nat. Prod.* **2017**, *80*, 1798.

Submitted: March 7, 2019

Accepted: April 5, 2019

č.	citace	ISSN
13	CAMPOS, LE, FM GARIBOTTO, E ANGELINA, J KOS , T TOMASIC, N ZIDER, D KIKELJ, T GONEC, P MARVANOVA, P MOKRY, J JAMPILEK, SE ALVAREZ a RD ENRIZ. Searching new structural scaffolds for BRAF inhibitors. An integrative study using theoretical and experimental techniques. <i>BIOORGANIC CHEMISTRY</i> [online]. 2019, 91 . Dostupné z: doi: 10.1016/j.bioorg.2019.103125	0045-2068



Searching new structural scaffolds for BRAF inhibitors. An integrative study using theoretical and experimental techniques

Ludmila E. Campos^{a,b}, Francisco M. Garibotto^{a,b}, Emilio Angelina^c, Jiri Kos^d, Tihomir Tomašič^e, Nace Zidar^e, Danijel Kikelj^e, Tomas Gonec^f, Pavlina Marvanova^f, Petr Mokry^f, Josef Jampilek^{d,g}, Sergio E. Alvarez^{a,b,*}, Ricardo D. Enriz^{a,b,*}

^a Facultad de Química, Bioquímica y Farmacia, Universidad Nacional de San Luis, Ejército de los Andes 950, 5700 San Luis, Argentina

^b Instituto Multidisciplinario de Investigaciones Biológicas (IMIBIO-SL), Ejército de los Andes 950, 5700 San Luis, Argentina

^c Laboratorio de Estructura Molecular y Propiedades, Área de Química Física, Departamento de Química, Facultad de Ciencias Exactas y Naturales y Agrimensura, Universidad Nacional del Nordeste, Avda. Libertad 5460, 3400 Corrientes, Argentina

^d Division of Biologically Active Complexes and Molecular Magnets, Regional Centre of Advanced Technologies and Materials, Faculty of Science, Palacky University Olomouc, Slechtitelu 27, 78371 Olomouc, Czech Republic

^e University of Ljubljana, Faculty of Pharmacy, Aškerčeva 7, 1000 Ljubljana, Slovenia

^f Department of Chemical Drugs, Faculty of Pharmacy, University of Veterinary and Pharmaceutical Sciences Brno, Palackeho 1, 61242 Brno, Czech Republic

^g Department of Analytical Chemistry, Faculty of Natural Sciences, Comenius University, Ilkovicova 6, 84215 Bratislava, Slovakia

ARTICLE INFO

Keywords:

BRAF inhibitors
Virtual screening
Synthesis
Bioassays
Molecular modeling

ABSTRACT

The identification of the V600E activating mutation in the protein kinase **BRAF** in around 50% of melanoma patients has driven the development of highly potent small inhibitors (BRAFi) of the mutated protein. To date, Dabrafenib and Vemurafenib, two specific BRAFi, have been clinically approved for the treatment of metastatic melanoma. Unfortunately, after the initial response, tumors become resistant and patients develop a progressive and lethal disease, making imperative the development of new therapeutic options. The main objective of this work was to find new BRAF inhibitors with different structural scaffolds than those of the known inhibitors. Our study was carried out in different stages; in the first step we performed a virtual screening that allowed us to identify potential new inhibitors. In the second step, we synthesized and tested the inhibitory activity of the novel compounds founded. Finally, we conducted a molecular modelling study that allowed us to understand interactions at the molecular level that stabilize the formation of the different molecular complexes.

Our theoretical and experimental study allowed the identification of four new structural scaffolds, which could be used as starting structures for the design and development of new inhibitors of BRAF. Our experimental data indicate that the most active compounds reduced significantly ERK $\frac{1}{2}$ phosphorylation, a measure of BRAF inhibition, and cell viability. Thus, from our theoretical and experimental results, we propose new substituted hydroxynaphthalenecarboxamides, *N*-(hetero)aryl-piperazinylhydroxyalkylphenylcarbamates, substituted piperazinylethanol and substituted piperazinylpropanediols as initial structures for the development of new inhibitors for BRAF. Moreover, by performing QTAIM analysis, we are able to describe in detail the molecular interactions that stabilize the different Ligand-Receptor complexes. Such analysis indicates which portion of the different molecules must be changed in order to obtain an increase in the binding affinity of these new ligands.

1. Introduction

The BRAF/MEK $\frac{1}{2}$ /ERK $\frac{1}{2}$ cascade is one of the major pathways deregulated in many types of cancer. Oncogenic mutations in BRAF occur in around 50% of melanoma patients but also in colon adenocarcinoma (5–12%), papillary thyroid carcinoma (39–69%), and others

[1,2]. Upon activation of this pathway, BRAF phosphorylates and activates the dual kinase MEK $\frac{1}{2}$, which in turn phosphorylates and activates its only target ERK $\frac{1}{2}$ at Tyr 204/187 and Thr202/185 residues. RAF family includes 3 members: ARAF, BRAF and CRAF, although oncogenic mutations occur mostly in BRAF gene. The majority of BRAF mutations consist in substitutions of valine for glutamic acid

* Corresponding authors at: Facultad de Química, Bioquímica y Farmacia, Universidad Nacional de San Luis and Instituto Multidisciplinario de Investigaciones Biológicas (IMIBIO-SL CONICET), Ejército de los Andes 950, 5700 San Luis, Argentina.

E-mail addresses: sealvarez98@gmail.com, sealvar@unsl.edu.ar (S.E. Alvarez), denriz@unsl.edu.ar (R.D. Enriz).

<https://doi.org/10.1016/j.bioorg.2019.103125>

Received 10 April 2019; Received in revised form 4 July 2019; Accepted 11 July 2019

Available online 12 July 2019

0045-2068/ © 2019 Elsevier Inc. All rights reserved.

(BRAF^{V600E}), or less frequently for lysine (BRAF^{V600K}), at position 600 leading to a constitutive active protein that does not require external stimuli to be activated [1–3]. To date, the U.S. Food and Drugs Administration have approved the use of two BRAF inhibitors (BRAFi), Vemurafenib [4] and Dabrafenib [5], and two MEK inhibitors (MEKi), trametinib and cobimetinib [6,7], for the treatment of metastatic melanoma. BRAFi and MEKi constitute the first-line treatment for BRAF^{V600E} mutated melanomas, however the development of acquired resistance invariably occurs, and in some cases no clinical benefit at all is observed [8,9]. Although many mechanisms of resistance have been reported, most of them involve the reactivation of ERK^{1/2} signaling [10–12]. Moreover, BRAFi therapy also induces paradoxical activation of ERK signaling in BRAF^{wt} tissue [13] that may promote the formation of benign tumors in the skin [14]. Resistance development and secondary effects to BRAFi therapy reduce the effectiveness and durability of the clinical response, and justify the search and design of new potential BRAFi.

The high sequence conservation within the large family of protein kinases makes it difficult to develop selective inhibitors for a particular member of the family. Furthermore, nearly all of the approved protein kinase antagonists are steady-state competitive enzyme inhibitors of ATP and they interact with the ATP-binding pocket which is well conserved among the family of protein kinases [15]. However, protein kinases have high plasticity and it is well known that kinase conformational state has a great impact in inhibitor potency and selectivity [16]. Therefore, conformational plasticity of kinases can be exploited to design inhibitors that target a specific kinase type in a particular conformational state.

BRAF has an active site (including the so called catalytic loop) to which both ATP and inhibitors bind. The conserved DFG triad shifts to an 'out' conformation where the phenylalanine side chain vacates a lipophilic "allosteric" pocket that is available to inhibitor binding (i.e. DFG-out conformation). Compounds that bind to kinase in DFG-out state are classified as type II inhibitors [17], in contrast to the active DFG-in conformation. In the latter case, PHE is flipped toward the allosteric pocket and inhibitors that target this conformation (Type I inhibitors) bind at the ATP site but do not penetrate the allosteric pocket and therefore do not depend on specific kinase conformations for binding. There is a small set of kinases including BRAF that achieves a peculiar variant of the DFG-in conformation in which a conserved salt bridge between a glutamate in α C-helix and a lysine in the β 3-sheet is broken. The disruption of this salt bridge causes an outward movement of the α C-helix (α C-helix-out) and renders the kinase in an inactive state despite the DFG triad residing in the 'in' conformation. Inhibitors that target the DFG-in α C-helix-out conformation are classified as type IIB while inhibitors that bind to the more typical inactive kinase conformation DFG-out are re-classified as type IIA inhibitors. Since only few kinases are able to perform this DFG-in, α C-helix-out conformation, inhibitors designed to target this particular kinase state have exhibited excellent selectivity towards the RAF kinase family. These inhibitors accommodate a propyl group in a small lipophilic pocket formed by the outward movement of α C-helix-out [18]. Vemurafenib is an example of a selective BRAF inhibitor that targets this kinase conformation.

Considering the important role of BRAF in processes related to cancer [1] and vemurafenib clinical limitations, the main objective of this work was to develop new inhibitors possessing different structural scaffolds than those of the already known inhibitors. Our study has been carried out in different stages; in the first step we performed a virtual screening that allowed us to identify potential new inhibitors. In the second step, we synthesized and tested the inhibitory activity of the novel compounds. Finally, we conducted a molecular modeling study that allowed us to understand interactions at the molecular level that stabilize the formation of the different molecular complexes. Fig. 1 shows an scheme of the various steps that have been carried out in this study.

2. Results and discussion

2.1. Structure-based approach to prioritize novel scaffolds as BRAF inhibitors

At the time we started this work, there were around 60 BRAF crystal structures available in the Protein Data Bank (PDB). Taking advantage of this structural information we pursued a structure-based drug design project searching for novel scaffolds that may function as BRAF inhibitors.

Structure-Based Virtual Screening (SBVS) strategies rely on the three dimensional structure of a target and on the ability of docking algorithms to predict the binding mode and the binding affinities of different compounds obtained from libraries.

As was previously remarked, protein kinases have high plasticity and several conformations, and it is well known that kinase conformational state has a great impact in inhibitor potency and selectivity [16]. BRAF crystal structures deposited in the PDB up to date cover the three more relevant kinase conformational states.

Fig. 2 shows superposition of BRAF in two of its conformational states, DFG-out (gray) and DFG-in α C-helix-out (cyan). In Fig. 2a, a type IIA inhibitor (gray sticks) accommodates a bulky aromatic group into the lipophilic pocket of DFG-out conformation (depicted as a gray surface) which is otherwise occluded in DFG-in like conformations. Thus, type IIA inhibitors that were designed to target the lipophilic pocket in DFG-out conformation would not bind properly at DFG-in conformations.

In contrast, in Fig. 2b, a type IIB inhibitor (cyan sticks) accommodates a small aliphatic group into a small lipophilic pocket created by the outward shift of α C-helix which disrupt the salt bridge between K483 and E501; such place can be occupied by the inhibitor in the DFG-in α C-helix-out conformation. This small but deep pocket is generally absent in DFG-in and DFG-out conformations in which the salt bridge holds α C-helix and β 3-sheet together. Therefore, in order to allow more structural variety among selected compounds, virtual screening libraries should be docked against representative structures from each of the BRAF conformational states (ensemble docking). In other words, if only one of the BRAF conformations are considered in docking calculations, we could miss inhibitors targeting that conformation but we would miss inhibitors that stabilize other relevant BRAF conformations.

2.1.1. Virtual screening and docking power assessment

The docking process is usually divided into two major steps: first, the correct placement of the ligand at the protein binding-site and second, the estimation of the ligand affinity by a scoring function [19]. Scoring functions launched with docking software are usually calibrated with structurally very diverse complexes because they are intended for general use in any bimolecular system of interest. In part because of their general nature, standard docking scoring functions often might fail either to recover ligand known binding affinities (scoring power) or poses (docking power) or might fail to rank ligands by their affinities (ranking power) or also recover known ligands from decoys libraries (screening power). Therefore, before undertaking the search for novel BRAF inhibitors, we considered it was prudent to perform a retrospective study with known BRAF inhibitors to evaluate performance of docking algorithm in our system of study.

Metrics employed to evaluate and tune docking performance depends on the intended use of docking programs. Docking, scoring, ranking or screening power can be tuned depending on the particular task and experimental information available. The scoring function optimal for the different tasks may have some overlap, although improvements in affinity prediction are not always related to improvements in the docking performance [20]. To test screening power we measured the ability of AutoDock4 [21] standard scoring function to retrieve BRAF inhibitors from a decoys library. The decoys library was

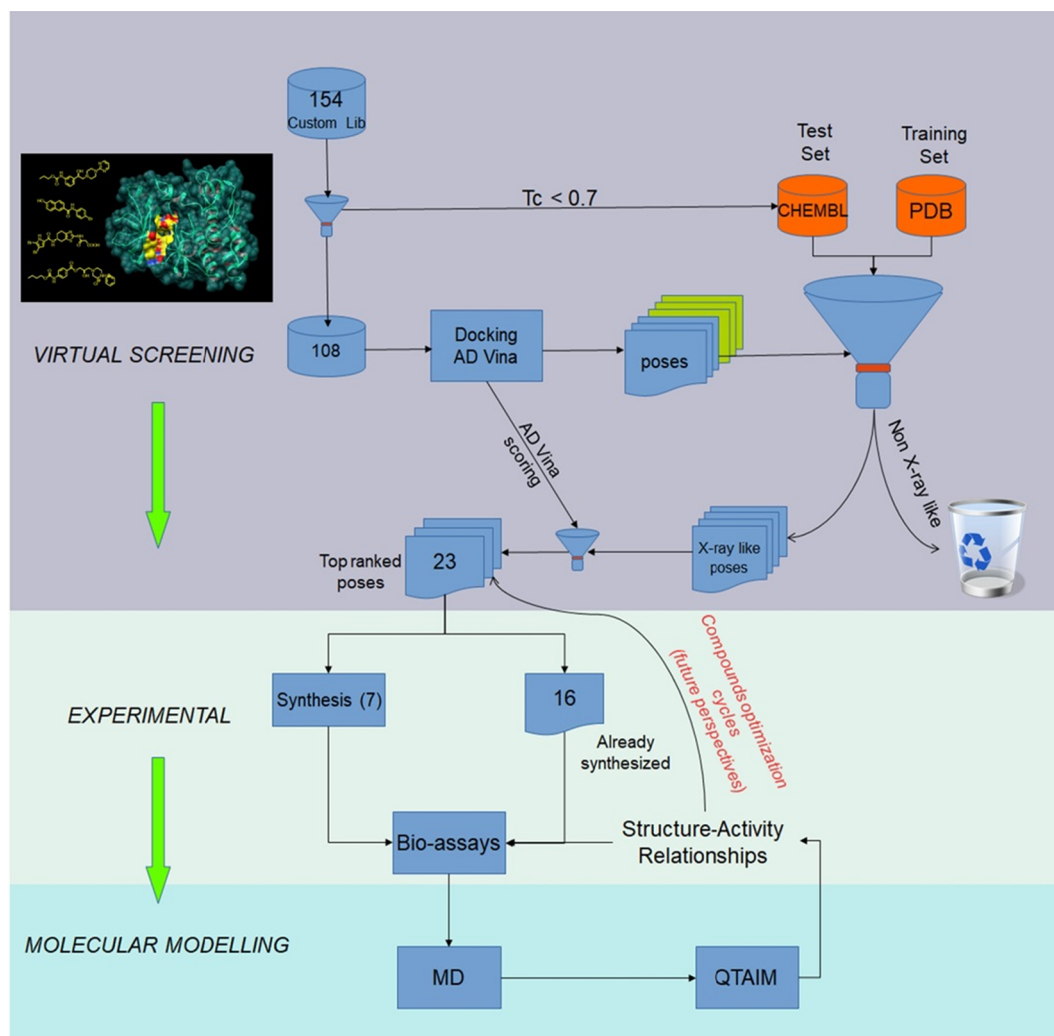


Fig. 1. Flow chart showing the various steps and techniques carried out in our study. The numbers inside the boxes indicate the number of compounds evaluated.

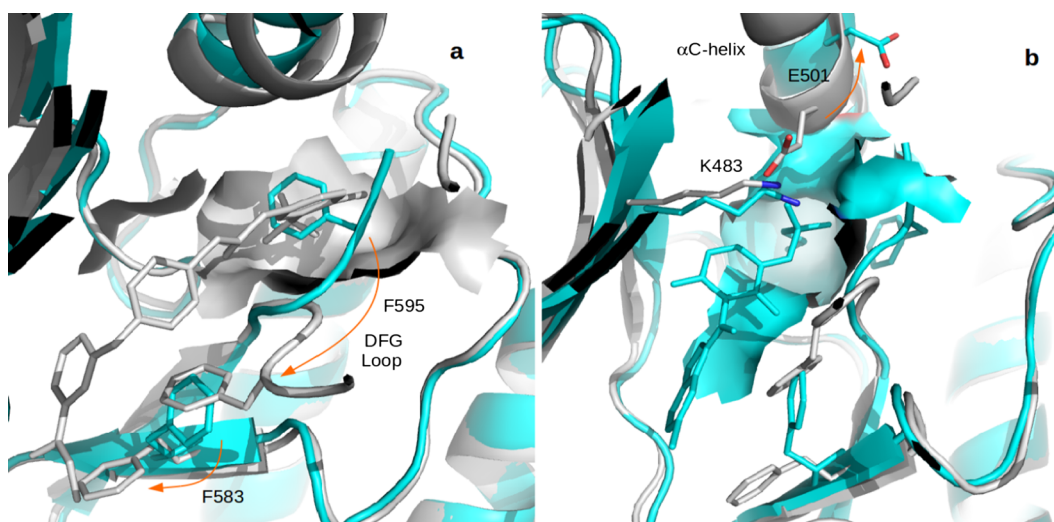


Fig. 2. Superposition of two conformations of BRAF (DFG-out is shown in grey color and DFG-in α C-helix-out in cyan). Figure a: Transition from DFG-in to DFG-out conformation. Figure b: Type IIB inhibitor induce an outward shift of α C-helix.

compiled by seeding about 40 known BRAF inhibitors into a larger set of presumably non-binding compounds (decoys) that were automatically generated with the DUD-E server [22]. Decoy molecules have similar physical properties than actual ligands so that enrichment is not

a mere separation by trivial physical characteristics, but are chemically distinct from ligands, so that they are likely to be non-binders.

BRAF inhibitors seeded into the decoys library were extracted from crystal structures of BRAF bound to inhibitors to later evaluate both

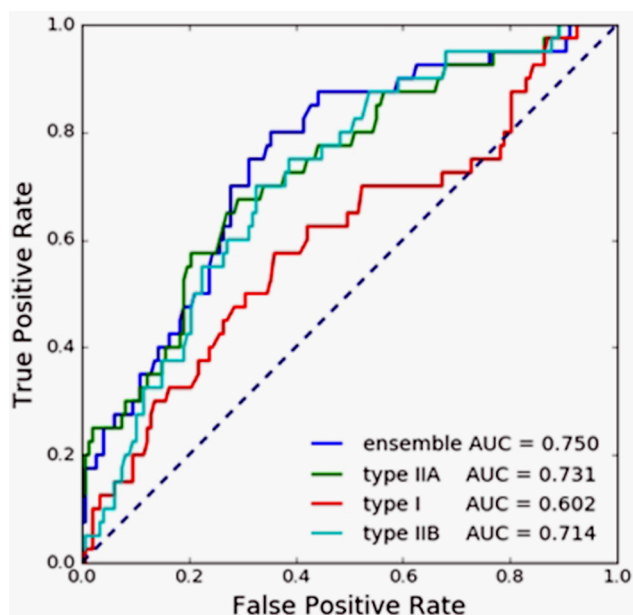


Fig. 3. Screening power evaluation of docking algorithms for retrieving known BRAF inhibitors from a decoys library.

docking power (i.e. by RMSD measurement) and screening power. Inhibitors were chosen considering that the three types of inhibitors are fairly represented within the inhibitors pool (i.e. types I, IIA and IIB are roughly in the same number). The decoy library was docked against a representative structure from each of the three most relevant BRAF conformational states, i.e. DFG-in, DFG-out and DFG-in α C-helix-out conformations. After docking the decoys library with AutoDock4, ROC (Receiver Operating Characteristic) curves were constructed and the Area Under the Curve (AUC) was computed. Fig. 3 depicts ROC curves and AUCs for virtual screening on each of the BRAF conformations as well as for the ensemble of BRAF conformations.

Ensemble docking helps to mitigate the lack of flexibility of docking receptor models by allowing docking a single ligand against multiple conformations of the protein and selecting the highest scoring binding mode from the ensemble of receptors. Any model with an AUC > 0.5 performs better than random in discriminating the most active compounds from less active ones. Unsurprisingly, the virtual screening (VS) prediction on the ensemble of BRAF conformations performs better than on single BRAF conformations (see AUCs in Fig. 3). This is in line with the fact that different types of BRAF inhibitors stabilize different conformations of the enzyme. As observed in the figure, the ensemble docking model performs reasonably well in the classification of the dataset (AUC ~ 0.75).

Moreover, since we know the experimental binding modes of the BRAF inhibitors in the decoys library we subsequently exploited that information to evaluate docking power, namely the ability of docking algorithm to predict the correct conformation of the ligand and placement in the receptor molecule (pose).

Docking power usually is evaluated by computing the root mean square deviation (RMSD) between the heavy atoms of the docked ligand and native crystal pose. Usually, a threshold of 2–3 Å RMSD is used to calculate the fraction of correct predictions.

Heat maps on Fig. 4a–c depict the RMSD values between crystallographic and docking poses of type IIA, type IIB and type I BRAF inhibitors, respectively. Each inhibitor was docked against the three relevant conformations of the enzyme and the conformation that achieves the best docking scoring is labeled with a green star.

As depicted in Fig. 4a, Type IIA inhibitors can reproduce their crystallographic poses (i.e. considering a 2–3 Å RMSD tolerance) only when they are docked to the DFG-out conformation of BRAF. This

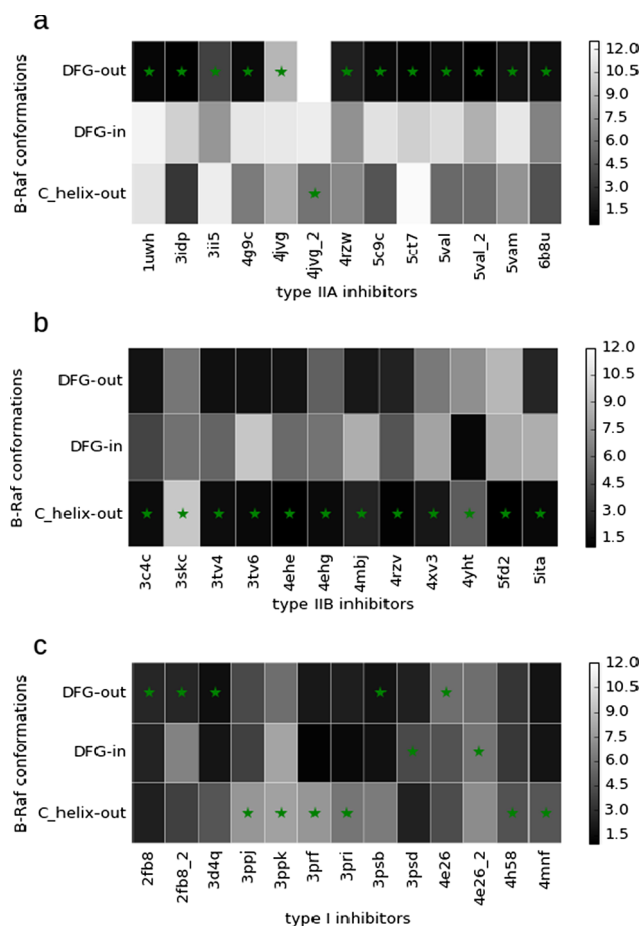


Fig. 4. Heat maps depicting RMSD differences between crystallographic and docking poses for type IIA (a), IIB (b) and type I (c) BRAF inhibitors as docked in the three relevant conformations of the enzyme. Best scoring conformation for each ligand is labeled with a green star. Ligands are named by the PDB ID of the BRAF native complex they belong to. Underscored PDB IDs represent different protonation states of the same ligand.

makes sense because type IIA inhibitors were designed to target the allosteric pocket that is otherwise occluded in DFG-in conformations. There is also a good correspondence between docking power and scoring, namely enzyme conformation achieving the best pose for a particular ligand is also the one that show the best energy score, as indicated by the green stars in Fig. 4a. In practice, that means that prospective virtual screening campaigns will likely prioritize candidates that reproduce known inhibitors binding modes and therefore that have more chance of being true positives upon experimental corroboration.

Similarly, most of Type IIB inhibitors are docked correctly in their native-like BRAF conformation, DFG-in α C-helix-out. These inhibitors have a hydrophobic tail attached to a sulfonamide group and target a small hydrophobic pocket created between β 3-sheet and α C-helix. In DFG-in conformation a conserved salt bridge between GLU501 and LYS483 holds together the α C-helix and the β 3-sheet and prevent the formation of the small hydrophobic pocket between both segments. This explains why Type IIB inhibitors cannot dock properly to BRAF in the DFG-in conformation (see Fig. 4b). Regarding DFG-out state, several type IIB inhibitors bind to this conformation in a native-like pose because they can accommodate the small hydrophobic tail in the adjacent allosteric pocket characteristic to that conformation without a significant degradation in the RMSD value.

On the other hand, and unlike previous BRAF inhibitors types, several type I inhibitors bind better to DFG-out or DFG-in α C-helix-out BRAF conformations than to its own DFG-in conformation. Moreover,

many of them cannot reproduce the crystallographic poses within a 2–3 Å RMSD tolerance in any of the BRAF conformations. Even though type I inhibitors do not perform as well as type IIA and IIB inhibitors, we consider that our proposed virtual screening protocol involving the three most relevant BRAF conformations performs well in terms of screening and docking power.

2.1.2. Pre-selection of candidate compounds and results of the virtual screening

Most kinase inhibitors discovered to date bind to kinase ATP binding cleft and roughly mimic the hydrogen bonds normally formed by the adenine, ribose and/or triphosphate moieties of ATP. Structure of ATP analog bound to kinase AKT1 (PDB code 1O6L) provides evidence about ATP binding mode at kinases ATP binding cleft. ATP binds in the cleft with the adenine ring forming hydrogen bonds with the kinase 'hinge', i.e. the segment that connects the amino- and carboxy-terminal kinase domains. The ribose and triphosphate groups enter in a tight channel and triphosphate moiety interacts with the activation segment that contains the common DFG motif, via two magnesium ions (PDB code 1O6L).

It is clear that the compounds selected for further testing should bear some structural resemblance to vemurafenib and other known ligands; i.e. part of the molecule mimicking adenine and other portion that mimics the triphosphate moiety. In addition some conformational flexibility could be convenient. Based on these considerations, we selected a group of 153 compounds including chalcones, acetogenins, protoberberines, nitrosopyrimidines, carbamates and carboxamides among others that already form part of our collection of compounds. We also include some new compounds (not reported yet) structurally related. The fingerprints of these 153 compounds were calculated using Open Babel [23], a chemical expert system mainly used for converting chemical file formats, and the results were compared with fingerprints obtained for the 40 compounds used previously to evaluate the docking "powers". Compounds that have a Tanimoto index (Tc) [19] greater than 0.7 were discarded. Note that the fingerprints are a way to encode the structure of a molecule in order to compare it with other compounds; whereas the Tc is a measure of the similarity between two structures ranging from 0 to 1. Based on Tc index, we selected 108 structurally diverse compounds which possess structural differences with respect to already-known BRAF inhibitors, justifying their further study. Each of the 108 compounds was docked against the three relevant conformations of the enzyme (ensemble docking). Then, the compounds were ranked according to the score achieved in the best enzyme conformation and the 30 top ranked compounds were selected. From these compounds, only the ones that bind in a pose that resemble the binding mode of known BRAF inhibitors like Vemurafenib (see below) were selected. Thus, 23 compounds were selected as potential inhibitors, while the remaining 7 were discarded because they unite in a different pose to that of the crystallized structures. All these 23 compounds have shown a better score when docked to the DFG-in α C-helix-out conformation of the enzyme, hence they were regarded as potential BRAF type IIB inhibitors.

2.2. Chemistry

Our model predicted 23 compounds as potential inhibitors of BRAF (Table 1). Those compounds were tested in an *in vitro* ERK1/2 phosphorylation assay as an indirect measure of BRAF inhibition in melanoma cells (results shown in the next section).

The compounds 1–8 were prepared by means of microwave-assisted synthesis in one step. Briefly, the carboxyl group was activated with phosphorus trichloride, and then aminolysis of acyl chloride by ring-substituted aniline in dry chlorobenzene yielded a final amide. All the compounds were purified by recrystallization from ethanol [24–26].

Synthesis and characterization of compounds 9–13 have been previously reported [27–30] (See *Supplementary Information*). These

compounds have been reported DNA gyrase inhibitors interacting with the ATP-binding site of the enzyme.

Reaction of 2- or 3- or 4-aminoacetophenone and a suitable alkyl chloroformate gave alkyl (2-/3-/4-acetylphenyl)carbamates 14a–21a, which reacted with bromine or with copper (II) bromide in chloroform/ethyl acetate to yield alkyl [2-/3-/4-(bromoacetyl)phenyl]carbamates 14b–21b; these compounds by treatment with different *N*-mono-substituted aryl(heteroaryl)piperazines provided the corresponding alkyl {2-/3-/4-[(4-aryl(heteroaryl)piperazin-1-yl)acetyl]phenyl}carbamates 14c–21c. Subsequent reduction of keto group using NaBH₄ provided target alkyl {2-/3-/4-[1-hydroxy-2-(4-aryl(heteroaryl)piperazin-1-yl)ethyl]phenyl}carbamates 14–21, see Scheme 1.

Studied 1-(3-{4-[(alkoxycarbonyl)amino]benzoyloxy}-2-hydroxypropyl)-4-phenylpiperazin-1-ium chlorides 22 and 23 were prepared by multiple-step reaction described in Scheme 2. Epoxides 22a and 23a were prepared from 4-aminobenzoic acid through reaction with propyl and methylchloroformates giving appropriate 4-[(alkoxycarbonyl)amino]benzoic acids. Chlorides of these acids formed by thionyl chloride treatment gave desired epoxides 22a and 23a after reaction with 2,3-epoxypropan-1-ol [31]. In the last step, final compounds 22 and 23 were prepared by a reaction of the epoxides with 1-(4-phenyl)piperazine and then converted to the hydrochloride salts using ethereal HCl to enhance their solubility in water [32].

2.3. Biological assays

Next, it was important to study whether or not these 23 compounds inhibit BRAF. Since the BRAF/MEK/ERK pathway is linear, it is possible to relate the BRAF activity to the levels of phosphorylated ERK (pERK) in a western blot assay. Indeed, ERK $\frac{1}{2}$ kinase is the only substrate of MEK $\frac{1}{2}$ that has been described to date [33]. To this end, Lu1205 melanoma cell line that express the mutant kinase BRAF^{V600E}, was employed. To establish the reliability of our model, we first tested the response of Lu1205 cells to the known BRAF^{V600E} inhibitor Vemurafenib. In line with previous reports, we show here that Vemurafenib strongly reduced ERK phosphorylation at both 1 and 10 μ M [34]. The effect of Vemurafenib is less pronounced after 48–72 h, probably indicating that ERK reactivation occurs, as was shown by other authors (Fig. 5) [35,36].

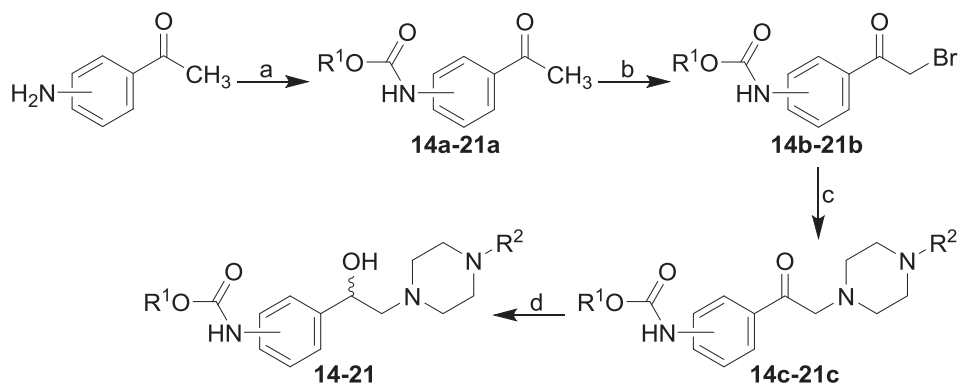
After determining that Lu1205 cells are responsive to Vemurafenib treatment as we expected and it is reported in literature, we considered that this cell model is appropriate for the following assays. Next, we evaluated the biological activity of the compounds listed in the Table 1. Since the goal of this study was to find new inhibitors of BRAF, we consider that 2 h treatment should be enough to show whether or not the new compounds have any noticeable activity. Thus, to perform a quick initial screening of BRAF kinase inhibition, we determined the phosphorylation of ERK in Lu1205 cells treated with the compounds at 10 μ M for 2 h by In-Cell Western (ICW) or western blot (Fig. 6).

As shown in Fig. 6, compounds 1, 2, 9, 10, 19–22 reduced ERK phosphorylation by more than 30% and were selected to perform a more detailed study. Compounds 17, 18 and 23, which did not show, or showed little inhibitory activity in the previous screening, were also included to verify the specificity of the compounds that did show activity. Next, Lu1205 cells were treated with the 11 selected compounds for 2 h at 10 and 1 μ M. Remarkably, all the compounds selected reduce ERK phosphorylation at different magnitude indicating that they have BRAF inhibitory activity, although only compounds 1, 2, 9, 19, 20–22 and 23 reduced significantly pERK suggesting that they have a stronger inhibitory effect (Fig. 7). It is important to notice that, although some compounds (ie. compound 17) decreased ERK phosphorylation, that reduction is not statistically significant.

Considering that BRAF^{V600E} is important in cell growth, we decide to determine whether or not the 11 selected compounds reduce cell viability as result of BRAF inhibition by using MTT assay. In order to determine the adequate experimental conditions, first we tested cell

Table 1
Structural features of compounds obtained from the virtual screening and evaluated as BRAF inhibitors.

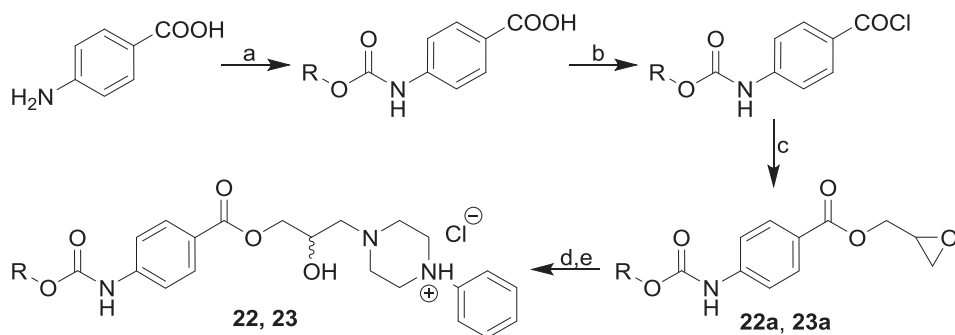
1		2	
3		4	
5		6	
7		8	
9		10	
11		12	
13		14	
15		16	
17		18	
19		20	
21		22	
23			



viability of Lu1205 cells treated with Vemurafenib 1 and 10 μ M at 48 and 72 h. As shown in Fig. 8A, Lu1205 cells treated with Vemurafenib proliferate less in comparison to the control both at 48 and 72 h. Furthermore, ICW was performed to corroborate that BRAF remains

inhibited at 48–72 h of Vemurafenib treatment (Fig. 8B). Since the results were similar at both 48 and 72 h, we decided to use only 72 h for the following experiments.

Subsequently, Lu1205 cells were treated with the 11 selected



Scheme 2. Synthesis of studied 1-(3-{4-[(alkoxycarbonyl)amino]benzoyloxy}-2-hydroxypropyl)-4-phenylpiperazin-1-ium chlorides **22** and **23**. R: Bu and Pr. *Reagents and conditions:* (a) ClCOOR, pyridine, acetone, reflux 3 h; (b) SOCl₂, toluene, reflux; (c) 2,3-epoxypropan-1-ol, THF, TEA, 0 °C then ambient temperature; (d) 1-(4-phenyl)piperazine, *i*-PrOH, reflux; (e) HCl, Et₂O, ambient temperature.

compounds at 1 and 10 μ M for 72 h. Our results revealed that only compounds **1** and **22** reduced significantly Lu1205 cell viability (Fig. 9).

In summary, we evaluated 23 compounds with different structural scaffolds. From the preliminary study we selected 11 compounds, of which 7 showed significant inhibitory activities. The results of the most exhaustive study show that these 7 compounds reduce ERK phosphorylation. These results indicate the good performance of our screening model. Compounds **1**, **9**, **20** and **22** have different scaffold and showed the most interesting activities. Among active compounds it is possible to clearly visualize four different types of structural scaffolds: (a) substituted hydroxynaphthalenecarboxamides (compounds **1** and **2**), N-(hetero)aryl-piperazinylhydroxyalkylphenylcarbamates (**9**), substituted piperazinylethanol (**19** and **20**) and substituted piperazinylpropanediols (**22** and **23**). Considering that these compounds have been obtained through a primary screening, their inhibitory activities can be considered quite strong and promising. In this sense, the inhibitory effect obtained for compounds **1** and **22** are very interesting since they showed a strong inhibitory activity even at relatively low concentrations (1 μ M). Furthermore, both compounds also reduced significantly cell viability, indicating that the inhibition of ERK signaling is accompanied by an anti-proliferative effect. Although these compounds have a strong inhibitory activity, their effects are weaker than that obtained for Vemurafenib. In the next section we report a molecular modeling study in which we evaluate the molecular interactions of the different L-R (Ligand-Receptor) complexes, which allows us to explain the different activities observed.

2.4. Molecular modeling

In order to understand at molecular level the behavior of these compounds, we conducted a molecular modeling study. The main objective of this study was to evaluate the molecular interactions that stabilize the different molecular complexes. This information could be very useful for the design and modification of these starting structures to obtain compounds with higher affinity for this protein. To this end, we selected a representative compound for each structural scaffold to make a comparative study for compounds **1**, **9**, **20** and **22**. We also

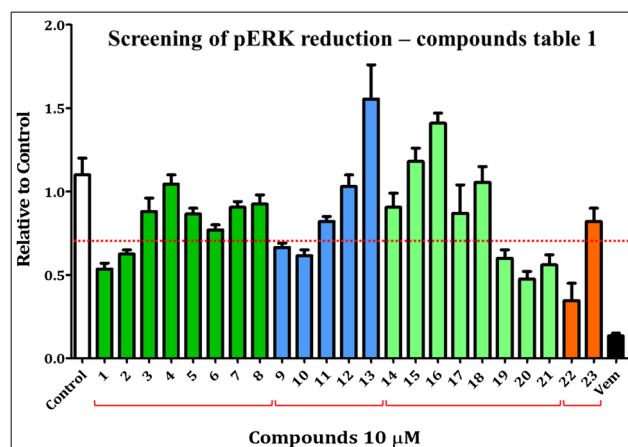


Fig. 6. Results obtained from the initial screening for compounds of Table 1. Substituted hydroxynaphthalenecarboxamides (dark green), N-(hetero)aryl-piperazinylhydroxyalkylphenylcarbamates (blue), substituted piperazinylethanol (light green), and substituted piperazinylpropanediols (orange). The red line indicates the cut between compounds with significant activity of the rest. The graph corresponds to the quantification of pERK of 2 experiments.

included in our study Vemurafenib, which allowed us to perform a comparative analysis of the different activities displayed by these molecules in relation to their structural differences.

The molecular modeling study was conducted in three different stages. First, we performed a docking analysis using the Autodock program [21]. In the second stage of this study, we carried out molecular dynamics (MD) simulations using the AMBER software package [37]. From the trajectories obtained with MD simulations, we performed an analysis per residue for the different compounds. Finally, to better understand the molecular interactions involved in the different L-R complexes, a Quantum Theory of Atoms In Molecules (QTAIM) study was carried out for the most representative structures. We have previously demonstrated the importance of these QTAIM studies for the understanding of the details of the different molecular interactions that stabilize or destabilize the various complexes [38–45].

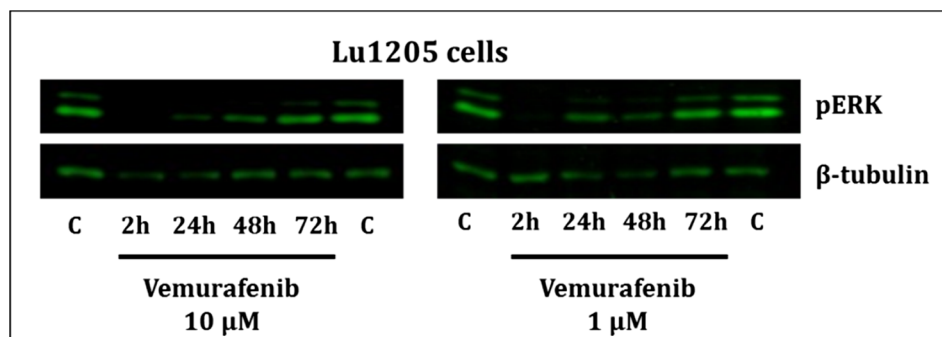


Fig. 5. Lu1205 melanoma cells were treated with 1 and 10 μ M of Vemurafenib or Control (untreated cells incubated with the carrier DMSO) at the indicated times. Proteins from cell lysates were separated by SDS-PAGE and transferred onto a nitrocellulose membrane. Membranes were incubated with the primary antibodies as indicated. The image is representative from at least 5 independent experiments.

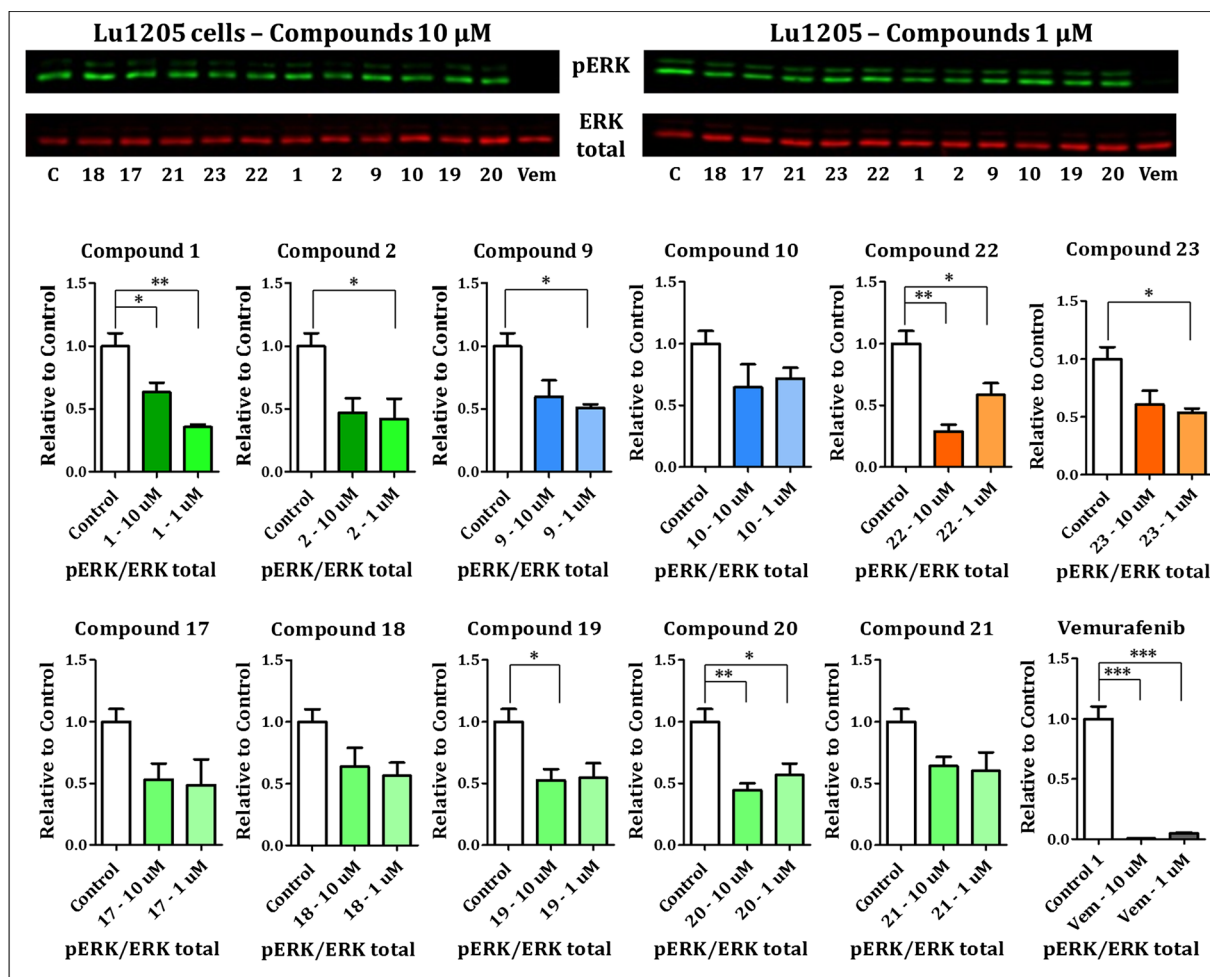


Fig. 7. Lu1205 melanoma cells were treated with the indicated compounds for 2 h at 1 and 10 μM . Proteins from cell lysates were separated by SDS-PAGE and transferred onto a nitrocellulose membrane. Membranes were incubated with the primary antibodies as indicated. The software Image Studio 5.2 was employed for the quantifications. Optical density of pERK band for each treatment was normalized to the respective ERK total band. pERK/ERK total relation for each treatment was relativized to pERK/ERK total relation of the control corresponding to untreated cells incubated with the carrier DMSO. Quantifications correspond to 3 independent experiments and the blots are representative from them. Statistic: One-way ANOVA and Tukey's post-test; (* $p \leq 0,05$; ** $p < 0,01$; *** $p \leq 0,001$).

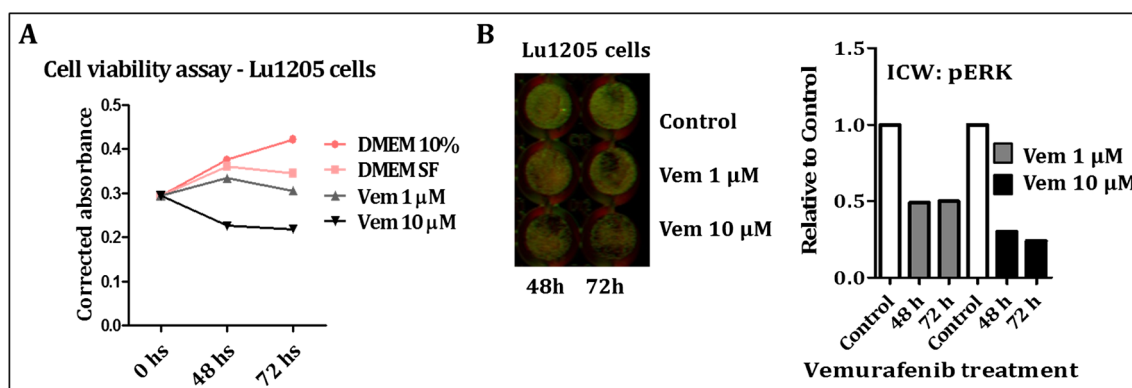


Fig. 8. Lu1205 cells cultured in 96-well plate were treated with Vemurafenib 1 and 10 μM or control. MTT reagent was added at the indicated times and incubated for 3 additional h. Then formazan product was dissolved and absorbance read at 540 nm (A). ICW was performed in parallel to MTT assay (B).

Analysis per residue obtained from molecular dynamics simulations allowed us to define the main interactions that stabilize the different complexes (Fig. 10). Our simulations indicate the importance of the following residues: ILE463, LYS483, LEU505, PHE516, ILE527, TRP531, GLN530, CYS532, PHE583, PHE595 and mainly ASP594 for binding of these ligands to BRAF. These results are in agreement with previously reported experimental data [46].

Superpositions of interactions obtained for compounds 1, 9, 20 and 22 with those displayed by Vemurafenib are shown in Fig. 10a–d. According to this data, it is evident that these compounds bind in a similar manner to Vemurafenib because they interact with essentially the same amino acids. However, these interactions are weaker than those shown for Vemurafenib along the simulations. These results are in agreement with the experimental data and might explain, at least in part, the lower

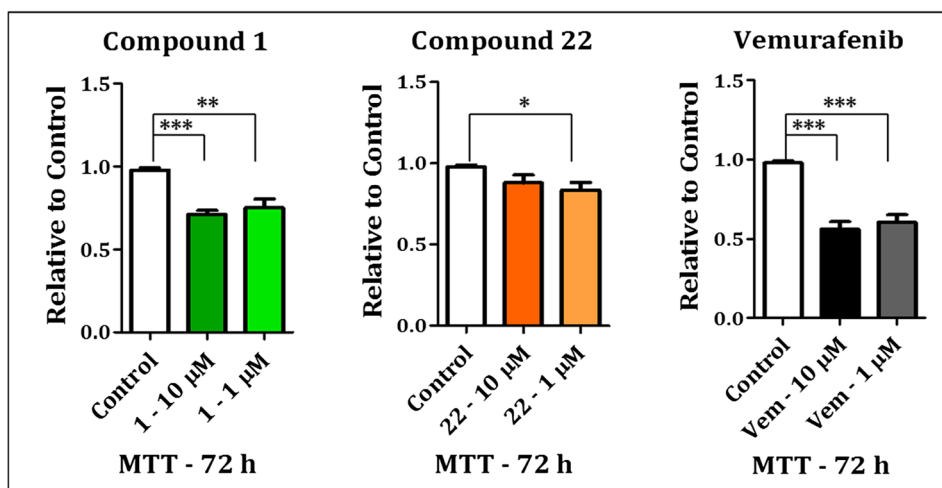


Fig. 9. Lu1205 cells cultured in 96-well plate were treated with the 11 compounds selected previously, Vemurafenib or control (DMSO), at 10 and 1 μ M. After 72 h of treatment, MTT reagent was added and incubated for 3 additional h. Then formazan product was dissolved and absorbance read at 540 nm. Each condition was assayed by 6 replicates and the results correspond to 3 independent experiments. One-way ANOVA and Tukey's post-test were performed.

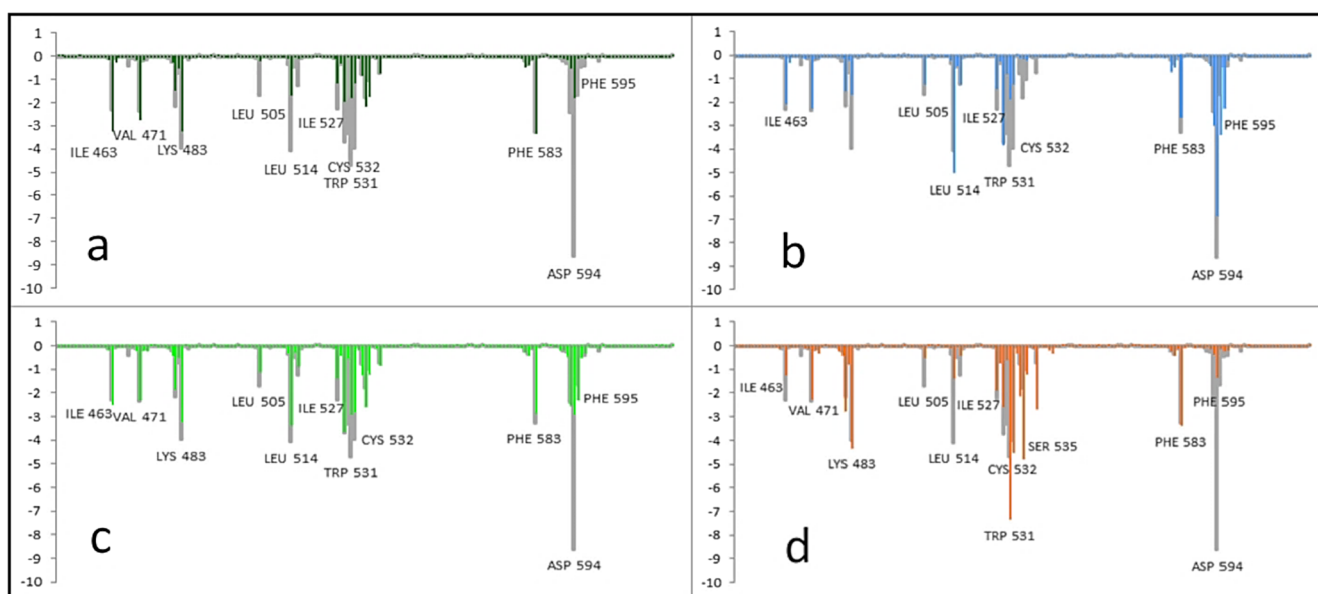


Fig. 10. Over imposed histograms showing the interaction energies of compounds **1** (dark green, a), **9** (light-blue, b), **20** (light-green, c) and **22** (orange, d) with the main amino acids involved in the complex formation. The histogram obtained for Vemurafenib is shown in gray in all the histograms for comparison.

inhibitory effects of the compounds reported here than Vemurafenib. Active compounds displayed their pharmacophoric portions in a closely related spatial form to that displayed by Vemurafenib [46]. This might be well appreciated in Fig. 11.

The main objective of our molecular modeling study is to evaluate the molecular interactions that stabilize the different ligand-enzyme complexes. It is well known that simulations of molecular dynamics are too crude, and that they might miss important information and many details involved in the stability of molecular complexes. Thus, we decided to conduct a QTAIM study that can better quantify the molecular interactions obtained for the different complexes. In fact, our research's group has been the pioneer in this type of studies and in many of them we have demonstrated the ability of QTAIM calculations to evaluate the molecular interactions for this type of complexes [38–45].

Fig. 12 shows the charge density sum at intermolecular bond critical points (BCPs). Inhibitors contributions to anchoring at the DFG-loop and hinge regions of ATP binding site are stacked on top of each other. As depicted in this figure, Vemurafenib is more strongly anchored to the enzyme ATP binding site than inhibitors reported here, as evidenced by the total height of stacked bars. Moreover, separate contributions to

anchoring at the Hinge and DFG-loop regions of ATP binding cleft tell us which interactions need to be optimized in order to increase binding affinity of the new inhibitors.

On the other hand, when comparing $\Sigma\rho$ values and inhibitory activities of moderate inhibitors as the ones reported here, no evident relationship is found. It should note that the four compounds reported here displayed similar inhibitory effect; however compounds **1** and **20** are more weakly anchored to the enzyme binding cleft according to the $\Sigma\rho$ values.

Separate contributions to anchoring at the Hinge and DFG-loop regions of ATP binding cleft (see Fig. 12) show that Vemurafenib as well as the two most active inhibitors reported here (**1** and **22**) show a stronger anchoring at the hinge region as compared to compounds **9** and **20**. Moreover, these inhibitors also have in common that anchoring at both DFG-loop and hinge has similar strength, namely they show a balanced anchoring at both ATP binding cleft regions.

Comparing ATP binding mode with those found for Vemurafenib and the new inhibitors from Molecular Dynamic simulations (Fig. 11) it is easy to identify which part of the inhibitors mimic the interactions of adenine and which other parts mimic the triphosphate (and less clearly ribose) interactions. Adenine moiety from ATP binds to the hinge

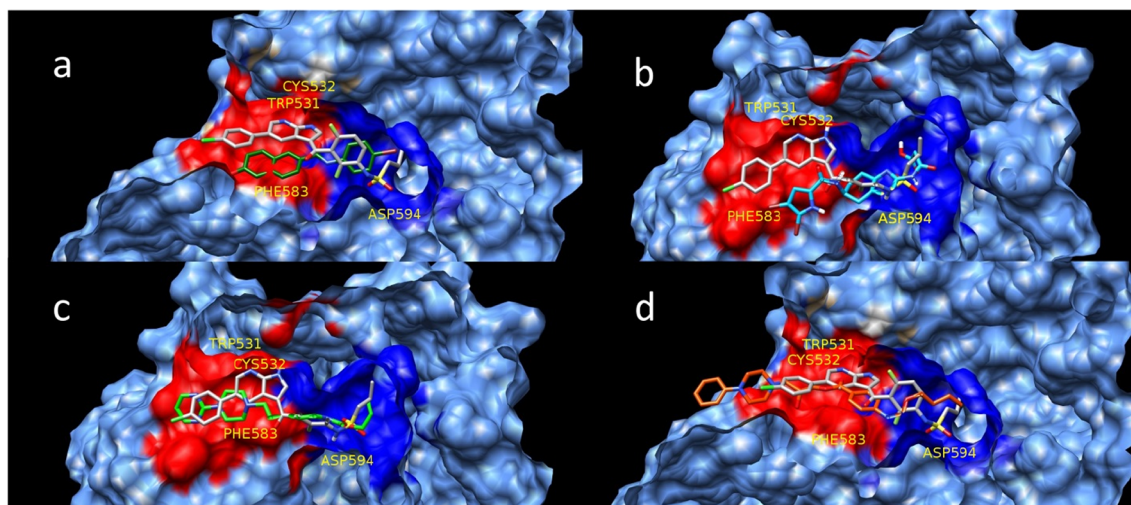


Fig. 11. View of the spatial ordering adopted by the different ligands in the active site of BRAF. Compounds **1** (dark green), **9** (light-blue), **20** (light-green) and **22** (orange) are over imposed with Vemurafenib in gray color. All these compounds are docked to a similar conformation of BRAF.

region of the binding cleft while triphosphate group binds to the DFG-loop. Therefore, the hinge and DFG-loop interacting parts of inhibitors are depicted in red and blue respectively, in the subsequent charge density molecular graphs.

The charge density molecular graphs in Fig. 13 displayed the main interactions of Vemurafenib at ATP binding site of BRAF kinase. For easy viewing, interactions of arylsulfonamide moiety that substitutes position 3 of the azaindole ring are shown in Fig. 13A whereas interactions of azaindole as well as its substituent at position 5 are depicted in Fig. 13B.

The sulfonamide moiety of Vemurafenib resembles ATP phosphate groups. In that way, it forms strong interactions with the DFG motif of the activation segment as long as it is in the “in” conformation. As shown in Fig. 13A, the sulfonamide oxygen atoms are connected through bond paths to the backbone of ASP594 while the amide proton is interacting with ASP594 side chain oxygen. The propyl tail of Vemurafenib is anchored in a hydrophobic pocket where it interacts with side chains of residues PHE595, ILE527, PHE516 and LEU505. The formation of this hydrophobic pocket is a consequence of the disruption of the conserved salt bridge between GLU501 and LYS483 that holds together the α C-helix and the β 3-sheet. The propyl tail of Vemurafenib

pushes out the α C-helix which in turn causes the salt bridge breaking and the formation of the hydrophobic pocket between α C-helix and β 3-sheet. The hydrophobic pocket is shown in surface representation in Fig. 13A. Moreover, LYS483 is stacked over the phenyl ring of the arylsulfonamide moiety and there are several bond paths connecting both groups. Moreover, PHE498 is also helps hold in place the phenyl ring as well as the sulfonamide moiety of Vemurafenib. This residue hangs over the binding cleft and usually do not interact directly with inhibitor because the conserved salt bridge blocks its access to the binding cleft. Thus, interactions of PHE498 are a feature specific to this type of DFG-in α C-helix-out BRAF conformation where the salt bridge is broken.

In that regard, the heterocyclic or azaindole ring of Vemurafenib mimics the interactions of ATP adenine ring and, as it was described in Fig. 13B, heterocyclic ring lies in the plane of the hinge loop and forms several interactions with backbone atoms of this loop. The pyridine nitrogen atom acts as hydrogen bond acceptor against the backbone amide hydrogen of CYS532 whereas the proton attached to pyrrole nitrogen acts as hydrogen bond donor against the carbonyl oxygen of GLN530. Other residues above and below the plane of the hinge loop also help to keep the heterocyclic ring in place by forming interaction with the π electrons of this ring. Above the plane of the hinge loop, side

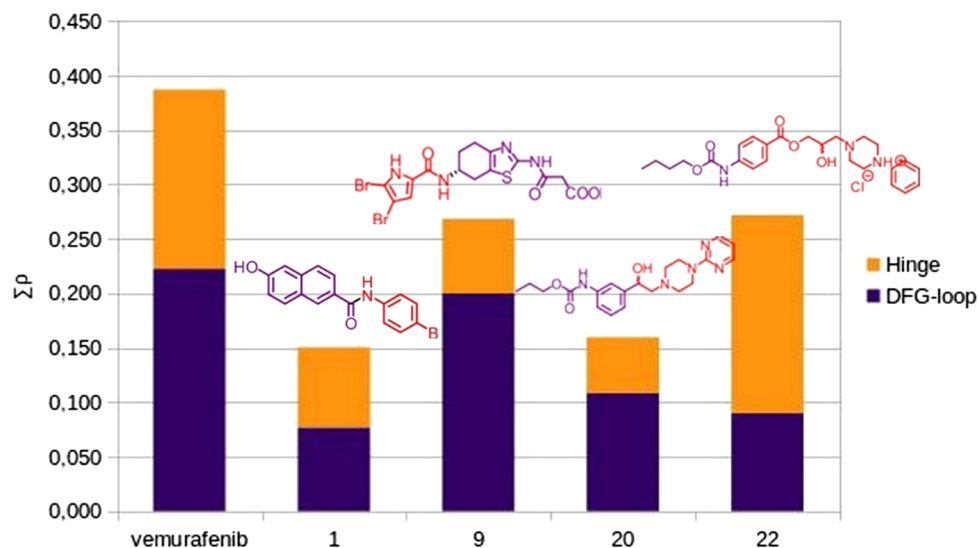


Fig. 12. Charge density sum at the intermolecular BCPs for complexes of BRAF with selected inhibitors. The interactions corresponding to the adenine-like moiety of inhibitors has been colored in orange, whereas the interactions of the inhibitors that resemble the ATP triphosphate interactions are depicted in magenta.

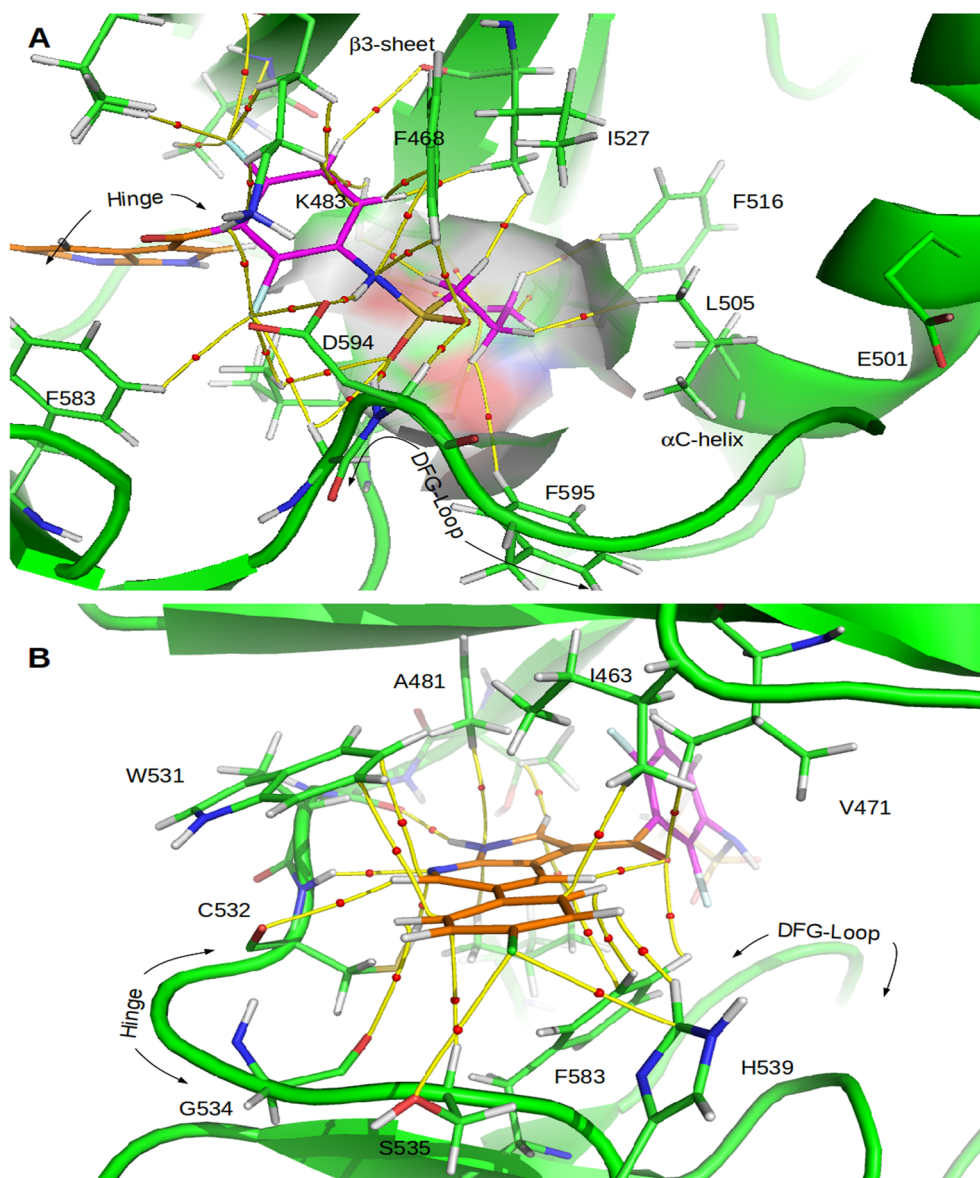


Fig. 13. Charge density molecular graphs depicting the molecular interactions of Vemurafenib at the ATP binding site. Yellow lines connecting the nuclei are the Bond Paths (BPs) and small red circles over them are the Bond Critical Points (BCPs). For easy viewing, interactions with DFG-loop and Hinge region are depicted separately in panels A and B, respectively. The interacting portions of DFG-loop and Hinge of Vemurafenib are colored in purple and orange, respectively.

chain of residues ILE463 and ALA481 act as hydrogen bond donor against the π system of the heterocyclic ring while side chain of TRP531 forms face to face stacking interactions with that ring. Below the plane of the hinge loop, PHE583 forms stacking interaction with azaindole ring and sulfhydryl proton from CYS532 acts as hydrogen bond donor against the pyridine nitrogen. The chlorophenyl ring attached to the azaindole also forms stacking interactions with PHE582 and TRP531.

Figs. 14–17 show the charge density molecular graphs of inhibitors reported in this work as they bind in the BRAF binding cleft.

As can be seen in Fig. 14, carboxylic acid oxygen atom of compound 9 forms strong interactions with backbone of DFG-loop that resemble interactions of sulfonamide oxygen atom of Vemurafenib with the same loop. In fact, DFG-loop interacting part of compound 9 is anchored with almost the same strength to the ATP binding cleft as Vemurafenib (Fig. 12). On the other hand, hinge interacting part of compound 9 fails in adopting the ATP adenine-like binding mode in which heterocycle lies in the same plane as the hinge backbone loop. Instead, the compound 9 brominated pyrrole ring is anchored above that plane with an interaction pattern similar to Vemurafenib but much weaker. It forms

stacking interactions with side chains of residues TRP531 and ILE463 above and PHE583 below the hinge plane, resembling interactions of Vemurafenib with the same residues. However, some of the strong interactions formed by Vemurafenib with the backbone of the hinge are either missed or very weak. It is evident that anchoring of compound 9 is driven by the DFG-loop interacting part of the inhibitor which might explain the deficient binding of the hinge interacting portion.

In a similar fashion, compound 20 (Fig. 15) also shows a deficient binding to enzyme hinge loop that can be explained in the same way as in compound 9 complex, namely it is the DFG-loop interacting part which governs the overall binding mode of the inhibitor (Fig. 12). In addition to interactions with backbone of DFG-loop, compound 20 is anchored in the hydrophobic pocket between α C-helix and β 3-sheet through its terminal *n*-butyl chain that resemble Vemurafenib *n*-propyl chain. Hydrophobic interactions formed by *n*-butyl chain are represented in the molecular graph of Fig. 15 by bond paths connecting hydrogen atoms of that chain with the same atoms of residues VAL501, LEU505, PHE516, ILE527 and PHE595. These hydrophobic interactions together make a non-negligible contribution to anchoring.

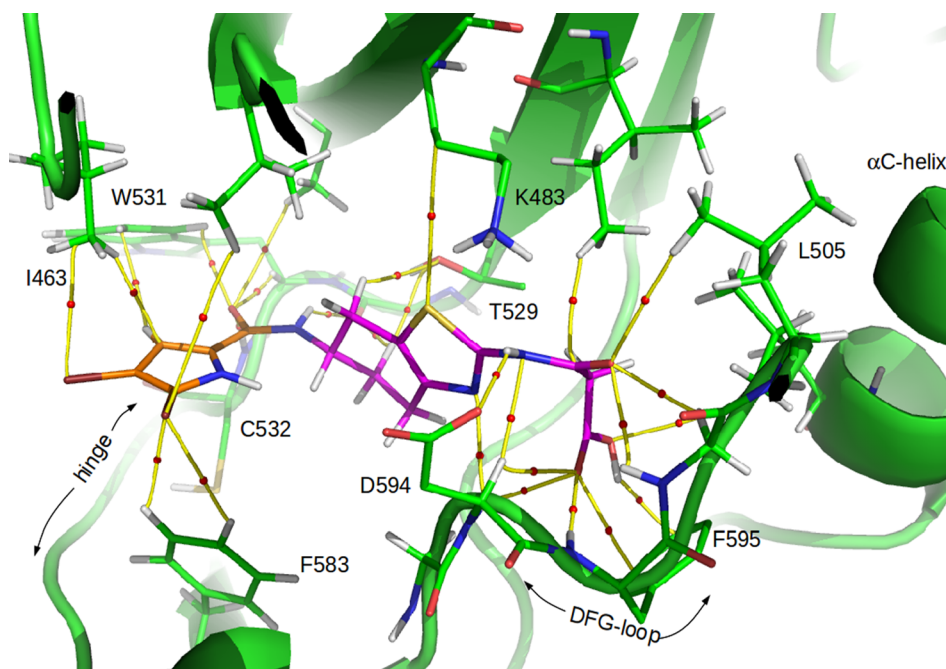


Fig. 14. Compound **9** interactions at the BRAF binding cleft. Topological elements of the charge density for the intermolecular interactions are depicted: bond paths in yellow lines and BCPs in red circles. The atoms of the inhibitor interacting with DFG-loop and hinge regions are colored in purple and orange, respectively.

Unlike to compounds **9** and **20**, the remaining inhibitors reported in this work, compounds **1** and **22** are either more strongly anchored to the hinge loop as in the case of **22** or show a balanced anchoring at both ATP binding cleft regions as in the case of **1**.

As evidenced in Fig. 16, hinge interacting ring of compound **1** lies close to the plane of the hinge region forming interactions with residues ILE463 and PHE583 above and below the plane, respectively. Additionally, hydroxyl group attached to β -naphthyl moiety of compound **1** is connected through several bond paths to the side chain of residues SER535 and SER536 from the hinge loop and also to HIS539. However, compound **1** lacks interactions with backbone of the hinge

characteristic of ATP adenine ring which explains its modest binding to that loop as compared to Vemurafenib. On the other side, bromophenyl moiety from DFG interacting part of compound **1** is anchored to the ATP binding cleft almost exclusively through hydrophobic interactions involving the bromine atom. This rather weak anchoring of DFG interacting part would allow a better positioning (and slightly stronger binding) of the hinge interacting part of compound **1** as compared to **9** and **20**. The modest improvement in hinge interacting part anchoring seems to be related to increased inhibition of the first compound with respect to the last ones.

Similarly than compound **1**, DFG-loop interacting part of compound

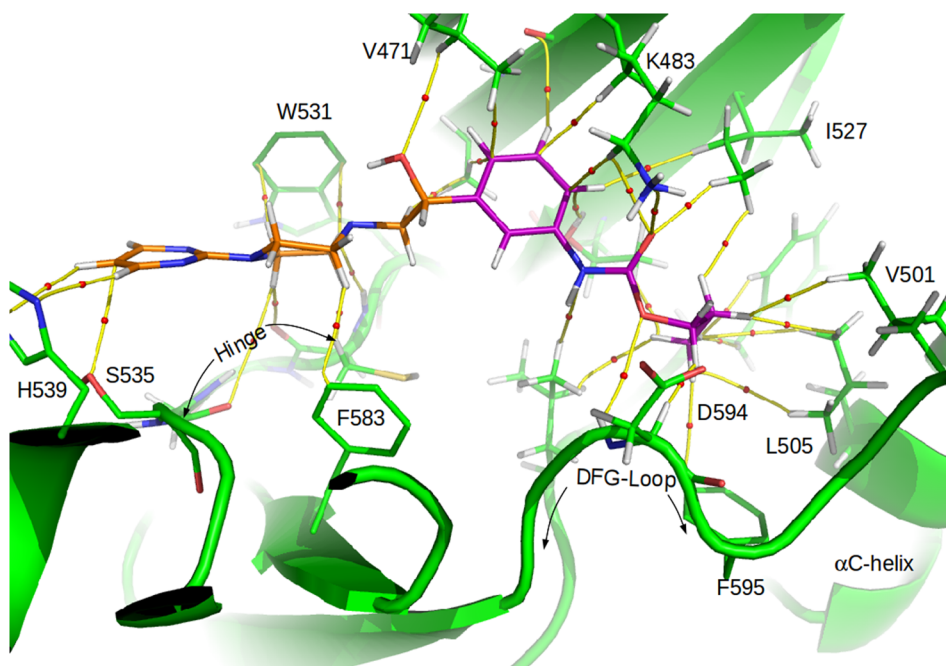


Fig. 15. Interactions of compound **20** at the BRAF binding cleft. Topological elements of the charge density for the intermolecular interactions are depicted: bond paths in yellow lines and BCPs in red circles. Inhibitor atoms interacting with DFG-loop and hinge regions colored in purple and orange, respectively.

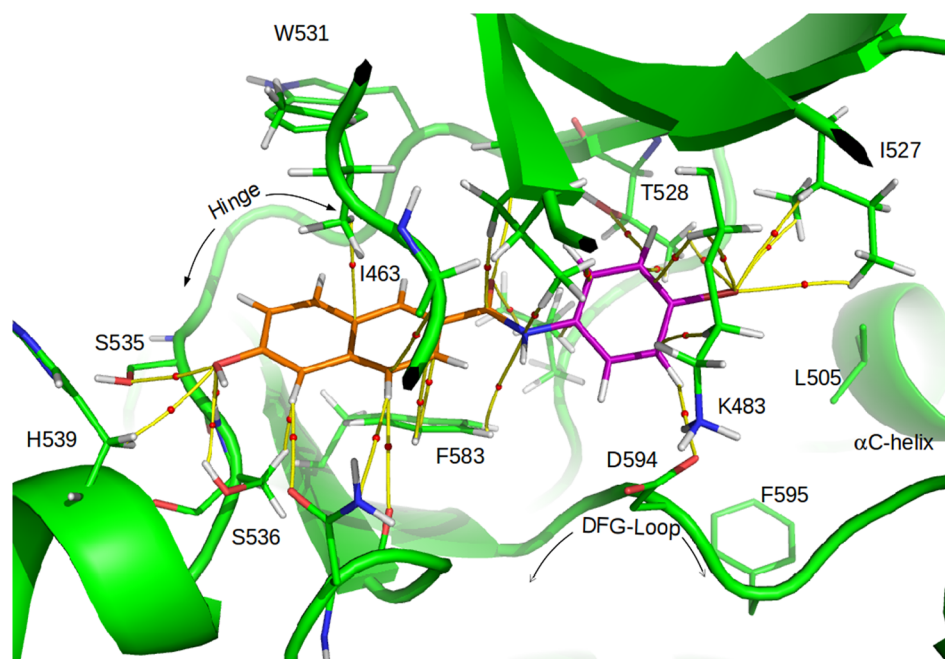


Fig. 16. Interactions of compound **1** at the BRAF binding cleft. Topological elements of the charge density for the intermolecular interactions are depicted: bond paths in yellow lines and BCPs in red circles. Inhibitor atoms interacting with DFG-loop and hinge regions colored in purple and orange, respectively.

22 (Fig. 17) binds to the ATP binding cleft mostly through weak non-polar interactions involving its *n*-butyl terminal chain. As shown in Fig. 12, anchoring of that portion of compound **22** is rather weak as compared with the binding strength of the hinge interacting part. Thus, the anchoring of compound **22** is driven by the interaction with the hinge region of the enzyme. Again, binding strength at the hinge region seems to correlate better with the inhibition activity than full inhibitor anchoring strength, since compound **22** is more active than **9** even when the total anchoring strength is almost the same for both inhibitors. Note that the only difference is that compound **22** is more strongly anchored to the hinge region while anchoring of **9** is driven by the DFG-loop interacting part, as discussed earlier.

3. Conclusions

The oncogenic kinase BRAF is mutated in many types of cancer, including melanoma, thyroid cancer, leukemia, colon cancer, among others. Particularly in melanoma, around 50% of patients harbor the mutated kinase BRAF^{V600E} that promotes cancer progression and development [1]. Melanoma is the deadliest form of skin cancer and according to the registers of the International Agency for Research in Cancer (IARC) its incidence has been growing in the last 20 years around the world (<http://gco.iarc.fr/>). Vemurafenib and Dabrafenib are two specific BRAF inhibitors that are approved for melanoma treatment. However resistance to anti BRAF therapy and secondary side effects limits its usefulness, making necessary the search of new inhibitors that could overcome these drawbacks.

Our theoretical and experimental study has allowed us to find four new structural scaffolds (eleven compounds), which could be used as excellent starting structures for the design and development of new inhibitors of BRAF. Such study was carried out in four steps: virtual screening, synthesis, bioassays and molecular modeling and has allowed us to propose compounds **1**, **9**, **20** and **22** as excellent starting structures for the development of new BRAF inhibitors. It should be noted that these compounds have been obtained from a primary screening and therefore their inhibitory activities can be considered as very significant and promising. In this sense hydroxynaphthalenecarboxamides, N-(hetero)aryl-piperazinyhydroxyalk-

ylphenylcarbamates, piperazinyethanols and piperazinypropandiols motifs represent novel cores for BRAF inhibitors and might find application to the design and development of new inhibitors.

Another interesting contribution of this work is the insight into details of certain structural aspects which are essential for understanding the formation of the complex ligand-BRAF interactions. Our QTAIM study has provided details on the molecular interactions that stabilize the formation of complexes of Vemurafenib with BRAF. Regarding the results obtained for the complexes of **1**, **9**, **20** and **22** with BRAF, such data give us an excellent guide to know which portions of these molecules should be modified in order to improve their affinity for the enzyme. It is important to remark that such information cannot be obtained using a simple method like the docking techniques or even only by using MD simulations. To obtain more detailed information about these molecular complexes, it is necessary to use more specific techniques, like for example QTAIM calculations. In fact the use of combined techniques: docking, MD simulations and QTAIM calculations, give us information about two important aspects: (i) why these novel compounds are less potent BRAF inhibitors than Vemurafenib, and (ii) crucial information about what portion of these compounds should be modified in order to increase their affinity for BRAF.

In summary, our findings provide useful information about novel structural scaffolds that reduce ERK phosphorylation and viability in BRAF^{V600E} melanoma cells. We expect that these scaffolds will serve as a start point to obtain better and more specific BRAF^{V600E} inhibitors that may potentially diminish resistance occurrence and improve the response and durability of current therapies against BRAF^{V600E}-harboring cancers.

4. Experimental section

4.1. Synthesis of N-(substituted phenyl)-hydroxynaphthalene-carboxamides 1–8

Described anilides **1**, **2** were characterized by Kos et al. [24], anilides **2–5** and **7** were characterized recently by Goncec et al. [25] and anilide **6** was characterized by Goncec et al. [26].

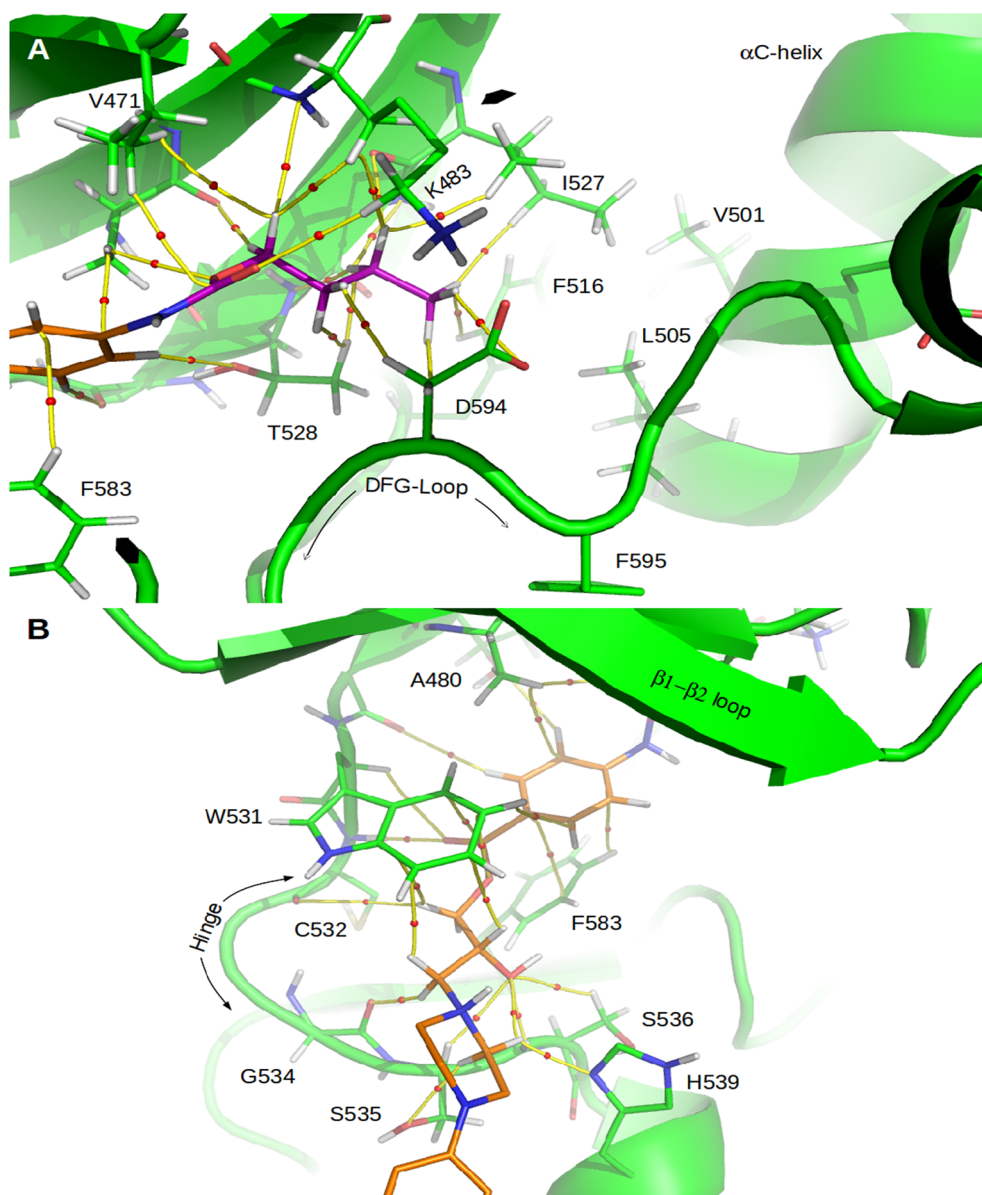


Fig. 17. Charge density molecular graphs depicting the molecular interactions of compound **22** at the ATP binding site. For easy viewing, interactions with DFG-loop and Hinge region are depicted separately in panels A and B, respectively.

4.2. Synthesis and characterization of compounds 9–13

Synthesis and characterization of compounds **9–13** have been previously reported [27–30] (See [Supplementary Information](#)).

4.3. Synthesis of compounds 14–21 (Scheme 1)

General information

Commercially available compounds were used as received, unless stated otherwise. Melting points were measured by a Kofler hot plate apparatus HMK (Franz KustnerNacht GK, Dresden, Germany) and are uncorrected. TLC was performed on silica gel 60 F₂₅₄ on aluminium plates (Merck, Darmstadt, Germany) and visualized with UV light (254 nm). Residues were purified by silica gel 60 (40–63 μm, Merck 9385) column chromatography. Infrared (IR) spectra were recorded on a Smart MIRacle™ ATR ZnSe for Nicolet™ Impact 410 Fourier-transform IR spectrometer (Thermo Scientific, West Palm Beach, FL, USA). The spectra were obtained by the accumulation of 256 scans with 2 cm⁻¹ resolution in the region of 4000–650 cm⁻¹. ¹H NMR and ¹³C NMR

spectra were standardly recorded at 25 °C in DMSO-*d*₆ as solvents on an Avance III 400 MHz FT-NMR spectrometers (Bruker, Karlsruhe, Germany). ¹H and ¹³C chemical shifts (δ) are reported in ppm. High-resolution mass spectra (HRMS) were measured using a high-performance liquid chromatograph DionexUltiMate® 3000 (Thermo Scientific, West Palm Beach, FL, USA) coupled with a LTQ Orbitrap XL™ Hybrid Ion Trap-Orbitrap Fourier Transform Mass Spectrometer (Thermo Scientific) with injection into HESI II in the positive or negative mode.

Butyl (3-acetylphenyl)carbamate(**15a–18a** = **21a**), butyl (4-acetylphenyl)carbamate(**19a**), butyl [3-(bromoacetyl)phenyl]carbamate (**15b–18b** = **21b**), butyl [4-(bromoacetyl)phenyl]carbamate (**19b**), butyl {3-[(4-(pyridine-4-yl)piperazin-1-yl)acetyl]phenyl}carbamate (**18c**), butyl {4-[(4-(pyridine-4-yl)piperazin-1-yl)acetyl]phenyl}carbamate (**19c**) and final butyl {3-[1-hydroxy-2-(4-(pyridine-4-yl)piperazin-1-yl)ethyl]phenyl}carbamate (**18**), butyl {4-[1-hydroxy-2-(4-(pyridine-4-yl)piperazin-1-yl)ethyl]phenyl}carbamate (**19**) were previously reported [44].

4.3.1. General procedure for the preparation of alkyl (2-/3-acetylphenyl) carbamates (**14a–21a**)

A solution of an appropriate alkyl chloroformate (37 mmol) in acetone (5 mL) was added dropwise to a stirred solution of 2-aminoacetophenone (5.00 g; 37 mmol) or 3-aminoacetophenone (5.00 g; 37 mmol) and pyridine (3.0 mL; 37 mmol) in acetone (20 mL), and then the mixture was heated to reflux for 3 h. The solvent was removed at reduced pressure, and the resulting solid was washed with water, and recrystallized from EtOH.

4.3.1.1. Ethyl (2-acetylphenyl)carbamate (14a). White solid, Yield 97%, m.p. 87–90 °C [90 °C [47,48]]. ¹H NMR (DMSO-*d*₆) δ 1.24 (t, 3H, -CH₃, *J* = 7.3 Hz), 2.63 (s, 3H, COCH₃), 4.10 (q, 2H, OCH₂-, *J* = 7.3 Hz), 7.15 (t, 1H, ArH, *J* = 7.7 Hz), 7.61 (t, 1H, ArH, *J* = 7.9 Hz), 8.03 (d, 1H, ArH, *J* = 7.7 Hz), 8.24 (d, 1H, ArH, *J* = 8.4 Hz), 10.99 (s, 1H, NH) [49]. ¹³C NMR (DMSO-*d*₆) δ 202.73, 152.93, 139.81, 134.42, 132.00, 122.28, 121.75, 118.52, 60.68, 28.44, 14.78.

4.3.1.2. Propyl (3-acetylphenyl)carbamate (20a). White solid, Yield 83%, m.p. 101–103 °C. ¹H NMR (DMSO-*d*₆) δ 0.94 (t, 3H, -CH₃, *J* = 7.5 Hz), 1.59–1.69 (m, 2H, -CH₂-), 2.53 (s, 3H, COCH₃), 4.06 (t, 2H, OCH₂-, *J* = 6.6 Hz), 7.44 (t, 1H, ArH, *J* = 7.9 Hz), 7.61 (d, 1H, ArH, *J* = 8.1 Hz), 7.70 (d, 1H, ArH, *J* = 8.1 Hz), 8.09 (s, 1H, ArH), 9.85 (s, 1H, NH). ¹³C NMR (DMSO-*d*₆) δ 197.45, 153.59, 139.60, 137.36, 128.96, 122.57, 122.27, 117.28, 65.73, 26.51, 21.76, 10.06.

4.3.2. General procedure for the preparation of alkyl [2-/3-(bromoacetyl)phenyl]carbamates (**14b–21b**)

Powdered CuBr₂ (80 mmol) was suspended in dry ethyl acetate (40 mL) and heated. Into a stirred refluxing suspension, a solution of appropriate alkyl (2-/3-acetylphenyl)carbamate (40 mmol) in chloroform (40 mL), was added dropwise and the mixture was refluxed for 8 h. Transformation of black CuBr₂ to white CuBr indicated completion of the reaction. Precipitate of CuBr was filtered off and the solvents were removed under reduced pressure. Solid crude products were recrystallized from *i*-PrOH.

4.3.2.1. Ethyl [2-(bromoacetyl)phenyl]carbamate (14b). White solid, Yield 79%, m.p. 102–104 °C [102–104 °C [50]]. ¹H NMR (DMSO-*d*₆) δ 1.26 (t, 3H, -CH₃, *J* = 7.3 Hz), 4.16 (q, 2H, OCH₂-, *J* = 7.3 Hz), 4.95 (s, 2H, CH₂Br), 7.19 (t, 1H, ArH, *J* = 7.7 Hz), 7.65 (t, 1H, ArH, *J* = 7.9 Hz), 8.01 (d, 1H, ArH, *J* = 8.1 Hz), 8.15 (d, 1H, ArH, *J* = 8.4 Hz), 10.55 (s, 1H, NH). ¹³C NMR (DMSO-*d*₆) δ 195.19, 153.03, 139.82, 134.76, 131.42, 122.09, 121.04, 119.42, 60.86, 35.01, 14.16.

4.3.2.2. Propyl [3-(bromoacetyl)phenyl]carbamate (20b). White solid, Yield 89%, m.p. 107–110 °C. ¹H NMR (DMSO-*d*₆) δ 0.93 (t, 3H, -CH₃, *J* = 7.3 Hz), 1.59–1.69 (m, 2H, -CH₂-), 4.05 (t, 2H, OCH₂-, *J* = 6.6 Hz), 4.88 (s, 2H, CH₂Br), 7.46 (t, 1H, ArH, *J* = 7.9 Hz), 7.67–7.74 (m, 2H, ArH), 8.10 (s, 1H, ArH), 9.90 (s, 1H, NH). ¹³C NMR (DMSO-*d*₆) δ 191.43, 153.59, 139.81, 134.51, 129.17, 123.30, 122.93, 117.61, 65.81, 33.70, 21.76, 10.13.

4.3.3. General procedure for preparation of alkyl {2-/3-[(4-arylpiperazin-1-yl)acetyl]phenyl} carbamates (**14c–21c**)

A solution of arylpiperazine (5.5 mmol) and triethylamine (0.8 mL; 5.5 mmol) in anhydrous THF (20 mL) was added dropwise to a stirred solution of an appropriate alkyl [2-/3-(bromoacetyl)phenyl]carbamate (5.5 mmol) in anhydrous THF (30 mL), and the mixture stirred for 3 h at ambient temperature. The solvents were removed under reduced pressure, and added chloroform (100 mL) and water. The organic phase was washed with additional water, dried over anhydrous sodium sulfate and the solvent removed under reduced pressure, to give a solid crude product, which was recrystallized from acetone.

4.3.3.1. Ethyl (2-[[4-(2-fluorophenyl)piperazin-1-yl]acetyl]phenyl) carbamate (14c). Yellow solid, Yield 93%, m.p. 138–142 °C. ¹H NMR (DMSO-*d*₆) δ 1.25 (t, 3H, -CH₃, *J* = 7.0 Hz), 2.66–2.70 (m, 4H, 2,6-piperazine), 2.99–3.06 (m, 4H, 3,5-piperazine), 3.91 (s, 2H, COCH₂N), 4.15 (q, 2H, OCH₂-, *J* = 7.1 Hz), 6.98–7.17 (m, 5H, ArH), 7.61 (t, 1H, ArH, *J* = 7.3 Hz), 8.09 (d, 1H, ArH, *J* = 8.1 Hz), 8.18 (d, 1H, ArH, *J* = 8.4 Hz), 10.89 (s, 1H, NH). ¹³C NMR (DMSO-*d*₆) δ 200.94, 154.87 (d, *J* = 242.8 Hz), 153.09, 139.73 (d, *J* = 8.4 Hz), 139.70, 134.27, 131.10, 124.67 (d, *J* = 3.0 Hz), 122.42, 122.14 (d, *J* = 7.6 Hz), 121.91, 119.17, 119.14 (d, *J* = 2.3 Hz), 115.78 (d, *J* = 20.5 Hz), 64.64, 60.74, 52.47, 49.97 (d, *J* = 3.1 Hz), 14.22.

4.3.3.2. Butyl (3-[[4-(4-fluorophenyl)piperazin-1-yl]acetyl]phenyl) carbamate (15c). Yellow solid, Yield 88%, m.p. 60–64 °C. ¹H NMR (DMSO-*d*₆) δ 0.92 (t, 3H, -CH₃, *J* = 7.3 Hz), 1.33–1.43 (m, 2H, -CH₂-), 1.58–1.66 (m, 2H, -CH₂-), 2.68–2.72 (m, 4H, 2,6-piperazine), 3.08–3.12 (m, 4H, 3,5-piperazine), 3.93 (s, 2H, COCH₂N), 4.11 (t, 2H, OCH₂-, *J* = 6.6 Hz), 6.93–7.08 (m, 4H, ArH), 7.44 (t, 1H, ArH, *J* = 8.1 Hz), 7.66–7.72 (m, 2H, ArH), 8.14 (s, 1H, ArH), 9.85 (s, 1H, NH). ¹³C NMR (DMSO-*d*₆) δ 196.19, 155.94 (d, *J* = 235.0 Hz), 153.57, 147.77 (d, *J* = 3.5 Hz), 139.57, 136.32, 128.90, 122.72, 122.10, 117.31, 117.05 (d, *J* = 7.6 Hz), 115.09 (d, *J* = 21.4 Hz), 63.37, 52.47, 48.73, 30.44, 18.46, 13.42.

4.3.3.3. Butyl [3-[[4-(trifluoromethyl)phenyl]piperazin-1-yl]acetyl]phenyl]carbamate (16c). White solid, Yield 81%, m.p. 105–109 °C. ¹H NMR (DMSO-*d*₆) δ 0.91 (t, 3H, -CH₃, *J* = 7.3 Hz), 1.33–1.42 (m, 2H, -CH₂-), 1.56–1.65 (m, 2H, -CH₂-), 2.68–2.72 (m, 4H, 2,6-piperazine), 3.28–3.33 (m, 4H, 3,5-piperazine), 3.95 (s, 2H, COCH₂N), 4.09 (t, 2H, OCH₂-, *J* = 6.6 Hz), 7.06 (d, 2H, ArH, *J* = 8.8 Hz), 7.43 (t, 1H, ArH, *J* = 7.7 Hz), 7.50 (d, 2H, ArH, *J* = 9.1 Hz), 7.65–7.70 (m, 2H, ArH), 8.13 (s, 1H, ArH), 9.85 (s, 1H, NH). ¹³C NMR (DMSO-*d*₆) δ 196.07, 153.56, 153.04, 139.55, 136.29, 128.89, 125.98 (q, *J* = 3.8 Hz), 124.90 (q, *J* = 270.1 Hz), 122.76, 122.07, 117.80 (q, *J* = 32.1 Hz), 117.32, 114.08, 63.91, 63.22, 52.09, 46.71, 30.43, 18.43, 13.37.

4.3.3.4. Butyl (3-[[4-(pyridin-2-yl)piperazin-1-yl]acetyl]phenyl)carbamate (17c). Yellow solid, Yield 83%, m.p. 148–152 °C. ¹H NMR (DMSO-*d*₆) δ 0.91 (t, 3H, -CH₃, *J* = 7.3 Hz), 1.33–1.43 (m, 2H, -CH₂-), 1.57–1.64 (m, 2H, -CH₂-), 2.59–2.63 (m, 4H, 2,6-piperazine), 3.47–3.51 (m, 4H, 3,5-piperazine), 3.87 (s, 2H, COCH₂N), 4.09 (t, 2H, OCH₂-, *J* = 6.6 Hz), 6.62 (dd, 1H, ArH, *J* = 7.1 Hz, *J* = 4.8 Hz), 6.81 (d, 1H, ArH, *J* = 8.2 Hz), 7.42 (t, 1H, ArH, *J* = 7.8 Hz), 7.51 (ddd, 1H, ArH, *J* = 8.7 Hz, *J* = 7.1 Hz, *J* = 2.1 Hz), 7.65 (d, 1H, ArH, *J* = 7.8 Hz), 7.70 (d, 1H, ArH, *J* = 8.2 Hz), 8.09–8.13 (m, 2H, ArH), 9.83 (s, 1H, NH). ¹³C NMR (DMSO-*d*₆) δ 196.44, 158.99, 153.66, 147.54, 139.66, 127.48, 136.41, 129.06, 122.71, 122.21, 117.28, 112.95, 107.04, 64.03, 63.65, 52.44, 44.54, 30.55, 18.60, 13.60.

4.3.3.5. Propyl (3-[[4-(pyrimidin-2-yl)piperazin-1-yl]acetyl]phenyl) carbamate (20c). White solid, Yield 78%, m.p. 98 °C. ¹H NMR (DMSO-*d*₆) δ 0.93 (t, 3H, -CH₃, *J* = 7.3 Hz), 1.60–1.70 (m, 2H, -CH₂-), 2.53–2.58 (m, 4H, 2,6-piperazine), 3.72–3.77 (m, 4H, 3,5-piperazine), 3.86 (s, 2H, COCH₂N), 4.05 (t, 2H, OCH₂-, *J* = 6.6 Hz), 6.61 (t, 1H, ArH, *J* = 4.8 Hz), 7.42 (t, 1H, ArH, *J* = 8.1 Hz), 7.63–7.72 (m, 2H, ArH), 8.12 (s, 1H, ArH), 8.35 (d, 2H, ArH, *J* = 4.8 Hz), 9.84 (s, 1H, NH). ¹³C NMR (DMSO-*d*₆) δ 196.41, 161.13, 157.81, 153.62, 139.58, 136.38, 128.95, 122.69, 122.12, 117.34, 109.98, 65.77, 63.56, 52.34, 43.16, 21.79, 10.14.

4.3.3.6. Butyl (3-[[4-(pyrimidin-2-yl)piperazin-1-yl]acetyl]phenyl) carbamate (21c). White solid, Yield 79%, m.p. 135–136 °C. ¹H NMR (DMSO-*d*₆) δ 0.90 (t, 3H, -CH₃, *J* = 7.3 Hz), 1.33–1.43 (m, 2H, -CH₂-), 1.56–1.66 (m, 2H, -CH₂-), 2.53–2.58 (m, 4H, 2,6-piperazine), 3.72–3.78 (m, 4H, 3,5-piperazine), 3.85 (s, 2H, COCH₂N), 4.08 (t, 2H, OCH₂-, *J* = 6.6 Hz), 6.60 (t, 1H, ArH,

$J = 4.8$ Hz), 7.41 (t, 1H, ArH, $J = 7.9$ Hz), 7.64–7.71 (m, 2H, ArH), 8.11 (s, 1H, ArH), 8.34 (d, 2H, ArH, $J = 4.8$ Hz), 9.83 (s, 1H, NH). ^{13}C NMR (DMSO- d_6) δ 196.41, 161.13, 157.79, 153.60, 139.58, 136.38, 128.95, 122.68, 122.12, 117.34, 109.98, 63.96, 63.56, 52.34, 43.17, 30.47, 18.50, 13.46.

4.3.4. General procedure for preparation of alkyl {2-/3-[1-hydroxy-2-(4-aryl)piperazin-1-yl]ethyl} phenyl} carbamates (**14–21**)

Solid sodium borohydride (0.30 g; 8.0 mmol) was added in small portions to a solution of the appropriate alkyl {2-/3-[(4-aryl)piperazin-1-yl]acetyl}phenyl} carbamate (4.0 mmol) in hot methanol (50 mL), and then the mixture was refluxed for 1 h. The solvent was removed under reduced pressure, and the residue was treated with distilled water (100 mL) and chloroform (100 mL). The organic phase was washed with additional water, dried over anhydrous sodium sulfate and solvent removed under reduced pressure to give a crude product, which was recrystallized from acetone.

4.3.4.1. Ethyl (2-(2-[4-(2-fluorophenyl)piperazin-1-yl]-1-hydroxyethyl} phenyl} carbamate (14**).** White solid, Yield 21%, m.p. 128–131 °C; IR (cm^{-1}): 3449 (ν NH), 2936 (ν_{as} CH₂), 2831 (ν_{s} CH₂), 1705 (ν C=O and δ NH), 1502 (ν CN), 1234 (ν_{as} COC), 1056 (ν_{s} CO); ^1H NMR (DMSO- d_6) δ 1.18 (t, 3H, -CH₃, $J = 7.0$ Hz), 2.54–2.70 (m, 6H, 2,6-piperazine; -CH₂N), 3.00–3.05 (m, 4H, 3,5-piperazine), 4.09 (q, 2H, OCH₂-, $J = 7.0$ Hz), 4.89–4.95 (m, 1H, -CH-), 5.51 (d, 1H, OH, $J = 3.7$ Hz), 6.93–7.22 (m, 6H, ArH), 7.42 (d, 1H, ArH, $J = 7.7$ Hz), 7.62 (d, 1H, ArH, $J = 7.7$ Hz), 9.83 (s, 1H, NH). ^{13}C NMR (DMSO- d_6) δ 154.80 (d, $J = 242.8$ Hz), 153.63, 139.65 (d, $J = 8.4$ Hz), 135.57, 135.55, 126.90, 126.32, 124.61 (d, $J = 3.0$ Hz), 123.42, 122.06 (d, $J = 7.6$ Hz), 121.98, 118.95 (d, $J = 2.3$ Hz), 115.77 (d, $J = 20.5$ Hz), 67.54, 65.60, 60.01, 53.32, 49.73 (d, $J = 3.1$ Hz), 14.39. HR-MS (Orbitrap): C₂₁H₂₇FN₃O₃ [M + H]⁺ calculated 388.2031 m/z , found 388.2038 m/z .

4.3.4.2. Butyl (3-{2-[4-(4-fluorophenyl)piperazin-1-yl]-1-hydroxyethyl} phenyl} carbamate (15**).** White solid, Yield 56%, m.p. 124–127 °C; IR (cm^{-1}): 3311 (ν NH), (ν_{as} CH₂) 2959, 2824 (ν_{s} CH₂), 1724 (ν C=O and δ NH), 1507 (ν CN), 1217 (ν_{as} COC), 1073 (ν_{s} CO); ^1H NMR (DMSO- d_6) δ 0.91 (t, 3H, -CH₃, $J = 7.3$ Hz), 1.33–1.43 (m, 2H, -CH₂-), 1.56–1.64 (m, 2H, -CH₂-), 2.36–2.53 (m, 2H, CH₂N), 2.63–2.67 (m, 4H, 2,6-piperazine), 3.07–3.12 (m, 4H, 3,5-piperazine), 4.07 (t, 2H, OCH₂-, $J = 6.6$ Hz), 4.66–4.72 (m, 1H, -CH-), 5.05 (d, 1H, OH, $J = 3.7$ Hz), 6.93–7.06 (m, 5H, ArH), 7.20 (t, 1H, ArH, $J = 8.1$ Hz), 7.33 (d, 1H, ArH, $J = 8.1$ Hz), 7.51 (s, 1H, ArH), 9.57 (s, 1H, NH). ^{13}C NMR (DMSO- d_6) δ 155.83 (d, $J = 235.0$ Hz), 153.57, 147.91 (d, $J = 3.5$ Hz), 145.24, 138.85, 128.08, 120.02, 116.90 (d, $J = 7.6$ Hz), 116.82, 115.99, 115.09 (d, $J = 21.4$ Hz), 69.88, 66.13, 63.66, 53.00, 48.91, 30.52, 18.49, 13.45. HR-MS (Orbitrap): C₂₃H₃₁FN₃O₃ [M + H]⁺ calculated 416.2344 m/z , found 416.2353 m/z .

4.3.4.3. Butyl [3-(1-hydroxy-2-{4-[4-(trifluoromethyl)phenyl]piperazin-1-yl}ethyl}phenyl} carbamate (16**).** White solid, Yield 84%, m.p. 130–133 °C; IR (cm^{-1}): 3297 (ν NH), 2959 (ν_{as} CH₂), 2823 (ν_{s} CH₂), 1698 (ν C=O and δ NH), 1553 (ν CN), 1234 (ν_{as} COC), 1068 (ν_{s} CO); ^1H NMR (DMSO- d_6) δ 0.91 (t, 3H, -CH₃, $J = 7.3$ Hz), 1.33–1.42 (m, 2H, -CH₂-), 1.56–1.64 (m, 2H, -CH₂-), 2.37–2.53 (m, 2H, CH₂N), 2.59–2.65 (m, 4H, 2,6-piperazine), 3.25–3.29 (m, 4H, 3,5-piperazine), 4.07 (t, 2H, OCH₂-, $J = 6.6$ Hz), 4.67–4.72 (m, 1H, -CH-), 5.08 (d, 1H, OH, $J = 3.7$ Hz), 6.98 (d, 1H, ArH, $J = 7.7$ Hz), 7.06 (d, 2H, ArH, $J = 8.8$ Hz), 7.24 (t, 1H, ArH, $J = 7.7$ Hz), 7.32 (d, 1H, ArH, $J = 7.7$ Hz), 7.49 (d, 2H, ArH, $J = 8.8$ Hz), 7.52 (s, 1H, ArH), 9.57 (s, 1H, NH). ^{13}C NMR (DMSO- d_6) δ 153.53, 153.18, 145.15, 138.81, 128.02, 125.95 (q, $J = 3.8$ Hz), 124.88 (q, $J = 270.1$ Hz), 119.98, 117.61 (q, $J = 32.1$ Hz), 116.78, 116.02, 113.92, 69.89, 65.98, 63.61, 52.67, 46.90, 30.49, 18.43, 13.39. HR-MS (Orbitrap): C₂₄H₃₁F₃N₃O₃ [M + H]⁺ calculated 466.2312 m/z , found 466.2319 m/z .

4.3.4.4. Butyl (3-{1-hydroxy-2-[4-(pyridin-2-yl)piperazin-1-yl]ethyl} phenyl} carbamate (17**).** White solid, Yield 78%, m.p. 112–144 °C; IR (cm^{-1}): 3320 (ν NH), 2959 (ν_{as} CH₂), 2808 (ν_{s} CH₂), 1699 (ν C=O and δ NH), 1542 (ν CN), 1227 (ν_{as} COC), 1074 (ν_{s} CO); ^1H NMR (DMSO- d_6) δ 0.91 (t, 3H, -CH₃, $J = 7.3$ Hz), 1.33–1.42 (m, 2H, -CH₂-), 1.56–1.63 (m, 2H, -CH₂-), 2.37–2.54 (m, 2H, CH₂N), 2.54–2.59 (m, 4H, 2,6-piperazine), 3.44–3.48 (m, 4H, 3,5-piperazine), 4.07 (t, 2H, OCH₂-, $J = 6.6$ Hz), 4.67–4.72 (m, 1H, -CH-), 5.05 (d, 1H, OH, $J = 3.7$ Hz), 6.62 (dd, 1H, ArH, $J = 6.9$ Hz, $J = 5.0$ Hz), 6.80 (d, 1H, ArH, $J = 8.7$ Hz), 6.98 (d, 1H, ArH, $J = 7.3$ Hz), 7.20 (t, 1H, ArH, $J = 7.8$ Hz), 7.32 (d, 1H, ArH, $J = 8.2$ Hz), 7.49–7.53 (m, 2H, ArH), 8.09–8.11 (m, 1H, ArH), 9.56 (s, 1H, NH). ^{13}C NMR (DMSO- d_6) δ 159.11, 153.64, 147.54, 145.37, 138.95, 137.44, 128.23, 120.09, 116.77, 115.98, 112.90, 107.04, 69.92, 66.41, 63.75, 52.94, 44.68, 30.62, 18.62, 13.62. HR-MS (Orbitrap): C₂₂H₃₁N₄O₃ [M + H]⁺ calculated 399.2391 m/z , found 399.2402 m/z .

4.3.4.5. Propyl (3-{1-hydroxy-2-[4-(pyrimidin-2-yl)piperazin-1-yl]ethyl} phenyl} carbamate (20**).** White solid, Yield 74%, m.p. 113–115 °C; IR (cm^{-1}): 3254 (ν NH), 2963 (ν_{as} CH₂), 2812 (ν_{s} CH₂), 1704 (ν C=O and δ NH), 1546 (ν CN), 1229 (ν_{as} COC), 1068 (ν_{s} CO); ^1H NMR (DMSO- d_6) δ 0.92 (t, 3H, -CH₃, $J = 7.3$ Hz), 1.57–1.67 (m, 2H, -CH₂-), 2.36–2.44 (m, 2H, CH₂N), 2.53–2.57 (m, 4H, 2,6-piperazine), 3.70–3.75 (m, 4H, 3,5-piperazine), 4.01 (t, 2H, OCH₂-, $J = 6.6$ Hz), 4.67–4.72 (m, 1H, -CH-), 5.05 (d, 1H, OH, $J = 3.7$ Hz), 6.59 (t, 1H, ArH, $J = 4.8$ Hz), 6.96 (d, 1H, ArH, $J = 7.3$ Hz), 7.19 (t, 1H, ArH, $J = 7.7$ Hz), 7.32 (d, 1H, ArH, $J = 7.9$ Hz), 7.49 (s, 1H, ArH), 8.30–8.37 (m, 2H, ArH), 9.56 (s, 1H, NH). ^{13}C NMR (DMSO- d_6) δ 161.20, 157.77, 153.60, 145.21, 138.87, 128.11, 120.04, 116.81, 116.02, 109.92, 69.83, 66.25, 65.49, 52.85, 43.31, 21.84, 10.16. HR-MS (Orbitrap): C₂₀H₂₈N₅O₃ [M + H]⁺ calculated 386.2187 m/z , found 386.2199 m/z .

4.3.4.6. Butyl (3-{1-hydroxy-2-[4-(pyrimidin-2-yl)piperazin-1-yl]ethyl} phenyl} carbamate (21**).** White solid, Yield 84%, m.p. 89–90 °C; IR (cm^{-1}): 3274 (ν NH), 2924 (ν_{as} CH₂), 2854 (ν_{s} CH₂), 1703 (ν C=O and δ NH), 1544 (ν CN), 1221 (ν_{as} COC), 1068 (ν_{s} CO); ^1H NMR (DMSO- d_6) δ 0.90 (t, 3H, -CH₃, $J = 7.3$ Hz), 1.33–1.42 (m, 2H, -CH₂-), 1.55–1.63 (m, 2H, -CH₂-), 2.37–2.50 (m, 2H, CH₂N), 2.53–2.67 (m, 4H, 2,6-piperazine), 3.68–3.76 (m, 4H, 3,5-piperazine), 4.06 (t, 2H, OCH₂-, $J = 6.6$ Hz), 4.68–4.72 (m, 1H, -CH-), 5.05 (d, 1H, OH, $J = 3.7$ Hz), 6.59 (t, 1H, ArH, $J = 4.8$ Hz), 6.96 (d, 1H, ArH, $J = 7.3$ Hz), 7.19 (t, 1H, ArH, $J = 7.7$ Hz), 7.32 (d, 1H, ArH, $J = 7.9$ Hz), 7.49 (s, 1H, ArH), 8.33–8.40 (m, 2H, ArH), 9.54 (s, 1H, NH). ^{13}C NMR (DMSO- d_6) δ 161.19, 157.76, 153.57, 145.20, 138.87, 128.10, 120.02, 116.79, 116.00, 109.90, 69.82, 66.24, 63.66, 52.84, 43.29, 30.53, 18.50, 13.46. HR-MS (Orbitrap): C₂₁H₃₀N₅O₃ [M + H]⁺ calculated 400.2343 m/z , found 400.2351 m/z .

4.4. Synthesis of compounds **22** and **23** (Scheme 2)

Synthesis, intermediates and compound target 4-[3-({4-[(butoxycarbonyl)amino]benzoyl}oxy)-2-hydroxypropyl]-1-phenylpiperazin-1-ium chloride (**22**) were described recently [31].

4.4.1. General procedure for preparation of 1-(3-{4-[(propoxycarbonyl)amino]benzoyloxy}-2-hydroxypropyl)-4-phenylpiperazin-1-ium chloride (**23**)

A mixture of oxiran-2-ylmethyl 4-[(propoxycarbonyl)amino]benzoate (**23a**) [29] (0.2 mol) and 1-(4-phenyl)piperazine (0.2 mol) in *i*-PrOH (150 mL) was heated at 80 °C for 4 h. The solvent was evaporated under reduced pressure, and the residing oil was dissolved in Et₂O. The solution of the base was converted to its chloride salt by addition of ethereal HCl. The piperazine salt was collected by filtration and recrystallized from *i*-PrOH to give white crystals.

4.4.1.1. 1-(2-hydroxy-3-{4-[(propoxycarbonyl)amino]benzoyloxy}propyl)-4-phenylpiperazin-1-ium chloride (23**).** White solid; Yield 59%;

m.p. 189–191 °C; FT-IR (ZnSe ATR, cm^{-1}): 3375 (ν NH), 3256 (ν OH), 2969 (ν CH), 2565 (ν NH^+), 1734 (ν C=O), 1702 (ν NHC = O), 1598 (ν_{ring} C=C); ^1H NMR (DMSO- d_6 , δ): 10.68 (s, 1H, $-\text{NH}^+$), 10.13 (s, 1H, $-\text{NH}$), 7.98 (d, $J = 8.7$, 2H, ArH), 7.63 (d, $J = 8.7$, 2H, ArH), 7.30–7.22 (m, 2H, ArH- N_{pip}), 7.02–6.98 (m, 2H, ArH- N_{pip}), 6.89–6.82 (m, 1H, ArH- N_{pip}), 6.07 (s, 1H, $-\text{OH}$), 4.50–4.42 (m, 1H, $-\text{CH}-$), 4.23–4.21 (m, 2H, $-\text{COOCH}_2-$), 4.06 (t, $J = 6.7$, 2H, OCH_2-), 3.83–3.61 (m, 4H, H_{pip}), 3.38–3.09 (m, 6H, H_{pip} + $-\text{CH}_2-\text{N}_{\text{pip}}$), 1.73–1.56 (m, 2H, $-\text{CH}_2-$), 0.93 (t, $J = 7.4$, 3H, $-\text{CH}_3$); ^{13}C NMR (50 MHz, DMSO- d_6 , δ): 165.0, 153.2, 149.0, 143.7, 130.1, 128.7, 122.5, 120.2, 117.0, 115.9, 65.8, 63.3, 58.9, 52.2, 51.2, 45.6, 21.7, 9.8; HR-MS (Orbitrap): $\text{C}_{24}\text{H}_{31}\text{N}_3\text{O}_5$ [M-H] calculated 440.2191 m/z, found 440.2199 m/z.

4.5. Bioassays

4.5.1. Reagents

Vemurafenib was used as a positive control. Stock solution of Vemurafenib (10 mM) and compounds of Table 1 (5 mM) were prepared in DMSO, aliquoted and preserved at -20 °C.

Primary antibodies to detect ERK total (1/2000) and pERK (T202-Y204, 1/1000) were purchased from Cell Signaling and prepared according to manufacturer specifications in TBS buffer (20 mM Tris pH 7.4, 0.9% NaCl) supplemented with 0.1% Tween-20 and 5% BSA (bovine serum albumin). Secondary antibodies conjugated to near-infrared fluorochromes (IRD, 1/30.000) were from Li-COR and prepared in TBS 0.1% Tween-20 and 3% fatty free milk as recommended by the manufacturer.

MTT reagent (3-(4,5-Dimethyl-2-thiazolyl)-2,5-diphenyl-2H-tetrazolium bromide, Sigma Aldrich) was prepared freshly according to the manufacturer instructions, as described elsewhere [51].

4.5.2. Cell culture

Lu1205 melanoma cell line was a generous gift of Dr. Pablo Bergami (Universidad de Maimónides) and was cultured in DMEM (Gibco) supplemented with 10% of fetal bovine serum (Natocor) at 37 °C in humidified atmosphere with 5% CO_2 , as described [52,53].

4.5.3. In-cell western blot (ICW)

Lu1205 cells were cultured in complete medium in 96-well plates at a density of 5.000 cells/well until 80–90% of confluence (48–72 h). Then the medium was replaced by fresh medium containing the testing compound at 1 and 10 μM and cultured for 2 h at 37 °C. ICW was performed according to standard protocols provided by Li-COR. Briefly, after the treatment, cells were fixed with ice-cold methanol (-20 °C) for 20 min and washed 3 times with PBS. Then each well was blocked with PBS 3% fatty free milk and 0.1% Tween-20 for 2 h and washed again for 5 min 5 times with PBS 0.1% Tween-20. Next, cells were incubated ON at 4 °C with a mix of primary antibodies anti-pERK (1/400) and anti-tubulin (1/800) prepared in PBS 5% BSA and 0.1% Tween-20. Secondary antibodies R800 and M680 prepared in PBS 3% fatty free milk and 0.1% Tween-20 (Li-COR, 1/1200) were incubated 1 h at room temperature. Plate was washed, dried and immediately scanned with Odyssey Clx scanner. Images were analyzed with Image Studio software.

4.5.4. Western blot

Western blot experiments were performed essentially as described Campos et al [52]. Lu1205 cells were seeded in 12-well plates at a density of 40.000 cells/well for 72 h. Then, the medium was replaced by fresh medium supplemented with the compounds of Table 1 at the final concentration of 1 and 10 μM and incubated 2 additional hours in the culture heater. Next, medium was discarded and cells were washed with ice-cold PBS and scraped into lysis buffer containing 20 mM Tris-HCl (pH 7.4), 1 mM EDTA, 150 mM NaCl, 1% Triton X-100, 1 mM β -mercaptoethanol, 1 mM Na_3VO_4 , and 1:2 protease inhibitor cocktail

(Roche). Lysates were incubated on ice for 1 h and centrifuged at 10.000 $\times g$ for 15 min. Proteins (30 μg) were separated by SDS-PAGE and blotted onto nitrocellulose. Membranes were blocked 1 h with TBS 0.1% Tween-20 and 3% fatty free milk, and incubated ON at 4 °C with specific primary antibodies as indicated. Immunopositive bands were detected with appropriate secondary antibodies (IRD, Li-COR, 1/30.000) incubated 1 h at room temperature. Membranes were scanned in Odyssey Clx and images analyzed with the software Image Studio 5.2. Results correspond to three independent experiments.

4.5.5. Cell viability assay

Lu1205 cells were cultured in 96-well plates at a density of 5.000 cells/well. The next day, culture medium was replaced by fresh medium containing compounds of Table 1 at the final concentration of 1 and 10 μM or control medium containing equal amount of DMSO and cultured for 72 h. The experiment was performed in six replicates for each concentration and each compound. MTT reagent was prepared freshly for each experiment. Briefly, MTT was dissolved in PBS (phosphate saline buffer) 5 mg/mL, vortexed 15' and sonicated 2' for five times. Then it was centrifuged at 12.000 $\times g$, 4 °C for 10' and the supernatant separated. Finally, MTT was diluted at 0.5 mg/mL in DMEM serum free and conserved at 4 °C for each experiment.

After addition of MTT reagent diluted in DMEM serum free cells were incubated three additional hours. Formazan was detected by reading the absorbance at 540 nm (Epoch). Average absorbance of each treatment (six replicates) was normalized with average absorbance of the respective control. Results correspond to three independent experiments.

4.5.6. Statistics

One way-ANOVA analyses and Tukey's post-test were used to determine the significance of western blot and cell viability bioassays.

4.6. Molecular modelling

4.6.1. Virtual screening

All the PDB files were downloaded from the protein data bank. In these structures BRAF is found as a dimer (i.e. chain A, B) which is the assembly needed for normal Ras-dependent RAF kinase activation. Since the ATP-binding site is far away from the dimer interface, only chain A from each structure was kept. Then, the monomers were structurally aligned by the protein backbone atoms, hydrogen atoms were added and the X-ray models were split into receptor, co-factors, water molecules and ligands which were saved separately.

Receptors and ligands were prepared for docking (i.e. PDB to PDBQT conversion) by using python scripts provided with the MGL Tools installation [21]. All docking calculations were performed with AutoDock4 program [21].

A single docking grid box was defined on the structurally aligned receptors in such a way that all the crystallographic ligands remain roughly in the box center. Default settings were used for other grid parameters.

Default GA search settings were used except for the number of poses generated that was set to 50 in the docking parameter file (i.e. $\text{ga_run} = 50$).

4.6.2. Computational details

4.6.2.1. MD simulations. We take the geometries obtained from the docking analysis and we soaked them in boxes of explicit water using the TIP3P model [54] and then were subjected to MD simulations. Such simulations were carried out by using the Amber software package [37] using periodic boundary conditions and cubic simulation cells. In these simulations we use the Particle Mesh Ewald method (PME) [55] with a grid spacing of 1.2 Å, a spline interpolation order of 4 Å and a real space direct sum cutoff of 10 Å. In order to obtain an integration time step of 2 fs, we applied the SHAKE algorithm. All the simulations were

performed at 310 K temperature and three MD simulations of 30 ns were conducted for each system under different starting velocity distribution functions. Thus, we obtained a total of 90 ns of simulation for each complex. The NPT ensemble was employed using Berendsen coupling to a baro/thermostat (target pressure 1 atm, relaxation time 0.1 ps). Post MD analysis was performed by using the program PTRAJ.

4.6.2.2. Quantum calculations setup. From the MD simulations we constructed reduced 3D model systems including the tested compounds and the main residues at the BRAF binding site. We only included in the different reduced models those side chains of the binding site possessing a $|\Delta G|$ value higher than 1.0 kcal/mol in the per residue analysis, together with each inhibitor.

4.6.2.3. QTAIM calculations. For the QTAIM analysis [56] we use the reduced models as input data, which was performed with the help of Multiwfn software [57]. We employed the Gaussian 16 package [58,59] for the computations and the calculations were carried out by using the B3LYP functional with dispersion correction (B3LYP-D) and 6-31G(d) as basis set. These calculations were selected considering the extension of the system in study because they ensures a reasonable compromise between the wave function quality required to obtain reliable values of the derivatives of $\rho(r)$ and the computation capability available [60].

Acknowledgements

This work was supported by grants from INC (Instituto Nacional del Cáncer-Argentina) to R.D.E., ANPCyT-Argentina PICT 2378-2014 to S.E.A. and CONICET, Argentina PIP916-2015 to S.E.A. Grants from Universidad Nacional de San Luis (UNSL-Argentina) partially supported this work. Dr. Ludmila Campos is a postdoctoral fellowship of CONICET-Argentina. This work was also partially supported by the Ministry of Education of the Czech Republic (LO1305) and by the Slovak Research and Development Agency (APVV-17-0373 and APVV-17-0318).

Appendix A. Supplementary material

Supplementary data to this article can be found online at <https://doi.org/10.1016/j.bioorg.2019.103125>.

References







- [1] M. Dankner, A.A.N. Rose, S. Rajkumar, P.M. Siegel, I.R. Watson, Classifying BRAF alterations in cancer: new rational therapeutic strategies for actionable mutations, *Oncogene* 37 (2018) 3183–3199, <https://doi.org/10.1038/s41388-018-0171-x> [pii].
- [2] Cancer, I. A. f. r. i. <https://www.iarc.fr/>, 2018.
- [3] P.T. Wan, et al., Mechanism of activation of the RAF-ERK signaling pathway by oncogenic mutations of B-RAF, *Cell* 116 (2004) 855–867 doi:S0092867404002156 [pii].
- [4] P.B. Chapman, et al., Improved survival with vemurafenib in melanoma with BRAF V600E mutation, *N. Engl. J. Med.* 364 (2011) 2507–2516, <https://doi.org/10.1056/NEJMoa1103782>.
- [5] A. Hauschild, et al., Dabrafenib in BRAF-mutated metastatic melanoma: a multicentre, open-label, phase 3 randomised controlled trial, *Lancet* 380 (2012) 358–365, [https://doi.org/10.1016/S0140-6736\(12\)60868-X](https://doi.org/10.1016/S0140-6736(12)60868-X) S0140-6736(12)60868-X [pii].
- [6] G.V. Long, et al., Dabrafenib and trametinib versus dabrafenib and placebo for Val600 BRAF-mutant melanoma: a multicentre, double-blind, phase 3 randomised controlled trial, *Lancet* 386 (2015) 444–451, [https://doi.org/10.1016/S0140-6736\(15\)60898-4](https://doi.org/10.1016/S0140-6736(15)60898-4) S0140-6736(15)60898-4 [pii].
- [7] J. Larkin, et al., Combined vemurafenib and cobimetinib in BRAF-mutated melanoma, *N. Engl. J. Med.* 371 (2014) 1867–1876, <https://doi.org/10.1056/NEJMoa1408868>.
- [8] S. Kakadia, et al., Mechanisms of resistance to BRAF and MEK inhibitors and clinical update of US Food and Drug Administration-approved targeted therapy in advanced melanoma, *Onco Targets Ther* 11 (2018) 7095–7107, <https://doi.org/10.2147/OTT.S182721ott-11-7095> [pii].
- [9] H. Shi, et al., Acquired resistance and clonal evolution in melanoma during BRAF inhibitor therapy, *Cancer Discov* 4 (2014) 80–93, <https://doi.org/10.1158/2159-8290.CD-13-0642>.
- [10] C. Montagut, et al., Elevated CRAF as a potential mechanism of acquired resistance to BRAF inhibition in melanoma, *Cancer Res.* 68 (2008) 4853–4861, <https://doi.org/10.1158/0008-5472.CAN-07-6787> 68/12/4853 [pii].
- [11] S.J. Heidorn, et al., Kinase-dead BRAF and oncogenic RAS cooperate to drive tumor progression through CRAF, *Cell* 140 (2010) 209–221, <https://doi.org/10.1016/j.cell.2009.12.040> S0092-8674(09)01626-2 [pii].
- [12] H. Shi, et al., Melanoma whole-exome sequencing identifies (V600E)B-RAF amplification-mediated acquired B-RAF inhibitor resistance, *Nat. Commun.* 3 (2012) 724, <https://doi.org/10.1038/ncomms1727> ncomms1727 [pii].
- [13] P.I. Poulikakos, C. Zhang, G. Bollag, K.M. Shokat, N. Rosen, RAF inhibitors transactivate RAF dimers and ERK signalling in cells with wild-type BRAF, *Nature* 464 (2010) 427–430, <https://doi.org/10.1038/nature08902> nature08902 [pii].
- [14] F. Su, et al., RAS mutations in cutaneous squamous-cell carcinomas in patients treated with BRAF inhibitors, *N. Engl. J. Med.* 366 (2012) 207–215, <https://doi.org/10.1056/NEJMoa1105358>.
- [15] R. Roskoski Jr., Classification of small molecule protein kinase inhibitors based upon the structures of their drug-enzyme complexes, *Pharmacol. Res.* 103 (2016) 26–48, <https://doi.org/10.1016/j.phrs.2015.10.021> S1043-6618(15)30129-8 [pii].
- [16] D.K. Treiber, N.P. Shah, Ins and outs of kinase DFG motifs, *Chem. Biol.* 20 (2013) 745–746, <https://doi.org/10.1016/j.chembiol.2013.06.001> S1074-5521(13)00214-7 [pii].
- [17] B. Agianian, E. Gavathiotis, Current insights of BRAF inhibitors in cancer, *J. Med. Chem.* 61 (2018) 5775–5793, <https://doi.org/10.1021/acs.jmedchem.7b01306>.
- [18] S. Wenglowsky, et al., Pyrazolopyridine inhibitors of B-Raf(V600E). Part 4: rational design and kinase selectivity profile of cell potent type II inhibitors, *Bioorg. Med. Chem. Lett.* 22 (2012) 6237–6241, <https://doi.org/10.1016/j.bmcl.2012.08.007> S0960-894X(12)00996-1 [pii].
- [19] W. Zheng, S.R. Johnson, in: *Cheminformatics Approaches to Virtual Screening* (ed The Royal Society of Chemistry), 2008, pp. 268–294.
- [20] E.J. Bjerrum, Machine learning optimization of cross docking accuracy, *Comput. Biol. Chem.* 62 (2016) 133–144, <https://doi.org/10.1016/j.compbiolchem.2016.04.005> S1476-9271(16)30021-4 [pii].
- [21] G.M. Morris, et al., AutoDock4 and AutoDockTools4: automated docking with selective receptor flexibility, *J. Comput. Chem.* 30 (2009) 2785–2791, <https://doi.org/10.1002/jcc.21256>.
- [22] M.M. Mysinger, M. Carchia, J.J. Irwin, B.K. Shoichet, Directory of useful decoys, enhanced (DUD-E): better ligands and decoys for better benchmarking, *J. Med. Chem.* 55 (2012) 6582–6594, <https://doi.org/10.1021/jm300687e>.
- [23] N.M. O'Boyle, et al., Open Babel: an open chemical toolbox, *J. Cheminform* 3 (2011) 33, <https://doi.org/10.1186/1758-2946-3-33> 1758-2946-3-33 [pii].
- [24] J. Kos, et al., Synthesis and antimycobacterial properties of ring-substituted 6-hydroxynaphthalene-2-carboxanilides, *Bioorg. Med. Chem.* 23 (2015) 2035–2043, <https://doi.org/10.1016/j.bmc.2015.03.018> S0968-0896(15)00185-6 [pii].
- [25] T. Goncec, et al., Halogenated 1-hydroxynaphthalene-2-carboxanilides affecting photosynthetic electron transport in photosystem II, *Molecules* 22 (2017), <https://doi.org/10.3390/molecules22101709> molecules22101709 [pii].
- [26] T. Goncec, et al., Antibacterial and herbicidal activity of ring-substituted 2-hydroxynaphthalene-1-carboxanilides, *Molecules* 18 (2013) 9397–9419, <https://doi.org/10.3390/molecules18089397> molecules18089397 [pii].
- [27] T. Tomasic, et al., Discovery of 4,5,6,7-tetrahydrobenzo[1,2-d]thiazoles as novel DNA gyrase inhibitors targeting the ATP-binding site, *J. Med. Chem.* 58 (2015) 5501–5521, <https://doi.org/10.1021/acs.jmedchem.5b00489>.
- [28] T. Tomasic, et al., Design, synthesis and biological evaluation of 4,5-dibromo-N-(thiazol-2-yl)-1H-pyrrole-2-carboxamide derivatives as novel DNA gyrase inhibitors, *Bioorg. Med. Chem.* 25 (2017) 338–349, <https://doi.org/10.1016/j.bmc.2016.10.038> S0968-0896(16)31093-8 [pii].
- [29] M. Gjorgjieva, et al., Discovery of Benzothiazole scaffold-based DNA gyrase B inhibitors, *J. Med. Chem.* 59 (2016) 8941–8954, <https://doi.org/10.1021/acs.jmedchem.6b00864>.
- [30] N. Zidar, et al., N-Phenyl-4,5-dibromopyrrolamides and N-phenylindolamides as ATP competitive DNA gyrase B inhibitors: design, synthesis, and evaluation, *J. Med. Chem.* 58 (2015) 6179–6194, <https://doi.org/10.1021/acs.jmedchem.5b00775>.
- [31] J. Tengler, et al., Synthesis and biological evaluation of 2-hydroxy-3-[(2-aryloxyethyl)amino]propyl 4-[(alkoxy)carbonyl]amino]benzoates, *Sci. World J.* 2013 (2013) 274570, <https://doi.org/10.1155/2013/274570>.
- [32] P. Marvanova, et al., Synthesis and characterization of new 3-(4-arylpiperazin-1-yl)-2-hydroxypropyl 4-propoxybenzoates and their hydrochloride salts, *Molecules* 21 (2016), <https://doi.org/10.3390/molecules21060707> molecules21060707 [pii].
- [33] I. Wortzel, R. Seger, The ERK cascade: distinct functions within various subcellular organelles, *Genes. Cancer* 2 (2011) 195–209, <https://doi.org/10.1177/1947601911407328> 10.1177_1947601911407328 [pii].
- [34] J. Tsai, et al., Discovery of a selective inhibitor of oncogenic B-Raf kinase with potent antimelanoma activity, *Proc. Natl. Acad. Sci. U.S.A.* 105 (2008) 3041–3046, <https://doi.org/10.1073/pnas.0711741105> 0711741105 [pii].
- [35] R.B. Corcoran, et al., EGFR-mediated re-activation of MAPK signaling contributes to insensitivity of BRAF mutant colorectal cancers to RAF inhibition with vemurafenib, *Cancer Discov.* 2 (2012) 227–235, <https://doi.org/10.1158/2159-8290.CD-11-0341>.
- [36] J.N. Sondergaard, et al., Differential sensitivity of melanoma cell lines with BRAFV600E mutation to the specific Raf inhibitor PLX4032, *J. Transl. Med.* 8 (2010) 39, <https://doi.org/10.1186/1479-5876-8-39> 1479-5876-8-39 [pii].
- [37] Amber 2014, 2014.
- [38] S.A. Andujar, et al., Searching the “biologically relevant” conformation of dopamine: a computational approach, *J. Chem. Inf. Model.* 52 (2012) 99–112, <https://doi.org/10.1021/ci2004225>.

- [39] E.L. Angelina, S.A. Andujar, R.D. Tosso, R.D. Enriz, N.M. Peruchena, Non-covalent interactions in receptor-ligand complexes. A study based on the electron charge density, *J. Phys. Org. Chem.* 27 (2014) 7.
- [40] L.J. Gutierrez, et al., New small-size peptides modulators of the exosite of BACE1 obtained from a structure-based design, *J. Biomol. Struct. Dyn.* 35 (2017) 413–426, <https://doi.org/10.1080/07391102.2016.1145143>.
- [41] J. Parraga, et al., Dopaminergic isoquinolines with hexahydrocyclopenta[*ij*]-isoquinolines as D2-like selective ligands, *Eur. J. Med. Chem.* 122 (2016) 27–42, <https://doi.org/10.1016/j.ejmech.2016.06.009> S0223-5234(16)30486-X [pii].
- [42] J. Parraga, et al., 2,3,9- and 2,3,11-trisubstituted tetrahydroprotoberberines as D2 dopaminergic ligands, *Eur. J. Med. Chem.* 68 (2013) 150–166, <https://doi.org/10.1016/j.ejmech.2013.07.036> S0223-5234(13)00484-4 [pii].
- [43] R.D. Tosso, et al., Molecular modeling study of dihydrofolate reductase inhibitors. Molecular dynamics simulations, quantum mechanical calculations, and experimental corroboration, *J. Chem. Inf. Model.* 53 (2013) 2018–2032, <https://doi.org/10.1021/ci400178h>.
- [44] M. Vettorazzi, et al., An integrative study to identify novel scaffolds for sphingosine kinase 1 inhibitors, *Eur. J. Med. Chem.* 139 (2017) 461–481, <https://doi.org/10.1016/j.ejmech.2017.08.017> S0223-5234(17)30620-7 [pii].
- [45] M. Vettorazzi, et al., Theoretical models to predict the inhibitory effect of ligands of sphingosine kinase 1 using QTAIM calculations and hydrogen bond dynamic propensity analysis, *J. Comput. Aided Mol. Des.* 32 (2018) 781–791, <https://doi.org/10.1007/s10822-018-0129-7> 10.1007/s10822-018-0129-7 [pii].
- [46] S. Wenglowky, et al., Highly potent and selective 3-N-methylquinazoline-4(3H)-one based inhibitors of B-Raf(V600E) kinase, *Bioorg. Med. Chem. Lett.* 24 (2014) 1923–1927, <https://doi.org/10.1016/j.bmcl.2014.03.007> S0960-894X(14)00223-6 [pii].
- [47] W.L.F.A.a.J.I.C. Smith, Quinazolines. Part VIII. Electronic effects in 2-substituted quinazolines, *J. Chem. Soc. C* 6 (1966).
- [48] F. Ishikawa, Y. Watanabe, J. Saegusa, Cyclic guanidines. IX. Synthesis of 2-amino-3,4-dihydroquinazolines as blood platelet aggregation inhibitors, *Chem Pharm Bull (Tokyo)* 28 (1980) 1357–1364.
- [49] R.K. Pandey, S.P. Dagade, M.K. Dongare, P. Kumar, Synthesis of carbamates using Yttria-Zirconia based lewis acid catalyst, *Synth. Commun.* 33 (2003) 9.
- [50] J.L. Garcia Ruano, C. Pedregal, J.H. Rodriguez, Synthesis and conformational analysis of the bioisosteres of oxisuran, *Anales de Quimica, Serie C: QuimicaOrganicaIBioquimica* 84 (1988) 9.
- [51] T. Mosmann, Rapid colorimetric assay for cellular growth and survival: application to proliferation and cytotoxicity assays, *J. Immunol. Methods* 65 (1983) 55–63 0022-1759(83)90303-4 [pii].
- [52] L.S. Campos, et al., Filamin a expression negatively regulates sphingosine-1-phosphate-induced NF-kappaB activation in melanoma cells by inhibition of Akt signaling, *Mol. Cell. Biol.* 36 (2016) 320–329, <https://doi.org/10.1128/MCB.00554-15> MCB.00554-15 [pii].
- [53] M.G. Castro, L.E. Campos, Y.I. Rodriguez, S.E. Alvarez, In vitro methods to study the modulation of migration and invasion by sphingosine-1-phosphate, *Methods Mol. Biol.* 1697 (2018) 117–131, https://doi.org/10.1007/7651_2017_51.
- [54] P. Mark, L. Nilsson, Structure and dynamics of the TIP3P, SPC, and SPC/E water models at 298 K, *J. Phys. Chem.* 105 (2001) 6.
- [55] T. Darden, D. York, L. Pedersen, Particle mesh Ewald: An N.log(*n*) method for Ewald sums in large systems, *J. Chem. Phys.* 98 (1993) 4.
- [56] R.F.W. Bader, Atoms in molecules, *Acc. Chem. Res.* 18 (1985) 7.
- [57] T. Lu, F. Chen, Multiwfn: a multifunctional wavefunction analyzer, *J. Comput. Chem.* 33 (2012) 580–592, <https://doi.org/10.1002/jcc.22885>.
- [58] Gaussian 09, 2009.
- [59] Gaussian 16, 2016.
- [60] E.E. Barrera Guisasola, et al., Pentameric models as alternative molecular targets for the design of new antiaggregant agents, *Curr. Protein Pept. Sci.* 17 (2016) 156–168 CPPS-EPUB-71511 [pii].

č.	citace	ISSN
14	HOSEK, J, J KOS , T STRHARSKY, L CERNA, P STARHA, J VANCO, Z TRAVNICEK, F DEVINSKY a J JAMPILEK. Investigation of Anti-Inflammatory Potential of N-Arylcinnamamide Derivatives. <i>MOLECULES</i> [online]. 2019, 24 (24). Dostupné z: doi: 10.3390/molecules24244531	1420-3049

Article

Investigation of Anti-Inflammatory Potential of *N*-Arylcinnamamide Derivatives

Jan Hošek ¹, Jiří Kos ¹, Tomáš Strhársky ¹, Lucie Černá ¹, Pavel Štarha ¹, Ján Vančo ¹,
Zdeněk Trávníček ¹, Ferdinand Devínsky ^{2,*} and Josef Jampílek ^{1,3,*}

¹ Division of Biologically Active Complexes and Molecular Magnets, Regional Centre of Advanced Technologies and Materials, Faculty of Science, Palacký University, Šlechtitelů 27, 78371 Olomouc, Czech Republic; jan.hosek@upol.cz (J.H.); jiri.kos@upol.cz (J.K.); tomas.strharsky01@upol.cz (T.S.); lucie.cerna02@upol.cz (L.Č.); pavel.starha@upol.cz (P.Š.); jan.vanco@upol.cz (J.V.); zdenek.travnicek@upol.cz (Z.T.)

² Faculty of Pharmacy, Comenius University, Odbojárov 10, 83232 Bratislava, Slovakia

³ Department of Analytical Chemistry, Faculty of Natural Sciences, Comenius University, Ilkovičova 6, 84215 Bratislava, Slovakia

* Correspondence: fdevinsky@gmail.com (F.D.); josef.jampilek@gmail.com (J.J.)

Received: 18 November 2019; Accepted: 10 December 2019; Published: 11 December 2019



Abstract: A series of sixteen ring-substituted *N*-arylcinnamanilides, previously described as highly antimicrobially effective against a wide spectrum of bacteria and fungi, together with two new derivatives from this group were prepared and characterized. Moreover, the molecular structure of (*2E*)-*N*-(2-bromo-5-fluorophenyl)-3-phenylprop-2-enamide as a model compound was determined using single-crystal X-ray analysis. All the compounds were tested for their anti-inflammatory potential, and most tested compounds significantly attenuated the lipopolysaccharide-induced NF-κB activation and were more potent than the parental cinnamic acid. (*2E*)-*N*-[2-Chloro-5-(trifluoromethyl)phenyl]-3-phenylprop-2-enamide, (*2E*)-*N*-(2,6-dibromophenyl)-3-phenylprop-2-enamide, and (*2E*)-*N*-(2,5-dichlorophenyl)-3-phenylprop-2-enamide demonstrated the highest inhibition effect on transcription factor NF-κB at the concentration of 2 μM and showed a similar effectiveness as the reference drug prednisone. Several compounds also decreased the level of TNF-α. Nevertheless, subsequent tests showed that the investigated compounds affect neither IκBα level nor MAPKs activity, which suggests that the *N*-arylcinnamanilides may have a different mode of action to prednisone. The modification of the C_(2,5)' or C_(2,6)' positions of the anilide core by rather lipophilic and bulky moieties seems to be preferable for the anti-inflammatory potential of these compounds.

Keywords: cinnamamides; X-ray structure; polypharmacology; anti-inflammatory potential

1. Introduction

Inflammation is physiological immune reaction against infectious agents or injury, and its main role is to eradicate the noxious agent and to restore tissue homeostasis [1]. Under normal conditions, inflammation is self-limiting, but when it is uncontrolled and continuous, chronic inflammatory phase can develop subsequently. Chronic inflammation is a hallmark of many diseases, including atherosclerosis [2], rheumatoid arthritis [3], psoriasis [4], cancer [5], chronic respiratory diseases [6,7], and type 2 diabetes mellitus [8].

To modulate and drive the inflammatory response and inflammation itself are big tasks of current medicine. One way of handling such conditions is the application of natural compounds and their derivatives. Natural material is a huge source of bioactive compounds [9,10], and many currently used

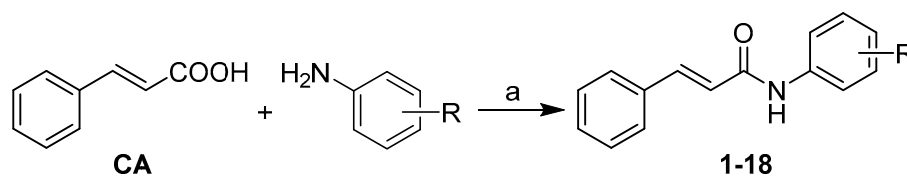
drugs are directly obtained from plants or fungi or are “nature-inspired” [11]. One such molecule is cinnamic acid (CA). It is a small organic molecule, which can be found in many kinds of plants in pure form or as a part of more complicated structures. CA and its natural and synthetic derivatives possess many interesting biological effects, such as antimicrobial [12,13], anticancer [14], anti-oxidant [13], and anti-inflammatory activities [15].

N-Arylcinnamides represent a group of synthetic derivatives of CA. This group of compounds possesses several potentially active moieties—styryl, amide (peptide-like [16]) bond, and aryl [17–22]. Thus, cinnamides can be considered as a privilege structure or a scaffold (a part) of more complex molecules in medicinal chemistry [23,24]. The series of *N*-arylcinnamide derivatives presented in this work was previously tested for their anti-microbial activity (compounds 1–15 and 17) [25,26], and three new derivatives 16 and 18 were prepared and characterized. Based on the concepts of polypharmacology, multifactorial diseases, and multitarget drugs [27], as well as the above-mentioned results, a group of eighteen *N*-arylcinnamides was chosen for the screening of their ability to moderate the inflammation-like reaction *in vitro*.

2. Results and Discussion

2.1. Chemistry

The investigated compounds (previously published compounds 1–15 and 17 [25] and two new compounds, 16 and 18) were prepared using a one-step microwave-assisted synthesis, see Scheme 1. Briefly, the carboxyl group of CA was activated with phosphorus trichloride, and then the aminolysis of an acyl chloride by a ring-substituted aniline in dry chlorobenzene gave a final anilide. All the target derivatives were purified by recrystallization from ethanol. The yields of the target compounds ranged from 65% to 91%.



R = H (1), 3-CH₃ (2), 4-CH₃ (3), 2-F (4), 3-F (5), 3-CF₃ (6), 2,5-CH₃ (7), 2,5-Cl (8), 2,6-Cl (9), 3,4-Cl (10), 3,5-Cl (11), 2,6-Br (12), 3,5-CF₃ (13), 2-F-5-Br (14), 2-Br-5-F (15), 2-Cl-4-Br (16), 2-Cl-5-CF₃ (17), 2-OCH₃-5-NO₂ (18)

Scheme 1. Synthesis of ring-substituted (2*E*)-*N*-aryl-3-phenylprop-2-enamides 1–18. Reagents and conditions: (a) PCl₃, chlorobenzene, MW, 20 min [25].

2.2. X-Ray Crystallography

Single crystal X-ray analysis revealed the molecular structure of (2*E*)-*N*-(2-bromo-5-fluorophenyl)-3-phenylprop-2-enamide (15), which is depicted in Figure 1. The crystal data and structure refinement for 15 are given in Table 1. The crystal structure consists of individual molecules, which are connected through strong N–H···O and weak C–H···O hydrogen bonds and via Br···O non-covalent contacts into 1D polymeric chains, see Figure 2 and Table 2. Moreover, the crystal structure is further stabilized by weak C–H···C hydrogen bonds and other non-covalent interactions of C···Br and C···C types connecting individual molecules into a 3D supramolecular structure. Both benzene rings (ring 1 = C4, C5, C6, C7, C8, C9, and ring 2 = C10, C11, C12, C13, C14, C15) are nearly ideally planar with the maximal deviation of 0.010(4) Å for the C11 atom from the least-squares planes fitted through the mentioned carbon atoms. The rings are mutually oriented by the dihedral angle of 47.0(2)°, and this value is substantially lower as compared to the values of 73.89(7)° and 79.46(7)° found for *N*-(2-fluorophenyl)cinnamamide [28] (in two crystallographically independent molecules with the asymmetric unit) and the value of 24.6(1)° found for *N*-(3-chlorophenyl)cinnamamide [29]. Moreover, there are also next two known

structures of halogenated *N*-phenylcinnamamides, i.e., *N*-(3,5-difluoro-4-chlorophenyl)cinnamide and *N*-(3,4-difluorophenyl)cinnamide [30], in which both aromatic rings are almost coplanar, with the dihedral angle of 0.54° and 2.04°, respectively. The selected bond lengths and angles of compound **15** are given in Table S1 in Supplementary Materials. Interestingly, the C1–O1 bond length is significantly longer (1.312(6) Å) than that of a typical double C=O bond (an average value of 1.235(7) Å was found by the analysis of 39 structures containing the *N*-phenylcinnamamide skeleton deposited in CSD, ver. 5.40, Aug 2019 update). This lengthening of this bond in compound **15** may be connected with the involvement of the O1 atom into non-covalent bonding (see Figure 2).

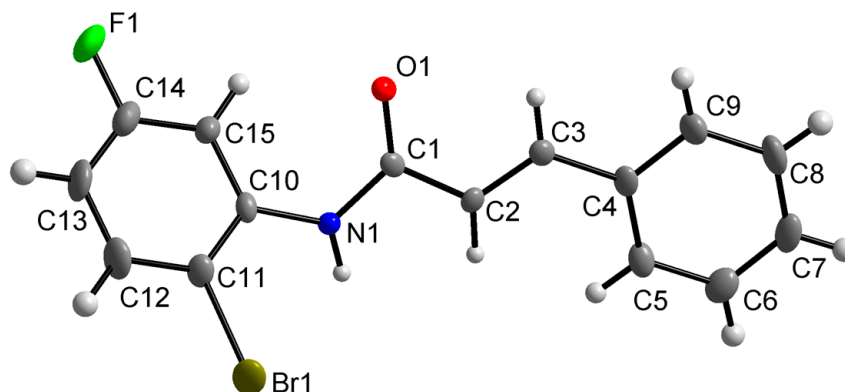


Figure 1. Molecular structure of (2*E*)-*N*-(2-bromo-5-fluorophenyl)-3-phenylprop-2-enamide (**15**). Non-H atoms are drawn as thermal ellipsoids at 50% probability level. H-atoms are not labelled and are displayed as balls in light-grey color.

Table 1. Crystal data and structure refinement for compound **15**.

Formula	C ₁₅ H ₁₁ BrFNO
Formula weight	320.16
Temperature	150(2) K
Wavelength	0.71073 Å
Crystal system	Monoclinic
Space group	<i>P</i> 2 ₁ / <i>c</i>
Unit cell dimensions	<i>a</i> = 9.410(3) Å, α = 90° <i>b</i> = 14.645(5) Å, β = 108.633(15)° <i>c</i> = 10.184(4) Å, γ = 90°
Volume	1329.9(8) Å ³
<i>Z</i>	4
Density (calculated)	1.599 g/cm ³
Absorption coefficient	3.093 mm ⁻¹
<i>F</i> (000)	640
Crystal size	0.140 × 0.140 × 0.060 mm
Theta range for data collection	2.284 to 24.999°
Index ranges	−11 ≤ <i>h</i> ≤ 11, −17 ≤ <i>k</i> ≤ 17, −12 ≤ <i>l</i> ≤ 12
Reflections collected	22311
Independent reflections	2339 [R(int) = 0.1233]
Absorption correction	Semi-empirical from equivalents
Refinement method	Full-matrix least-squares on <i>F</i> ²
Data/restraints/parameters	2339/0/160
Goodness-of-fit on <i>F</i> ²	1.067
Final <i>R</i> indices [<i>I</i> > 2σ(<i>I</i>)]	<i>R</i> ₁ = 0.0523, <i>wR</i> ₂ = 0.1295
<i>R</i> indices (all data)	<i>R</i> ₁ = 0.0746, <i>wR</i> ₂ = 0.1391
Largest diff. peak and hole	1.162 and −1.065 e.Å ⁻³

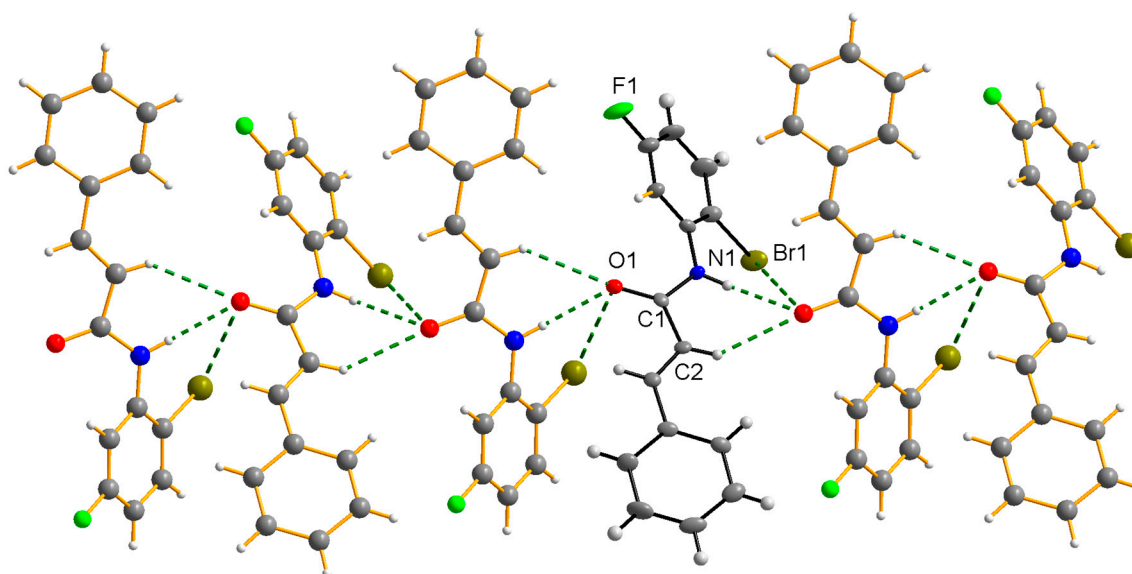


Figure 2. Part of the crystal structure of (2E)-N-(2-bromo-5-fluorophenyl)-3-phenylprop-2-enamide (**15**) showing N–H···O hydrogen bonds and Br···O non-covalent contacts (dashed green lines), connecting individual molecules into infinite polymeric chains.

Table 2. Parameters of selected non-covalent contacts (in Å and °) in the crystal structure of compound **15**.

D–H···A	d(D–H)	d(H···A)	d(D···A)	<(DHA)
N(1)–H(1)···O(1)(i)	0.88	2.20	3.065(5)	167.5
C(2)–H(2)···O(1)(i)	0.95	2.71	3.507(6)	141.8
Br(1)···O(1)(i)	–	–	3.346(3)	–

Symmetry transformations used to generate equivalent atoms: (i) $x, -y+1/2, z+1/2$.

2.3. In Vitro Cell Viability Assay

The panel of tested compounds was evaluated for their cytotoxicity against THP1-Blue™ NF-κB cells, see Table 3 and Figure S1 in Supplementary Materials for more information about dose-response curves. Compounds **10** (R = 3,4-Cl), **11** (R = 3,5-Cl), and **13** (3,5-CF₃) showed the lowest IC₅₀ values of 6.28 ± 2.32 , 2.43 ± 1.06 , and 2.17 ± 1.19 μM, respectively. The moderate cytotoxicity against THP1-Blue™ NF-κB cells was found in case of compound **6** (3-CF₃) with IC₅₀ = 11.60 ± 1.13 μM. All these compounds were also previously identified to have moderate influence on cell viability in different cancer cell lines [25].

The obtained results of cytotoxicity correlate with the log *k* and Clog *P* parameters calculated in the work of Pospisilova et al. [25]—the higher values of log *k* and Clog *P* parameters are, the higher IC₅₀ values are, for example, compound **6** (log *k* = 0.4859, IC₅₀ = 11.60 μM) >>>> compound **10** (log *k* = 0.6821, IC₅₀ = 6.28 μM) >> compound **11** (log *k* = 0.8155, IC₅₀ = 2.43 μM) ≈ compound **13** (log *k* = 0.9814, IC₅₀ = 2.17 μM). Naturally, these observations correspond with distributive parameters π (see Table 3), a constant characterizing hydrophobicity (lipophilicity contribution) of individual moieties, substituents, and substructures in some skeleton [31,32]; compound **6** (π_{Ar} = 2.73) >>>> compound **10** (π_{Ar} = 2.77) >> compound **11** (π_{Ar} = 2.90) ≈ compound **13** (π_{Ar} = 3.98). Nevertheless, di-substitution with highly lipophilic and electron-withdrawing substituents (Cl or CF₃) on the C_{(3,5)'} or C_{(3,4)'} positions of the anilide ring seems to be the most important for achieving a high antiproliferative effect. On the other hand, these facts correspond with the high antitubercular and antistaphylococcal potency of those agents as described recently [25].

Table 3. List of ring-substituted *N*-arylcinnamanilides **1–18** and their influence on the viability of THP1-Blue™ NF-κB cell line (IC₅₀ [μM] ± SEM of three independent measurements), NF-κB inhibition [%] in comparison with the starting cinnamic acid (CA), predicted values of distributive parameters π, and molar volume (MV [cm³]) of anilide (Ar).

Comp.	R	IC ₅₀ [μM] ± SEM	NF-κB inhibition [%]	π _{Ar} ^a	MV ^a [cm ³]
1	H	>30	0 ^b	1.76	80.88
2	3-CH ₃	>30	9.00 ^b	2.22	97.11
3	4-CH ₃	>30	8.50 ^b	2.22	97.11
4	2-F	>30	2.87 ^b	2.26	85.90
5	3-F	>30	9.67 ^b	1.78	85.90
6	3-CF ₃	11.60 ± 1.13	16.67 ^b	2.73	113.57
7	2,5-CH ₃	>30	14.78 ^b	2.68	113.27
8	2,5-Cl	>30	22.50 ^b	2.73	103.54
9	2,6-Cl	>30	14.11 ^b	2.72	103.54
10	3,4-Cl	6.28 ± 2.32	10.89 ^c	2.77	103.54
11	3,5-Cl	2.43 ± 1.06	16.22 ^c	2.90	103.54
12	2,6-Br	>30	23.12 ^b	2.85	107.33
13	3,5-CF ₃	2.17 ± 1.19	19.67 ^c	3.98	145.57
14	2-F-5-Br	>30	19.67 ^b	2.87	99.09
15	2-Br-5-F	>30	17.78 ^b	2.28	99.09
16	2-Cl-4-Br	>30	13.67 ^b	3.09	105.44
17	2-Cl-5-CF ₃	>30	27.12 ^b	3.28	124.72
18	2-OCH ₃ -5-NO ₂	>30	17.56 ^b	1.12	115.77
CA	–	>30	11.44 ^b	–	–

^a calculated using ACD/Percepta ver. 2012 (Advanced Chemistry Development, Inc., Toronto, ON, Canada),

^b concentration of compounds 2 μM, ^c concentration of compounds 0.5 μM.

2.4. Inhibition of NF-κB Activity and Cell Signaling In Vitro

Cinnamic acid alone and several CA derivatives demonstrated the ability to influence the activity or expression of the pro-inflammatory transcription factor NF-κB in previous studies [15,33]. The effect of *N*-arylcinnamamide derivatives with the modified cinnamyl phenyl ring on NF-κB activity was studied by Chen et al. [23] as well as by Jan et al. [34], but the effect of derivatives with the unchanged cinnamyl moiety is described here for the first time. Apart from compounds **1** and **4**, all anilides were able to significantly attenuate the lipopolysaccharide (LPS)-induced NF-κB activation by 10% to 27% in the non-toxic concentrations of 2 and 0.5 μM (used for compounds **10** (R = 3,4-Cl), **11** (R = 3,5-Cl), **13** (R = 3,5-CF₃) with the lowest cell viability), see Figure 3. Moreover, most *N*-arylcinnamamide derivatives were more active than the parental CA. The highest inhibitory effect on NF-κB activity was observed for (*2E*)-*N*-[2-chloro-5-(trifluoromethyl)phenyl]-3-phenyl-prop-2-enamide (**17**), which was comparable with prednisone (PDS) applied at the same concentration level of 2 μM. The overall results indicate that monosubstituted *N*-arylcinnamanilides show lower inhibitory effect on NF-κB activity than the di-substituted ones. (*2E*)-3-Phenyl-*N*-[3-(trifluoromethyl)phenyl]prop-2-enamide (**6**), with bulky CF₃ substitution of the anilide ring, is the only exception.

The electron σ parameters of individual substituents (listed in Pospisilova et al. [25]) play only a secondary role in this matter; however, it can be stated that the electron-withdrawing properties of the anilide substituent seem to be more advantageous. On the other hand, the position of the substituents on the anilide ring, lipophilicity, and bulkiness influence the activity of the compounds significantly. C_(2,5)' or C_(2,6)' di-substitutions by bulky substituents are preferred. The dependences of the inhibition of NF-κB on the lipophilicity expressed by distributive π parameters of the whole anilide ring and on

the molar volume of the whole anilide ring are illustrated in Figure 4, where the discussed compounds are shown, with the exception of toxic compounds 10, 11, 13, and compound 18 (R = 2-OCH₃-5-NO₂), which is excluded due to the completely different nature of the substituents compared to the rest (that are methyls or halogens). Figure 4A,B show the trends of the increasing ability to inhibit NF- κ B with increasing distributive π parameters (correlation coefficient $r = 0.7892$, $n = 14$) as well as anilide ring bulkiness ($r = 0.8118$, $n = 14$).

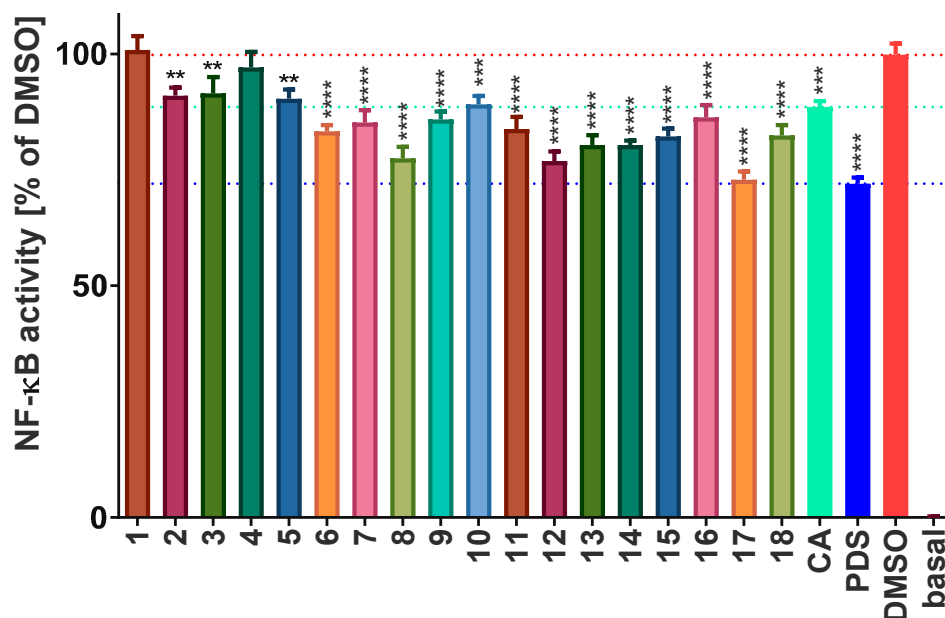


Figure 3. Effect of the tested compounds on the activity of transcription factor NF- κ B. THP1-Blue™ NF- κ B cells were pretreated by compounds (2 μ M; or 0.5 μ M for 10, 11, and 13) or prednisone (PDS; 2 μ M) dissolved in DMSO at indicated concentrations for 1 h. Then, lipopolysaccharide (LPS) 1 μ g/mL was added to trigger the NF- κ B activation. The activity of NF- κ B was measured 24 h after LPS stimulation using QuantiBlue™ assay. Graph represents mean \pm SEM. Red dotted line show value of DMSO-only treated group, azur dotted line CA treated group, and blue dotted line PDS treated group. ** indicates statistical significance ($p < 0.01$) to DMSO group; *** indicates statistical significance ($p < 0.001$) to DMSO group **** indicates statistical significance ($p < 0.0001$) to DMSO group.

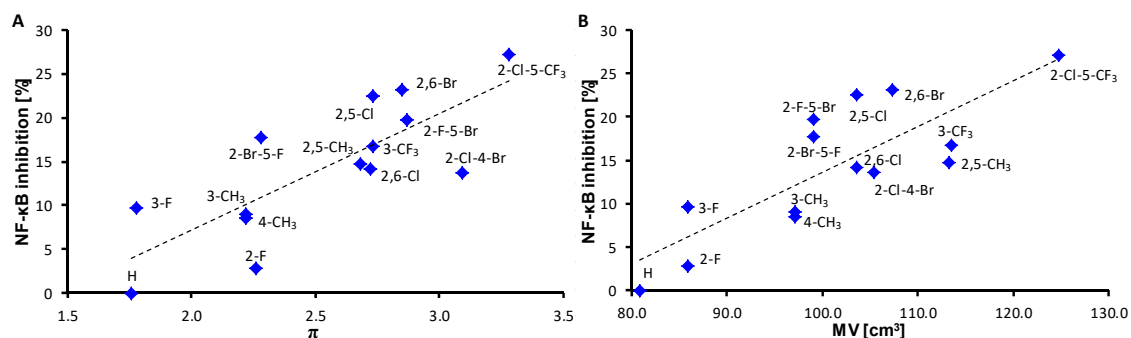


Figure 4. Dependence of NF- κ B inhibition [%] on lipophilicity contributions of anilide rings expressed as distributive π parameters (A) and on molar volumes (MV [cm^3]) of the whole anilide rings (B).

To confirm the effect of the most potent compound 17 on NF- κ B, the analysis of its nuclear translocation was performed (see Figure 5). There is visible nuclear translocation of NF- κ B after LPS stimulation. This movement was slightly affected by 17. It is in agreement with observed inhibition of NF- κ B activity and it can delineate the possible mechanisms of action.

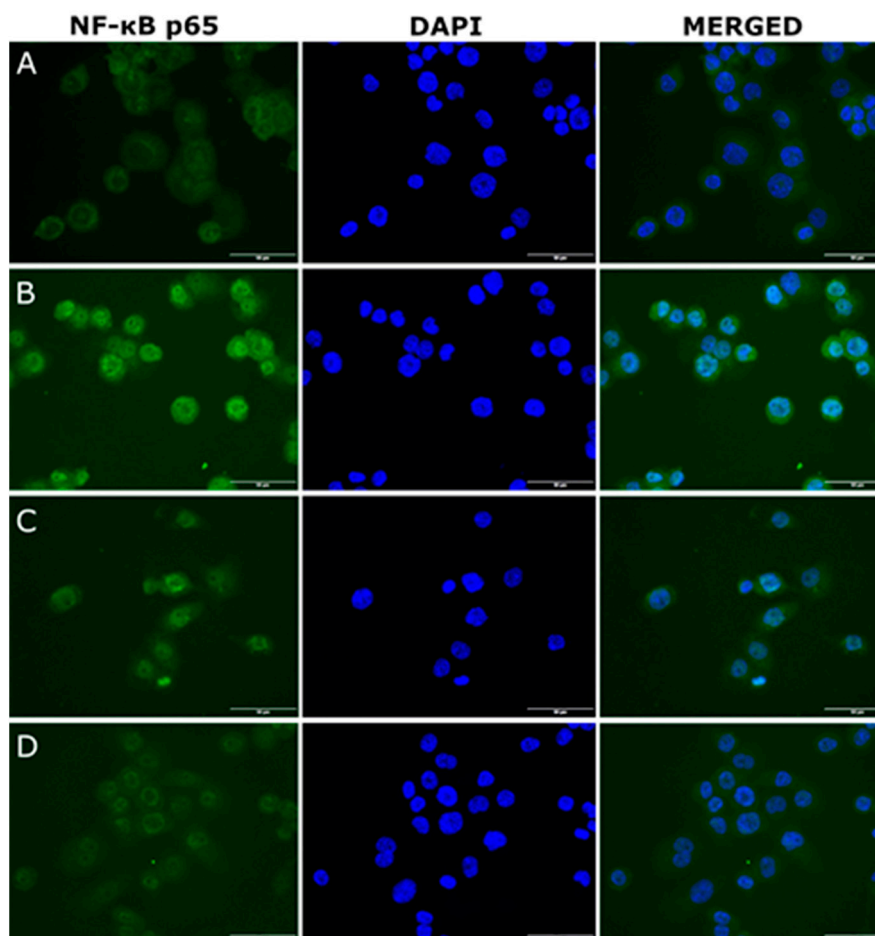


Figure 5. Effect of **17** ($R = 2\text{-Cl-5-CF}_3$) and prednisone on the cellular distribution of transcription factor NF- κ B. THP1-Blue™ NF- κ B cells were pretreated by **17** $2\ \mu\text{M}$ (**D**) or prednisone (PDS; $2\ \mu\text{M}$) (**C**), or by pure DMSO (**A,B**) for 1 h. Then, lipopolysaccharide (LPS) $1\ \mu\text{g/mL}$ was added to activate the NF- κ B (**B–D**). Control cell remained without LPS (**A**). The cellular distribution of NF- κ B was observed 1 h after LPS stimulation using fluorescent microscope.

Having discovered the high ability of compounds **17** ($R = 2\text{-Cl-5-CF}_3$) and **8** ($R = 2,5\text{-Cl}$) to moderate the activity of NF- κ B, we decided to elucidate further their mechanism of action and compare it with CA used as the reference compound. The activity of NF- κ B is driven by the level of its inhibitor I κ B and by the activity of several mitogen-activated protein kinases (MAPKs), especially p38 and c-Jun *N*-terminal kinase (JNK) [35,36], as well as ERK [37]. The influence of CA on NF- κ B and MAPKs expression and activity was described previously [38,39], the same as for some cinnamides [23]. Our results showed no effect of compounds **17**, **8**, and CA on the I κ B α levels and MAPKs activity, see Figure 6. Similar effects were also referred for a synthetic derivative of CA, WK2-16 ((*E*)-*N*-hydroxy-4-methoxy-2-(biphenyl-4-yl)cinnamide) [34,40]. It was proposed that WK2-16 could influence transcription factors YY-1 and STAT-1/-3. However, the discrepancy between the NF- κ B inhibition and unobserved alteration of the above-mentioned signaling pathways could be also explained by a different mode of action as compared to known anti-inflammatory drugs, like PDS. It can be hypothesized that the tested *N*-arylcinnamanilides might act either via the inhibition of the nuclear translocation of NF- κ B (as was described above), or influence its binding to DNA [41,42], or act by epigenetic regulation [43]. A combination of more than one mechanism of action is not excluded as well.

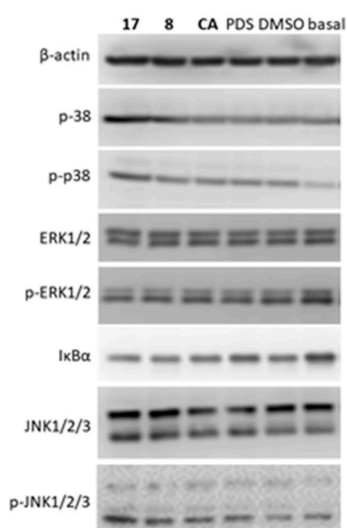


Figure 6. Effect of *N*-arylcinnamamide derivatives on the activation of MAPKs. THP1-Blue™ NF- κ B cells were pretreated by compounds or PDS (2 μ M) for 1 h, then LPS (1 μ g/mL) was added to trigger the inflammatory signaling. Cells were collected 30 min after LPS stimulation and selected proteins were detected by Western blot and immunodetection.

2.5. Inhibition of TNF- α Secretion

To verify the effect of tested compounds on NF- κ B activity, the secretion of TNF- α , which is under its transcription control [44], was measured. CA is known for its ability to attenuate the production of this pro-inflammatory cytokine in vitro and in vivo [45,46]. In our experiment, pure CA did not affect the TNF- α production, see Figure 7. This could be caused by the usage of a very low, but pharmacologically relevant concentration of 2 μ M. On the other hand, compounds **12** (R = 2,6-Br), **6** (R = 3-CF₃), and **17** (R = 2-Cl-5-CF₃) that showed the highest inhibitory effect on NF- κ B were able to significantly decrease the level of TNF- α by 10%, 10.4%, and 12.4%, respectively. This correlates with the observed attenuation of NF- κ B, when compound **17** reached the greatest effect. However, the effect of PDS was notably higher—the reduction of TNF- α by 70.3%. In case of NF- κ B inhibition, the tested compounds are comparable with PDS, but PDS is more effective in TNF- α decreasing. This indicates that the modes of action of PDS and the discussed *N*-arylcinnamanilides are different.

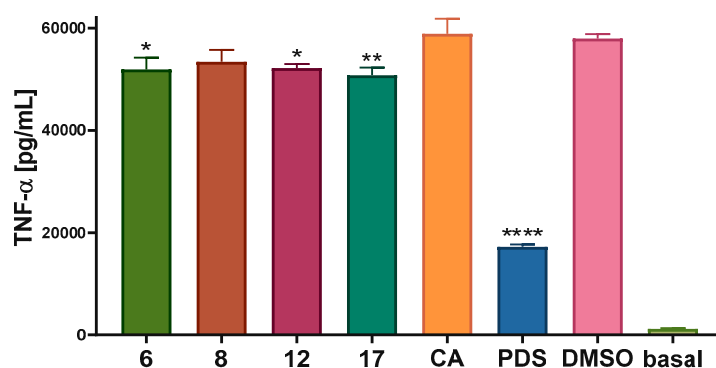


Figure 7. Effect of *N*-arylcinnamamide derivatives on the secretion of TNF- α . THP1-Blue™ NF- κ B cells were differentiated to macrophages by PMA. Such cells were pretreated by compounds or PDS (2 μ M) for 1 h, then LPS (1 μ g/mL) was added to trigger the inflammatory signaling. Cultivation medium was collected 24 h after LPS stimulation, and the amount of TNF- α was measured by the ELISA technique. Graph represents mean \pm SEM. * indicates statistical significance ($p < 0.05$) to DMSO group; ** indicates statistical significance ($p < 0.01$) to DMSO group **** indicates statistical significance ($p < 0.0001$) to DMSO group.

3. Materials and Methods

3.1. Chemistry

3.1.1. General Information

All reagents were purchased from Merck (Sigma-Aldrich, St. Louis, MO, USA) and Alfa (Alfa-Aesar, Ward Hill, MA, USA). Reactions were performed using a CEM Discover SP microwave reactor (CEM, Matthews, NC, USA). Melting points of **16** and **18** were determined on an apparatus STA 449 F1 Jupiter (NETZSCH, Selb, Germany). Infrared (IR) spectra were recorded on an UATR Zn/Se for a Spectrum Two™ Fourier-transform IR spectrometer (PerkinElmer, Waltham, MA, USA). The spectra were obtained by the accumulation of 32 scans with 4 cm⁻¹ resolution in the region of 4000–400 cm⁻¹. All ¹H- and ¹³C-NMR spectra were recorded on a JEOL JNM-ECA 600II NMR spectrometer (600 MHz for ¹H and 150 MHz for ¹³C, Jeol, Tokyo, Japan) in dimethyl sulfoxide-*d*₆ (DMSO-*d*₆). ¹H and ¹³C chemical shifts (δ) are reported in ppm. High-resolution mass spectra were measured using a high-performance liquid chromatograph Dionex UltiMate® 3000 (Thermo Scientific, West Palm Beach, FL, USA) coupled with an LTQ Orbitrap XL™ Hybrid Ion Trap-Orbitrap Fourier Transform Mass Spectrometer (Thermo Scientific) equipped with a HESI II (heated electrospray ionization) source in the positive mode.

3.1.2. Synthesis

Cinnamic acid (3.37 mM) was suspended at room temperature in dry chlorobenzene (20 mL) inside a microwave tube, where phosphorus trichloride (1.7 mM) and the corresponding aniline derivative (3.37 mM) were added dropwise. Following this step, a magnetic stirrer was added to the tube and the reaction mixture was transferred to the microwave reactor at 120 °C for 20 min, where the synthesis at elevated pressure was performed. After the mixture was cooled to 60 °C, the solvent was evaporated in vacuum. A solid residue was washed with 2 M HCl, and a crude product was recrystallized, using 96% ethanol first, and then using 50% ethanol.

The *N*-arylcinnamanilides **1–15** and **17** were prepared and characterized previously by Pospisilova et al. [25].

(*2E*)-*N*-(4-bromo-2-chlorophenyl)-3-phenylprop-2-enamide (**16**). Yield 65%; Mp 169 °C; IR (cm⁻¹): 3265, 3069, 3028, 1654, 1619, 1575, 1523, 1470, 1381, 1336, 1282, 1183, 969, 860, 825, 758, 709, 696, 647, 630, 567, 552, 506; ¹H-NMR (DMSO-*d*₆), δ: 9.57 (s, 1H), 7.93 (d, *J* = 8.7 Hz, 1H), 7.80 (d, *J* = 2.3 Hz, 1H), 7.66–7.60 (m, 3H), 7.57 (dd, *J* = 8.7 Hz, 2.3 Hz, 1H), 7.48–7.41 (m, 3H), 7.12 (d, *J* = 16 Hz, 1H), see Figure S2; ¹³C-NMR (DMSO-*d*₆), δ: 164.01, 141.21, 134.63, 134.60, 131.64, 130.49, 130.01, 129.04, 127.89, 126.66, 121.57, 116.86, see Figure S3; HR-MS: [M + H]⁺ calculated 335.9785 *m/z*, found 335.9784 *m/z*, see Figure S4.

(*2E*)-*N*-(2-methoxy-5-nitrophenyl)-3-phenylprop-2-enamide (**18**). Yield 78%; Mp 209 °C; IR (cm⁻¹): 3421, 3356, 1683, 1595, 1524, 1511, 1476, 1449, 1420, 1340, 1271, 1163, 1139, 1079, 1022, 978, 823, 769, 746, 710, 637, 591; ¹H-NMR (DMSO-*d*₆), δ: 9.74 (s, 1H), 9.22 (d, *J* = 2.7 Hz, 1H), 8.04 (dd, *J* = 9.1 Hz, 2.7 Hz, 1H), 7.66–7.60 (m, 3H), 7.48–7.40 (m, 3H), 7.30 (s, 1H), 7.27 (d, *J* = 6.9 Hz, 1H), 4.03 (s, 3H), see Figure S5; ¹³C-NMR (DMSO-*d*₆), δ: 164.39, 154.10, 141.06, 140.37, 134.74, 129.95, 129.02, 128.03, 127.89, 122.08, 120.25, 115.38, 110.93, 56.79, see Figure S6; HR-MS: [M + H]⁺ calculated 299.1026 *m/z*, found 299.1020 *m/z*, see Figure S7.

3.2. X-Ray Crystallography

Crystals of (*2E*)-*N*-(2-bromo-5-fluorophenyl)-3-phenylprop-2-enamide (**15**) suitable for a single X-ray analysis were prepared by the slow evaporation of ethanol from the solution of compound **15** at 4 °C. The diffraction data were collected on a D8 QUEST diffractometer (Bruker) equipped with a PHOTON 100 CMOS detector, using Mo-Kα radiation (λ = 0.71073 Å). The data collection and reduction were performed using the APEX3 software [47]. The structure was solved by a direct method

(SHELXS) and refined using the Bruker SHELXTL software package [48]. The benzene ring, involving C4, C5, C6, C7, C8, and C9 atoms, was refined with a riding group fitting (AFIX 66) with the fixed C–C bonds (1.39 Å). All H-atoms were found from difference Fourier maps and refined using a riding model, with C–H = 0.95 Å for (CH) and 0.88 Å for (NH) and with $U_{\text{iso}}(\text{H}) = 1.2 U_{\text{eq}}(\text{CH}, \text{NH})$. The graphics were drawn, and additional structural calculations were performed by the DIAMOND [49] software.

Crystallographic data has been deposited with the Cambridge Crystallographic Data Centre under CCDC deposition number 1957819. Copies of this information may be obtained free of charge from the Director, CCDC, 12 Union Road, Cambridge CB2 1EY, UK (fax: +44-1223-336033; e-mail: deposit@ccdc.cam.ac.uk or [www:http://www.ccdc.cam.ac.uk](http://www.ccdc.cam.ac.uk)).

3.3. Cell Cultivation

THP1-Blue™ NF-κB cell line was purchased from Invivogen (San Diego, CA, USA). Cells were cultured in RPMI 1640 medium (Merck, Darmstadt, Germany) containing stabilized 2 mM L-glutamine (Merck) supplemented with antibiotics [100 U/mL penicillin and 100 mg/mL streptomycin (Merck)] and 10% FBS (Merck). The cultures were passaged twice a week. Cells were kept in an incubator at 37 °C in a water-saturated atmosphere of air containing 5% CO₂.

The viability of the used cell lines (5th–18th passage) was over 95% for each experiment. The cell number and viability were determined by staining with Trypan Blue solution. Cells were counted manually using a haemocytometer and an optical microscope. Cells that remained unstained were considered viable, while light red cells were considered non-viable. The viability percentage was calculated as the ratio of the number of all viable cells to the number of all cells.

3.4. Cell Viability Determination

The cell viability was determined as was described previously [50]. Briefly, THP1-Blue™ NF-κB cells (500,000 cells/mL) were washed by PBS, resuspended in a serum-free RPMI 1640 medium and seeded into 96-well plates (100 µL/well, i.e., 50,000 cells per each well). After 2 h, tested compounds (30–0.47 µM) dissolved in DMSO were added to the cells. The final concentration of DMSO was 0.1% (v/v) in each well. Measurements were taken after 24 h incubation with the tested substances. Viability was measured by the Cell Proliferation Reagent kit WST-1 (Roche Diagnostics, Basel, Switzerland) according to the manufacturer's manual. The amount of formazan formed, which corresponded to the number of metabolically active cells in the culture, was calculated as a percentage of the control cells, which were treated only with serum-free RPMI 1640 medium and were assigned as 100%. The IC₅₀ values were calculated by four-parameter logistic (4PL) analysis from obtained viability curves.

3.5. Determination of NF-κB Activity

The activity of NF-κB transcription factors was evaluated on THP1-Blue™ NF-κB cells as described previously [50,51]. Briefly, cells were transferred into serum-free RPMI 1640 medium as was delineated above in Section 3.4. All tested compounds were added 2 h later in non-toxic concentration 2 µM but compounds **10**, **11**, and **13** in concentration 0.5 µM. After 1 h of incubation of the treated cells with the samples, cells were stimulated by lipopolysaccharide (LPS) from *E. coli* 0111:B4 (Merck) dissolved in serum-free RPMI 1640 medium (1 µg/mL). After 24 h of incubation, 20 µL of cultivation medium was mixed with 200 µL of Quanti-Blue™ medium (Invivogen) and incubated according to the manufacturer's instructions at 37 °C for 30–40 min. The activity of NF-κB was determined as secretion of embryonic alkaline phosphatase spectrophotometrically in a Tecan Infinite M200 (Tecan, Männedorf Switzerland) at 650 nm and compared with an untreated control (100%).

3.6. Immunocytochemical Analysis of NF-κB Nuclear Migration

To differentiate THP1-Blue™ NF-κB monocytes into macrophages, the cells were stimulated with phorbol myristate acetate (PMA) at the final concentration of 50 ng/mL, as was described previously [51,52]. Cells were seeded into 8-well cell culture glass slide (SPL, Korea) at the concentration

of 500,000 cells/mL, 150,000 cells per well. The compound **17** was added at the final concentration of 2 μ M, and 1 h later, the cells were activated by LPS (1 μ g/mL). After 1h, the culture slide was washed with PBS and fixed with 4% formaldehyde. The cells were permeabilized by 0.1% Triton X-100 (*v/v*; Merck) and blocked with 3% bovine serum albumin (BSA, Merck) dissolved in PBS. The primary antibody NF- κ B p65 (Abcam, Cambridge, UK; product No. ab16502) at concentration 2.5 μ g/mL was used for overnight incubation at 4 °C. After that, secondary anti-rabbit antibody labeled with Alexa Fluor[®] 488 (Cell Signaling; product No. 4412; dilution 1:1000) was added for 1 h in dark, and the nuclei were stained using 0,5 μ g/mL DAPI (Merck) for 5 min. The wells were washed three-times between the mentioned steps with PBS. The coverslip was mounted with VectaShield mounting (Vector laboratories, Burlingame, CA, USA) medium and sealed with the nail polish. The nail polish was allowed to dry at 4 °C and the translocation of NF- κ B was observed by fluorescence microscopy.

3.7. Signaling Pathway Analysis

The level of I κ B and the amount of activated (phosphorylated) mitogen-activated protein (MAP) kinase p38, ERK1/2, and JNK was determined on the THP1-Blue[™] NF- κ B, in a way similar to that described previously [53]. Briefly, cells cultivated in serum-free medium were pretreated with the tested compounds (**8**, **17**, cinnamic acid, or prednisone) at concentration 2 μ M. One hour later, 1 μ g/mL of LPS was added, and after 30 min the cells were collected into ice-cold Mammalian Cell Lysis Buffer (Abcam, Cambridge, UK) with phosphatase inhibitors PhosSTOP (Roche, Mannheim, Germany). Cell lysates were centrifuged 3000 g/5 min/4 °C and supernatants were mixed with 5 \times Laemmli reducing buffer [250 mM Tris-HCl pH 6.8, 10% (*w/v*) SDS, 30% (*v/v*) glycerol, 5% (*v/v*) β -mercaptoethanol, 0.04% (*w/v*) bromphenol blue], and incubated at 95 °C for 5 min. To separate the proteins, 10 μ g of the proteins was loaded onto a 12% polyacrylamide gel and then transferred electrophoretically to PVDF (polyvinylidene fluoride) membranes that were subsequently blocked using 5% BSA dissolved in TBST buffer [150 mM NaCl, 10 mM Tris base, and 0.1% (*v/v*) Tween-20]. The membranes were incubated at 4 °C for 16 h with primary anti-I κ B- α (Cell Signaling; product No. 4814; dilution 1:1,000), anti-p44/42 MAPK (ERK1/2) (Cell Signaling; product No. 9102; dilution 1:1,000), anti-phospho-p44/42 MAPK (ERK1/2) (Cell Signaling; product No. 9101; dilution 1:1,000), anti-JNK1/2/3 (Abcam; product No. ab179461; dilution 1:1,000), anti-phospho-JNK1/2/3 (Abcam; product No. ab76572; dilution 1:5,000), anti-p38 MAPK (Cell Signaling; product No. 8690; dilution 1:1,000), anti-phospho-p38 MAPK (Cell Signaling; product No. 9210; dilution 1:1,000), and anti- β -actin (Santa Cruz, Aachen, Germany; product No. sc-47778; dilution 1:5000) antibodies. After washing, the secondary anti-mouse and anti-rabbit IgG antibodies (Cell Signaling, products No. 7076S and 7074P2) were diluted 1:2000 and applied to the membranes, which were incubated for 1 h at the laboratory temperature. The amount of bound secondary antibody was determined using WesternSure[®] PREMIUM Chemiluminescent Substrate (LI-COR, Lincoln, NE, USA). Chemiluminescence was detected using a LI-COR C-DiGit chemiluminescence imaging system (LI-COR).

3.8. Differentiation Monocytes into Macrophages and Evaluation of TNF- α Secretion

Differentiated THP1-Blue[™] NF- κ B macrophages (see the chapter 3.6) were pre-treated for 1 h with 2 μ M solutions of the tested compounds **8**, **12**, **6**, **17**, cinnamic acid, and prednisone dissolved in DMSO, or only the vehicle [0.1% (*v/v*) DMF solution]. The inflammatory-like response was triggered by adding 1 μ g/mL of LPS from *E. coli* 0111:B4 (Sigma-Aldrich) to the pre-treated macrophages; the control cells were left without LPS treatment. After 24 h, the supernatants were collected and the concentration of TNF- α was measured using a Human TNF- α ELISA Kit (Diaclone, Besançon, France), according to the manufacturer's manual.

3.9. Statistical Analysis

Statistical analysis was carried out in GraphPad Prism 8.0.1 (San Diego, CA, USA). Outliers were identified by the ROUT statistical method (Q = 5%) and excluded for further analysis. Data were

expressed as mean \pm SEM. Groups were compared with the help of the one-way ANOVA test followed by Fisher's LSD multiple comparison test. The value $p < 0.05$ was assigned as statistically significant.

4. Conclusions

A series of eighteen ring-substituted *N*-arylcinnamanilides was designed. The molecular structure of (2*E*)-*N*-(2-bromo-5-fluorophenyl)-3-phenylprop-2-enamide (**15**) as a model compound was determined by single-crystal X-ray diffraction. All the compounds were screened for their anti-inflammatory potential at the pharmacologically relevant, non-toxic concentration of 2 μ M, only least viable compounds **10** (R = 3,4-Cl), **11** (R = 3,5-Cl), and **13** (3,5-CF₃), which IC₅₀ ranged from 2.17 to 6.28 μ M on THP1-Blue™ NF- κ B cell line, were tested at the concentration level of 0.5 μ M. It seems that cell viability is mainly affected by di-substitution on the C_{(3,5)'} or C_{(3,4)'} positions by Cl and/or CF₃, i.e., groups with highly lipophilic and strong electron-withdrawing properties. Thus, although it would be advantageous to obtain compounds with both antimicrobial and anti-inflammatory activity, compounds **10**, **11**, and **13** were excluded from further study because of this undesirable cytotoxic effect. Most tested compounds significantly attenuated the LPS-induced NF- κ B activation. They were more potent than the parental cinnamic acid. (2*E*)-*N*-[2-Chloro-5-(trifluoromethyl)phenyl]-3-phenylprop-2-enamide (**17**), (2*E*)-*N*-(2,6-dibromophenyl)-3-phenylprop-2-enamide (**12**), and (2*E*)-*N*-(2,5-dichlorophenyl)-3-phenyl-prop-2-enamide (**8**) demonstrated the highest activity within the series that was comparable with prednisone. Compounds **12** and **17** also decreased the level of TNF- α , which correlates with the observed attenuation of NF- κ B. On the other hand, subsequent tests showed that the investigated compounds did not affect I κ B α level and MAPKs activity as expected. Based on above-mentioned fact, it can be hypothesized that the investigated *N*-arylcinnamanilides may have a different mode of action, which may consist of the nuclear translocation of NF- κ B inhibition, or affect its binding to DNA, or act by epigenetic regulation, while the combinations of these effects are not excluded. In conclusion, it can be stated that anti-inflammatory activity (while minimizing antiproliferative activity) is positively influenced by di-substitution on the C_{(2,5)'} or C_{(2,6)'} positions by rather lipophilic and preferably bulky moieties that causes the anilide ring to rotate, resulting in a non-planar configuration of the entire system, as confirmed by the crystal structure.

Supplementary Materials: The supplementary materials are available online.

Author Contributions: J.K. and T.S. synthesized the compounds. P.Š. characterized the compounds. J.H. and L.Č. performed biological screening. Z.T. and J.V. performed X-Ray study. J.J. designed the compounds. J.H., Z.T., J.J. and F.D. wrote the paper.

Funding: This study was supported by the Slovak Research and Development Agency (APVV-17-0373) and by the Ministry of Education, Youth and Sports of the Czech Republic (LO1305). Knowledge gained within project ITMS 26240120034 of the Center of Excellence in Security Research (CEBV) has been used in the results.

Conflicts of Interest: The authors declare no conflict of interest.

References

1. Medzhitov, R. Origin and physiological roles of inflammation. *Nature* **2008**, *454*, 428–435. [[CrossRef](#)] [[PubMed](#)]
2. Libby, P. Inflammation in atherosclerosis. *Nature* **2002**, *420*, 868–874. [[CrossRef](#)] [[PubMed](#)]
3. McInnes, I.B.; Schett, G. Cytokines in the pathogenesis of rheumatoid arthritis. *Nat. Rev. Immunol.* **2007**, *7*, 429–442. [[CrossRef](#)] [[PubMed](#)]
4. Nickoloff, B.J.; Nestle, F.O. Recent insights into the immunopathogenesis of psoriasis provide new therapeutic opportunities. *J. Clin. Invest.* **2004**, *113*, 1664–1675. [[CrossRef](#)] [[PubMed](#)]
5. Grivennikov, S.I.; Greten, F.R.; Karin, M. Immunity, inflammation, and cancer. *Cell* **2010**, *140*, 883–899. [[CrossRef](#)]
6. Barnes, P.J. Immunology of asthma and chronic obstructive pulmonary disease. *Nat. Rev. Immunol.* **2008**, *8*, 183–192. [[CrossRef](#)]

7. Jampilek, J.; Dolezal, M.; Opletalova, V.; Hartl, J. 5-Lipoxygenase, leukotrienes biosynthesis and potential antileukotrienic agents. *Curr. Med. Chem.* **2006**, *13*, 117–129. [CrossRef]
8. Shoelson, S.E.; Herrero, L.; Naaz, A. Obesity, inflammation, and insulin resistance. *Gastroenterology* **2007**, *132*, 2169–2180. [CrossRef]
9. Atanasov, A.G.; Waltenberger, B.; Pferschy-Wenzig, E.M.; Linder, T.; Wawrosch, C.; Uhrin, P.; Temml, V.; Wang, L.; Schwaiger, S.; Heiss, E.H.; et al. Discovery and resupply of pharmacologically active plant-derived natural products: A review. *Biotechnol. Adv.* **2015**, *33*, 1582–1614. [CrossRef]
10. Zhang, H.J.; Jampilek, J. Anti-infective drug discovery based on diversified plant natural compounds. *Curr. Org. Chem.* **2017**, *21*, 1775–1776. [CrossRef]
11. Newman, D.J.; Cragg, G.M. Natural products as sources of new drugs from 1981 to 2014. *J. Nat. Prod.* **2016**, *79*, 629–661. [CrossRef] [PubMed]
12. Guzman, J.D. Natural cinnamic acids, synthetic derivatives and hybrids with antimicrobial activity. *Molecules* **2014**, *19*, 19292–19349. [CrossRef] [PubMed]
13. Sova, M. Antioxidant and antimicrobial activities of cinnamic acid derivatives. *Mini-Rev. Med. Chem.* **2012**, *12*, 749–767. [CrossRef] [PubMed]
14. De, P.; Baltas, M.; Bedos-Belval, F. Cinnamic acid derivatives as anticancer agents – a review. *Curr Med Chem* **2011**, *18*, 1672–1703. [CrossRef] [PubMed]
15. Liao, J.C.; Deng, J.S.; Chiu, C.S.; Hou, W.C.; Huang, S.S.; Shie, P.H.; Huang, G.J. Anti-Inflammatory activities of cinnamomum cassia constituents in vitro and in vivo. *Evid-Based Compl. Alt.* **2012**, *2012*, 429320. [CrossRef]
16. Choudhary, A.; Raines, R.T. An evaluation of peptide-bond isosteres. *ChemBioChem* **2011**, *12*, 1801–1807. [CrossRef]
17. Mrozek-Wilczkiewicz, A.; Kalinowski, D.; Musiol, R.; Finster, J.; Szurko, A.; Serafin, K.; Knas, M.; Kamalapuram, S.K.; Kovacevic, Z.; Jampilek, J.; et al. Investigating anti-proliferative activity of styrylazanaphthalenes and azanaphthalenediones. *Bioorg. Med. Chem.* **2010**, *18*, 2664–2671. [CrossRef]
18. Imramovsky, A.; Pesko, M.; Kralova, K.; Vejsova, M.; Stolarikova, J.; Vinsova, J.; Jampilek, J. Investigating spectrum of biological activity of 4- and 5-chloro-2-hydroxy-N-[2-(arylamino)-1-alkyl-2-oxoethyl]-benzamides. *Molecules* **2011**, *16*, 2414–2430. [CrossRef]
19. Imramovsky, A.; Pesko, M.; Ferriz, J.M.; Kralova, K.; Vinsova, J.; Jampilek, J. Photosynthesis—Inhibiting efficiency of 4-chloro-2-(chlorophenylcarbamoyl)phenyl alkylcarbamates. *Bioorg. Med. Chem. Lett.* **2011**, *21*, 4564–4567. [CrossRef]
20. Zadrazilova, I.; Pospisilova, S.; Masarikova, M.; Imramovsky, A.; Ferriz, J.M.; Vinsova, J.; Cizek, A.; Jampilek, J. Salicylanilide carbamates: Promising antibacterial agents with high in vitro activity against methicillin-resistant *Staphylococcus aureus* (MRSA). *Eur. J. Pharm. Sci.* **2015**, *77*, 197–207. [CrossRef]
21. Mahesh, S.; Tang, K.C.; Raj, M. Amide bond activation of biological molecules. *Molecules* **2018**, *23*, 2615. [CrossRef] [PubMed]
22. Michnova, H.; Pospisilova, S.; Gonec, T.; Kapustikova, I.; Kollar, P.; Kozik, V.; Musiol, R.; Jendrzewska, I.; Vanco, J.; Trávníček, Z.; et al. Bioactivity of methoxylated and methylated 1-hydroxynaphthalene-2-carboxanilides: Comparative molecular surface analysis. *Molecules* **2019**, *24*, 2991. [CrossRef] [PubMed]
23. Chen, G.Z.; Zhang, Y.L.; Liu, X.; Fang, Q.L.; Wang, Z.; Fu, L.L.; Liu, Z.G.; Wang, Y.; Zhao, Y.J.; Li, X.K.; et al. Discovery of a New inhibitor of myeloid differentiation 2 from cinnamide derivatives with anti-inflammatory activity in sepsis and acute lung injury. *J. Med. Chem.* **2016**, *59*, 2436–2451. [CrossRef] [PubMed]
24. Gaikwad, N.; Nanduri, S.; Madhavi, Y.V. Cinnamamide: An insight into the pharmacological advances and structure-activity relationships. *Eur. J. Med. Chem.* **2019**, *181*, 111561. [CrossRef] [PubMed]
25. Pospisilova, S.; Kos, J.; Michnova, H.; Kapustikova, I.; Strharsky, T.; Oravec, M.; Moricz, A.M.; Bakonyi, J.; Kauerova, T.; Kollar, P.; et al. Synthesis and spectrum of biological activities of novel *N*-arylcinnamamides. *Int. J. Mol. Sci.* **2018**, *19*, 2318. [CrossRef]
26. Pospisilova, S.; Kos, J.; Michnova, H.; Strharsky, T.; Cizek, A.; Jampilek, J. *N*-Arylcinnamamides as antistaphylococcal agents. In Proceedings of the 4th International Electronic Conference on Medicinal Chemistry (ECMC-4), 1–30 November 2018; Available online: <https://sciforum.net/manuscripts/5576/slides.pdf> (accessed on 17 November 2019).

27. Mangoni, A.A.; Guillou, C.; Vanden Eynde, J.J.; Hulme, C.; Jampilek, J.; Li, W.; Prokai-Tatrai, K.; Rautio, J.; Collina, S.; Tuccinardi, T.; et al. Breakthroughs in medicinal chemistry: New targets and mechanisms, new drugs, new hopes—4. *Molecules* **2019**, *24*, 130. [[CrossRef](#)]
28. Saeed, A.; Khera, R.A.; Simpson, J. N-(2-Fluorophenyl)cinnamamide. *Acta Cryst. E* **2010**, *66*, o533–o534. [[CrossRef](#)]
29. Nissa, M.N.; Aravindan, P.G.; Kasinath, V.; Gopalakrishnan, G.; Merazig, H.; Velmurugan, D. Crystal structures of 2-chloro cinnamoyl phenolate (I) and 3-chloro cinnamanilide (II). *Cryst. Res. Technol.* **2004**, *39*, 643–649. [[CrossRef](#)]
30. Skolyapova, A.D.; Selivanova, G.A.; Tretyakov, E.V.; Bogdanova, T.F.; Shchegoleva, L.N.; Bagryanskaya, I.Y.; Gurskaya, L.Y.; Shteingarts, V.D. Interaction of polyfluorinated 2-chloroquinolines with ammonia. *Tetrahedron* **2017**, *73*, 1219–1229. [[CrossRef](#)]
31. Hansch, C.; Leo, A.; Unger, S.H.; Kim, K.H.; Nikaitani, D.; Lien, E.J. “Aromatic” substituent constants for structure-activity correlations. *J. Med. Chem.* **1973**, *16*, 1207–1216. [[CrossRef](#)]
32. Kucerova-Chlupacova, M.; Opletalova, V.; Jampilek, J.; Dolezel, J.; Dohnal, J.; Pour, M.; Kunes, J.; Vorisek, V. New hydrophobicity constants of substituents in pyrazine rings derived from RP-HPLC study. *Coll. Czech. Chem. Commun.* **2008**, *73*, 1–18. [[CrossRef](#)]
33. Adewoyin, M.; Mohsin, S.M.N.; Arulseivan, P.; Hussein, M.Z.; Fakurazi, S. Enhanced anti-inflammatory potential of cinnamate-zinc layered hydroxide in lipopolysaccharide-stimulated RAW 264.7 macrophages. *Drug Des. Dev. Ther.* **2015**, *9*, 2475–2484. [[CrossRef](#)]
34. Jan, J.S.; Chou, Y.C.; Cheng, Y.W.; Chen, C.K.; Huang, W.J.; Hsiao, G. The novel HDAC8 inhibitor WK2-16 attenuates lipopolysaccharide-activated matrix metalloproteinase-9 expression in human monocytic cells and improves hypercytokinemia in vivo. *Int. J. Mol. Sci.* **2017**, *18*, 1394. [[CrossRef](#)] [[PubMed](#)]
35. Perkins, N.D.; Gilmore, T.D. Good cop, bad cop: The different faces of NF-kappa B. *Cell. Death Differ.* **2006**, *13*, 759–772. [[CrossRef](#)] [[PubMed](#)]
36. Hoesel, B.; Schmid, J.A. The complexity of NF-kappa B signaling in inflammation and cancer. *Mol. Cancer* **2013**, *12*, 86. [[CrossRef](#)]
37. Arthur, J.S.C.; Ley, S.C. Mitogen-activated protein kinases in innate immunity. *Nat. Rev. Immunol.* **2013**, *13*, 679–692. [[CrossRef](#)]
38. Tsai, C.M.; Sun, F.M.; Chen, Y.L.; Hsu, C.L.; Yen, G.C.; Weng, C.J. Molecular mechanism depressing PMA-induced invasive behaviors in human lung adenocarcinoma cells by cis- and trans-cinnamic acid. *Eur. J. Pharm. Sci.* **2013**, *48*, 494–501. [[CrossRef](#)]
39. Kim, M.S.; Kim, J.Y. Cinnamon subcritical water extract attenuates intestinal inflammation and enhances intestinal tight junction in a Caco-2 and RAW264.7 co-culture model. *Food Funct.* **2019**, *10*, 4350–4360. [[CrossRef](#)]
40. Lin, F.L.; Yen, J.L.; Kuo, Y.C.; Kang, J.J.; Cheng, Y.W.; Huang, W.J.; Hsiao, G. HDAC8 inhibitor WK2-16 therapeutically targets lipopolysaccharide-induced mouse model of neuroinflammation and microglial activation. *Int. J. Mol. Sci.* **2019**, *20*, 410. [[CrossRef](#)]
41. D’Acquisto, F.; May, M.J.; Ghosh, S. Inhibition of nuclear factor kappa B (NF-kB): An emerging theme in anti-inflammatory therapies. *Mol. Interv.* **2002**, *2*, 22–35. [[CrossRef](#)]
42. Liu, T.; Zhang, L.Y.; Joo, D.; Sun, S.C. NF-kappa B signaling in inflammation. *Signal Transduct. Target Ther.* **2017**, *2*, 17023. [[CrossRef](#)] [[PubMed](#)]
43. Wierda, R.J.; Geutskens, S.B.; Jukema, J.W.; Quax, P.H.A.; van den Elsen, P.J. Epigenetics in atherosclerosis and inflammation. *J. Cell. Mol. Med.* **2010**, *14*, 1225–1240. [[CrossRef](#)] [[PubMed](#)]
44. Zelova, H.; Hosek, J. TNF-alpha signalling and inflammation: Interactions between old acquaintances. *Inflamm. Res.* **2013**, *62*, 641–651. [[CrossRef](#)] [[PubMed](#)]
45. Chakrabarti, S.; Jana, M.; Roy, A.; Pahan, K. Upregulation of suppressor of cytokine signaling 3 in microglia by cinnamic acid. *Curr. Alzheimer Res.* **2018**, *15*, 894–904. [[CrossRef](#)]
46. Xu, F.; Wang, F.; Wen, T.Q.; Sang, W.T.; He, X.Y.; Li, L.; Zeng, N. Protective effect of cinnamic acid in endotoxin-poisoned mice. *Phytother. Res.* **2017**, *31*, 1946–1953. [[CrossRef](#)]
47. Bruker Apex3; Bruker AXS Inc.: Madison, WI, USA, 2015. Available online: <https://www.bruker.com/products/x-ray-diffraction-and-elemental-analysis/single-crystal-x-ray-diffraction/sc-xrd-software/apex3.html> (accessed on 17 November 2019).
48. Sheldrick, G.M. Crystal structure refinement with SHELXL. *Acta Crystallogr. C* **2015**, *71*, 3–8. [[CrossRef](#)]

49. Brandenburg, K. *Diamond Version 4.6.0.*; Crystal Impact GbR: Bonn, Germany, 2019.
50. Plavcova, Z.; Salamunova, P.; Salon, I.; Stepanek, F.; Hanus, J.; Hosek, J. Curcumin encapsulation in yeast glucan particles promotes its anti-inflammatory potential in vitro. *Int. J. Pharm.* **2019**, *568*, 118532. [[CrossRef](#)]
51. Vančo, J.; Trávníček, Z.; Hošek, J.; Suchý, P. In vitro and in vivo anti-inflammatory active copper(II)-lawsone complexes. *PLoS ONE* **2017**, *12*, e0181822. [[CrossRef](#)]
52. Brezani, V.; Lelakova, V.; Hassan, S.T.S.; Berchova-Bimova, K.; Novy, P.; Kloucek, P.; Marsik, P.; Dall'Acqua, S.; Hosek, J.; Smejkal, K. Anti-Infectivity against herpes simplex virus and selected microbes and anti-inflammatory activities of compounds isolated from *Eucalyptus globulus* Labill. *Viruses* **2018**, *10*, E360. [[CrossRef](#)]
53. Leláková, V.; Šmejkal, K.; Jakubczyk, K.; Veselý, O.; Landa, P.; Václavík, J.; Bobál, P.; Pížová, H.; Temml, V.; Steinacher, T.; et al. Parallel in vitro and in silico investigations into anti-inflammatory effects of non-prenylated stilbenoids. *Food Chem.* **2019**, *285*, 431–440. [[CrossRef](#)]

Sample Availability: Samples of the compounds are available from the authors.



© 2019 by the authors. Licensee MDPI, Basel, Switzerland. This article is an open access article distributed under the terms and conditions of the Creative Commons Attribution (CC BY) license (<http://creativecommons.org/licenses/by/4.0/>).

č.	citace	ISSN
15	BAK, A, <i>J KOS*(corresponding author)*</i> , H MICHNOVA, T GONEC, S POSPISILOVA, V KOZIK, A CIZEK, A SMOLINSKI a J JAMPILEK. Consensus-Based Pharmacophore Mapping for New Set of N-(disubstituted-phenyl)-3-hydroxyl-naphthalene-2-carboxamides. <i>INTERNATIONAL JOURNAL OF MOLECULAR SCIENCES</i> [online]. 2020, 21 (18). Dostupné z: doi: 10.3390/ijms21186583	1422-0067



Article

Consensus-Based Pharmacophore Mapping for New Set of *N*-(disubstituted-phenyl)-3-hydroxyl-naphthalene-2-carboxamides

Andrzej Bak ^{1,*} , Jiri Kos ^{2,*} , Hana Michnova ² , Tomas Gonec ³ , Sarka Pospisilova ² , Violetta Kozik ¹ , Alois Cizek ⁴ , Adam Smolinski ⁵ and Josef Jampilek ²

¹ Department of Chemistry, University of Silesia, Szkolna 9, 40007 Katowice, Poland; violetta.kozik@us.edu.pl

² Division of Biologically Active Complexes and Molecular Magnets, Regional Centre of Advanced Technologies and Materials, Faculty of Science, Palacky University, Slechtitelu 27, 78371 Olomouc, Czech Republic; michnova.hana@gmail.com (H.M.); sharka.pospisilova@gmail.com (S.P.); josef.jampilek@gmail.com (J.J.)

³ Department of Chemical Drugs, Faculty of Pharmacy, Masaryk University, Palackeho 1, 60200 Brno, Czech Republic; t.gonec@seznam.cz

⁴ Department of Infectious Diseases and Microbiology, Faculty of Veterinary Medicine, University of Veterinary and Pharmaceutical Sciences, Palackeho 1946/1, 61242 Brno, Czech Republic; cizeka@vfu.cz

⁵ Central Mining Institute, Pl. Gwarków 1, 40-166 Katowice, Poland; smolin@gig.katowice.pl

* Correspondence: andrzej.bak@us.edu.pl (A.B.); jiri.kos@upol.cz (J.K.)

Received: 3 August 2020; Accepted: 7 September 2020; Published: 9 September 2020



Abstract: A series of twenty-two novel *N*-(disubstituted-phenyl)-3-hydroxynaphthalene-2-carboxamide derivatives was synthesized and characterized as potential antimicrobial agents. *N*-[3,5-bis(trifluoromethyl)phenyl]- and *N*-[2-chloro-5-(trifluoromethyl)phenyl]-3-hydroxynaphthalene-2-carboxamide showed submicromolar (MICs 0.16–0.68 μ M) activity against methicillin-resistant *Staphylococcus aureus* isolates. *N*-[3,5-bis(trifluoromethyl)phenyl]- and *N*-[4-bromo-3-(trifluoromethyl)phenyl]-3-hydroxynaphthalene-2-carboxamide revealed activity against *M. tuberculosis* (both MICs 10 μ M) comparable with that of rifampicin. Synergistic activity was observed for the combinations of ciprofloxacin with *N*-[4-bromo-3-(trifluoromethyl)phenyl]- and *N*-(4-bromo-3-fluorophenyl)-3-hydroxynaphthalene-2-carboxamides against MRSA SA 630 isolate. The similarity-related property space assessment for the congeneric series of structurally related carboxamide derivatives was performed using the principal component analysis. Interestingly, different distribution of mono-halogenated carboxamide derivatives with the $-CF_3$ substituent is accompanied by the increased activity profile. A symmetric matrix of Tanimoto coefficients indicated the structural dissimilarities of dichloro- and dimethoxy-substituted isomers from the remaining ones. Moreover, the quantitative sampling of similarity-related activity landscape provided a subtle picture of favorable and disallowed structural modifications that are valid for determining activity cliffs. Finally, the advanced method of neural network quantitative SAR was engaged to illustrate the key 3D steric/electronic/lipophilic features of the ligand-site composition by the systematic probing of the functional group.

Keywords: hydroxynaphthalenecarboxamides; lipophilicity; antistaphylococcal activity; antitubercular activity; MIC; MTT assay; CoMSA; IVE-PLS; similarity-activity landscape index

1. Introduction

The comprehensive specification of the target-ligand interaction content in the rational drug design is a computationally intense issue that requires at least four German G's: Geschick (skill),

Geduld (patience), Geld (money), and Glück (luck) [1]. Hence, the decision-making process of hit identification→lead generation→lead optimization→candidate nomination in the synthetic efforts during drug discovery ought to be supported by a variety of advanced in silico approaches. On the whole, the computer-assisted manipulation of host-guest structures can be dichotomized into direct target-dependent (structure-based) as well as indirect drug-related (ligand-based) methodologies [2]. Unfortunately, there is no a priori guideline based on which a procedure performs best in the search for promising drug molecule for a given disease; therefore, the integrated (collaborative) approach is advisable to advocate chemical intuition [3]. Whenever no structure or model of the target molecule is accessible at the atomic level the pharmacophore-guided concept can be employed for mapping of the binding/active site [4]. The inspiration for pharmacophoric pattern study stems loosely from the intermolecular recognition concept assuming that interchangeable groups that are similar in size, shape, or electronic distribution are likely to induce similar effects on binding affinities (neighbor behavior) [5]. Conceptually, the straightforward tenet of substituent interchangeability and complementarity inherently favors the similarity principle, especially in structure-activity (SAR) modeling, where congeneric series of molecules should exhibit similar pharmacological profile [6]. In this context, validation is one of those words . . . that is constantly used and seldom defined as was stated by Feinstein [7]. Obviously, a comprehensive mapping of the topology and/or topography of a compound into the property-based chemical space (CS) is not feasible in principal as was noticed by an anonymous reviewer, since it is estimated that up to 10^{100} structures can be synthesized with potentially 10^{60} small molecules of less than 30 non-hydrogen atoms and up to 10^{40} pharmacologically relevant compounds [8]. Hence, only a limited exploration of the factual chemical space (FCS) is achievable (10^8), mainly employing structurally-related structures [9,10]. On the other hand, the clever management of pharmacophore-related information can provide hints that might be incorporated at the synthesis stage.

Basically, the pseudoreceptor mapping of pharmacophoric features can be classified into similarity-driven and hypothesis-related approaches, respectively [11]. Roughly speaking, the hypothesis-based procedures employ frequently machine learning techniques conjugated with variable selection/weighting algorithms to prioritize robust linear or non-linear SAR models [12]. The quantitative comparison of ligand surfaces using electrostatic potential maps (CoMSA) and field-based descriptors (CoMFA) can provide a more realistic picture of mutual drug-receptor recognition phenomena; however, it is only a crude approximation of the underlying biological reality [13,14]. On the other hand, the similarity principle is still questionable since similarity depends strongly on both descriptor and/or similarity score used. Despite some drawbacks, distance-related similarity searching with a numerical measure of the intermolecular resemblance between two objects, each described by a number of attributes, contributes favorably in SAR practice [15]. Obviously, certain molecular signatures such as lipophilicity can correlate with bioavailability, therefore in silico filters are meaningful in restricting the values of structural or physicochemical descriptors to ADMET-friendly property space [16]. Estimation of the sustainable equilibrium between ADMET-related properties and desirable drug affinity to the receptor can be illustrated graphically by enhancement of the planar (2D) similarity-driven projection with activity data to form a biological response surface [17]. Intuitively, SAR landscapes are not homogenous in nature, but rather heterogeneously distributed regions resembling more rugged topography of Poland's Tatra Mountains than the gently rolling Flint Hills of Kansas [18]. Chemically, smooth and flat regions of SAR landscape indicate areas where subtle structural changes are accompanied by tiny variations in biological response according to the similarity principle. Conversely, sharp and non-uniform areas called activity cliffs highlight structurally-related compounds that are characterized by exorbitant changes in potency to target (magic methyl phenomenon) [19]. From the drug hunter's perspective, successful exploration of jagged landscape parts provides a guideline to a non-trivial question about the structural modifications that boost or demolish the biological activity. In fact, a range of similarity metrics and fingerprint representation is employed

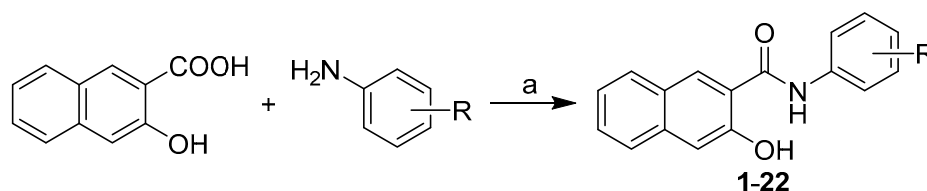
to numerically quantify the SAR smoothness, for instance, the structure-activity landscape index (SALI) [20].

Hydroxynaphthalenecarboxanilide scaffolds make it possible to design a wide variety of compounds, especially with anti-infective [21–26] and antineoplastic activity [27,28]. 3-Hydroxynaphthalene-2-carboxanilides (which are direct radical analogs of salicylanilides) were investigated as well [29,30]. The activity of these structurally simple compounds is dependent on the mutual position of the carboxamide and the phenolic moieties [21–28,31,32]. In other words, various substitutions of the crucial phenolic motif determine a spectrum of different biological activities. Roughly speaking, the carboxamide fragment that mimics a peptide bond seems to be pivotal for the binding affinity, since a compound is bound to its targets using this molecular anchor. One can assume that the anilide part of the molecule has a direct impact also on the physicochemical properties and binding strength of the tested compounds to the potential target. As a matter of fact, hydroxynaphthalenecarboxanilide analogs can be classified as multi-target compounds, since they are able to affect various target structures, especially in microbial pathogens (similarly to salicylanilides) [33]. These types of compounds are able to inhibit glucose uptake, oxidative phosphorylation, two-component regulatory systems of bacteria, interleukin-12p40 production, various bacterial enzymes, respectively. Moreover, they can bind to protein kinase epidermal growth factor receptor, destruct the cellular proton gradient as proton shuttles, etc. [34]. Thus, based on the experience with various substituents on the aniline core a series of novel 22 *N*-(disubstituted-phenyl)-3-hydroxynaphthalene-2-carboxamides, was synthesized and in vitro tested against several microbial strains [26,35–37]. The similarity related property space assessment for the set of carboxamide derivatives was performed using the principal component analysis (PCA) [38,39]. Moreover, the quantitative sampling of similarity related activity landscape provided a subtle picture of favorable and disallowed structural modifications that are valid for determining the activity cliffs [40]. Finally, the complex approach of the machine learning using neural network was employed in quantitative SAR to specify the potentially valid 3-dimensional steric/electronic/ lipophilic features of the ligand-receptor composition by the systematic sampling of the functional group resulting in the production of an averaged selection-driven pharmacophore pattern [26].

2. Results and Discussion

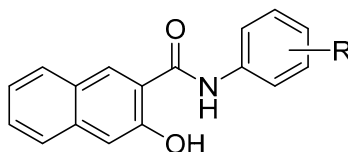
2.1. Synthesis and Physicochemical Properties

All studied *N*-(disubstituted-phenyl)-3-hydroxynaphthalene-2-carboxamides were prepared according to Scheme 1 as described previously by Kos et al. [31]. The condensation of 3-hydroxynaphthalene-2-carboxylic acid with appropriate disubstituted anilines using phosphorus trichloride in dry chlorobenzene under microwave conditions gave a series of target 3-hydroxy-*N*-arylnaphthalene-2-carboxanilides 1–22 (see Table 1).



Scheme 1. Synthesis of *N*-(disubstituted-phenyl)-3-hydroxynaphthalene-2-carboxamides 1–22. Reagents and conditions: (a) PCl₃, chlorobenzene, microwave reactor, 45 min [31].

Table 1. Compositions of *N*-disubstituted 3-hydroxynaphthalene-2-carboxanilides, in vitro antistaphylococcal activities MIC [μ M] compared to ampicillin (AMP) and ciprofloxacin (CPX), in vitro antitubercular activity MIC [μ M] compared to isoniazid (INH) and rifampicin (RIF).



No.	R	MIC [μ M]				
		SA	MRSA 63718	MRSA SA 630	MRSA SA 3202	MT
1.	2,5-OCH ₃	198	792	792	792	792
2.	3,5-OCH ₃	198	792	792	792	792
3.	2,5-CH ₃	879	879	879	879	256
4.	2,6-CH ₃	27.4	54.9	27.4	27.4	54.9
5.	3,5-CH ₃	879	879	879	879	110
6.	2,5-F	856	856	856	856	879
7.	2,6-F	26.7	856	53.4	107	107
8.	3,5-F	856	856	214	856	53.4
9.	2,5-Cl	770	770	770	770	770
10.	2,6-Cl	193	385	385	385	385
11.	3,4-Cl	770	770	770	770	770
12.	3,5-Cl	770	770	770	770	12.0
13.	3,5-CF ₃	0.158	0.626	0.158	0.626	10.0
14.	3-CF ₃ -4-CH ₃	741	371	741	371	741
15.	3-CF ₃ -4-F	11.4	11.4	11.4	11.4	22.9
16.	3-CF ₃ -4-Br	2.43	4.78	4.78	4.78	9.75
17.	3-F-4-Br	5.54	5.54	5.54	5.54	11.1
18.	5-CF ₃ -2-F	11.4	11.4	11.4	11.4	11.4
19.	5-CF ₃ -3-F	11.4	11.4	11.4	11.4	11.4
20.	5-CF ₃ -2-Cl	0.342	0.684	0.342	0.342	10.9
21.	4-CF ₃ -3-F	5.72	5.72	5.72	5.72	11.4
22.	4-CF ₃ -2-Br	624	624	624	624	624
AMP	–	5.72	45.8	45.8	45.8	–
CPX	–	0.751	48.3	48.3	48.3	–
INH	–	–	–	–	–	36.5
RIF	–	–	–	–	–	9.72

SA = *Staphylococcus aureus* ATCC 29213; MRSA = clinical isolates of methicillin-resistant *S. aureus* 63718, SA 630, and SA 3202 (National Institute of Public Health, Prague, Czech Republic); MT = *Mycobacterium tuberculosis* H37Ra ATCC 25177.

2.2. In Vitro Antimicrobial Activity

The biological screening of all the compounds was performed against the reference and quality control strain *Staphylococcus aureus* ATCC 29213, three clinical isolates of methicillin-resistant *S. aureus* (MRSA) [41], and against *Mycobacterium tuberculosis* H37Ra ATCC 25177. The efficiency of the compounds was expressed as the minimum inhibitory concentrations (MICs), that are defined for bacteria as 90% (IC₉₀) reduction of growth in comparison with the control (see Table 1). The MIC (IC₉₀) value is routinely and widely used in bacterial assays as a standard detection limit according to the Clinical and Laboratory Standards Institute (CLSI) [42,43]. Based on the range of observed MIC values, it can be summarized that compounds expressed a wide range of potencies. Some of them, especially substituted by a trifluoromethyl moiety were much more active than standards, clinically used drugs. *N*-[3,5-bis(Trifluoromethyl)phenyl]- (13) and *N*-[2-chloro-5-(trifluoromethyl)-phenyl]-3-hydroxynaphthalene-2-carboxamide (20) showed submicromolar (MICs 0.16–0.68 μ M) antistaphylococcal activity; and compounds 16–19 and 21 demonstrated antistaphylococcal activity

ranging from 2.4 to 11.5 μM . As MICs against MRSA isolates were, in fact, comparable with the MIC values observed against methicillin-susceptible *S. aureus* ATCC 29213, it could be assumed that the presence of *mecA* gene did not affect the activity of these compounds [44].

The same compounds, i.e., **13**, *N*-[4-bromo-3-(trifluoromethyl)phenyl]-3-hydroxy-naphthalene-2-carboxamide (**16**), **12**, and **17–21** showed activity against *M. tuberculosis* ranging from 9.75 to 12.0 μM and comparable with that of rifampicin. Therefore, a standard MTT (3-(4,5-dimethylthiazol-2-yl)-2,5-diphenyltetrazolium bromide) assay was performed with the chosen most effective compounds against *M. tuberculosis* H37Ra. The MTT test can be used to assess cell growth by measuring respiration. The MTT measured viability of mycobacterial cells less than 70% after exposure to the MIC values for each tested compound is considered as a positive result of this assay. This low level of cell viability indicates inhibition of cell growth by inhibition of respiration [45,46]. It can be concluded that compounds **12** (R = 3,5-Cl, 27%), **13** (R = 3,5-CF₃, 6%), **19** (R = 5-CF₃-3-F, 41%), **20** (R = 5-CF₃-2-Cl, 5%), and **21** (R = 4-CF₃-3-F, 46%) showed the viability of *M. tuberculosis* that was significantly less than 70% at the tested concentration equal to MICs [47].

Based on the above findings, it can be assumed that one mechanisms of actions of these so-called multi-target compounds appears to be the inhibition of bacterial respiration by the inhibition of ATP synthase (F₀F₁ complex) or cytochrome bc1 [21–26,48]. In addition, the structurally-related molecules can destroy the cellular proton gradient as proton shuttles that is evidenced by their ability to inhibit photosynthetic electron transport (PET) in chloroplasts [29–31,49–51]. In fact, a good correlation was found between PET inhibition and the antibacterial/antimycobacterial activities [52,53]). It seems that other possible sites of action in bacterial cells are possible; therefore, further studies at the molecular level are needed.

2.3. Molecular Similarity Assessment

The similarity-guided evaluation of the activity profile for the congeneric series of structurally-related *N*-(disubstituted-phenyl)-3-hydroxynaphthalene-2-carboxamide derivatives was performed using the principal component analysis (PCA) on the pool of 2762 descriptors generated by Dragon 6.0 software, where constant or nearly constant descriptors (standard deviation < 0.0001) were *a priori* excluded (overall 2123 variables) [54]. The multi-dimensional data were arranged in $X_{22 \times 2762}$ matrix with columns and rows representing variables and molecules, respectively. The centered and standardized data were subsequently subjected to PCA, where compression efficiency is directly related to the quantity of uncorrelated variables. The high percentage of total variance described by the first three principal components (72.69%) suggests that variables are highly inter-correlated. The first two PCs characterized 65.36% of the overall variance; therefore, the projection of the selected properties on the plane defined by the first two PCs with respect to carboxamide chemotype was conducted as illustrated in Figure 1.

Despite the fact, that carboxamide derivatives **1–22** have a common chemotype based on hydroxynaphthalene ring, peptide-like linker, and phenyl substituent, mainly two heterogeneous structural subfamilies can be formed along the PC1: the first one (PC1 < 0) with compounds **3–12**, **17** and the second group (PC1 > 0) containing the remaining ones (see Figure 1a). It is noticeable that very active compound **13** occupies a distinct location of the PC1 vs. PC2 plane, while fairly potent compounds group together (20 < PC1 < 40), as shown in Figure 1b. Interestingly, different distribution of mono-halogenated carboxamide derivatives with the –CF₃ substituent (molecules **15**, **16**, **18–22**) is accompanied by the increased activity profile (see Figure 1b).

In fact, the majority of the investigated carboxamides do not strictly obey the Lipinski's Rule of Five (Ro5), where the set of threshold values was imposed on the specific molecular descriptors (MW ≤ 500, HBD ≤ 5, HBA ≤ 10, clogP ≤ 5) to specify drug-like property space (see Figure 2a); however, a good drug-like score does not make a molecule a drug and vice versa [55–57]. On the other hand, the violations of any two of the Ro5 conditions reduces the probability of a compound to be orally bioavailable as suggested anonymous Reviewer. Clearly, ADMET-friendly properties

such as lipophilicity are meaningful in the context of specific ligand-receptor interactions; therefore, the lipophilic profile for the analyzed set of compounds is displayed in Figure 2b.

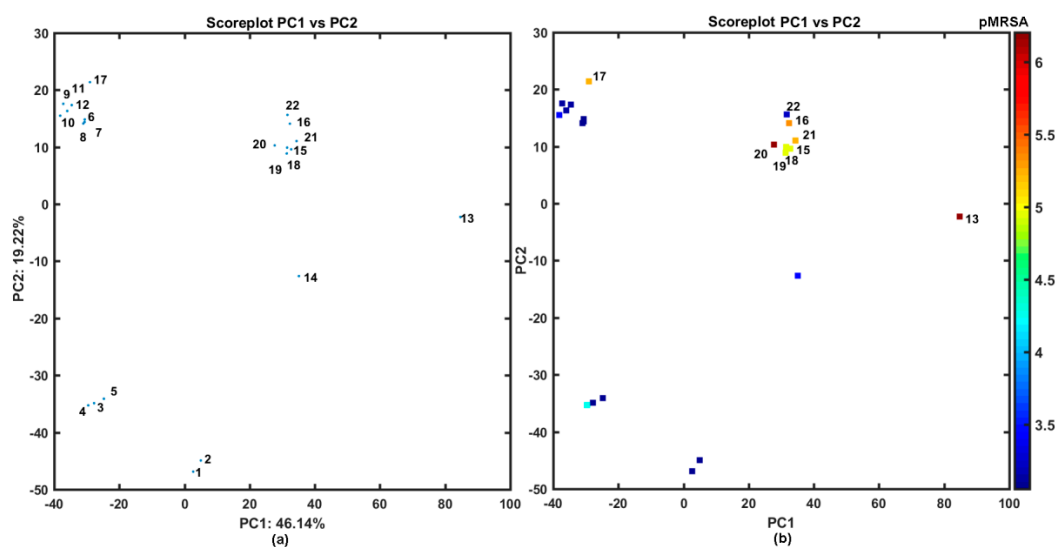


Figure 1. Projection of carboxamides 1–22 on plane defined by first vs. second principal components for Dragon descriptors (a) with MRSA activity in logarithmic scale (b) colors code numerical values of pMRSA activity. Molecules with pMRSA > 4 are numerically labeled.

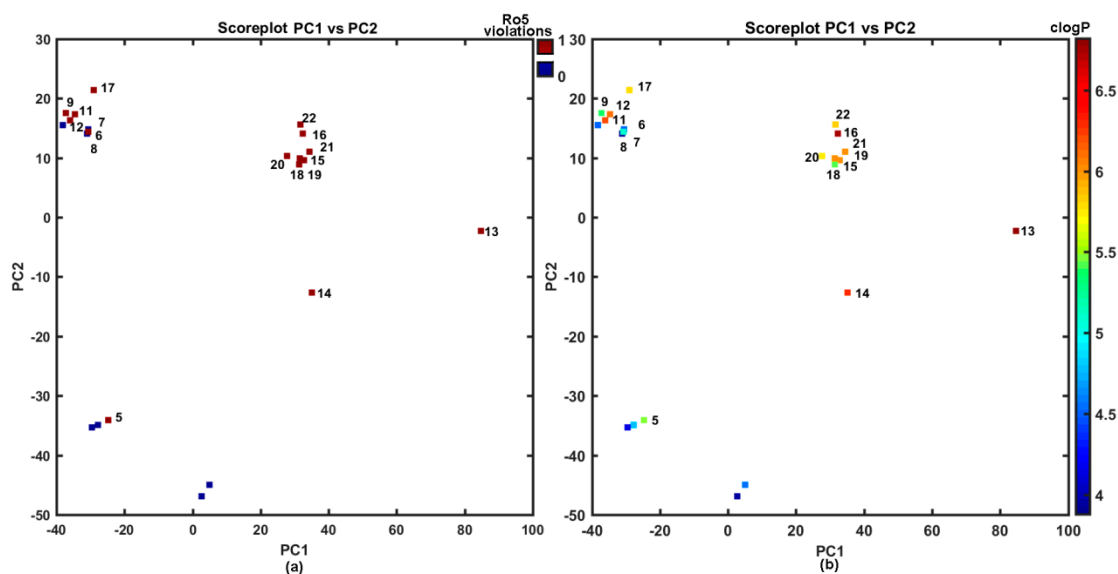


Figure 2. Projection of carboxamides 1–22 on the plane defined by first vs. second principal components for Dragon descriptors with Ro5 rule violations (a) and calculated lipophilicity clogP (b) colors code numerical values of clogP and Ro5 violations. Molecules with Ro5 violation and clogP > 5 are numerically labeled.

Unarguably, the core of many SAR-based methods is the similarity principle in the structural space assuming that similar compounds are expected to display similar physicochemical and biological properties. Conceptually, medicinal chemists have adopted a simplified view that similarity between two objects can be quantitatively expressed by the function of common features [58]. Despite obvious oversimplification of the similarity quantification (e.g., some similarity scores exhibit size-dependent behavior), it is still a powerful concept, where the number of molecular characteristics might be denoted by a bit-string representation (sometimes augmented with the scaling coefficients). The pair-wise descriptor-based structural resemblance/relatedness can be numerically evaluated by a variety of

relative distance metrics (Hamming or Euclidean measures) or absolute comparison using Tanimoto coefficient calculated for OpenBabel fingerprints. The distribution of Tanimoto coefficients for the analyzed set of compounds was investigated revealing that the greatest frequency was recorded in the range of $0.65 < T < 0.70$, respectively. A triangular matrix of $T_{22 \times 22}$ in Figure 3 indicates the structural dissimilarities of dichloro-substituted (compounds 9–12) and dimethoxy-substituted (compounds 1, 2) isomers from the remaining ones that confirm our previous PCA findings (see Figure 1a). On the other hand, in the Tanimoto matrix compound 13 is high similar to compounds 14–22, but PCA showed a different result as indicated by an anonymous reviewer. It should be noted that the PCA-based similarity analysis is performed in the reduced PC1 vs. PC2 space, that describes 65% of the overall variance.

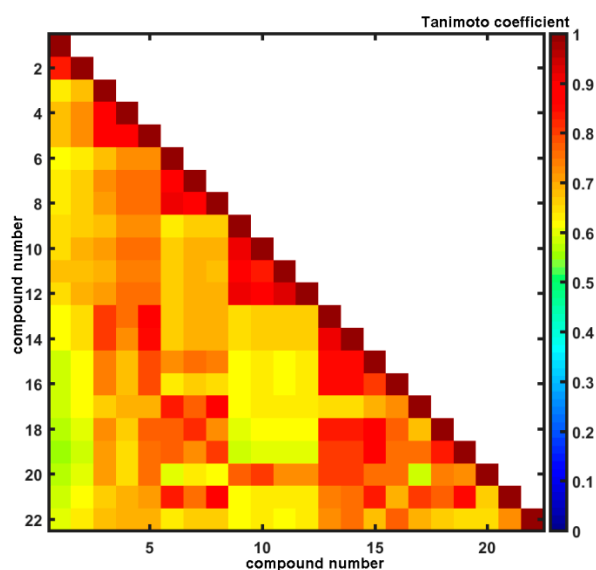


Figure 3. Triangular matrix of Tanimoto coefficients for 1–22 carboxamides.

The 2D image of molecular similarity augmented with biological affinity profile provides a coherent visualization tool for the systematic illumination of SAR trends (continuity areas and/or activity cliffs) in the form of the structure-activity landscape indexes (SALI) [13–16]. The greater density of compounds that cover the factual chemical space (FCS) the more accurate specification of activity cliffs; however even relatively sparse sampling of FCS can be sufficient to construct a reliable activity landscape. As a matter of fact, the detection of sharply non-uniform regions that form steep cliffs in the activity landscape depends critically on the availability of structurally-related compounds with discernible variations in the biological response data. It is obvious that for closely related molecules (e.g., stereoisomers where $T \rightarrow 1$) $SALI \rightarrow \infty$; therefore, such values were substituted by the largest SALI value. Figure 4a presents the symmetrical grayscale heatmap of SALI for the investigated set of carboxamides, where axes correspond to a molecule number sorted according to increasing affinity ATCC 29213 ($\Delta pATCC = 3.75$) with a legend indicating the range of SALI values. In fact, two types of spots can be noticed on the heatmap: the white representing the highest numerical SALI values and the black that indicate minimal ones, respectively.

Located at the right lower part of the SALI plane (or symmetrically positioned in the upper left part) are pairs of molecules that potentially form the activity cliff that is formally manifested via demolition of activity for similar structures (lighter spots in Figure 4a). Interestingly, the substitution of hydrogen atoms in methyl groups of molecule 5 with fluorine resulted in the boost of potency observed for molecule 13. Moreover, the potent molecule 13 is accompanied by inactive molecule 14, where one trifluoromethyl group was isomerically (*meta*→*ortho*) replaced with one methyl substituent. The mentioned structural modifications, that unfavorably affect the affinity profile, can be tracked down on the neighborhood plot (see Figure 4b), where the structurally-related pairs of molecules

($T > 0.85$) are plotted versus differences in the biological activity and color-coded by higher SALI values as well. It seems, that further dense sampling of rough regions (the upper right corner) in the numerical SALI plane ($T > 0.75$ and $pIC_{50} > 2$) is necessary to specify the valid SAR boundaries for the investigated series of carboxamides.

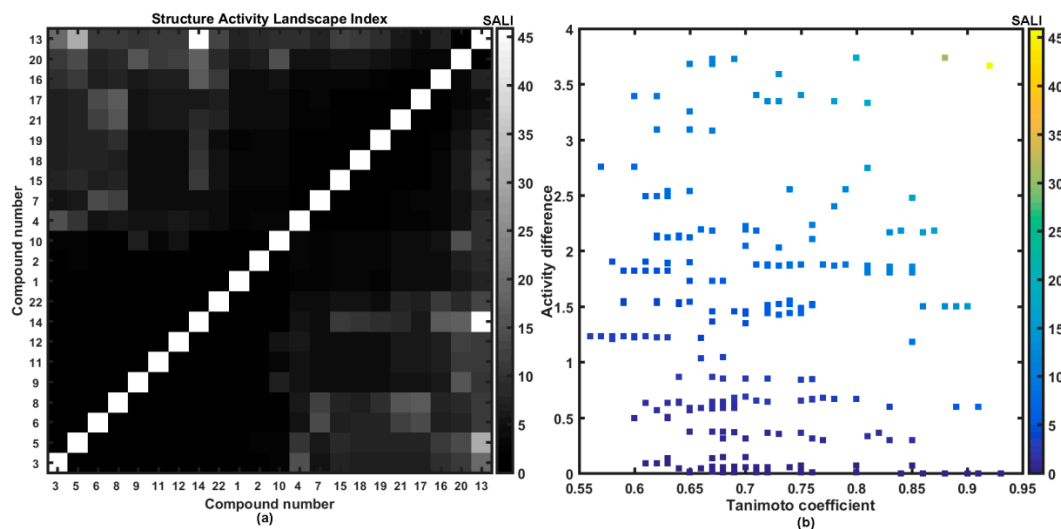


Figure 4. Grayscaled SALI plot with compounds ordered with increasing ATCC 29213 activities (a) and neighboring plot (b) for 1–22 carboxamides.

2.4. Probability-Driven Pharmacophore Mapping

In order to explore the key 3D steric/electronic/lipophilic features of the ligand-site composition the systematic probing of the functional group complementarity inevitably led to the introduction of pharmacophore concept in SAR studies [59]. In the simplest case, the relative arrangement of pharmacophoric properties is specified for the homogenous subfamily of compounds that share the common structural scaffold (chemotype). In reality, drug hunters aspire to enhance the SAR applicability domain for non-congeneric series of molecules, but accurate *de novo* prediction of modeled property for the entire universe of chemicals (CS) is still an elusive and enigmatic operation. Moreover, the model robustness and predictive power are strongly dependent on the training/test subset division, but no correlation between good retrospective performance and good prospective performance was observed (Kubinyi paradox) [60,61]. In fact, there are no specific rules to place particular molecules into the training/test groups; therefore, multiple and interchangeable training/test assignment was proposed for the probability-oriented pharmacophore mapping stemming from stochastic model validation (SMV) approach [3,5,13,57]. Fortunately, the CPU-intense PLS calculations were viable for the entire pool of systematically generated training/test populations ($C_{22}^8 \approx 3 \times 10^5$) for CoMSA MRSA 63718 modeling. The frequency distribution of test compounds for models with preferable $q_{cv}^2 \geq 0.5$ and $q_{test}^2 \geq 0.5$ parameters (more efficient than flipping a coin) revealed that active (17 and 20) and inactive (9 and 22) molecules were noticeably over-represented. The preferential over-representation of some compounds in the test set suggests the possibility of optional (or random) generation of better models; therefore, the investigation of all possible training/test set combinations seems advisable. In other words, better models were recorded for training sets depleted of the indicated molecules. Additionally, an averaged selection-driven pharmacophore pattern was produced based on the regions of the pretty high model ability and predictability according to the IVE-PLS (iterative variable elimination partial least squares) procedure described elsewhere [62]. A listing of spatial zones with favorable and unfavorable contributions of CoMSA descriptors is provided in Figure 5.

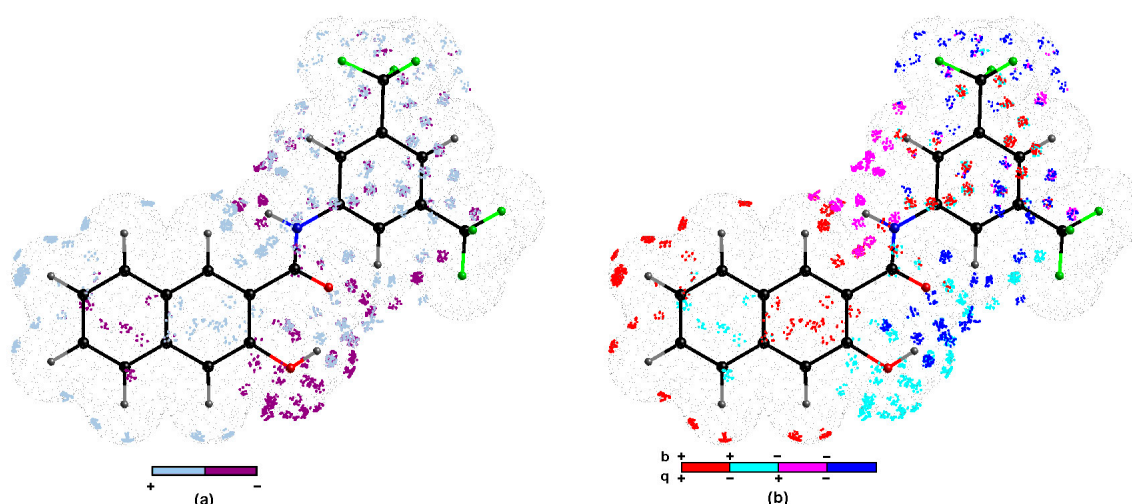


Figure 5. Spatial sectors with largest contribution into MRSA potency selected by CoMSA IVE-PLS for 14/8 training/test set samplings. Colors code their contribution (a) and four possible combination of mean charge q and correlation coefficient b values (b) 1–22 carboxamides. Reference compound **13** was illustrated as the most potent molecule.

The impact of the surface/charge descriptors on the ligand-site affinity is indicated by the regions of positive and negative potency contribution (Figure 5a) and four combinations of charge values versus the mean regression coefficients (Figure 5b), respectively. It is not straightforward to translate pharmacophore-related points of the space into the corresponding pseudoreceptor model with privileged zones, that hypothetically harbors putative drug molecule, while the bundle of steric and electrostatic features was specified on the averaged surface of the receptor-selective ligand molecules. The three-dimensional distribution plot shown in Figure 5a demonstrates the contribution of hydroxynaphthalene ring, peptide-like linker, and phenyl group. Oddly enough, the negatively charged surface areas of the hydroxyl substituent contribute unfavorably, mainly due to steric and/or electronic factors, while the gray 3D polyhedrals surrounding carbonyl groups depict the spatial areas that were foreseen as favorable (see Figure 5a,b). Noticeably, the dominant gray spheres in the close proximity of position 3 in the phenyl group (Figure 5a) correspond well with the increased electron density on fluorine atoms of the $-CF_3$ substituent, that confirms the tendency recorded for carboxamide derivative, where activity profile for meta substitution can be basically ranked as trifluoromethyl \gg methyl. Similarly, the negatively charged substituent directly attached to the phenyl group at position 5 contributes favorably to carboxamides binding affinity as suggested by dark blue zones in Figure 5a and data recorded in Table 1, respectively. In fact, the interpretation of an average pharmacophore pattern is common for a set of congeneric subfamilies, and provides subtle hints useful at the stage of structure-related activity modifications. In fact, no particular pharmacophore interaction was indicated as dominant; however, the pharmacophore visualization based on the consensus 3D QSAR modeling provides the spatial map of chemical groups/atoms potentially relevant for increasing/decreasing the activity profile of the analyzed molecules.

2.5. Advanced Antimicrobial Evaluation

2.5.1. Combined Effect

The most potent antistaphylococcal compounds **13**, **16**, **17**, **20**, and **21** were studied in combination with ciprofloxacin to evaluate their potential additive effect on the resistant isolate MRSA SA 630 of a given antibacterial chemotherapeutic. The method of minimal fractional inhibitory concentration index (FICI) in a microtitration plate was used. $FICI \leq 0.5$ means synergy; $0.5 < FICI < 1$ means

additivity; $1 \leq \text{FICI} < 4$ means indifference; and $\text{FICI} \geq 4$ means antagonism, respectively [63,64]. All the results are included in Table 2.

Synergistic activity was observed for the combinations of compounds **16** and **17** with ciprofloxacin (CPX) against MRSA SA 630. The combination of compound **21** with CPX showed additivity against this isolate as well. Combinations of all tested compounds with oxacillin (OXA) were indifferent. This indifference shows no interference of the tested compounds with *mecA* gene and can exclude interaction with the cell wall. The mechanism of resistance to CPX in MRSA SA 630 has not yet been precisely described. Generally, the common mechanism of resistance to fluoroquinolones is active efflux; so, a possible explanation of synergy may be inhibition of efflux pumps.

Table 2. Effect of tested compounds in combination with ciprofloxacin (CPX) and oxacillin (OXA) against isolate MRSA SA 630. MICs ($\mu\text{g/mL}$) of compounds alone and observed in the synergy experiment are shown in parentheses. In the case of additivity and synergy, concentrations of tested compound/CPX ($\mu\text{g/mL}$) providing this effect are shown.

Combination (MIC [$\mu\text{g/mL}$])	FIC Index	Comb. Effect (MICs [$\mu\text{g/mL}$])
Comp. 13 + CPX (0.125/128)	1.000	IND
Comp. 16 + CPX (8/128)	0.375	SYN 1/32
Comp. 17 + CPX (1/128)	0.500	SYN 0.25/32
Comp. 20 + CPX (0,5/128)	1.004	IND
Comp. 21 + CPX (0.125/128)	0.75	ADD 0.0625/32; 0.03125/64
Comp. 13 + OXA (0.125/64)	1.004	IND
Comp. 16 + OXA (8/64)	1.000	IND
Comp. 17 + OXA (1/64)	1.125	IND
Comp. 20 + OXA (0,5/64)	1.002	IND
Comp. 21 + OXA (0,125/64)	1.125	IND

FIC = fractional inhibitory concentration; IND = indifference; ADD = additivity; SYN = synergy.

2.5.2. Time-Kill Assay

Compounds **16**, **17**, **20**, and **21** were chosen for the evaluation of the dynamics of the antibacterial activity by the time-kill curves method against *S. aureus* ATCC 29213 and MRSA SA 3202 (Figure 6). Compound **13** was not included in this experiment by reason of too low MIC, which is limiting for this methodology. The activity was tested at concentrations equal to $1\times\text{MIC}$, $2\times\text{MIC}$, and $4\times\text{MIC}$ at timepoints 0, 4, 6, 8, and 24 h from the beginning of incubation.

Most of the tested compounds had a bacteriostatic effect. The activity of the compound **16** depended on the concentration; the static effect was observed at concentration $4\times\text{MIC}$ at 4 and 6 h after the start of incubation for *S. aureus* ATCC 29213 and at 4, 6, and 8 h for MRSA SA 3202. The increase in the amount of CFU at 24 h could be caused by the selection of resistant mutants. Compound **17** showed the highest effect at 8 h for both tested strains. In the case of *S. aureus* ATCC 29213, there is only a small difference between concentrations at that timepoint. On the other hand, the most active concentration against MRSA SA 3202 was $2\times\text{MIC}$. Compound **20** showed concentration dependence with the highest effect at $4\times\text{MIC}$ at 6 h for *S. aureus* ATCC 29213 and 4 h for MRSA SA 3202. Bactericidal effect ($\geq \log_{10}3$ decrease) was observed only in the case of compound **21** at concentrations $2\times\text{MIC}$ and $4\times\text{MIC}$ at 24 h of incubation against *S. aureus* ATCC 29213. All the tested concentrations of this compound showed at least 90% killing at 8 and 24 h of incubation against this strain. In the case of MRSA SA 3202, 90% killing at all the three concentrations at 8 h of incubation was also observed; the concentration $4\times\text{MIC}$ at 24 h timepoint showed actually 99% killing. Both strains showed time-dependent killing.

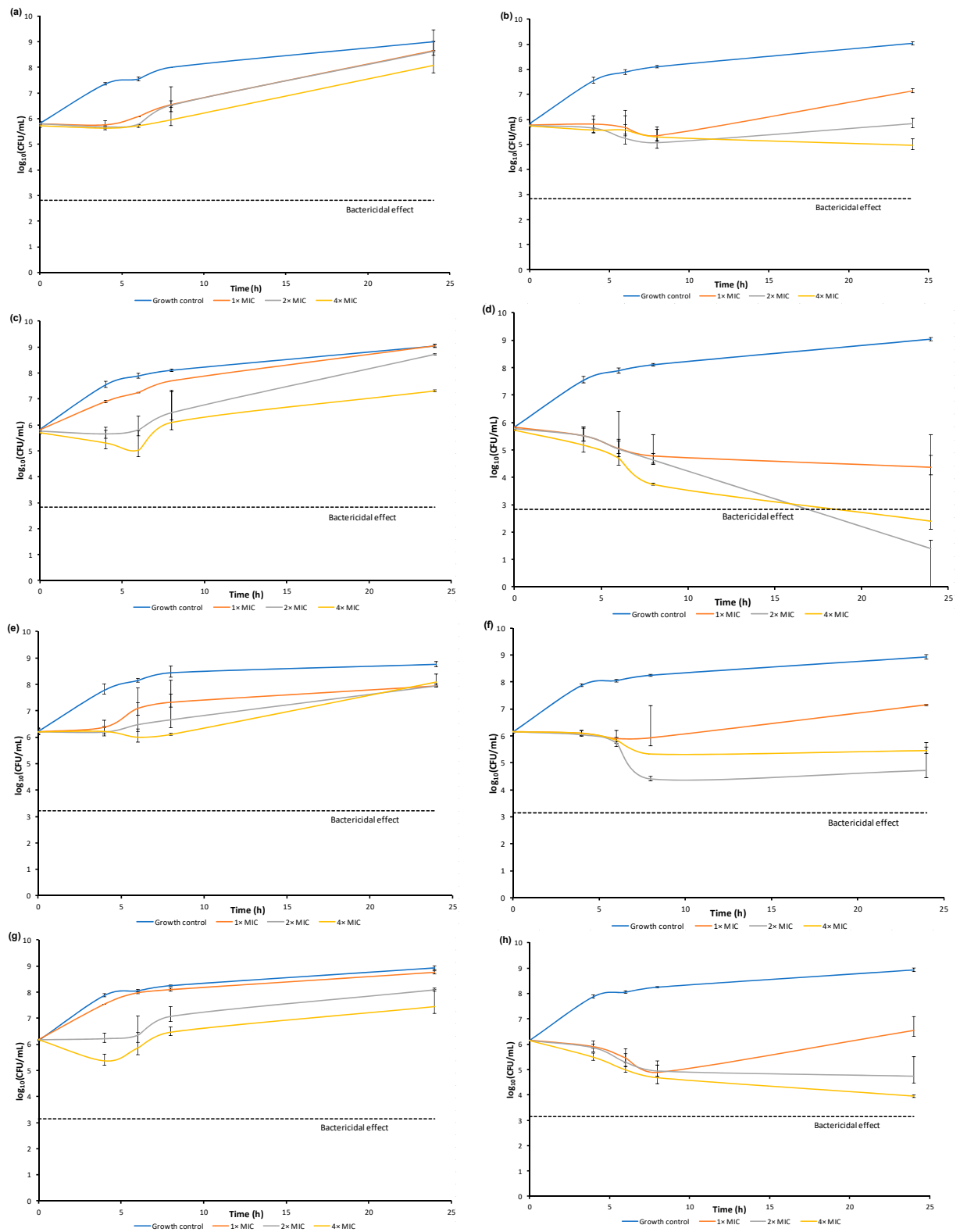


Figure 6. Comparison of dynamics of antibacterial activity of selected compounds **16**, **17**, **20**, **21** against *S. aureus* ATCC 29213 (a–d) and MRSA SA 3202 (e–h).

3. Materials and Methods

3.1. General Methods

All reagents were purchased from Merck (Sigma-Aldrich, St. Louis, MO, USA) and Alfa (Alfa-Aesar, Ward Hill, MA, USA). Reactions were conducted using a CEM Discover SP microwave reactor (CEM, Matthews, NC, USA). The melting points were specified using a Kofler hot-plate apparatus HMK (Franz Kustner Nacht KG, Dresden, Germany) and are maintained uncorrected. Infrared (IR) spectra were recorded with Smart MIRacle™ ATR ZnSe for Nicolet™ Impact 410 Fourier-transform IR spectrometer (Thermo Scientific, West Palm Beach, FL, USA). The spectra were received by the accumulation of 256 scans with 2 cm^{-1} resolution in the region of $4000\text{--}650\text{ cm}^{-1}$. All ^1H - and ^{13}C -NMR spectra were recorded using an Agilent VNMRs 600 MHz system (600 MHz for ^1H and 150 MHz for ^{13}C ; Agilent Technologies, Santa Clara, CA, USA) in dimethyl sulfoxide- d_6 (DMSO- d_6). ^1H and ^{13}C chemical shifts (δ) are reported in ppm. High-resolution mass spectra were measured using a high-performance liquid chromatograph Dionex UltiMate® 3000 (Thermo Scientific) coupled with an LTQ Orbitrap XL™ Hybrid Ion Trap-Orbitrap Fourier Transform Mass Spectrometer (Thermo Scientific) equipped with a HESI II (heated electrospray ionization) source in the positive mode.

3.2. Chemistry

General Procedure for Synthesis of Carboxamide Derivatives 1–22

3-Hydroxynaphthalene-2-carboxylic acid (1.0 g, 5.3 mM) was suspended in dry chlorobenzene (30 mL) at ambient temperature and phosphorus trichloride (0.23 mL, 2.7 mM, 0.5 eq.), and the corresponding substituted aniline (5.3 mM, 1 eq.) was added dropwise. The reaction mixture was transferred to the microwave reactor, where the synthesis was conducted (1st phase: 10 min, $100\text{ }^\circ\text{C}$, 100 W; 2nd phase: 15 min, $120\text{ }^\circ\text{C}$, 500 W; 3rd phase: 20 min, $130\text{ }^\circ\text{C}$, 500 W). Subsequently, the mixture was cooled to $60\text{ }^\circ\text{C}$, and hence the solvent was removed to dryness under reduced pressure. The residue was washed with hydrochloric acid and water. The crude product was recrystallized from EtOH.

N-(2,5-Dimethoxyphenyl)-3-hydroxynaphthalene-2-carboxamide (1). Yield 57%; Mp $186\text{--}188\text{ }^\circ\text{C}$; IR (cm^{-1}): 3425, 2934, 2836, 1604, 1592, 1538, 1490, 1445, 1434, 1280, 1217, 1183, 1144, 1050, 1024, 872, 862, 785, 751, 737, 711; ^1H -NMR (DMSO- d_6), δ : 11.79 (s, 1H), 11.13 (s, 1H), 8.70 (s, 1H), 8.24 (s, 1H), 7.98 (d, 1H, $J = 8.1\text{ Hz}$), 7.78 (d, 1H, $J = 8.1\text{ Hz}$), 7.52 (t, 1H, $J = 7.1\text{ Hz}$), 7.37 (t, 1H, $J = 7.3\text{ Hz}$), 7.36 (s, 1H), 7.03 (dd, 1H, $J = 9.2\text{ Hz}$, $J = 1.5\text{ Hz}$), 6.66 (ddd, 1H, $J = 9.2\text{ Hz}$, $J = 7.7\text{ Hz}$, $J = 1.5\text{ Hz}$), 3.87 (s, 3H), 3.74 (s, 3H); ^{13}C -NMR (DMSO- d_6), δ : 162.8, 153.2, 152.5, 142.7, 135.9, 132.7, 129.0, 128.8, 128.3, 127.2, 125.6, 123.9, 121.3, 111.7, 110.7, 107.5, 106.9, 56.6, 55.3; HR-MS: $[\text{M} - \text{H}]^+$ calculated 322.1074 m/z , found 322.1080 m/z .

N-(3,5-Dimethoxyphenyl)-3-hydroxynaphthalene-2-carboxamide (2). Yield 80%; Mp $179\text{--}184\text{ }^\circ\text{C}$; IR (cm^{-1}): 3115, 1645, 1623, 1606, 1558, 1478, 1455, 1341, 1318, 1269, 1227, 1198, 1156, 1061, 948, 838, 811, 799, 767, 678; ^1H -NMR (DMSO- d_6), δ : 11.26 (s, 1H), 10.52 (s, 1H), 8.46 (s, 1H), 7.92 (d, 1H, $J = 8.1\text{ Hz}$), 7.76 (d, 1H, $J = 8.4\text{ Hz}$), 7.51 (t, 1H, $J = 7.5\text{ Hz}$), 7.36 (t, 1H, $J = 7.3\text{ Hz}$), 7.32 (s, 1H), 7.04 (d, 2H, $J = 1.8\text{ Hz}$), 6.31 (t, 1H, $J = 1.8\text{ Hz}$), 3.76 (s, 6H); ^{13}C -NMR (DMSO- d_6), δ : 165.7, 160.5, 153.6, 140.2, 135.7, 130.5, 128.7, 128.1, 126.9, 125.8, 123.8, 122.1, 110.5, 98.7, 96.0, 55.2; HR-MS: $[\text{M} - \text{H}]^+$ calculated 322.1074 m/z , found 322.1081 m/z .

N-(2,5-Dimethylphenyl)-3-hydroxynaphthalene-2-carboxamide (3). Yield 84%; Mp $209\text{--}212\text{ }^\circ\text{C}$; IR (cm^{-1}): 3328, 3013, 1633, 1621, 1597, 1577, 1538, 1519, 1493, 1446, 1413, 1361, 1326, 1287, 1262, 1221, 1174, 1067, 1000, 957, 917, 849, 800, 775, 730, 682; ^1H -NMR (DMSO- d_6), δ : 11.83 (s, 1H), 10.49 (s, 1H), 8.66 (s, 1H), 7.95 (d, 1H, $J = 8.1\text{ Hz}$), 7.80 (s, 1H), 7.78 (d, 1H, $J = 8.4\text{ Hz}$), 7.52 (t, 1H, $J = 7.3\text{ Hz}$), 7.37 (t, 1H, $J = 7.3\text{ Hz}$), 7.36 (s, 1H), 7.17 (d, 1H, $J = 7.7\text{ Hz}$), 6.94 (d, 1H, $J = 7.7\text{ Hz}$), 2.31 (s, 3H), 2.28 (s, 3H); ^{13}C -NMR (DMSO- d_6), δ : 164.5, 153.6, 136.2, 135.9, 135.4, 131.5, 130.2, 128.9, 128.3, 127.0, 126.9, 125.7, 125.6, 123.9, 123.9, 120.7, 110.7, 20.8, 17.4; HR-MS: $[\text{M} - \text{H}]^+$ calculated 290.11756 m/z , found 290.11829 m/z .

N-(2,6-Dimethylphenyl)-3-hydroxynaphthalene-2-carboxamide (**4**). Yield 83%; Mp 192–196 °C; IR (cm⁻¹): 3054, 1652, 1635, 1622, 1590, 1509, 1470, 1446, 1393, 1358, 1346, 1269, 1229, 1168, 1070, 953, 936, 916, 869, 842, 776, 750, 712, 671; ¹H-NMR (DMSO-*d*₆), δ: 11.73 (s, 1H), 10.24 (s, 1H), 8.63 (s, 1H), 7.92 (d, 1H, *J* = 7.7 Hz), 7.78 (d, 1H, *J* = 8.1 Hz), 7.53 (t, 1H, *J* = 7.3 Hz), 7.37 (t, 1H, *J* = 7.3 Hz), 7.34 (s, 1H), 7.16 (s, 3H), 2.25 (s, 6H); ¹³C-NMR (DMSO-*d*₆), δ: 166.6, 155.0, 136.0, 135.4, 134.5, 130.0, 128.7, 128.3, 127.8, 126.9, 126.7, 125.8, 123.8, 119.7, 110.7, 18.1; HR-MS: [M – H]⁺ calculated 290.1176 *m/z*, found 290.1183 *m/z*.

N-(3,5-Dimethylphenyl)-3-hydroxynaphthalene-2-carboxamide (**5**). Yield 83%; Mp 184–186 °C; IR (cm⁻¹): 3303, 3042, 2011, 2916, 1635, 1621, 1598, 1557, 1519, 1454, 1396, 1358, 1335, 1224, 1210, 1169, 1145, 916, 870, 838, 772, 744, 711, 685; ¹H-NMR (DMSO-*d*₆), δ: 11.41 (s, 1H), 10.48 (s, 1H), 8.52 (s, 1H), 7.92 (d, 1H, *J* = 8.1 Hz), 7.77 (d, 1H, *J* = 8.4 Hz), 7.52 (t, 1H, *J* = 7.1 Hz), 7.40 (s, 2H), 7.36 (t, 1H, *J* = 7.3 Hz), 7.33 (s, 1H), 6.79 (s, 1H), 2.29 (s, 6H); ¹³C-NMR (DMSO-*d*₆), δ: 165.6, 153.9, 138.2, 137.8, 135.8, 130.5, 128.7, 128.2, 126.9, 125.8, 125.6, 123.8, 121.5, 118.3, 110.6, 21.1; HR-MS: [M – H]⁺ calculated 290.1176 *m/z*, found 290.1185 *m/z*.

N-(2,5-Difluorophenyl)-3-hydroxynaphthalene-2-carboxamide (**6**). Yield 53%; Mp 264 °C; IR (cm⁻¹): 3057, 1652, 1630, 1598, 1561, 1516, 1489, 1444, 1391, 1360, 1346, 1285, 1272, 1245, 1222, 1184, 1145, 1064, 1015, 972, 949, 908, 889, 862, 833, 807, 795, 765, 736, 716; ¹H-NMR (DMSO-*d*₆), δ: 11.93 (s, 1H); 11.11 (s, 1H), 8.68 (s, 1H), 8.30 (ddd, 1H, *J* = 3.2 Hz, *J* = 6.2 Hz, *J* = 10.3 Hz), 7.99 (d, 1H, *J* = 8.2 Hz), 7.78 (d, 1H, *J* = 8.3 Hz), 7.54 (ddd, 1H, *J* = 1.1 Hz, *J* = 6.8 Hz, *J* = 8.3 Hz), 7.41 (ddd, 1H, *J* = 5.1 Hz, *J* = 9.1 Hz, *J* = 10.6 Hz), 7.38 (ddd, 1H, *J* = 1.2 Hz, *J* = 6.8 Hz, *J* = 8.2 Hz), 7.37 (s, 1H), 7.00–7.04 (m, 1H); ¹³C-NMR (DMSO-*d*₆), δ: 163.6, 157.9 (dd, *J* = 1.7 Hz, *J* = 238.4 Hz), 152.5, 148.8 (dd, *J* = 2.4 Hz, *J* = 239.1 Hz), 136.1, 132.7, 129.1, 128.6, 127.6 (t, *J* = 12.4 Hz), 127.2, 125.7, 124.1, 120.4, 116.1 (dd, *J* = 10.0 Hz, *J* = 22.1 Hz), 110.9, 110.4 (dd, *J* = 8.0 Hz, *J* = 24.3 Hz), 108.7 (d, *J* = 29.9 Hz); HR-MS: [M + H]⁺ calculated 300.0830 *m/z*, found 300.0832 *m/z*.

N-(2,6-Difluorophenyl)-3-hydroxynaphthalene-2-carboxamide (**7**). Yield 78%; Mp 194–198 °C; IR (cm⁻¹): 3357, 1662, 1628, 1596, 1511, 1466, 1304, 1285, 1213, 1147, 1134, 1009, 899, 830, 788, 778, 747; ¹H-NMR (DMSO-*d*₆), δ: 11.48 (s, 1H), 10.41 (s, 1H), 8.61 (s, 1H), 7.94 (d, 1H, *J* = 8.1 Hz), 7.78 (d, 1H, *J* = 8.1 Hz), 7.54 (t, 1H, *J* = 7.0 Hz), 7.33–7.44 (m, 4H), 7.25 (t, 1H, *J* = 7.9 Hz); ¹³C-NMR (DMSO-*d*₆), δ: 166.0, 157.9 (dd, *J* = 247.3 Hz, *J* = 5.3 Hz), 154.1, 136.2, 131.2, 128.9, 128.7 (t, *J* = 19.8 Hz), 128.5, 126.8, 125.9, 125.8, 123.9, 119.4, 114.2 (t, *J* = 16.7 Hz), 112.0 (m); HR-MS: [M – H]⁺ calculated 298.0674 *m/z*, found 298.0681 *m/z*.

N-(3,5-Difluorophenyl)-3-hydroxynaphthalene-2-carboxamide (**8**). Yield 79%; Mp 273–276 °C; IR (cm⁻¹): 3103, 1645, 1626, 1608, 1574, 1564, 1479, 1439, 1345, 1308, 1268, 1225, 1208, 1169, 1118, 999, 989, 855, 829, 767, 740; ¹H-NMR (DMSO-*d*₆), δ: 11.05 (s, 1H), 10.80 (s, 1H), 8.38 (s, 1H), 7.93 (d, 1H, *J* = 8.0 Hz), 7.76 (d, 1H, *J* = 8.4 Hz), 7.51–7.62 (m, 3H), 7.38 (t, 1H, *J* = 7.5 Hz), 7.34 (s, 1H), 6.99 (t, 1H, *J* = 8.0 Hz); ¹³C-NMR (DMSO-*d*₆), δ: 165.8, 162.4 (dd, *J* = 241.3 Hz, *J* = 15.2 Hz), 153.0, 141.2 (t, *J* = 13.7 Hz), 135.7, 130.6, 128.7, 128.2, 126.9, 125.8, 123.8, 122.8, 110.5, 103.0 (m), 98.93 (t, *J* = 25.8 Hz); HR-MS: [M – H]⁺ calculated 298.0674 *m/z*, found 298.0685 *m/z*.

N-(2,5-Dichlorophenyl)-3-hydroxynaphthalene-2-carboxamide (**9**). Yield 72%; Mp 252 °C; IR (cm⁻¹): 3187, 1637, 1623, 1590, 1580, 1519, 1470, 1455, 1404, 1359, 1347, 1313, 1265, 1204, 1174, 1140, 1090, 1073, 1047, 1017, 979, 960, 916, 867, 846, 808, 769, 750, 707; ¹H-NMR (DMSO-*d*₆), δ: 12.03 (s, 1H), 11.28 (s, 1H), 8.71 (s, 1H), 8.67 (d, 1H, *J* = 2.5 Hz), 7.99 (d, 1H, *J* = 8.2 Hz), 7.78 (d, 1H, *J* = 8.2 Hz), 7.60 (d, 1H, *J* = 8.6 Hz), 7.53 (ddd, 1H, *J* = 1.2 Hz, *J* = 6.8 Hz, *J* = 8.3 Hz), 7.38 (s, 1H), 7.37 (ddd, 1H, *J* = 1.1 Hz, *J* = 6.8 Hz, *J* = 8.2 Hz), 7.25 (dd, 1H, *J* = 2.6 Hz, *J* = 8.6 Hz); ¹³C-NMR (DMSO-*d*₆), δ: 163.5, 152.4, 136.5, 136.1, 133.0, 132.1, 130.6, 129.1, 128.7, 127.2, 125.7, 124.5, 124.0, 121.39, 121.35, 120.3, 110.9; HR-MS: [M + H]⁺ calculated 332.0240 *m/z*, found 332.0243 *m/z*.

N-(2,6-Dichlorophenyl)-3-hydroxynaphthalene-2-carboxamide (**10**). Yield 73%; Mp 283–284 °C; IR (cm⁻¹): 3209, 1623, 1614, 1570, 1515, 1463, 1450, 1433, 1405, 1328, 1236, 1205, 1155, 970, 912, 818, 793, 783, 771,

745, 704, 679; $^1\text{H-NMR}$ (DMSO- d_6) δ : 11.57 (s, 1H), 10.66 (s, 1H), 8.66 (s, 1H), 7.95 (d, 1H, $J = 8.2$ Hz), 7.79 (d, 1H, $J = 8.2$ Hz), 7.62 (d, 2H, $J = 8.2$ Hz), 7.53 (ddd, 1H, $J = 7.8$ Hz, $J = 6.9$ Hz, 1.0 Hz), 7.43 (t, 1H, $J = 8.2$ Hz), 7.37 (ddd, 1H, $J = 8.2$ Hz, $J = 6.9$ Hz, $J = 0.9$ Hz), 7.35 (s, 1H); $^{13}\text{C-NMR}$ (DMSO- d_6), δ : 165.8, 153.6, 136.0, 134.1, 133.3, 131.1, 129.3, 128.9, 128.8, 128.2, 126.8, 125.9, 125.6, 123.9, 120.4; HR-MS: $[\text{M} + \text{H}]^+$ calculated 332.0240 m/z , found 332.0238 m/z .

N-(3,4-Dichlorophenyl)-3-hydroxynaphthalene-2-carboxamide (**11**). Yield 76%; Mp 278–279 °C; IR (cm^{-1}): 3080, 1622, 1605, 1589, 1566, 1545, 1474, 1449, 1396, 1377, 1358, 1344, 1240, 1207, 1172, 1134, 1073, 1024, 955, 925, 898, 852, 837, 826, 771, 748, 680; $^1\text{H-NMR}$ (DMSO- d_6) δ : 11.09 (s, 1H), 10.75 (s, 1H), 8.41 (s, 1H), 8.18 (d, 1H, $J = 2.3$ Hz), 7.93 (d, 1H, $J = 8.2$ Hz), 7.77 (d, 1H, $J = 8.2$ Hz), 7.72 (dd, 1H, $J = 8.9$ Hz, $J = 12.3$ Hz), 7.64 (d, 1H, $J = 8.7$ Hz), 7.51 (ddd, 1H, $J = 7.8$ Hz, $J = 6.9$ Hz, $J = 0.9$ Hz), 7.36 (ddd, 1H, $J = 8.2$ Hz, $J = 6.9$ Hz, $J = 0.9$ Hz), 7.33 (s, 1H); $^{13}\text{C-NMR}$ (DMSO- d_6), δ : 165.8, 153.2, 138.8, 135.7, 131.0, 130.7, 130.5, 128.7, 128.2, 126.9, 125.8, 125.3, 123.8, 122.5, 121.4, 120.3, 110.5; HR-MS: $[\text{M} + \text{H}]^+$ calculated 332.0240 m/z , found 332.0242 m/z .

N-(3,5-Dichlorophenyl)-3-hydroxynaphthalene-2-carboxamide (**12**). Yield 70%; Mp 252 °C; IR (cm^{-1}): 3087, 1646, 1630, 1583, 1547, 1447, 1409, 1396, 1375, 1345, 1329, 1269, 1254, 1204, 1172, 1147, 1115, 1092, 1072, 1017, 993, 938, 917, 905, 867, 861, 836, 802, 788, 764, 741, 723, 688; $^1\text{H-NMR}$ (DMSO- d_6) δ : 11.04 (s, 1H), 10.75 (s, 1H), 8.39 (s, 1H), 7.92 (d, 1H, $J = 8.2$ Hz), 7.89 (d, 2H, $J = 1.7$ Hz), 7.77 (d, 1H, $J = 8.3$ Hz), 7.51 (ddd, 1H, $J = 1.2$ Hz, $J = 6.8$ Hz, $J = 8.3$ Hz), 7.36 (ddd, 1H, $J = 1.1$ Hz, $J = 6.8$ Hz, $J = 8.2$ Hz), 7.34 (t, 1H, $J = 1.7$ Hz), 7.34 (s, 1H); $^{13}\text{C-NMR}$ (DMSO- d_6), δ : 165.9, 153.1, 141.0, 135.7, 134.1, 130.5, 128.7, 128.2, 126.8, 125.8, 123.8, 123.0, 122.6, 118.3, 110.5; HR-MS: $[\text{M} + \text{H}]^+$ calculated 332.0240 m/z , found 332.0244 m/z .

N-[3,5-bis(Trifluoromethyl)phenyl]-3-hydroxynaphthalene-2-carboxamide (**13**). Yield 57%; Mp 232–235 °C; IR (cm^{-1}): 3256, 1651, 1631, 1601, 1578, 1568, 1473, 1384, 1357, 1346, 1274, 1162, 1120, 1113, 943, 883, 866, 836, 765, 744, 707, 682; $^1\text{H-NMR}$ (DMSO- d_6), δ : 11.05 (s, 1H), 10.99 (s, 1H), 8.50 (s, 2H), 8.41 (s, 1H), 7.93 (d, 1H, $J = 8.1$ Hz), 7.84 (s, 1H), 7.78 (d, 1H, $J = 8.4$ Hz), 7.52 (t, 1H, $J = 6.6$ Hz), 7.34–7.40 (m, 2H); $^{13}\text{C-NMR}$ (DMSO- d_6), δ : 166.4, 153.2, 140.6, 135.8, 130.8 (q, $J = 32.8$ Hz), 130.6, 128.6, 128.2, 126.8, 125.9, 123.9, 123.3 (q, $J = 272.4$ Hz), 122.6, 120.0 (q, $J = 3.6$ Hz), 116.6 (sep, $J = 3.4$ Hz), 110.5; HR-MS: $[\text{M} - \text{H}]^+$ calculated 398.0610 m/z , found 398.0620 m/z .

3-Hydroxy-*N*-[4-methyl-3-(trifluoromethyl)phenyl]naphthalene-2-carboxamide (**14**). Yield 68%; Mp 251–252 °C; IR (cm^{-1}): 3135, 1638, 1607, 1553, 1502, 1450, 1398, 1361, 1316, 1204, 1169, 1141, 1113, 1052, 1008, 955, 920, 900, 867, 837, 770, 749, 726; $^1\text{H-NMR}$ (DMSO- d_6) δ : 11.19 (s, 1H), 10.73 (s, 1H), 8.46 (s, 1H), 8.20 (d, 1H, $J = 1.9$ Hz), 7.92 (d, 1H, $J = 8.2$ Hz), 7.89 (dd, 1H, $J = 1.9$ Hz, $J = 8.3$ Hz), 7.77 (d, 1H, $J = 8.3$ Hz), 7.51 (ddd, 1H, $J = 1.2$ Hz, $J = 6.8$ Hz, $J = 8.3$ Hz), 7.44 (d, 1H, $J = 8.3$ Hz), 7.36 (ddd, 1H, $J = 1.1$ Hz, $J = 6.8$ Hz, $J = 8.2$ Hz), 7.33 (s, 1H), 2.42 (s, 3H); $^{13}\text{C-NMR}$ (DMSO- d_6), δ : 166.0, 153.6, 136.8, 135.8, 132.7, 131.1 (q, $J = 1.7$ Hz), 130.4, 128.7, 128.2, 127.5 (q, $J = 29.3$ Hz), 126.9, 125.8, 124.4 (q, $J = 273.8$ Hz), 123.8, 122.0, 117.4 (q, $J = 5.9$ Hz), 110.6, 18.3 (q, $J = 1.9$ Hz); HR-MS: $[\text{M} + \text{H}]^+$ calculated 346.1049 m/z , found 346.1055 m/z .

N-[4-Fluoro-3-(trifluoromethyl)phenyl]-3-hydroxynaphthalene-2-carboxamide (**15**). Yield 72%; Mp 231–232 °C; IR (cm^{-1}): 3101, 1639, 1613, 1575, 1498, 1453, 1421, 1397, 1361, 1344, 1321, 1273, 1254, 1229, 1206, 1179, 1144, 1123, 1053, 959, 925, 903, 868, 839, 814, 771, 753, 732, 679; $^1\text{H-NMR}$ (DMSO- d_6) δ : 11.10 (s, 1H), 10.81 (s, 1H), 8.43 (s, 1H), 8.29 (dd, 1H, $J = 2.6$ Hz, $J = 6.5$ Hz), 8.05 (ddd, 1H, $J = 3.0$ Hz, $J = 4.2$ Hz, $J = 8.9$ Hz), 7.92 (d, 1H, $J = 8.2$ Hz), 7.77 (d, 1H, $J = 8.3$ Hz), 7.55 (dd, 1H, $J = 9.0$ Hz, $J = 10.5$ Hz), 7.51 (ddd, 1H, $J = 1.2$ Hz, $J = 6.8$ Hz, 8.3 Hz), 7.36 (ddd, 1H, $J = 1.2$ Hz, $J = 6.8$ Hz, $J = 8.2$ Hz), 7.34 (s, 1H); $^{13}\text{C-NMR}$ (DMSO- d_6), δ : 166.0, 154.8 (dq, $J = 2.1$ Hz, $J = 250.3$ Hz), 153.4, 135.8, 135.4 (d, $J = 2.9$ Hz), 130.4, 128.7, 128.2, 126.8, (d, $J = 8.1$ Hz), 126.5, 125.8, 123.8, 122.5 (dq, $J = 1.1$, 272.1 Hz), 122.2, 118.4 (q, $J = 4.9$ Hz), 117.7 (d, $J = 21.4$ Hz), 116.5 (dq, $J = 13.4$, 32.4 Hz), 110.5; HR-MS: $[\text{M} + \text{H}]^+$ calculated 350.0799 m/z , found 350.0801 m/z .

N-[4-Bromo-3-(trifluoromethyl)phenyl]-3-hydroxynaphthalene-2-carboxamide (**16**). Yield 62%; Mp 234–235 °C; IR (cm⁻¹): 3161, 1637, 1622, 1602, 1549, 1478, 1451, 1395, 1359, 1313, 1264, 1208, 1176, 1151, 1127, 1105, 1021, 957, 924, 896, 867, 836, 770, 750, 721; ¹H-NMR (DMSO-*d*₆) δ: 11.07 (s, 1H), 10.86 (s, 1H), 8.42 (s, 1H), 8.37 (d, 1H, *J* = 2.5 Hz), 7.97 (dd, 1H, *J* = 2.5 Hz, *J* = 8.7 Hz), 7.92 (d, 1H, *J* = 8.2 Hz), 7.88 (d, 1H, *J* = 8.7 Hz), 7.77 (d, 1H, *J* = 8.3 Hz), 7.51 (ddd, 1H, *J* = 1.2 Hz, *J* = 6.8 Hz, *J* = 8.3 Hz), 7.36 (ddd, 1H, *J* = 1.2 Hz, *J* = 6.8 Hz, *J* = 8.2 Hz), 7.34 (s, 1H); ¹³C-NMR (DMSO-*d*₆) δ: 166.1, 153.3, 138.6, 135.8, 135.5, 130.5, 128.7, 128.6 (q, *J* = 30.5 Hz), 128.2, 126.9, 125.8, 125.1, 123.8, 122.9 (q, *J* = 273.1 Hz), 122.5, 119.3 (q, *J* = 5.8 Hz), 112.2 (q, *J* = 1.8 Hz), 110.5; HR-MS: [M + H]⁺ calculated 409.9998 *m/z*, found 410.0005 *m/z*.

N-(4-Bromo-3-fluorophenyl)-3-hydroxynaphthalene-2-carboxamide (**17**). Yield 72%; Mp 255–256 °C; IR (cm⁻¹): 3053, 1634, 1619, 1599, 1557, 1486, 1447, 1400, 1356, 1344, 1270, 1244, 1221, 1207, 1168, 1145, 1128, 1078, 1043, 963, 915, 871, 844, 817, 771, 749, 704; ¹H-NMR (DMSO-*d*₆) δ: 11.10 (s, 1H), 10.78 (s, 1H), 8.41 (s, 1H), 7.95 (dd, 1H, *J* = 2.3 Hz, *J* = 11.4 Hz), 7.93 (d, 1H, *J* = 8.3 Hz), 7.76 (d, 1H, *J* = 8.3 Hz), 7.69 (dd, 1H, *J* = 8.2 Hz, *J* = 8.7 Hz), 7.52 (ddd, 1H, *J* = 0.7 Hz, *J* = 2.4 Hz, *J* = 8.9 Hz), 7.51 (ddd, 1H, *J* = 1.3 Hz, *J* = 6.8 Hz, *J* = 8.3 Hz), 7.36 (ddd, 1H, *J* = 1.2 Hz, *J* = 6.8 Hz, *J* = 8.2 Hz), 7.33 (s, 1H); ¹³C-NMR (DMSO-*d*₆) δ: 165.8, 158.1 (d, *J* = 242.4 Hz), 153.2, 139.9 (d, *J* = 10.2 Hz), 135.7, 133.3 (d, *J* = 1.2 Hz), 130.6, 128.7, 128.2, 126.9, 125.8, 123.8, 122.5, 101.5 (d, *J* = 21.0 Hz), 108.2 (d, *J* = 27.1 Hz), 117.6 (d, *J* = 3.0 Hz), 110.5; HR-MS: [M + H]⁺ calculated 360.0030 *m/z*, found 360.0036 *m/z*.

N-[2-Fluoro-5-(trifluoromethyl)phenyl]-3-hydroxynaphthalene-2-carboxamide (**18**). Yield 77%; Mp 222–223 °C; IR (cm⁻¹): 3276, 1656, 1632, 1619, 1568, 1521, 1498, 1468, 1442, 1396, 1345, 1321, 1263, 1248, 1215, 1204, 1165, 1148, 1126, 1072, 926, 917, 904, 888, 865, 812, 765, 746, 716; ¹H-NMR (DMSO-*d*₆) δ: 11.92 (s, 1H), 11.16 (s, 1H), 8.83 (dd, 1H, *J* = 1.6 Hz, *J* = 7.1 Hz), 8.67 (s, 1H), 7.98 (d, 1H, *J* = 8.2 Hz), 7.57–7.62 (m, 2H), 7.78 (d, 1H, *J* = 8.3 Hz), 7.53 (ddd, 1H, *J* = 1.2 Hz, *J* = 6.8 Hz, *J* = 8.3 Hz), 7.38 (ddd, 1H, *J* = 1.1 Hz, *J* = 6.8 Hz, *J* = 8.2 Hz), 7.38 (s, 1H); ¹³C-NMR (DMSO-*d*₆) δ: 164.0, 154.5 (d, *J* = 249.9 Hz), 152.6, 136.1, 132.7, 129.1, 128.7, 127.5 (d, *J* = 11.5 Hz), 125.8, 127.2, 125.5 (dq, *J* = 3.1 Hz, *J* = 32.2 Hz), 124.1, 123.8 (q, *J* = 272.3 Hz), 121.9 (dq, *J* = 3.9 Hz, 8.7 Hz), 120.4, 118.9 (m), 116.4 (d, *J* = 20.9 Hz), 110.9; HR-MS: [M + H]⁺ calculated 350.0799 *m/z*, found 350.0802 *m/z*.

N-[3-Fluoro-5-(trifluoromethyl)phenyl]-3-hydroxynaphthalene-2-carboxamide (**19**). Yield 66%; Mp 245–247 °C; IR (cm⁻¹): 3094, 1647, 1623, 1575, 1564, 1482, 1458, 1436, 1397, 1358, 1347, 1327, 1254, 1217, 1207, 1171, 1149, 1128, 1099, 1003, 995, 922, 894, 875, 867, 858, 840, 799, 766, 745; ¹H-NMR (DMSO-*d*₆) δ: 11.01 (s, 1H); 10.93 (s, 1H); 8.40 (s, 1H); 8.05 (s, 1H); 8.00 (d, 1H, *J* = 11.0 Hz); 7.93 (d, 1H, *J* = 8.2 Hz); 7.77 (d, 1H, *J* = 8.2 Hz); 7.51 (dd, 1H, *J* = 8.2 Hz, 6.9 Hz); 7.43 (d, 1H, *J* = 8.2 Hz); 7.37 (t, 1H, *J* = 7.2 Hz); 7.34 (s, 1H); ¹³C-NMR (DMSO-*d*₆) δ: 166.1; 162.1 (d, *J* = 244.2 Hz); 153.1; 141.4 (d, *J* = 11.6 Hz); 135.8; 131.0 (td, *J* = 33.2 Hz, 10.1 Hz); 130.6; 128.7; 128.2; 126.9; 125.9; 123.8; 123.3 (qd, *J* = 273.1 Hz, 4.3 Hz); 122.8; 112.6 (m); 110.5 (d, *J* = 26.0 Hz); 110.5; 107.5 (m); HR-MS: [M + H]⁺ calculated 350.0799 *m/z*, found 350.0791 *m/z*.

N-[2-Chloro-5-(trifluoromethyl)phenyl]-3-hydroxynaphthalene-2-carboxamide (**20**). Yield 60%; Mp 185–188 °C; IR (cm⁻¹): 3193, 1642, 1622, 1601, 1586, 1544, 1519, 1425, 1329, 1253, 1204, 1167, 1150, 1119, 1080, 1046, 916, 895, 873, 848, 826, 770, 752; ¹H-NMR (DMSO-*d*₆) δ: 12.09 (s, 1H), 11.41 (s, 1H), 8.98 (d, 1H, *J* = 2.2 Hz), 8.72 (s, 1H), 7.99 (d, 1H, *J* = 8.1 Hz), 7.82 (d, 1H, *J* = 7.7 Hz), 7.78 (d, 1H, *J* = 8.1 Hz), 7.50–7.57 (m, 2H), 7.33–7.41 (m, 2H); ¹³C-NMR (DMSO-*d*₆) δ: 163.7, 152.5, 136.3, 136.2, 133.1, 130.5, 129.2, 128.7, 128.4 (q, *J* = 32.0 Hz), 127.1, 126.8 (q, *J* = 1.5 Hz), 125.7, 124.1, 123.7 (q, *J* = 272.4 Hz), 121.3 (q, *J* = 3.9 Hz), 120.3, 118.2 (q, *J* = 3.8 Hz), 110.9; HR-MS: [M – H]⁺ calculated 364.0347 *m/z*, found 364.0355 *m/z*.

N-[3-Fluoro-4-(trifluoromethyl)phenyl]-3-hydroxynaphthalene-2-carboxamide (**21**). Yield 61%; Mp 273–274 °C; IR (cm⁻¹): 3061, 1622, 1605, 1557, 1451, 1432, 1417, 1398, 1360, 1342, 1317, 1271, 1244, 1210, 1174, 1120, 1069, 1047, 977, 962, 945, 915, 873, 860, 842, 815, 772, 754, 732, 702; ¹H NMR (CDCl₃) δ: 11.05 (s, 1H), 10.96 (s, 1H), 8.39 (s, 1H), 8.02 (dd, 1H, *J* = 1.4 Hz, *J* = 13.5 Hz), 7.94 (d, 1H, *J* = 8.2 Hz), 7.78 (t, 1H, *J* = 8.6 Hz), 7.77 (d, 1H, *J* = 8.3 Hz), 7.71 (dd, 1H, *J* = 1.4 Hz, *J* = 8.7 Hz), 7.51 (ddd, 1H,

$J = 1.2$ Hz, $J = 6.8$ Hz, $J = 8.3$ Hz), 7.36 (ddd, 1H, $J = 1.2$, $J = 6.8$ Hz, $J = 8.2$ Hz), 7.34 (s, 1H); ^{13}C -NMR (DMSO- d_6), δ : 166.0, 159.2 (dq, $J = 2.0$ Hz, $J = 250.6$ Hz), 152.9, 144.5 (d, $J = 11.4$ Hz), 135.8, 130.7, 107.5 (d, $J = 25.4$ Hz), 128.7, 128.2, 127.8 (m), 126.9, 125.8, 123.8, 122.9, 122.8 (q, $J = 271.1$ Hz), 115.6 (d, $J = 1.4$ Hz, $J = 8.7$ Hz), 111.0 (dq, $J = 12.5$, 32.6 Hz), 110.5; HR-MS: $[\text{M} + \text{H}]^+$ calculated 350.0799 m/z , found 350.0801 m/z .

N-[2-Bromo-4-(trifluoromethyl)phenyl]-3-hydroxynaphthalene-2-carboxamide (**22**). Yield 67%; Mp 231–233 °C; IR (cm^{-1}): 3225, 3093, 1643, 1626, 1601, 1588, 1541, 1492, 1451, 1404, 1359, 1319, 1274, 1212, 1169, 1120, 1078, 1042, 955, 919, 894, 871, 838, 803; ^1H NMR (CDCl_3) δ : 12.09 (s, 1H); 11.32 (s, 1H); 8.76 (d, 1H, $J = 8.9$ Hz); 8.73 (s, 1H); 8.12 (s, 1H); 8.01 (d, 1H, $J = 8.2$ Hz); 7.85 (dd, 1H, $J = 8.2$ Hz, $J = 1.4$ Hz); 7.79 (d, 1H, $J = 8.2$ Hz); 7.56–7.53 (m, 1H); 7.40 (s, 1H); 7.39–7.73 (m, 1H); ^{13}C -NMR (DMSO- d_6), δ : 163.6; 152.5; 140.4; 136.2; 133.2; 129.6 (q, $J = 4.3$ Hz); 129.2; 128.8; 127.2; 125.7; 125.7 (q, $J = 4.3$ Hz); 125.2 (q, $J = 33.2$ Hz); 124.1; 123.4 (q, $J = 271.7$ Hz); 122.4; 120.3; 113.4; 110.9; HR-MS: $[\text{M} + \text{H}]^+$ calculated 409.9998 m/z , found 409.9988 m/z .

3.3. Biological Testing

3.3.1. In Vitro Antibacterial Evaluation

The synthesized compounds were evaluated for in vitro antibacterial activity against representatives of multidrug-resistant bacteria and clinical isolates of methicillin-resistant *Staphylococcus aureus* (MRSA) 63718, SA 630, and SA 3202 that were obtained from the National Institute of Public Health (Prague, Czech Republic) [41]. *S. aureus* ATCC 29213 was used as a reference and quality control strain. Ampicillin and ciprofloxacin (Sigma, St. Louis, MO, USA) were employed as the standard. Prior to testing, each strain was passaged onto nutrient agar (Oxoid, Basingstoke, UK) with 5% of bovine blood, and bacterial inocula were prepared by suspending a small portion of a bacterial colony in sterile phosphate-buffered saline (pH 7.2–7.3). The cell density was adjusted to 0.5 McFarland units using a densitometer (Densi-La-Meter, LIAP, Riga, Latvia). This inoculum was diluted to reach the final concentration of bacterial cells 5×10^5 CFU/mL in the wells. The compounds were dissolved in DMSO (Sigma), and the final concentration of DMSO in the cation-adjusted Mueller–Hinton (CaMH) broth (Oxoid) did not exceed 2.5% of the total solution composition. The final concentrations of the evaluated compounds ranged from 256 to 0.008 $\mu\text{g/mL}$. The broth dilution micro-method, modified according to the NCCLS (National Committee for Clinical Laboratory Standards) guidelines in Mueller–Hinton (MH) broth, was used to determine the minimum inhibitory concentration (MIC) [42]. Drug-free controls, sterility controls, and controls consisting of MH broth and DMSO alone were included. The determination of results was performed visually after 24 h of static incubation in the darkness at 37 °C in an aerobic atmosphere. The results are reported in Table 1.

3.3.2. In Vitro Antimycobacterial Assessment

Mycobacterium tuberculosis ATCC 25177/H37Ra was grown in Middlebrook broth (MB), supplemented with Oleic-Albumin-Dextrose-Catalase (OADC) supplement (Difco, Lawrence, KS, USA). At log phase growth, a culture sample (10 mL) was centrifuged at 15,000 rpm/20 min using a bench top centrifuge (MPW-65R, MPW Med Instruments, Warszawa, Poland). Following the removal of the supernatant, the pellet was washed in fresh Middlebrook 7H9GC broth and resuspended in fresh, ODAC-supplemented MB (10 mL). The turbidity was adjusted to match McFarland standard No. 1 (3×10^8 CFU) with MB broth. A further 1:10 dilution of the culture was then performed in MB broth. The antimicrobial susceptibility of *M. tuberculosis* was investigated in a 96-well plate format. In these experiments, sterile deionized water (300 μL) was added to all outer-perimeter wells of the plates to minimize evaporation of the medium in the test wells during incubation. Each evaluated compound (100 μL) was incubated with *M. tuberculosis* (100 μL). Dilutions of each compound were prepared in duplicate. For all synthesized compounds, final concentrations ranged from 128 to 4 $\mu\text{g/mL}$. All compounds were dissolved in DMSO, and subsequent dilutions were made in supplemented MB.

The plates were sealed with Parafilm and incubated at 37 °C for 14 days. Following incubation, a 10% addition of alamarBlue (Difco) was mixed into each well, and readings at 570 nm and 600 nm were taken, initially for background subtraction and subsequently after 24 h reincubation. The background subtraction is necessary for strongly colored compounds, where the color may interfere with the interpretation of any color change. For noninterfering compounds, a blue color in the well was interpreted as the absence of growth, and a pink color was scored as growth. Isoniazid and rifampicin (Sigma) used as positive control, as it is a clinically used antitubercular drug. The results are shown in Table 1.

3.3.3. MTT Assay

The percent inhibition was determined through the MTT assay. Compounds were prepared according to the previously described procedure and diluted in MB broth for *M. tuberculosis* ATCC 25177/H37Ra. *M. tuberculosis* ATCC 25177/H37Ra was suspended in ODAC supplemented MB at 1.0 McFarland and then diluted 1:10, using MB as a diluent. The diluted mycobacteria (50 µL) were added to each well containing the compound to be investigated. Diluted mycobacteria in broth free from inhibiting compounds were employed as the growth control. All compounds were prepared in duplicate. Plates were incubated at 37 °C for 7 days for *M. tuberculosis*. After the incubation period, 10% well volume of MTT (3-(4,5-dimethylthiazol-2-yl)-2,5-diphenyltetrazolium bromide) reagent (Sigma) was added into each well and the plates were incubated at 37 °C for 4 h in dark for mycobacteria. Subsequently, 100 µL of 17% sodium dodecyl sulfate in 40% dimethylformamide was added to each well. The plates were read at 570 nm. The absorbance readings for cells grown in the presence of the tested compounds were compared with those representing uninhibited cell growth to specify the relative percent inhibition. The percent viability is calculated through the comparison of a measured value and that of the uninhibited control: % viability = $OD_{570E}/OD_{570P} \times 100$, where OD_{570E} is the reading from the compound-exposed cells, while OD_{570P} is the reading from the uninhibited cells (positive control). Cytotoxic potential is evaluated by percent viability <70% [44–46,64].

3.3.4. Combined Effect with Clinically Used Drugs

For the synergy effect study, a method of fractional inhibitory concentration was engaged. A tested compound (A) and antibiotic (B) (ciprofloxacin and oxacillin, purchased from Sigma) were diluted in the microtitration plate in cation adjusted Mueller–Hinton (CaMH) broth to get an original combination of concentrations in every well. Row H was employed for the evaluation of MIC(A); column 12 was applied for assessment of MIC(B). The plate was inoculated by the bacterial suspension to reach a final concentration of 5×10^5 CFU/mL in the wells. The fractional inhibitory concentration index (FICI) was measured using the concentrations in the first nonturbid (clear) well found in each row and column along with the turbidity/nonturbidity interface. To interpret the combined effect, the lowest FICI was used [60]. A $\Sigma FICI \leq 0.5$ means synergy; $0.5 < \Sigma FICI < 1$ means additivity; $1 \leq \Sigma FICI < 4$ means indifference; and $\Sigma FICI \geq 4$ means antagonism, respectively [61]. The tests were made in duplicate, and the results were averaged. The results are reported in Table 2.

3.3.5. Dynamic of Antibacterial Activity

The method of time-kill curves was employed to investigate the bactericidal effect of the specified compounds [65]. The experiment was conducted with *S. aureus* ATCC 29213 and MRSA SA 3202 isolate. The compounds were diluted in CaMH broth to reach concentrations equal to 1×MIC, 2×MIC, and 4×MIC, respectively. The tubes were inoculated by bacterial inoculum in the exponential phase of growth to get a final concentration of 7.5×10^6 CFU/mL. The tubes were incubated statically at 37 °C. Immediately after inoculation and after 4, 6, 8, and 24 h, 100 µL of the sample was serially diluted (1:10) in phosphate-buffered saline. Subsequently, 2×20 µL from each dilution were put onto an MH agar plate and cultivated at 37 °C for 24 h. After incubation, the CFUs of dilutions containing 5–50 colonies were counted. Results were expressed as a decrease of $\log_{10}(\text{CFU})$ in each time compared

to the starting inoculum. Bactericidal effect is specified as a $-3\log$ decrease of CFU/mL compared to the growth control at timepoint 0. The test was performed in duplicate on two separate occasions, and the results were averaged. The growth curves with error bars are illustrated in Figure 6.

3.4. Theoretical Calculations

3.4.1. Model Building and Molecular Modeling

CACTVS/csed and CORINA editors were engaged to produce each structural model and its initial spatial geometry. OpenBabel (inter)change file format converter was employed for data conversion as well. Sybyl-X 2.0/Certara software package running on an HP Z200 workstation with a Debian 10.0 operating system was used to conduct the molecular modeling simulations. The initial compound geometry optimization with MAXMIN2 module was performed using the standard Tripos force field (POWELL conjugate gradient algorithm) with a 0.01 kcal/mol energy gradient convergence criterion. The specification of the electrostatic potential values based on the partial atomic charges was carried out with the Gasteiger–Hückel method implemented in Sybyl-X. One 13-ordered atom trial alignment on the most active molecule **13** according to the active analog approach (AAA) was used in the FIT method to cover the entire bonding topology in the maximal common structure (MCS).

SONNIA software was applied for simulation of 10×10 to 30×30 SOMs with a winning distance ranging from 0.2 to 2.0 in CoMSA analysis. Cartesian coordinates of the molecular surfaces were used as input to Kohonen SOM network to generate a 2D map of the electrostatic potential (MEP) for the set of superimposed molecules. The output maps were reshaped into a 100- to 900-element vectors that were subsequently transformed by the PLS method implemented in the MATLAB environment [66].

3.4.2. Similarity-Driven Activity Landscape

The quantitative sampling of similarity-related activity landscape delivers a subtle picture of favorable and disallowed structural modifications that are valid for the specification of the activity cliffs [11]. The smoothness of this surface can be numerically quantified using structure-activity landscape index (SALI) calculated according to the following formula:

$$SALI_{x,y} = \frac{|A_x - A_y|}{1 - sim(x,y)} \quad (1)$$

where A_x and A_y are activity profiles for the x -th and y -th molecule and $sim(x,y)$ is the similarity estimation between the corresponding molecules [13–16]. The combination of the pairwise dissimilarity and absolute discrepancies in the molecular activities assigns the score to the specific spot of the response surface. The negligible impact of the specific similarity metric on the overall appearance of the symmetric SALI matrix has been observed; therefore, Tanimoto coefficient was applied in the fingerprint-based similarity analysis [14]. In this case, the structural relatedness between molecules library is usually estimated using a function mapping (dis)similarities between the pairs of bitstring descriptors given by the following equation:

$$T(x,y) = \frac{n_{xy}}{(n_x + n_y - n_{xy})} \quad (2)$$

where n_{xy} is the number of bits set into 1 shared in the fingerprint of the molecule x and y , n_x is the number of bits set into 1 in the molecule x , n_y is the number of bits set into 1 in the molecule y , respectively. Top-ranked objects are supposed to have similar properties, although the validity of this assumption is fairly questionable because 70% of compounds with $T(x,y) > 0.85$ to an active analog have a comparatively low opportunity of being active in the same way [67]. A relatively sparse sampling of chemistry space may be sufficient to identify the potential activity cliffs.

3.4.3. Selection-Driven Surface Analysis

The hypothesis-based similarity in a structural space can be expressed by the number of descriptors that capture information about the pharmacophore pattern. Some machine learning techniques combined with weighting and selecting algorithms were applied to specify the minimal set of pharmacophoric features potentially valid for ligand-site interactions [59]. A meaningful comparison of the shape/charge intensities produced on the molecular surface and values of target affinity can be performed using comparative molecular surface analysis (CoMSA) [68]. A self-organizing network (SOM) is composed of a single layer of neurons arranged in a 2D plane with well-defined topology [69]. The closely related objects are located in the proximal neurons of the square map because a neural network automatically adapts itself to the input data. In other words, a planar image of the multidimensional property space is generated, where objects located in neighboring neurons possess theoretically similar properties—most groups have a distinct location in specific regions of the map. The presence of electrostatic and/or steric features, that are potentially valid for ligand-receptor complementarity and recognition, can be detected using the recurrent variable selection method conjugated with the PLS procedure (IVE-PLS) [70]. Briefly, the whole computer implementation includes four stages: (1) standard PLS analysis with LOO-CV to assess the performance of the PLS model, (2) elimination of a matrix column with the lowest $abs(mean(b)/std(b))$ value, (3) standard PLS analysis of the new matrix without the column eliminated in stage (2), (4) recurrent repetition of stages (1)–(3) to maximize the LOO parameter. In order to estimate the model robustness and SAR predictive power, the multiple interchangeable division of the dataset into training/test subsets was applied. The descriptor-driven consensus pharmacophore pattern is derived on the basis of the validated models; however, our models are not expected to be predictive externally—extrapolation might be elusive [71]. The chosen training/test samplings within highly populated areas of $q_{cv}^2 > 0.5$ versus $q_{test}^2 > 0.5$ performance were selected to produce ‘an average’ pharmacophore. On the contrary to the standard procedure for a single training/test subset, an attempt was taken to specify a common ensemble of variables that contribute (un)-favorably to the observed activity simultaneously in all chosen models. Thus, the columns annotated with the highest stability $abs(mean(b)/std(b))$ for each of the chosen models were identified using the IVE-PLS methodology. The cumulative sum of common columns for the selected models was specified and normalized to the range of [0–1]. The relative contribution of each variable is weighted by the magnitude and sign of the corresponding regression coefficient; therefore, color code signs of the descriptor affect/influence compound potency. The sign of influence is color-coded depicting not only the regions with a positive and/or negative activity contribution, but also four possible combinations of a mean charge/correlation coefficient, respectively. A simplified visual inspection of the generated pharmacophore pattern gives a clear 3D picture of the regions that should be modified to modulate the biological activity [59].

4. Conclusions

A series of twenty-two novel multi-target *N*-(disubstituted-phenyl)-3-hydroxynaphthalene-2-carboxamide derivatives were synthesized and characterized by the set of in vitro potency profiles. *N*-[3,5-bis(trifluoromethyl)phenyl]-3-hydroxynaphthalene-2-carboxamide (**13**) and *N*-[2-chloro-5-(trifluoromethyl)phenyl]-3-hydroxynaphthalene-2-carboxamide (**20**) demonstrated high activity against methicillin-resistant *S. aureus* isolates in the range of MICs from 0.16 to 0.68 μ M. Compound **13** and *N*-[4-bromo-3-(trifluoromethyl)phenyl]-3-hydroxynaphthalene-2-carboxamide (**16**) showed activity against *M. tuberculosis* (both MICs approx. 10 μ M) comparable with rifampicin. Synergistic in vitro studies showed an increase in activity of ciprofloxacin in combinations with compound **16** or *N*-(4-bromo-3-fluorophenyl)-3-hydroxynaphthalene-2-carboxamides (**17**) against MRSA SA 630 isolate, which could be related to the inhibition of efflux pumps. The similarity-related property space assessment for the congeneric series of structurally related carboxamide derivatives was performed using the principal component analysis. It is noticeable that very active *N*-[3,5-bis(trifluoromethyl)phenyl]-3-hydroxynaphthalene-2-carboxamide (**13**) occupies a distinct

location of the PC1 vs. PC2 plane, while fairly potent compounds are grouped together. Interestingly, different distribution of mono-halogenated carboxamide derivatives with the $-CF_3$ substituent (compounds **15**, **16**, **18–22**) is accompanied by the increased activity profile. Moreover, the quantitative sampling of similarity-related activity landscape provided a subtle picture of favorable and disallowed structural modifications that are valid for determining the activity cliffs. A symmetric matrix of Tanimoto coefficients indicated the structural dissimilarities of dichloro-substituted (compounds **9–12**) and dimethoxy-substituted (compounds **1**, **2**) isomers from the remaining ones. The potent compound **13** ($R = 3,5-CF_3$) is accompanied by inactive 3-hydroxy-*N*-[4-methyl-3-(trifluoromethyl)phenyl]naphthalene-2-carboxamide (**14**) where one trifluoromethyl group was isomerically (*meta*→*orto*) replaced with one methyl substituent. It seems that further dense sampling of rough regions (the upper right corner) in the numerical SALI plane ($T > 0.75$ and $pIC_{50} > 2$) is necessary to specify valid SAR boundaries for the investigated series of carboxamides. An advanced method of neural network quantitative SAR was engaged to illustrate the key 3D steric/electronic/lipophilic features of the ligand-site composition by the systematic probing of the functional group. On the other hand, it cannot be expected that even robust and validated models can reliably predict the modeled property for the entire universe of chemicals; therefore, the application boundary should be investigated using similarity concept and biological surface analysis. From a philosophical point of view, it is impossible to specify an absolute measure of predictivity, as it considerably depends on the selection of datasets and the statistical approach that is engaged, but the great advantage of the QSAR paradigm lies not in the extrapolation, as was stated by Hansch [14]. Combining molecular similarity concept with hypothesis-based pharmacophore mapping may enhance the probability of finding potent compounds in drug discovery projects.

Author Contributions: J.K. and T.G. synthesized and characterized the compounds. H.M., S.P. and A.C. performed biological screening. J.J. designed the compounds. A.B. and V.K. and A.S. performed theoretical calculations, CoMSA, PCA, IVE-PLS. A.B. and J.J. wrote the paper. All authors have read and agreed to the published version of the manuscript.

Funding: This study was supported by the Ministry of Education of the Czech Republic (project LO1305) and Palacky University in Olomouc (IGA_PrF_2020_023).

Acknowledgments: The authors thank Johann Gasteiger for facilitating access to the SONNIA programs. We would like to acknowledge the OpenEye and OpenBabel Scientific Software for providing free academic licenses.

Conflicts of Interest: The funders had no role in the design of the study; in the collection, analyses, or interpretation of data; in the writing of the manuscript, or in the decision to publish the results.

References

1. Valent, P.; Groner, B.; Schumacher, U.; Superti-Furga, G.; Busslinger, M.; Kralovics, R.; Zielinski, C.; Penninger, J.M.; Kerjaschki, D.; Stingl, G.; et al. Paul Ehrlich (1854–1915) and his contributions to the foundation and birth of translational medicine. *J. Innate Immun.* **2016**, *8*, 111–120. [[CrossRef](#)] [[PubMed](#)]
2. Devillers, J. Methods for building QSARs. *Methods Mol. Biol.* **2013**, *930*, 3–27. [[PubMed](#)]
3. Bak, A.; Pizova, H.; Kozik, V.; Vorcakova, K.; Kos, J.; Treml, J.; Odehnalova, K.; Oravec, M.; Imramovsky, A.; Bobal, P.; et al. SAR-mediated similarity assessment of the property profile for new, silicon-based AChE/BChE inhibitors. *Int. J. Mol. Sci.* **2019**, *20*, 5385. [[CrossRef](#)] [[PubMed](#)]
4. Colquhoun, D. The quantitative analysis of drug–receptor interactions: A short history. *Trends Pharmacol. Sci.* **2006**, *27*, 149–157. [[CrossRef](#)]
5. Bak, A.; Kozik, V.; Malik, I.; Jampilek, J.; Smolinski, A. Probability-driven 3D pharmacophore mapping of antimycobacterial potential of hybrid molecules combining phenylcarbamoyloxy and *N*-arylpiperazine fragments. *SAR QSAR Environ. Res.* **2018**, *29*, 801–821. [[CrossRef](#)]
6. Hann, M.; Oprea, T. Pursuing the leadlikeness concept in pharmaceutical research. *Curr. Opin. Chem. Biol.* **2004**, *8*, 255–263. [[CrossRef](#)]
7. Grammatica, P. Principles of QSAR models validation: Internal and external. *Qsar Comb. Sci.* **2007**, *26*, 694–701. [[CrossRef](#)]
8. Golbraikh, A.; Tropsha, A. Beware of q^2 ! *J. Mol. Graph. Mod.* **2002**, *20*, 269–276. [[CrossRef](#)]

9. Merlot, C.; Domine, D.; Cleva, C.; Church, D.J. Chemical substructures in drug discovery. *Drug Discov. Today* **2003**, *8*, 594–602. [[CrossRef](#)]
10. Reymond, J.L.; van Deursen, R.; Blum, L.C.; Ruddigkeit, L. Chemical space as a source for new drugs. *MedChemComm* **2010**, *1*, 30–38. [[CrossRef](#)]
11. Peltason, L.; Bajorath, J. Systematic computational analysis of structure-activity relationships: Concepts, challenges and recent advances. *Future Med. Chem.* **2009**, *1*, 451–466. [[CrossRef](#)] [[PubMed](#)]
12. Polanski, J.; Bak, A.; Gieleciak, R.; Magdziarz, T. Modeling robust QSAR. *J. Chem. Inf. Model.* **2003**, *46*, 2310–2318. [[CrossRef](#)] [[PubMed](#)]
13. Bak, A.; Kozik, V.; Smolinski, A.; Jampilek, J. Multidimensional (3D/4D-QSAR) probability-guided pharmacophore mapping: Investigation of activity profile for a series of drug absorption promoters. *RSC Adv.* **2016**, *6*, 76183–76205. [[CrossRef](#)]
14. Kubinyi, H. *Hansch Analysis and Related Approaches*; Wiley-VCH Verlag GmbH: Weinheim, Germany, 1993.
15. Maggiora, G.M.; Shanmugasundaram, V. Molecular similarity measures. *Methods Mol. Biol.* **2011**, *672*, 39–100.
16. Van de Waterbeemd, H.; Gifford, E. ADMET in silico modelling: Towards prediction paradise? *Nat. Rev. Drug Discov.* **2003**, *2*, 192–204. [[CrossRef](#)]
17. Lopez-Lopez, E.; Prieto-Martínez, F.D.; Medina-Franco, J.L. Activity landscape and molecular modeling to explore the SAR of dual epigenetic inhibitors: A focus on G9a and DNMT1. *Molecules* **2018**, *23*, 3282. [[CrossRef](#)]
18. Guha, R.; Van Drie, J.H. Assessing how well a modeling protocol captures a structure—Activity landscape. *J. Chem. Inf. Model.* **2008**, *48*, 1716–1728. [[CrossRef](#)]
19. Bajorath, J.; Peltason, L.; Wawer, M.; Guha, R.; Lajiness, M.S.; Van Drie, J.H. Navigating structure—Activity landscapes. *Drug Discov. Today* **2009**, *14*, 698–705. [[CrossRef](#)]
20. Hu, H.; Stumpfe, D.; Bajorath, J. Systematic identification of target set-dependent activity cliffs. *Future Sci. OA* **2019**, *5*, 363. [[CrossRef](#)]
21. Gonec, T.; Kos, J.; Zadrazilova, I.; Pesko, M.; Keltosova, S.; Tengler, J.; Bobal, P.; Kollar, P.; Cizek, A.; Kralova, K.; et al. Antimycobacterial and herbicidal activity of ring-substituted 1-hydroxynaphthalene-2-carboxanilides. *Bioorg. Med. Chem.* **2013**, *21*, 6531–6541. [[CrossRef](#)]
22. Gonec, T.; Kos, J.; Zadrazilova, I.; Pesko, M.; Govender, R.; Keltosova, S.; Chambel, B.; Pereira, D.; Kollar, P.; Imramovsky, A.; et al. Antibacterial and herbicidal activity of ring-substituted 2-hydroxynaphthalene-1-carboxanilides. *Molecules* **2013**, *18*, 9397–9419. [[CrossRef](#)] [[PubMed](#)]
23. Gonec, T.; Zadrazilova, I.; Nevin, E.; Kauerovala, T.; Pesko, M.; Kos, J.; Oravec, M.; Kollar, P.; Coffey, A.; O'Mahony, J.; et al. Synthesis and biological evaluation of N-alkoxyphenyl-3-hydroxynaphthalene-2-carboxanilides. *Molecules* **2015**, *20*, 9767–9787. [[CrossRef](#)] [[PubMed](#)]
24. Kos, J.; Nevin, E.; Soral, M.; Kushkevych, I.; Gonec, T.; Bobal, P.; Kollar, P.; Coffey, A.; O'Mahony, J.; Liptaj, T.; et al. Synthesis and antimycobacterial properties of ring-substituted 6-hydroxynaphthalene-2-carboxanilides. *Bioorg. Med. Chem.* **2015**, *23*, 2035–2043. [[CrossRef](#)] [[PubMed](#)]
25. Gonec, T.; Pospisilova, S.; Kauerovala, T.; Kos, J.; Dohanosova, J.; Oravec, M.; Kollar, P.; Coffey, A.; Liptaj, T.; Cizek, A.; et al. N-Alkoxyphenylhydroxynaphthalenecarboxamides and their antimycobacterial activity. *Molecules* **2016**, *21*, 1068. [[CrossRef](#)]
26. Michnova, H.; Pospisilova, S.; Gonec, T.; Kapustikova, I.; Kollar, P.; Kozik, V.; Musiol, R.; Jendrzewska, I.; Vanco, J.; Travnicek, Z.; et al. Bioactivity of methoxylated and methylated 1-hydroxynaphthalene-2-carboxanilides: Comparative molecular surface analysis. *Molecules* **2019**, *24*, 2991. [[CrossRef](#)]
27. Kauerovala, T.; Kos, J.; Gonec, T.; Jampilek, J.; Kollar, P. Antiproliferative and pro-apoptotic effect of novel nitro-substituted hydroxynaphthalenyls on human cancer cell lines. *Int. J. Mol. Sci.* **2016**, *17*, 1219. [[CrossRef](#)]
28. Kauerovala, T.; Gonec, T.; Jampilek, J.; Hafner, S.; Gaiser, A.K.; Syrovets, T.; Fedr, R.; Soucek, K.; Kollar, P. Ring-substituted 1-hydroxynaphthalene-2-carboxanilides inhibit proliferation and trigger mitochondria-mediated apoptosis. *Int. J. Mol. Sci.* **2020**, *21*, 3416. [[CrossRef](#)]
29. Imramovsky, A.; Pesko, M.; Kralova, K.; Vejsova, M.; Stolarikova, J.; Vinsova, J.; Jampilek, J. Investigating spectrum of biological activity of 4- and 5-chloro-2-hydroxy-N-[2-(arylamino)-1-alkyl-2-oxoethyl]-benzamides. *Molecules* **2011**, *16*, 2414–2430. [[CrossRef](#)]
30. Pauk, K.; Zadrazilova, I.; Imramovsky, A.; Vinsova, J.; Pokorna, M.; Masarikova, M.; Cizek, A.; Jampilek, J. New derivatives of salicylamides: Preparation and antimicrobial activity against various bacterial species. *Bioorg. Med. Chem.* **2013**, *21*, 6574–6581. [[CrossRef](#)]

31. Kos, J.; Zadrazilova, I.; Pesko, M.; Keltosova, S.; Tengler, J.; Gonec, T.; Bobal, P.; Kauerovala, T.; Oravec, M.; Kollar, P.; et al. Antibacterial and herbicidal activity of ring-substituted 3-hydroxynaphthalene-2-carboxanilides. *Molecules* **2013**, *18*, 7977–7997. [[CrossRef](#)]
32. Kos, J.; Kapustikova, I.; Clements, C.; Gray, A.I.; Jampilek, J. 3-Hydroxynaphthalene-2-carboxanilides and their antitrypanosomal activity. *Monatsh. Chem.* **2018**, *149*, 887–892. [[CrossRef](#)]
33. DrugBank—Niclosamide. Available online: <https://www.drugbank.ca/drugs/DB06803> (accessed on 27 August 2020).
34. Gajdar, J.; Tsami, K.; Michnova, H.; Gonec, T.; Brazdova, M.; Soldanova, Z.; Fojta, M.; Jampilek, J.; Barek, J.; Fischer, J. Electrochemistry of ring-substituted 1-hydroxynaphthalene-2-carboxanilides: Relation to structure and biological activity. *Electrochim. Acta* **2020**, *332*, 135485. [[CrossRef](#)]
35. Pospisilova, S.; Kos, J.; Michnova, H.; Kapustikova, I.; Strharsky, T.; Oravec, M.; Moricz, A.M.; Bakonyi, J.; Kauerovala, T.; Kollar, P.; et al. Synthesis and spectrum of biological activities of novel *N*-arylcinnamamides. *Int. J. Mol. Sci.* **2018**, *19*, 2318. [[CrossRef](#)] [[PubMed](#)]
36. Spaczynska, E.; Mrozek-Wilczkiewicz, A.; Malarz, K.; Kos, J.; Gonec, T.; Oravec, M.; Gawecki, R.; Bak, A.; Dohanosova, J.; Kapustikova, I.; et al. Design and synthesis of anticancer 1-hydroxynaphthalene-2-carboxanilides with p53 independent mechanism of action. *Sci. Rep.* **2019**, *9*, 6387. [[CrossRef](#)]
37. Gonec, T.; Kos, J.; Pesko, M.; Dohanosova, J.; Oravec, M.; Liptaj, T.; Kralova, K.; Jampilek, J. Halogenated 1-hydroxynaphthalene-2-carboxanilides affecting photosynthetic electron transport in photosystem II. *Molecules* **2017**, *22*, 1709. [[CrossRef](#)]
38. Likus-Cieslik, J.; Smolinski, A.; Pietrzykowski, M.; Bak, A. Sulphur contamination impact on seasonal and surface water chemistry on a reforested area of a former sulphur mine. *Land Degrad. Dev.* **2019**, *30*, 212–225. [[CrossRef](#)]
39. Bak, A.; Kozik, V.; Smolinski, A.; Jampilek, J. In silico estimation of basic activity-relevant parameters for a set of drug absorption promoters. *SAR QSAR Environ. Res.* **2017**, *28*, 427–449. [[CrossRef](#)]
40. Hann, M.M.; Keserü, G.M. Finding the sweet spot: The role of nature and nurture in medicinal chemistry. *Nat. Rev. Drug Discov.* **2012**, *11*, 355–365. [[CrossRef](#)] [[PubMed](#)]
41. Zadrazilova, I.; Pospisilova, S.; Masarikova, M.; Imramovsky, A.; Ferriz, J.M.; Vinsova, J.; Cizek, A.; Jampilek, J. Salicylanilide carbamates: Promising antibacterial agents with high in vitro activity against methicillin-resistant *Staphylococcus aureus* (MRSA). *Eur. J. Pharm. Sci.* **2015**, *77*, 197–207. [[CrossRef](#)]
42. National Committee for Clinical Laboratory Standards. *Methods for Dilution Antimicrobial Susceptibility Tests for Bacteria that Grow Aerobically*, 11th ed.; M07; NCCLS: Wayne, PA, USA, 2018.
43. National Committee for Clinical Laboratory Standards. *Susceptibility Testing of Mycobacteria, Nocardiae, and Other Aerobic Actinomycetes*, 3rd ed.; Approved Standard, M24; Approved Standard, M24; NCCLS: Wayne, PA, USA, 2020.
44. Nubel, U.; Dordel, J.; Kurt, K.; Strommenger, B.; Westh, H.; Shukla, S.K.; Zemlickova, H.; Leblois, R.; Wirth, T.; Jombart, T.; et al. A timescale for evolution, population expansion, and spatial spread of an emerging clone of methicillin-resistant *Staphylococcus aureus*. *PLoS Pathog.* **2010**, *6*, e1000855. [[CrossRef](#)]
45. Measuring Cell Viability/Cytotoxicity. Dojindo EU GmbH, Munich, Germany. Available online: <https://www.dojindo.eu.com/Protocol/Dojindo-Cell-Proliferation-Protocol.pdf> (accessed on 27 August 2020).
46. Bueno, J. Antitubercular in vitro drug discovery: Tools for begin the search. In *Understanding Tuberculosis—New Approaches to Fighting Against Drug Resistance*; IntechOpen: Rijeka, Croatia, 2012; pp. 147–168.
47. International Organization for Standardization. *ISO 10993-5:2009 Biological Evaluation of Medical Devices Part 5: Tests for in Vitro Cytotoxicity*; International Organization for Standardization: Geneva, Switzerland, 2009; last revision 2017.
48. Jampilek, J. Design and discovery of new antibacterial agents: Advances, perspectives, challenges. *Curr. Med. Chem.* **2018**, *25*, 4972–5006. [[CrossRef](#)]
49. Imramovsky, A.; Pesko, M.; Ferriz, J.M.; Kralova, K.; Vinsova, J.; Jampilek, J. Photosynthesis—Inhibiting efficiency of 4-chloro-2-(chlorophenylcarbamoyl)phenyl alkylcarbamates. *Bioorg. Med. Chem. Lett.* **2011**, *21*, 4564–4567. [[CrossRef](#)] [[PubMed](#)]
50. Kralova, K.; Perina, M.; Waisser, K.; Jampilek, J. Structure-activity relationships of *n*-benzylsalicylamides for inhibition of photosynthetic electron transport. *Med. Chem.* **2015**, *11*, 156–164. [[CrossRef](#)]

51. Gonec, T.; Kralova, K.; Pesko, M.; Jampilek, J. Antimycobacterial N-alkoxyphenylhydroxynaphthalenecarboxamides affecting photosystem II. *Bioorg. Med. Chem. Lett.* **2017**, *27*, 1881–1885. [[CrossRef](#)] [[PubMed](#)]
52. Kos, J.; Zadrazilova, I.; Nevin, E.; Soral, M.; Gonec, T.; Kollar, P.; Oravec, M.; Coffey, A.; O'Mahony, J.; Liptaj, T.; et al. Ring-substituted 8-hydroxyquinoline-2-carboxanilides as potential antimycobacterial agents. *Bioorg. Med. Chem.* **2015**, *23*, 4188–4196. [[CrossRef](#)] [[PubMed](#)]
53. Jampilek, J.; Kralova, K.; Pesko, M.; Kos, J. Ring-substituted 8-hydroxyquinoline-2-carboxanilides as photosystem II inhibitors. *Bioorg. Med. Chem. Lett.* **2016**, *26*, 3862–3865. [[CrossRef](#)] [[PubMed](#)]
54. Todeschini, R.; Consonni, V. *Molecular Descriptors for Chemoinformatics*; Wiley-VCH Verlag GmbH & Co. KgaA: Weinheim, Germany, 2010.
55. Ertl, P.; Schuffenhauer, A. Estimation of synthetic accessibility score of drug-like molecules based on molecular complexity and fragment contributions. *J. Cheminform.* **2009**, *1*, 8. [[CrossRef](#)]
56. Clark, D.E.; Pickett, S.E. Computational methods for the prediction of 'drug-likeness'. *Drug Discov. Today* **2000**, *5*, 49–58. [[CrossRef](#)]
57. Pizova, H.; Havelkova, M.; Stepankova, S.; Bak, A.; Kauerova, T.; Kozik, V.; Oravec, M.; Imramovsky, A.; Kollar, P.; Bobal, P.; et al. Proline-based carbamates as cholinesterase inhibitors. *Molecules* **2017**, *22*, 1969. [[CrossRef](#)]
58. Holliday, J.D.; Salim, N.; Whittle, M.; Willett, P. Analysis and display of the size dependence of chemical similarity coefficients. *J. Chem. Inf. Comput. Sci.* **2003**, *43*, 819–828. [[CrossRef](#)]
59. Gieleciak, R.; Magdziarz, T.; Bak, A.; Polanski, J. Modeling robust QSAR. 1. Coding molecules in 3D-QSAR—From a point to surface sectors and molecular volumes. *J. Chem. Inf. Model.* **2005**, *45*, 1447–1455. [[CrossRef](#)] [[PubMed](#)]
60. Stouch, T.R.; Kenyon, J.R.; Johnson, S.R.; Chen, X.Q.; Doweiko, A.; Li, Y. In silico ADME/Tox: Why models fail. *J. Comput. Aided Mol. Des.* **2003**, *17*, 83–92. [[CrossRef](#)] [[PubMed](#)]
61. Doweiko, A.M. QSAR: Dead or alive? *J. Comput. Aided Mol. Des.* **2008**, *22*, 81–89. [[CrossRef](#)]
62. Bak, A.; Polanski, J. Modeling robust QSAR 3: SOM-4D-QSAR with iterative variable elimination IVE-PLS: Application to steroid, azo dye, and benzoic acid series. *J. Chem. Inf. Model.* **2007**, *47*, 1469–1480. [[CrossRef](#)] [[PubMed](#)]
63. Schwalbe, R.; Steele-Moore, L.; Goodwin, A.C. *Antimicrobial Susceptibility Testing Protocols*, 1st ed.; CRC Press: Boca Raton, FL, USA, 2007.
64. Bonapace, C.R.; Bosso, J.A.; Friedrich, L.V.; White, R.L. Comparison of methods of interpretation of checkerboard synergy testing. *Diagn. Microbiol. Infect. Dis.* **2002**, *44*, 363–366. [[CrossRef](#)]
65. Abate, G.; Mshana, R.N.; Miorner, H. Evaluation of a colorimetric assay based on 3-(4,5-dimethylthiazol-2-yl)-2,5-diphenyl tetrazolium bromide (MTT) for rapid detection of rifampicin resistance in *Mycobacterium tuberculosis*. *Int. J. Tuberc. Lung Dis.* **1998**, *2*, 1011–1016.
66. Stanton, D.T. QSAR and QSPR model interpretation using partial least squares (PLS) analysis. *Curr. Comput. Aided Drug Des.* **2012**, *8*, 107–127. [[CrossRef](#)]
67. Xie, X.Q.; Chen, J.Z. Data mining a small molecule drug screening representative subset from NIH PubChem. *J. Chem. Inf. Model.* **2008**, *48*, 465–475. [[CrossRef](#)]
68. Polanski, J.; Gieleciak, R.; Magdziarz, T.; Bak, A. GRID formalism for the comparative molecular surface analysis: Application to the CoMFA benchmark steroids, azo dyes, and HEPT derivatives. *J. Chem. Inf. Comput. Sci.* **2004**, *44*, 1423–1435. [[CrossRef](#)]
69. Zupan, J.; Gasteiger, J. *Neural Networks and Drug Design for Chemists*, 2nd ed.; Wiley-VCH: Weinheim, Germany, 1999.
70. Centner, V.; Massart, D.L.; de Noord, O.E.; de Jong, S.; Vandeginste, B.M.V.; Sterna, C. Elimination of uninformative variables for multivariate calibration. *Anal. Chem.* **1996**, *68*, 3851–3858. [[CrossRef](#)]
71. Dearden, J.C.; Cronin, M.T.; Kaiser, K.L. How not to develop a quantitative structure-activity or structure-property relationship (QSAR/QSPR)? *Sar Qsar Environ. Res.* **2009**, *20*, 241–266. [[CrossRef](#)] [[PubMed](#)]

Sample Availability: Samples of the compounds are available from the authors.








© 2020 by the authors. Licensee MDPI, Basel, Switzerland. This article is an open access article distributed under the terms and conditions of the Creative Commons Attribution (CC BY) license (<http://creativecommons.org/licenses/by/4.0/>).

č.	citace	ISSN
16	KOS, J , A BAK, V KOZIK, T JANKECH, T STRHARSKY, A SWIETLICKA, H MICHNOVA, J HOSEK, A SMOLINSKI, M ORAVEC, F DEVINSKY, M HUTTA a J JAMPILEK. Biological Activities and ADMET-Related Properties of Novel Set of Cinnamanilides. <i>MOLECULES</i> [online]. 2020, 25 (18). Dostupné z: doi: 10.3390/molecules25184121	1420-3049

Article

Biological Activities and ADMET-Related Properties of Novel Set of Cinnamanilides †

Jiri Kos ¹, Andrzej Bak ^{2,*} , Violetta Kozik ², Timotej Jankech ³, Tomas Strharsky ¹, Aleksandra Swietlicka ², Hana Michnova ¹, Jan Hosek ¹ , Adam Smolinski ⁴ , Michal Oravec ⁵, Ferdinand Devinsky ⁶ , Milan Hutta ³ and Josef Jampilek ^{3,*} 

¹ Regional Centre of Advanced Technologies and Materials, Faculty of Science, Palacky University, Slechtitelu 27, 78371 Olomouc, Czech Republic; jiri.kos@upol.cz (J.K.); tomas.strharsky01@upol.cz (T.S.); michnova.hana@gmail.com (H.M.); jan.hosek@upol.cz (J.H.)

² Department of Chemistry, University of Silesia, Szkolna 9, 40007 Katowice, Poland; violetta.kozik@us.edu.pl (V.K.); aswietlicka@us.edu.pl (A.S.)

³ Department of Analytical Chemistry, Faculty of Natural Sciences, Comenius University, Ilkovicova 6, 84215 Bratislava, Slovakia; timotej.jankech@gmail.com (T.J.); milan.hutta@uniba.sk (M.H.)

⁴ Central Mining Institute, Pl. Gwarkow 1, 40166 Katowice, Poland; smolin@gig.katowice.pl

⁵ Global Change Research Institute CAS, Belidla 986/4a, 60300 Brno, Czech Republic; oravec.m@czechglobe.cz

⁶ Faculty of Pharmacy, Comenius University, Odbojarov 10, 83232 Bratislava, Slovakia; devinsky@fpharm.uniba.sk

* Correspondence: andrzej.bak@us.edu.pl (A.B.); josef.jampilek@gmail.com (J.J.)

† Preliminary results presented at the 23rd International Electronic Conference on Synthetic Organic Chemistry, 15 November–15 December 2019; Available online: <https://ecsoc-23.sciforum.net/>.

Academic Editor: Julio A. A. Seijas Vázquez

Received: 24 August 2020; Accepted: 8 September 2020; Published: 9 September 2020



Abstract: A series of nineteen novel ring-substituted *N*-arylcinnamanilides was synthesized and characterized. All investigated compounds were tested against *Staphylococcus aureus* as the reference strain, two clinical isolates of methicillin-resistant *S. aureus* (MRSA), and *Mycobacterium tuberculosis*. (2*E*)-*N*-[3-Fluoro-4-(trifluoromethyl)phenyl]-3-phenylprop-2-enamide showed even better activity (minimum inhibitory concentration (MIC) 25.9 and 12.9 μ M) against MRSA isolates than the commonly used ampicillin (MIC 45.8 μ M). The screening of the cell viability was performed using THP1-Blue™ NF- κ B cells and, except for (2*E*)-*N*-(4-bromo-3-chlorophenyl)-3-phenylprop-2-enamide (IC₅₀ 6.5 μ M), none of the discussed compounds showed any significant cytotoxic effect up to 20 μ M. Moreover, all compounds were tested for their anti-inflammatory potential; several compounds attenuated the lipopolysaccharide-induced NF- κ B activation and were more potent than the parental cinnamic acid. The lipophilicity values were specified experimentally as well. In addition, in silico approximation of the lipophilicity values was performed employing a set of free/commercial clogP estimators, corrected afterwards by the corresponding pK_a calculated at physiological pH and subsequently cross-compared with the experimental parameters. The similarity-driven property space evaluation of structural analogs was carried out using the principal component analysis, Tanimoto metrics, and Kohonen mapping.

Keywords: cinnamamides; synthesis; antistaphylococcal activity; MTT assay; cytotoxicity; lipophilicity; PCA; IVE-PLS; quantitative structure-property relationships

1. Introduction

Inflammatory diseases of visceral organs, joints, bones, etc. can be based on an infectious or autoimmune basis, but the body always aims to eradicate noxious agents and restore tissue homeostasis [1]. A bacterial infection is often connected with severe inflammatory diseases such as

bronchial asthma [2], gingivitis, periodontitis [3], systemic lupus erythematosus [4], and even with cancer [5]. Because the bacterial infection can trigger inflammation, which can cause subsequent damage of surrounding tissue [6], it seems advantageous to follow a multi-target approach in drug design and try to prepare molecules with dual antimicrobial and anti-inflammatory activity. Multi-target drug discovery represents an innovative approach of medicinal chemistry to overcome a crisis in drug design, reflected in the small number of newly approved drugs. This approach is based on the concepts of privileged scaffolds, polypharmacology, and multifactorial diseases [7–12]. Thus, multi-target drugs can be designed for the simultaneous treatment of, for example, autoimmune, inflammatory, and invasive diseases. From pharmaco-economic and patients' comfort point of view, it seems favorable to treat both a cause and a consequence (bacterial infection and inflammation) simultaneously with one active substance.

Cinnamic acids are one of such privileged multi-target structures that occur naturally in all plants [13–15]. Cinnamic acids as well as hydroxy- and phenyl-substituted derivatives of cinnamic acids have been widely investigated due to their significant and varied biological effects including anti-inflammatory, antioxidant, hepatoprotective, antidiabetic, antidepressant/anxiolytic, antifungal, antibacterial, antiviral, and anticancer effects [16–24]. Derivatives of cinnamic acids are also used as agricultural fungicides [25]. Ring-substituted *N*-arylcinnamanilides were recently synthesized and tested for their antibacterial, antimycobacterial, anti-inflammatory potential and antifungal activity as well as for their activity related to the inhibition of photosynthetic electron transport (PET) in spinach (*Spinacia oleracea* L.) chloroplasts [26–28]. Since the *N*-phenylcinnamamide skeleton can be considered as a privileged scaffold providing multi-target agents, new di-, tri-, and tetra-halogenated *N*-arylcinnamanilides were prepared.

The biopharmaceutical profile of a compound is increasingly relevant for characterizing both the pharmacokinetic (ADMET) and pharmacodynamic aspects of drug–receptor/enzyme interactions [29,30]. The ADMET-friendly design of molecular *in vivo* permeability and cell bioaccumulation belongs to the field of the quantitative structure–property relationships (QSPR), where the physicochemical properties of a compound are the mathematical function of the chemical composition/constitution [31,32]. In this context, lipophilicity and its quantitative descriptor ($\log P$) that often correlates well with the bioactivity of compounds indicate the differential partitioning of a neutral compound between two immiscible solvents (*n*-octanol/water) under equilibrium conditions [33,34]. The existing experimental lipophilicity dataset is negligible (3×10^4) when compared to the enormous number of compounds under design; therefore, the reliable measure/estimation of lipophilicity is a valid requirement at the early stages of drug design [35]. Hence, an attractive alternative for lipophilicity estimation is *in silico* predictive protocols due to the additive-constitutive nature of the $\log P$ descriptor [36]. Regrettably, the comparative evaluation of implemented computational algorithms (linear or non-linear) revealed that the practical development of magic bullet (a global model for a diverse set of structural types) is dubious—the quality of lipophilicity estimation varies noticeably depending on the chemical type under consideration [37]. In order to eliminate a consequential uncertainty (over-/under-estimation) of $\log P$ value, a possible vast range of *in silico* predictors should be engaged and compared with the available experimental data. As a matter of fact, early lipophilicity profiling (theoretical and/or empirical) might facilitate better decision-making in the hit→lead→seed→drug route and eradicate bad actors (false positive hits) at early stages of drug design/development according to the “fail fast, fail cheap” concept [38]. Due to the inaccuracy of $\log P$ prediction, the potential exclusion of prospective drug molecules (false negative hits) at the preliminary step of drug discovery might happen using the Ro5 rule [39].

Depending on the target location and the track of administration, chemicals are exposed to pH variations in the physiological environment (pH = 2–12). In the case of non-ionizable compounds, only neutral species exist; however, the majority of commercial pharmaceuticals contain an ionizable moiety—approximately 75% are basic, and 20% are acidic [40]. In fact, even partial ionization of a molecule results in the depletion of calculated/measured lipophilicity; therefore, the distribution

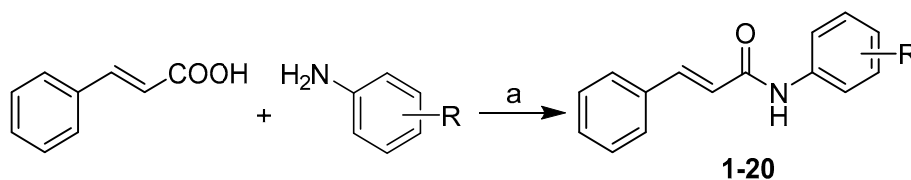
coefficient $\log D_{pH}$ (the pH dependent version of $\log P$) should be taken into consideration [41]. In fact, $\log D_{pH}$ potentially accumulates errors due to the $\log P$ and dissociation constant (pK_a) estimations according to the following formulas: $\log D_{pH} = \log P - \log[1 + 10^{(pH-pK_a)}]$ for acids and $\log D_{pH} = \log P - \log[1 + 10^{(pK_a-pH)}]$ for bases [42]. On the other hand, in many systems, ionic species enter the non-aqueous phase, and therefore a more rigorous approach would be appropriate, but this is beyond the scope of this paper.

In the presented study, a set of cinnamic acid anilide derivatives was synthesized, investigated for biological activity, and characterized by a series of experimental lipophilicity values generated using reversed-phase high-performance liquid (RP-HPLC) and reversed-phase thin-layer chromatography (RP-TLC). The similarity-related property space evaluation for the congeneric series of structurally-based analogs was carried out using the principal component analysis (PCA). Moreover, the *in silico* approximation of the lipophilic values for the ensemble of anilides 1–20 was performed employing a set of free/commercial $\text{clog}P$ estimators, corrected afterwards by the corresponding pK_a calculated at physiological pH and subsequently cross-compared with the experimental parameter. The mean values of the selected molecular descriptors that average over the chosen calculation methods were subsequently correlated with the $\log D_{7.4}$ parameter, namely consensus $\text{clog}P$. Finally, the similarity-driven investigation using Tanimoto metrics and Kohonen mapping was conducted revealing some structural dissimilarities within the analyzed series of compounds.

2. Results and Discussion

2.1. Synthesis and Biological Screening

All compounds were synthesized from cinnamic acid in a microwave reactor: The carboxyl group was converted with phosphorus trichloride to acyl chloride, which then reacted with the appropriately substituted aniline to give the desired product (Scheme 1). The structures and biological activities are reported in Table 1, and empirically evaluated lipophilicity using RP-HPLC and RP-TLC are listed in Table 2.



Scheme 1. Synthesis of ring-substituted (2*E*)-*N*-aryl-3-phenylprop-2-enamides 1–20. Reagents and conditions: (a) PCl_3 , chlorobenzene, MW (max. 500 W), 130 °C, 30 min [26,28].

2.1.1. In Vitro Antimicrobial Evaluation

The investigated compounds were tested on their antistaphylococcal activity against three clinical isolates of methicillin-resistant *Staphylococcus aureus* (MRSA) and *S. aureus* ATCC 29213 as the reference and quality control strain. Moreover, all compounds were tested against *Mycobacterium tuberculosis* ATCC 25177/H37Ra (see Table 1). As a matter of fact, all compounds showed very limited antimicrobial activity with the exception of compound 10 ($R = 3\text{-F-}4\text{-CF}_3$) that revealed a significant effect against both *S. aureus* and MRSA isolates. It confirmed our previous findings, where compounds with CF_3 moiety showed high antistaphylococcal and antitubercular activity [26,27]. Consequently, it was expected that other compounds with the CF_3 motif, such as 13 ($R = 2\text{-Br-}5\text{-CF}_3$) and 19 ($R = 2,6\text{-Br-}4\text{-CF}_3$) or compound 6 ($R = 3,4,5\text{-Cl}$), derived from 3,5-Cl (highly effective against *M. tuberculosis*) should have similar activity [26]. Unfortunately, only molecule 10 turned out to be active. Because the minimum inhibitory concentrations (MICs) of compound 10 are the same against both *S. aureus* and MRSA isolates (25.9 and 12.9 μM), it can be speculated concerning the specific activity against *Staphylococcus* sp. In addition,

all compounds were verified against the reference strain *Enterococcus faecalis* ATCC 29212 and three vanA-carrying vancomycin-resistant *E. faecalis* (VRE) isolates; however no activity was recorded.

It should be emphasized that besides MIC values, minimum bactericidal concentrations (MBCs) were also determined for compound **10**. All MBC values were equal to the MIC values, indicating that compound **10** showed not only bacteriostatic but bactericidal activity. In fact, a tested compound is classified as bactericidal if the ratio of its MBC/MIC values is ≤ 4 [43].

Finally, 3-(4,5-dimethylthiazol-2-yl)-2,5-diphenyltetrazolium bromide (MTT) assay of effective antistaphylococcal compound **10** was conducted as well. The MTT test is employed to assess cell growth by measuring respiration. The MTT measured viability of bacterial cells less than 70% [44] after the exposure to the MIC values of tested compound is considered as a positive result of this assay, because this low level of cell viability indicates the inhibition of cell growth by the inhibition of respiration [45]. It can be concluded that compound **10** showed a significant decrease in viability to $13.4 \pm 0.1\%$, which is far below the limit of 70% viability of *S. aureus* ATCC 29213 at the tested concentration equal to MIC (i.e., $25.9 \mu\text{M}$ ($8 \mu\text{g/mL}$)).

Table 1. Structure of ring-substituted (2E)-N-aryl-3-phenylprop-2-enamides **1–20**, in vitro anti-*Staphylococcus* activities' minimum inhibitory concentration (MIC; μM) in comparison with standard ampicillin (AMP), in vitro antitubercular activity MIC (μM) in comparison with standard isoniazid (INH), and their influence on viability of THP1-Blue™ NF- κ B cell line (IC_{50} (μM) \pm SEM, n = 6).

Comp.	R	MIC (μM)				Tox IC_{50} (μM) \pm SEM
		SA	MRSA 63718	MRSA SA 630	Mtb	
1 *	H	>1146	>1146	>1146	286	>20
2	2,4,6-F	>924	>924	>924	>462	>20
3	3,4,5-F	462	>924	>924	>462	>20
4	2,4-Cl	>880	>880	>880	>440	>20
5	2,4,5-Cl	>790	>790	>790	>395	>20
6	3,4,5-Cl	>790	>790	>790	>395	>20
7	2,4-Br	>677	>677	>677	>339	>20
8	2-F-5-Cl	931	>931	>931	>465	>20
9	3-F-4-Br	>805	>805	805	>403	>20
10	3-F-4-CF ₃	25.9	25.9	12.9	>414	>20
11	3-Cl-4-Br	>766	192	192	>383	6.5 \pm 1.0
12	2-Br-4-Cl	>766	>766	>766	>383	>20
13	2-Br-5-CF ₃	>696	>696	>696	>348	>20
14	2-CF ₃ -4-F	>828	>828	>828	>414	>20
15	2-CF ₃ -4-Cl	>788	>788	>788	>394	>20
16	2-CF ₃ -4-Br	>696	>696	>696	>348	>20
17	2-CF ₃ -4-NO ₂	>762	>762	>762	>381	>20
18	3-CF ₃ -4-NO ₂	>762	>762	>762	>381	>20
19	2,6-Br-4-CF ₃	>574	>574	>574	>287	>20
20	2,6-Br-3-Cl-4-F	>595	>595	>595	>298	>20
AMP	–	5.72	45.8	45.8	–	–
INH	–	–	–	–	36.6	–

* compound was described in reference [26]; SA = *Staphylococcus aureus* ATCC 29213; MRSA = clinical isolates of methicillin-resistant *S. aureus* 63,718 and SA 630 (National Institute of Public Health, Prague, Czech Republic); Mtb = *Mycobacterium tuberculosis* H37Ra.

Table 2. Experimentally found lipophilicity determined using HPLC and TLC approaches for *N*-arylcinnamanilides 1–20.

Comp.	R	RP-HPLC			RP-TLC		
		Logk ^a	logD ^b	logD ^c	R _M ^d	R _M ^e	R _M ^f
1	H	0.0270	0.1251	0.1090	−0.5087	0.2848	0.4038
2	2,4,6-F	−0.0831	0.0260	0.0107	−0.6536	0.1218	0.1951
3	3,4,5-F	0.4893	0.5495	0.5274	−0.4206	0.6074	0.5495
4	2,4-Cl	0.5278	0.5885	0.5685	−0.3933	0.6546	0.5495
5	2,4,5-Cl	0.8373	0.8879	0.8647	−0.2497	0.9695	0.9832
6	3,4,5-Cl	0.9671	1.0104	0.9897	−0.1870	1.0852	1.1306
7	2,4-Br	0.6152	0.6704	0.6518	−0.3098	0.7331	0.7295
8	2-F-5-Cl	0.3692	0.4334	0.4154	−0.4711	0.5411	0.5495
9	3-F-4-Br	0.5025	0.5597	0.5408	−0.4081	0.6797	0.6895
10	3-F-4-CF ₃	0.5789	0.6327	0.6095	−0.5032	0.7923	0.5960
11	3-Cl-4-Br	0.6611	0.7126	0.6912	−0.3376	0.8388	0.8181
12	2-Br-4-Cl	0.5476	0.6064	0.5860	−0.4072	0.6553	0.6484
13	2-Br-5-CF ₃	0.5561	0.6157	0.5936	−0.4325	0.7194	0.5619
14	2-CF ₃ -4-F	0.1607	0.2426	0.2220	−0.6797	0.3011	0.1330
15	2-CF ₃ -4-Cl	0.4113	0.4741	0.454	−0.6102	0.5305	0.3219
16	2-CF ₃ -4-Br	0.4683	0.5316	0.5105	−0.5624	0.5730	0.4273
17	2-CF ₃ -4-NO ₂	0.3794	0.4431	0.3989	−0.5633	0.4998	0.4311
18	3-CF ₃ -4-NO ₂	0.5004	0.5571	0.5098	−0.4804	0.6927	0.6160
19	2,6-Br-4-CF ₃	0.4321	0.4941	0.4731	−0.5206	0.5301	0.3733
20	2,6-Br-3-Cl-4-F	0.3139	0.3922	0.3699	−0.5541	0.4320	0.4138

^a 72:28 MeOH:H₂O; ^b 72:28 MeOH:NaOAc buffer (pH 7.4); ^c 72:28 MeOH: NaOAc buffer (pH 6.5); ^d 100% MeOH, ^e 72:28 MeOH:H₂O; ^f 72:28 MeOH: NaOAc buffer (pH 7.4).

2.1.2. In Vitro Cell Viability and Anti-Inflammatory Potential

In vitro cell viability of all the compounds was estimated using the human THP1-Blue™ NF-κB cell line. Almost all tested compounds showed insignificant cytotoxic effect (IC₅₀ > 20 μM) (Table 1) with exception of molecule **11** (R = 3-Cl-4-Br, IC₅₀ = 6.5 ± 1.0 μM). It seems that the disubstitution of C_(3,4) by highly lipophilic and electron-withdrawing moieties (combination of chlorine and bromine) is critical for the toxic effect of the analyzed series of compounds.

With respect to the used THP1-Blue™ NF-κB cells, the anti-inflammatory potential of compounds was evaluated in order to modulate the activity of the pro-inflammatory transcription nuclear factor (NF)-κB (see Figure 1). After lipopolysaccharide (LPS) stimulation, compounds **14** (R = 2-CF₃-4-F), **18** (R = 3-CF₃-4-NO₂), and **20** (R = 2,6-Br-3-Cl-4-F) showed the highest attenuation of the activity of this transcription factor within the studied set of compounds; however, the decrease was approximately 9%, which was lower compared to the previously verified cinnamides [28]. On the other hand, the half concentration of tested compounds was used in the study. As a matter of fact, compounds **2** (R = 2,4,6-F), **4** (R = 2,4-Cl), **5** (R = 2,4,5-Cl), and **10** (R = 3-F-4-CF₃) significantly increased the activity of NF-κB by 10–15%, respectively. It seems that the position and type of substituents on phenyl ring is important for tuning pro-/anti-inflammatory potential of cinnamic acid anilides, which confirms similar observations in our previous study, where the substitution of *ortho* and *meta* positions of the anilide ring by rather lipophilic and bulky moieties was preferred for the anti-inflammatory potential [28].

Surprisingly, the insignificant anti-inflammatory potential of compound **13** (R = 2-Br-5-CF₃) is disappointing, because its chlorinated analogue showed promising activity [28]. It can be hypothesized that the investigated *N*-arylcinnamanilides may have a different mode of action, which may be the nuclear translocation of NF-κB inhibition, or affecting its binding to DNA, or acting by epigenetic regulation, while combinations of these effects are not excluded.

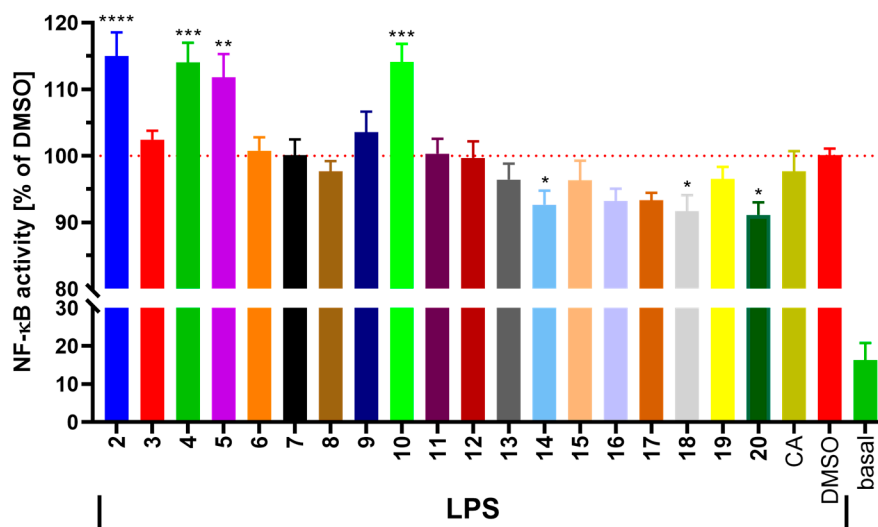


Figure 1. Effect of tested compounds on activity of transcription factor NF- κ B. THP1-Blue™ NF- κ B cells were pretreated by compounds (1 μ M) dissolved in dimethyl sulfoxide (DMSO) for 1 h. Then, lipopolysaccharide (LPS) 1 μ g/mL was added to trigger the NF- κ B activation. The activity of NF- κ B was measured 24 h after LPS stimulation using QuantiBlue™ assay. The graph represents mean \pm SEM (n = 9). The red dotted line shows the value of the DMSO-only treated group. Groups were compared with the help of the one-way ANOVA test followed by Fisher's LSD multiple comparison test. * indicates statistical significance ($p < 0.05$) to DMSO group; ** indicates statistical significance ($p < 0.01$) to DMSO group; *** indicates statistical significance ($p < 0.001$) to DMSO group; **** indicates statistical significance ($p < 0.0001$) to DMSO group. CA—cinnamic acid.

2.2. Similarity-Driven Property Evaluation

The similarity-guided assessment of the property profile for the group of structurally alike compounds was conducted for the congeneric set of cinnamic acid anilide analogues. The a priori calculation of molecular descriptors, regarded as the result of mathematical transformation of chemical information encoded within a symbolic representation of a molecule is crucial for the compound's bioavailability and hence critical for the prospective drug candidate properties. The gold standard of ADMET-tailored property approximation is the generation of statistically robust models, where a property is a function of the chemical structure, that are capable of making accurate quantitative predictions, including those of molecular binding affinity, metabolic/pharmacokinetic/pharmacodynamics fate, or environmental ecotoxicology. The molecular descriptors are essentially estimated based on the molecular structure as intuitive roadmaps even before the synthesis of the molecule has been rationalized. In fact, the majority of topological descriptors is highly intercorrelated; therefore, it is necessary to employ the linear (e.g., PCA) or non-linear (e.g., neural network) techniques to reduce the data dimensionality and illustrate the object similarity in the orthogonal basis using the pair-wise descriptor-based structural resemblance/relatedness measure of the intermolecular resemblance between two objects (e.g., Euclidean metric) [46]. Initially, the principal component analysis (PCA) was performed on the pool of 2567 descriptors calculated using Dragon 6.0 program, where constant and nearly constant variables (standard deviation $< 10^{-4}$) were a priori eradicated. Subsequently, the multidimensional matrix was generated ($X_{20 \times 2567}$) with rows and columns representing variables (descriptors) and objects (molecules), respectively. The PCA procedure was employed on the centered and standardized dataset. The compression efficacy of the PCA method is strictly related to the number of uncorrelated variables; therefore, the high percentage of total variance explained by the first three principal components (PC1 + PC2 + PC3 = 77.98%) implies, that descriptors are highly inter-correlated. In fact, first two PCs described 71.44% of the total variance; hence, the chosen properties were projected on the plane specified by the PC1 versus PC2-predicted scores as illustrated in Figure 2a.

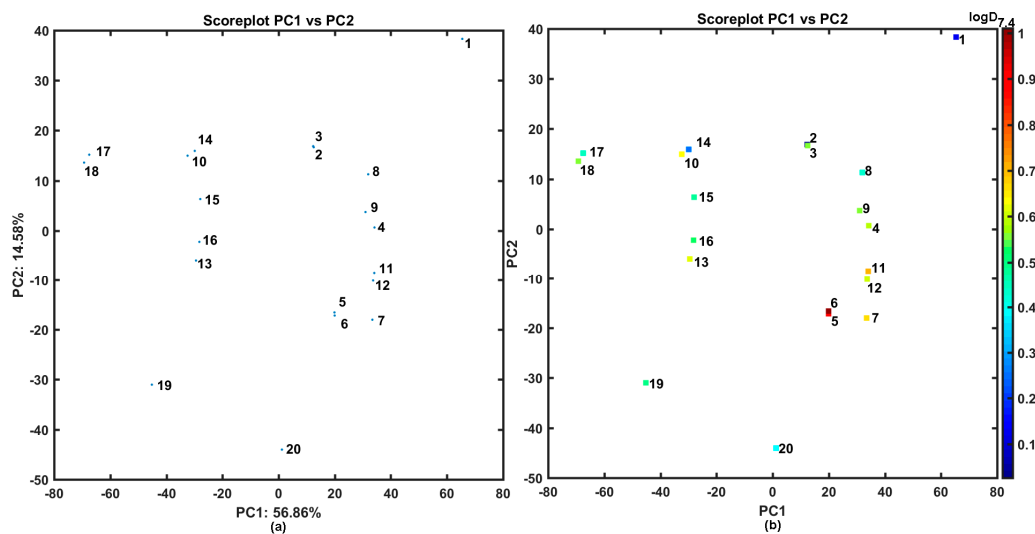


Figure 2. Projection of cinnamic acid anilides 1–20 on plane defined by first vs. second principal components for Dragon descriptors (a) with experimental $\log D_{7.4}$ (b). Colors code numerical values of $\log D$ at pH = 7.4.

Basically, two subfamilies can be formed along the positive and negative values of PC1 for the analyzed 1–20 anilides that share a common chemotype based on styrene-containing motif, peptide-like linker, and phenyl R-substituted ring. The first group (PC1 > 0) contains di/tri/tetra-halogenated analogues (objects 2–9, 11, 12, 20), while the second one (PC1 < 0) is composed of mono-trifluoromethyl-based molecules (objects 10, 13–19). Interestingly, compounds 19 and 20 are located distinctly along the second principal component (PC2 < -30). Not surprisingly, unsubstituted (only hydrogenated) molecule 1 is separated from the remaining ones. The similarity-driven analysis of the empirical lipophilicity at the physiological pH = 7.4 is illustrated on the PC1 vs. PC2 plane. In fact, the most lipophilic molecules 5–7 and 11 are grouped together as shown in Figure 2b.

On the whole, the vast number of the investigated anilides abide the Lipinski's Rule of Five (Ro5), where the ADMET-friendly properties are confined by the liminal values imposed on the specific molecular descriptors ($MW \leq 500$, $HBD \leq 5$, $HBA \leq 10$, $\text{clogP} \leq 5$). Interestingly, the Ro5 violation observed for molecules depicted in Figure 3a is strictly related with the calculated lipophilicity values ($\text{clogP} > 5$). Despite the drug-like property space is still a questionable concept, because a good drug-like score does not make a molecule a drug and vice versa, the Ro5 rule might be handy in differentiating a prospective drug from a non-drug molecule [47]. Moreover, almost all tested compounds showed very low cytotoxic effect ($IC_{50} > 20 \mu M$) as presented in Figure 3b and Table 1. Compound 11 ($IC_{50} = 6.5 \mu M$) is the visible exception, which is also annotated with Ro5 violation. As mentioned above, it seems that the $C_{(3,4)'}$ disubstitution by chlorine and bromine is critical for the viability of cells unlike the disubstitution of $C_{(2,4)'}$ positions. Since the lipophilicity is regarded as a meaningful property in the context of pharmacokinetic and pharmacodynamic drug-receptor interactions, the lipophilic profiles of the analyzed anilide analogues were thoroughly investigated.

From the drug hunter perspective, the justifiable precariousness of the validity of lipophilicity estimation can arise, using a variety of theoretical approaches, because some methods for the theoretical calculation of lipophilicity might be more or less suitable for specific/heterogeneous series of compounds. In other words, the non-trivial question arises how to single out the best-suited method or combination of methods for clogP estimation of new compounds. It is known that a jack of all trades is a master of none; therefore, it seems advisable not to rely solely on one clogP estimator, but rather a combination of methods should be engaged with subsequent comparison of the results with the experimental data. Hence, a consensus procedure for clogP prediction was previously proposed based on a consensus methodology that was adopted from the structure-based studies, where many docking programs and scoring functions can be employed [48–50]. Thus, *in silico* approximation of the lipophilic values for

the ensemble of anilides 1–20 was performed employing a set of free/commercial clogP estimators such as clogPS, Molinspirations, OSIRIS, HyperChem 7.0, Sybyl-X, MarvinSketch 15, ACD/ChemSketch 2015, Dragon 6.0, Kowwin, XlogP3, ChemDraw, and ACD/Percepta (Table S1 in Supplementary Materials). Moreover, the deduced clogP values were corrected afterwards by the corresponding pK_a calculated at specific pH using ACD/Percepta/pKa Classic module (Table S2 in Supplementary Materials). The obtained clogD_{pH} does not differ significantly from clogP specified by distinct *in silico* principles, because the investigated molecules do not contain an ionizable moiety. Furthermore, the $\text{clogD}_{7.4}$ findings were inter-correlated with each other and cross-compared with the empirical $\text{logD}_{7.4}$ values as illustrated by the triangular matrix of linear correlations parameters in Figure 4.

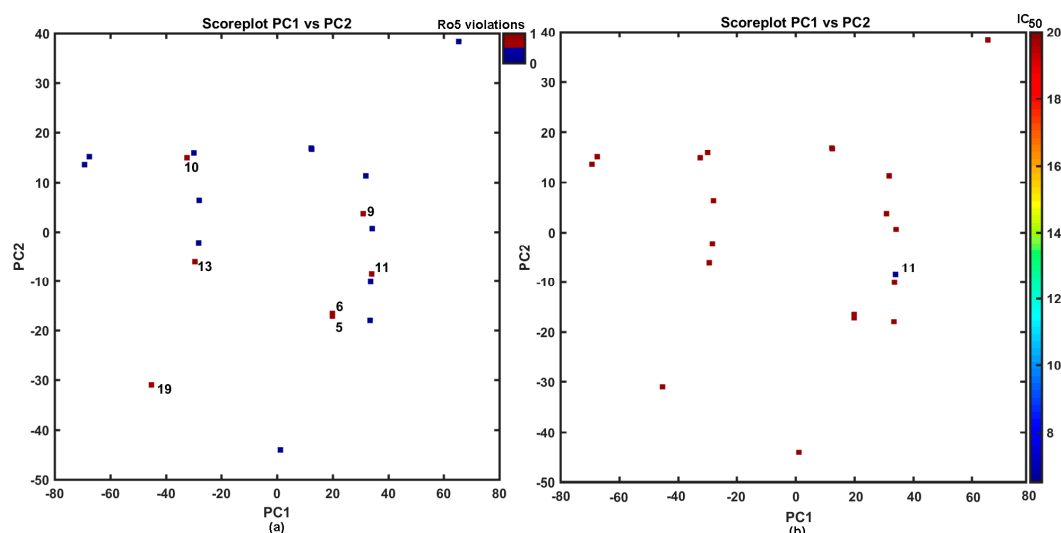


Figure 3. Projection of cinnamic acid anilides 1–20 on a plane defined by first vs. second principal components for Dragon descriptors with Ro5 rule violations (a) and cytotoxic effect IC_{50} (b). Colors code numerical values of Ro5 violations and IC_{50} .

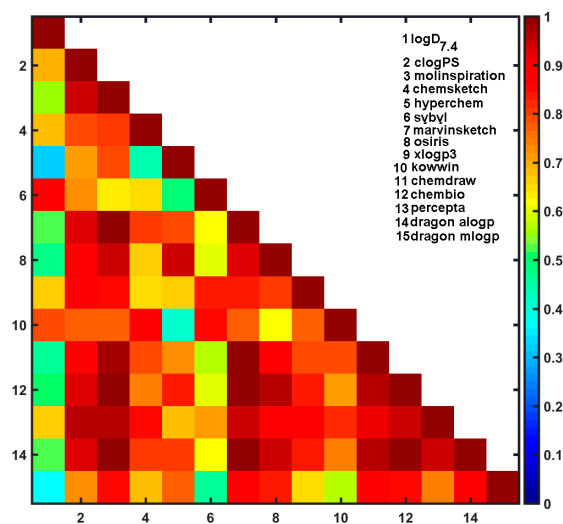


Figure 4. Matrix of correlation coefficients of linear relationships between experimental and calculated $\text{logD}_{7.4}$ lipophilicity specified using different programs.

In fact, relatively good correlation ($r > 0.65$) between experimental $\text{logD}_{7.4}$ and model-predicted $\text{clogD}_{7.4}$ values was recorded for clogPS, ChemSketch, Sybyl, XlogP3, and Kowwin estimators. On the other hand, rather poor correlation ($r \leq 0.4$) was revealed for data provided by HyperChem and Dragon predictors (see Figure 4). The noticeable variations in logD estimation at given pH probably resulted from different computational algorithms (atom/fragment- or descriptor-based) implemented in the

software and/or training data engaged at the training stage. Obviously, prediction of the individual lipophilic contribution of each group/atom (sometimes augmented by the structural correction factors) is as good as the modeling data used at the training stage of model generation [51]. In other words, the poorer performance of some predictors focuses on issues arising from the lipophilicity estimation for the in house collection of molecules with structural features uncovered by chemical classes of compounds in the training subset—a wide range of chemical space is still not covered [52]. Luckily, usually a few empirically measured values are sufficient to produce reliable lipophilicity estimation for structurally related series of molecules. Hence, the integrated $\text{clogD}_{7.4}$ matrix ($X_{20 \times 14}$) and empirical $\text{logD}_{7.4}$ were subjected to the backward elimination PLS-based procedure (IVE) indicating Sybyl-X, XlogP3, Kowwin, ACD/Percepta, and HyperChem as valid contributors to the final QSPR model ($q_{cv}^2 = 0.72$, $q_{test}^2 = 0.9$, $A_{opt} = 7$). The mean and median values of the selected estimators that averaged over the chosen $\text{clogD}_{7.4}$ values were subsequently correlated with the experimental parameter with correlation coefficient 0.65, because not only the best inter-correlated $\text{clogD}_{7.4}$ values were specified in the consensus clogP approach.

The similarity tenet in the chemical space (CS) is the core of many SAR-driven procedures, where structurally alike molecules are expected to display similar physicochemical and/or pharmacological properties [53]. Conceptually, a numerical measure of molecular diversity between two objects can be quantitatively expressed by a bit-string representation (sometimes augmented with the scaling coefficients) in the function of (un-)common features. Unarguably, it is still a powerful concept despite some obvious oversimplification of the similarity quantification (e.g., some similarity scores exhibit size-dependent behavior) [54]. The pairwise relatedness between descriptor-guided structures can be numerically evaluated by a variety of relative distance metrics (e.g., Hamming or Euclidean measures) or absolute comparison using Tanimoto coefficient calculated for molecular fingerprints (e.g., OpenBabel) [55]. The distribution of Tanimoto coefficients for the ensemble of investigated anilides 1–20 is illustrated in Figure 5a, where the highest frequency was recorded in the pretty wide range of $0.55 < T < 0.75$. The detailed inspection of the symmetric Tanimoto coefficient matrix ($T_{20 \times 20}$) in Figure 5b reveals the structural dissimilarities of nitro-substituted isomers (compounds 17 and 18) as compared with the remaining ones that confirms our previous PCA (PC1 < -60) findings (see Figure 2a). Interestingly, mono-bromo/chloro- substituted isomers (molecules 11 and 12) indicate the structural similarity to di-/tri-bromo/chloro- substituted positional isomers (compounds 4–9) as was also shown in Figure 2a (PC1 > 20). Unfortunately, the similarity investigation did not provide valuable hints that could explain the noticeable variations in the toxic effect exerted by molecule 11 (see Figure 3b) and the remaining ones.

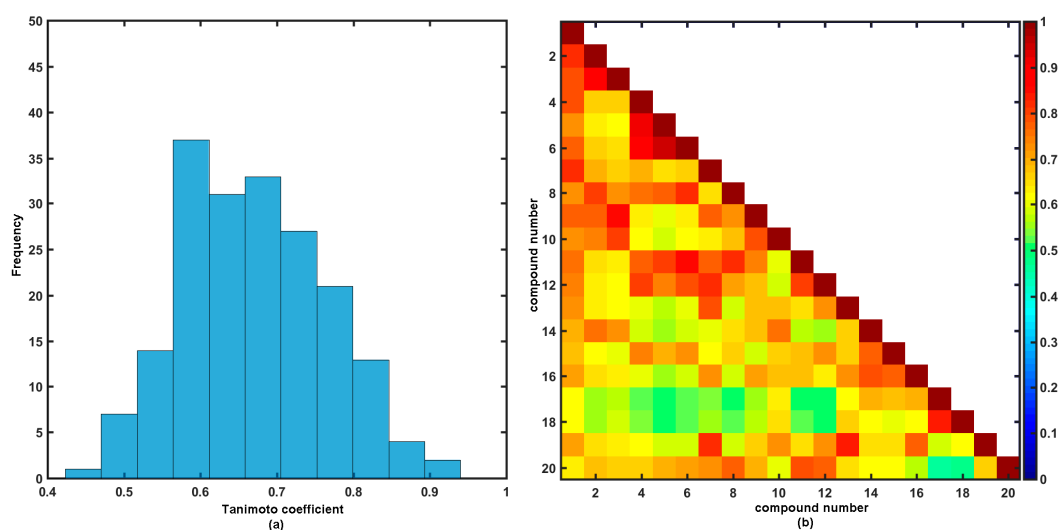


Figure 5. Distribution of Tanimoto coefficients (a) and triangular matrix of Tanimoto coefficients (b) for 1–20 anilides.

Comparative Molecular Shape Analysis

The molecular shape analysis of the cinnamic acid anilides was performed, because the molecular electrostatics and lipophilicity are two important properties used in the rational drug design. Firstly, the 11-ordered atom trial alignment of the most active molecule **10** (active analogue approach, AAA) was applied to cover the entire bonding topology in the maximal common structure (MCS) in the FIT method as illustrated in Figure 6.

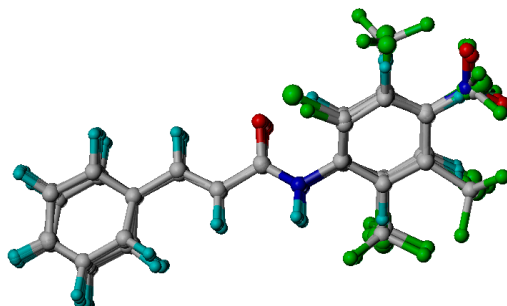


Figure 6. Superimposition of 1–20 anilides according to AAA hypothesis.

Secondly, the molecular electrostatic potentials (MESP) on the Connolly surface were specified to provide information on the charge distribution of the substituted anilides. The interrelation between electrostatic and lipophilicity potentials on molecular surfaces was reported previously [56]. The electron-rich positions seem to appear at low, possibly negative, electrostatic potential energy values (see Figure 7). In other words, low MESP values indicate molecular areas susceptible to electrophilic attack (nucleophilic positions), while greater electrostatic values correspond to electrophilic positions. Noticeably, the negative MESP values (dark blue areas) in the close proximity of the substituted anilide ring seem to contribute to the MIC activity of molecule **10**. Obviously, the introduction and composition of electronegative or electropositive substituents have an impact on the lipophilicity values as well.

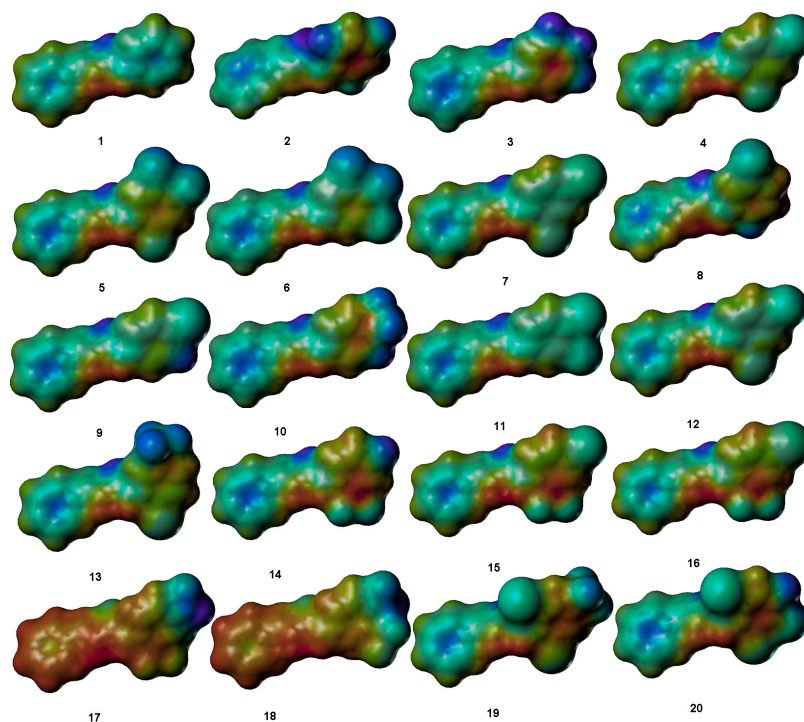


Figure 7. Molecular electrostatic potential topography of 1–20 anilides. Blue color codes negative values; red color codes positive MESP values.

The spatial MESP distribution does not provide a practical tool for molecular comparison; therefore, simpler, comparative 2D Kohonen maps of the entire molecular surface were generated [57]. Self-organizing Kohonen neural mapping (SOM) is a nonlinear projection procedure that reduces the input data dimensionality (e.g., converts 3D objects to 2D), while preserving the topological relationships between the input and output data [58]. Moreover, a trained network can be engaged to project the specified molecular property (expressed as a vector) by generating a 2D color-coded clustering pattern called a feature map. The SOM algorithm was employed to generate an electrostatic potential map in the form of a two-dimensional topographic pattern produced from input signals (points) that were sampled randomly at the molecular surface as illustrated in Figure 8. The substitution of the anilide ring by a rather bulky motif (e.g., -CF₃) was preferred for the anti-inflammatory potential and lipophilic compound property; therefore, a mono-trifluoro-methyl-based molecule with highly electronegative substituent (e.g., -F) was chosen as a template (the most active molecule 10) to proceed the remaining (counter-template) molecules. The structural inconsistencies (dissimilarities) within the analyzed set of compounds are indicated by the number of inactive (empty/white) neurons in the map (see Figure 8). Unfortunately, there are no clear and visible variations in the surface charge distribution within 40 × 40 maps between substituted analogues, with exception of molecules 17 and 18. Not surprisingly, the lowest number of non-active neurons of the comparative maps (less than 200 out of 1600) is prescribed to the similarly substituted (position 3 and 4 of the anilide ring) molecules 9, 11, and 18.

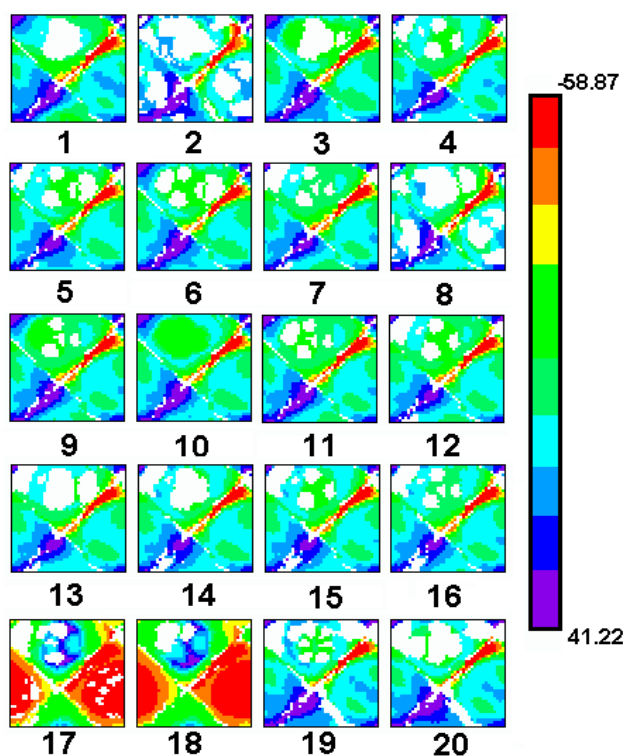


Figure 8. Comparative SOM 40 × 40 maps for 1–20 anilides. Colors code MESP values, white color indicates non-active neurons.

3. Materials and Methods

3.1. Chemistry

3.1.1. General Information

All reagents were purchased from Merck (Sigma-Aldrich, St. Louis, MO, USA) or Alfa (Alfa-Aesar, Ward Hill, MA, USA). Reactions were performed using a CEM Discover SP microwave reactor (CEM,

Matthews, NC, USA). Melting points were determined on an apparatus Stuart SMP10 (Stone, UK) and are uncorrected. Infrared (IR) spectra were recorded on an ATR Zn/Se for a Nicolet™ iS 5 FT-IR spectrometer (Thermo Fisher Scientific, West Palm Beach, FL, USA). The spectra were obtained by the accumulation of 64 scans with 4 cm^{-1} resolution in the region of $4000\text{--}400\text{ cm}^{-1}$. All ^1H - and ^{13}C -NMR spectra were recorded on a JEOL JNM-ECA 600II NMR spectrometer (600 MHz for ^1H and 150 MHz for ^{13}C , Jeol, Tokyo, Japan) in dimethyl sulfoxide- d_6 (DMSO- d_6); ^1H and ^{13}C chemical shifts (δ) are reported in ppm. High-resolution mass spectra were measured using a high-performance liquid chromatograph Dionex UltiMate® 3000 (Thermo Scientific, West Palm Beach, FL, USA) coupled with an LTQ Orbitrap XL™ Hybrid Ion Trap-Orbitrap Fourier Transform Mass Spectrometer (Thermo Scientific) equipped with a HESI II (heated electrospray ionization) source in the negative mode.

3.1.2. Synthesis

Cinnamic acid (3.37 mM) was suspended at room temperature in dry chlorobenzene (20 mL) inside a microwave tube, where phosphorus trichloride (1.7 mM) and the corresponding aniline derivative (3.37 mM) were added dropwise. Following this step, a magnetic stirrer was added to the tube and the reaction mixture was transferred to the microwave reactor (max. 500 W) at $130\text{ }^\circ\text{C}$ for 30 min, where the synthesis at elevated pressure was performed. After the mixture was cooled to $60\text{ }^\circ\text{C}$, the solvent was evaporated in vacuum. A solid residue was washed with 2M HCl, and a crude product was recrystallized, using 96% ethanol first, and then 50% ethanol [26,28].

(2E)-N-Phenyl-3-phenylprop-2-enamide (1) was described previously by Pospisilova et al. [26].

(2E)-3-Phenyl-N-(2,4,6-trifluorophenyl)prop-2-enamide (2), Yield 72%; Mp $134\text{--}136\text{ }^\circ\text{C}$; IR (cm^{-1}): 3244, 3078, 3024, 1659, 1631, 1612, 1525, 1443, 1336, 1239, 1177, 1124, 1045, 999, 972, 861, 843, 764, 751, 705, 666, 612, 572, 533, 513, 481; ^1H -NMR (DMSO- d_6), δ : 9.91 (s, 1H), 7.65–7.64 (m, 2H), 7.61 (d, $J = 15.8\text{ Hz}$, 1H), 7.47–7.41 (m, 3H), 7.32 (t, $J = 8.2\text{ Hz}$, 2H), 6.85 (d, $J = 15.8\text{ Hz}$, 1H); ^{13}C -NMR (DMSO- d_6), δ : 163.95, 159.93 (d, $J = 245.7\text{ Hz}$), 157.88 (ddd, $J = 250.0\text{ Hz}$, 15.9 Hz, 8.7 Hz), 141.19, 134.44, 130.02, 129.03, 127.87, 120.35, 111.48 (td, $J = 17.3\text{ Hz}$, $J = 5.8\text{ Hz}$), 100.95 (m) (Figure S1); HR-MS: $\text{C}_{15}\text{H}_9\text{ONF}_3$ [$\text{M} - \text{H}$] $^-$ calculated 276.0642 m/z , found 276.0634 m/z (Figure S2).

(2E)-3-Phenyl-N-(3,4,5-trifluorophenyl)prop-2-enamide (3), Yield 74%; Mp $169\text{--}171\text{ }^\circ\text{C}$; IR (cm^{-1}): 3303, 1661, 1617, 1545, 1530, 1451, 1426, 1338, 1238, 1208, 1195, 1044, 1013, 976, 858, 848, 805, 770, 761, 717, 642, 628, 561, 509, 481; ^1H -NMR (DMSO- d_6), δ : 10.58 (s, 1H), 7.64–7.67 (m, 5H), 7.46–7.41 (m, 3H), 6.74 (d, $J = 15.8\text{ Hz}$, 1H); ^{13}C -NMR (DMSO- d_6), δ : 164.02, 150.09 (ddd, $J = 244.2\text{ Hz}$, $J = 10.1\text{ Hz}$, $J = 5.8\text{ Hz}$), 141.33, 135.56 (td, $J = 11.6\text{ Hz}$, $J = 4.3\text{ Hz}$), 134.70 (dt, $J = 244.2\text{ Hz}$, $J = 15.9\text{ Hz}$), 134.38, 130.10, 129.05, 127.89, 121.25, 103.45 (m) (Figure S3); HR-MS: $\text{C}_{15}\text{H}_9\text{ONF}_3$ [$\text{M} - \text{H}$] $^-$ calculated 276.0642 m/z , found 276.0633 m/z (Figure S4).

(2E)-N-(2,4-Dichlorophenyl)-3-phenylprop-2-enamide (4), Yield: 62%; Mp $159\text{--}161\text{ }^\circ\text{C}$; IR (cm^{-1}): 3264, 3071, 3027, 1654, 1620, 1578, 1524, 1471, 1448, 1380, 1335, 1283, 1238, 1202, 1182, 1144, 1099, 1072, 1053, 1029, 1005, 999, 969, 858, 826, 787, 757, 725, 710, 697, 658, 632, 560, 559, 513, 488, 445; ^1H -NMR (DMSO- d_6), δ : 9.78 (s, 1H), 7.98 (d, $J = 8.9\text{ Hz}$, 1 H), 7.69 (d, $J = 2.1\text{ Hz}$, 1H), 7.65–7.64 (m, 2H), 7.62 (d, $J = 15.8\text{ Hz}$, 1H), 7.47–7.41 (m, 4H), 7.11 (d, $J = 15.8\text{ Hz}$, 1H); ^{13}C -NMR (DMSO- d_6), δ : 164.02, 141.17, 134.62, 134.21, 129.99, 129.09, 129.05, 128.95, 127.88, 127.59, 126.57, 126.43, 121.54 (Figure S5); HR-MS: $\text{C}_{15}\text{H}_{10}\text{ONCl}_2$ [$\text{M} - \text{H}$] $^-$ calculated 290.01450 m/z , found 290.0140 m/z (Figure S6).

(2E)-3-Phenyl-N-(2,4,5-trichlorophenyl)prop-2-enamide (5), Yield: 52%; Mp $170\text{--}172\text{ }^\circ\text{C}$; IR (cm^{-1}): 3265, 3107, 3061, 3011, 1656, 1629, 1600, 1568, 1511, 1456, 1446, 1364, 1281, 1248, 1202, 1181, 1129, 1074, 1031, 962, 942, 880, 855, 798, 756, 729, 706, 688, 675, 631, 579, 564, 499, 465, 448; ^1H -NMR (DMSO- d_6), δ : 9.85 (s, 1H), 8.33 (s, 1H), 7.94 (s, 1H), 7.66–7.65 (m, 2H), 7.64 (d, $J = 15.8\text{ Hz}$, 1H), 7.48–7.42 (m, 3H), 7.16 (d, $J = 15.8\text{ Hz}$, 1H); ^{13}C -NMR (DMSO- d_6), δ : 164.23, 141.68, 135.18, 134.52, 130.55, 130.12, 129.84,

129.05, 127.95, 126.89, 125.31, 124.45, 121.29 (Figure S7); HR-MS: $C_{15}H_9ONCl_3$ $[M - H]^-$ calculated 323.9755 m/z , found 323.9751 m/z (Figure S8).

(2*E*)-3-Phenyl-*N*-(3,4,5-trichlorophenyl)prop-2-enamide (**6**), Yield: 75%; Mp 237–239 °C; IR (cm^{-1}): 3157, 3080, 1655, 1613, 1583, 1513, 1433, 1378, 1337, 1281, 1245, 1196, 1188, 1148, 1011, 998, 967, 944, 880, 860, 815, 762, 711, 685, 617, 602, 575, 536, 483; 1H -NMR (DMSO- d_6), δ : 10.62 (s, 1H), 7.95 (s, 2H), 7.65–7.62 (m, 3H), 7.47–7.42 (m, 3H), 6.74 (d, $J = 15.8$ Hz, 1H); ^{13}C -NMR (DMSO- d_6), δ : 164.16, 141.63, 139.28, 134.31, 132.91, 130.20, 129.08, 127.96, 123.40, 121.14, 119.19 (Figure S9); HR-MS: $C_{15}H_9ONCl_3$ $[M - H]^-$ calculated 323.9755 m/z , found 323.9752 m/z (Figure S10).

(2*E*)-*N*-(2,4-Dibromophenyl)-3-phenylprop-2-enamide (**7**), Yield: 49%; Mp 180–182 °C; IR (cm^{-1}): 3263, 2980, 2888, 1653, 1620, 1575, 1521, 1464, 1446, 1376, 1336, 1280, 1240, 1203, 1184, 1080, 1040, 1007, 967, 859, 825, 766, 755, 711, 688, 643, 619, 566, 546, 501, 472, 440; 1H -NMR (DMSO- d_6), δ : 9.68 (s, 1H), 7.94 (d, $J = 2.1$ Hz, 1H), 7.78 (d, $J = 8.9$ Hz, 1H), 7.65–7.60 (m, 4H), 7.47–7.41 (m, 3H), 7.06 (d, $J = 15.8$ Hz, 1H); ^{13}C -NMR (DMSO- d_6), δ : 163.93, 141.13, 135.88, 134.61, 134.55, 130.98, 129.99, 129.05, 127.88, 127.73, 121.50, 117.97, 117.66 (Figure S11); HR-MS: $C_{15}H_{10}ONBr_2$ $[M - H]^-$ calculated 377.9134 m/z , found 377.9106 m/z (Figure S12).

(2*E*)-*N*-(5-Chloro-2-fluorophenyl)-3-phenylprop-2-enamide (**8**), Yield: 59%; Mp 118–120 °C; IR (cm^{-1}): 3244, 3188, 3119, 3042, 1663, 1622, 1612, 1541, 1481, 1415, 1343, 1268, 1253, 1202, 1182, 1112, 996, 915, 871, 808, 761, 737, 679, 646, 574, 566, 502, 485, 454; 1H -NMR (DMSO- d_6), δ : 10.13 (s, 1H), 8.31 (dd, $J = 6.9$ Hz, $J = 2.7$ Hz, 1H), 7.64–7.61 (m, 3H), 7.47–7.41 (m, 3H), 7.35 (dd, $J = 11.0$ Hz, $J = 8.9$ Hz, 1H), 7.22–7.19 (m, 1H), 7.11 (d, $J = 15.8$ Hz, 1H); ^{13}C -NMR (DMSO- d_6), δ : 164.22, 151.55 (d, $J = 245.6$ Hz), 141.31, 134.58, 130.04, 129.06, 128.02 (d, $J = 2.9$ Hz), 127.89 (d, $J = 13.0$ Hz), 127.87, 124.14 (d, $J = 7.2$ Hz), 122.23, 121.48, 116.98 (d, $J = 21.7$ Hz) (Figure S13); HR-MS: $C_{15}H_{10}ONClF$ $[M - H]^-$ calculated 274.0440 m/z , found 274.0435 m/z (Figure S14).

(2*E*)-*N*-(4-Bromo-3-fluorophenyl)-3-phenylprop-2-enamide (**9**), Yield: 69%; Mp 146–148 °C; IR (cm^{-1}): 3405, 1673, 1625, 1598, 1514, 1473, 1450, 1414, 1333, 1302, 1240, 1204, 1190, 1155, 1135, 1045, 988, 976, 944, 868, 857, 812, 780, 763, 738, 707, 683, 642, 572, 564, 544, 518, 518; 1H -NMR (DMSO- d_6), δ : 10.55 (s, 1H), 7.89 (dd, $J = 8.9$ Hz, $J = 4.0$ Hz, 1H), 7.67–7.61 (m, 4H), 7.47–7.41 (m, 3H), 7.36 (dd, $J = 8.9$ Hz, $J = 2.1$ Hz, 1H), 6.79 (d, $J = 15.8$ Hz, 1H); ^{13}C -NMR (DMSO- d_6), δ : 163.95, 158.08 (d, $J = 242.8$ Hz), 141.13, 140.43 (d, $J = 10.1$ Hz), 134.48, 133.41, 130.06, 129.08, 127.88, 121.54, 116.59 (d, $J = 2.9$ Hz), 107.19 (d, $J = 26.0$ Hz), 100.83 (d, $J = 21.7$ Hz) (Figure S15); HR-MS: $C_{15}H_{10}ONBrF$ $[M - H]^-$ calculated 317.9935 m/z , found 317.9929 m/z (Figure S16).

(2*E*)-*N*-[3-Fluoro-4-(trifluoromethyl)phenyl]-3-phenylprop-2-enamide (**10**), Yield 69%; Mp 139–141 °C; IR (cm^{-1}): 8336, 1671, 1624, 1560, 1521, 1506, 1452, 1424, 1413, 1338, 1319, 1205, 1192, 1162, 1117, 1049, 996, 970, 666, 827, 767, 763, 738, 710, 633, 603, 565, 536, 507, 484; 1H -NMR (DMSO- d_6), δ : 10.78 (s, 1H), 7.95 (dd, $J = 13.7$ Hz, 1H), 7.75 (t, $J = 8.6$ Hz, 1H), 7.67 (d, $J = 15.8$ Hz, 1H), 7.68–7.65 (m, 2H), 7.54 (d, $J = 8.2$ Hz, 1H), 7.48–7.42 (m, 3H), 6.82 (d, $J = 15.8$ Hz, 1H); ^{13}C -NMR (DMSO- d_6), δ : 164.33, 159.20 (dq, $J = 248.5$ Hz, $J = 2.9$ Hz), 144.96 (d, $J = 11.6$ Hz), 141.74, 134.36, 130.20, 129.08, 127.95, 127.87 (m), 122.82 (q, $J = 271.7$ Hz), 121.25, 114.75, 110.57 (qd, $J = 31.8$ Hz, $J = 11.6$ Hz), 106.65 (d, $J = 26.1$ Hz) (Figure S17); HR-MS: $C_{16}H_{10}ONF_4$ $[M - H]^-$ calculated 308.0704 m/z , found 308.0695 m/z (Figure S18).

(2*E*)-*N*-(4-Bromo-3-chlorophenyl)-3-phenylprop-2-enamide (**11**), Yield: 61%; Mp 170–172 °C; IR (cm^{-1}): 3282, 3097, 2980, 2888, 1663, 1627, 1579, 1521, 1470, 1449, 1376, 1338, 1288, 1253, 1229, 1180, 1113, 1071, 968, 882, 861, 808, 761, 711, 679, 676, 577, 561, 496, 482; 1H -NMR (DMSO- d_6), δ : 10.51 (s, 1H), 8.11 (d, $J = 2.1$ Hz, 1H), 7.72 (d, $J = 8.2$ Hz, 1H), 7.65–7.61 (m, 3H), 7.50 (dd, $J = 8.6$ Hz, $J = 2.4$ Hz, 1H), 7.47–7.41 (m, 3H), 6.78 (d, $J = 15.8$ Hz, 1H); ^{13}C -NMR (DMSO- d_6), δ : 163.94, 141.13, 139.92, 134.47, 133.95, 133.09,

130.07, 129.08, 127.88, 121.53, 120.31, 119.45, 114.48 (Figure S19); HR-MS: $C_{15}H_{10}ONBrCl$ $[M - H]^-$ calculated 333.9640 m/z , found 333.9635 m/z (Figure S20).

(2E)-N-(2-Bromo-4-chlorophenyl)-3-phenylprop-2-enamide (**12**), Yield: 68%; Mp 173–175 °C; IR (cm^{-1}): 3258, 2980, 2888, 1653, 1621, 1572, 1524, 1465, 1447, 1380, 1336, 1279, 1263, 1238, 1201, 1180, 1093, 1039, 1006, 999, 969, 858, 824, 775, 757, 714, 700, 653, 632, 568, 551, 512; 1H -NMR (DMSO- d_6), δ : 9.69 (s, 1H), 7.84–7.82 (m, 2H), 7.65–7.64 (m, 2H), 7.62 (d, $J = 15.8$ Hz, 1H), 7.49 (dd, $J = 8.6$ Hz, $J = 2.4$ Hz, 1H), 7.47–7.41 (m, 3H), 7.07 (d, $J = 15.8$ Hz, 1H); ^{13}C -NMR (DMSO- d_6), δ : 163.94, 141.08, 135.50, 134.60, 131.87, 129.96, 129.72, 129.02, 128.05, 127.85, 127.38, 121.49, 117.69 (Figure S21); HR-MS: $C_{15}H_{10}ONBrCl$ $[M - H]^-$ calculated 333.9640 m/z , found 333.9635 m/z (Figure S22).

(2E)-N-[2-Bromo-5-(trifluoromethyl)phenyl]-3-phenylprop-2-enamide (**13**), Yield 59%; Mp 134–135 °C; IR (cm^{-1}): 3270, 1658, 1631, 1606, 1529, 1467, 1423, 1329, 1262, 1170, 1112, 1078, 1035, 963, 928, 894, 856, 816, 759, 709, 685, 643, 615, 560, 491, 454; 1H -NMR (DMSO- d_6), δ : 9.84 (s, 1H), 8.26 (d, $J = 1.4$ Hz, 1H), 7.94 (d, $J = 8.2$ Hz, 1H), 7.67–7.65 (m, 2H), 7.65 (d, $J = 15.8$ Hz, 1H), 7.49–7.42 (m, 4H), 7.14 (d, $J = 15.8$ Hz, 1H); ^{13}C -NMR (DMSO- d_6), δ : 164.25, 141.54, 137.26, 134.54, 134.06, 130.08, 129.06, 128.59 (q, $J = 31.8$ Hz), 127.94, 123.71 (q, $J = 273.1$ Hz), 122.77 (q, $J = 4.3$ Hz), 122.07 (q, $J = 2.9$ Hz), 121.35, 120.81 (Figure S23); HR-MS: $C_{16}H_{10}ONBrF_3$ $[M - H]^-$ calculated 367.9903 m/z , found 367.9893 m/z (Figure S24).

(2E)-N-[4-Fluoro-2-(trifluoromethyl)phenyl]-3-phenylprop-2-enamide (**14**), Yield 76%; Mp 145–147 °C; IR (cm^{-1}): 3257, 3086, 1653, 1622, 1521, 1492, 1429, 1332, 1316, 1271, 146, 1174, 1127, 1119, 1049, 974, 914, 883, 865, 845, 823, 761, 745, 727, 709, 691, 664, 652, 569, 539, 499, 481; 1H -NMR (DMSO- d_6), δ : 9.79 (s, 1H), 7.67 (dd, $J = 8.9$ Hz, $J = 2.7$ Hz, 1H), 7.65–7.63 (m, 2H), 7.61–7.58 (m, 2H), 7.59 (d, $J = 15.8$ Hz, 1H), 7.46–7.40 (m, 3 H), 6.97 (d, $J = 15.8$ Hz, 1H); ^{13}C -NMR (DMSO- d_6), δ : 164.79, 159.51 (d, $J = 245.7$ Hz), 140.86, 134.55, 132.54 (d, $J = 8.7$ Hz), 131.76 (d, $J = 2.9$ Hz), 129.92, 129.02, 127.81, 126.40 (qd, $J = 31.8$ Hz, $J = 10.1$ Hz), 122.67 (qd, $J = 274.6$ Hz, $J = 2.9$ Hz), 121.18, 120.00 (d, $J = 21.7$ Hz), 113.72 (dq, $J = 26.0$ Hz, $J = 5.8$ Hz) (Figure S25); HR-MS: $C_{16}H_{10}ONF_4$ $[M - H]^-$ calculated 308.0704 m/z , found 308.0696 m/z (Figure S26).

(2E)-N-[4-Chloro-2-(trifluoromethyl)phenyl]-3-phenylprop-2-enamide (**15**), Yield 71%; Mp 165–167 °C; IR (cm^{-1}): 3268, 3083, 3030, 1655, 1624, 1584, 1522, 1483, 1449, 1410, 1337, 1306, 1277, 1268, 1243, 1171, 1122, 1109, 1052, 967, 890, 872, 857, 833, 810, 761, 711, 696, 684, 562, 539, 509; 1H -NMR (DMSO- d_6), δ : 9.80 (s, 1H), 7.84 (d, $J = 2.1$ Hz, 1H), 7.79 (dd, $J = 8.6$ Hz, $J = 2.4$ Hz, 1H), 7.69 (d, $J = 8.9$ Hz, 1H), 7.65–7.64 (m, 2H), 7.60 (d, $J = 15.8$ Hz, 1H), 7.47–7.41 (m, 3H), 7.00 (d, $J = 15.8$ Hz, 1H); ^{13}C -NMR (DMSO- d_6), δ : 164.65, 141.13, 134.52, 134.38, 132.96, 131.51, 130.67, 129.98, 129.03, 127.86, 126.26 (q, $J = 5.8$ Hz), 125.72 (q, $J = 30.3$ Hz), 122.7 (q, $J = 273.1$ Hz), 121.12 (Figure S27); HR-MS: $C_{16}H_{10}ONClF_3$ $[M - H]^-$ calculated 324.0409 m/z , found 324.0399 m/z (Figure S28).

(2E)-N-[4-Bromo-2-(trifluoromethyl)phenyl]-3-phenylprop-2-enamide (**16**), Yield 64%; Mp 176–178 °C; IR (cm^{-1}): 3289, 3083, 3030, 1657, 1624, 1525, 1481, 1404, 1338, 1305, 1278, 1265, 1247, 1172, 1160, 1124, 1052, 967, 889, 866, 831, 760, 747, 710, 682, 631, 560, 529, 501, 463; 1H -NMR (DMSO- d_6), δ : 9.78 (s, 1H), 7.94 (m, 1H), 7.92 (dd, $J = 8.2$ Hz, $J = 2.1$ Hz, 1H), 7.65–7.62 (m, 3H), 7.60 (d, $J = 15.8$ Hz, 1H), 7.46–7.41 (m, 3H), 7.00 (d, $J = 15.8$ Hz, 1H); ^{13}C -NMR (DMSO- d_6), δ : 164.59, 141.16, 135.94, 134.81 (q, $J = 2.9$ Hz), 134.52, 131.64, 129.99, 129.03, 129.02 (q, $J = 5.8$ Hz), 127.86, 125.87 (q, $J = 30.3$ Hz), 122.60 (q, $J = 273.1$ Hz), 121.12, 118.62 (Figure S29); HR-MS: $C_{16}H_{10}ONBrF_3$ $[M - H]^-$ calculated 367.9903 m/z , found 367.9894 m/z (Figure S30).

(2E)-N-[4-Nitro-2-(trifluoromethyl)phenyl]-3-phenylprop-2-enamide (**17**), Yield 61%; Mp 164–166 °C; IR (cm^{-1}): 3314, 3086, 1662, 1620, 1594, 1544, 1505, 1449, 1424, 1338, 1319, 1277, 1172, 1112, 1052, 1000, 973, 921, 901, 854, 840, 790, 760, 744, 709, 686, 604, 592, 560; 1H -NMR (DMSO- d_6), δ : 9.95 (s, 1H), 8.54 (dd, $J = 8.9$ Hz, $J = 2.7$ Hz, 1H), 8.47 (d, $J = 2.7$ Hz, 1H), 8.17 (d, $J = 8.9$ Hz, 1H), 7.68 (d, $J = 15.8$ Hz,

1H), 7.68–7.67 (m, 2H), 7.48–7.43 (m, 3H), 7.17 (d, $J = 15.8$ Hz, 1H); ^{13}C -NMR (DMSO- d_6), δ : 164.64, 143.84, 142.29, 141.30, 134.41, 130.25, 129.06, 128.84, 128.04, 127.96, 122.50 (q, $J = 30.3$ Hz), 122.48 (q, $J = 273.10$ Hz), 122.27 (q, $J = 4.3$ Hz), 120.91 (Figure S31); HR-MS: $\text{C}_{16}\text{H}_{10}\text{O}_3\text{N}_2\text{F}_3$ $[\text{M} - \text{H}]^-$ calculated 335.0649 m/z , found 335.0637 m/z (Figure S32).

(2E)-N-[4-Nitro-3-(trifluoromethyl)phenyl]-3-phenylprop-2-enamide (**18**), Yield 60%; Mp 181–183 °C; IR (cm^{-1}): 3314, 3086, 1662, 1620, 1594, 1544, 1505, 1424, 1338, 1319, 1277, 1247, 1172, 1112, 1052, 983, 921, 901, 854, 840, 790, 760, 750, 709, 686, 645, 604, 593, 560, 505; ^1H -NMR (DMSO- d_6), δ : 11.03 (s, 1H), 8.38 (d, $J = 2.1$ Hz, 1H), 8.23 (d, $J = 8.9$ Hz, 1H), 8.13 (dd, $J = 8.9$ Hz, $J = 2.1$ Hz, 1H), 7.70 (d, $J = 15.8$ Hz, 1H), 7.67–7.66 (m, 2H), 7.48–7.43 (m, 3H), 6.81 (d, $J = 15.8$ Hz, 1H); ^{13}C -NMR (DMSO- d_6), δ : 164.54, 143.95, 142.27, 141.30, 134.23, 130.35, 129.10, 128.04, 127.84, 123.02 (q, $J = 33.2$ Hz), 122.07 (q, $J = 273.1$ Hz), 120.94, 117.32 (q, $J = 5.8$ Hz) (Figure S33); HR-MS: $\text{C}_{16}\text{H}_{10}\text{O}_3\text{N}_2\text{F}_3$ $[\text{M} - \text{H}]^-$ calculated 335.0649 m/z , found 335.0635 m/z (Figure S34).

(2E)-N-[2,6-Dibromo-4-(trifluoromethyl)phenyl]-3-phenylprop-2-enamide (**19**), Yield 78%; Mp 227–229 °C; IR (cm^{-1}): 3086, 2970, 2855, 1655, 1613, 1520, 1450, 1395, 1340, 1303, 1197, 1167, 1132, 1096, 1072, 1010, 984, 881, 862, 768, 743, 715, 692, 666, 566, 497; ^1H -NMR (DMSO- d_6), δ : 10.36 (s, 1H), 8.19 (s, 2H), 7.67–7.66 (m, 2H), 7.64 (d, $J = 15.8$ Hz, 1H), 7.47–7.42 (3H), 6.90 (d, $J = 15.8$ Hz, 1H); ^{13}C -NMR (DMSO- d_6), δ : 163.42, 141.14, 140.13, 134.38, 130.08, 129.99 (q, $J = 33.2$ Hz), 129.16 (q, $J = 4.3$ Hz), 129.07, 127.88, 124.96, 122.29 (q, $J = 273.1$ Hz), 120.45 (Figure S35); HR-MS: $\text{C}_{16}\text{H}_9\text{ONBr}_2\text{F}_3$ $[\text{M} - \text{H}]^-$ calculated 445.9008 m/z , found 445.9002 m/z (Figure S36).

(2E)-N-(2,6-Dibromo-3-chloro-4-fluorophenyl)-3-phenylprop-2-enamide (**20**), Yield: 74%; Mp 234–235 °C; IR (cm^{-1}): 3197, 3001, 1656, 1664, 1611, 1571, 1523, 1442, 1357, 1339, 1296, 1285, 1206, 1179, 1113, 988, 979, 854, 784, 763, 753, 723, 696, 684, 640, 581, 562, 530, 486, 442; ^1H -NMR (DMSO- d_6), δ : 10.26 (s, 1H), 8.07 (d, $J = 8.9$ Hz, 1H), 7.67–7.65 (m, 2H), 7.62 (d, $J = 15.8$ Hz, 1H), 7.47–7.42 (m, 3H), 6.87 (d, $J = 15.8$ Hz, 1H); ^{13}C -NMR (DMSO- d_6), δ : 163.64, 156.15 (d, $J = 252.9$ Hz), 141.25, 134.40, 134.28 (d, $J = 2.9$ Hz), 130.04, 129.07, 127.85, 126.30, 122.82 (d, $J = 10.1$ Hz), 121.30 (d, $J = 20.2$ Hz), 120.52, 119.79 (d, $J = 24.6$ Hz) (Figure S37); HR-MS: $\text{C}_{15}\text{H}_8\text{ONBr}_2\text{FCl}$ $[\text{M} - \text{H}]^-$ calculated 429.8651 m/z , found 429.8648 m/z (Figure S38).

3.2. Biological Testing

3.2.1. In Vitro Antibacterial Evaluation

The synthesized compounds were evaluated for their in vitro antibacterial activity against representatives of multidrug-resistant bacteria, clinical isolates of methicillin-resistant *Staphylococcus aureus* (MRSA) 63718, and SA 630 that were obtained from the National Institute of Public Health (Prague, Czech Republic). *S. aureus* ATCC 29213 was used as the reference and quality control strain. Ampicillin (Sigma, St. Louis, MO, USA) was employed as the standard. All compounds and controls were prepared in triplicate. The screening was performed as described previously [26]. The results are summarized in Table 1. Antibacterial activity was assessed by determining MIC and MBC values. The broth microdilution method was applied. MIC values were determined in a microtiter plate. Aliquots from this plate were subcultivated on the Petri dish with Mueller-Hinton broth for the determination of MBC [43].

3.2.2. In Vitro Antimycobacterial Evaluation

The assessment of the in vitro antimycobacterial activity of the compounds was performed against *Mycobacterium tuberculosis* H37Ra/ATCC 25177 by means of the methodology described recently (e.g., [26]). Isoniazid (Sigma) was used as the standard. All compounds and controls were prepared in triplicate. The results are summarized in Table 1.

3.2.3. MTT Assay

A compound was diluted in Mueller-Hinton broth to achieve the desired final concentrations of 0.5 and 1 µg/mL, respectively. *S. aureus* ATCC 29213 bacterial suspension in sterile distilled water at 0.5 McFarland was diluted 1:3. Inocula were added to each well by a multi-inoculator. Diluted bacteria in broth free from inhibiting compounds were used as the growth control. The procedure was performed three times. Plates were incubated at 37 °C for 24 h. After the incubation period, 10% well volume of MTT (3-(4,5-dimethylthiazol-2-yl)-2,5-diphenyltetrazolium bromide) reagent (Sigma) was mixed into each well and incubated at 37 °C for 1 h. Then 100 µL of 17% sodium dodecyl sulphate in 40% dimethylformamide was added to each well. The plates were read at 570 nm. The absorbance readings from the cells grown in the presence of the tested compounds were compared with uninhibited cell growth to determine relative percent inhibition. The percent inhibition was determined through the MTT assay. The percent viability is calculated through the comparison of a measured value and that of the uninhibited control: % viability = $OD_{570E}/OD_{570P} \times 100$, where OD_{570E} is the reading from the compound-exposed cells, while OD_{570P} is the reading from the uninhibited cells (positive control). Cytotoxic potential is determined by a percent viability of <70% [43,59].

3.2.4. In Vitro Cell Viability Assay

The cytotoxic effect of the tested compounds was specified on THP1-Blue™ NF-κB cell line (Invivogen; San Diego, CA, USA), as described previously [28]. Briefly, cells resuspended in serum-free RPMI 1640 medium (Merck, Darmstadt, Germany) supplemented with antibiotics (100 U/mL penicillin and 100 mg/mL streptomycin (Merck)) and 10% FBS (Merck) were seeded into 96-well plates (100 µL/well, i.e., 50,000 cells per each well). After 2 h, tested compounds dissolved in DMSO (1.25–20 µM) were added to the cells. The final concentration of DMSO was 0.1% (v/v) in each well. The viability analysis was performed after 24 h incubation with the tested substances using the WST-1 Cell Proliferation Reagent kit (Roche Diagnostics, Basel, Switzerland) according to the manufacturer's manual. The amount of formazan formed, which corresponded to the number of metabolically active cells in the culture, was calculated as a percentage of the control cells, which were treated only with serum-free RPMI 1640 medium and were assigned as 100%. The IC₅₀ values were calculated by four-parameter logistic (4PL) analysis from obtained viability curves by GraphPad Prism 8.0.1 (San Diego, CA, USA) software. The results are summarized in Table 1 as mean ± SEM (n = 6).

3.2.5. Determination of NF-κB Activity

To evaluate the anti-inflammatory potential of novel compounds, their ability to attenuate the lipopolysaccharide (LPS)-activated pro-inflammatory transcription nuclear factor (NF)-κB was measured as was described previously [28]. Briefly, THP1-Blue™ NF-κB cells were pretreated by tested compounds dissolved in DMSO in the non-toxic concentration 1 µM for 1 h. After LPS (1 µg/mL) stimulation, the NF-κB activity was evaluated by Quanti-Blue medium (Invivogen) according to the manufacturer's instructions. The results from 3 independent experiments performed in triplicate (n = 9) were analyzed by GraphPad Prism 8.0.1 software. The outlying values were excluded by ROUT algorithms (Q = 5%).

3.3. Lipophilicity Determination by RP-HPLC (Capacity Factor k' /Calculated log k')

The HPLC separation system Merck Hitachi LaChrom Elite® equipped with a Merck Hitachi LaChrom Elite® L-2455 Diode-Array Detector (Hitachi High Technologies America, San Jose, CA, USA) was used. A chromatographic column Symmetry® C18 5 µm, 4.6 × 250 mm, Part No. W21751W016 (Waters Corp., Milford, MA, USA) was used. The HPLC separation process was monitored by the EZ CHROM Elite® software (Hitachi High Technologies America). The total flow of the column was 1.0 mL/min, injection 10 µL, column temperature 40 °C, and sample temperature 10 °C. The detection wavelength 214 nm was chosen. A KI methanolic solution was used for the dead time (t_0) determination.

Retention times (t_R) were measured in minutes. Isocratic elution by a mixture of Metanol Chromasolv™ (Honeywell, St. Louis, MO, USA) (72%) and H₂O-HPLC Mili-Q grade (Labconco, Kansas City, MO, USA) (28%) as a mobile phase was used for the determination of capacity factor k , while isocratic elution by a mixture of Metanol Chromasolv™ (Honeywell) (72%) and NaOAc buffer, pH 6.5 and 7.4 (28%) as a mobile phase were used for the determination of distribution coefficients $D_{6.5}$ and $D_{7.4}$. The capacity factors and distribution coefficients were calculated according to the formula $k(D) = (t_R - t_D)/t_D$, where t_R is the retention time of the solute and t_D is the dead time obtained using an unretained analyte. Each experiment was repeated three times. The calculated $\log k$, $\log D_{6.5}$, and $\log D_{7.4}$ values of individual compounds are shown in Table 1.

3.4. Lipophilicity Determination by RP-TLC

R_M values were determined from the RP-18 TLC measurements. The solutions of compounds in Metanol Chromasolv™ (Honeywell) were spotted on a RP-TLC plate (Silica gel Nano-SIL C18-100 UV 254, 10 × 10 cm, Macherey-Nagel, Duren, Germany), 1.5 cm from the edge. The volatiles were carefully evaporated, and the plate was developed by MeOH (100%) or MeOH: H₂O-HPLC (72:28 *v/v*) or MeOH: NaOAc buffer, pH 7.4 (72:28 *v/v*). After drying, the spots were visualized under UV ($\lambda = 365$ nm). R_M data were obtained from equation: $R_M = \log(1/R_f - 1)$. Each experiment was repeated three times. The R_M values of individual compounds are shown in Table 1.

3.5. Model Building and Experimental vs. Theoretical Lipophilicity Prediction

CACTVS/csed and CORINA editors were engaged to produce each structural model and its initial spatial geometry. OpenBabel (inter)change file format converter was employed for data conversion. Sybyl-X 2.0/Certara software package running on a HP Z200 workstation with a Debian 10.0 operating system was used to conduct the molecular modeling simulations. The initial compound geometry optimization with MAXMIN2 module was performed using the standard Tripos force field (POWELL conjugate gradient algorithm) with a 0.01 kcal/mol energy gradient convergence criterion. The specification of the electrostatic potential values based on the partial atomic charges was carried out with the Gasteiger–Hückel method implemented in Sybyl-X.

An ensemble of freely/commercially available *in silico* predictors can be engaged to specify theoretically the numerical value of partition coefficients ($\log P$) as follows:

AlogPS—algorithm implemented by Tetko et al. [37] based on atom-type electrotopological-state (E-state) indices and neural networks (NN);

milogP—procedure proposed by Molinspiration for practical $\log P$ calculations of almost all organic molecules as a sum of fragment-based contributions and correction factors;

ClogP—fragment-based approach for estimation of lipophilicity based on structure-dependent correction values retrieved from Hansch and Leo's database that is implemented in Sybyl/Centara software;

HyperChem $\log P$ —an atom-additive method that estimates lipophilicity using the individual atomic contribution based on procedure proposed by Ghose, Prichett and Crippen;

MarvinSketch $\log P$ —the overall lipophilicity of a molecule is composed of the contributing values of its atom types that were redefined to accommodate electron delocalization and contributions of ionic forms;

ChemSketch $\log P$ —a comprehensive fragment-based algorithm with high quality models built using empirical data. Well-characterized $\log P$ contributions have been compiled for atoms; structural fragments and intramolecular interactions provided for more than 12×10^3 experimental $\log P$ values;

Dragon AlogP—statistical estimators of the Ghose-Crippen-Viswanadhan model were specified on the basis of known experimental $\log P$ for the training set of 8364 compounds. The overall approach of the lipophilic atomic-based constant is estimated with the contribution of 115 atom types;

Dragon MlogP—the calculated partition coefficient includes VdW volume and Moriguchi polar parameters as correction factors. A regression MlogP model is based on 13 structural parameters that were rated on the training group of 1,230 organic molecules;

Kowwin—estimates the log octanol-water partition coefficient of chemicals using the atom/fragment contribution protocol;

XlogP3—an atom-additive procedure with well-defined correction factors that engages an optimized atom typing approach calibrated on a big training set;

OSIRIS clogP—in house approach based on the cumulative sum of atom contributions calculated for more than 5000 compounds with experimentally measured logP values as a training set. Predicting engine distinguishes 369 atom types;

ChemDraw clogP—the combination of Classic and GALAS algorithms for the prediction of partition coefficient based on a training set of $>11 \times 10^3$ compounds provides coverage for a broad chemical space;

Percepta clogP—based on $>12 \times 10^3$ of empirical logP values with the algorithm that uses the principal of isolating carbons.

In order to detect the redundant descriptors in QSAR/QSPR studies, several methods of variable selection/elimination have been proposed, including the uninformative variable elimination (UVE-PLS), as well as its modifications, namely iterative variable elimination (IVE-PLS) [60]. Overall, the entire algorithm comprises of the following stages:

Stage 1. Standard PLS analysis with LOO-CV to evaluate the performance of the PLS model

Stage 2. Elimination of the matrix column with the lowest $\text{abs}(\text{mean}(b)/\text{std}(b))$ value

Stage 3. Standard PLS analysis of the new matrix without the column eliminated in Stage 2.

Stage 4. Iterative repetition of the Stages 1–3 to maximize the LOO q_{cv}^2 .

3.6. Similarity Assessment Using PCA and Tanimoto Coefficient

The proper mapping of the molecular diversity in the theoretically infinite chemical space ($CS \approx 10^{60}$ – 10^{200}) into the corresponding property space basically requires the multi-dimensional description of a molecule by a set of structural (S) and physicochemical (P) properties organized in a vector [61]. The molecular distribution of the experimental-based (FCS) and virtual-derived (VCS) compounds/models might be graphically displayed using the human friendly 2D/3D plots, e.g., in the procedure called Principal Component Analysis (PCA) [62]. PCA is a linear projection method designed to model multivariate data with a relatively small number of so-called principal components (scores and loadings) constructed in order to maximize the variance description of input data [63]. The PCA model with f principal components for a data matrix X can be presented as follows:

$$X = TP^T + E \quad (1)$$

where X is a data matrix with m objects and n variables, T is the score matrix with dimensions $(m \times f)$, P^T is a transposed matrix of loadings with dimensions $(f \times n)$ and E is a matrix of the residual variance $(m \times n)$ that is not explained by the first f principal components. Basically, the first few principal components often capture interesting information about the data structure and uncover groups of objects.

The structural relatedness between molecule library is usually estimated using a function mapping (dis)similarities between the pairs of bit-string descriptors given by the Tanimoto equation as follows:

$$T(x, y) = \frac{n_{xy}}{(n_x + n_y - n_{xy})} \quad (2)$$

where n_{xy} is the number of bits set into 1 shared in the fingerprint of molecules x and y , n_x is the number of bits set into 1 in molecule x , n_y is the number of bits set into 1 in molecule y . Top-ranked objects are supposed to have similar properties, although the validity of this assumption is fairly

questionable, because 70% of compounds with $T(x, y) > 0.85$ to an active analog have comparatively low probability of being active in the same way [64].

4. Conclusions

A set of 20 cinnamic acid anilides (1 published recently and 19 newly synthesized) was investigated in relation to their biological activities and characterized by a series of experimental lipophilicity values generated using RP-HPLC and RP-TLC methods. All compounds were tested against the reference strain *Staphylococcus aureus*, two MRSA clinical isolates, and *Mycobacterium tuberculosis*. (2*E*)-*N*-[3-Fluoro-4-(trifluoromethyl)phenyl]-3-phenylprop-2-enamide (**10**) showed comparable or even better activity than the ampicillin. It was found that the activity of compound **10** is bactericidal. The screening of the cell viability performed using THP1-Blue™ NF-κB cells demonstrated that only (2*E*)-*N*-(4-bromo-3-chlorophenyl)-3-phenylprop-2-enamide (**11**) showed significant cytotoxic effect. Moreover, all compounds were tested for their anti-inflammatory potential; (2*E*)-*N*-(2,6-dibromo-3-chloro-4-fluorophenyl)-3-phenylprop-2-enamide (**20**) attenuated the lipopolysaccharide-induced NF-κB activation and was more potent than the parental cinnamic acid. Unfortunately, the design of compound that combines both high antimicrobial activity and anti-inflammatory effect is a great challenge; compounds with preferential anilide ring substitution at the *meta* positions and optionally in combination with *para* show the highest antimicrobial activity, while the *ortho* position optionally in combination with *meta* are anti-inflammatory preferential. The similarity-related property space evaluation for the congeneric series of structural analogues was carried out using the principal component analysis (PCA). Moreover, the *in silico* approximation of the lipophilic values for the ensemble of anilides **1–20** was performed employing a set of free/commercial clogP estimators, subsequently corrected using the corresponding pK_a calculated at physiological pH and subsequently cross-compared with the experimental parameter. The mean and median value of the selected estimators that averaged over the chosen logD_{7.4} values were subsequently correlated with the experimental parameter with correlation coefficient of 0.65, because not only the best inter-correlated clogD_{7.4} values were specified in the consensus clogP approach. Finally, the similarity-driven investigation using Tanimoto metrics was conducted revealing the structural dissimilarities of nitro-substituted isomers (compounds **17** (R = 2-CF₃-4-NO₂) and **18** (R = 3-CF₃-4-NO₂)) as compared with the remaining ones, which confirms our previous PCA findings. Interestingly, mono-bromo/chloro-substituted isomers (compounds **11** (R = 3-Cl-4-Br) and **12** (R = 2-Br-4-Cl)) indicate the structural similarity to di/tri-bromo/chloro-substituted positional isomers (molecules **4–9**). Unfortunately, the similarity investigation did not provide valuable hints that could explain the noticeable variations in the toxic effect exerted by molecule **11** (IC₅₀ = 6.5 μM on THP1-Blue™ NF-κB cells) and the remaining ones. In general, the distribution coefficient provides a more realistic estimation of lipophilicity in the relevant pH environments; therefore, logD_{pH} ought to be preferentially engaged in the QSPR study, especially for compounds that are likely to ionize in physiological media. Based on this study, the antiproliferative/antineoplastic activity of compound **11** will be investigated, while the rest of the tested compounds will be studied in relation to their antimicrobial and anti-inflammatory activities.

Supplementary Materials: The following are available online, Table S1: Theoretically estimated partition coefficient calculated by set of alternative methods for anilides **1–20**. Table S2: Theoretically estimated pK_a calculated by ACD/Percepta/pK_a for anilides **1–20**. Figure S1: ¹³C-NMR (DMSO-*d*₆) spectrum of (2*E*)-3-phenyl-*N*-(2,4,6-trifluorophenyl)prop-2-enamide (**2**). Figure S2: HR-MS record of (2*E*)-3-phenyl-*N*-(2,4,6-trifluorophenyl)prop-2-enamide (**2**). Figure S3: ¹³C-NMR (DMSO-*d*₆) spectrum of (2*E*)-3-phenyl-*N*-(3,4,5-trifluorophenyl)prop-2-enamide (**3**). Figure S4: HR-MS record of (2*E*)-3-phenyl-*N*-(3,4,5-trifluorophenyl)prop-2-enamide (**3**). Figure S5: ¹³C-NMR (DMSO-*d*₆) spectrum of (2*E*)-*N*-(2,4-dichlorophenyl)-3-phenylprop-2-enamide (**4**). Figure S6: HR-MS record of (2*E*)-*N*-(2,4-dichlorophenyl)-3-phenylprop-2-enamide (**4**). Figure S7: ¹³C-NMR (DMSO-*d*₆) spectrum of (2*E*)-3-phenyl-*N*-(2,4,5-trichlorophenyl)prop-2-enamide (**5**). Figure S8: HR-MS record of (2*E*)-3-phenyl-*N*-(2,4,5-trichlorophenyl)prop-2-enamide (**5**). Figure S9: ¹³C-NMR (DMSO-*d*₆) spectrum of (2*E*)-3-phenyl-*N*-(3,4,5-trichlorophenyl)prop-2-enamide (**6**). Figure S10: HR-MS record of (2*E*)-3-phenyl-*N*-(3,4,5-trichlorophenyl)prop-2-enamide (**6**). Figure S11: ¹³C-NMR (DMSO-*d*₆) spectrum of (2*E*)-*N*-(2,4-dibromophenyl)-3-phenylprop-2-enamide (**7**). Figure S12: HR-MS record of (2*E*)-*N*-(2,4-dibromophenyl)-3-phenylprop-

2-enamide (7). Figure S13: ^{13}C -NMR (DMSO- d_6) spectrum of (2E)-N-(5-chloro-2-fluorophenyl)-3-phenylprop-2-enamide (8). Figure S14: HR-MS record of (2E)-N-(5-chloro-2-fluorophenyl)-3-phenylprop-2-enamide (8). Figure S15: ^{13}C -NMR (DMSO- d_6) spectrum of (2E)-N-(4-bromo-3-fluorophenyl)-3-phenylprop-2-enamide (9). Figure S16: HR-MS record of (2E)-N-(4-bromo-3-fluorophenyl)-3-phenylprop-2-enamide (9). Figure S17: ^{13}C -NMR (DMSO- d_6) spectrum of (2E)-N-[3-fluoro-4-(trifluoromethyl)phenyl]-3-phenylprop-2-enamide (10). Figure S18: HR-MS record of (2E)-N-[3-fluoro-4-(trifluoromethyl)phenyl]-3-phenylprop-2-enamide (10). Figure S19: ^{13}C -NMR (DMSO- d_6) spectrum of (2E)-N-(4-bromo-3-chlorophenyl)-3-phenylprop-2-enamide (11). Figure S20: HR-MS record of (2E)-N-(4-bromo-3-chlorophenyl)-3-phenylprop-2-enamide (11). Figure S21: ^{13}C -NMR (DMSO- d_6) spectrum of (2E)-N-(2-bromo-4-chlorophenyl)-3-phenylprop-2-enamide (12). Figure S22: HR-MS record of (2E)-N-(2-bromo-4-chlorophenyl)-3-phenylprop-2-enamide (12). Figure S23: ^{13}C -NMR (DMSO- d_6) spectrum of (2E)-N-[2-bromo-5-(trifluoromethyl)phenyl]-3-phenylprop-2-enamide (13). Figure S24: HR-MS record of (2E)-N-[2-bromo-5-(trifluoromethyl)phenyl]-3-phenylprop-2-enamide (13). Figure S25: ^{13}C -NMR (DMSO- d_6) spectrum of (2E)-N-[4-fluoro-2-(trifluoromethyl)phenyl]-3-phenylprop-2-enamide (14). Figure S26: HR-MS record of (2E)-N-[4-fluoro-2-(trifluoromethyl)phenyl]-3-phenylprop-2-enamide (14). Figure S27: ^{13}C -NMR (DMSO- d_6) spectrum of (2E)-N-[4-chloro-2-(trifluoromethyl)phenyl]-3-phenylprop-2-enamide (15). Figure S28: HR-MS record of (2E)-N-[4-chloro-2-(trifluoromethyl)phenyl]-3-phenylprop-2-enamide (15). Figure S29: ^{13}C -NMR (DMSO- d_6) spectrum of (2E)-N-[4-bromo-2-(trifluoromethyl)phenyl]-3-phenylprop-2-enamide (16). Figure S30: HR-MS record of (2E)-N-[4-bromo-2-(trifluoromethyl)phenyl]-3-phenylprop-2-enamide (16). Figure S31: ^{13}C -NMR (DMSO- d_6) spectrum of (2E)-N-[4-nitro-2-(trifluoromethyl)phenyl]-3-phenylprop-2-enamide (17). Figure S32: HR-MS record of (2E)-N-[4-nitro-2-(trifluoromethyl)phenyl]-3-phenylprop-2-enamide (17). Figure S33: ^{13}C -NMR (DMSO- d_6) spectrum of (2E)-N-[4-nitro-3-(trifluoromethyl)phenyl]-3-phenylprop-2-enamide (18). Figure S34: HR-MS record of (2E)-N-[4-nitro-3-(trifluoromethyl)phenyl]-3-phenylprop-2-enamide (18). Figure S35: ^{13}C -NMR (DMSO- d_6) spectrum of (2E)-N-[2,6-dibromo-4-(trifluoromethyl)phenyl]-3-phenylprop-2-enamide (19). Figure S36: HR-MS record of (2E)-N-[2,6-dibromo-4-(trifluoromethyl)phenyl]-3-phenylprop-2-enamide (19). Figure S37: ^{13}C -NMR (DMSO- d_6) spectrum of (2E)-N-(2,6-dibromo-3-chloro-4-fluorophenyl)-3-phenylprop-2-enamide (20). Figure S38: HR-MS record of (2E)-N-(2,6-dibromo-3-chloro-4-fluorophenyl)-3-phenylprop-2-enamide (20).

Author Contributions: J.K., T.S. and F.D. synthesized the compounds. M.O., T.J., M.H. analyzed the compounds. H.M. and J.H. performed biological screening. J.J. designed the compounds. A.B., V.K., A.S. (Adam Smolinski) and A.S. (Aleksandra Swietlicka) performed theoretical lipophilicity calculations, PCA, IVE-PLS. A.B. and J.J. wrote the paper. All authors have read and agreed to the published version of the manuscript.

Funding: This study was supported by the Slovak Research and Development Agency (APVV-17-0373) and by Palacky University Olomouc (IGA_PrF_2020_023). Knowledge gained within project APVV-0516-12 has been used in the results. M.O. was supported by SustES (CZ.02.1.01/0.0/0.0/16_019/0000797).

Acknowledgments: We would like to acknowledge the OpenEye and OpenBabel Scientific Software for providing free academic licenses.

Conflicts of Interest: The authors declare no conflict of interest.

References

1. Medzhitov, R. Origin and physiological roles of inflammation. *Nature* **2008**, *454*, 428–435. [[CrossRef](#)]
2. Oehling, A.K. Bacterial infection as an important triggering factor in bronchial asthma. *J. Investig. Allergol. Clin. Immunol.* **1999**, *9*, 6–13.
3. Sreenivasan, P.K.; Gaffar, A. Antibacterials as anti-inflammatory agents: Dual action agents for oral health. *Antonie Van Leeuwenhoek* **2008**, *93*, 227–239. [[CrossRef](#)] [[PubMed](#)]
4. Qiu, C.C.; Caricchio, R.; Gallucci, S. Triggers of autoimmunity: The role of bacterial infections in the extracellular exposure of lupus nuclear autoantigens. *Front. Immunol.* **2019**, *10*, 2608. [[CrossRef](#)] [[PubMed](#)]
5. Van Elsland, D.; Neefjes, J. Bacterial infections and cancer. *EMBO Rep.* **2018**, *19*, e46632. [[CrossRef](#)]
6. Chen, L.; Deng, H.; Cui, H.; Fang, J.; Zuo, Z.; Deng, J.; Li, Y.; Wang, X.; Zhao, L. Inflammatory responses and inflammation-associated diseases in organs. *Oncotarget* **2017**, *9*, 7204–7218. [[CrossRef](#)] [[PubMed](#)]
7. Vasaikar, S.; Bhatia, P.; Bhatia, P.G.; Yaiw, K.C. Complementary approaches to existing target based drug discovery for identifying novel drug targets. *Biomedicines* **2016**, *4*, 27. [[CrossRef](#)] [[PubMed](#)]
8. Ul Islam, N.; Amin, R.; Shahid, M.; Amin, M.; Zaib, S.; Iqbal, J. A multi-target therapeutic potential of *Prunus domestica* gum stabilized nanoparticles exhibited prospective anticancer, antibacterial, urease-inhibition, anti-inflammatory and analgesic properties. *BMC Complement. Altern. Med.* **2017**, *17*, 276. [[CrossRef](#)]
9. Brullo, C.; Massa, M.; Rapetti, F.; Alfei, S.; Bertolotto, M.B.; Montecucco, F.; Signorello, M.G.; Bruno, O. New hybrid pyrazole and imidazopyrazole antiinflammatory agents able to reduce ROS production in different biological targets. *Molecules* **2020**, *25*, 899. [[CrossRef](#)]

10. Ramsay, R.R.; Popovic-Nikolic, M.R.; Nikolic, K.; Uliassi, E.; Bolognesi, M.L. A perspective on multi-target drug discovery and design for complex diseases. *Clin. Transl. Med.* **2018**, *7*, 3. [CrossRef]
11. Bolognesi, M.L. Polypharmacology in a single drug: Multitarget drugs. *Curr. Med. Chem.* **2013**, *20*, 1639–1645. [CrossRef] [PubMed]
12. Talevi, A. Multi-target pharmacology: Possibilities and limitations of the “skeleton key approach” from a medicinal chemist perspective. *Front. Pharmacol.* **2015**, *6*, 205. [CrossRef] [PubMed]
13. Bräse, S. *Privileged Scaffolds in Medicinal Chemistry: Design, Synthesis, Evaluation*; Royal Society of Chemistry: Cambridge, UK, 2016.
14. Gaikwad, N.; Nanduri, S.; Madhavi, Y.V. Cinnamamide: An insight into the pharmacological advances and structure-activity relationships. *Eur. J. Med. Chem.* **2019**, *181*, 111561. [CrossRef] [PubMed]
15. Das, A.B.; Goud, V.V.; Das, C. Phenolic compounds as functional ingredients in beverages. In *Value-Added Ingredients and Enrichments of Beverages*; Grumezescu, A.M., Holban, A.M., Eds.; Woodhead Publishing: Duxford, UK; Elsevier: Duxford, UK, 2019; pp. 285–323.
16. Sharma, P. Cinnamic acid derivatives: A new chapter of various pharmacological activities. *J. Chem. Pharm. Res.* **2011**, *3*, 403–423.
17. Peperidou, A.; Kapoukranidou, D.; Kontogiorgis, C.; Hadjipavlou-Litina, D. Multitarget molecular hybrids of cinnamic acids. *Molecules* **2014**, *19*, 20197–20226. [CrossRef]
18. Peperidou, A.; Pontiki, E.; Hadjipavlou-Litina, D.; Voulgari, E.; Avgoustakis, K. Multifunctional cinnamic acid derivatives. *Molecules* **2017**, *22*, 1247. [CrossRef]
19. Guzman, J.D. Natural cinnamic acids, synthetic derivatives and hybrids with antimicrobial activity. *Molecules* **2014**, *19*, 19292–19349. [CrossRef]
20. Lima, T.C.; Ferreira, A.R.; Silva, D.F.; Lima, E.O.; de Sousa, D.P. Antifungal activity of cinnamic acid and benzoic acid esters against *Candida albicans* strains. *Nat. Prod. Res.* **2018**, *32*, 572–575. [CrossRef]
21. Dolab, J.G.; Lima, B.; Spaczynska, E.; Kos, J.; Cano, N.H.; Feresin, G.; Tapia, A.; Garibotto, F.; Petenatti, E.; Olivella, M.; et al. Antimicrobial activity of *Annona emarginata* (Schltdl.) H. Rainer and most active isolated compound against clinically important bacteria. *Molecules* **2018**, *23*, 1187. [CrossRef]
22. Pontiki, E.; Peperidou, A.; Fotopoulos, I.; Hadjipavlou-Litina, D. Cinnamate hybrids: A unique family of compounds with multiple biological activities. *Curr. Pharm. Biotechnol.* **2018**, *19*, 1019–1048. [CrossRef]
23. Silva, A.T.; Bento, C.M.; Pena, A.C.; Figueiredo, L.M.; Prudencio, C.; Aguiar, L.; Silva, T.; Ferraz, R.; Gomes, M.S.; Teixeira, C.; et al. Cinnamic acid conjugates in the rescuing and repurposing of classical antimalarial drugs. *Molecules* **2019**, *25*, 66. [CrossRef]
24. Martinez, M.D.; Riva, D.A.; Garcia, C.; Duran, F.J.; Burton, G. Synthesis and antibacterial activity of difluoromethyl cinnamoyl amides. *Molecules* **2020**, *25*, 789. [CrossRef] [PubMed]
25. Fungicide Resistance Action Committee. *FRAC Code List© 2020: Fungal Control Agents Sorted by Cross Resistance Pattern and Mode of Action*; Fungicide Resistance Action Committee, CropLife International: Brussels, Belgium, 2020.
26. Pospisilova, S.; Kos, J.; Michnova, H.; Kapustikova, I.; Strharsky, T.; Oravec, M.; Moricz, A.M.; Bakonyi, J.; Kauerova, T.; Kollar, P.; et al. Synthesis and spectrum of biological activities of novel *N*-arylcinnamamides. *Int. J. Mol. Sci.* **2018**, *19*, 2318. [CrossRef] [PubMed]
27. Pospisilova, S.; Kos, J.; Michnova, H.; Strharsky, T.; Cizek, A.; Jampilek, J. *N*-Arylcinnamamides as Antistaphylococcal Agents. In Proceedings of the 4th International Electronic Conference on Medicinal Chemistry, ECMC-4, 1–30 November 2018; p. 5576. Available online: <https://sciforum.net/manuscripts/5576/slides.pdf> (accessed on 4 August 2020).
28. Hosek, J.; Kos, J.; Strharsky, T.; Cerna, L.; Starha, P.; Vanco, J.; Travnicek, Z.; Devinsky, F.; Jampilek, J. Investigation of anti-inflammatory potential of *n*-arylcinnamide derivatives. *Molecules* **2019**, *24*, 4531. [CrossRef] [PubMed]
29. Veber, D.F.; Johnson, S.R.; Cheng, H.Y.; Smith, B.R.; Ward, K.W.; Kopple, K.D. Molecular properties that influence the oral bioavailability of drug candidates. *J. Med. Chem.* **2002**, *45*, 2615–2623. [CrossRef] [PubMed]
30. Van de Waterbeemd, H.; Gifford, E. ADMET in silico modeling: Towards prediction paradise? *Nat. Rev. Drug Discov.* **2003**, *2*, 192–204. [CrossRef] [PubMed]
31. Fukunishi, Y.; Nakamura, H. Definition of drug-likeness for compound affinity. *J. Chem. Inf. Model.* **2011**, *51*, 1012–1016. [CrossRef]

32. Lipinski, C.A.; Lombardo, F.; Dominy, B.W.; Feeney, P.J. Experimental and computational approaches to estimate solubility and permeability in drug discovery and development settings. *Adv. Drug Deliv. Rev.* **2001**, *46*, 3–26. [[CrossRef](#)]
33. Bak, A.; Kozik, V.; Smolinski, A.; Jampilek, J. In silico estimation of basic activity-relevant parameters for a set of drug absorption promoters. *SAR QSAR Environ. Res.* **2017**, *28*, 427–449. [[CrossRef](#)]
34. Arnott, J.A.; Planey, S.L. The influence of lipophilicity in drug discovery and design. *Expert Opin. Drug Discov.* **2012**, *7*, 863–875. [[CrossRef](#)]
35. Efremov, R.G.; Chugunov, A.O.; Pyrkov, T.V.; Priestle, J.P.; Arseniev, A.S.; Jacoby, E. Molecular lipophilicity in protein modeling and drug design. *Curr. Med. Chem.* **2007**, *14*, 393–415. [[CrossRef](#)] [[PubMed](#)]
36. Mannhold, R.; Poda, G.I.; Ostermann, C.; Tetko, I.V. Calculation of molecular lipophilicity: State-of-the-art and comparison of logP methods on more than 96,000 compounds. *J. Pharm. Sci.* **2009**, *3*, 861–864. [[CrossRef](#)] [[PubMed](#)]
37. Tetko, I.; Poda, G.I. Application of ALOGPS 2.1 to predict logD distribution coefficient for Pfizer proprietary compounds. *J. Med. Chem.* **2004**, *47*, 5601–5604. [[PubMed](#)]
38. Lipinski, C.A. Lead- and drug-like compounds: The rule-of-five revolution. *Drug Discov. Today Technol.* **2004**, *1*, 337–341. [[CrossRef](#)] [[PubMed](#)]
39. Kah, M.; Brown, C.D. LogD: Lipophilicity for ionisable compounds. *Chemosphere* **2008**, *72*, 1401–1408. [[CrossRef](#)] [[PubMed](#)]
40. Bhal, S.K.; Kassam, K.; Peirson, I.G.; Pearl, G.M. The rule of five revisited: Applying logD in place of logP in drug-likeness filters. *Mol. Pharm.* **2007**, *40*, 556–560. [[CrossRef](#)]
41. Xing, L.; Glen, C. Novel methods for the prediction of logP, pKa and logD. *J. Chem. Inf. Comput. Sci.* **2002**, *42*, 796–805. [[CrossRef](#)]
42. Rupp, M.; Körner, R.; Tetko, I.V. Predicting the pKa of small molecules. *Comb. Chem. High Throughput Screen.* **2011**, *14*, 307–327. [[CrossRef](#)]
43. Zadrazilova, I.; Pospisilova, S.; Masarikova, M.; Imramovsky, A.; Ferriz, J.M.; Vinsova, J.; Cizek, A.; Jampilek, J. Salicylanilide carbamates: Promising antibacterial agents with high in vitro activity against methicillin-resistant *Staphylococcus aureus* (MRSA). *Eur. J. Pharm. Sci.* **2015**, *77*, 197–207. [[CrossRef](#)]
44. International Organization for Standardization. *ISO 10993-5:2009 Biological Evaluation of Medical Devices Part 5: Tests for In Vitro Cytotoxicity*; International Organization for Standardization: Geneva, Switzerland, 2009; last revision 2017.
45. Grella, E.; Kozłowska, J.; Grabowiecka, A. Current methodology of MTT assay in bacteria—A review. *Acta Histochem.* **2018**, *120*, 303–311. [[CrossRef](#)]
46. Bender, A.; Scheiber, J.; Jenkins, J.L.; Sukuru, S.C. How similar are similarity searching methods? A principal component analysis of molecular descriptor space. *J. Chem. Inf. Model.* **2009**, *49*, 108–119. [[CrossRef](#)]
47. Fialkowski, M.; Bishop, K.J.M.; Chubukov, V.A.; Campbell, C.J.; Grzybowski, B.A. Architecture and evolution of organic chemistry. *Angew. Chem. Int. Ed.* **2005**, *44*, 7263–7269. [[CrossRef](#)] [[PubMed](#)]
48. Bak, A.; Pizova, H.; Kozik, V.; Vorcakova, K.; Kos, J.; Tremel, J.; Odehnalova, K.; Oravec, M.; Imramovsky, A.; Bobal, P.; et al. SAR-mediated similarity assessment of the property profile for new, silicon-based AChE/BChE inhibitors. *Int. J. Mol. Sci.* **2019**, *20*, 5385. [[CrossRef](#)] [[PubMed](#)]
49. Bak, A.; Kozik, V.; Malik, I.; Jampilek, J.; Smolinski, A. Probability-driven 3D pharmacophore mapping of antimycobacterial potential of hybrid molecules combining phenylcarbamoyloxy and N-arylpiperazine fragments. *SAR QSAR Environ. Res.* **2018**, *29*, 801–821. [[CrossRef](#)]
50. Pizova, H.; Havelkova, M.; Stepankova, S.; Bak, A.; Kauerova, T.; Kozik, V.; Oravec, M.; Imramovsky, A.; Kollar, P.; Bobal, P.; et al. Proline-based carbamates as cholinesterase inhibitors. *Molecules* **2017**, *22*, 1969. [[CrossRef](#)]
51. Martel, S.; Gillerat, F.; Carosati, E.; Maiarelli, D.; Tetko, I.V.; Mannhold, R.; Carrupt, P.A. Large, chemically diverse dataset of logP measurements for benchmarking studies. *Eur. J. Pharm. Sci.* **2013**, *48*, 21–29. [[CrossRef](#)] [[PubMed](#)]
52. Tetko, I.V. Computing chemistry on the web. *Drug Discov. Today* **2005**, *10*, 1497–1500. [[CrossRef](#)]
53. Peltason, L.; Bajorath, J. Systematic computational analysis of structure-activity relationships: Concepts, challenges and recent advances. *Future Med. Chem.* **2009**, *1*, 451–466. [[CrossRef](#)]
54. Maggiora, G.M.; Shanmugasundaram, V. Molecular similarity measures. *Methods Mol. Biol.* **2011**, *672*, 39–100. [[PubMed](#)]

55. Holliday, J.D.; Salim, N.; Whittle, M.; Willett, P. Analysis and display of the size dependence of chemical similarity coefficients. *J. Chem. Inf. Comput. Sci.* **2003**, *43*, 819–828. [[CrossRef](#)] [[PubMed](#)]
56. Rozas, I.; Du, Q.; Arteca, G.A. Interrelation between electrostatic and lipophilicity potentials on molecular surfaces. *J. Mol. Graph.* **1995**, *13*, 98–108. [[CrossRef](#)]
57. Zupan, J.; Gasteiger, J. *Neural Networks and Drug Design for Chemists*, 2nd ed.; Wiley-VCH: Weinheim, Germany, 1999.
58. Bak, A.; Wyszomirski, M.; Magdziarz, T.; Smolinski, A.; Polanski, J. Structure-based modeling of dye-fiber affinity with SOM-4D-QSAR paradigm: Application to set of anthraquinone derivatives. *Comb. Chem. High Throughput Screen.* **2014**, *17*, 485–502. [[CrossRef](#)]
59. Michnova, H.; Pospisilova, S.; Gonec, T.; Kapustikova, I.; Kollar, P.; Kozik, V.; Musiol, R.; Jendrzewska, I.; Vanco, J.; Travnicek, Z.; et al. Bioactivity of methoxylated and methylated 1-hydroxynaphthalene-2-carboxanilides: Comparative molecular surface analysis. *Molecules* **2019**, *24*, 2991. [[CrossRef](#)] [[PubMed](#)]
60. Bak, A.; Polanski, J. Modeling robust QSAR 3: SOM-4D-QSAR with iterative variable elimination IVE-PLS: Application to steroid, azo dye, and benzoic acid series. *J. Chem. Inf. Model.* **2007**, *47*, 1469–1480. [[CrossRef](#)] [[PubMed](#)]
61. Polanski, J.; Bak, A.; Gieleciak, R.; Magdziarz, T. Modeling robust QSAR. *J. Chem. Inf. Model.* **2003**, *46*, 2310–2318. [[CrossRef](#)] [[PubMed](#)]
62. Bak, A.; Kozik, V.; Smolinski, A.; Jampilek, J. Multidimensional (3D/4D-QSAR) probability-guided pharmacophore mapping: Investigation of activity profile for a series of drug absorption promoters. *RSC Adv.* **2016**, *6*, 76183–76205. [[CrossRef](#)]
63. Bak, A.; Kozik, V.; Kozakiewicz, D.; Gajcy, K.; Strub, D.J.; Swietlicka, A.; Stepankova, S.; Imramovsky, A.; Polanski, J.; Smolinski, A.; et al. Novel benzene-based carbamates for AChE/BChE inhibition: Synthesis and ligand/structure-oriented SAR study. *Int. J. Mol. Sci.* **2019**, *20*, 1524. [[CrossRef](#)]
64. Xie, X.Q.; Chen, J.Z. Data mining a small molecule drug screening representative subset from NIH PubChem. *J. Chem. Inf. Model.* **2008**, *48*, 465–475. [[CrossRef](#)]

Sample Availability: Samples of the compounds are available from the authors.



© 2020 by the authors. Licensee MDPI, Basel, Switzerland. This article is an open access article distributed under the terms and conditions of the Creative Commons Attribution (CC BY) license (<http://creativecommons.org/licenses/by/4.0/>).

č.	citace	ISSN
17	CAMPOS, LE, F GARIBOTTO, E ANGELINA, J KOS , T GONEC, P MARVANNOVA, M VETTORAZZI, M ORAVEC, I JENDRZEJEWSKA, J JAMPILEK, SE ALVAREZ a RD ENRIZ. Hydroxynaphthalenecarboxamides and substituted piperazinypropandiols, two new series of BRAF inhibitors. A theoretical and experimental study. <i>BIOORGANIC CHEMISTRY</i> [online]. 2020, 103 . Dostupné z: doi: 10.1016/j.bioorg.2020.104145	0045-2068



ELSEVIER

Contents lists available at ScienceDirect

Bioorganic Chemistry

journal homepage: www.elsevier.com/locate/bioorg

Hydroxynaphthalenecarboxamides and substituted piperazinypropandiols, two new series of BRAF inhibitors. A theoretical and experimental study

Ludmila E. Campos^a, Francisco Garibotto^a, Emilio Angelina^b, Jiri Kos^c, Tomas Gonec^d,
 Pavlina Marvanova^d, Marcela Vettorazzi^a, Michal Oravec^e, Izabela Jendrzewska^f,
 Josef Jampilek^c, Sergio E. Alvarez^{a,*}, Ricardo D. Enriz^{a,*}

^a Facultad de Química, Bioquímica y Farmacia, Universidad Nacional de San Luis, Instituto Multidisciplinario de Investigaciones Biológicas (IMIBIO-SL), Ejército de los Andes 950, 5700 San Luis, Argentina

^b Laboratorio de Estructura Molecular y Propiedades, Área de Química Física, Departamento de Química, Facultad de Ciencias Exactas y Naturales y Agrimensura, Universidad Nacional del Nordeste, Avda. Libertad 5460, (3400) Corrientes, Argentina

^c Regional Centre of Advanced Technologies and Materials, Faculty of Science, Palacky University, Slechtitelu 27, 78371 Olomouc, Czech Republic

^d Department of Chemical Drugs, Faculty of Pharmacy, Masaryk University, Palackeho 1, 612 00 Brno, Czech Republic

^e Global Change Research Institute CAS, Belidla 986/4a, 603 00 Brno, Czech Republic

^f Institute of Chemistry, University of Silesia, Szkolna 9, 40007 Katowice, Poland

ARTICLE INFO

Keywords:

BRAF inhibitors
 Melanoma
 Molecular modeling
 Cell viability
 ERK phosphorylation

ABSTRACT

The oncogenic mutated kinase BRAF^{V600E} is an attractive molecular target because it is expressed in several human cancers, including melanoma. To present, only three BRAF small inhibitors are approved by the FDA for the treatment of patients with metastatic melanoma: Vemurafenib, Dabrafenib and Encorafenib. Although many protocol treatments have been probed in clinical trials, BRAF inhibition has a limited effectiveness because patients invariably develop resistance and secondary toxic effects associated with the therapy. These limitations highlight the importance of designing new and better inhibitors with different structures that could establish different interactions in the active site of the enzyme and therefore decrease resistance progress.

Considering the data from our previous report, here we studied two series of derivatives of structural scaffolds as potential BRAF inhibitors: hydroxynaphthalenecarboxamides and substituted piperazinypropandiols. Our results indicate that structural analogues of substituted piperazinypropandiols do not show significantly better activities to that previously reported. In contrast, the hydroxynaphthalenecarboxamides derivatives significantly inhibited cell viability and ERK phosphorylation, a measure of BRAF activity, in Lu1205 BRAF^{V600E} melanoma cells. In order to better understand these experimental results, we carried out a molecular modeling study using different combined techniques: docking, MD simulations and quantum theory of atoms in molecules (QTAIM) calculations. Thus, by using this approach we determined that the molecular interactions that stabilize the different molecular complexes are closely related to Vemurafenib, a well-documented BRAF inhibitor. Furthermore, we found that bi-substituted compounds may interact more strongly respect to the mono-substituted analogues, by establishing additional interactions with the DFG-loop at the BRAF-active site. On the bases of these results we synthesized and tested a new series of hydroxynaphthalenecarboxamides bi-substituted. Remarkably, all these compounds displayed significant inhibitory effects on the bioassays performed. Thus, the structural information reported here is important for the design of new BRAF^{V600E} inhibitors possessing this type of structural scaffold.

1. Introduction

After the publication in 2002 of the first article describing an oncogenic BRAF mutant protein [1,2], intense efforts have been centered in the development of selective and potent BRAF inhibitors. Certainly, US Food and Drug Administration (FDA) support the use of two

BRAF^{V600E} inhibitors for the treatment of metastatic melanoma: Vemurafenib (Zelboraf) and Dabrafenib (Tafinlar), approved in 2011 and 2013, respectively [3,4]. Although both drugs showed an impressive success rate in melanoma patients, durability of response remains an issue because the tumor quickly becomes resistant [5]. On the other hand, many cancers are intrinsically resistant to these compounds or

* Corresponding authors.

E-mail addresses: sealvarez98@gmail.com (S.E. Alvarez), denriz@unsl.edu.ar (R.D. Enriz).

<https://doi.org/10.1016/j.bioorg.2020.104145>

Received 16 April 2020; Received in revised form 17 June 2020; Accepted 24 July 2020

Available online 28 July 2020

0045-2068/ © 2020 Elsevier Inc. All rights reserved.

show limited benefits. For example, it has been shown that colorectal and thyroid BRAF^{V600E} tumors are resistant to Vemurafenib and Dabrafenib [6,7]. Recently, on the basis of COLUMBUS trial, FDA has approved a new BRAF inhibitor named Encorafenib (Array Biopharma) administered with a MEK inhibitor for the treatment of metastatic melanoma [8,9].

In the past few years, a large number of new BRAF inhibitors have been developed [10]. Intense investigations on the biochemical and cellular effects of these new BRAF inhibitors have enlarged our understanding on their mechanisms of action [11]. It has been widely reported that BRAF inhibitors induce allosteric structural rearrangements, locking their target kinases in discrete conformations and resemble inactive or active kinase states of the α C-helix and DFG motif [12,13]. Such conformations allow to classify inhibitors as type I (α C-helix-IN/DFG-IN), type II (α C-helix-IN/DFG-OUT), or type II/2 (α C-helix-OUT/DFG-IN) [14,15]. Both Vemurafenib and Dabrafenib belong to type II/2 inhibitors. A recent work from Agianian and Gavathiotis show the different zones in which BRAF inhibitors would be linked [16]. Moreover, a large number of structures have been classified as first, second and third generation BRAF inhibitors.

Although BRAF is an excellent molecular target for searching new anticancer agents, its anomalous or unusual behavior implies a severe drawback for the development of new inhibitors [17–19]. While the inhibitors suppressed tumors harboring BRAF^{V600E} or other BRAF mutants, they paradoxically activate RAF activity and downstream ERK signaling (RAF inhibitor paradox or “paradoxical activation”) in tumors expressing BRAF wild type (BRAF^{WT}) [20,21]. The general consensus is that type I inhibitors exhibit more paradoxical activation, followed by type II and type II/2. The model of “paradoxical activation” described above explains the clinical effectiveness of the current FDA approved α C-OUT RAF inhibitors Vemurafenib and Dabrafenib [22]. Moreover, paradox breakers constitute a new class of BRAF inhibitors that could inhibit BRAF^{V600E} but not promotes paradoxical activation of MAPK signaling [23]. Encorafenib is the latest BRAF inhibitor FDA-approved, and in fact has shown significantly less paradoxical effects compared to Vemurafenib and Dabrafenib in patients treated with these drugs [24]. These evidences point that the rational design of new BRAF inhibitors with different structural scaffolds may establish distinct interactions with the enzyme and hence reduce resistance and paradoxical effects in order to achieve a durable response.

It is clearly evident that new BRAF inhibitors with different structural scaffolds that can bind to the enzyme in a different manner are needed. Certainly, we have recently reported a study conducted through a virtual screening in which we found three different structural scaffolds with significant inhibitory activities on BRAF [25]. These series are: 1*H*-pyrrol-2-ylcarbonylamino-1,3-benzothiazol-2-ylamino oxo carboxylic acids (Fig. 1, compounds type A), substituted piperazinylpropanediols (Fig. 1, compounds Type B) and hydroxynaphthalenecarboxamides (Fig. 1, compounds type C). From these three series of compounds, molecules 3 and 22 shown in Fig. 1 exhibited the most significant inhibitory effect. Here, we report a deeper study on two of these series by using several analogues of compounds 3 and 22. Using molecular modeling studies we established a structure–activity relationship in these series of compounds. In addition, to gain a better understanding of the mechanisms of action at molecular level, we have carried out an exhaustive study about molecular interactions that stabilize the different ligand–receptor (L-R) complexes. Such information is of great value to perform future structural changes in these compounds that could potentially improve their affinity with the enzyme.

2. Experimental section

2.1. Chemistry

All reagents were purchased from Merck (Sigma-Aldrich, St. Louis,

MO, USA) and Alfa (Alfa-Aesar, Ward Hill, MA, USA). Reactions were performed using a CEM Discover SP microwave reactor (CEM, Matthews, NC, USA). TLC experiments were performed on alumina-backed silica gel 40 F254 plates (Merck, Darmstadt, Germany). The plates were illuminated under UV (254 nm) and evaluated in iodine vapour. Melting points were determined on a Koflerhot-plate apparatus (HMK Franz KustnerNacht BG, Dresden, Germany) and are uncorrected. Infrared (IR) spectra were recorded on a Smart MIRacle ATR ZnSe for Nicolet Impact 410 FT-IR spectrometer (Thermo Scientific, West Palm Beach, FL, USA). The spectra were obtained by the accumulation of 64 scans with 2 cm⁻¹ resolution in the region of 4000–650 cm⁻¹. All ¹H- and ¹³C NMR spectra were recorded on a JEOL JNM-ECA 600II NMR spectrometer (600 MHz for ¹H and 150 MHz for ¹³C, Jeol, Tokyo, Japan) in dimethyl sulfoxide-*d*₆ (DMSO-*d*₆), ¹H and ¹³C chemical shifts (δ) are reported in ppm. Mass spectra were measured using a LTQ Orbitrap Hybrid Mass Spectrometer (Thermo Electron Corporation) with direct injection into an APCI source (400 °C) in the positive or negative mode.

1-(3-{4-[(Butoxycarbonyl)amino]benzoyloxy}-2-hydroxypropyl)-4-phenylpiperazin-1-ium chloride (3) was described by Vettoraziet *al* [26]. 1-{2-Hydroxy-3-[(4-alkoxybenzoyl)oxy]propyl}-4-arylpiperazinediium dichlorides compounds 4–7 were published by Marvanovaet *al* [27] and 1-(2-hydroxy-3-[(4-(2-propoxyethoxy)benzoyl)oxy]propyl)-4-phenylpiperazinediium dichloride (compound 8) was published by Marvanovaet *al* [28]. Described anilides 9–11 [29], 12 [30], 15–17 [31], 18 and 19 [32], and 20–25 [33] were characterized recently.

General procedures for synthesis of *N*-(substituted phenyl)naphthalene-carboxamides. The appropriate naphthalenecarboxylic acid (5.3 mM) was suspended in dry chlorobenzene (30 mL) at ambient temperature and phosphorus trichloride (2.7 mM, 0.5 eq.), and the corresponding substituted aniline (5.3 mM, 1 eq.) was added dropwise. The reaction mixture was transferred to the microwave reactor at 130 °C for 40 min, where the synthesis was performed. Then the mixture was cooled to 40 °C, and then the solvent was removed to dryness under reduced pressure. The residue was washed with 2 M HCl. The crude product was recrystallized from EtOH.

***N*-(3,5-Dichlorophenyl)-2-hydroxynaphthalene-1-carboxamide (13).** Yield 67%; mp 246–249 °C; IR (cm⁻¹): 3362, 1646, 1586, 1538, 1514, 1448, 1436, 1403, 1352, 1312, 1299, 1262, 1231, 1211, 1114, 1066, 838, 806, 795, 745, 665; ¹H NMR (DMSO-*d*₆), δ : 10.77 (s, 1H), 10.26 (s, 1H), 7.90 (d, 2H, *J* = 4.4 Hz), 7.86 (d, 2H, *J* = 7.7 Hz), 7.67 (d, 1H, *J* = 8.4 Hz), 7.48 (td, 1H, *J* = 7.8, *J* = 1.1 Hz), 7.34 (td, 1H, *J* = 7.5 Hz, *J* = 1.1 Hz), 7.33 (s, 1H), 7.26 (d, 1H, *J* = 8.8 Hz); ¹³C NMR (DMSO-*d*₆), δ : 166.42, 151.87, 141.81, 134.14, 131.18, 130.66, 128.04, 127.34, 127.23, 123.19, 123.17, 122.54, 118.28, 117.70, 117.32; HR-MS: for C₁₇H₁₀NO₂Cl₂[M-H]⁺ calculated 330.00831 *m/z*, found 330.00946 *m/z*.

2-Hydroxy-*N*-(3,4,5-trichlorophenyl)naphthalene-1-carboxamide (14). Yield 69%; mp 182–186 °C; IR (cm⁻¹): 3359, 3275, 1646, 1625, 1579, 1567, 1511, 1505, 1434, 1382, 1372, 1302, 1273, 1235, 1189, 1151, 966, 855, 810, 787, 749, 699, 867, 657; ¹H NMR (DMSO-*d*₆), δ : 10.82 (s, 1H), 10.27 (br. s, 1H), 8.08 (s, 2H), 7.88 (t, 2H, *J* = 9.2 Hz), 7.67 (d, 1H, *J* = 8.4 Hz), 7.47 (ddd, 1H, *J* = 8.5 Hz, *J* = 6.8 Hz, *J* = 1.3 Hz), 7.31–7.38 (m, 1H), 7.26 (d, 1H, *J* = 9.0 Hz); ¹³C NMR (DMSO-*d*₆), δ : 166.49, 151.93, 139.50, 132.90, 131.14, 130.78, 128.04, 127.32, 127.26, 123.35, 123.19, 123.16, 119.18, 118.26, 117.48; HR-MS: for C₁₇H₉NO₂Cl₃ [M-H]⁺ calculated 363.96934 *m/z*, found 363.97052 *m/z*.

***N*-[2,4-bis(Trifluoromethyl)phenyl]-6-hydroxynaphthalene-2-carboxamide (26).** Yield 42%; mp 167–169 °C; IR (cm⁻¹): 3304, 1654, 1628, 1529, 1343, 1314, 1279, 1253, 1182, 1166, 1118, 1080, 1056, 914, 861, 841, 803, 764, 742, 675, 654; ¹H NMR (DMSO-*d*₆), δ : 10.38 (s, 1H), 10.15 (br. s, 1H), 8.48 (s, 1H), 8.15 (d, *J* = 8.9 Hz, 1H), 8.13 (s, 1H), 7.94 (d, *J* = 8.9 Hz, 1H), 7.92 (dd, *J* = 8.6 Hz, *J* = 1.7 Hz, 1H), 7.89 (d, *J* = 8.2 Hz, 1H), 7.83 (d, *J* = 8.2 Hz, 1H), 7.22 (d, *J* = 2.1 Hz,

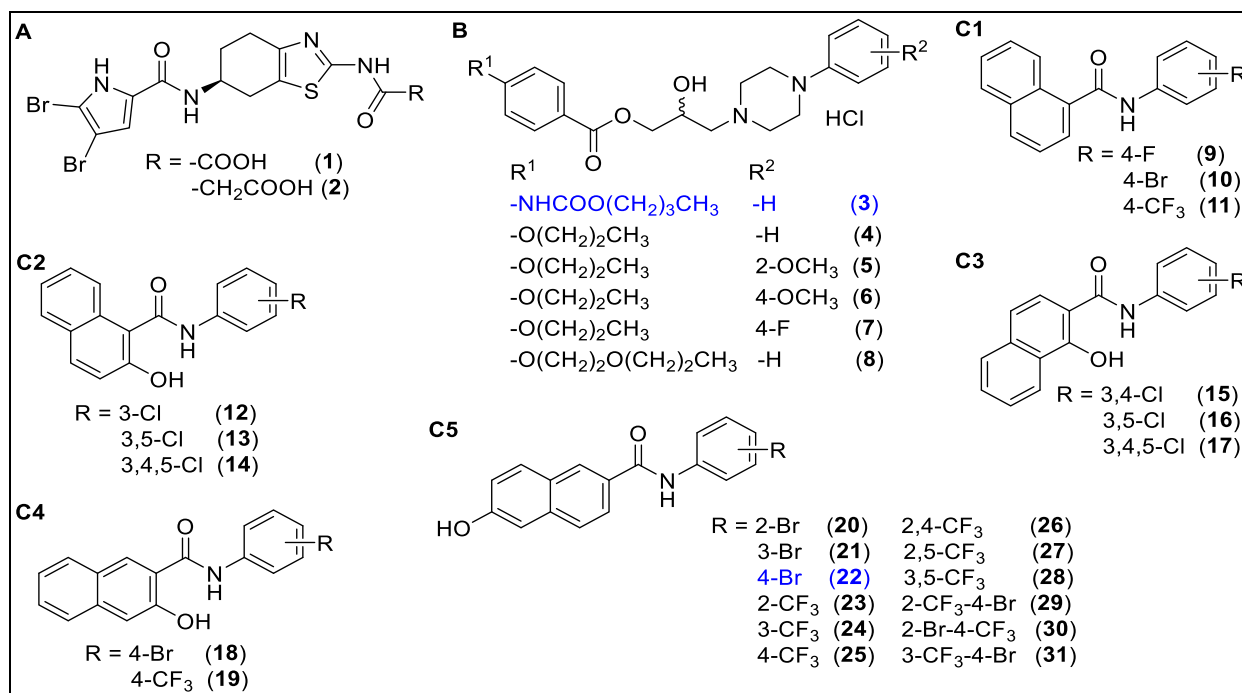


Fig. 1. Structures of investigated compounds.

1H), 7.20 (dd, $J = 8.9$ Hz, $J = 2.1$ Hz, 1H); ¹³C NMR (DMSO-*d*₆), δ : 166.56, 157.34, 140.14, 136.53, 131.99, 130.88, 130.13 (q, $J = 2.9$ Hz), 128.46, 127.47, 127.44 (q, $J = 33.2$ Hz), 126.67 (q, $J = 30.3$ Hz), 126.56, 126.30, 124.47, 123.99–123.87 (m, 1C), 123.40 (q, $J = 271.7$), 122.89 (q, $J = 273.1$), 119.70, 108.72; HR-MS: for C₁₉H₁₀NO₂F₆ [M-H]⁻ calculated 398.06212 *m/z*, found 398.06271 *m/z*.

N-[2,5-bis(Trifluoromethyl)phenyl]-6-hydroxynaphthalene-2-carboxamide (27). Yield 49%; mp179–180 °C; IR (cm⁻¹): 3361, 1609, 1591, 1534, 1494, 1433, 1393, 1336, 1313, 1284, 1260, 1181, 1121, 1085, 1042, 935, 870, 861, 835, 750; ¹H NMR (DMSO-*d*₆), δ : 10.38 (s, 1H), 10.14 (s, 1H), 8.48 (s, 1H), 8.07 (d, $J = 8.2$ Hz, 1H), 8.03 (s, 1H), 7.94–7.92 (m, 3H), 7.82 (d, 1H), 7.22–7.19 (m, 2H); ¹³C NMR (DMSO-*d*₆), δ : 168.71, 157.30, 137.30, 136.51, 133.18 (q, $J = 33.2$ Hz), 130.86, 129.89 (q, $J = 30.3$ Hz), 128.42, 128.26 (q, $J = 4.3$ Hz), 127.93–127.85 (m, 1C), 127.52, 128.55, 126.25, 124.51, 124.13–124.05 (m, 1C), 123.18 (q, $J = 273.1$ Hz), 122.94 (q, $J = 274.6$ Hz), 119.68, 108.72; HR-MS: for C₁₉H₁₀NO₂F₆ [M-H]⁻ calculated 398.06212 *m/z*, found 398.06243 *m/z*.

N-[3,5-bis(Trifluoromethyl)phenyl]-6-hydroxynaphthalene-2-carboxamide (28). Yield 46%; mp214–215 °C; IR (cm⁻¹): 3325, 3124, 1628, 1561, 1473, 1427, 1374, 1273, 1200, 1166, 1129, 950, 932, 885, 841, 824, 809, 697, 682, 662; ¹H NMR (DMSO-*d*₆), δ : 10.88 (s, 1H), 10.17 (s, 1H), 8.57 (s, 2H), 8.53 (d, $J = 0.9$ Hz, 1H), 7.96–7.94 (m, 2H), 7.83 (d, $J = 8.7$ Hz, 1H), 7.80 (s, 1H), 7.22–7.19 (m, 2H); ¹³C NMR (DMSO-*d*₆), δ : 166.34, 157.47, 141.37, 136.60, 130.89, 130.65 (q, $J = 33.2$ Hz), 128.49, 127.82, 126.49, 126.34, 124.50, 123.34 (q, $J = 273.1$ Hz), 119.80–119.70 (m, 2C), 116.20–116.06 (m, 1C), 108.77; HR-MS: for C₁₉H₁₀NO₂F₆ [M-H]⁻ calculated 398.06212 *m/z*, found 398.06268 *m/z*.

N-[4-Bromo-2-(trifluoromethyl)phenyl]-6-hydroxynaphthalene-2-carboxamide (29). Yield 45%; mp209–211 °C; IR (cm⁻¹): 3260, 1613, 1577, 1519, 1502, 1475, 1435, 1407, 1394, 1355, 1297, 1286, 1266, 1200, 1164, 1115, 1049, 909, 887, 859, 819, 808, 764, 726, 681; ¹H NMR (DMSO-*d*₆), δ : 10.20 (s, 1H), 10.12 (s, 1H), 8.46 (s, 1H), 8.00 (d, $J = 1.8$ Hz, 1H), 7.96 (dd, $J = 8.7$ Hz, 2.3 Hz, 1H), 7.92 (d, $J = 8.7$ Hz, 1H), 7.90 (dd, $J = 8.2$ Hz, $J = 1.4$ Hz, 1H), 7.81 (d, $J = 8.7$ Hz, 1H), 7.55 (d, $J = 8.2$ Hz, 1H), 7.21–7.17 (m, 2H); ¹³C

NMR (DMSO-*d*₆), δ : 166.49, 157.23, 136.43, 136.09, 135.57 (q, $J = 1.9$ Hz), 133.35, 130.83, 129.28 (q, $J = 5.8$ Hz), 128.31, 127.86 (q, $J = 29.9$ Hz), 127.66, 126.56, 126.22, 124.47, 122.67 (q, $J = 273.6$ Hz), 119.64, 119.63, 108.69; HR-MS: for C₁₈H₁₀O₂NBrF₃ [M-H]⁻ calculated 407.98524 *m/z*, found 407.98630 *m/z*.

N-[2-Bromo-4-(trifluoromethyl)phenyl]-6-hydroxynaphthalene-2-carboxamide (30). Yield 42%; mp184–186 °C; IR (cm⁻¹): 3263, 1662, 1680, 1579, 1521, 1486, 1471, 1436, 1393, 1317, 1263, 1195, 1165, 1117, 1076, 1041, 966, 945, 887, 879, 863, 834, 805, 742, 687; ¹H NMR (DMSO-*d*₆), δ : 10.21 (s, 1H), 10.15 (s, 1H), 8.53 (s, 1H), 8.12 (d, $J = 0.9$ Hz, 1H), 7.96–7.91 (m, 3H), 7.83 (d, $J = 8.7$ Hz, 2H), 7.22–7.18 (m, 2H); ¹³C NMR (DMSO-*d*₆), δ : 165.53, 157.36, 140.75, 136.55, 130.91, 129.66 (q, $J = 3.9$ Hz), 128.51, 128.25, 127.62, 127.34 (q, $J = 32.8$ Hz), 126.57, 126.32, 125.15 (q, $J = 3.9$ Hz), 124.48, 123.29 (q, $J = 273.6$ Hz), 119.86, 119.69, 108.72; HR-MS: for C₁₈H₁₀O₂NBrF₃ [M-H]⁻ calculated 407.98524 *m/z*, found 407.98571 *m/z*.

N-[4-Bromo-3-(trifluoromethyl)phenyl]-6-hydroxynaphthalene-2-carboxamide (31). Yield 60%; mp198–201 °C; IR (cm⁻¹): 3353, 3282, 1664, 1632, 1601, 1538, 1506, 1428, 1315, 1266, 1237, 12008, 1174, 1133, 1123, 1020, 908, 887, 870, 836, 802, 764, 742, 715, 672, 648; ¹H NMR (DMSO-*d*₆), δ : 10.68 (s, 1H), 10.14 (s, 1H), 8.49 (s, 1H), 8.4 (d, $J = 2.7$ Hz, 1H), 8.09 (dd, $J = 8.7$ Hz, $J = 2.3$ Hz, 1H), 7.94 (d, $J = 8.7$ Hz, 1H), 7.93 (dd, $J = 8.7$ Hz, $J = 1.8$ Hz, 1H), 7.87 (d, $J = 9.1$ Hz, 1H), 7.82 (d, $J = 8.7$ Hz, 1H), 7.21–7.18 (m, 2H); ¹³C NMR (DMSO-*d*₆), δ : 166.09, 157.35, 139.40, 136.48, 135.40, 130.87, 128.44 (q, $J = 30.8$ Hz), 128.35, 128.16, 126.51, 126.27, 124.88, 124.55, 122.94 (q, $J = 272.6$ Hz), 119.69, 119.18 (q, $J = 5.8$ Hz), 111.65 (q, $J = 1.9$ Hz), 108.74; HR-MS: for C₁₈H₁₀O₂NBrF₃ [M-H]⁻ calculated 407.98524 *m/z*, found 407.98549 *m/z*.

2.2. Bioassays

2.2.1. Reagents

Stock solutions of Vemurafenib and compounds tested in the present work were prepared in sterile DMSO, properly aliquoted and preserved at -20 °C. Vemurafenib was included in all the experiments as a

positive control of pERK and viability inhibition.

Anti-ERK total (dilution 1/2000) and phospho-ERK (T202-Y204, dilution 1/1000) antibodies were obtained from Cell Signaling (Danvers, MA, USA) and prepared in TBS buffer (20 mM Tris pH 7.4 and 0.9% NaCl) supplemented with 5% BSA (bovine serum albumin) and 0.1% Tween-20. Secondary antibodies conjugated to near-infrared fluorochromes (IRD, dilution 1/30.000) were from Li-COR (Lincoln, NE, USA) and prepared as indicated [25].

A stock solution of 5 mg/mL of MTT (3-(4,5-Dimethyl-2-thiazolyl)-2,5-diphenyl-2H-tetrazolium bromide, Sigma Aldrich) viability reagent was prepared freshly in PBS by five consecutive cycles of 15' vortexing and 2' sonication. After centrifugation at 12.000 xg, 4 °C for 10', the supernatant was recovered and MTT reagent diluted 1:10 in DMEM serum free and stored at 4 °C as described previously [25].

2.2.2. Cell culture

Lu1205 BRAF^{V600E} (mutant) melanoma cells were used to perform all the bioassays. Cells were cultured in Dulbecco's Modified Eagle's Media (DMEM, Gibco) supplemented with 10% of fetal bovine serum (Natocor), as described previously [25]. Cells were obtained from Dr. Pablo Bergami (Universidad de Maimónides, Buenos Aires, Argentina).

2.2.3. Western blot

Western blot experiments were performed essentially as described [25]. Briefly, 40.000 Lu1205 cells/well were seeded in 12-well plates and grown for 72 h. Medium was replaced by fresh medium containing the compound (1 and 10 μM), and cells cultured for 2 additional hours at 37 °C. Cells were washed with ice-cold PBS and scraped into lysis buffer containing 20 mM Tris-HCl (pH 7.4), 1 mM EDTA, 150 mM NaCl, 1% Triton X-100, 1 mM β-mercaptoethanol, 1 mM Na₃VO₄, and 1:2 protease inhibitor cocktail (Roche). Lysates were incubated on ice for 1 h and centrifuged at 10.000 xg for 15 min to remove cellular debris. Equal amounts of proteins (30 μg) were separated by SDS-PAGE and then transblotted to nitrocellulose, blocked with 3% nonfat dry milk for 1 h at room temperature, and then incubated overnight at 4 °C with specific primary antibodies as indicated in each figure. Immunoreactive signals were detected by 1 h-incubation at room temperature with appropriate secondary antibodies (IRD, Li-COR, 1/30.000). After scanning in Odyssey Clx device, optical densities of pERK bands were quantified and normalized to their respective total ERK bands with Image Studio 5.2 Software.

2.2.4. Cell viability assay

All the viability experiments were performed in sextuplicates for each concentration and each compound as reported [25]. In brief, 5000 Lu1205 cells/well were grown for 18 h in 96-well plates and after that, the medium was replaced by fresh medium containing the indicated compounds (final concentration 1 and 10 μM) or DMSO vehicle and cultured for another 72 h. Lu1205 cells were then incubated for 3 additional hours in 110 μl of 0.5 mg/ml solution of MTT. Formazan was solubilized with DMSO and the concentration detected by absorbance at 540 nm (Epoch). Average absorbance of each treatment (six replicates) was normalized with average absorbance of the respective control.

2.2.5. Statistics

One way-ANOVA analysis and Tukey's post-test were used to determine the significance of western blot and cell viability bioassays.

2.3. Molecular modeling

2.3.1. Docking study

The docking simulations were carried out using AutoDock 4.2 [34]. In all simulations the following parameters were used: initial population of trial ligands was constituted by 250 individuals; maximum number of generations was set to 2.7×10^4 . The maximum number of

energy evaluations was 10.0×10^6 . All other run parameters were maintained at their default setting. The 3D affinity map was a cube which size was chosen depending on the size of the binding pocket of each system. The points were separated by 0.375 Å and centered at the active site of the different molecular targets. The resulting docked conformations were clustered into families by the backbone RMSD (root mean square deviation) of 2 Å. Considering that the docking calculations suggest several modes of binding for each compound and the binding energies between the clusters are similar, the leader of the most populated cluster was selected for further study.

2.3.2. Refinement of the anchoring

After docking calculations, the complexes were refined by performing molecular dynamics simulations. Antechamber Software in the AmberTools package [35] was used to generate the parameters for MD simulations considering ff99SB and GAFF force fields [36,37]. All MD simulations were performed with the Amber 16 software package (All-atoms force field ff99SB) using periodic boundary conditions for constant volume and cubic simulation cells [38]. Each model was soaked in a truncated octahedral periodic box of TIP3P water molecules. The distance between the edges of the water box and the closest atom of the solutes was at least 10 Å. Sodium or chloride ions (depending on the complex) were added to neutralize the charge of the system. The entire system was subjected to energy minimization. The particle mesh Ewald method (PME) [39] was applied using a grid spacing of 1.2 Å, a spline interpolation order of 4 and a real space direct sum cutoff of 10 Å. The SHAKE algorithm was applied allowing for an integration time step of 2 fs. MD simulations were carried out at 310 K temperature. Three MD simulations of 30 ns were conducted for each system under different starting velocity distribution functions; thus, in total 90 ns were simulated for each complex. The NPT ensemble was employed using Berendsen coupling to a baro/thermostat (target pressure 1 atm, relaxation time 0.1 ps). Post MD analysis was carried out with program CPPTRAJ [40].

2.3.3. Binding energy calculations

The MM-PBSA and MM-GBSA protocol was applied to each MD trajectory in order to calculate the relative binding energies of the different complexes. The MM-PBSA and MM-GBSA method was used in a hierarchical strategy, and the details of this method have been presented elsewhere [41]. This protocol was applied to 15,000 equidistant snapshots extracted from the last 25.0 ns of the dynamics in triplicate and was used within the one-trajectory approximation.

Briefly, the binding free energy (ΔG_{bind}) resulting from the formation of a L-R complex between a ligand (L) and a receptor (R) is calculated as:

$$\Delta G_{\text{bind}} = \Delta E_{\text{MM}} + \Delta G_{\text{solv}} - T\Delta S \quad (1)$$

$$\Delta E_{\text{MM}} = \Delta E_{\text{internal}} + \Delta E_{\text{electrostatic}} + \Delta E_{\text{vdW}} \quad (2)$$

$$\Delta G_{\text{solv}} = \Delta G_{\text{PB}} + \Delta G_{\text{SA}} \quad (3)$$

where ΔE_{MM} , ΔG_{solv} , and $-T\Delta S$ are the changes in the gas phase MM energy, the solvation free energy, and the conformational entropy upon binding, respectively. ΔE_{MM} includes $\Delta E_{\text{internal}}$ (bond, angle, and dihedral energies), $\Delta E_{\text{electrostatic}}$ (electrostatic), and ΔE_{vdW} (van der Waals) energies. ΔG_{solv} is the sum of electrostatic solvation energy (polar contribution), ΔG_{PB} , and the non-electrostatic solvation component (nonpolar contribution), ΔG_{SA} . Polar contribution is calculated using the PB model, while the nonpolar energy is estimated by solvent accessible surface area. The conformational entropy change $-T\Delta S$ is usually computed by normal mode analysis, but in this study the entropy contributions were not calculated due to the computational cost involved in such calculations.

2.3.4. Selection of the input structures for QTAIM analysis

It is important to keep in mind that QTAIM calculations are

performed over static geometries, while ligand-receptor binding is a consequence of an assembly of conformations. Therefore the choice on which structure or structures must be considered in the analysis is a very important decision. To solve this problem, clustering technique was carried out using the CPTRAJ program, included in the AmberTools package. The last 25 ns of each trajectory were analyzed resulting in a total of 5,000 frames. Thus, a total of 15,000 frames were evaluated. The representative structure of the cluster most populated for each complex was employed as input structure for the QTAIM analysis.

2.3.5. Construction of reduced models employed in QTAIM analysis.

Reduced models are necessary since the inhibitors that interact in the different active sites constitute a molecular system that is too large for precise calculations of quantum mechanics. By using a reduced model, the complexities of considering the whole biological system are avoided. Therefore, a better understanding of the inherent electronic properties of the complexes can be obtained. To determine which amino acids should be included in the reduced model, two conditions were established: i) to consider all those amino acids that are within a radius of 5 Å of distance of each of the ligand atoms and ii) to have significant interactions with the ligand. Thus, only those amino acids involved in the interactions that form the different L-R complexes were included; however, we must be sure that all the important interactions have been considered. To gain more detailed information about the molecular interactions (MI) driving the linkages of the ligands into the different active sites, the structure affinity relationship was carried out by using analysis per residue from MM-GBSA calculations. All the water molecules within a 5 Å radius were also included in the reduced model. Reduced 3D model systems representing the different L-R binding pocket of the selected zone were constructed from MD simulations; such reduced model was constructed as follow:

Ile463, Ala481, Lys483, Glu501, Leu505, Phe516, Ile527, Gln530, Trp531, Cys532, Ser535, Ser536, His539, Phe582, Phe583, Asp594 and Phe595.

2.3.6. QTAIM calculations (Molecular interactions (MI)).

Topological analysis of the electron density constitutes a powerful tool to evaluate the electronic properties of the molecular systems of biological interest and allows for a deep examination of the molecular interactions. This methodology has been successfully applied in the study of the properties of a variety of conventional and unconventional HBs, aromatic HBs, and π - π stacking [42–44]. A very important point is that from the QTAIM, it is possible to determine in an unequivocal way the different strong and weak interactions between two atoms observing the existence of bond critical points (BCPs) and their respective bond paths. It should be noted that this detailed analysis is not possible from the evaluation of the geometrical parameters (bond, distance and angles).

Here, we only present the essential theoretical information that is needed for the understanding of the QTAIM calculations performed in our study because the use of topological concepts in the description of intra/intermolecular interactions is well documented in the standard literature [45–48]. More details about these types of calculations can be obtained from references [49,50].

Charge density topological analysis based in the QTAIM was performed on the different reduced models to evaluate the L–R interactions. These calculations were performed with the help of Multiwfn and AIMAll software [51,52]. The wave function used as input for these calculations were computed with the Gaussian 16 package [53] by employing the B3LYP functional [38,54,55], with dispersion correction (B3LYP-D [56]), and 6-31G(d) as a basis set. The empirical dispersion correction for the B3LYP functional was applied by invoking the IOp 3/124 = 3 keyword in Gaussian 16. The topological properties of a scalar field such as $\rho(r)$ are summarized in terms of their critical points, i.e., the points where $\Delta\rho(r) = 0$. Critical points are classified

according to their type (ω , σ) by stating their rank, ω , and signature, σ . The rank is equal to the number of nonzero eigenvalues of the Hessian matrix of $\rho(r)$ at rc , while the signature is the algebraic sum of the signs of the eigenvalues of this matrix. Critical points of (3, –1) and (3, +1) type describe saddle points, while the (3, –3) is a maximum and (3, +3) is a minimum in the field. Among these critical points, the (3, –1) or bond critical points are the most relevant ones since they are found between any two atoms linked by a chemical bond.

2.3.7. Some concepts useful in theory of atoms in molecules

The electron charge density, $\rho(r)$, is a physical quantity that has a definite value at each point in space. QTAIM analysis is based on the critical points (CPs) of this electronic density distribution. The gradient vector of the charge density ($\Delta\rho(r)$) vanishes at these points, which are characterized by the three eigenvalues (λ_1 , λ_2 , and λ_3) of the Hessian matrix of the charge density. In the topological distribution of the electronic charge density, three topological features or elements appear as a consequence of the interaction between two atoms: (a) a bond critical point (BCP), (b) a bond path (BP), and (c) an interatomic surface (IAS). A BCP has two negative eigenvalues and a positive eigenvalue. The two negative eigenvalues of the Hessian matrix (λ_1 and λ_2) measure the degree of contraction of the charge density at BCP ($\rho(r)$) perpendicular to the bond toward the critical point, while the positive eigenvalue (λ_3) measures the degree of contraction parallel to the bond and from the BCP toward each of the neighboring nuclei. As mentioned above, the eigenvectors associated with the eigenvalue λ_3 define a unique pair of trajectories of $\Delta\rho(r)$ that originate in the (3, –1) BCP, each of which terminates at the nucleus of one of the neighboring atoms (3, –3). This pair of trajectories defines a line through space along which the electron density is a maximum with respect to any neighboring line forming an atomic interaction line (AIL) or bond path. Each bond path is homeomorphically mirrored by a virial path, a line of maximum negative potential energy density linking the same nuclei. Thus, the presence of a bond path and its associated virial path provides a universal indicator of bonding between the atoms so linked. Three other critical point types can be defined in the topology of $\rho(r)$: (3, +1) or the ring critical point, RCP; (3, –3) or the nuclear critical point, NCP, associated with the nuclei; and (3, +3) or the cage critical point, CCP. This last CP type appears when several rings topologically describe a cage.

3. Results and discussion

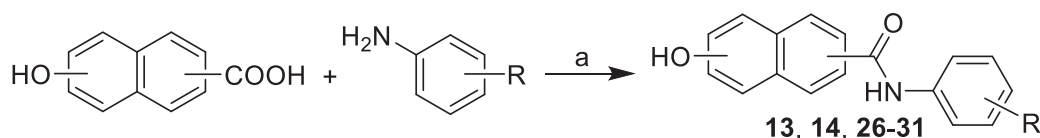
3.1. Synthesis of compounds 13, 14 and 26–31

Studied 1-[3-(4-substituted-benzoyloxy)-2-hydroxypropyl]-4-phenylpiperazin-1-ium chlorides **3–8** were prepared by multiple-step synthesis described recently [26–28]. New compounds **13**, **14** as well as **26–31** were prepared according to Scheme 1 similarly as previously described anilides **9–12**, **15–25** [29–33]. Briefly, the condensation of naphthalenecarboxylic acid with appropriate ring-substituted aniline using phosphorus trichloride in dry chlorobenzene under microwave conditions gave a target substituted *N*-arylnaphthalene-carbox-anilides **13**, **14**, **26–31**.

3.2. Biological assays

3.2.1. Substituted piperazinylethanol and substituted piperazinypropandiols (compounds 3–8)

We have recently reported compounds **3** and **22** (Fig. 1) as potential inhibitors of BRAF [25]. These compounds were obtained from a virtual screening investigation. In the present study, we have taken these two molecules as starting structures for the search of new BRAF inhibitors. First, we evaluated analogues of compound **3** and therefore we use the previously reported compounds **4–8**. Note that these compounds are closely related to compound **3** in which structural changes had been



Scheme 1. Synthesis of ring-substituted naphthalene-carboxanilides **13**, **14**, **26–31**: (a) PCl_3 , chlorobenzene, microwave irradiation (MW) [29–33].

introduced at both extremes of the molecule. Therefore, these compounds fit very well for our purposes. Our next step was to determine the phosphorylation of ERK in Lu1205 cells treated with these new compounds at $10\ \mu\text{M}$ for 2 h by western blot. It is important to note that these bioassays do not categorically guarantee that the compounds have direct effects on BRAF; they allow making an extrapolation based on the levels of ERK phosphorylation, which is a downstream target of BRAF. Although an additional support to the possible effect on BRAF are the results obtained from molecular modeling simulations; specific BRAF activity determination is required to clearly confirm the effect of the compounds on BRAF.

Although all compounds reduce significantly ERK phosphorylation at concentrations of $10\ \mu\text{M}$ (see Fig. 2A), only compound **5** showed an inhibitory effect at lower concentration ($1\ \mu\text{M}$) (see figure S1A as supporting information). In parallel, we evaluated the effects of these compounds in cellular viability. Our results showed that none of these compounds have a significant effect on cell viability at concentrations of $10\ \mu\text{M}$ or $1\ \mu\text{M}$ (Fig. 2B and S1B). Based on these results, we decided to focus our efforts on the other compounds reported here, the hydroxynaphthalenecarboxamides derivatives.

3.2.2. Substituted hydroxynaphthalenecarboxamides (compounds 9–25)

To find new inhibitors with this structural scaffold, we decided to take our previously reported compound **22** as the starting structure. Our research group has previously published different compounds structurally related to **22**. They are compounds **9–11** (type C1, Fig. 1 [29]), **12–14** (type C2, Fig. 1 [30]), **15–17** (type C3, Fig. 1 [31]), **18** and **19** (type C4, Fig. 1 [32]) and compounds **20–25** (type C5, Fig. 1

[33]). It must be pointed out that compounds **13** and **14** were synthesized exclusively for this study and therefore they are described here for the first time; the rest of the compounds have been previously reported as indicated. Taking the advantage of having these compounds available in our laboratory, we determined their potential inhibitory activities. It is important to highlight that compound **22** has been recently reported in our previous article [25], however it was evaluated once again as a positive control, to verify the reliability of our bioassays. Compounds used in this study were selected in such a way that they allow us to evaluate at least two different aspects from the structural point of view of the ligand: a) presence and position of the OH group at the naphthalene moiety; b) type and position of substituents in the benzene group.

Fig. 3 shows the results obtained for the phosphorylation of ERK in Lu1205 cells treated with compounds **9–25** at $10\ \mu\text{M}$ for 2 h by western blot. These results clearly show that only compounds **20–25** (type C5) significantly reduce ERK phosphorylation at concentrations of $10\ \mu\text{M}$. The rest of the tested compounds did not show significant activities.

Altogether, these data suggest several conclusions from the structural point of view of the ligand. The lack of activity obtained for compounds **9–11** shows that the presence of the OH group at the naphthalene moiety might be important for the inhibitory effect in these compounds; however the lack of activity of compounds **12–19** clearly indicates that not only the presence of an OH group is necessary, but its spatial position appears to be important. It should be noted that compounds **12–19** have the OH group in different positions at the naphthalene moiety and none of them showed significant inhibitory effect at $10\ \mu\text{M}$. Moreover, the presence of a substituent with

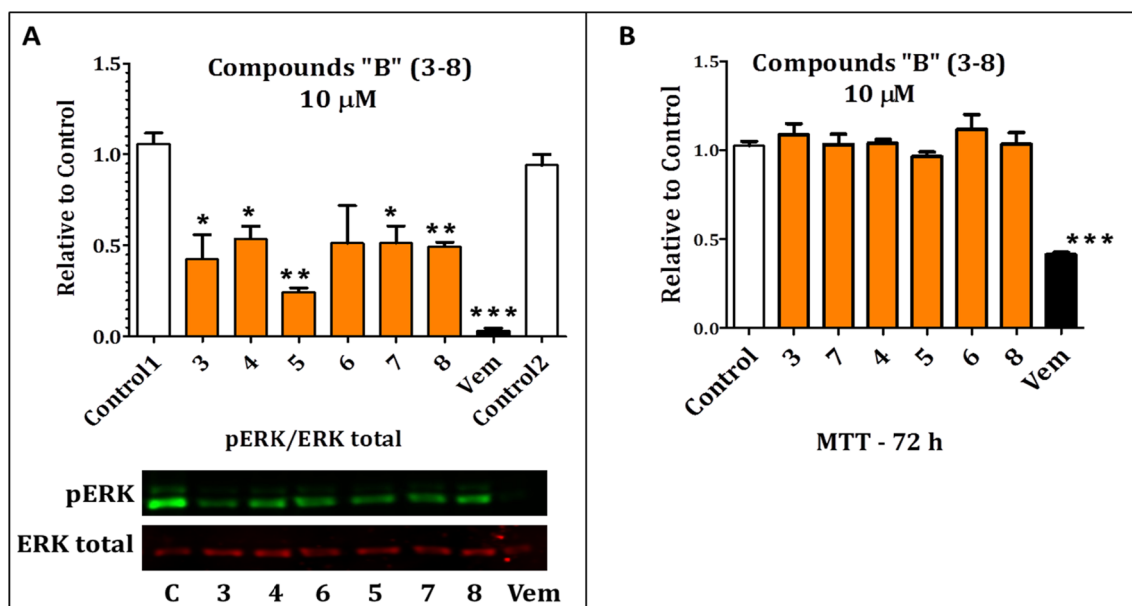


Fig. 2. Lu1205 melanoma cells were treated with compounds type B (**3–8**, orange bars), control (carrier DMSO, white bars) or Vemurafenib (Vem, black bars) at $10\ \mu\text{M}$ for 2 h (A) or 72 h (B). A) Proteins from the cell lysates were separated by SDS-PAGE and then western blot was performed by using specific antibodies against pERK and ERK total. Image Studio 5.2 was used to make the quantification of each band and establish the relation pERK/ERK total respect to the control. A representative western blot is shown. B) Cell viability was determined by the reduction of the MTT reagent. Crystals were dissolved in DMSO and absorbance was measured at 540 nm in the spectrophotometer. Absorbance of each treatment was normalized to the Absorbance of the control. The results are shown as the mean \pm SEM of 3 independent experiments. Statistics: One-way ANOVA and Tukey post-test (* $p < 0.05$; ** $p < 0.01$; *** $p < 0.001$). (For interpretation of the references to colour in this figure legend, the reader is referred to the web version of this article.)

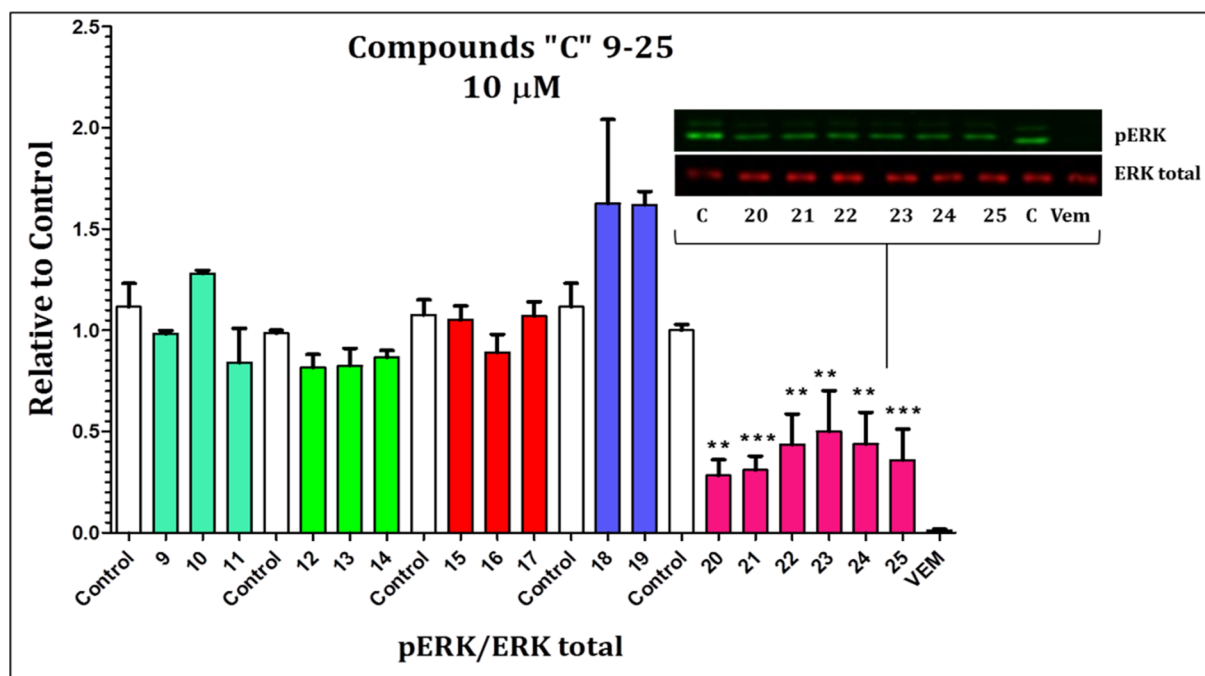


Fig. 3. Lu1205 melanoma cells were treated with compounds “C” 9–25 (C1 cyan bars; C2 green bars; C3 red bars; C4 blue bars; C5 pink bars), control (carrier DMSO, white bars) or Vemurafenib (black bars) at 10 μM for 2 h. Proteins from the cell lysates were separated by SDS-PAGE and then immunoblot was performed by using pERK and ERK total specific antibodies. Image Studio 5.2 was used to make the quantification of each band and establish the relation pERK/ERK total respect to the control. The results are shown as the mean \pm SEM of 3 independent experiments. Statistics: One-way ANOVA and Tukey post-test (* $p < 0.05$; ** $p < 0.01$; *** $p < 0.001$). A representative western blot of active compounds 20–25 is shown. (For interpretation of the references to colour in this figure legend, the reader is referred to the web version of this article.)

electronegative characteristics (such as Br or CF_3) might improve the activity of these series of compounds. Certainly, all the active compounds possess substituents with those characteristics at the benzene ring (type C5, compounds 20–25). Considering that only compounds 20–25 did show inhibitory effect, they were also tested at 1 μM . Remarkably, all these compounds reduced ERK phosphorylation at this concentration (Fig. 4A) but only compounds 21 and 22 also reduced significantly cell viability of Lu1205 melanoma cells (Fig. 4B). These data suggest that they are potential new anti-carcinogenic agents.

3.3. Molecular modeling study

In order to understand more deeply our experimental results, a molecular modeling study was developed. We carried out this study in four steps using different modeling techniques. First, we conducted a docking study; in the second step we performed simulations using molecular dynamics calculations. With these data we performed an analysis by residue and lastly, quantum mechanics calculations were made to evaluate in detail the molecular interactions that stabilize the different ligand-receptor complexes.

As expected, the docking study indicates that compound 21 is bound in a spatial arrangement in a similar fashion to that previously reported for compound 22 [25]. It should be noted that Vemurafenib displays a similar spatial ordering as well (Fig. 5 [25]).

Molecular dynamics calculations allowed us to perform an analysis per residue for the different series of compounds to understand the biological results obtained for these compounds. The histogram obtained for compound 21 is shown in Fig. 6A. The interactions of compound 21 are mainly with Asp594 and Lys483 (slightly less with the last one). The other interactions that stabilize the formation of this complex are noticeably more weak (Ile463, Val471, Ala481, Thr529 and Phe583). It is important to highlight the high similarity between the histograms of compound 21 and Vemurafenib (see Fig. 6A and 6B). In fact, considering just these simulations, we could expect that

compound 21 would show the same inhibitory effect as Vemurafenib, however its activity, although significant, is much lower. In the next section, we explore a possible explanation for this performance by carrying out a more detailed analysis of the molecular interactions.

Histograms obtained for compounds 10 and 18 are shown in Fig. 6C and 6D, respectively. These histograms emphasize the clear differences between active compounds (Fig. 6A and B) from those with marginal activity or inactive (compounds 9–19, Fig. 6C and D).

Although the interactions observed for these inactive compounds 10 and 18 are almost the same to those obtained for compound 21 and Vemurafenib, such interactions are markedly weaker. Note that most of these interactions do not reach 2 Kcal/mol and none of them reach 3.8 Kcal/mol. In particular, those interactions with Asp594 and Lys483 are significantly weaker compared to the observed in active compounds. These results are in agreement with our experimental data. Similar histograms were obtained for the rest of the inactive compounds (data not shown). In order to better understand the behavior of ligands, we have recently shown that it is helpful to analyze the molecular interactions of the different complexes employing more accurate calculations. For this purpose, combined MD/QTAIM (quantum theory of atoms in molecules) calculations are extremely useful for detailing the molecular interactions of different ligand-receptor complexes [49,50]. Therefore, we perform a QTAIM analysis for the most representative complexes of these compounds.

3.4. Topological analysis of the charge density

QTAIM analysis consists in the mapping of the gradient vector field ∇ on top of the charge density (ρ) of the system to give rise to the topological elements of the charge density, two of which we are mainly concerned in here: the Bond Critical Points (BCPs) at the complex intermolecular interface and the Bond Paths (BPs) that connect the BCP to bonded atoms of the ligand and the protein. Unlike the geometrical parameters (i.e. bond distance and angle and also types of atoms

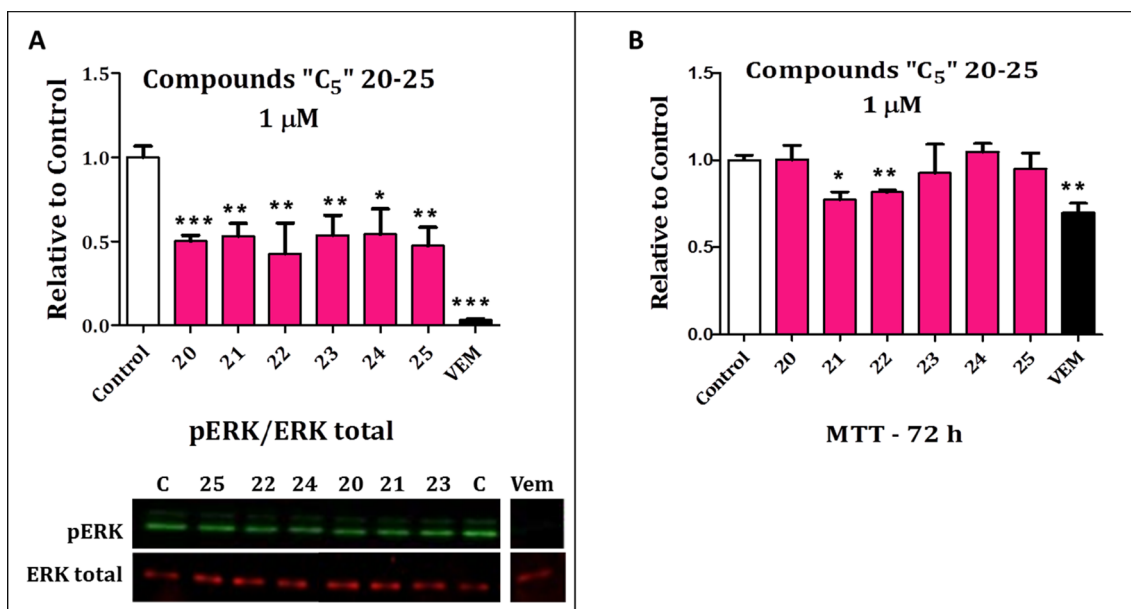


Fig. 4. Lu1205 melanoma cells were treated with compounds "C₅" 20–25 (pink bars), control (carrier DMSO, white bars) or Vemurafenib (black bars) at 1 μM for 2 h (A) or 72 h (B). A) Proteins from the cell lysates were separated by SDS-PAGE and then immunoblot was performed by using specific antibodies against pERK and ERK total. Image Studio 5.2 was used to make the quantification of each band and establish the relation pERK/ERK total respect to the control. A representative western blot is shown. B) MTT reagent was added and incubated 3 h additionally. Formazan crystals were dissolved in DMSO and absorbance was measured at 540 nm. Each treatment was normalized to the control. The results are shown as the mean ± SEM of 3 independent experiments. Statistics: One-way ANOVA and Tukey post-test (*p < 0.05; **p < 0.01; ***p < 0.001). (For interpretation of the references to colour in this figure legend, the reader is referred to the web version of this article.)

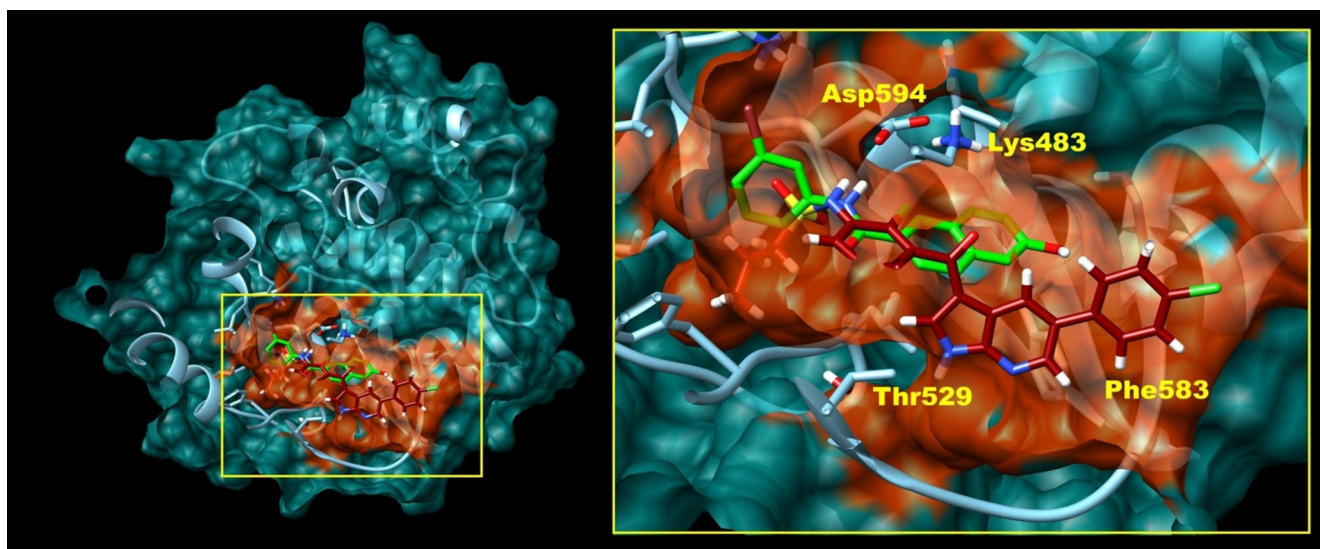


Fig. 5. Spatial view of the ordering adopted by compound 21 (green) and Vemurafenib (dark red) in the active site of BRAF. (For interpretation of the references to colour in this figure legend, the reader is referred to the web version of this article.)

involved) for describing non covalent interactions, QTAIM does not rely on any arbitrary criteria for deciding whether an interaction is actually formed or not: the sole presence of a BCP and the corresponding BPs between two atoms guarantee the existence of the interaction. Conversely, if no BCP and BPs is observed, then it is a fact that those atoms are not interacting with each other. Therefore, QTAIM allows detecting weak intermolecular interactions, mostly involving hydrophobic moieties which lack of well-defined geometrical limits.

Fig. 7 depicts the charge density molecular graph of compound 21 bound to BRAF.

As shown in Fig. 7, an intricate network of interactions holds compound 21 within the binding cleft of the enzyme. Since the charge

density value at the BCP of the interaction is a measure of the strength of that interaction, the sum of charge density values for all the intermolecular interactions gives an estimate of the overall strength of the binding. Similarly, the sum of charge density values corresponding to all the interactions of a particular functional group of the ligand with enzyme atoms is a measure of the anchoring of that group to the binding cleft.

Bar plot in Fig. 8 shows the charge density sum corresponding to interactions of Vemurafenib and compound 21 with BRAF. As expected, Vemurafenib is anchored to the BRAF binding cleft several times more strongly than compound 21, a finding that correlates very well with results of the ERK phosphorylation assays discussed above.

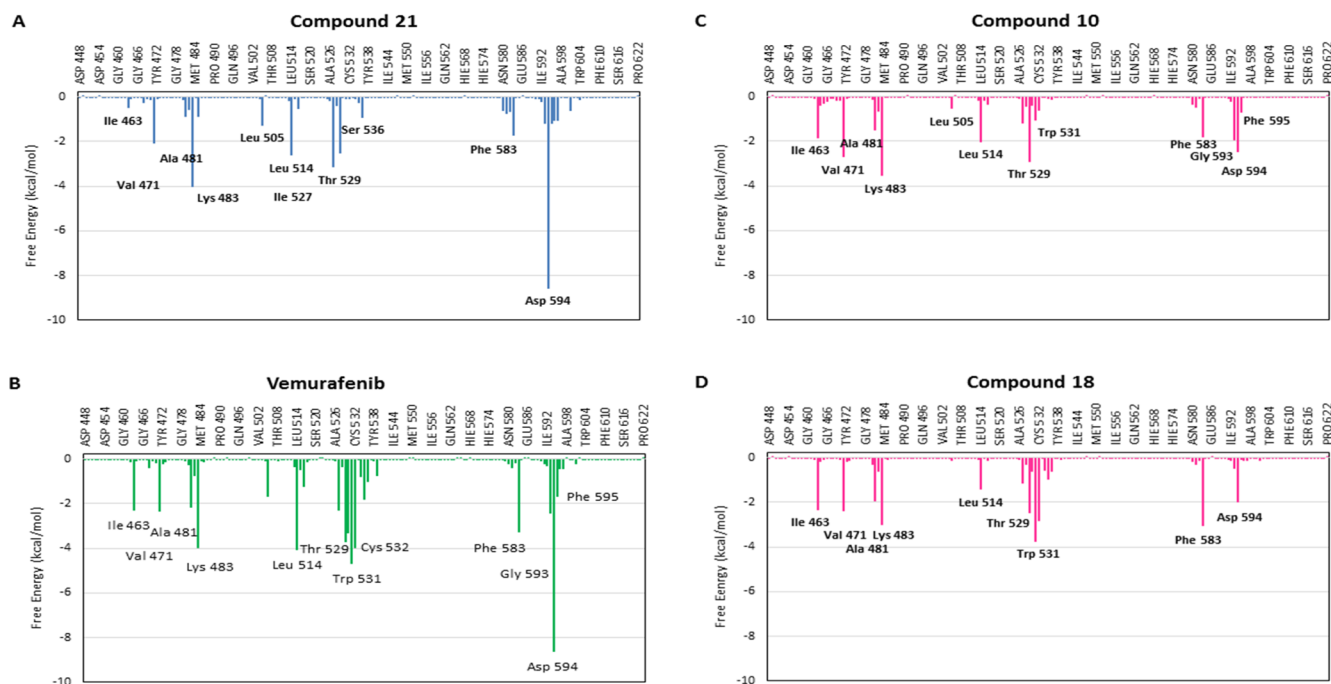


Fig. 6. Histograms for compounds **21** (A), Vemurafenib (B), **10** (C) and **18** (D) show the interaction energies with the main amino acids that participate in the formation of the complex enzyme-ligand.

Furthermore, Vemurafenib binds more strongly than compound **21** to both regions of the enzyme, i.e. DFG loop as well as the hinge region. [Figure S2](#) shows a superposition of the binding modes of compound **21**, Vemurafenib (PDB code = 3OG7) and a very close analog of ATP (PDB code = 6U2G).

It is clearly visible the Y-shaped bifurcated binding cleft of BRAF in

which ATP analog shares with compound **21** and Vemurafenib the same binding site on the Hinge region. However they target different sides of the binding cleft bifurcation around the DFG loop region. As can be seen, both Vemurafenib and compound **21** target a deep pocket that remains unexplored by ATP enzyme substrate.

Despite the quite similar binding mode of Vemurafenib and

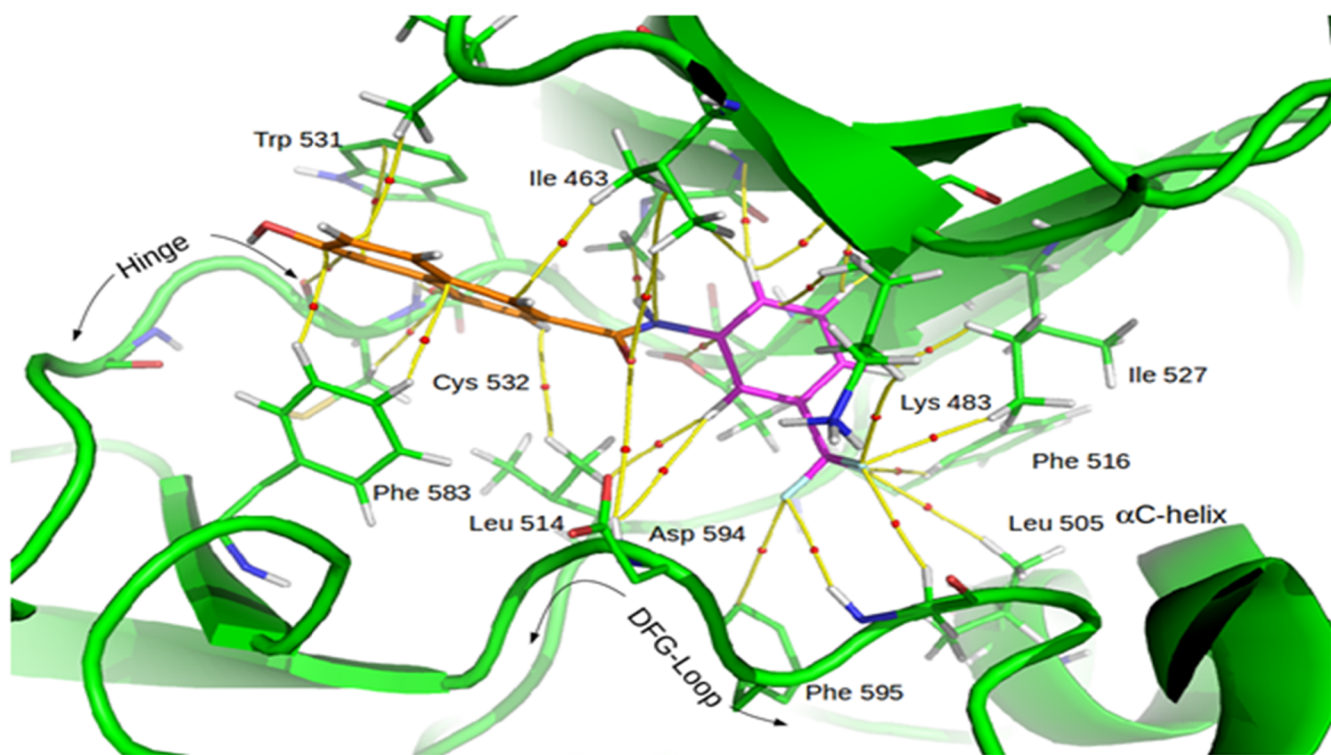


Fig. 7. Charge density molecular graph of compound **21** bound to BRAF. BCPs and BPs for the complex intermolecular interactions are shown in red spheres and yellow lines, respectively. The interacting parts of compound **21** with DFG-loop and Hinge are colored in purple and orange, respectively. (For interpretation of the references to colour in this figure legend, the reader is referred to the web version of this article.)

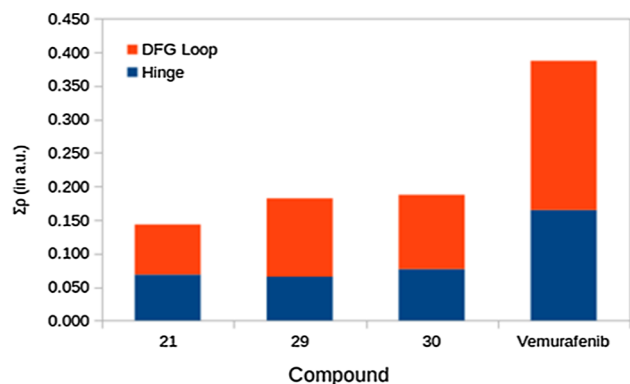


Fig. 8. Charge density sum ($\Sigma\rho$) for interactions of Vemurafenib and compounds 21, 29 and 30 with BRAF. Total charge density sum (i.e. full height of stacked bars) is decomposed in interactions with the Hinge and DFG loop regions of BRAF binding cleft. Results obtained for compounds 29 and 30 are shown here but they are discussed in section 3.5.

compound 21, the first one is able to form much stronger interactions than compound 21, as evidenced by the bar plot in Fig. 8. Accordingly, in what follows we discuss the differences in the intermolecular interactions profiles of both inhibitors to uncover such differences. To help in the discussion, we have included the molecular graph of Vemurafenib at the BRAF binding cleft (Figure S3). A very similar graph has been reported by us in Campos, *et al* [25]. We have recalculated this complex using the same methodology employed here to homogenize the results. However, it should be noted that the results obtained are closely related to those previously reported. By comparing the molecular graphs in Figure 7 and S3 one can see that the residues involved in the binding of compound 21 and Vemurafenib are basically the same.

Fig. 9 shows the intermolecular interaction profiles for complexes of BRAF with compound 21 and Vemurafenib.

While residues involved in the anchoring of both compounds are almost the same as argued above, there are significant differences in quantitative terms, namely several of the involved residues interact much more strongly with Vemurafenib than with compound 21. This is particularly true for interactions with key residue Asp594 from DFG loop and also with Gln530 and Cys532 from the hinge loop. Additionally, Vemurafenib forms other interactions with hinge residues like Gly534, Ser535 and His539 that are not formed for compound 21.

Moreover, residues Lys483 and Phe468 from β -sheet motif that

conform the roof of the binding cleft are strongly interacting with Vemurafenib while only forms weak contacts with compound 21 (i.e. as in the case of Lys483) or do not interact at all with it (i.e. as in the case of Phe468). These last interactions help to keep β -sheet motif close to the DFG loop thus allowing formation of salt bridge between Lys483 and Asp594 which in turn stabilizes the DFG-in/ α -helix- out conformation of BRAF when it is bound to Vemurafenib.

On the other hand, as compound 21 is not able to form stable interactions with residue Phe468 and Lys483, the β -sheet motif moves away from the DFG loop and the salt bridge between Lys483 and Asn594 gets broken. Salt bridge disruption together with the fact that compound 21 only interacts weakly with DFG loop residues like Asp594 suggest that this loop could move quite freely between in and out conformation of BRAF. Thus, we hypothesize that if we were able to simulate complex of BRAF with compound 21 for long enough time in the microsecond/millisecond time scale, DFG loop would move from in to out conformation and compound 21 would eventually end up expelled from BRAF binding cleft in this process. In contrast, in the case of Vemurafenib, this conformational transition should take more time to occur (if it actually does at all) because the DFG loop is more tightly hold in the DFG-in conformation by direct interactions with the inhibitor as well as by the salt bridge with Lys483.

3.5. Bi-substituted hydroxynaphthalenecarboxamides (compounds 26–31)

At this stage of our study and based on our results obtained from molecular modeling, we wondering if bi-substituted compounds could have any advantage compared to the mono-substituted derivatives. The simulations previously shown indicate that BRAF binding site has enough space to properly accommodate another substituent on the benzene ring of the inhibitors. Thus, we decided to perform a molecular modeling study for bi-substituted derivatives. To this end, we selected compounds that had bromine atom and trifluoromethyl substituents at different spatial positions.

The histograms obtained for bi-substituted derivatives are shown in Figure S4. It can be clearly seen that histograms of compounds 29 and 30 have a very similar profile to those obtained for compound 21 and Vemurafenib (compare Figures S2D-E with 6A and 6B). Similar histograms were obtained for compounds 26, 27, 28 and 31 which are shown in Figure S2 as supporting information.

Furthermore, MD/QTAIM study revealed very interesting results for these compounds. For instance, the total $\rho(r)$ values obtained for

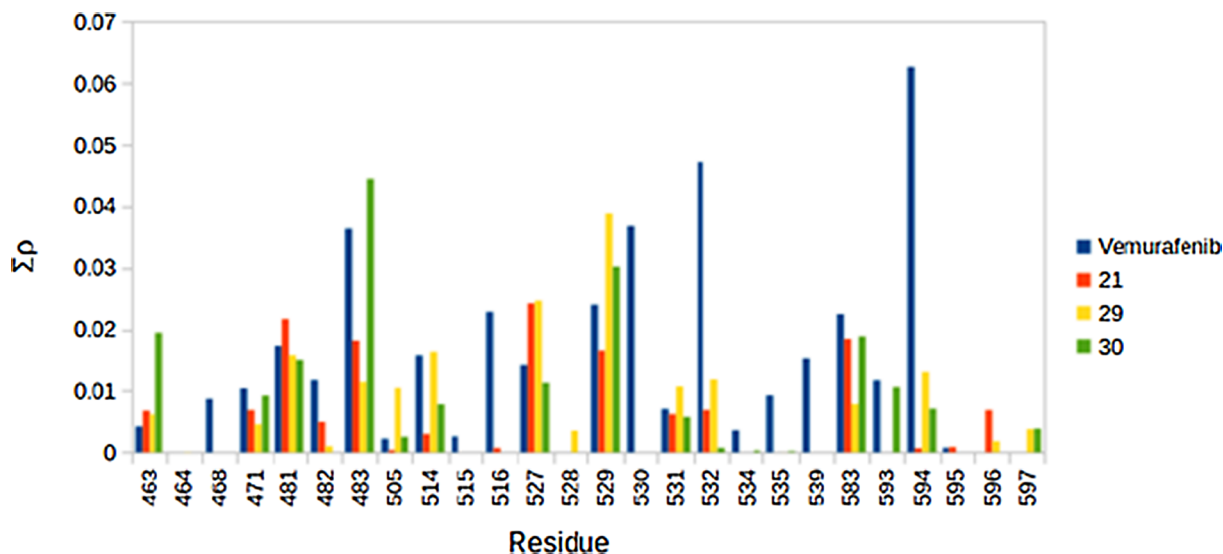


Fig. 9. Per-residue charge density sum (in atomic units) of the intermolecular interactions in complexes of BRAF with compounds 21, 29, 30 and Vemurafenib. Results obtained for compounds 29 and 30 are shown here but they are discussed in section 3.5.

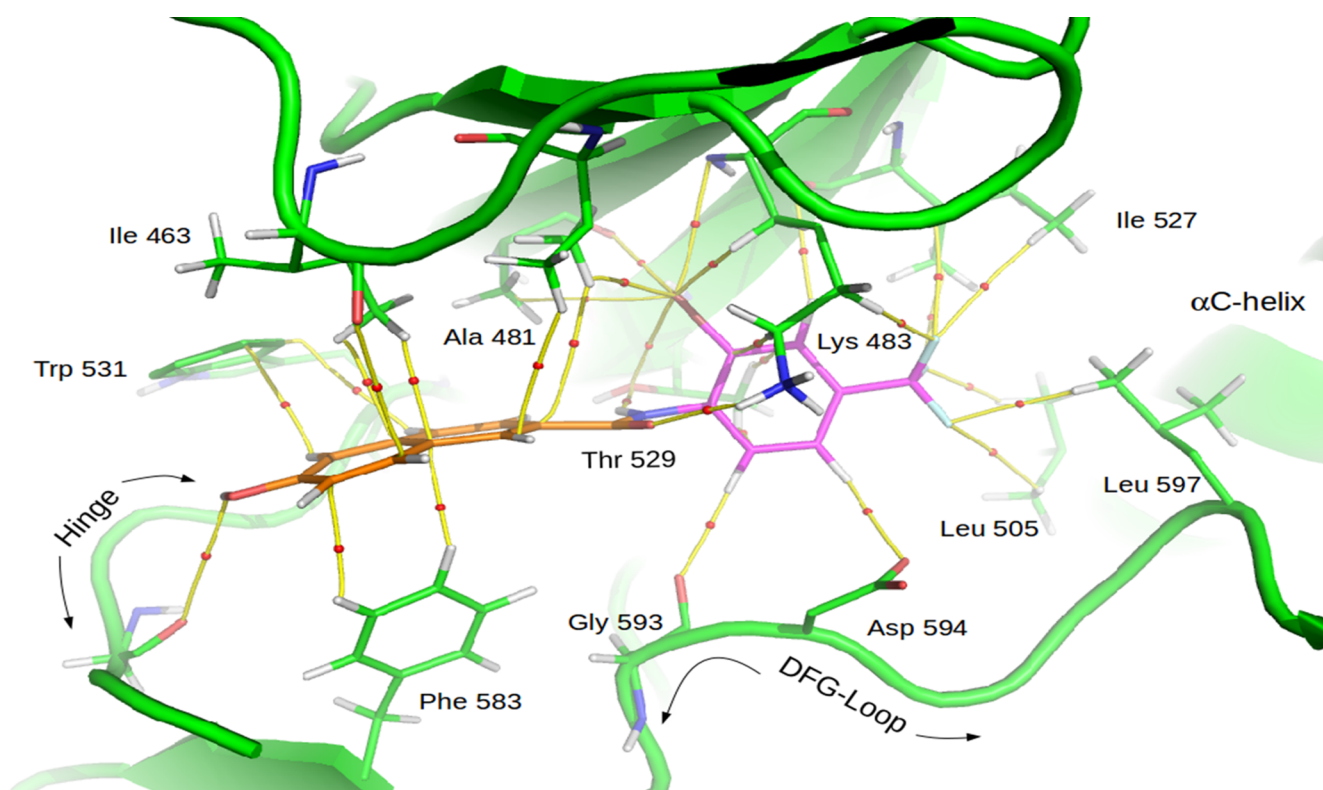


Fig. 10. Charge density molecular graph of compound **30** bound to BRAF. BCPs and BPs for the complex intermolecular interactions are shown in red spheres and yellow lines, respectively. The interacting parts of compound **30** with DFG-loop and Hinge are colored in purple and orange, respectively. (For interpretation of the references to colour in this figure legend, the reader is referred to the web version of this article.)

compounds **29** and **30** are slightly higher than those of **21** but at the same time lower than those of Vemurafenib (Fig. 8). An interesting point to remark is that the blue portion of compounds **29** and **30** is almost the same as that of compound **21**, however the red portion of bi-substituted compounds is higher compared to **21** (see Fig. 8). This is expected since the increased interaction in this portion of the molecule is due to the interactions produced by the two groups included in the benzene ring. This can be better observed in Fig. 10 in which these interactions have been analyzed residue by residue. The strongest interactions of Vemurafenib with respect to compounds **29** and **30** can also be clearly seen in this figure. Simulations and calculations were performed for six compounds (**26–31**) although only the results of **29** and **30** are shown here by a space issue.

Compound **30** shows a binding mode very similar to that of compound **21** at BRAF binding cleft. Actually, structural superposition of both complexes shows that, except for the substituents at the benzene rings, ligand atoms are almost perfectly superimposed (data not shown). In other words, the incorporation of a second substituent on the benzene ring significantly increases the anchoring of compound **30** but without affecting its overall binding mode. This finding is further supported by Fig. 8, which shows that the binding to BRAF hinge region through the ligand hydroxynaphthyl group is not affected by number and position of substituents. However, the anchoring at the DFG loop region does increase markedly upon the incorporation of a second substituent. The increase in anchoring strength of compound **30** as compared to compound **21** is related to the greater number of interactions that both substituents can achieve together.

As can be seen in the molecular graph of Fig. 10, there are several bond paths connecting the bromine atom at benzene ring to residues Ala481, Lys483 and Thr529 from the β -sheet motif. At the same time, the trifluoromethyl substituent fills the hydrophobic pocket originated by the outward shift of the α C-helix where it forms several hydrophobic interactions with residues Leu505, Ile527 and Leu597. To better

understand the conformational changes that take place in the binding site, we construct Figure S6 which shows a superposition of BRAF bound to compounds **21**, **30** and Vemurafenib as well as BRAF in DFG-out conformation. Based on these results, we decided to synthesize and measure the biological activity of these six compounds.

3.5.1. Experimental corroboration

Based on the results discussed in the previous section, our next step was to synthesize and evaluate the six new bi-substituted derivatives (compounds **26–31**). Details of synthesis were discussed in section 3.1. Notably, all these new compounds showed significant inhibitory activity on BRAF (see Fig. 11A and S5A). In fact, these compounds not only showed a significant inhibitory effect on BRAF at both concentrations tested (10 and 1 μ M), but also reduced viability of Lu1205 melanoma cells (see Fig. 11B and S5B).

It is important to remark that these compounds displayed stronger activities in comparison to compound **21** and those previously reported [25]. Moreover, these results constitute an additional support to our molecular modeling study since they are in complete agreement with their predictions. These compounds, although showing less activity than Vemurafenib, are more active than compound **21** and the other mono-substituted compounds in the series.

4. Conclusions

Recently, we reported two new structural scaffolds as potential inhibitors of BRAF; both series of compounds were studied in greater depth in the present work. Our results indicate that structural analogues of the previously reported compound **3** do not show significantly better activities to that previously reported for this compound which was chosen as starting structure. In contrast, the results obtained for hydroxynaphthalenecarboxamides were more successful. We report here new compounds possessing this structural scaffold with significant

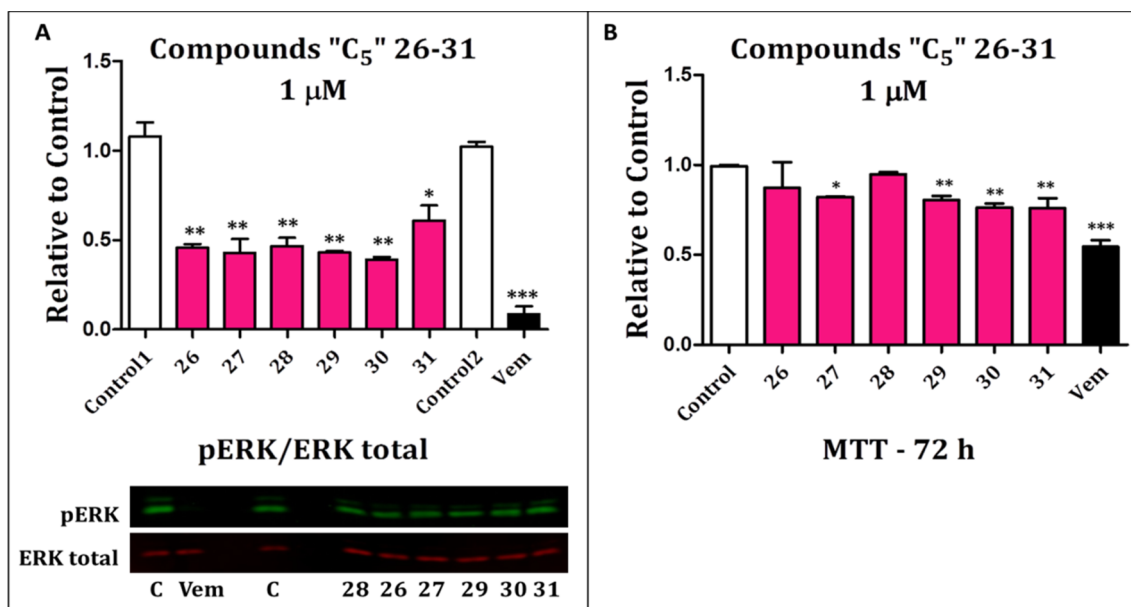


Fig. 11. Lu1205 melanoma cells were treated with compounds “C₅” 26–31 (pink bars), control (carrier DMSO, white bars) or Vemurafenib (Vem, black bars) at 1 μ M for 2 h (A) or 72 h (B). A) Proteins from the cell lysates were separated by SDS-PAGE and then immunoblot was performed by using specific antibodies against pERK and ERK total. Image Studio 5.2 was used to make the quantification of each band and establish the relation pERK/ERK total respect to the control. A representative western blot is shown. B) MTT reagent was added and incubated for 3 additional hours. DMSO was employed to dissolve the formazan crystals and the absorbance was measured at 540 nm. Each treatment was normalized to the control. The results are shown as the mean \pm SEM of 3 independent experiments. Statistics: One-way ANOVA and Tukey post-test (* p < 0.05; ** p < 0.01; *** p < 0.001).

inhibitory activity on BRAF. Among these derivatives, compounds 21, 22 and six new bi-substituted derivatives (26–31) are those that showed the strongest inhibitory activities. In addition, these compounds also reduce notably the cell viability of Lu1205 melanoma cells and therefore they are good candidates for further development. In the same line, bi-substituted compounds seem to have structural advantages with respect to the mono-substituted analogues.

In order to better understand these experimental results, we carried out a molecular modeling study using different combined techniques. While simulations using simple techniques such as docking and MD simulations allowed us to explain which the best structural scaffold is, such results are not appropriate to explain why some compounds within the same series displayed different activities. These explanations were obtained from the combined MD/QTAIM calculations that allowed us to explain in detail the molecular interactions that stabilize the different molecular complexes reported here.

On the other hand, QTAIM results of the new compounds are in agreement to those observed for Vemurafenib, explaining the lower activity obtained for the compounds reported here with respect to the drug used as reference. This structural information is important for the design and development of new BRAF inhibitors possessing this type of structural scaffold.

Declaration of Competing Interest

The authors declare that they have no known competing financial interests or personal relationships that could have appeared to influence the work reported in this paper.

Acknowledgements

This work was supported by grants from INC (Instituto Nacional del Cáncer-Argentina) to R.D.E., ANPCyT-Argentina PICT 2378-2014 to S.E.A. and CONICET, Argentina PIP916-2015 to S.E.A. Grants from Universidad Nacional de San Luis (UNSL-Argentina) partially supported this work. Dr. Ludmila Campos is a postdoctoral fellowship of

CONICET-Argentina. This work was also partially supported by the Ministry of Education of the Czech Republic (LO1305) and Palacky University in Olomouc (IGA_PrF_2020_023). M.O. was supported by SustES (CZ.02.1.01/0.0/0.0/16_019/0000797). We thank Dr. Pablo Bergami (Universidad de Maimónides, Buenos Aires) for generously provide us Lu1205 melanoma cell line.

Appendix A. Supplementary data

Supplementary data to this article can be found online at <https://doi.org/10.1016/j.bioorg.2020.104145>.

References




- [1] H. Davies Y et al, Mutations of the BRAF gene in human cancer, *Nature*, pp. 949-54, 2002.
- [2] M.L. Turski, S.J. Vidwans, F. Janku, I. Garrido-Laguna, J. Munoz, R. Schwab, V. Subbiah, J. Rodon, R. Kurzrock, Genomically Driven Tumors and Actionability across Histologies: BRAF-Mutant Cancers as a Paradigm, *Molecular Cancer Therapeutics* 15 (4) (2016) 533–547, <https://doi.org/10.1158/1535-7163.MCT-15-0643>.
- [3] K. Young, A. Minchom, Y.J. Larkin, BRIM-1, -2 and -3 Trials: Improved Survival With Vemurafenib in Metastatic Melanoma Patients With a BRAF(V600E) Mutation, *Future Oncol.*, pp. 499-507, 2012.
- [4] J.J. Luke, K.T. Flaherty, A. Ribas, Y.G.V. Long, Targeted agents and immunotherapies: optimizing outcomes in melanoma, *Nat. Rev. Clin. Oncol.* (2017) 463–482.
- [5] S.J. Welsh, H. Rizos, R.A. Scolyer, Y.G.V. Long, Resistance to combination BRAF and MEK inhibition in metastatic melanoma: Where to next? *European Journal of Cancer* (2016) 76–85.
- [6] D. Barras, BRAF Mutation in Colorectal Cancer: An Update., *Biomark. Cancer.* (2015) 9–12.
- [7] K. B. Kim, M. E. Cabanillas, A. J. Lazar, Y.S. I. Sherman, Clinical Responses to Vemurafenib in Patients with Metastatic Papillary Thyroid Cancer Harboring BRAFV600E Mutation, *Thyroid*, p. 1277–1283, 2013.
- [8] R. Dummer, P. A. Ascierto, H. J. Gogas, A. Arance, Y.K. T. Flaherty, Overall survival in patients with BRAF-mutant melanoma receiving encorafenib plus binimetinib versus vemurafenib or encorafenib (COLUMBUS): a multicentre, open-label, randomised, phase 3 trial, *The Lancet Oncology*, pp. 1315-1327, 2018.
- [9] Reinhard Dummer, Paolo A Ascierto, Helen J Gogas, Ana Arance, Mario Mandala, Gabriella Liszkay, Claus Garbe, Dirk Schadendorf, Ivana Krajsova, Ralf Gutzmer, Vanna Chiarion-Sileni, Caroline Dutriaux, Jan Willem B de Groot, Naoya Yamazaki, Carmen Loquai, Laure A Moutouh-de Parseval, Michael D Pickard, Victor Sandor,

- Caroline Robert, Keith T Flaherty, Encorafenib plus binimetinib versus vemurafenib or encorafenib in patients with BRAF-mutant melanoma (COLUMBUS): a multi-centre, open-label, randomised phase 3 trial, *The Lancet Oncology* 19 (5) (2018) 603–615, [https://doi.org/10.1016/S1470-2045\(18\)30142-6](https://doi.org/10.1016/S1470-2045(18)30142-6).
- [10] A.A. Samatar, Y.P.I. Poulidakos, Targeting RAS–ERK signalling in, *Nature Reviews Drug Discovery* (2014) 928–942.
- [11] X. Wang, Y.K. Schleicher, Conformation-specific Inhibitors of Raf Kinases, *Enzymes*, pp. 41–66, 2013.
- [12] H. Lavoie, Y.M. Therrien, Regulation of RAF Protein Kinases in ERK Signalling, *Nat Rev Mol Cell Biol* (2015) 281–298.
- [13] Z. Karoulia, Y. Wu, T. A. Ahmed, Q. Xin, Y.P. I. Poulidakos, Integrated Model of RAF Inhibitor Action Predicts Inhibitor Activity against Oncogenic BRAF Signaling, *Cancer Cell*, p. 485–498, 2017.
- [14] S.-H. Chen, Y. Zhang, R. D. Van Horn, T. Yin, Y.S.-B. Peng, That Function as Homodimers and Are Sensitive to Inhibition by RAF Dimer Inhibitor LY3009120, *Cancer Discovery*, p. 300–315, 2016.
- [15] Hugo Lavoie, Neroshan Thevakumar, Gwenaëlle Gavory, John J Li, Abbas Padeganeh, Sébastien Guiral, Jean Duchaine, Daniel Y L Mao, Michel Bouvier, Frank Sicheri, Marc Therrien, Inhibitors that stabilize a closed RAF kinase domain conformation induce dimerization, *Nat Chem Biol* 9 (7) (2013) 428–436, <https://doi.org/10.1038/nchembio.1257>.
- [16] B. Agianian, Y.E. Gavathiotis, Current Insights of BRAF Inhibitors in Cancer, *J. Med. Chem.* (2018) 5775–5793.
- [17] Sonja J. Heidorn, Carla Milagre, Steven Whittaker, Arnaud Nourry, Ion Niculescu-Duvas, Nathalie Dhomen, Jahan Hussain, Jorge S. Reis-Filho, Caroline J. Springer, Catrin Pritchard, Richard Marais, Kinase-Dead BRAF and Oncogenic RAS Cooperate to Drive Tumor Progression through CRAF, *Cell* 140 (2) (2010) 209–221, <https://doi.org/10.1016/j.cell.2009.12.040>.
- [18] Poulidakos I. Poulidakos, Chao Zhang, Gideon Bollag, Kevan M. Shokat, Neal Rosen, RAF inhibitors transactivate RAF dimers and ERK signalling in cells with wild-type BRAF, *Nature* 464 (7287) (2010) 427–430, <https://doi.org/10.1038/nature08902>.
- [19] Georgia Hatzivassiliou, Kyung Song, Ivana Yen, Barbara J. Brandhuber, Daniel J. Anderson, Ryan Alvarado, Mary J.C. Ludlam, David Stokoe, Susan L. Gloor, Guy Vigers, Tony Morales, Ignacio Aliagas, Bonnie Liu, Steve Sideris, Klaus P. Hoefflich, Bijay S. Jaiswal, Somasekar Seshagiri, Hartmut Koeppen, Marcia Belvin, Lori S. Friedman, Shiva Malek, RAF inhibitors prime wild-type RAF to activate the MAPK pathway and enhance growth, *Nature* 464 (7287) (2010) 431–435, <https://doi.org/10.1038/nature08833>.
- [20] M. Holderfield, M.M. Deuker, F. McCormick, Y.M. McMahon, Targeting RAF kinases for cancer therapy: BRAF-mutated melanoma and beyond, *Nat. Rev. Cancer* (2014) 455–467.
- [21] N. Cope, C. Candelora, K. Wong, S. Kumar, Y.Z. Wang, Mechanism of BRAF Activation Through Biochemical Characterization of the Recombinant Full-Length Protein, *Chembiochem*, pp. 1988–1997, 2018.
- [22] Zoi Karoulia, Yang Wu, Tamer A. Ahmed, Qisheng Xin, Julien Bollard, Clemens Krepler, Xuwei Wu, Chao Zhang, Gideon Bollag, Meenhard Herlyn, James A. Fagin, Amaia Lujambio, Evripidis Gavathiotis, Poulidakos I. Poulidakos, An Integrated Model of RAF Inhibitor Action Predicts Inhibitor Activity against Oncogenic BRAF Signaling, *Cancer Cell* 30 (3) (2016) 501–503, <https://doi.org/10.1016/j.ccell.2016.08.008>.
- [23] C. Zhang, W. Spevak, Y. Zhang, E.A. Burton, Y.G. Bollag, RAF inhibitors that evade paradoxical MAPK pathway activation, *Nature* 526 (2015) 583–586.
- [24] C.H. Adelman, G. Ching, L. Du, R.C. Saporito, Y.K.Y. Tsai, Comparative profiles of BRAF inhibitors: the paradox index as a predictor of clinical toxicity, *Oncotarget* 7 (21) (2016) 30453–30460.
- [25] L.E. Campos, F.M. Garibotto, E. Angelina, J. Kos, Y.R.D. Enriz, Searching New Structural Scaffolds for BRAF Inhibitors. An Integrative Study using theoretical and experimental techniques, *Bioorganic Chemistry* (2019).
- [26] M. Vettorazzi, E. Angelina, S. Lima, T. Gonec, Y.R.D. Enriz, An integrative study to identify novel scaffolds for sphingosine kinase 1 inhibitors, *Europ. J. Med. Chem.* (2017) 461–481.
- [27] P. Marvanova, T. Padrtova, T. Pekarek, J. Brus, Y.J. Jampilek, Synthesis and characterization of new 3-(4-arylpiperazin-1-yl)-2-hydroxypropyl 4-propoxybenzoates and their hydrochloride salts, *Molecules*, pp. 4–7, 2016a.
- [28] P. Marvanova, T. Padrtova, K. Odehmalova, O. Hosik, Y.P. Mokry, Synthesis and determination of physicochemical properties of new 3-(4-arylpiperazin-1-yl)-2-hydroxypropyl 4-alkoxyethoxy-benzoates, *Molecules*, pp. 1682–1688, 2016b.
- [29] T. Gonec, J. Kos, E. Nevin, R. Govender, Y.J. Jampilek, Preparation and biological properties of ring-substituted naphthalene-1-carboxanilides, *Molecules*, p. 9–11, 2014.
- [30] T. Gonec, J. Kos, I. Zadrazilova, M. Pesko, Y.J. Jampilek, Antibacterial and herbicidal activity of ring-substituted 2-hydroxynaphthalene-1-carboxanilides, *Molecules*, pp. 9397–9419, 2013.
- [31] T. Gonec, J. Kos, M. Pesko, J. Dohanosova, Y.J. Jampilek, Halogenated 1-hydroxynaphthalene-2-carboxanilides affecting photosynthetic electron transport in photosystem II, *Molecules*, pp. 15–17, 2017.
- [32] J. Kos, I. Zadrazilova, M. Pesko, S. Keltosova, Y.J. Jampilek, Antibacterial and herbicidal activity of ring-substituted 3-hydroxynaphthalene-2-carboxanilides, *Molecules*, pp. 7977–7997, 2013.
- [33] J. Kos, E. Nevin, M. Soral, I. Kushkevych, Y.J. Jampilek, Synthesis and antimycobacterial properties of ring-substituted 6-hydroxynaphthalene-2-carboxanilides, *Bioorg. Med. Chem.* (2015) 20–25.
- [34] G.M. Morris, R. Huey, W. Lindstrom, M.F. Sanner, Y.A.J. Olson, AutoDock4 and AutoDockTools4: automated docking with selective receptor flexibility, *J. Comput. Chem.* (2009) 2785–2791.
- [35] AMBER 2014, 2014.
- [36] K. Lindorff-Larsen, S. Piana, K. Palmo, P. Maragakis, Y.D. E. Shaw, Improved Side-Chain Torsion Potentials for the Amber ff99SB Protein Force Field, *Proteins*, p. 1950–1958, 2010.
- [37] J. Wang, R.M. Wolf, J.W. Caldwell, P.A. Kollman, Y.D.A. Case, Development and Testing of a General Amber Force Field, *J. Comput. Chem.* (2004) 1157–1174.
- [38] A.D. Becke, Density-functional Thermochemistry. III. The Role of Exact Exchange, *J. Chem. Phys.* (1993) 5648–5652.
- [39] U. Essmann, L. Perera, Y.M.L. Berkowitz, Smooth Particle Mesh Ewald Method, *J. Chem. Phys.* (1995).
- [40] D. R. Roe, Y.T. E. Cheatham, PTRAJ and CPPTRAJ: Software for Processing and Analysis of Molecular Dynamics Trajectory Data, *J. Chem. Theory Comput.*, p. 3084–3095, 2013.
- [41] S. Genheden, Y.U. Ryde, The MM/PBSA and MM/GBSA Methods to Estimate Ligand-Binding Affinities, *Expert Opin. Drug Discov.* (2015) 449–461.
- [42] U. Koch, Y.P.L. Popelier, Characterization of C–H–O Hydrogen Bonds on the Basis of the Charge Density, *J. Phys. Chem.* (1995) 9747–9754.
- [43] C.F. Matta, N. Castillo, Y.R.J. Boyd, Extended Weak Bonding Interactions in DNA: π -Stacking (Base – Base), Base – Backbone, and Backbone – Backbone Interactions, *J. Phys. Chem.* (2005) 563–578.
- [44] R. A. Mosquera, M. J. Moa, L. Estevez, M. Mandado, Y.A. M. Graña, An Electron Density-Based Approach to the Origin of Stacking Interactions, de Quantum Biochemistry, Weinheim, Germany, Ed. WILEY-VCH Verlag GmbH & Co, 2010, pp. 365–387.
- [45] R.F.W. Bader, Atoms in molecules, *Acc. Chem. Res.* (1985) 9–15.
- [46] R.F. Bader, A quantum theory of molecular structure and its applications, *Chem. Rev.* (1991) 893–928.
- [47] R. F. Bader, The Quantum Mechanical Basis of Conceptual Chemistry, *Monatshefte für Chemie*, p. 819–854, 2005.
- [48] R.F. Bader, Atoms in Molecules, *Encycl. Comput. Chem.* (1998).
- [49] S.A. Andujar, R.D. Tosso, F.D. Suvire, E. Angelina, Y.R.D. Enriz, Searching the “Biologically Relevant” Conformation of Dopamine: A Computational Approach, *J. Chem. Inf. Model.* (2012) 99–112.
- [50] R.D. Tosso, S.A. Andujar, L. Gutierrez, E. Angelina, Y.R.D. Enriz, Molecular Modeling Study of Dihydrofolate Reductase Inhibitors. Molecular Dynamics Simulations, Quantum Mechanical Calculations, and Experimental Corroboration, *J. Chem. Inf. Model.* (2013) 2018–2032.
- [51] F. Chen, Multiwfn: A multifunctional wavefunction analyzer, *J. Comput.*, pp. 580–592, 2012.
- [52] T. A. Keith, T. G. S. AIMAll (Version 19.02.13), Overl. Park KS, USA, 2019.
- [53] M. J. Frisch, G. W. Trucks, H. B. Schlegel, G. E. Scuseria, Y.D. J. Fox, Gaussian 16, Revision B.01, 2016, Wallingford CT, 2016.
- [54] C. Lee, W. Yang, Y.R.G. Parr, Development of the Colle-Salvetti Correlation-Energy Formula into a Functional of the Electron Density, *Phys. Rev. B. Condens. Matter* (1988) 785–789.
- [55] W.J. Hehre, R. Ditchfield, Y.J.A. Pople, Self-Consistent Molecular Orbital Methods. XII. Further Extensions of Gaussian—Type Basis Sets for Use in Molecular Orbital Studies of Organic Molecules, *J. Chem. Phys.* (1972).
- [56] S. Grimme, Semiempirical GGA-Type Density Functional Constructed with a Long-Range Dispersion Correction, *J. Comput. Chem.* (2006) 1787–1799.

č.	citace	ISSN
18	<p>KOS, J*(corresponding author)*, T GONEC, M ORAVEC, I JENDRZEJEWSKA a J JAMPILEK. Photosynthesis-Inhibiting Activity of N-(Disubstituted-phenyl)-3-hydroxynaphthalene-2-carboxamides. <i>MOLECULES</i> [online]. 2021, 26(14). Dostupné z: doi:10.3390/molecules26144336</p>	1420-3049

Article

Photosynthesis-Inhibiting Activity of *N*-(Disubstituted-phenyl)-3-hydroxynaphthalene-2-carboxamides [†]

Jiri Kos ^{1,*} , Tomas Gonec ² , Michal Oravec ³, Izabela Jendrzewska ⁴ and Josef Jampilek ⁵ 

¹ Department of Biochemistry, Faculty of Medicine, Masaryk University, Kamenice 5, 62500 Brno, Czech Republic

² Department of Chemical Drugs, Faculty of Pharmacy, Masaryk University, Palackeho tr. 1946/1, 61200 Brno, Czech Republic; t.gonec@seznam.cz

³ Global Change Research Institute of the Czech Academy of Sciences, Belidla 986/4a, 60300 Brno, Czech Republic; oravec.m@czechglobe.cz

⁴ Institute of Chemistry, University of Silesia, Szkolna 9, 40007 Katowice, Poland; izabela.jendrzewska@us.edu.pl

⁵ Department of Analytical Chemistry, Faculty of Natural Sciences, Comenius University, Ilkovicova 6, 84215 Bratislava, Slovakia; josef.jampilek@gmail.com

* Correspondence: jirikos85@gmail.com

[†] Preliminary results presented at the 24th International Electronic Conference on Synthetic Organic Chemistry, 15 November–15 December 2020. Available online: <https://ecsoc-24.sciforum.net/>.

Abstract: A set of twenty-four 3-hydroxynaphthalene-2-carboxanilides, disubstituted on the anilide ring by combinations of methoxy/methyl/fluoro/chloro/bromo and ditrifluoromethyl groups at different positions, was prepared. The compounds were tested for their ability to inhibit photosynthetic electron transport (PET) in spinach (*Spinacia oleracea* L.) chloroplasts. *N*-(3,5-Difluorophenyl)-, *N*-(3,5-dimethylphenyl)-, *N*-(2,5-difluorophenyl)- and *N*-(2,5-dimethylphenyl)-3-hydroxynaphthalene-2-carboxamides showed the highest PET-inhibiting activity (IC₅₀ ~ 10 μM) within the series. These compounds were able to inhibit PET in photosystem II. It has been found that PET-inhibiting activity strongly depends on the position of the individual substituents on the anilide ring and on the lipophilicity of the compounds. The electron-withdrawing properties of the substituents contribute towards the PET activity of these compounds.

Keywords: hydroxynaphthalene-carboxamides; PET inhibition; spinach chloroplasts; structure-activity relationships



Citation: Kos, J.; Gonec, T.; Oravec, M.; Jendrzewska, I.; Jampilek, J. Photosynthesis-Inhibiting Activity of *N*-(Disubstituted-phenyl)-3-hydroxynaphthalene-2-carboxamides. *Molecules* **2021**, *26*, 4336. <https://doi.org/10.3390/molecules26144336>

Academic Editor: Julio A. A. Seijas Vázquez

Received: 5 June 2021

Accepted: 14 July 2021

Published: 17 July 2021

Publisher's Note: MDPI stays neutral with regard to jurisdictional claims in published maps and institutional affiliations.



Copyright: © 2021 by the authors. Licensee MDPI, Basel, Switzerland. This article is an open access article distributed under the terms and conditions of the Creative Commons Attribution (CC BY) license (<https://creativecommons.org/licenses/by/4.0/>).

1. Introduction

Due to population growth, there is a constant pressure on farmers to multiply yields to ensure sufficient food. On the other hand, this challenge is difficult to meet due to deteriorating conditions for agriculture, such as the loss of quality agricultural land, desiccation or, conversely, heavy rains and floods, climate change and the rise of many plant and crop destroyers. One way to combat pathogens of plants is to use pesticides to help farmers increase productivity per hectare by protecting plants from pests, diseases and weeds. For example, food crops must compete with approximately 30,000 weed species. Herbicides are still used widely around the world because manual weeding has never been an effective method of weed control, especially when large-scale farming is used. Herbicides are often used instead of tillage because the use of herbicides reduces erosion, fuel consumption, greenhouse gas emissions and nutrient leakage, and saves water compared to plowing. Of course, the question remains as to what extent the negative chemical effects of herbicides harm non-target organisms and degrade soil and water resources [1–3].

Herbicides can be classified according to the type/chemical structure of the active ingredient, mechanism of action, method and time of application, mobility, type of formulation or residual effect [4–6]. There are currently about 20 different mechanisms of action of

herbicides [4–11], but over 50% of commercially available herbicides act by reversibly binding to photosystem II (PS II), resulting in disruption of photosynthetic electron transport (PET) [4,6–8]. PS II uses light energy to oxidize water and reduce plastoquinone, which consists of parts Q_A and Q_B . The plastoquinone Q_A acting as a single electron acceptor is permanently bound to PS II; the plastoquinone Q_B acting as a two-electron acceptor is loosely bound; after reduction, it separates from the reaction center and diffuses into the hydrophobic membrane nucleus, the Q_B binding site being occupied by the oxidized molecule plastoquinone [12]. Herbicides belonging to inhibitors of PS II inhibit photosynthetic electron transfer (PET) by binding to the Q_B binding niche on the D_1 protein of the PS II complex in chloroplast thylakoid membranes, leading to inhibition of PET from Q_A to Q_B , blocking CO_2 fixation and inhibition of ATP production [6,9–11].

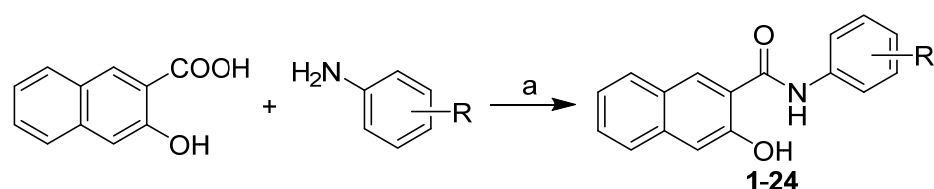
Studies of large libraries of structurally diverse PS II inhibitors have confirmed the hydrophobic nature of the binding domain, with lipophilicity being the dominant determinant of Hill inhibitory activity [12–18]. Significant amounts of herbicides acting as PET inhibitors in PS II contain an amide (–CONH–) and/or carbamate (–HNCOO–) bond in their structure that is capable of forming hydrogen bonds between the amide/carbamate group and target proteins in the photosynthetic centers of thylakoid membranes, leading to conformational changes and PET inhibition [19–25]. Both the *N*- and *O*-terminal ends of the CONH linker are substituted and the substituents further modify the bond properties and strength of the basic scaffold [26]. Amides are thought to be inhibitors of PS II, causing the displacement of Q_B from its binding pocket in the D_1 protein [27], and halogenated substituents have been found to contribute to increased PET inhibitory activity [18,23,24,28–30].

Our team has long been investigating the effects of a wide range of variously substituted naphthalenecarboxanilides [23,24,27,29–31] and quinolinecarboxanilides [32] on PS II. A series of ring-monosubstituted anilides of 3-hydroxynaphthalene-2-carboxylic acid was published by Kos et al. [29] and some interesting biological activity was found, including herbicidal activity. Since monosubstituted derivatives of 3-hydroxy-*N*-arylnaphthalene-2-carboxanilides showed PET inhibition in spinach chloroplasts (*Spinacia oleracea* L.), select new, variously disubstituted, derivatives were evaluated for their PET-inhibiting activity.

2. Results and Discussion

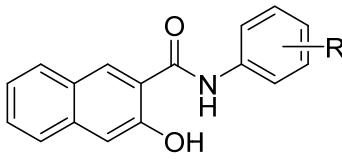
2.1. Chemistry

All compounds were prepared by the reaction of 3-hydroxynaphthalene-2-carboxylic acid with appropriate disubstituted anilines with the addition of phosphorus trichloride in dry chlorobenzene under microwave conditions (Scheme 1) [29,31], which resulted in a series of target *N*-(disubstituted-phenyl)-3-hydroxynaphthalene-2-carboxamides **1–24**, see Table 1.



Scheme 1. Synthesis of 3-hydroxy-*N*-arylnaphthalene-2-carboxanilides **1–24**. Reagents and conditions: (a) PCl_3 , chlorobenzene, MW, 45 min [29,31].

Table 1. Structure of ring-disubstituted 3-hydroxynaphthalene-2-carboxanilides **1–24**, calculated values of Clog *P* for compounds, electronic σ parameters of anilide (Ar) and IC₅₀ [μ M] values related to photosynthetic electron transport (PET) inhibition in spinach chloroplasts of tested compounds in comparison with the 3-(3,4-dichlorophenyl)-1,1-dimethylurea (DCMU) standard.



Comp.	R	Clog <i>P</i> ²	$\sigma_{(Ar)}$ ³	PET Inhibition IC ₅₀ [μ M]
1 ¹	2,5-OCH ₃	3.9563	0.08	183
2 ¹	3,5-OCH ₃	4.5463	0.93	24.5
3 ¹	2,5-CH ₃	4.7942	0.59	11.6
4 ¹	2,6-CH ₃	4.1442	0.58	28.5
5 ¹	3,5-CH ₃	5.4442	0.59	9.9
6 ¹	2,5-F	4.4799	1.24	11.2
7 ¹	2,6-F	3.8799	1.44	78.7
8 ¹	3,5-F	5.0799	1.12	9.8
9 ¹	2,5-Cl	5.3699	1.22	321
10 ¹	2,6-Cl	4.5199	1.33	156
11 ¹	3,4-Cl	6.0999	1.19	47.5
12 ¹	3,5-Cl	6.2199	1.11	39.2
13	2,4-Br	5.6399	1.11	296
14	2,5-Br	5.6399	1.23	161
15 ¹	3,5-CF ₃	6.8207	1.05	15.9
16	2-OCH ₃ -5-F	4.2725	0.14	79.1
17	2-F-6-OCH ₃	3.6725	0.16	507
18	3-F-5-OCH ₃	4.8625	0.99	31.6
19	2-Cl-5-OCH ₃	4.5825	1.13	171
20	2-F-4-Cl	5.0499	1.17	1405
21 ¹	3-F-4-Br	5.7999	1.16	527
22 ¹	3-F-5-CF ₃	6.0131	1.04	31.0
23 ¹	2-Cl-5-CF ₃	5.7331	1.19	13.2
24 ¹	2-Br-4-CF ₃	5.8531	1.32	621
DCMU	–	–	–	2.1

¹ Compounds described in [31]; ² ChemBioDraw Ultra 13.0 (CambridgeSoft, PerkinElmer Inc., MA, USA); ³ calculated using ACD/Percepta ver. 2012 (Advanced Chemistry Development, Toronto, ON, Canada).

Lipophilicity is an extremely important parameter in the design of any biologically active compound, as it primarily ensures sufficient penetration across biological membranes to reach the target site of action [33]. In general, it can be stated that a higher value of lipophilicity is required for agrochemicals acting in plant leaves due to the permeability of a stronger and more lipophilic cuticle [34]. Lipophilicity, expressed as Clog *P* values (predicted by ChemBioDraw Ultra 13.0), of the investigated compounds is listed in Table 1. Clog *P* values ranged from 3.6 (compound **17**, R = 2-F-6-OCH₃) to 6.8 (compound **15**, R = 3,5-CF₃). When comparing the general effect of substituents at the same positions on lipophilicity, the order of the groups with respect to the increasing contribution of lipophilicity is as follows: OCH₃ < F < CH₃ < Cl < Br < CF₃; thus, in general, any substitution by a fluorine or methoxy moiety significantly decreases lipophilicity. In addition to the type of substituent, their mutual position on the aniline ring also has a significant effect on the lipophilicity value. For example, in series with dichlorinated derivatives, lipophilicity increases as follows: 2.6 < 2.5 < 3.4 < 3.5. In series with different moieties of disubstituted compounds, the Clog *P* values are significantly decreased when a fluorine or methoxy moiety is introduced, especially in positions C₍₂₎' and C₍₆₎', as mentioned above. The predicted Clog *P* values are presented in the illustrated order in Figure 1, where they

are simultaneously divided into three groups according to the nature of the substitution. The first group consists of methoxy-, methyl- and fluoro-disubstituted compounds 1–8; the second group consists of dichloro, dibromo and 3,5-CF₃ derivatives 9–15; and derivatives 16–24, disubstituted by two different substituents, are in the third group. This division proves important for the description of PET inhibition, see below.

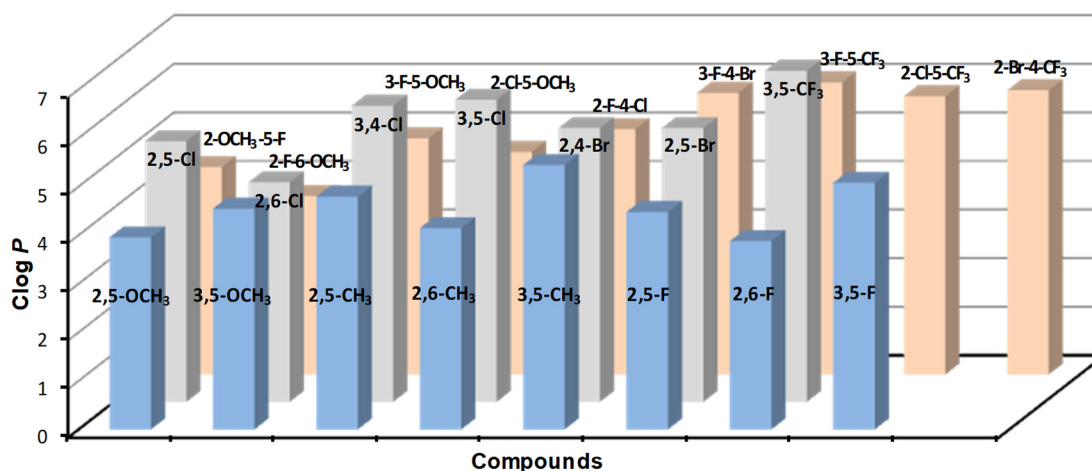


Figure 1. Graphical comparison of lipophilicity of investigated compounds expressed as Clog *P*, predicted by ChemBioDraw Ultra 13.0.

Electronic contributions of substituents are another important parameter, especially for substituted aromatic rings (anilines, phenols). The electron σ parameters of the whole substituted anilide ring, predicted by the ADC/Percepta program, are listed in Table 1. As with the lipophilicity values, the σ values are in a wide range. Based on the results of the prediction program, the weakest electron-withdrawing properties have the substitution 2,5-OCH₃-Ph of compound 1 ($\sigma = 0.08$), while the strongest electron-withdrawing properties have fluoro-substituted derivative 7 (2,6-F-Ph, $\sigma = 1.44$). These values affect the electron density at the amide linker and thus the overall binding to the putative site of action of these compounds, which is on the acceptor side of PS II, at the section between P₆₈₀ (primary donor of PS II) and Q_B [23–25,29].

2.2. Inhibition of Photosynthetic Electron Transport (PET) in Spinach Chloroplasts

The PET-inhibition of the studied compounds was expressed by the negative logarithm of the IC₅₀ value (concentration (in μ M) of the compounds causing a 50% decrease in the oxygen evolution rate relative to the untreated control). The evaluated disubstituted 3-hydroxynaphthalene-2-carboxanilides showed a wide range of PET inhibition in spinach (*Spinacia oleracea* L.) chloroplasts with the IC₅₀ values ranging from 9.8 to 1405 μ M, see Table 1. *N*-(3,5-Difluorophenyl)-(8) and *N*-(3,5-dimethylphenyl)-(5), *N*-(2,5-difluorophenyl)-(6) and *N*-(2,5-dimethylphenyl)-(3) 3-hydroxynaphthalene-2-carboxamides demonstrated the highest PET-inhibiting activity (IC₅₀ ~ 10 μ M) within the whole investigated series. Acceptable activity was also found for *N*-(2-chloro-5-trifluoromethylphenyl)-(23) and *N*-(3,5-ditrifluoromethylphenyl)-3-hydroxynaphthalene-2-carboxamides (15) with IC₅₀ 13.2 and 15.9 μ M, respectively. On the other hand, derivatives 21 (3-F-4-Br), 24 (2-Br-4-CF₃) and 20 (R = 2-F-4-Cl) were completely inactive (IC₅₀ = 527, 621 and 1405 μ M, respectively).

The results of this screening indicate that the position of the substituents is crucial for the activity, with the 3,5 positions being the most preferred (i.e., both *meta* positions are substituted). However, 2,5-disubstituted derivatives also showed PET-inhibiting activity when substituted with moieties with suitable properties, including electronic properties and lipophilicity. As mentioned above, lipophilicity tends to affect biological activity. The dependence of the PET-inhibiting activity, expressed as $\log(1/IC_{50} [M])$, of the investigated

compounds in spinach chloroplasts on lipophilicity (Clog *P*) is shown in Figure 2A. It can be stated that most of the evaluated compounds substituted by OCH₃/CH₃/F can be traced to a quasi-parabolic dependence with the optimum Clog *P* ca. 5. The active compounds have a range of lipophilicity values from 4.4 to 5.7. On the other hand, a linear dependence can be observed for the dichloro-, dibromo- and bis(trifluoromethyl)-substituted compounds, i.e., markedly lipophilic groups. The inhibition of PET increases with increasing lipophilicity.

Figure 2B shows the dependence of the PET-inhibiting activity, expressed as log(1/IC₅₀ [M]), on the electronic $\sigma_{(Ar)}$ properties of the whole anilide substituents. As can be seen, electronic properties play a secondary role compared to lipophilicity and substituent position; however, the quasi-parabolic (for OCH₃/CH₃/F substituted compounds) or linear (for disubstituted compounds by Cl/Br/CF₃ moieties) trend is evident. It can be stated that electron-withdrawing properties in the range of $\sigma_{(Ar)}$ from approximately 0.6 to 1.2 are preferred.

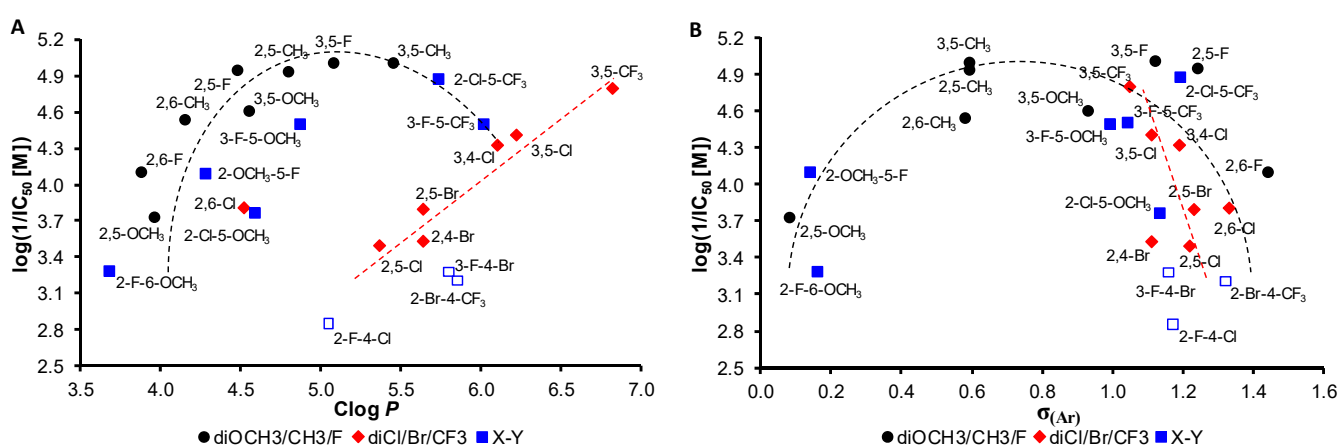


Figure 2. Dependence of PET-inhibiting activity log(1/IC₅₀ [M]) of all discussed compounds 1–24 in spinach chloroplasts on lipophilicity expressed as Clog *P* (A) and electronic σ parameters of whole *N*-aryl part of individual anilides (B). Empty squares are not involved in SAR discussion due to their inactivity.

Based on the structural similarity of the test compounds to previously performed experiments with salicylanilides or hydroxynaphthanilides, the same mechanism of action can be supposed, i.e., inhibition on the acceptor side of PS II, at the section between P₆₈₀ (primary donor of PS II) and plastoquinone Q_B [20–24,27,29–31]. Furthermore, it should be noted that plastoquinone Q_B on the acceptor side of PS II has been found to be the site of inhibitory action of other amide-based derivatives [6,13–15,25,35], such as *N*-phenylpyrazine-2-carboxamides [19], *N*-substituted 2-aminobenzothiazoles [22] or 8-hydroxyquinoline-2-carboxanilides [32].

3. Materials and Methods

3.1. General Information

All reagents were purchased from Merck (Sigma-Aldrich, St. Louis, MO, USA) and Alfa (Alfa-Aesar, Ward Hill, MA, USA). Reactions were performed using a CEM Discover SP microwave reactor (CEM, Matthews, NC, USA). The melting points were determined on a Kofler hot-plate apparatus HMK (Franz Kustner Nacht KG, Dresden, Germany) and are uncorrected. Infrared (IR) spectra were recorded on a Smart MIRacle™ ATR ZnSe for Nicolet™ Impact 410 Fourier-transform IR spectrometer (Thermo Scientific, West Palm Beach, FL, USA). The spectra were obtained by the accumulation of 256 scans with 2 cm⁻¹ resolution in the region of 4000–650 cm⁻¹. All ¹H- and ¹³C-NMR spectra were recorded in dimethyl sulfoxide-*d*₆ (DMSO-*d*₆) at 600 MHz for ¹H and 150 MHz for ¹³C, on an Agilent VNMRs 600 MHz system (Agilent Technologies, Santa Clara, CA, USA). The ¹H and ¹³C chemical shifts (δ) are reported in ppm. High-resolution mass spectra were measured using

a high-performance liquid chromatograph Dionex UltiMate[®] 3000 (Thermo Scientific, West Palm Beach, FL, USA) coupled with an LTQ Orbitrap XL[™] Hybrid Ion Trap-Orbitrap Fourier Transform Mass Spectrometer (Thermo Scientific) equipped with a HESI II (heated electrospray ionization) source in positive and negative mode.

3.2. Synthesis

General Procedure for the Synthesis of *N*-(Disubstituted phenyl)-3-hydroxynaphthalene-2-carboxamides **1–24**

3-Hydroxynaphthalene-2-carboxylic acid (0.5 g, 2.65 mM) was suspended in dry chlorobenzene (20 mL) at ambient temperature and phosphorus trichloride (0.12 mL, 1.35 mM), and the corresponding substituted aniline (2.65 mM) was added dropwise. The reaction mixture was transferred to the microwave reactor, where the synthesis was performed (1st phase: 10 min, 100 °C; 2nd phase: 15 min, 120 °C; 3rd phase: 20 min, 130 °C; max 500 W). The mixture was then cooled to 60 °C, and the solvent was removed under reduced pressure. The residue was washed sequentially with hydrochloric acid and water, and the crude product was recrystallized from EtOH. All the compounds are presented in Table 1.

The synthesis and analytical data for anilides **1–12**, **15** and **21–24** were described previously [31].

N-(2,4-Dibromophenyl)-3-hydroxynaphthalene-2-carboxamide (**13**). Yield 56%; mp 241–243 °C; IR (cm⁻¹): 3221; 1641; 1625; 1603; 1575; 1524; 1462; 1448; 1398; 1363; 1345; 1321; 1290; 1240; 1206; 1175; 1146; 1081; 1035; 951; 913; 878; 867; 846; 825; 791; 767; 737; 688; ¹H NMR (DMSO-*d*₆), δ: 11.97 (s, 1H), 11.07 (s, 1H), 8.70 (s, 1H), 8.42 (d, *J* = 8.8 Hz, 1H), 7.99 (d, *J* = 8.2 Hz, 1H), 7.97 (d, *J* = 2.2 Hz, 1H), 7.78 (d, *J* = 8.3 Hz, 1H), 7.66 (dd, *J* = 2.2 Hz, *J* = 8.8 Hz, 1H), 7.53 (ddd, *J* = 1.2 Hz, *J* = 6.8 Hz, *J* = 8.3 Hz, 1H), 7.38 (s, 1H), 7.37 (ddd, *J* = 1.1 Hz, *J* = 6.8 Hz, *J* = 8.2 Hz, 1H); ¹³C NMR (DMSO-*d*₆), δ: 163.6, 152.6, 136.2, 136.1, 134.4, 132.8, 131.3, 129.1, 128.6, 127.2, 125.7, 124.4, 124.0, 120.4, 116.3, 114.9, 110.8; HR-MS C₁₇H₁₂O₂NBr₂ [M + H]⁺ calculated 419.9229 *m/z*, found 419.9237 *m/z*.

N-(2,5-Dibromophenyl)-3-hydroxynaphthalene-2-carboxamide (**14**). Yield 49%; mp 233–235 °C; IR (cm⁻¹): 3190; 1636; 1622; 1597; 1568; 1506; 1447; 1393; 1360; 1344; 1250; 1192; 1174; 1147; 1080; 1069; 1029; 962; 915; 902; 868; 848; 796; 770; 750; 736; ¹H NMR (DMSO-*d*₆), δ: 12.02 (s, 1H), 11.14 (s, 1H), 8.74 (d, *J* = 2.3 Hz, 1H), 8.71 (s, 1H), 8.00 (d, *J* = 8.2 Hz, 1H), 7.79 (d, *J* = 8.3 Hz, 1H), 7.69 (d, *J* = 8.5 Hz, 1H), 7.54 (ddd, *J* = 1.2 Hz, *J* = 6.8 Hz, *J* = 8.3 Hz, 1H), 7.39 (s, 1H), 7.38 (ddd, *J* = 1.1 Hz, *J* = 6.8 Hz, *J* = 8.2 Hz, 1H), 7.32 (dd, *J* = 2.4 Hz, *J* = 8.5 Hz, 1H); ¹³C NMR (DMSO-*d*₆), δ: 163.6, 152.5, 138.1, 136.2, 134.2, 133.0, 129.1, 128.7, 128.1, 127.2, 125.7, 125.0, 124.0, 120.9, 120.3, 112.7, 110.8; MS C₁₇H₁₂O₂NBr₂ [M + H]⁺ calculated 419.9229 *m/z*, found 419.9239 *m/z*.

N-(5-Fluoro-2-methoxyphenyl)-3-hydroxynaphthalene-2-carboxamide (**16**). Yield 80%; mp 198–203 °C; IR (cm⁻¹): 3194, 1640, 1625, 1615, 1601, 1538, 1488, 1432, 1393, 1356, 1346, 1249, 1214, 1176, 1148, 1065, 1038, 975, 866, 838, 786, 731, 711; ¹H-NMR (DMSO-*d*₆), δ: 11.86 (s, 1H), 11.25 (s, 1H), 8.70 (s, 1H), 8.40 (dd, *J* = 11.0 Hz, *J* = 3.3 Hz, 1H), 7.93 (d, *J* = 8.1 Hz, 1H), 7.78 (d, *J* = 8.4 Hz, 1H), 7.53 (t, *J* = 7.5 Hz, 1H), 7.37 (s, 1H), 7.36 (t, *J* = 7.5 Hz, 1H), 7.12 (dd, *J* = 9.2 Hz, *J* = 5.1 Hz, 1H), 6.92 (td, *J* = 8.6 Hz, *J* = 3.3 Hz, 1H), 3.92 (s, 3H); ¹³C-NMR (DMSO-*d*₆), δ: 163.0, 156.0 (d, *J* = 232.2 Hz), 152.4, 144.8 (d, *J* = 1.8 Hz), 136.0, 132.9, 129.1, 129.0 (d, *J* = 12.9 Hz), 128.5, 127.2, 125.7, 123.9, 121.0, 111.7 (d, *J* = 9.1 Hz), 110.8, 109.0 (d, *J* = 22.8 Hz), 106.9 (d, *J* = 29.6 Hz), 57.0; HR-MS: C₁₈H₁₃FNO₃ [M – H]⁻ calculated 310.0885 *m/z*, found 310.0881 *m/z*.

N-(2-Fluoro-6-methoxyphenyl)-3-hydroxynaphthalene-2-carboxamide (**17**). Yield 66%; mp 138–144 °C; IR (cm⁻¹): 3259, 2836, 1651, 1622, 1596, 1532, 1515, 1506, 1466, 1438, 1279, 1249, 1216, 1167, 1146, 1087, 900, 873, 834, 789, 767, 747, 728; ¹H-NMR (DMSO-*d*₆), δ: 11.76 (s, 1H), 10.22 (s, 1H), 8.69 (s, 1H), 7.93 (d, *J* = 8.8 Hz, 1H), 7.78 (d, *J* = 8.4 Hz, 1H), 7.54 (t, *J* = 7.3 Hz, 1H), 7.30–7.40 (m, 3H), 6.99 (d, *J* = 8.4 Hz, 1H), 6.94 (t, *J* = 9.0 Hz, 1H), 3.84 (s, 3H); ¹³C-NMR (DMSO-*d*₆), δ: 166.3, 158.1 (d, *J* = 246.4 Hz), 155.8 (d, *J* = 5.3 Hz), 154.6, 136.2, 131.0, 128.9,

128.5, 128.2 (d, $J = 10.7$ Hz), 126.8, 125.8, 123.9, 118.7, 113.7 (d, $J = 15.3$ Hz), 110.9, 107.9 (d, $J = 26.4$ Hz), 107.7, 56.3; HR-MS: $C_{18}H_{13}FNO_3$ $[M - H]^-$ calculated 310.0885 m/z , found 310.0880 m/z .

N-(3-Fluoro-5-methoxyphenyl)-3-hydroxynaphthalene-2-carboxamide (**18**). Yield 59%; mp 227–230 °C; IR (cm^{-1}): 3147, 1644, 1622, 1595, 1557, 1520, 1456, 1448, 1359, 1261, 1224, 1212, 1191, 1141, 1129, 1063, 999, 987, 872, 858, 816, 767, 745, 690; 1H -NMR (DMSO- d_6), δ : 11.12 (s, 1H), 10.64 (s, 1H), 8.41 (s, 1H), 7.93 (d, $J = 8.4$ Hz, 1H), 7.76 (d, $J = 8.1$ Hz, 1H), 7.51 (t, $J = 7.0$ Hz, 1H), 7.32–7.40 (m, 3H), 7.21 (s, 1H), 6.62 (d, $J = 11.0$ Hz, 1H), 3.78 (s, 3H); ^{13}C -NMR (DMSO- d_6), δ : 165.7, 162.9 (d, $J = 238.5$ Hz), 160.7 (d, $J = 12.9$ Hz), 153.3, 140.6 (d, $J = 13.7$ Hz), 135.7, 130.5, 128.7, 128.1, 126.9, 125.8, 123.8, 122.5, 110.5, 102.0 (d, $J = 2.0$ Hz), 99.4 (d, $J = 27.3$ Hz), 97.0 (d, $J = 25.0$ Hz), 55.6; HR-MS: $C_{18}H_{13}FNO_3$ $[M - H]^-$ calculated 310.0885 m/z , found 310.0881 m/z .

N-(2-Chloro-5-methoxyphenyl)-3-hydroxynaphthalene-2-carboxamide (**19**). Yield 58%; mp 187–188 °C; IR (cm^{-1}): 3177, 2954, 2834, 1638, 1624, 1598, 1539, 1462, 1447, 1427, 1358, 1305, 1274, 1262, 1220, 1167, 1147, 1135, 1063, 1028, 960, 916, 866, 845, 787, 771, 745, 719; 1H -NMR (DMSO- d_6), δ : 11.97 (s, 1H), 11.17 (s, 1H), 8.73 (s, 1H), 8.25 (d, $J = 2.9$ Hz, 1H), 7.99 (d, $J = 8.2$ Hz, 1H), 7.78 (d, $J = 8.3$ Hz, 1H), 7.53 (ddd, $J = 8.3$ Hz, $J = 6.8$ Hz, $J = 1.2$ Hz, 1H), 7.46 (d, $J = 8.8$ Hz, 1H), 7.38 (ddd, $J = 8.2$ Hz, $J = 6.8$ Hz, $J = 1.2$ Hz, 1H), 7.38 (s, 1H), 6.78 (dd, $J = 8.8$ Hz, $J = 3.0$ Hz, 1H), 3.80 (s, 3H); ^{13}C -NMR (DMSO- d_6), δ : 163.4, 158.5, 152.5, 136.1, 132.9, 129.6, 129.1, 128.6, 127.2, 125.7, 124.0, 120.6, 114.2, 110.8, 110.4, 108.0, 55.5; HR-MS: $C_{18}H_{15}ClNO_3$ $[M + H]^+$ calculated 328.0735 m/z , found 328.0737 m/z .

N-(4-Chloro-2-fluorophenyl)-3-hydroxynaphthalene-2-carboxamide (**20**). Yield 75%; mp 267–269 °C; IR (cm^{-1}): 3194, 1647, 1627, 1601, 1552, 1489, 1449, 1414, 1393, 1357, 1338, 1259, 1207, 1174, 1147, 1118, 1064, 951, 918, 897, 870, 841, 820, 767, 740, 722, 667; 1H NMR (DMSO- d_6) δ : 11.85 (s, 1H), 10.97 (s, 1H), 8.66 (s, 1H), 8.37 (t, $J = 8.7$ Hz, 1H), 7.97 (d, $J = 8.2$ Hz, 1H), 7.77 (d, $J = 8.3$ Hz, 1H), 7.56 (dd, $J = 2.4$ Hz, $J = 10.8$ Hz, 1H), 7.52 (ddd, $J = 1.2$ Hz, $J = 6.8$ Hz, $J = 8.3$ Hz, 1H), 7.37 (ddd, $J = 1.1$ Hz, $J = 6.8$ Hz, $J = 8.2$ Hz, 1H), 7.36 (s, 1H), 7.34 (ddd, $J = 1.2$ Hz, $J = 2.4$ Hz, $J = 8.8$ Hz, 1H). ^{13}C NMR (DMSO- d_6), δ : 163.8, 152.8 (d, $J = 247.5$ Hz), 152.8, 136.1, 132.4, 129.0, 128.5, 127.9 (d, $J = 10.0$ Hz), 127.1, 125.7, 125.7 (d, $J = 10.7$ Hz), 124.9 (d, $J = 3.4$ Hz), 124.0, 123.6, 120.4, 115.9 (d, $J = 23.1$ Hz), 110.9; HR-MS: $C_{17}H_{12}ClFNO_2$ $[M + H]^+$ calculated 316.0535 m/z , found 316.0535 m/z .

3.3. Study of Inhibition of Photosynthetic Electron Transport (PET) in Spinach Chloroplasts

Chloroplasts were prepared from spinach (*Spinacia oleracea* L.) according to Kralova et al. [36]. Screening was performed as described previously [e.g., 19–25,31]. A selective herbicide 3-(3,4-dichlorophenyl)-1,1-dimethylurea, DCMU (Diuron[®], Merck, Darmstadt, Germany) was used as a standard. The results are summarized in Table 1.

4. Conclusions

A series of 3-hydroxynaphthalene-2-carboxanilides substituted with two similar or different atoms or groups on the anilide ring was prepared under microwave-assisted conditions and tested for their ability to inhibit photosynthetic electron transport (PET) in spinach (*Spinacia oleracea* L.) chloroplasts. *N*-(3,5-Difluorophenyl)-3-hydroxynaphthalene-2-carboxamide (**8**), *N*-(3,5-dimethylphenyl)-3-hydroxynaphthalene-2-carboxamide (**5**), *N*-(2,5-difluorophenyl)-3-hydroxynaphthalene-2-carboxamide (**6**) and *N*-(2,5-dimethylphenyl)-3-hydroxynaphthalene-2-carboxamide (**3**) exhibited the highest PET-inhibiting activity with their IC_{50} values ranging from 9.8 to 11.6 μ M. The $C_{(3,5)}$ and $C_{(2,5)}$ disubstituted isomers were found to be the most active among the test compounds. Furthermore, for diOCH₃/diCH₃/diF substituted derivatives, a Clog P value of approximately 5 is important, while for diCl/diBr/diCF₃ substituted derivatives, PET inhibition increases with increasing lipophilicity to a Clog P value of 6.8 of *N*-(3,5-ditrifluoromethylphenyl)-3-hydroxynaphthalene-2-carboxamides (**15**) with $IC_{50} = 15.9$ μ M. The electronic properties of the substituents play a complementary role and the electron-withdrawing properties

($\sigma_{(Ar)}$ ca. 0.6 to 1.2) for PET activity seem to be more advantageous. Based on the structural similarity of the investigated compounds with previously published isomers, it can be concluded that these hydroxynaphthanilides inhibit PET in photosystem II.

Author Contributions: J.K., T.G. and I.J. synthesized and characterized the compounds. M.O. performed analytical measurement. J.K. performed biological screening. J.J. designed the compounds. J.K., T.G. and J.J. wrote the paper. All authors have read and agreed to the published version of the manuscript.

Funding: This study was supported by the Slovak Research and Development Agency (projects APVV-17-0373 and APVV-17-0318). This work is based on use of Large Research Infrastructure CzeCOS supported by the Ministry of Education, Youth and Sports of the Czech Republic within the CzeCOS program, grant number LM2018123; M.O. was supported by SustES—Adaptation strategies for sustainable ecosystem services and food security under adverse environmental conditions, project no. CZ.02.1.01/0.0/0.0/16_019/0000797.

Institutional Review Board Statement: Not applicable.

Informed Consent Statement: Not applicable.

Data Availability Statement: Data is contained within the article.

Conflicts of Interest: The authors declare no conflict of interest.

References

1. Importance & Benefits of Pesticides. CropLife International: Brussels, Belgium, 2020. Available online: <https://pesticidefacts.org/topics/necessity-of-pesticides/> (accessed on 19 May 2021).
2. Gianessi, L.P. The increasing importance of herbicides in worldwide crop production. *Pest. Manag. Sci.* **2013**, *69*, 1099–1105. [CrossRef] [PubMed]
3. Gianessi, L.; Williams, A. The importance of herbicides for natural resource conservation in the USA. In *Convergence of Food Security, Energy Security and Sustainable Agriculture*; Songstad, D., Hatfield, J., Tomes, D., Eds.; Springer: Heidelberg, Germany, 2014; pp. 333–350.
4. Classification of Herbicides. Weed Management in Horticulture Crops. Available online: <http://ecoursesonline.iasri.res.in/mod/page/view.php?id=12032> (accessed on 19 May 2021).
5. Forouzes, A.; Zand, E.; Soufizadeh, S.; Foroushani, S.S. Classification of herbicides according to chemical family for weed resistance management strategies—An update. *Weed Res.* **2015**, *55*, 334–358. [CrossRef]
6. Herbicide Resistance Action Committee. HRAC Mode of Action Classification 2020 Map. Available online: <https://hracglobal.com/tools/hrac-mode-of-action-classification-2020-map> (accessed on 19 May 2021).
7. Draber, W.; Tietjen, K.; Kluth, J.F.; Trebst, A. Herbicides in photosynthesis research. *Angew. Chem.* **1991**, *3*, 1621–1633. [CrossRef]
8. Tischer, W.; Strotmann, H. Relationship between inhibitor binding by chloroplasts and inhibition of photosynthetic electron-transport. *Biochim. Biophys. Acta* **1977**, *460*, 113–125. [CrossRef]
9. Trebst, A.; Draber, W. Structure activity correlations of recent herbicides in photosynthetic reactions. In *Advances in Pesticide Science*; Greissbuehler, H., Ed.; Pergamon Press: Oxford, UK, 1979; pp. 223–234.
10. Bowyer, J.R.; Camilleri, P.; Vermaas, W.F.J. *Herbicides, Topics in Photosynthesis*; Baker, N.R., Percival, M.P., Eds.; Elsevier: Amsterdam, The Netherlands, 1991; pp. 27–85.
11. Izawa, S. Acceptors and donors for chloroplast electron transport. In *Methods in Enzymology*; Part, C., Colowick, P., Kaplan, N.O., Eds.; Academic Press: New York, NY, USA; London, UK, 1980; pp. 413–434.
12. Whitmarsh, J. Electron transport and energy transduction. In *Photosynthesis: A Comprehensive Treatise*; Raghavendra, A.S., Ed.; Cambridge University Press: Cambridge, UK, 1998; pp. 87–110.
13. Jablonkai, I. Molecular mechanism of action of herbicides. In *Herbicides—Mechanisms and Mode of Action*; Abd El-Ghany Hasaneen, M.N., Ed.; IntechOpen: Rijeka, Croatia, 2011; Chapter 1. Available online: <https://www.intechopen.com/books/herbicides-physiology-of-action-and-safety/modes-of-action-of-different-classes-of-herbicides> (accessed on 19 May 2021).
14. Sherwani, S.I.; Arif, I.A.; Khan, H.A. Modes of action of different classes of herbicides. In *Herbicides—Physiology of Action, and Safety*; Price, A., Kelton, J., Sarunaite, L., Eds.; IntechOpen: Rijeka, Croatia, 2015; Chapter 8. Available online: <https://www.intechopen.com/books/herbicides-physiology-of-action-and-safety/modes-of-action-of-different-classes-of-herbicides> (accessed on 19 May 2021).
15. Huppatz, J.L.; McFadden, H.G. Understanding the topography of the photosystem II herbicide binding niche: Does QSAR help? *Z. Naturforsch.* **1993**, *48*, 140–145. [CrossRef]
16. Lambrea, M.D.; Russo, D.; Polticelli, F.; Scognamiglio, V.; Antonacci, A.; Zobnina, V.; Campi, G.; Rea, G. Structure/function/dynamics of photosystem II plastoquinone binding sites. *Curr. Protein Pept. Sci.* **2014**, *15*, 285–295. [CrossRef] [PubMed]

17. Trebst, A. Inhibitors in the functional dissection of the photosynthetic electron transport system. *Photosynth. Res.* **2007**, *92*, 217–224. [[CrossRef](#)]
18. Teixeira, R.R.; de Andrade Barros, M.V.; Bressan, G.C.; Siqueira, R.P.; Dos Santos, F.S.; Bertazzini, M.; Kiralj, R.; Ferreira, M.M.C.; Forlani, G. Synthesis, theoretical studies, and effect on the photosynthetic electron transport of trifluoromethyl arylamides. *Pest. Manag. Sci.* **2017**, *73*, 2360–2371. [[CrossRef](#)]
19. Dolezal, M.; Zitko, J.; Osicka, Z.; Kunes, J.; Vejsova, M.; Buchta, V.; Dohnal, J.; Jampilek, J.; Kralova, K. Synthesis, antimycobacterial, antifungal and photosynthesis-inhibiting activity of chlorinated N-phenylpyrazine-2-carboxamides. *Molecules* **2010**, *15*, 8567–8581. [[CrossRef](#)] [[PubMed](#)]
20. Imramovsky, A.; Pesko, M.; Kralova, K.; Vejsova, M.; Stolarikova, J.; Vinsova, J.; Jampilek, J. Investigating spectrum of biological activity of 4- and 5-chloro-2-hydroxy-N-[2-(arylamino)-1-alkyl-2-oxoethyl]benzamides. *Molecules* **2011**, *16*, 2414–2430. [[CrossRef](#)]
21. Imramovsky, A.; Pesko, M.; Monreal-Ferriz, J.; Kralova, K.; Vinsova, J.; Jampilek, J. Photosynthesis-inhibiting efficiency of 4-chloro-2-(chlorophenylcarbamoyl)phenyl alkyl-carbamates. *Bioorg. Med. Chem. Lett.* **2011**, *21*, 4564–4567. [[CrossRef](#)]
22. Fajkusova, D.; Pesko, M.; Keltosova, S.; Guo, J.; Oktabec, Z.; Vejsova, M.; Kollar, P.; Coffey, A.; Csollei, J.; Kralova, K.; et al. Anti-infective and herbicidal activity of N-substituted 2-aminobenzothiazoles. *Bioorg. Med. Chem.* **2012**, *20*, 7059–7068. [[CrossRef](#)]
23. Gonec, T.; Kos, J.; Zadrazilova, I.; Pesko, M.; Keltosova, S.; Tengler, J.; Bobal, P.; Kollar, P.; Cizek, A.; Kralova, K.; et al. Antimycobacterial and herbicidal activity of ring-substituted 1-hydroxynaphthalene-2-carboxanilides. *Bioorg. Med. Chem.* **2013**, *21*, 6531–6541. [[CrossRef](#)]
24. Gonec, T.; Kos, J.; Pesko, M.; Dohanosova, J.; Oravec, M.; Liptaj, T.; Kralova, K.; Jampilek, J. Halogenated 1-Hydroxynaphthalene-2-Carboxanilides Affecting Photosynthetic Electron Transport in Photosystem II. *Molecules* **2017**, *22*, 1709. [[CrossRef](#)]
25. Bak, A.; Pizova, H.; Kozik, V.; Vorcakova, K.; Kos, J.; Tremel, J.; Odehnalova, K.; Oravec, M.; Imramovsky, A.; Bobal, P.; et al. SAR-mediated Similarity Assessment of the Property Profile for New, Silicon-Based AChE/BChE Inhibitors. *Int. J. Mol. Sci.* **2019**, *20*, 5385. [[CrossRef](#)] [[PubMed](#)]
26. Pattabiraman, V.R.; Bode, J.W. Rethinking amide bond synthesis. *Nature* **2011**, *480*, 471–479. [[CrossRef](#)] [[PubMed](#)]
27. Gonec, T.; Zadrazilova, I.; Nevin, E.; Kauerovala, T.; Pesko, M.; Kos, J.; Oravec, M.; Kollar, P.; Coffey, A.; O'Mahony, J.; et al. Synthesis and biological evaluation of N-alkoxyphenyl-3-hydroxynaphthalene-2-carboxanilides. *Molecules* **2015**, *20*, 9767–9787. [[CrossRef](#)] [[PubMed](#)]
28. Teixeira, R.R.; Pereira, J.L.; Pereira, W.L. Photosynthetic inhibitors. In *Applied Photosynthesis*; Najafpour, M., Ed.; InTech: Rijeka, Croatia, 2012; pp. 3–22.
29. Kos, J.; Zadrazilova, I.; Pesko, M.; Keltosova, S.; Tengler, J.; Gonec, T.; Bobal, P.; Kauerovala, T.; Oravec, M.; Kollar, P.; et al. Antibacterial and herbicidal activity of ring-substituted 3-hydroxynaphthalene-2-carboxanilides. *Molecules* **2013**, *18*, 7977–7997. [[CrossRef](#)] [[PubMed](#)]
30. Gonec, T.; Kos, J.; Zadrazilova, I.; Pesko, M.; Govender, R.; Keltosova, S.; Chambel, B.; Pereira, D.; Kollar, P.; Imramovsky, A.; et al. Antibacterial and herbicidal activity of ring-substituted 2-hydroxynaphthalene-1-carboxanilides. *Molecules* **2013**, *18*, 9397–9419. [[CrossRef](#)]
31. Gonec, T.; Kralova, K.; Pesko, M.; Jampilek, J. Antimycobacterial N-alkoxyphenylhydroxynaphthalene-carboxamides affecting photosystem II. *Bioorg. Med. Chem. Lett.* **2017**, *27*, 1881–1885. [[CrossRef](#)]
32. Jampilek, J.; Kralova, K.; Pesko, M.; Kos, J. Ring-substituted 8-hydroxyquinoline-2-carboxanilides as photosystem II inhibitors. *Bioorg. Med. Chem. Lett.* **2016**, *26*, 3862–3865. [[CrossRef](#)] [[PubMed](#)]
33. Bak, A.; Kos, J.; Michnova, H.; Gonec, T.; Pospisilova, S.; Kozik, V.; Cizek, A.; Smolinski, A.; Jampilek, J. Similarity-driven pharmacophore mapping for series of N-(disubstituted-phenyl)-3-hydroxynaphthalene-2-carboxamides. *Int. J. Mol. Sci.* **2020**, *21*, 6583. [[CrossRef](#)] [[PubMed](#)]
34. Kerns, E.H.; Di, L. *Drug-Like Properties: Concepts. Structure Design and Methods: From ADME to Toxicity Optimization*; Academic Press: San Diego, CA, USA, 2008.
35. Jampilek, J. Potential of agricultural fungicides for antifungal drug discovery. *Expert Opin. Drug Dis.* **2016**, *11*, 1–9. [[CrossRef](#)] [[PubMed](#)]
36. Masarovicova, E.; Kralova, K. Approaches to measuring plant photosynthesis activity. In *Handbook of Photosynthesis*, 2nd ed.; Pessaraki, M., Ed.; Taylor & Francis Group: Boca Raton, FL, USA, 2005; pp. 617–656.